Vol. 63 October, 1959 No. 10

# THE JOURNAL OF PHYSICAL CHEMISTRY

(Registered in U. S. Patent Office)

## CONTENTS


**33rd NATIONAL COLLOID SYMPOSIUM, MINNEAPOLIS, MINNESOTA, JUNE 18–20, 1959**

**Wayne H. Martin and Quentin Van Winkle:** A Study of the Transference Method for the Determination of Counterion Association with Polyelectrolytes and its Application to Poly-4-vinyl-N, *n*-Butylpyridinium Bromide in HBr Solutions ..... 1539
**John R. Cann:** On the Behavior of Serum Albumin in Acidic Perchlorate Solutions ..... 1545
**E. Matijevic, D. Broadhurst and M. Kerker:** On Coagulation Effects of Highly Charged Counter Ions ..... 1552
**Chester T. O'Konski, Koshiro Yoshioka and William H. Orttung:** Electric Properties of Macromolecules. IV. Determination of Electric and Optical Parameters from Saturation of Electric Birefringence in Solutions ..... 1558
**Wilfried Heller, Englebert Rowe, Robert Berg, and John H. L. Watson:** Effect of Partial Coagulation Upon the Size Distribution Curve in Heterodisperse Colloidal Systems ..... 1566
**Robert L. Baldwin:** Boundary Spreading in Sedimentation Velocity Experiments. VI. A Better Method for Finding Distributions of Sedimentation Coefficient when the Effects of Diffusion are Large ..... 1570
**K. E. Van Holde:** The Sedimentation Velocity of Osmium Tetroxide in Aqueous Solution ..... 1574
**E. Glen Richards and Howard K. Schachman:** Ultracentrifuge Studies with Rayleigh Interference Optics. I. General Application ..... 1578
**Rodes Trautman and Sydney S. Breese, Jr.:** Moving Boundary Theory Applied to Preparative Ultracentrifugation ..... 1592
**Riyad R. Irani:** The Interpretation of Abnormalities in the Log-Normal Distribution of Particle Size ..... 1603
**Marjorie J. Vold:** Sediment Volume and Structure in Dispersions of Anisometric Particles ..... 1608
**H. R. Heydegger and H. N. Dunning:** A Radiotracer Study of Adsorption of an Ethylene Oxide-Propylene Oxide Condensate on Quartz Powders ..... 1613
**L. H. Little:** Infrared Spectra of Hydrocarbons Adsorbed on Silica Supported Metal Oxides ..... 1616
**Aage Solbakken and Lloyd H. Reyerson:** Sorption and Magnetic Susceptibility Studies on Nitric Oxide-Silica Gel Systems at a Number of Temperatures ..... 1622
**Yung-Fang Yu, J. J. Chessick and A. C. Zettlemoyer:** Adsorption Studies on Metals. VIII. Monofunctional Organic Molecules on Reduced and Oxide-Coated Nickel and Copper ..... 1626
**J. L. Shereshefsky and Bibhuti R. Mazumder:** The Adsorption of Some Gases on Evaporated Metal Films and on Oxidized Films of Nickel. 1630
**William H. Wade and Norman Hackerman:** Heats of Immersion. II. Calcite and Kaolinite—The Effect of Pretreatment ..... 1639
**Irving Fatt and Mohamed A. Selim:** Chromatographic Frontal Advance of an Adsorbate that has an Adsorption Maximum ..... 1641
**Charles G. Dodd and O. Gerald Kiel:** Evaluation of Monte Carlo Methods in Studying Fluid–Fluid Displacements and Wettability in Porous Rocks ..... 1646
**Wasyl S. Hnojewyj and Lloyd H. Reyerson:** The Sorption of $H_2O$ and $D_2O$ by Lyophilized Lysozyme ..... 1653
**Rulon E. Johnson, Jr.:** Conflicts between Gibbsian Thermodynamics and Recent Treatments of Interfacial Energies in Solid-Liquid-Vapor Systems ..... 1655
**K. B. Deshpande and C. E. Marshall:** An Interpretation of Electrochemical Measurements on a Montmorillonite Clay ..... 1659
**C. E. Marshall and G. Garcia:** Exchange Equilibria in a Carboxylic Resin and in Attapulgite Clay ..... 1663
**E. L. Talbot:** The Surface Tension of Perfluoro Sulfonates in Strong and Oxidizing Acid Media ..... 1666
**Sydney Ross and J. P. Olivier:** A New Method for the Determination of Critical Micelle Concentrations of Un-ionized Association Colloids in Aqueous or in Non-aqueous Solution ..... 1671
**Paul Becher:** Non-ionic Surface-Active Compounds. I. Critical Micelle Concentrations of Water-Soluble Ether-Alcohols ..... 1675
**Jack H. Schulman, Walter Stoeckenius and Leon M. Prince:** Mechanism of Formation and Structure of Micro Emulsions by Electron Microscopy ..... 1677
**Sydney Ross, E. S. Chen, Paul Becher, and H. J. Ranauto:** Spreading Coefficients and Hydrophile-Lipophile Balance of Aqueous Solutions of Emulsifying Agents ..... 1681
**F. M. Fowkes, G. S. Ronay and M. J. Schick:** Monolayers in Equilibrium with Lenses of Oil on Water. II. Dependence of Equilibrium Pressures on pH and on Concentration of Surfactant ..... 1684
**Melvin H. Gottlieb:** Bubble Stability in Dimethyl Silicone Solutions ..... 1687
**Henri L. Rosano and Gerhart Karg:** The Desorption of Sodium Dodecyl Sulfate Spread on an Aqueous Substrate ..... 1692

**Karol J. Mysels and L. H. Princen:** Light Scattering by Some Laurylsulfate Solutions ..... 1696
**T. S. Smith and E. A. Smith:** Nuclear Magnetic Shielding of $F^{19}$ in Some Chlorofluorocarbons ..... 1701
**Eric Baum:** Integration of the Rate Equation for a Second Order Reaction in an Adiabatic Flow System ..... 1704
**W. Fuller:** Hydrogen Bond Lengths and Angles Observed in Crystals ..... 1705
**K. L. Sutherland:** Collector-Depressant Equilibria in Flotation ..... 1717
**Arthur Veis and Joan Anesey:** Configurational Transitions in Gelatins in Non-Aqueous Solutions ..... 1720
**J. R. Thomas:** Sonic Degradation of High Polymers in Solution ..... 1725
**J. W. Shepard and John P. Ryan:** A Radioactive Tracer Study of the Adsorption of Fluorinated Compounds on Solid Planar Surfaces. I. Perfluorooctanoic Acid ..... 1729
**Gordon B. Skinner and Robert A. Ruehrwein:** Shock Tube Studies on the Pyrolysis and Oxidation of Methane ..... 1736
**David A. Yphantis:** Ultracentrifugal Molecular Weight Averages during the Approach to Equilibrium ..... 1742
**E. K. Storms and N. H. Krikorian:** The Variation of Lattice Parameter with Carbon Content of Niobium Carbide ..... 1747
**F. Jona:** Preparation and Dielectric Properties of Synthetic Boracite-Like Compounds ..... 1750
**Willis A. Rosser, Jr. and Henry Wise:** The Kinetics of Oxidation of HBr ..... 1753
**A. A. Miller:** Radiation Chemistry of Polyvinyl Chloride ..... 1755
**Louis Watts Clark:** The Effect of Monocarboxylic Acids and their Derivatives on the Trichloroacetate Ion ..... 1760
**Leo A. Wall, Daniel W. Brown and Roland E. Florin:** Atoms and Free Radicals by Gamma Irradiation at 4.2° K ..... 1762
**Gideon Czapski, Joshua Jortner and Gabriel Stein:** The Oxidation of Iodide Ions in Aqueous Solution by Atomic Hydrogen ..... 1769
**C. W. Bjorklund, J. G. Reavis, J. A. Leary and K. A. Walsh:** Phase Equilibria in the Binary Systems $PuCl_3$–NaCl and $PuCl_3$–LiCl ..... 1774
**E. R. Nightingale, Jr., and R. F. Benck:** Viscosity of Aqueous Sodium Fluoride and Sodium Periodate Solutions. Ionic Energies and Entropies of Activation for Viscous Flow ..... 1777

**Notes**

**L. H. Princen and Karol J. Mysels:** Some Effects of Lauryl Alcohol on Light Scattering by Sodium Lauryl Sulfate ..... 1781
**James D. Ray:** The Conversion of Nitrogen Dioxide to Nitric Oxide ..... 1782
**R. N. Barfield:** The Viscosity of Diethylamine–Water Mixtures ..... 1783

# THE JOURNAL OF PHYSICAL CHEMISTRY

(Registered in U. S. Patent Office)



Published monthly by the American Chemical Society at 20th and Northampton Sts., Easton, Pa.

Second-class mail privileges authorized at Easton, Pa. This publication is authorized to be mailed at the special rates of postage prescribed by Section 131.122.

The *Journal of Physical Chemistry* is devoted to the publication of selected symposia in the broad field of physical chemistry and to other contributed papers.

Manuscripts originating in the British Isles, Europe and Africa should be sent to F. C. Tompkins, The Faraday Society, 6 Gray's Inn Square, London W. C. 1, England.

Manuscripts originating elsewhere should be sent to W. Albert Noyes, Jr., Department of Chemistry, University of Rochester, Rochester 20, N. Y.

Correspondence regarding accepted copy, proofs and reprints should be directed to Assistant Editor, Allen D. Bliss, Department of Chemistry, Simmons College, 300 the Fenway, Boston 15, Mass.

Business Office: Alden H. Emery, Executive Secretary, American Chemical Society, 1155 Sixteenth St., N. W., Washington 6, D. C.

Advertising Office: Reinhold Publishing Corporation, 430 Park Avenue, New York 22, N. Y.

Articles must be submitted in duplicate, typed and double spaced. They should have at the beginning a brief Abstract, in no case exceeding 300 words. Original drawings should accompany the manuscript. Lettering at the sides of graphs (black on white or blue) may be pencilled in and will be typeset. Figures and tables should be held to a minimum consistent with adequate presentation of information. Photographs will not be printed on glossy paper except by special arrangement. All footnotes and references to the literature should be numbered consecutively and placed in the manuscript at the proper places. Initials of authors referred to in citations should be given. Nomenclature should conform to that used in *Chemical Abstracts*, mathematical characters marked for italic, Greek letters carefully made or annotated, and subscripts and superscripts clearly shown. Articles should be written as briefly as possible consistent with clarity and should avoid historical background unnecessary for specialists.

*Notes* describe fragmentary or incomplete studies but do not otherwise differ fundamentally from articles and are subjected to the same editorial appraisal as are articles. In their preparation particular attention should be paid to brevity and conciseness. Material included in Notes must be definitive and may not be republished subsequently.

*Communications to the Editor* are designed to afford prompt preliminary publication of observations or discoveries whose value to science is so great that immediate publication is imperative. The appearance of related work from other laboratories is in itself not considered sufficient justification for the publication of a Communication, which must in addition meet special requirements of timeliness and significance. Their total length may in no case exceed 500 words or their equivalent. They differ from Articles and Notes in that their subject matter may be republished.

Symposium papers should be sent in all cases to Secretaries of Divisions sponsoring the symposium, who will be responsible for their transmittal to the Editor. The Secretary of the Division by agreement with the Editor will specify a time after which symposium papers cannot be accepted. The Editor reserves the right to refuse to publish symposium articles, for valid scientific reasons. Each symposium paper may not exceed four printed pages (about sixteen double spaced typewritten pages) in length except by prior arrangement with the Editor.

Remittances and orders for subscriptions and for single copies, notices of changes of address and new professional connections, and claims for missing numbers should be sent to the American Chemical Society, 1155 Sixteenth St., N. W., Washington 6, D. C. Changes of address for the *Journal of Physical Chemistry* must be received on or before the 30th of the preceding month.

Claims for missing numbers will not be allowed (1) if received more than sixty days from date of issue (because of delivery hazards, no claims can be honored from subscribers in Central Europe, Asia, or Pacific Islands other than Hawaii), (2) if loss was due to failure of notice of change of address to be received before the date specified in the preceding paragraph, or (3) if the reason for the claim is "missing from files."

Subscription Rates (1959): members of American Chemical Society, $8.00 for 1 year; to non-members, $16.00 for 1 year. Postage free to countries in the Pan American Union; Canada, $0.40; all other countries, $1.20. Single copies, current volume, $1.35; foreign postage, $0.15; Canadian postage $0.05. Back volumes (Vol. 56–59) $15.00 per volume; (starting with Vol. 60) $18.00 per volume; foreign postage, per volume $1.20, Canadian, $0.15; Pan-American Union, $0.25. Single copies: back issues, $1.75; for current year, $1.35; postage, single copies: foreign, $0.15; Canadian, $0.05; Pan American Union, $0.05.

The American Chemical Society and the Editors of the *Journal of Physical Chemistry* assume no responsibility for the statements and opinions advanced by contributors to This Journal.

The American Chemical Society also publishes *Journal of the American Chemical Society, Chemical Abstracts, Industrial and Engineering Chemistry, Chemical and Engineering News Analytical Chemistry, Journal of Agricultural and Food Chemistry, Journal of Organic Chemistry* and *Journal of Chemical and Engineering Data*. Rates on request.

W. E. Harris, W. H. McFadden and R. G. McIntosh: Chemical Effects of (n,γ)-Activation of Bromine in the Alkyl Bromides: A New Method for Determination of Organic Retention ..... 1784
J. L. Barton and H. Bloom: The Molecular Weight of Sodium and Potassium Chloride Vapors ..... 1785
F. Pizzarello: Purification of Lithium Iodide by Zone Melting ..... 1785
S. R. Gunn, L. G. Green and A. I. Von Egidy: The Heat of Chlorination of Dibboron Tetrachloride ..... 1787
T. W. Gilbert, Jr.: Determination of Association Equilibria by the Method of Continuous Variations ..... 1788
A. C. Makrides: Thermal Aging of Silica Gels ..... 1789
Elmer J. Badin: The Reaction between Titanium Tetrachloride and Aluminum Triethyl ..... 1791
Gundolf Kohlmaier and B. S. Rabinovitch: Kinetics of Thermal Isomerization of *para*-Tolyl Isocyanide ..... 1793

THE JOURNAL OF
PHYSICAL CHEMISTRY

(Registered in U. S. Patent Office) 

VOLUME 63 OCTOBER 20, 1959 NUMBER 10

# A STUDY OF THE TRANSFERENCE METHOD FOR THE DETERMINATION OF COUNTERION ASSOCIATION WITH POLYELECTROLYTES AND ITS APPLICATION TO POLY-4-VINYL-N,*n*-BUTYLPYRIDINIUM BROMIDE IN HYDROGEN BROMIDE SOLUTIONS

BY WAYNE H. MARTIN AND QUENTIN VAN WINKLE

*Department of Chemistry, The Ohio State University, Columbus, Ohio*

*Received March 6, 1959*

Some limitations of the transference method for study of degree of ionization ($\alpha$) of polyelectrolytes are discussed. For PVPBr in HBr, where the polyion and simple ion of like charge ($H^+$) have greatly differing mobilities, the "mixture effect" of Onsager and Fuoss causes large errors to be introduced in the values of $\alpha$ for finite concentrations of HBr. At zero HBr concentration, it was found that $\alpha$ decreases from 0.57 at zero PVPBr concentration to a constant value of 0.25 at concentrations of PVPBr above 0.5%.

## Introduction

A critical study of the transference method for determining the extent of counterion association in polyelectrolyte systems has revealed that the method cannot be used without some assumption concerning the values of the ionic conductivities in the polyelectrolyte solution.

In the method as originally used by Wall and associates,[2-4] it is assumed that the ionic conductivities of both counterions and by-ions are the same as in a simple binary electrolyte solution, and that these conductivities are additive, together with the conductivity of the polyion, to give the observed conductance of the solution. The validity of this assumption should be questioned, especially for polyelectrolytes in the presence of added salts, since it has been shown both theoretically and experimentally[5] that the observed conductance in an arbitrary mixture of ions is less than the value obtained by adding the individual ionic conductivities as measured in simple binary solutions. This "mixture effect" disappears as the ionic strength of the solution approaches zero, and as the mobilities of the various ions of like charge approach each other.

The most critical test of Wall's method would therefore be to apply it to fairly concentrated solutions of a system in which the mobilities of the polyion and its by-ion differ significantly. Poly-4-vinyl-N,*n*-butylpyridinium bromide (PVPBr) in HBr solutions is suitable for such a test, because the mobilities of $PVP^+$ and $H^+$ differ by a factor of ten, and the solutions can be analyzed readily for $H^+$ and $Br^-$.

## Experimental

**Preparation and Analysis of Solutions.**—Vinylpyridine was polymerized by a procedure adapted from Fuoss and Strauss.[6]

Chemical analysis of the PVPBr gave a formula of $C_{11.04}H_{18.08}N_{1.000}Br_{1.004}$ as compared to the theoretical formula $C_{11}H_{16}NBr$. Titration with $AgNO_3$ and NaOH indicate that 97.75% of the nitrogen atoms are quaternized with butyl bromide, and the additional 2.25% are quaternized with HBr. Light scattering studies on unquaternized PVP gave $\bar{M}_W$ = 116,000. Assuming 100% quaternization, the molecular weight of the PVPBr would be 267,000, corresponding to a weight average degree of polymerization of 1100.

Studies were made on the solutions shown in Table II. Exact concentrations of the solutions were determined by analysis and are given in Tables I and II. The Volhard method was used for $Br^-$ analysis. The $H^+$ was titrated with 0.02 *N* NaOH using phenolphthalein as an indicator: two samples of each solution were analyzed in most cases.

The concentration of $PVP^+$ was obtained from $C_P = C_{Br} - C_H$ where $C_{Br}$ and $C_H$ are the concentrations of $Br^-$ and $H^+$ in the same units. All analyses were made on a

(1) From the Ph.D. dissertation of Wayne H. Martin, The Ohio State University, 1958.

(2) F. T. Wall and R. H. Doremus, *ibid.*, **76**, 1557 (1954).

(3) (a) J. R. Huizenga, P. F. Grieger and F. T. Wall, *J. Am. Chem. Soc.*, **72**, 2636 (1950); (b) **72**, 4228 (1950).

(4) F. T. Wall and M. J. Eitel, *ibid.*, **79**, 1556 (1957).

(5) L. Onsager and R. M. Fuoss, THIS JOURNAL, **36**, 2689 (1932).

(6) R. M. Fuoss and U. P. Strauss, *J. Polymer Sci.*, **3**, 246 (1948).

TABLE I

VALUES OF $r$, $\Lambda'_{Br}$, $\Lambda'_{H}$ AND $t'_{H}$ FOR THE VARIOUS HBr SOLUTIONS USED AS SOLVENT

| $C_{HBr}$ | $r$ | $\Lambda'_{Br}$ | $\Lambda'_{H}$ | $t'_{H}$ |
|---|---|---|---|---|
| 0.04065 | 0.21317 | 70.90 | 333.21 | 0.82429 |
| .02504 | .21492 | 72.13 | 336.04 | .82310 |
| .01020 | .21756 | 73.99 | 340.29 | .82131 |
| .00500 | .21911 | 75.10 | 342.85 | .82027 |
| .00250 | .22028 | 75.92 | 344.73 | .81948 |
| .000439[a] | .22202 | 77.16 | 347.87 | .81832 |
| .000306[a] | .22224 | 77.31 | 348.18 | .81817 |

[a] Estimated values of free HBr present for solutions of 1 and 0.5% PVPBr in water. The PVPBr is partially quaternized (2.25%) with HBr rather than butyl bromide, and part of this HBr is hydrolyzed in water, as indicated by $p$H measurements. The hydrolysis was negligible in HBr solutions.

weight basis (equivalents per 1000 g. solution) and were converted to equivalents per 1000 g. of water for the transference calculations.

**Apparatus and Procedures.**—The transference cell consisted of a modified Hittorf apparatus with several right angle bends inserted to help eliminate convection currents. The anode, middle and cathode compartments had volumes of 60, 30 and 70 ml., respectively. Vent tubes facilitated draining the various compartments without mixing.

The electrodes were of bright platinum wire (20 gauge), the anode being a coil made from a 3 cm. length, while the cathode was only 2 mm. long, in order to minimize adsorption of the polymer on the cathode. The electrodes were held in place by rubber stoppers which also contained stopcocks. During a run the stopcocks were left open to permit escape of gases and were closed at the end of the run.

The quantity of electricity passed through the cell was measured accurately by means of two iodine coulometers, one in series with each electrode.

During the transference experiments the cell was immersed in a water-bath maintained at 25.00 ± 0.01°. The cell was mounted on a hydraulic lift to permit removal from the bath with a minimum of vibration.

A Jones-type bridge manufactured by Leeds and Northrup Company was used for the conductance measurements. The cells were designed according to the recommendations of Jones and Bollinger,[7] but in order to minimize adsorption of polymer on the electrodes, the latter were not platinized.

Two cells were used, one having a cell constant of 39.968, and the other a cell constant of 2.8247. The cell constants were accurately determined before each series of measurements by using a standard 0.01 demal KCl solution.

All resistance measurements were made at 1000 cycles per second with the cell in a water-bath which was maintained at 25.000 ± 0.005°.

## Theoretical

**Calculation of Degree of Association from Transference Experiments.**—The discussion will be limited to only one species of polymeric ion in solutions with counterions present either in the free state or in the bound state, with no intermediate states.

The polymeric ion will be designated by the subscript p, the counterions by the subscript c, and the by-ions (ions of same sign as the polyion) by the subscript b.

It will be helpful to consider the solutions to be made up by dissolving the polyelectrolyte, $PC_n$, in a solution of the simple, symmetrical electrolyte BC.

These symbols will be used

$\alpha$ = fractional charge per monomer unit (identical with the degree of dissociation for a weak electrolyte)

(7) G. Jones and G. M. Bollinger, *J. Am. Chem. Soc.*, **53**, 411 (1931).

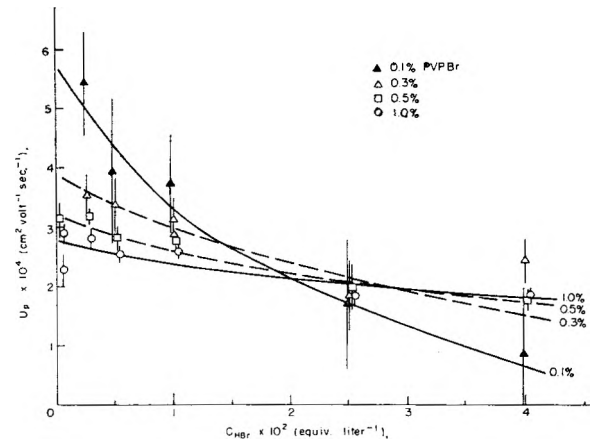


Fig. 1a.—Variation of mobility with HBr at constant PVPBr concentration.

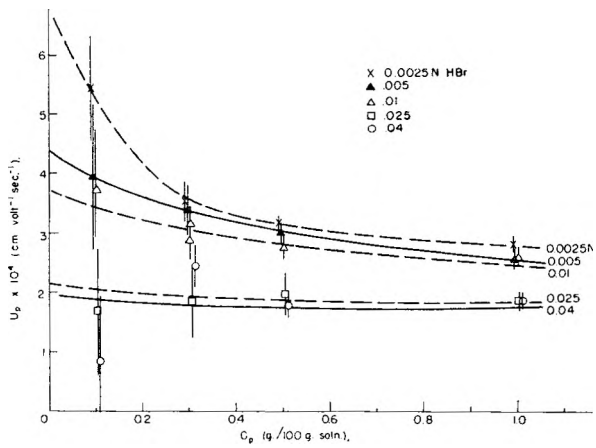


Fig. 1b.—Variation of mobility with $C_p$ at constant HBr concentration.

$1 - \alpha$ = degree of association of the counterion C with the polyion

$t_i$ = transference number of ion i

$Q_i$ = net increase in the no. of equiv.[9] of ion i in the cathode compartment during a transference expt.

$n$ = no. of equiv. of electricity passed through the cell during a transference expt.

$C_i$ = stoichiometric concn. of the ion i in equiv.[9] per l.

$K$ = specific conductance of the polymer soln.

$K_i$ = ionic specific conductance of ion i in the polymer soln.

$\Lambda_i$ = ionic equiv. conductance of ion i in the polymer soln.

$K'$, $K_i'$, $\Lambda'$, $\Lambda_i'$, $t_i'$, etc., are the same quantities as defined above, except that the primed quantities refer to the simple electrolyte soln. BC in which the polyelectrolyte was dissolved, while the unprimed quantities refer to the polymer soln.

$r = t_c'/t_b'$ = ratio of the counterion transference no. to that of the by-ion in the simple electrolyte soln. in which the polymer is dissolved

The transference number of the polyion can be defined as the fraction of the charge carried

$$t_p = \frac{\alpha Q_p}{n} = \frac{K_p}{K} \qquad (1)$$

Using

$$K_p = K - K_b - K_c \qquad (2)$$

and following the derivation of Wall[1,8]

(8) F. T. Wall, J. J. Ondrejcin and M. Pikramenou, *ibid.*, **73**, 2821 (1951).

(9) For the polymeric ion "one equivalent" is the same as a monomole, or one mole of monomer units.

TABLE II

EXPERIMENTAL DATA[a]

| $C_P$, % | $C_{HBr}$, equiv./l. | $t_H$ | $Q_P$, meq. | $n$, meq. | $\mathcal{J}_P$, meq./10 g. soln. | $K \times 10^3$, mho/cm. |
|---|---|---|---|---|---|---|
| 0.1 | 0.0025 | 0.701 | 0.0150 | 0.07892 | 0.04129 | 1.1414 |
| | .005 | .753 | .0106 | .14218 | .04155 | 2.1185 |
| | .01 | .7947 | .0148 | .42924 | .04017 | 4.2088 |
| | .025 | .8119 | .0052 | .76214 | .04251 | 10.170 |
| | .04 | .8150 | .0028 | 1.2945 | .04200 | 16.297 |
| 0.3 | 0.0025 | 0.606 | 0.0304 | 0.09723 | 0.12384 | 1.3535 |
| | .005 | .700 | .0271 | .15560 | .12233 | 2.2984 |
| | .01 | .7519 | .0347 | .44621 | .12180 | 4.3696 |
| | .01 | .7532 | .0376 | .44041 | .12179 | 4.3462 |
| | .025 | .7972 | .0122 | .56159 | .12503 | 10.276 |
| | .04 | .8019 | .0267 | 1.4978 | .12353 | 16.357 |
| 0.5 | 0 | 0.117 | 0.0209 | 0.02232 | 0.20532 | 0.64572 |
| | 0 | .165 | .0239 | .02522 | .20345 | 0.65215 |
| | 0.0025 | .512 | .0520 | .12285 | .22133 | 1.6041 |
| | .005 | .631 | .0529 | .21886 | .20857 | 2.5048 |
| | .01 | .7185 | .0540 | .44396 | .20547 | 4.4987 |
| | .025 | .7783 | .0213 | .56240 | .20495 | 10.363 |
| | .04 | .7943 | .0370 | 1.7380 | .20631 | 16.415 |
| 1 | 0 | 0.123 | 0.0279 | 0.03814 | 0.40942 | 1.2352 |
| | 0 | .099 | .0335 | .03600 | .41157 | 1.2427 |
| | 0.0025 | .373 | .0638 | .11960 | .41083 | 2.0908 |
| | .005 | .528 | .0680 | .19913 | .41128 | 2.9604 |
| | .01 | .6463 | .0936 | .45132 | 40883 | 4.8993 |
| | .025 | .7452 | .0459 | .66797 | 40692 | 10.616 |
| | .04 | .7687 | .0725 | 1.6197 | 41134 | 16.538 |

[a] Each of the quantities tabulated contains two doubtful figures.

$$\alpha = \frac{10^3K - C_b\Lambda_b - C_b\Lambda_c}{\frac{10^3Q_pK}{n} + C_p\Lambda_c} \qquad (3)$$

Equations 2 and 3 are strictly valid only if the conductivities are determined in the polymer solution. If the concentration of by-ions in the solution can be determined, then the transference number of the by-ion in the polymer solution can be calculated from the transference data, and the conductance of the by-ions can be obtained from (4)

$$\Lambda_b = \frac{10^3K_b}{C_b} = \frac{10^3t_bK}{C_b} \qquad (4)$$

where $K$ is the experimentally measured conductance of the solution.

The counterion conductance cannot be determined from an expression similar to equation 4, however, because some of the counterions migrate with the polyion, and thus $t_c$ is dependent on $\alpha$. Several methods will now be discussed which will lead to approximate values of $\alpha$.

**Method (i).**—The easiest assumption to make from the experimental point of view is that Kohlrausch's rule of independent migration of ions is valid, and thus $\Lambda_b$ and $\Lambda_c$ can be obtained from data on simple binary electrolytes. This is the method used by Wall and co-workers.[1-4]

$\Lambda_c$ should be evaluated from data on a simple binary electrolyte in which the concentration is equal to the total concentration of free counterions in the polyelectrolyte solution, which is given by

$$(C_c)_{free} = C_b + \alpha C_p \qquad (5)$$

Literature data are lacking on HBr solutions, but theoretical equations are available which give $\Lambda_i$ as a function of concentration. Such an equation should give more accurate results than Hittorf-type transference experiments. The equation of Robinson and Stokes[10,11] used was for a 1-1 electrolyte.

$$\Lambda_i = \Lambda_i^0 - (B_i\Lambda_i^0 + {}^1/_2B_2)\frac{\sqrt{C}}{1 + Ba\sqrt{C}} \qquad (6)$$

where $B = 0.3286$, $B_1 = 0.2289$ and $B_2 = 60.32$. The quantity $a$ is the ion size parameter in Å., for which a value of 5.10 was used. This compares well with the value of 5.18 obtained for HBr over the range 0.1–1.0 molal from activity coefficient data.[12] Values of 78.14 and 349.81 were used for $\Lambda^0_{Br}$ and $\Lambda^0_H$. The values of $\Lambda_H$ obtained from the above equation are tabulated in Table I under the column labeled $\Lambda_H'$.

The values of $\alpha$ and $\Lambda_c$ must be adjusted by a series of successive approximations using equations 3, 5 and 6.

**Method (ii).**—This method is similar to method (i) except that enough additional experimental data are obtained to calculate the actual value of by-ion conductance $\Lambda_b$ in the polyelectrolyte solution, using equation 4. $\Lambda_c$ is still obtained from data on simple electrolyte solutions, however.

Equation 3 may be used to calculate $\alpha$ by this method, but the values of $\alpha$ and $\Lambda_c$ must be adjusted by a series of successive approximations as in method (i).

**Method (iii).**—The conductance of the by-ions

(10) R. A. Robinson and R. H. Stokes, "Electrolyte Solutions," Academic Press, New York, N. Y., 1955, p. 150.

(11) Literature data are lacking for HBr, but for HCl the values of $\Lambda_{Cl}$ calculated from this equation agree with observed values within 0.07% for a 0.01 $N$ solution and within 0.6% for a 0.1 $N$ solution.

(12) R. A. Robinson and R. H. Stokes, ref. 10, p. 247.

in the polyelectrolyte solution can be determined from equation 4. It then may be assumed that $\Lambda_c$ and $\Lambda_b$ are decreased in the same proportion on addition of the polyelectrolyte. Thus

$$\frac{\Lambda_c}{\Lambda_c'} = \frac{\Lambda_b}{\Lambda_b'} \qquad (7)$$

When equations 4 and 7 are substituted into equation 3, the expression for $\alpha$ becomes

$$\alpha = \frac{10^3K - C_b\Lambda_b(1+r)}{\frac{10^3Q_pK}{n} + C_pr\Lambda_b} = \frac{1 - t_b - rt_b}{\frac{Q_p}{n} + \frac{C_prt_b}{C_b}} \qquad (8)$$

The quantity $r$ is the ratio $t_c/t_b$ in the simple electrolyte solution BC, and may be determined from a separate transference experiment on the simple salt solution. In the present investigation $r$ was calculated from an equation for the variation of transference number with concentration. For a 1-1 electrolyte such an equation may be written[13]

$$t_i = \frac{\Lambda_i^0 - {}^1/_2B_2\frac{\sqrt{C}}{1+Ka}}{\Lambda^0 - B_2\frac{\sqrt{C}}{1+Ka}} \qquad (9)$$

where $B_2 = 60.32$, and $Ka = 0.3286\sqrt{C}$, $a$ being the ion size parameter in Å. A value of $5 \times 10^{14}$ was used for $a$, as in the preceding section.

In calculating $r$, the denominator of equation 9 cancels, and the expression for $r$ becomes

$$r = \frac{t_C'}{t_b'} = \frac{\Lambda_C^0 - {}^1/_2B_2\frac{\sqrt{C}}{1+Ka}}{\Lambda_b^0 - {}^1/_2B_2\frac{\sqrt{C}}{1+Ka}} \qquad (10)$$

Values of $r$ calculated from this equation and of $t_H'$ calculated from equation 9 are given in Table I for each of the HBr solutions used as solvent.

**Method (iv).**—Experimentally it is found that $\Lambda_b$ is decreased when a polyelectrolyte PC is added to a solution of the simple electrolyte BC. From the considerations of Onsager and Fuoss,[5] the presence of polyelectrolyte is expected to produce a smaller decrease in the conductivity of the counterions C than the observed decrease in the conductivity of the by-ions B, and thus

$$\frac{\Lambda_c}{\Lambda_c'} = x \times \frac{\Lambda_b}{\Lambda_b'} \qquad (11)$$

where $x$ is a number greater than one. The only difficulty with this method is that the values of $\alpha$ are very sensitive to small changes in $x$, and the quantity $x$ cannot be considered as constant over a wide range of experimental conditions.

This method can best be used in conjunction with method (iii) to indicate the direction and to estimate the magnitude of corrections which should be applied to values of $\alpha$ obtained by method (iii).

Equation 8 can be used to calculate $\alpha$ by this method if the quantity $r$ is replaced by $xr$.

**Calculation of the Polyion Mobility.**—According to Svensson,[15] the constituent mobility of an ion may be defined in terms of a transference experiment as the mass transported relative to some plane of reference per unit time, unit cross section of the tube, unit field strength and unit concentration of the constituent. In terms of the nomenclature used here, the expression for $u_P$ can be written

$$u_P = \frac{10^3Q_pK}{C_pnF} \qquad (12)$$

In equation 12, $C_P$ should be expressed in equivalents per liter of solution, but since the analyses are made on a weight basis, $C_P$ will be expressed in equivalents per 1000 grams of solution in the calculations. The error introduced by doing this is much smaller than the other experimental errors

## Results and Discussion

The experimental data are presented in Table II. Table III gives a comparison of the values of $\alpha$ obtained by each of the four methods described, as well as values of $u_P$, the polyion mobility. Blank spaces in Table III indicate that the numerator in the expression for $\alpha$ was negative. In method (iv), the numerator becomes negative for high values of $x$. It should be noted that method (iii) is merely a special case of method (iv) in which $x = 1$. Three significant figures are given for both $\alpha$ and $u_P$, but an analysis of errors indicates that two of these three figures are doubtful, the error decreasing with increasing $C_P$. In Figs. 1 and 2 the errors in $u_P$ and $\alpha$ are represented by the length of the vertical lines through the points.

**Mobility Data.**—In considering the influence of $C_{HBr}$ and $C_P$ on the mobility of the polyion, two factors are expected to play an important role. One is a decrease in the effective size of the polyion due to a change in shape upon the addition of a simple electrolyte such as HBr, as shown by viscosity studies.[16] This decrease in size would tend to increase the mobility with increasing HBr concentration. The second factor is a change in $\alpha$, and thus the charge on the polyion. By analogy with systems of simple weak electrolytes, one would expect $\alpha$ to decrease as HBr is added, because of the common-ion effect. A decrease in $\alpha$ with added HBr would tend to decrease the mobility of the polyion.

An examination of Fig. 1a reveals that the polyion mobility does decrease with increasing HBr, and thus the effect of charge on the mobility must be greater than that of shape. Furthermore, since the polyion mobility is obtained directly from experimental quantities with no assumptions involved, the decrease in mobility with HBr concentration is unequivocal evidence that $\alpha$ decreases with increasing HBr concentration.

**Comparison of the Values of $\alpha$ Calculated by the Four Methods.**—An examination of Table IV reveals that method (i) gives the expected decrease in $\alpha$ with HBr, but the values do not tend to become constant at high HBr as expected, and in many cases the numerator of the expression for $\alpha$ is negative. This is the result of using values of $\Lambda_b$ and $\Lambda_c$ which are too large, thus making $\alpha$ (i) smaller than the true value of $\alpha$.

Table III and Fig. 2a show that methods (ii) and (iii) give an increase in $\alpha$ with increasing HBr concentration, which is indeed surprising. This in-

(13) R. A. Robinson and R. H. Stokes, ref. 10, p. 157.

(14) $t_H$ is not very sensitive to the choice of $a$. For 0.02 $N$ HBr, $t_H$ varies from 0.8229 to 0.8226 as $a$ is varied from 4.00 to 5.40.

(15) H. Svensson, *Acta Chem. Scand.*, **2**, 841 (1948).

(16) R. M. Fuoss and U. P. Strauss, *J. Polymer Sci.*, **3**, 602 (1948).

TABLE III

CALCULATED VALUES OF $\alpha$ AND $u_P$

| $C_P$ | $C_{HBr}$ | $10^4 u_P$[a] | $\alpha$ (i) | $\alpha$ (ii) | $\alpha$ (iii) | $\alpha$ (iv) with $x$ = 1.01 | 1.05 | 1.20 |
|---|---|---|---|---|---|---|---|---|
| 0.1 | 0.0025 | 5.44 | 0.171 | 0.289 | 0.325 | 0.320 | 0.299 | 0.229 |
| | .005 | 3.94 | .061 | .319 | .387 | .377 | .337 | .205 |
| | .01 | 3.74 | ... | .252 | .316 | .297 | .225 | ... |
| | .025 | 1.69 | ... | .293 | .373 | .324 | .129 | ... |
| | .04 | 0.87 | ... | .412 | .562 | .473 | .124 | ... |
| 0.3 | 0.0025 | 3.54 | 0.225 | 0.256 | 0.267 | 0.264 | 0.252 | 0.211 |
| | .005 | 3.39 | .161 | .242 | .267 | .262 | .244 | .186 |
| | .01 | 2.89 | .118 | .271 | .309 | .301 | .269 | .166 |
| | .01 | 3.15 | .097 | .255 | .295 | .287 | .257 | .157 |
| | .025 | 1.85 | .050 | .254 | .294 | .276 | .205 | ... |
| | .04 | 2.45 | ... | .316 | .390 | .363 | .258 | ... |
| 0.5 | 0 | 3.05 | 0.241 | 0.255 | 0.320 | 0.318 | 0.309 | 0.281 |
| | 0 | 3.15 | .244 | .243 | .236 | .234 | .227 | .204 |
| | 0.0025 | 3.18 | .239 | .257 | .264 | .261 | .251 | .217 |
| | .005 | 3.01 | .195 | .258 | .282 | .278 | .264 | .217 |
| | .01 | 2.76 | .135 | .253 | .287 | .281 | .260 | .188 |
| | .025 | 1.98 | .078 | .271 | .297 | .299 | .253 | .103 |
| | .04 | 1.76 | ... | .282 | .335 | .317 | .246 | .017 |
| 1 | 0 | 2.29 | 0.267 | 0.268 | 0.259 | 0.257 | 0.249 | 0.223 |
| | 0 | 2.91 | .254 | .259 | .294 | .292 | .284 | .257 |
| | 0.0025 | 2.81 | .232 | .273 | .289 | .287 | .277 | .245 |
| | .005 | 2.55 | .218 | .256 | .276 | .273 | .261 | .225 |
| | .01 | 2.58 | .171 | .249 | .276 | .273 | .258 | .209 |
| | .025 | 1.86 | .111 | .254 | .287 | .280 | .253 | .164 |
| | .04 | 1.86 | .032 | .267 | .320 | .310 | .273 | .142 |

[a] $u_P$ is given in cm.$^2$ sec.$^{-1}$ volt$^{-1}$.

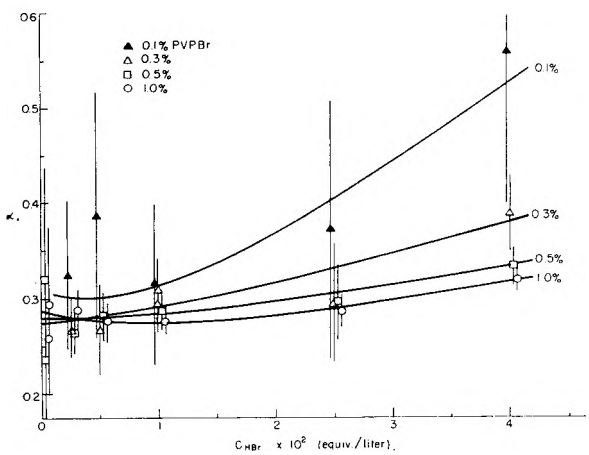


Fig. 2a.—Influence of $C_{HBr}$ on $\alpha$ as calculated by method (iii).

crease is difficult to explain, and it cannot be real, for the mobility data, which are free from assumptions, show unequivocally that $\alpha$ decreases with increasing HBr concentration.

Figures 2b and 2c show the influence of $C_{HBr}$ on $\alpha$ as calculated by method (iv). For low values of $x$ the curves go through a minimum, *i.e.*, they decrease with increasing $C_{HBr}$ at first, but as the HBr concentration is increased further, the curves begin to rise. The increase in $\alpha$ at higher HBr concentrations can be removed by increasing the value of $x$, and the curves approach the expected shape at sufficiently high values of $x$. As $C_P$ is increased, higher values of $x$ are required to prevent the curves from rising in more concentrated HBr solutions, values of $x$ = 1.05, 1.12, 1.15 and 1.20 being necessary to prevent the rise in solutions for which $C_P$ = 0.1, 0.3, 0.5 and 1%, respectively.

Method (iv), which takes into account the fact that $\Lambda_{Br}$ in the polyelectrolyte solution is less than in an HBr solution, gives the correct shape to the curves if the proper value of the parameter $x$ is used. Unfortunately the quantity $x$ depends on both $C_P$ and $C_H$ and is too complex a function to evaluate.

Since the "mixture effect" should disappear at zero HBr concentration, all four methods should give the same values of $\alpha$ at $C_{HBr}$ = 0. Although there is considerable error in the extrapolations, this prediction is correct within the experimental error. The extrapolated values are shown in Fig. 2d.

**Comparison of $\alpha$ Values with Those Obtained by E.M.F. Measurements.**—Ritchey[17] determined the degree of association of $Br^-$ with $PVP^+$ in the absence of HBr from e.m.f. measurements on concentration cells.

The $\alpha$ *vs.* $C_{HBr}$ curves of the present investigation must be extrapolated to $C_{HBr}$ = 0 before a comparison with Ritchey's results can be made. The extrapolation can best be made by using the curves obtained from method (iv) (Figs. 2b and 2c). The extrapolated values of $\alpha$ depend slightly on the value used for $x$, and therefore an average value was taken, with the curves having the correct shape being weighted more heavily than those which curved upward at high HBr concentrations.

There is considerable error introduced in the extrapolations, as there was in Ritchey's method II.

(17) W. Ritchey, Master's thesis, The Ohio State University, 1953.

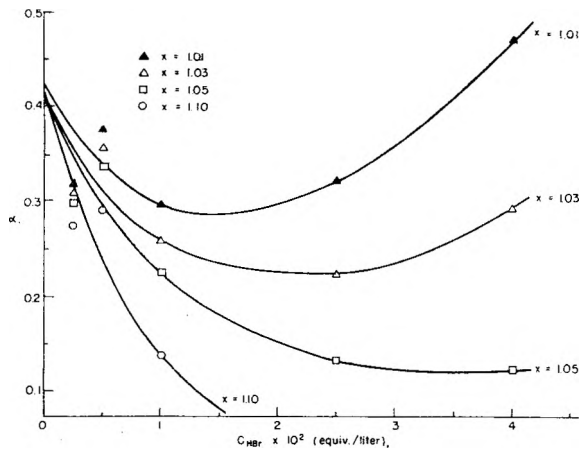


Fig. 2b.—Effect of $x$ on the curves of $\alpha$ *vs.* $C_{HBr}$ as calculated by method (iv) for 0.1% PVPBr.

The extrapolated values of $\alpha$ are plotted as a function of $C_P$ in Fig. 2d, however, and it may be seen that there is good agreement between these values and Ritchey's values which are plotted on the same graph.

**Application to Other Polyelectrolyte Systems.**—Wall and Eitel[4] neutralized polyacrylic acid (PAA) with NaOH, and studied the association of $Na^+$ with the $PAA^-$ ion in the presence of NaCl by the transference method. They used only one polymer concentration and measured $\alpha$ as a function of NaCl concentration for different degrees of neutralization, $\alpha$ being calculated by method (i).

For the case of complete neutralization of the PAA with NaOH, Wall's data have been used to calculate $\alpha$ by means of methods (ii), (iii) and (iv). The results of these calculations are presented in Table IV.

TABLE IV

COMPARISON OF $\alpha$-VALUES OBTAINED BY METHODS (i), (ii), (iii) AND (iv) FOR SODIUM POLYACRYLATE IN NaCl SOLUTIONS[a]

| $C_{NaCl}$ | $\alpha$ (i) | $\alpha$ (ii) | $\alpha$ (iii) | $\alpha$ (iv) $x = 1.10$ |
|---|---|---|---|---|
| 0.00905 | 0.355 | 0.367 | 0.361 | 0.334 |
| .0302 | .328 | .346 | .341 | .300 |
| .0453 | .307 | .329 | .324 | .274 |
| .0604 | .310 | .341 | .339[b] | .274 |

[a] The values of $\alpha$ (i) were obtained by Wall and Eitel.[4] Other values were calculated from their data. $C_P$ = 0.0695 for all the solutions (PAA completely neutralized with NaOH). [b] This value becomes 0.319 if method (iv) is used with $x$ = 1.03, and 0.306 with $x$ = 1.05.

It may be seen that the values of $\alpha$ obtained by the four different methods show much better agreement for this system than for PVPBr in HBr solutions. This is not surprising, because the "mixture effect" on the values of $\Lambda_i$ becomes zero as the mobilities of the various ions of like charge approach each other. Both Wall's sodium polyacrylate and the PVPBr used in the present investigation had mobilities of about $3 \times 10^{-4}$ cm.$^2$ volt$^{-1}$ sec.$^{-1}$. The mobilities of $H^+$ and $Cl^-$ are about $3.6 \times 10^{-3}$ and $7.9 \times 10^{-4}$ cm.$^2$ volt$^{-1}$ sec.$^{-1}$, respectively, so it is evident that the mixture effect will be much greater in the PVPBr–HBr system than in the NaPAA–NaCl system.

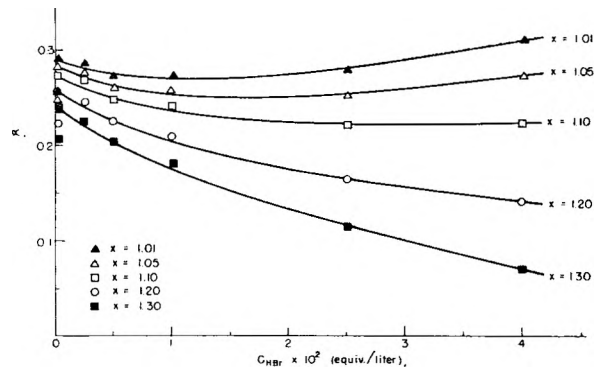


Fig. 2c.—Effect of $x$ on the curves of $\alpha$ *vs.* $C$ as calculated by method (iv) for 1% PVPBr.

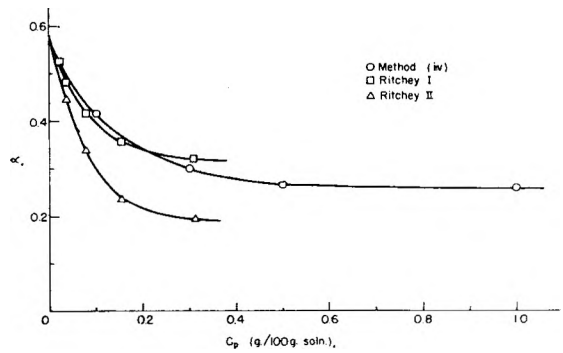


Fig. 2d.—Extrapolated values of $\alpha$ as a function of $C_p$ at $C_{HBr} = 0$.

Comparing the values of $\alpha$ as obtained by the four different methods on the NaPAA–NaCl system, several points should be noted. First of all it should be recalled that the values obtained by method (i) are too low, due to the nature of the approximations involved. The results obtained by methods (ii) and (iii) are only slightly higher than those obtained by (i), while the values obtained by method (iv) with $x$ = 1.10 are less than those obtained by method (i). Since the values obtained by method (iv) decrease with increasing $x$, it is evident that 1.10 is too large a value of $x$, since the correct value of $\alpha$ must be greater than $\alpha$ (i). This emphasizes the fact that $x$ is not a constant and must increase with increasing NaCl concentration.

**Conclusions.**—The transference method has been found to give reasonably accurate values of degree of ionization ($\alpha$) in polyelectrolyte systems for which the following conditions are met: (1) the polyion and counterion mobilities are of the same order of magnitude; (2) the concentration of added salt is less than 0.05 $N$.

For PVPBr in HBr, where the polyion and simple ion of like charge ($H^+$) have greatly differing mobilities, the "mixture effect" causes large errors to be introduced in the values of $\alpha$ at finite concentrations of HBr.

## DISCUSSION

Q. VAN WINKLE.—A question has been raised about the effect of charge. There is certainly a very high charge density on the polymer coil. None of the theories, presently available, is adequate for explaining the ionization behavior of polyelectrolytes. We have not made any attempts to develop a theory to explain the behavior reported here.

# ON THE BEHAVIOR OF SERUM ALBUMIN IN ACIDIC PERCHLORATE SOLUTIONS[1]

BY JOHN R. CANN

*Contribution No. 85 from the Department of Biophysics, Florence R. Sabin Laboratories, University of Colorado Medical Center, Denver, Colorado*

*Received March 2, 1959*

When the *p*H of a bovine serum albumin (BSA) solution in 0.15 *M* $NaClO_4$ is lowered from 4.7 to about 4.1 no precipitation occurs, but on lowering the *p*H further to a value of 3.7 a heavy precipitate develops immediately. The precipitate redissolves progressively as the *p*H is lowered still further and is completely redissolved at *p*H 3.2–2.3. Following dissolution of the precipitate, a new precipitate slowly forms at the low *p*H values. Although the various precipitates redissolve at *p*H's above about 4.5, it has been shown that the protein suffers irreversible damage as a result of prolonged exposure to acidic perchlorate solutions. The implications of these findings for the structure of BSA in acidic media are discussed. Precipitation at *p*H 3.0 is readily reversed by heating when the reaction occurs at 0° but is irreversible at 36°. The over-all rate of precipitation exhibits a strong minimum at about 26°. The kinetics of precipitation are explicable in terms of the reaction scheme: $P + nClO_4^- \rightleftarrows P(ClO_4^-)_n \rightleftarrows I \rightarrow I'$, where the symbol P denotes the "expanded" BSA molecule and $P(ClO_4^-)_n$, a protein–perchlorate complex. The protein–perchlorate complex is assumed to undergo some structural change leading to a reversibly precipitated protein I which in turn is converted irreversibly to another insoluble form I', *via* a reaction occurring in the precipitate. Whereas the rate of reversible precipitation decreases with increasing temperature, the rate of the reaction $I \rightarrow I'$ increases. The action of perchlorate does not appear to be oxidative in nature.

## Introduction

The sedimentation behavior of conalbumin and γ-pseudoglobulin in acidic media exhibits a complex type of variation with changes in either *p*H or ionic strength of the solution.[2-5] Under certain conditions (*e.g.*, ionic strength 0.1 NaCl, *p*H changing from 7 to 3.1) these proteins undergo configurational changes which affect their sedimentation constants, but which usually are without influence on their molecular weights. With properly chosen type and concentration of salt, however, acid *p*H's also can cause aggregation. At *p*H 3 these proteins aggregate at high but not low NaCl concentration and at lower concentrations of other supporting electrolytes. The effectiveness of univalent anions in aggregating the protein increases in the order $Cl^-$, $Br^-$, $NO_3^-$ and $ClO_4^-$.

Bovine serum albumin (BSA) also undergoes configurational changes in acidic media,[6,7] and it would be of interest to study possible aggregation of this protein in different supporting electrolytes. Preliminary experiments designed to study the sedimentation behavior of BSA in acidic perchlorate solutions revealed that under certain conditions of $NaClO_4$ concentration, the protein precipitates from solution when the *p*H is lowered from the isoionic point to a value less than about 4. The purpose of this paper is to present the results of a systematic investigation of this phenomenon and to discuss the implications of these observations for the structure of BSA in acidic media.

(1) Supported in part by research grant No. E-1482 from the National Institute of Allergy and Infectious Diseases of the National Institutes of Health, Public Health Service; and in part by the Damon Runyon Fund and the American Cancer Society.

(2) R. A. Phelps and J. R. Cann, *Arch. Biochem. Biophys.*, **61**, 51 (1956).

(3) J. R. Cann and R. A. Phelps, *Biochim. Biophys. Acta*, **26**, 378 (1957).

(4) J. R. Cann and R. A. Phelps, *J. Am. Chem. Soc.*, **77**, 4266 (1955).

(5) R. A. Phelps and J. R. Cann, *Biochim. Biophys. Acta*, **23**, 149 (1957).

(6) J. T. Yang and J. F. Foster, *J. Am. Chem. Soc.*, **76**, 1588 (1954).

(7) C. Tanford, J. G. Buzzell, D. G. Rands and S. A. Swanson, *ibid.*, **77**, 6421 (1955).

## Experimental

**Materials.**—The bovine serum albumin was Armour's crystallized bovine plasma albumin, Lot No. S68004. Reagent grade chemicals were used.

**Methods.**—Concentrated stock solutions of BSA were prepared by dissolving the protein in water and then dialyzing *vs.* water for about 18 hours at 7°. Portions of the stock solution were diluted with concentrated $NaClO_4$ solutions to give the desired protein and perchlorate concentrations. The *p*H was adjusted with 0.5 *M* HCl. The *p*H of the solutions were measured at room temperature with a Beckman Model G *p*H meter. The solutions were then brought to the desired temperature in a constant temperature bath. A crushed ice-bath was used at 0°. Below 26°, the temperature was maintained constant to ±0.1° or better during the entire time-course of precipitation. At 26° and above, the temperature was constant to ±0.1 during measurements of initial rates of precipitation, but temperature fluctuations as large as ±0.5° sometimes occurred during long-term experiments.

After precipitation had occurred for the desired length of time, the reaction mixture was clarified by rapid centrifugation. Since the precipitates formed at low temperatures redissolved on raising the temperature, care was taken to centrifuge the sample at the temperature of precipitation. Samples precipitated at other temperatures were centrifuged at room temperature. During early stages of precipitation at 34 and 36° difficulty was encountered in completely clarifying the solutions since precipitation continued during centrifugation. Accordingly, in all cases, the reaction time was taken as the time that elapsed from the start of the experiment to completion of centrifugation. The supernatants were diluted with ionic strength 0.1 phosphate buffer at *p*H 7.1 and analyzed for their protein content. In those cases where the supernatants were turbid after centrifugation, the solutions clarified on dilution with buffer.

Protein concentrations were determined spectrophotometrically at 2800Å. with a Beckman model DU spectrophotometer. A solution of BSA which had been precipitated from 0.3 *M* $NaClO_4$ at about *p*H 3 and then redissolved at about *p*H 6, gave an optical density which was the same, within experimental error, as the value expected for a solution of BSA never exposed to low *p*H's.

In control experiments BSA did not precipitate from its solution in 0.15 *M* NaCl, *p*H 3.0, during 3 hours at 26.2° and 2 hours at 1.0°.

Viscosity measurements were made at 25.1 ± 0.01° and 1.0 ± 0.01°.

## Results and Discussion

**Precipitation Curves.**—In our first set of experiments, the *p*H's of different samples of 0.94% solution of BSA in 0.3 *M* $NaClO_4$ were lowered from the isoionic *p*H of 5.56 to values in the range 5.15 to

2.05. Precipitation did not occur between the isoionic *p*H and *p*H 4.3, but when the *p*H was lowered further a precipitate formed immediately. After aging for 0.5 hour at room temperature, the various samples were clarified by centrifugation and the supernatants analyzed for their protein content. A precipitation curve was then constructed by plotting the per cent. of protein precipitated *vs.* the *p*H. As shown in Fig. 1, the precipitation curve rises sharply from zero precipitation at *p*H 4.3 to a maximum of essentially complete precipitation at about *p*H 3.6. The per cent. precipitated then decreases very slightly as the *p*H is lowered still further to a value of about 2.0.

Acid-precipitation curves were also determined for other concentrations of $NaClO_4$, and the nature of the curves was found to be strongly dependent upon the perchlorate concentration. Thus, while the curve obtained in 0.2 *M* $NaClO_4$ was similar to that in 0.3 *M* $NaClO_4$ (depending upon the *p*H about 10 to 30% less precipitate was formed at the lower perchlorate concentration), no immediate precipitation occurred in 0.1 *M* $NaClO_4$ even at *p*H 2.2 and only a strong Tyndall effect developed when a solution at *p*H 3.0 was aged at room temperature for 24 hours. The curve obtained in 0.15 *M* $NaClO_4$ is of particular interest since it differs markedly from those at other perchlorate concentrations in several important respects. When the *p*H of a BSA solution in 0.15 *M* $NaClO_4$ is lowered from 4.66 to 4.06 no precipitation occurs, but on lowering the *p*H further to a value of 3.7 a heavy precipitate develops immediately. In contrast to the behavior in 0.2 and 0.3 *M* $NaClO_4$, this precipitate redissolves progressively as the *p*H is lowered still further and is completely redissolved at *p*H 3.15–2.32.[8] Consequently, as shown in Fig. 1, the immediate-precipitation curve is approximately bell-shaped. A second interesting feature of the precipitation behavior in 0.15 *M* $NaClO_4$ is the slow development of a new precipitate at low *p*H values following dissolution of the original precipitate formed at high *p*H's. Thus, for example, when a solution of BSA in 0.15 *M* $NaClO_4$ was acidified with HCl, the precipitate that formed on passing through the *p*H range 4 to 3.7 completely redissolved on passing from *p*H 3.7 to 2.99. Within about a minute following dissolution of the precipitate, the *p*H 2.99 solution once again assumed a bluish hue and precipitation ensued. During the next 3 hours 44% of the protein precipitated out of solution and in 23 hours, 68%. The rate of this second precipitation is dependent upon *p*H. Thus, in the *p*H range 3.7 to 3.3, partial dissolution of the precipitate, formed at higher *p*H values, is followed by reprecipitation at such a rapid rate that quantitative determination of the immediate precipitation curve in this region was impossible. This accounts for the broken-line portion of the bell-shaped precipitation curve shown in Fig. 1.

It appeared desirable as a first step toward the elucidation of this complex behavior to construct a precipitation curve for aged acidic solutions of protein. Samples of a solution of BSA in 0.15 *M* $NaClO_4$ were adjusted to the desired *p*H values and allowed to age at room temperature for 4 days. The samples were then centrifuged and the supernatants analyzed for their protein content. The resultant precipitation curve, Fig. 1, shows three *p*H regions of interest: (a) the *p*H range 4.66 to 4.18 in which no precipitation occurs; (b) the *p*H range 4.18 to about 3.3 in which precipitation passes through a maximum; and (c) the range from 3.3 to about 2.3 in which precipitation increases continuously when the *p*H is lowered.

These results indicate that, depending upon *p*H, BSA can exist in at least three distinct forms. In the *p*H range 4.7 to 4.2 the protein exists in a form which is soluble in 0.15 to 0.3 *M* $NaClO_4$. At a *p*H of about 4.2 the protein apparently undergoes some structural alteration which changes its solubility properties such that the protein now precipitates in 0.15 to 0.3 *M* $NaClO_4$. A second structural alteration occurs when the *p*H is further lowered to a value of about *p*H 3.7. This third form of BSA is initially soluble in 0.15 *M* $NaClO_4$ but slowly undergoes some further change in structure which results in slow precipitation of the protein. (The possibility that the bell-shaped, immediate precipitation curve in 0.15 *M* $NaClO_4$ simply represents isoelectric precipitation seems to be eliminated by the fact that BSA does not show isoelectric precipitation in 0.15 *M* KCl.)

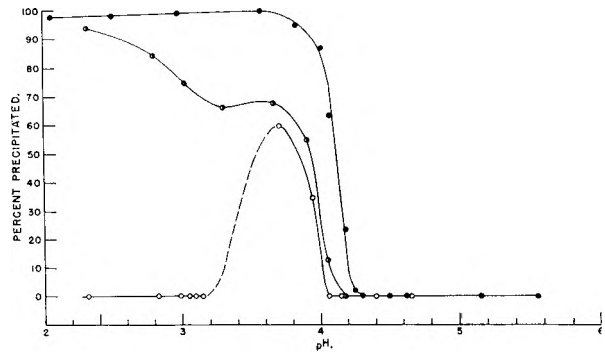


Fig. 1.—Precipitation curves for BSA in acidic perchlorate solutions: ●, 0.3 *M* $NaClO_4$, aged 0.5 hour at room temperature; ○, immediate precipitation in 0.15 *M* $NaClO_4$ (points at *p*H 4.06, 3.94 and 3.70 obtained within 0.5 hour after adjusting *p*H); ◑, 0.15 *M* $NaClO_4$, aged 4 days at room temperature.

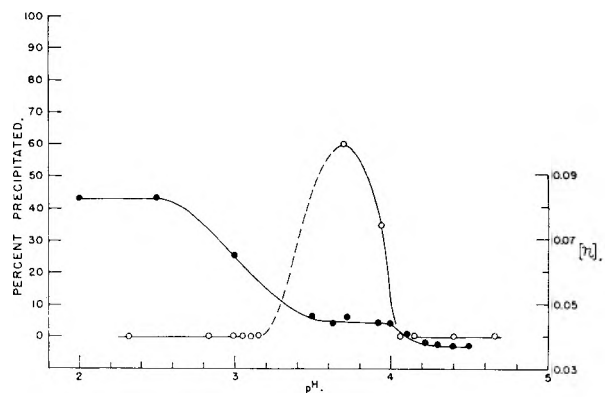


Fig. 2.—Comparison of immediate precipitation curve for BSA in 0.15 *M* $NaClO_4$ with intrinsic viscosities $[\eta]$ in 0.15 *M* KCl: ○, precipitation curve; ●, intrinsic viscosities of Tanford and co-workers.[7]

(8) If the solution is held at a *p*H value between 3.8 and 3.5 for too long a time before lowering the *p*H to 3.0, the precipitate does not completely redissolve.

These three forms of BSA may correspond to the compact isoionic form, the "expandable" form and the "expanded" form of the protein. The existence of these latter three structurally different forms of BSA is indicated by viscosity, optical rotation and light scattering measurements on solutions of the protein in NaCl–HCl and KCl–HCl.[6,7] It is of interest to compare the immediate precipitation curve of BSA in 0.15 *M* $NaClO_4$ with the viscosity data of Tanford and his co-workers[7] on the same protein in 0.15 *M* KCl. This comparison is made in Fig. 2. The viscosity data have been interpreted as follows[7]: between *p*H 10.5 and 4.3 BSA exists in a compact form held together by a network of bonds involving the side-chain groups of the protein. Near *p*H 4.2 the titration of some of the side chains results in transition to an "expandable" form. This form undergoes continuous expansion, increasing with charge and decreasing with ionic strength, so as to reduce the electrostatic free energy. The comparison made in Fig. 2 suggests that the compact form is soluble in 0.15 to 0.3 *M* $NaClO_4$; the "expandable" form is insoluble in these media, while the "expanded" molecule is soluble. However, the "expanded" molecule must undergo some further change in structure which results in precipitation in perchlorate solutions. This change proceeds slowly in 0.15 *M* $NaClO_4$ but rapidly in 0.3 *M* $NaClO_4$. Tanford and his co-workers[7] have also observed a slow, molecular change in the "expanded" molecule as evidenced by a slow increase in viscosity of its solutions in 0.15 *M* KCl.

**On the Reversibility of Precipitation.**—The protein which precipitates from acidic perchlorate solutions redissolves at higher *p*H values. For example, about 99% of the protein precipitates from its solution in 0.3 *M* $NaClO_4$ when the *p*H is adjusted to *p*H 2.9. When the *p*H of the acidic solution and its precipitate was readjusted to a value of 4.5 by the addition of 0.5 *M* NaOH, the precipitate redissolved completely to give a clear solution. Furthermore, the protein could be precipitated and redissolved in this manner several times in succession. While all the precipitates formed under the various conditions described above redissolved when suspended in *p*H 7.1 phosphate buffer of ionic strength 0.1, fresh precipitates dissolved much more readily than aged ones. Sometimes the aged precipitates gave solutions at *p*H 7.1 which showed a Tyndall effect but the bluish hue gradually disappeared on standing at room temperature. Precipitates formed at higher temperatures (34–36°) also dissolved in *p*H 7.1 buffer with some difficulty.

Despite the fact that all of the various precipitates formed below *p*H 4 redissolved at higher *p*H's, it can be shown that the protein suffers some irreversible damage as a result of exposure to acidic perchlorate solution for a prolonged period of time. This is illustrated by the following experiment: a sample of BSA in 0.15 *M* $NaClO_4$ was adjusted to *p*H 3.0. As in previous experiments, the precipitate formed in the *p*H range 4 to 3.7, redissolved at lower *p*H's. The clear, *p*H 3.0 solution was aged for 5 hours at 26° during which time about 55% of the protein precipitated from solution. The sample then was centrifuged. The precipitate was redissolved in an appropriate volume of *p*H 7.1 phosphate buffer, ionic strength 0.1, dialyzed overnight *vs.* buffer, and then dialyzed *vs.* water. This material will be referred to as the "precipitated portion." The supernatant obtained by centrifugation of the aged acidic sample was adjusted to *p*H 6 with NaOH, dialyzed *vs.* water, concentrated by pervaporation and dialyzed once more *vs.* water. This material will be referred to as the "non-precipitated portion." The acid-precipitation behavior of a 1% solution of each of these materials in 0.15 *M* $NaClO_4$ was determined. When the *p*H of the solution of "precipitated portion" was lowered to a value of about 3.7, heavy precipitation occurred immediately. However, in contrast to BSA, which had not been exposed previously to low *p*H's, the precipitate did not redissolve, at least to any great extent, when the *p*H was lowered further to a value of 2.7. This shows that the protein suffered irreversible damage during its first acid-precipitation. In contrast, the "non-precipitated portion" behaved similarly to, although not identically with, BSA which had not been exposed previously to low *p*H's. Thus, when the *p*H of the perchlorate solution of the "non-precipitated portion" was adjusted to about 3.7, immediate precipitation occurred. The precipitate redissolved when the *p*H was lowered further to a value of 3.0, and a new precipitate then appeared. However, the initial rate of the new precipitation was about three times that observed with BSA never exposed previously to low *p*H's. It must be concluded, therefore, that even the portion of BSA which has not had time to precipitate at *p*H 3.0 in 5 hours has nevertheless undergone some irreversible change in structure during that time.

**Kinetics of Precipitation.**—In order to gain insight into the mechanism of precipitation of BSA from its acidic perchlorate solutions, it seemed advisable to investigate the kinetics of precipitation. The rate of precipitation of the protein from its solution in 0.15 *M* $NaClO_4$ at *p*H 4 to 3.7, is very rapid. However, the precipitation which occurs at *p*H 3.0 following dissolution of the precipitate which formed as the *p*H of the solution passed through the range 4 to 3.7, is sufficiently slow to permit kinetic studies. The rate of precipitation at *p*H 3.0, 0.15 *M* $NaClO_4$, shows a curious dependence upon temperature. Whereas the rate of precipitation increases with increasing temperature in the range 26 to 36.3°, the rate increases with decreasing temperature in the range 26 to 0°. Furthermore, while the precipitate formed at 36.3° does not redissolve when the temperature is lowered to 26°, the precipitate formed at 0° largely redissolves at 15.5°. The kinetics of precipitation in each of these temperature ranges will be considered separately and then a possible reaction scheme will be discussed.

The results of measurements on the rate of precipitation at 26.0 and 36.3° are presented in Fig. 3 which is a semi-logarithmic plot of the fraction of protein remaining in solution *vs.* the time in hours. Clearly, the precipitation process does not follow

simple first-order reaction kinetics. Although the semi-logarithmic plots are linear, within experimental error, during early stages of precipitation (during precipitation of about 30% of the protein at 26° and about 65% at 36.3°), they deviate markedly from linearity during the further course of precipitation. During this latter stage the rate of precipitation becomes progressively smaller than the rate expected for a first-order reaction.[9] The question naturally arises as to whether the decrease in the logarithmic rate of precipitation with time is simply an artifact arising from a change in *p*H during the course of reaction. The reaction mixtures were unbuffered, and the rate of precipitation is sensitive to *p*H. However, this possibility is eliminated by the observation that the *p*H of the precipitating mixture does not change during 17 hours at 26°. A second possibility is that BSA is heterogeneous with respect to its rate of precipitation from acidic perchlorate solutions. The following experiment was designed to test this explanation: a sample of BSA in 0.15 *M* $NaClO_4$, *p*H 3.0, was allowed to precipitate for 5 hours. The sample then was centrifuged. The supernatant was adjusted to *p*H 6, dialyzed *vs.* water, concentrated by pervaporation and then dialyzed once more *vs.* water. This is the "non-precipitated portion" of BSA discussed in the section "On the Reversibility of Precipitation." If the "non-precipitated portion" were a slowly precipitating fraction of BSA, then one would expect this material to precipitate very slowly during a second exposure to 0.15 *M* $NaClO_4$ at *p*H 3.0. Furthermore, the time-course of precipitation should be more nearly linear than that obtained with the original BSA. Actually, precipitation of this material was rapid and the rate curve had the same shape as observed with the original BSA. However, the situation is complicated by the fact that the initial specific rate of precipitation of the "non-precipitated portion" was about three times the rate shown by the original BSA. Nevertheless, these results would seem to eliminate the possibility that BSA is heterogeneous with respect to precipitation rate.

One plausible explanation of the shape of the rate curves is that the protein precipitates in accordance with a scheme such as

$$P \rightleftarrows I \longrightarrow I' \qquad (1)$$

where the symbol P denotes soluble protein; I, reversibly precipitated proteins; and I′, irreversibly precipitated protein. It is assumed that the first precipitate to form can reconvert to soluble protein, and that this reversibly precipitated protein is in turn transformed irreversibly into a structurally-different insoluble form. The last reaction is assumed to occur in the precipitate. With the proper choice of rate constants such a scheme will give a semi-logarithmic rate curve similar in shape to those shown in Fig. 3 and describable by a sum of two exponential rate terms with constant coefficients. Although our rate data are not adequately represented by such a kinetic expression (a sum of three exponential rate terms with constant coefficients does give a reasonable fit), it must be remembered that the soluble protein suffers irreversible damage during prolonged exposure to acidic perchlorate solution so that departures from a simple reaction scheme such as that shown above are to be expected. If the precipitation process does indeed involve a reversible step, then it is conceivable that some of the precipitate formed at a given temperature might redissolve at a lower temperature. Actually, this is not the case. None of the precipitate formed during 11 minutes at 36.3° (about 61% of the protein) redissolved when the temperature was lowered to 26° even after remaining at the lower temperature for 1 hour. In fact, during this time precipitation continued but at the much reduced rate expected at the lower temperature. Of course, the reaction scheme given above is not necessarily inconsistent with this observation. Whether or not any reversibly precipitated protein present at the higher temperature redissolves at the lower one, would depend upon the effect of temperature on the equilibrium constant for the reaction P ⇆ I. If the lower temperature shifts the equilibrium position in favor of I, then reversibly precipitated protein would not redissolve. Direct experimental evidence for such an equilibrium will be presented shortly.

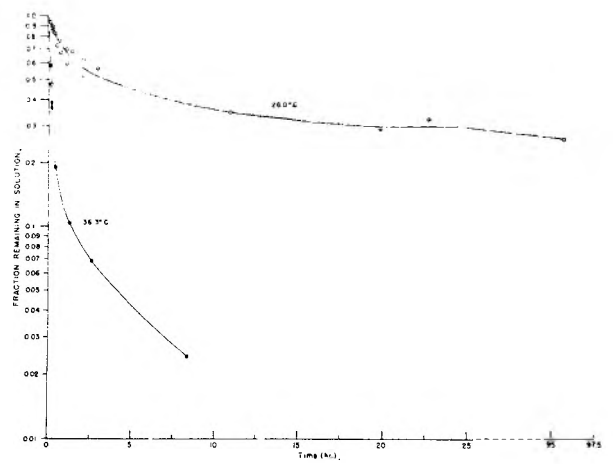

Fig. 3.—Time-course of precipitation in 0.15 *M* $NaClO_4$ at *p*H 3.0.

The initial stage of precipitation in the temperature range under consideration has been examined in some detail. Within experimental error, the initial specific rate of precipitation at 26° (*i.e.*, the initial rate of precipitation per unit concentration of protein) is independent of the protein concentration over the range 0.2 to 2.4%. This indicates a first-order reaction with respect to protein concentration. In contrast, the specific rate of precipitation is extremely sensitive to perchlorate concentration. Thus, at 26°, BSA does not precipitate from its 0.1 *M* $NaClO_4$ solution at *p*H 3.0 in 3.5 hours, and only a strong Tyndall effect develops in 24 hours. On the other hand, precipitation occurs too rapidly in 0.2 *M* $NaClO_4$ to permit kinetic measurements. In fact, at this perchlorate concentration it is impossible to separate the various processes

(9) Precipitation does not follow a second-order rate law, and the absence of an induction period seems to eliminate the possibility that aggregation of the protein in solution is rate limiting at this *p*H. (There might be an induction period at lower *p*H's, but this possibility has not been investigated systematically.)

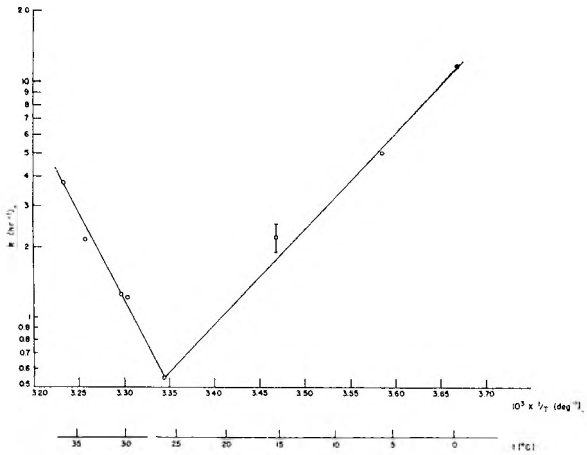

Fig. 4.—Semi-logarithmic plot of initial specific rates of precipitation *vs.* temperature.

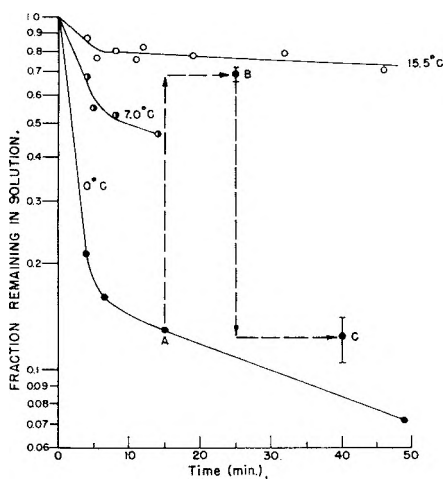


Fig. 5.—Time-course of precipitation in 0.15 *M* $NaClO_4$ at *p*H 3.0. The broken-line curve is explained in the text.

which occur as the *p*H of the solution is lowered from the isoionic point to *p*H 3.0. Despite this strong dependence of the rate on perchlorate concentration, it was possible to get some idea as to the order of the precipitation process with respect to perchlorate concentration by measuring the initial specific rates at 36.3° in 0.13 *M* and in 0.15 *M* $NaClO_4$, *p*H 3.0. It was found that the initial specific rate approximately doubles on increasing the perchlorate concentration by even this small amount. This indicates that, within the experimental error of these measurements, the process is fourth or fifth order with respect to perchlorate. Finally, the rate of precipitation in 0.15 *M* $NaClO_4$ is very sensitive to temperature. The initial rate at 36.3° is almost seven times the rate at 26°. Initial specific rates at various temperatures are presented in Fig. 4. An activation energy of about 34 kcal./mole was calculated for the temperature range 26 to 36°. Such a large activation energy suggests that precipitation occurs as a result of profound changes occurring in the structure of the protein molecule.

The kinetics of precipitation at temperatures below 26° are in striking contrast to those described for the temperature range 26 to 36°. Rate measurements at 15.5, 7.0 and 0° are presented in Fig. 5. "Initial" specific rates of precipitation at these temperatures are shown in Fig. 4. As indicated, the rate shown for 15.5° is subject to considerable uncertainty, and those at 7.0 and 0° must be considered as minimum values since precipitation proceeds so fast at these temperatures that the actual initial rates cannot be measured. In any event, the data reveal several important features of the precipitation process. The first of these is the negative temperature coefficient at low temperatures. Thus, as the temperature is lowered from 26 to 0°, the rate of precipitation increases by at least a factor of 20. The rate at 0° is at least 3 times the rate at 36.3°.

As found for higher temperatures, the rate of precipitation at 0° is extremely sensitive to perchlorate concentration. Whereas precipitation is very rapid in 0.15 *M* $NaClO_4$, no precipitation occurred during 24 hours in 0.1 *M* $NaClO_4$.

An important property of precipitation at 0° is its reversibility with respect to temperature. This is illustrated by the broken-line curve, ABC, shown in Fig. 5. About 87% of the protein precipitates during the first 15 minutes at 0° (point A). If at this time the temperature of the reaction mixture is raised to 15.5°, approximately two-thirds of the precipitate dissolves rapidly. After 10 minutes at 15.5° only about 30% of the protein remains as a precipitate (point B). If at this time the temperature is once again lowered to 0° the protein rapidly reprecipitates and after 15 minutes at 0° (point C) the amount of precipitate is about the same as obtained during the initial 15 minute exposure to this temperature. The amount of precipitate remaining after the reaction mixture at 0° is warmed to 15.5° appears to be significantly lower than the amount expected from the rate measurements at the higher temperature. This is attributed to some irreversible precipitation at 0°. These results indicate that the shape of the rate curves at low temperatures reflects a rapid approach to equilibrium complicated by slow formation of some irreversibly precipitated material. Furthermore, the equilibrium between soluble and precipitated proteins shifts in favor of precipitate when the temperature is lowered from 15.5 to 0°. These findings support our interpretation of the shape of the rate curves obtained in the temperature range 26 to 36°, but it must be concluded that only a relatively small fraction of the high-temperature precipitate is of the reversible type formed at 0°.

The question naturally arises whether the action of perchlorate ions on BSA is simply oxidative in nature. Experiments with other anions seem to eliminate this possibility. Thus, when the *p*H of a BSA solution in 0.3 *M* NaCNS was lowered from the isoionic point to about *p*H 3, a heavy precipitate formed rapidly. No immediate precipitation occurred when the *p*H of a BSA solution in 0.15 *M* NaCNS was adjusted to *p*H 2.7. However, a precipitate developed slowly on standing at room temperature: the solution was very turbid after 3 hours and gave a heavy precipitate in 18 hr. At 36°, both precipitation and gelation occurred. The protein also precipitated from its solution in 0.3 *M* NaI,

*p*H 3.0. The rate of precipitation at room temperature was faster than in 0.15 *M* $NaClO_4$, and the rate was greater at 36° than at room temperature.

The simplest reaction scheme which can account for the kinetics of precipitation over the entire temperature range 0 to 36°, appears to be

$$P + nClO_4^- \underset{A}{\rightleftharpoons} P(ClO_4^-)_n \underset{B}{\rightleftharpoons} I \longrightarrow I' \quad (2)$$

where the symbol P denotes the "expanded" BSA molecule and $P(ClO_4^-)_n$, a protein–perchlorate complex. The protein–perchlorate complex is assumed to undergo some structural change leading to a reversibly precipitated protein I which in turn is converted to another insoluble form I′ *via* a reaction occurring in the precipitate. The observed temperature dependence of the rate of precipitation can be understood qualitatively by assuming that the change in enthalpy for binding of perchlorate ions by the protein is negative and that the reaction I → I′ has a large activation energy. At low temperatures, equilibrium B in eq. 2 is established rather rapidly but the reaction I → I′ occurs very slowly. At higher temperatures, equilibrium A is shifted in favor of P and consequently the rate of formation of I will be decreased. At still higher temperatures, the reaction I → I′ becomes increasingly important and consequently the over-all rate of precipitation passes through a minimum with increasing temperature.[10]

One possible explanation of these data involves binding of perchlorate ions to at least two different kinds of sites on the protein. Experiments carried out at 36.3° indicate that *n* is about 4 or 5. This finding presents certain problems since the average number of perchlorate ions bound by a molecule of BSA at *p*H 3 must certainly be very much larger than 4 or 5. Measurements on the binding of perchlorate ion by serum albumin are limited to isoionic protein[11,12] but some idea as to the probable extent of binding at *p*H 3 can be obtained from data on the binding of other ions. Thus, isoionic serum albumin, either bovine or human, in 0.15 *M* salt solution binds an average of about 10 chloride, 20 perchlorate or 23 thiocyanate ions per molecule while serum albumin at *p*H 3.0–3.2 binds an average of about 30 chloride or 60 thiocyanate ions per molecule.[11–15] From these data one would expect BSA at *p*H 3 to bind an average of about 50 perchlorate ions per molecule. If this is so, then practically all of the protein molecules should be in the form of complexes containing at least 5 perchlorate ions. It is possible, of course, that BSA possesses several sets of perchlorate-binding sites, each set having a different affinity for the ion, and that at least 4 or 5 ions must react with one particular set of sites in order for the precipitation process to occur. These sites would presumably have a very low affinity for perchlorate ion. On the other hand, it is not necessary to postulate special binding sites if it is assumed that all protein–perchlorate complexes can undergo a structural change leading to precipitation at a rate which increases as the number of perchlorate ions in the complex increases. In this event, the dependence of the rate of precipitation upon perchlorate concentration is not subject to the usual interpretation. Thus, for example, at 0° where irreversible precipitation is of secondary importance, the "apparent order of the reaction with respect to perchlorate concentration" is, according to this method, equal to the difference between the average number of bound perchlorate ions in the activated states of the precipitation reactions and the average number bound by the soluble protein.[16] In either event, it is conceivable that perchlorate ions exert their effect by altering the charge distribution and thus the electrostatic forces within the "expanded" BSA molecule.

Another possible explanation of the behavior of BSA in acidic perchlorate solutions is as follows. Binding of perchlorate ions to groups on the surface of the protein molecule in 0.15 *M* $NaClO_4$ at first solubilizes the "expanded" form of BSA at room temperature, Figs. 1 and 2. It is supposed that the bound perchlorate ions then diffuse into the hydrophobic interior of the protein molecule, and as a result their solubilization effect is lost. Examination of the influence of various anions on the thermodynamic properties of aqueous solutions of non-electrolytes is pertinent to this explanation. It is particularly interesting that perchlorate ions salt-in argon into aqueous solution, whereas other anions salt-out argon.[17] Likewise, $HClO_4$ salts-in while HCl salts-out benzene.[18] The effectiveness of the anions of various sodium salts in salting-out benzene decreases in the order $OH^-$, $Cl^-$, $Br^-$, $NO_3^-$, $ClO_4^-$ and $I^-$.[18] Also, $NaClO_4$ and NaI salt phenylthiourea[19] and γ-butyrolactone[20] into aqueous solutions, whereas electrolytes such as NaCl salt-out these substances. Apparently, perchlorate ions, like iodide ions which also cause slow precipitation of BSA at *p*H 3, prefer a relatively hydrophobic environment. Perchlorate ion is generally a poor complexing agent, and at first glance it seems surprising that it is bound by proteins to such a large extent.[4,11,12] Perhaps this binding can be understood in terms of a tendency of perchlorate ions to

(10) Another reaction scheme which has been considered, postulates that in 0.15 *M* $NaClO_4$ at *p*H 3.0, BSA can exist in two structurally-different interconvertible forms which precipitate by different mechanisms. A rapidly established, temperature dependent equilibrium between the two forms was assumed. It also was assumed that the low-temperature form precipitates reversibly and the high-temperature form, irreversibly. This scheme lost its attractiveness when we observed that the reduced specific viscosities of 0.8–0.9% BSA solutions in 0.15 *M* KCl at *p*H 3.0 were the same, within experimental error, at 1.0 as at 25.1°. This result indicates that the configuration of the "expanded" BSA molecule is insensitive to temperature. Of course, this does not exclude the possibility that BSA undergoes configurational changes in 0.15 *M* $NaClO_4$, pH 3.0, as a result of changing the temperature.

(11) G. Scatchard and E. S. Black, THIS JOURNAL, **53**, 88 (1949).

(12) C. W. Carr, *Arch. Biochim. Biophys.*, **40**, 286 (1952).

(13) G. Scatchard, I. H. Scheinberg and S. H. Armstrong, Jr., *J. Am. Chem. Soc.*, **72**, 535 (1950).

(14) G. Scatchard, I. H. Scheinberg and S. H. Armstrong, Jr., *ibid.*, **72**, 540 (1950).

(15) R. A. Alberty and H. H. Marvin, Jr., *ibid.*, **73**, 3220 (1951).

(16) R. B. Simpson and W. Kauzmann, *ibid.*, **75**, 5139 (1953).

(17) Personal communication from the late Professor John G. Kirkwood who suggested this explanation of the data.

(18) W. F. McDevit and F. A. Long, *J. Am. Chem. Soc.*, **74**, 1773 (1952).

(19) Merle Randall and C. F. Failey, *Chem. Revs.*, **4**, 285 (1927).

(20) F. A. Long, W. F. McDevit and F. B. Dunkle, THIS JOURNAL, **55**, 813 (1951).

escape from a relatively unfavorable, aqueous environment.

Finally, one is impressed by the similarities between the kinetics of precipitation of BSA from acidic perchlorate solutions and the urea denaturation of β-lactoglobulin[21] and ovalbumin.[16] Further analysis is required to determine whether these agents produce their respective effects *via* mechanisms at least partially similar.

## DISCUSSION

C. T. O'KONSKI (University of California at Berkeley).—Before doing work at low *p*H, were your samples de-ionized?

J. R. CANN.—Our BSA solutions were dialyzed *vs.* water but were not de-ionized on an ion-exchange column.

C. T. O'KONSKI.—I'd like to call your attention to an electric birefringence study of BSA, which includes measurements in acidic media using de-ionized samples (S. Kruse and C. T. O'Konski Abstracts, National Meeting, Am. Chem. Soc., April, 1958; *J. Am. Chem. Soc.*, in press). We observed aggregation at low *p*H in samples which were not de-ionized. In the relatively stable de-ionized material, the rotary diffusion constant seems to increase when *p*H goes from 5 to 2.5. This suggests that the longest dimension of the (asymmetric) macromolecule is slightly decreased by acid, contrary to an earlier view that BSA is spherical and swells isotropically at low *p*H. The explanation offered by Dintzis (Ph.D. Thesis, Harvard Univ., 1952) for the effect of de-ionization on the properties of BSA is that some fatty acid is removed by de-ionization. Perhaps the most remarkable indication of change is the fact that the slope of the curve of specific Kerr constant *vs.* concentration changes sign upon de-ionization, indicating a changed mode of interaction in dilute solutions. This may be very important in considering the kinetics of precipitation, and it appears that studies of the de-ionized material should be made.

(21) L. K. Christensen, *Compt. rend. Lab. Carlsberg, Sér. chim.*, **28**, 37 (1952).

J. R. CANN.—I agree with Dr. O'Konski that our experiments on the kinetics of precipitation should be extended to BSA de-ionized by passage through a mixed-bed ion-exchange column and, perhaps also, by electrodialysis. I suspect, however, that both of these materials may also show complex kinetics. Although de-ionized BSA is quite resistant to aggregation in acidic KCl solutions of low ionic strength, it does aggregate at high ionic strengths like those used in our experiments [ref. 7: M. J. Kronman, M. D. Stern and S. N. Timasheff, THIS JOURNAL, **60**, 829 (1956); S. N. Timasheff and R. J. Gibbs, *Arch. Biochem. Biophys.*, **70**, 547 (1957)].

Dr. O'Konski's important observations on the configurational changes which BSA undergoes at low *p*H are consistent with the results of small-angle X-ray scattering experiments on BSA solutions (M. Champagne, V. Luzzati and A. Nicolaieff, *J. Am. Chem. Soc.*, **80**, 1002 (1958)). Our changing views concerning the behavior of BSA in acidic solutions reflect the present state of knowledge of protein structure. In any event, it is apparent that we are dealing with a three-stage process: a rapidly occurring configurational change at about *p*H 4.2; a rapid change in configuration which occurs continuously over the *p*H range 3.7 to 2 and which is, in turn, followed by slow aggregation in high ionic strength KCl solutions and measurably slow precipitation in 0.15 *M* $NaClO_4$.

L. A. ROMO (du Pont Company).—To understand the stoichiometry and kinetics of the reaction, it would have been well to do the following: (*1*) Titrate and follow conductivity of the protein with perchloric acid as a function of *p*H. These measurements would have permitted you to establish the amount of $ClO_4^-$ bound by the protein and the charge distribution. (*2*) Back titrate the acid protein with a base and see whether there is hysteresis in the curve. This hysteresis should be related to the denaturation of the protein—also the viscosity data could be interpreted better with the results obtained by these experiments.

J. R. CANN.—I agree that measurements of this type will help elucidate the mechanisms of interaction of BSA with perchlorate ions in acidic media.

# ON COAGULATION EFFECTS OF HIGHLY CHARGED COUNTERIONS[1]

BY E. MATIJEVIĆ, D. BROADHURST AND M. KERKER

*Clarkson College of Technology, Potsdam, New York*

*Received March 6, 1959*

Sols whose charge had been reversed by 9-tungstophosphoric acid were coagulated by simple mono-, di-, tri- and tetravalent cations. These sols, which were originally positively charged, behaved as normal negative sols to the above coagulating cations. The influence upon the coagulation concentration of a number of procedures for preparing the recharged sols was investigated. The coagulation concentration of a hexol for negative silver halide sols has been determined at several *p*H values. At low *p*H, the hexol exhibits a coagulation concentration consistent with ionization to a hexavalent species. Just as had been found previously for highly charged anions, the highly charged hexol cation causes reversal of charge on the colloidal particles. The availability of critical coagulation concentrations of highly charged ions has made possible a detailed comparison of coagulation data with the requirements of existing quantitative expressions for the Schulze–Hardy rule. The validity of the theories of Derjaguin–Landau–Verwey–Overbeek, of Whetham and of Težak in relation to these coagulation data has been discussed.

## Introduction

There are very few published data available on the coagulation of lyophobic hydrosols by highly charged ions (charge > 4). According to the Schulze–Hardy rule, such ions should behave as very strong coagulating agents since the coagulation efficiency increases markedly with increasing charge of counterions in solution.

We have shown[2,3] recently that some of the heteropoly acids are fully ionized at low concentration and give rise to anions of high charge, *viz.*, 4 to 7. Accordingly, we have employed them in the coagulation of positive silver halide hydrosols. These heteropoly anions cause a reversal of the colloidal particle charge as is common for highly charged counterions. In this work we have investigated the effects when such sols, recharged with 9-tungstophosphoric acid, were coagulated with mono-, di-, tri- and tetravalent counterions. These investigations were performed in order to obtain some information on the properties of the stability region of recharged sols and also the influence of the size of primary particles and the charge of the stabilizing ion on the critical coagulation concentration of the coagulating ions.

A second aspect of this work has been to obtain coagulation data for negative sols by highly charged ions. For this we have used a hexol which at low *p*H gives hexavalent cations. The coagulation concentration in this case was comparable with that obtained with hexavalent anions using positive sols.

There is a definite difference in the quantitative expression of the Schulze–Hardy rule derived from the theory of Derjaguin and Landau[4] and Verwey and Overbeek[5] on the one hand, and those given by Whetham[6] and by Težak[7–9] on the other. The difference becomes more pronounced as the valency of the counterions increases. Therefore, we have used the new coagulation data of highly charged counterions which we have obtained to test these theories of the mechanism of coagulation.

## Experimental

**9-Tungstophosphoric acid** was prepared and purified as described previously.[10] A pure sample of **tris-(bis-ethylenediamine-chromium(III)-μ-diol)-chromium(III) chloride (Hexol)** was kindly given to us by Professor G. Schwarzenbach. All other chemicals were of the highest commercial purity grades, and when necessary were further purified by usual methods. The water was doubly distilled, the second distillation being carried out in an all-Pyrex still. All glassware was thoroughly cleaned and steamed before use.

In order to avoid losses of the hexol from the very dilute solutions by adsorption on glass, the following procedure was adopted. A freshly prepared solution was permitted to stand in a volumetric flask for several hours and then discarded. The flask was drained and weighed. After that a fresh solution of the same concentration was made up in the same flask and used for measurements. Fresh solutions of the hexol were prepared every few days since aging effects have been noticed if solutions were kept over longer periods of time.

The coagulation effects were explored using silver halide sols *in statu nascendi*. The determination of the critical coagulation concentrations and the experimental technique of measuring the rate of coagulation have been described previously.[11,2]

For *p*H measurements, a Beckman *p*H meter Model G with glass electrodes was used. The scale of the meter was calibrated with appropriate buffer solutions.

## Results

**1. Coagulation Effects with Heteropoly Ions.**—The coagulation effects of a number of heteropoly ions, including 9-tungstophosphate, have been described previously.[2,3] At higher concentrations of heteropoly ion a stability limit appears, above which the sols are only very slightly turbid—even much less turbid than the sols below the *critical coagulation concentration* of the heteropoly ions. This indicates that above the stability limit, the particles are exceedingly small, even smaller than can be seen in the ultramicroscope. This behavior is typical for higher valent counterions ($\geqslant 3$ for positive sols and $\geqslant 4$ for negative sols) and it is believed that this is due to the adsorption of the

(1) Supported by the U. S. Atomic Energy Commission Contract No. AT(30-1)-1801.

(2) E. Matijević and M. Kerker, THIS JOURNAL, **62**, 1271 (1958).

(3) E. Matijević and M. Kerker, *J. Am. Chem. Soc.*, submitted for publication.

(4) B. Derjaguin and L. Landau, *Acta Physicochim. USSR*, **14**, 633 (1941).

(5) E. J. W. Verwey and J. Th. G. Overbeek, "Theory of the Stability of Lyophobic Colloids," Elsevier, New York, N. Y., 1948.

(6) W. C. D. Whetham, *Phil. Mag.*, [5] **48**, 474 (1899).

(7) B. Težak, *Z. physik. Chem.*, **A191**, 270 (1942); *Arhiv kem.*, **22**, 26 (1950); B. Težak and E. Matijević, *ibid.*, **19**, 29 (1947); B. Težak, E. Matijević, K. F. Schulz, J. Kratohvil, M. Mirnik and V. B. Vouk, *Disc. Faraday Soc.*, **18**, 63, 194 (1954).

(8) B. Težak, E. Matijević and K. F. Schulz, THIS JOURNAL, **59**, 769 (1955).

(9) E. Matijević, K. F. Schulz and B. Težak, *Croat. Chem. Acta*, **28**, 81 (1956).

(10) E. Matijević and M. Kerker, *J. Am. Chem. Soc.*, **81**, 1307 (1959).

(11) B. Težak, E. Matijević and K. Schulz, THIS JOURNAL, **55**, 1575 (1951).

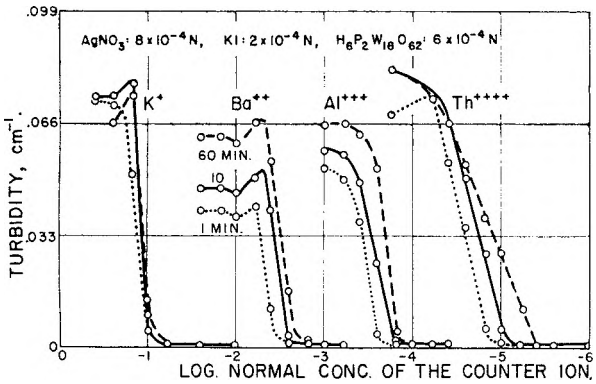


Fig. 1.—Coagulation curves of $KNO_3$, $Ba(NO_3)_2$, $Al(NO_3)_3$ and $Th(NO_3)_4$ for recharged silver iodide sol 1, 10 and 60 minutes after mixing the reacting components. The recharging was performed with the 9-tungstophosphoric acid.

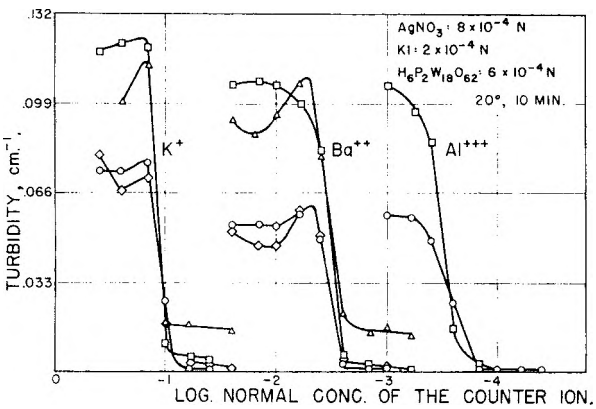


Fig. 2.—Coagulation curves of $KNO_3$, $Ba(NO_3)_2$ and $Al(NO_3)_3$ recharged for silver iodide sols with 9-tungstophosphoric acid (9-TPA) and prepared in different ways: circles, [$AgNO_3$] + [KI, 9-TPA, coag. electr.]; diamonds, [$AgNO_3$, 9-TPA] + [KI, coag. electr.]; triangles, [$AgNO_3$, KI] + [9-TPA, coag. electr.]; squares, [$AgNO_3$, KI] + [9-TPA] + [coag. electr.].

highly valent counterions, with a corresponding reversal of charge of the colloidal particles.

In order to establish that this region actually consists of recharged particles, we have tried to coagulate such stabilized solutions. If primary particles are present they should be negatively charged and therefore coagulated by cations.

Figure 1 gives the 1, 10 and 60 minutes coagulation curves for $K^+$, $Ba^{++}$, $Al^{+++}$ and $Th^{++++}$ for a silver iodide sol recharged with the 9-tungstophosphate ion at a concentration well into the stability region ($AgNO_3$, $8 \times 10^{-4}$ *N*; KI, $2 \times 10^{-4}$ *N*; $H_6P_2W_{18}O_{62}$, $6 \times 10^{-4}$ *N*). The coagulation effect is very obvious; even the validity of the Schulze–Hardy rule in this system appears unambiguously.

In these experiments the silver nitrate solution was in one test-tube and the solution of all other components (KI, $H_6P_2W_{18}O_{62}$ and coagulating electrolyte) was in another test-tube. The two solutions were mixed and the changes in turbidity observed. In such a case, the presence of the highly charged heteropoly ion may influence all stages of the formation of the solid phase prior to coagulation. In order to investigate this influence we have performed a number of experiments in which the sequence of mixing the solutions to the same final concentrations was varied.

Figure 2 summarizes these data. Circles denote the same systems as in Fig. 1. The curves denoted with diamonds were obtained by mixing of solutions which contained $AgNO_3$ + $H_6P_2W_{18}O_{62}$ in one test-tube and KI + coagulating electrolyte in the other test-tube. For curves marked with triangles, solutions of KI and $AgNO_3$ were first mixed forming negatively charged silver iodide. After one minute the solution of $H_6P_2W_{18}O_{62}$ + coagulating electrolyte was added and the turbidity measured. Finally, the squares denote results where three steps were employed. Firstly silver iodide was formed, then heteropoly ion added and finally the coagulating electrolyte was mixed with the recharged sol. Similar effects were obtained with a silver bromide sol.

From Fig. 2 it appears that the coagulation concentrations are only slightly influenced by the way the sols are prepared. The only difference is in the magnitude of the turbidity of the coagulated sols.

**2. Coagulation Effects with Hexols.**—Figure 3 represents a typical coagulation curve obtained when negative silver bromide sol was coagulated with the hexol. Although the hexol chloride was used, the chloride ion is present at too low a concentration to influence the sol formation. In any case it has been shown that more soluble halides do not change the precipitation picture of less soluble ones.[12,13] The recharging of the sol takes place at a very low concentration (which depends on *p*H). The recharged sols are stable over a long period of time as seen from the 48- and 72-hour curves. At these later times the stability limit is somewhat shifted toward higher hexol concentrations, but eventually reaches a limiting value. The turbidity of the coagulation region has dropped at the longer times due to the sedimentation of the coagulated particles.

There is very little difference in turbidities of the coagulation region from 10 to 60 minutes. Therefore, the 10-minute curves are used in subsequent plots. This is important in order to compare the data obtained in the presence of NaOH with that in acid for reasons to be explained below.

The *p*H of the systems in Fig. 3 is given with full dots. In the coagulation region the *p*H stays constant at 5.2. We have noticed that both the coagulation limit and the coagulation region change with *p*H. With decreasing *p*H the critical coagulation concentration becomes lower. We have ascribed this effect to the dissociation of hexol at higher *p*H's.

A complete presentation of the coagulation effects of the hexol on silver bromide sol in excess of KBr for various *p*H values is given in Fig. 4. The lower curve represents the coagulation limit and the upper the stabilization limit. The region in between is where the hexol acts as a coagulant. The different acidities were obtained by adding nitric acid and the *p*H always refers to the value at the coagulation limit.

When caustic soda was added in order to obtain

(12) B. Černicki and B. Težak, *Croat. Chem. Acta*, **28**, 13 (1956).
(13) M. Biff and B. Težak, *ibid.*, **30**, 9 (1958).

high *p*H values two effects were noted. Firstly, the *p*H of the resultant solutions was considerably lower than calculated. It remained constant for about 15 minutes, but after that a continuous drop could be noted indicating the decomposition of hexol. It was for this reason, as mentioned above, that for these coagulation measurements we have used only data obtained up to 10 minutes after mixing the solutions. Secondly, the coagulation curves showed an appreciably lower turbidity at *p*H's higher than 7. Although the coagulation process of NaOH seems to be somewhat complicated, we have included a few points obtained above *p*H 7 since they do fit well into the general trend of the curves. At the lowest *p*H values the influence of $H^+$ itself on the stability limit becomes significant. The coagulation limit, however, is influenced only inasmuch as the ionization of hexol increases. The coagulation values approach a limiting value which is about the same as the critical coagulation concentration for the hexavalent 9-tungstophosphate ion. This would indicate that the hexol is also hexavalent. The slight increase of the coagulation concentration at lowest *p*H is very probably a result of the presence of the large amount of $HNO_3$ which causes a super-additivity effect with the hexol.[14] A result obtained with a silver iodide sol is denoted with squares showing that there is not a significant difference between AgBr and AgI sols when coagulated with hexol.

Kruyt and Troelstra[15] have reported the recharging concentrations of a hexol-nitrate for silver iodide sol. At comparable *p*H values, their results are similar to ours but they do not cover the range of *p*H that we have worked with. Thus, they did not detect the minimum in Fig. 4. Furthermore, they do not mention the aging effects in NaOH media which we have found. They expressed the opinion that the hexol ion should be treated as a combination of six monovalent ions. Our coagulation results definitely show that this assumption cannot apply and that hexol ion, at least at very high dilutions critical for coagulation, behaves as a polyvalent ion.

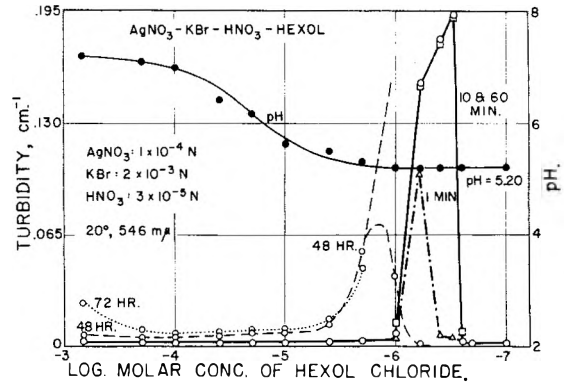


Fig. 3.—Coagulation curves of hexol chloride for silver bromide sol *in statu nascendi* 1, 10, 60 minutes, 48 and 72 hours after mixing the reacting components. *p*H values are denoted with full dots.

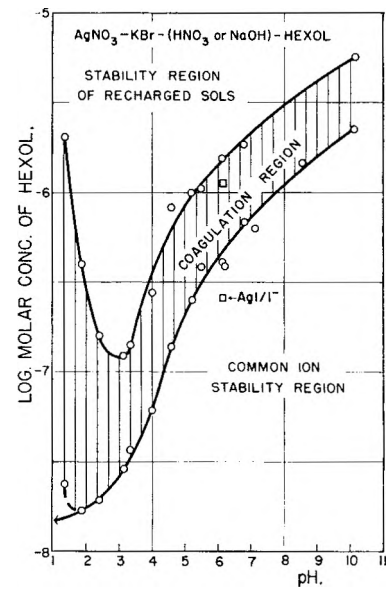


Fig. 4.—The *p*H–log molar concentration plot of the system $AgNO_3$ ($1 \times 10^{-4}$ *N*)–KBr ($2 \times 10^{-3}$ *N*)–$HNO_3$ or NaOH (varied)–hexol chloride. Hatched area represents the coagulation region. Upper curve gives the stability limit due to recharging of the sol. The lower curve is the coagulation limit of hexol ion for the silver bromide sol.

## Discussion

**1. Coagulation of Recharged Sols.**—The ability to coagulate silver halide sols stabilized in excess of 9-tungstophosphoric acid with cations shows that the stability of these sols is due to the adsorption of heteropoly anions onto the originally positive silver halide particles. The coagulation concentrations of $K^+$, $Ba^{++}$, $Al^{+++}$ and $Th^{++++}$ (Fig. 1) for these recharged sols are in very good agreement with values obtained when simple negatively charged silver bromide sols are coagulated with the same counterions.[8,9] This indicates that the original valency of a stabilizing ion plays a subordinate role and that, when adsorbed, every stabilizing ion acts as if it were monovalent toward its counterion in solution. This effect was found previously[16] but not with so highly charged counterions as in the present case, indicating a general validity of this effect.

Furthermore, the coagulation concentration does not depend on the manner of the preparation of sols (Fig. 2). The preparative procedure does result in different turbidities for the coagulated systems which in turn are dependent upon the size of the scattering particles. Thus, the systems coagulated *in statu nascendi*, *i.e.*, when the sol is formed in the presence of both the heteropoly and the coagulating ions, consist of a large number of small particles, whereas the sols which were first prepared, and then recharged and coagulated contain a smaller number of larger particles. Obviously the presence of heteropoly ions influences the nucleation process preventing the growth of nuclei by adsorption on their surface as soon as they reach a critical size. This, however, does not influence the coagulation process which seems to be insensitive to the size of the primary particles. These experiments

(14) Wo. Ostwald and K. Hoffmann, *Kolloid-Z.*, **80**, 186 (1937); B. Težak, E. Matijević, K. F. Schulz, R. Halassy and I. Kostinčer, *Proc. Int. Conf. of Surface Activity*, **3**, 607 (1957).

(15) H. R. Kruyt and S. A. Troelstra, *Kolloid-Beihefte*, **54**, 262 (1943).

(16) E. Matijević and N. Pavković, *Kolloid-Z.*, **159**, 1 (1958).

certainly obviate earlier objections[17] to the use of the method *in statu nascendi* for obtaining coagulation data since they definitely show that both the sols coagulated in the nascent state and sols firstly prepared and then coagulated give the same coagulation effects. The explanation for the similarity of behavior in the two cases is given elsewhere.[18,19]

**2. Coagulation with Highly Charged Counterions.**—In order to evaluate the coagulation effects of highly charged counterions we shall compare their coagulation concentrations with coagulation concentrations of lower valent counterions obtained with the same sols and try to see whether the results fit the requirements of existing theories of the stability of lyophobic colloids.

Such an approach is justified only if two conditions are fulfilled: (a) that we actually have in the solution free ions of the assumed valency, and (b) that all the coagulation effects to be compared are of the same character.

We have recently established the basicity of a number of heteropoly acids and that they are fully ionized in dilute solutions.[3] It appears from the coagulation value for the hexol at high acidities that this ion becomes fully charged at the extremely low concentrations employed in these experiments.

The shape of the coagulation curves, the magnitude of the turbidities and the rate of the coagulation processes obtained with the highly charged counterions are strictly comparable with coagulation effects of lower valent counterions for the same sols. They are definitely different from coagulation effects with ions where the coagulation is caused primarily by adsorption of counterions on the solid–liquid interface, *viz.*, *adsorption coagulation*.[20] Some adsorption effects recently have been observed even with simple ions of lower valencies.[21,22] However, from the behavior of the systems considered here there is no indication that we are dealing with adsorption coagulation in this case.

It is well known that the critical coagulation concentration of an ion also depends on its size. For this reason, the best approach in comparing the data for ions of different valencies is (a) to eliminate the effect of the size or (b) to compare ions of comparable sizes.

In an earlier paper, it was shown that the effect of size decreases with increasing charge of the counter ion and is already negligible with four-valent counterions.[8,9] The heteropoly and hexol ions employed are highly charged compact spheres with not excessively large radii, these being of the order of 5–6 Å.[23–25] It is therefore fair to assume that even though they are somewhat larger than the lower valent ions with which they are being compared, that the effect of the ionic size can be neglected. At the dilutions employed in coagulation measurements with the hexol and heteropoly ions the distances between polyvalent ions and the phase boundary becomes so large that the charge distribution on the polyvalent ions ceases to be of any influence and we are in effect dealing with point charges.

The size independent critical coagulation concentrations of mono-, di-, tri- and tetravalent cations for silver bromide sols[8,9] are presented in Table I. In addition, the value for hexol has been added.

TABLE I

$[Ag^+]$, $1 \times 10^{-4}$ $N$; $[Br^-]$, $2 \times 10^{-3}$ $N$

| Counterion | $C_{coag.}$, $N$ |
|---|---|
| Monovalent | $1.8 \times 10^{-1}$ |
| Divalent | $5.3 \times 10^{-3}$ |
| Trivalent | $1.1 \times 10^{-4}$ |
| Tetravalent | $4.0 \times 10^{-6}$ |
| Hexavalent | $8.7 \times 10^{-8}$ |

For coagulation of positively charged sols the problem is more difficult since the number of suitable ions available, especially for purposes of determining size effects, is considerably less.

The coagulation concentrations of a number of anions for positive silver bromide sols are listed in Table II including the references where the data are found.

TABLE II

$[Ag^+]$, $8 \times 10^{-4}$ $N$; $[Br^-]$, $2 \times 10^{-4}$ $N$

| Counterion | Charge | $C_{coag.}$, $N$ | Ref. |
|---|---|---|---|
| Nitrate | −1 | $1.8 \times 10^{-2}$ | 26 |
| Sulfate | −2 | $5.4 \times 10^{-4}$ | 27 |
| Citrate | −3 | $8.0 \times 10^{-6}$ | 28 |
| 12-Tungstosilicate | −4 | $6.0 \times 10^{-7}$ | 2 |
| 9-Tungstophosphate | −6 | $2.2 \times 10^{-7}$ | 2 |
| 12-Tungstophosphate | −7 | $6.7 \times 10^{-8}$ | 2 |

We have repeated the experiments with nitrate and sulfate ions and have obtained the same results. In the case of the three lower valent ions, *viz.*, nitrate, sulfate and citrate, the sizes are comparable, especially when one takes the shape factors into consideration. We already have pointed out that the size influence becomes less important for the higher valent ions. For this reason we have taken data from Table II for further treatment without correcting for ionic sizes. Actually only one of the three theoretical treatments which we will consider treats the ionic size effects (Težak).

The expression derived from the Derjaguin–Landau–Verwey–Overbeek theory for the variation of coagulation concentration with charge of the counterion ($C_1$ = concn. of the monovalent counterion, etc.) is

$$C_1:C_2:C_3:C_4:C_5:C_6 = 1:(1/2)^6:(1/3)^6:(1/4)^6:(1/5)^6:(1/6)^6 \quad (1)$$

Whetham's equation has the form

$$C_1:C_2:C_3:C_4:C_5:C_6 = 1:1/x:1/x^2:1/x^3:1/x^4:1/x^5 \quad (2)$$

(17) S. A. Troelstra, discussion remark, *Kolloid Z.*, **146**, 73 (1956).
(18) K. F. Schulz and B. Težak, *Arhiv kem.*, **26**, 187 (1954).
(19) E. Matijević, *Kolloid-Z.*, **146**, 74 (1956).
(20) E. Matijević and R. H. Ottewill, *J. Colloid Sci.*, **13**, 242 (1958).
(21) J. Lijklema, Thesis, Utrecht, 1957.
(22) K. F. Schulz and M. J. Herak, *Croat. Chem. Acta*, **30**, 127 (1958).
(23) A. F. Wells, "Structural Inorganic Chemistry," Oxford University Press, New York, N. Y., 1950.
(24) W. Hückel, "Structural Chemistry of Inorganic Compounds," Elsevier, New York, 1950.
(25) T. Kurucsev, A. M. Sargeson and B. O. West, THIS JOURNAL, **61**, 1567 (1957).
(26) H. Herak and B. Težak, *Arhiv kem.*, **25**, 87 (1953).
(27) J. Herak and B. Težak, *ibid.*, **26**, 1 (1954).
(28) B. Težak, *et al.*, THIS JOURNAL, **57**, 301 (1953).

The equation given by Težak includes the ionic size and is

$$z_0 d + r = {}_s d(\log C_{fix} - \log C_{coag}) \qquad (3)$$

where $r_i$ denotes the radius of the coagulating ion and $z$ its valency, ${}_c d$ is the critical distance in Bjerrum's equation for ion pair formation,[29] $C_{coag}$ is the critical coagulation concentration and ${}_s d$ and $C_{fix}$ are constants specific for each colloidal system. If radius is taken zero or constant, the equation reduces to

$$\log C_{coag} = \frac{{}_c d}{{}_s d} z + \log C_{fix} \qquad (4)$$

which gives a linear relationship between the logarithm of the coagulation concentration and the valency of counterions.

We do not intend to make use of Ostwald's or Freundlich's expressions[30] since we have shown earlier that they do not fit the data even qualitatively.[9,31]

We have summarized the results for negative sols in Fig. 5 and for positive sols in Fig. 6. The experimental data from Tables I and II are represented by the points. The dashed line represent the trend given by equation 1 and the full line gives that required by equations 2 and 4. In all cases the monovalent counterion was taken as the reference point for calculations.

There is very good agreement between the experimental data and the calculations made from Whetham's and Težak's equations for counterions of valencies up to four with both negative and positive sols. Higher valent counterions give a higher coagulation concentration than predicted by these theories. The function calculated from the Derjaguin–Landau–Verwey–Overbeek theory has a quite different trend. It begins to deviate markedly from the experimental data even for the four valent counterions and for higher charged ions requires considerably greater coagulation concentrations than were obtained experimentally.

A possible explanation for the failure of equation 1 to fit the experimental data may be due to the fact that this equation was derived for symmetrical electrolytes, whereas in our case all electrolytes used had a monovalent accompanying ion (nebenion). There are a few data available on the influence of mono- and divalent accompanying ions upon the coagulation concentration of various counterions.[32] They indicate that this influence is rather small, but it would be very difficult to predict what would happen for a 4–4 or even 6–6 valent electrolyte. However, it may be noted that $Al_2(SO_4)_3$ and $Th(SO_4)_2$ are better coagulating agents than respective nitrates so that the trend is opposite to what would be needed to comply with equation 1.

In a more recent paper Derjaguin[33] suggested that for higher valent counterions ($z = 3$) the sixth-power in Eq. (1) should be replaced by the eighth-power. This would bring the theoretical curve based on his theory much closer to our experimental results (for counterions of charges 4 and higher) as well as to the curve obtained from Težak's equation.

Težak's equation predicts lower coagulation concentrations than were obtained experimentally for highly charged counterions. His approach is based on ion pair interactions in which the distribution of ions in the solution plays a major role. Assuming the ideal case of uniform distribution, the plot of interionic distances against the logarithm of concentration shows that the interionic distances increase very fast with dilution.[34] This would indicate that the critical distribution of highly charged ions which causes coagulation is reached at

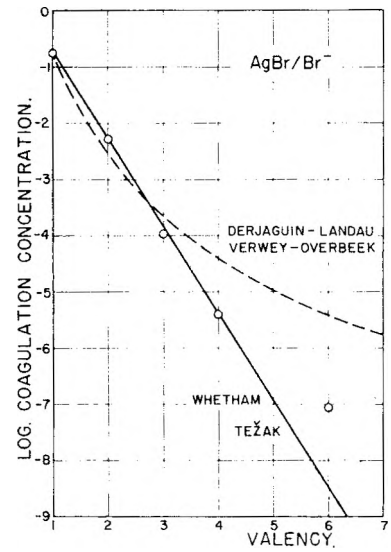


Fig. 5.—The relationship between the valency of the coagulating cations and the logarithm of their coagulation concentrations for a negative silver bromide sol. The dots represent the experimental results. The dashed line is the function as obtained from the Derjaguin–Landau–Verwey–Overbeek expression, the full line gives the relationship predicted by Whetham and by Težak.

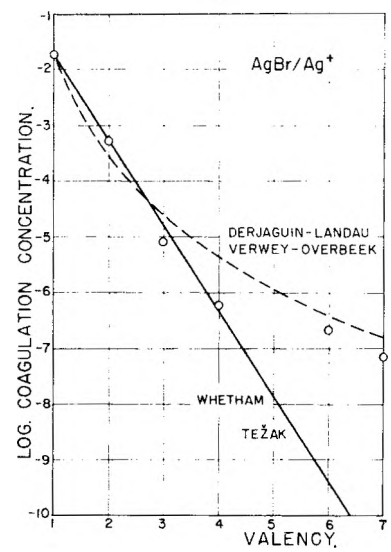


Fig. 6.—The same relationship as in Fig. 5 for coagulating anions on positive silver bromide sol.

(29) H. S. Harned and B. B. Owen, "The Physical Chemistry of Electrolytic Solutions," 3rd edition, Reinhold Publ. Corp., New York, N. Y., 1958, p. 70 ff.

(30) Wo. Ostwald, *Kolloid. Z.*, **26**, 28, 69 (1920); **85**, 34 (1938); **88**, 1 (1939); THIS JOURNAL, **42**, 981 (1938).

(31) B. Težak, E. Matijević and K. Schulz, *Arhiv kem.*, **20**, 1 (1948).

(32) E. Matijević, *Chimia (Switz.)*, **9**, 287 (1955).

(33) B. V. Derjaguin, I. I. Abricosova and E. M. Lifschitz, *Quart. Revs. (London)*, **10**, 295 (1956).

(34) B. Težak, *Arhiv kem.*, **21**, 96 (1949).

higher concentrations and therefore the sol becomes less sensitive toward the higher charged counterions, just as we have found, and it would be expected that the critical coagulation concentrations would be relatively higher than would be predicted on the basis of a comparison with lower valent coagulating ions.

**Acknowledgment.**—We are greatly indebted to Professor G. Schwarzenbach (Zürich) for a generous gift of hexol chloride.

## DISCUSSION

J. J. BIKERMAN (Massachusetts Institute of Technology).—I have two remarks to make. First, Dr. Matijević did not mention the work by Kruyt who measured coagulation by "hexol" or similar ions and tried to extend the Schulze–Hardy rule to hexavalent cations.

E. MATIJEVIĆ (Clarkson College of Technology).—Kruyt and Troelstra's work is cited in our paper.[15] They did not determine the coagulation concentration of hexol; the emphasis was on the limit for reversal of charge.

J. J. BIKERMAN.—The other remark concerns the final concentration of the coagulating ion. In every theory of coagulation by ions only the final concentration is important. If the initial concentration of "hexol" was, *e.g.*, $10^{-8}N$, it may have been lowered to $10^{-10}N$ by reaction with the protective or similar effects.

E. MATIJEVIĆ.—The concentrations of the counterion in solution could be decreased in two ways: (*1*) by forming an insoluble compound with stabilizing ion; (*2*) by adsorption on the solid phase. We have found that the solubility of silver sols of the heteropoly compounds used is very high, thus eliminating the first possibility. We keep in mind the possibility of adsorption and hope to do some adsorption determinations using $P^{32}$ labeled tungstophosphoric acids. Very recently Dr. Schulz[35] has measured the adsorption of thorium ions on positive and negative silver halide sols employing the tracer technique. He has found a rather strong adsorption of thorium on positive sols and a much lower adsorption on negative sols. Obviously more experimental data are needed to clarify the problem of adsorption of counterions.

L. A. ROMO.—The use of ionic radii factors is an attempt to introduce a capacity correction factor. It would seem more significant to work with $r^2$ or $r^3$. The equation as is hasn't much significance. One could do away with a radius factor and still get the same final results. For instance in such cases as $Ca^{++}$ and $Na^{+}$, this $r$ factor has no value because their radii are the same.

E. MATIJEVIĆ.—In Težak's approach the critical distance between the stabilizing ion and the counter ion as calculated using Bjerrum's equation for ion-pair formation plays the decisive role. The concentration necessary for an ion to reach the critical distance is influenced by its radius. Therefore, it is correct to use the radius as shown in Eq. 3. A given radius, for ions of different valencies, exerts the same absolute contribution to the critical distance but its relative contribution decreases with increasing valency of the counter ion.

(35) K. F. Schultz and M. J. Herak, *Croat. Chem. Acta*, **30**, 127 1958.

# ELECTRIC PROPERTIES OF MACROMOLECULES. IV. DETERMINATION OF ELECTRIC AND OPTICAL PARAMETERS FROM SATURATION OF ELECTRIC BIREFRINGENCE IN SOLUTIONS

BY CHESTER T. O'KONSKI, KOSHIRO YOSHIOKA AND WILLIAM H. ORTTUNG[1]

*Department of Chemistry, University of California, Berkeley*

*Received March 2, 1959*

The theory of electric birefringence in solutions of rigid axially symmetric dipolar molecules is extended to strong fields. The saturation behavior is computed for various ratios of permanent to induced moment contributions to the birefringence. By fitting the experimental birefringence saturation results to a theoretical curve, the electrical parameters and the optical anisotropy factor of the molecule can be separately determined. The birefringence buildup in strong fields and the decay are treated. Experimental saturation data are presented for a rigid polyelectrolyte (tobacco mosaic virus), a rigid polypeptide (poly-γ-benzyl-L-glutamate) and a flexible polyelectrolyte (sodium polyethylene sulfonate). The first exhibits saturation characteristic of a large electrical polarizability, and the second and the third most closely fit permanent dipole moment saturation. Molecular constants were obtained, and are in satisfactory agreement with values obtained by other methods, where data are available.

## Introduction

The recent development of the transient electric birefringence method has facilitated the characterization of rigid macromolecules through measurements of their rotational diffusion constant,[2-6] and through determination of their electrical properties in those cases where their optical properties could be determined from other measurements.[7,8]

In principle, it is possible to subject a dilute solution of macromolecules to an electric field of sufficient intensity to obtain complete orientation. Under these conditions, measurement of the birefringence is a direct measure of the optical anisotropy of the molecules with respect to the axis of orientation. Then, from measurements of the Kerr constant obtained in the ordinary way, one may compute the pertinent electrical anisotropy factor, which is of interest in the elucidation of the macromolecular structure.

In the actual case, complete orientation of the macromolecules cannot be achieved because of the disorienting effect of Brownian motion, and it becomes necessary to extrapolate the measurements by some suitable method. As will be shown, the nature of the birefringence saturation curve depends upon the electric polarization mechanism which is responsible for the orientation. Therefore, it is necessary to calculate saturation functions for appropriate models so that experimental results may be interpreted.

In this article it will be shown that the theory of the saturation of electric birefringence can be put into a convenient form for interpretation of saturation data on axially symmetric macromolecules. The early theoretical papers on electric birefringence considered mainly the effect of small applied fields.[8] Gans[9] considered arbitrarily large electric fields for pure induced moment and pure permanent moment orientation. He obtained a birefringence saturation function only for pure permanent dipole orientation. Peterlin and Stuart[10] developed a theory of birefringence for insulating suspensions and obtained a birefringence saturation equation for induced moment orientation.

In this research, birefringence saturation in the case of mixed orienting mechanisms is treated and compared with the pure permanent moment and the pure induced moment orientation behavior. Tables and graphs of saturation functions and methods of analyzing experimental data are presented. Approximate equations are developed for the birefringence transient resulting from the application of a saturating square voltage pulse.

Saturation measurements have been made in this Laboratory on poly-γ-benzyl-L-glutamate[11] (PBLG), tobacco mosaic virus (TMV) and sodium polyethylene sulfonate[12] (NaPES). The first of these displayed a saturation behavior in agreement with permanent dipole moment orientation. The dipole moment and the optical anisotropy factor of the molecule have been evaluated and compared with results from other types of measurements. For TMV, the birefringence saturation confirms an induced polarization mechanism and the optical and electrical properties were determined. With respect to saturation, it was found that PES ions behave as if they have a permanent dipole moment. A tentative explanation is offered for this. Very few experimental results on electric birefringence saturation could be found in the literature. Some relatively weak saturation effects previously observed[3] are discussed.

## Theory

The electric anisotropy of a molecule in a solution causes the interaction energy of the molecule with the applied field to depend upon the angle between the molecular axis and the applied field; hence, the angular distribution of molecular directions becomes non-random in the presence of the field. In the

(1) Bell Telephone Laboratories Fellow, 1957–1958.

(2) H. Benoit, *Ann. phys.*, **6**, 561 (1951); *J. chim. phys.*, **49**, 517 (1952).

(3) (a) C. T. O'Konski and B. H. Zimm, *Science*, **111**, 113 (1950).

(4) C. T. O'Konski and A. J. Haltner, *J. Am. Chem. Soc.*, **78**, 3604 (1956).

(5) I. Tinoco, *ibid.*, **77**, 3476 (1955).

(6) C. T. O'Konski and A. J. Haltner, *ibid.*, **79**, 5634 (1957).

(7) I. Tinoco, *ibid.*, **79**, 4336 (1957).

(8) (a) P. Langevin, *Le Radium*, **7**, 249 (1910); *Compt. rend.*, **151**, 475 (1910); (b) M. Born, *Ann. Physik*, **55**, 177 (1918).

(9) R. Gans, *ibid.*, **64**, 481 (1921).

(10) A. Peterlin and H. A. Stuart, *Z. Physik*, **112**, 129 (1939); also "Hand- und Jahrbuch der chemischen Physik," Bd. 8, Abt. 1B, Leipzig, 1943.

(11) C. T. O'Konski and W. H. Orttung, *J. Am. Chem. Soc.*, in press.

(12) K. Yoshioka and C. T. O'Konski, *J. Polymer Sci.*, unpublished.

following calculation rigid molecules are considered which have an axis of symmetry for their electric, optical and hydrodynamic properties. The assumption of a hydrodynamic axis of symmetry is used only in the calculation of transient effects. This assumption is less restrictive than the assumption of a specific model, such as a cylinder or an ellipsoid of revolution. Further, it is assumed that the solution is so dilute that interaction effects can be neglected.

The fundamental equation for the birefringence of a dilute solution of axially symmetric particles has been given by Peterlin and Stuart[10]

$$\frac{1}{C_v}\frac{\Delta n}{n} = \frac{2\pi}{n^2}(g_1 - g_2)\int_0^\pi f(\theta) \times \frac{3\cos^2\theta - 1}{2} \times 2\pi \sin\theta \, d\theta \quad (1)$$

where

$C_v$ = volume fraction of particles
$\Delta n = n_{\parallel} = n_{\perp}$, the birefringence
$n$ = index of refraction of the soln.
$g_1 - g_2$ = optical anisotropy factor,[10] the subscripts 1 and 2 referring to the symmetry and transverse axes, respectively
$f(\theta)$ = angular orientation distribution function
$\theta$ = angle between particle symmetry axis and the axis of anisotropy, in this case, the field direction

To compute the orientation distribution function, an expression for the energy of interaction of the particle with the external electric field $E$ is required. For an axially symmetric particle with dipole moment $\mu$ along the symmetry axis in the solvent, the dipole interaction energy may be written

$$U_1 = -\mu E B_1 \cos\theta \quad (2a)$$

where

$B_1$ = an internal field function = $E_{1_{int}}/E_1$
$E_1$ = $E\cos\theta$ = component of external field along the symmetry axis
$E_{1_{int}}$ = resulting internal field at the dipole, with field and dipole assumed to be colinear

For ellipsoids of revolution in insulating media, $B_1$ has been evaluated[13]

$$B_1 = 1/[1 + (\epsilon_1 - \epsilon_0)L_1/4\pi\epsilon_0]$$

where $L_1$ is an elliptic integral, and $\epsilon_1$ and $\epsilon_0$ are dielectric constants of particle and solvent, respectively. If the solution and ellipsoid are conducting, the internal field function is the same at low frequencies except that the specific conductivities, $\kappa_1$ and $\kappa_0$, replace $\epsilon_1$ and $\epsilon_0$.[14]

The induced dipole interaction energy may be written

$$U_2 = -\frac{1}{2}(\alpha_1 - \alpha_2)E^2\cos^2\theta \quad (2b)$$

where, for insulating media,[10] the coefficients $\alpha_1$ and $\alpha_2$ are the excess polarizabilities of the particle in the solvent. For conducting media the coefficients involve the conductivities as well as dielectric properties; they have been derived for steady-state conduction.[14] The total interaction energy is

$$U = U_1 + U_2 \quad (2c)$$

### A. Steady-state Birefringence in a Saturating Field.

—For the steady state, the distribution function is given by

$$f(\theta) = \frac{e^{-U/kT}}{\int_0^\pi e^{-U/kT}\, 2\pi \sin\theta \, d\theta} = \frac{e^{\beta u + \gamma u^2}}{2\pi\int_{-1}^{+1} e^{\beta u + \gamma u^2}\, du} \quad (3)$$

where we have introduced the notation

$$u = \cos\theta$$
$$\beta = \mu E B_1/kT \quad (4)$$
$$\gamma = (\alpha_1 - \alpha_2)E^2/2kT \quad (5)$$

The integral in the denominator of eq. 3 may be evaluated as

$$\int_{-1}^{+1} e^{\beta u + \gamma u^2}\, du = e^{-\beta^2/4\gamma}\int_{-1}^{+1} e^{(\sqrt{\gamma}u + \beta/2\sqrt{\gamma})^2}\, du \quad (6)$$

Making the substitution

$$X = \sqrt{\gamma}u + \beta/2\sqrt{\gamma} \quad (7)$$

one obtains

$$\int_{-1}^{+1} e^{\beta u + \gamma u^2}\, du = 1/\sqrt{\gamma}e^{-\beta^2/4\gamma}\int_{t_1}^{t_2} e^{X^2}\, dX \quad (8)$$

where $t_1 = \beta/2\sqrt{\gamma} - \sqrt{\gamma}$ and $t_2 = \beta/2\sqrt{\gamma} + \sqrt{\gamma}$, respectively. Using the definition (9)

$$E(t) = \int_0^t e^{X^2}\, dX \quad (9)$$

the integral may be written

$$\int_{-1}^{+1} e^{\beta u + \gamma u^2}\, du = (1/\sqrt{\gamma})e^{-\beta^2/4\gamma}\,[E(t_2) - E(t_1)] \quad (10)$$

A table of $E(t)$ was given by Terrill and Sweeny.[15]

Introducing eq. 3 into eq. 1, one has

$$\frac{1}{C_v}\frac{\Delta n}{n} = \frac{2\pi}{n^2}(g_1 - g_2)\Phi(\beta,\gamma) \quad (11)$$

where

$$\Phi(\beta,\gamma) = \frac{3\int_{-1}^{+1} u^2 e^{\beta u + \gamma u^2}\, du}{2\int_{-1}^{+1} e^{\beta u + \gamma u^2}\, du} - \frac{1}{2} \quad (12)$$

Making the substitution expressed by eq. 7, we can evaluate the integral in the numerator. Thus

$$\int_{-1}^{+1} u^2 e^{\beta u + \gamma u^2}\, du = \frac{e^{-\beta^2/4\gamma}}{\gamma\sqrt{\gamma}}\left[\int_{t_1}^{t_2} X^2 e^{X^2}\, dX - \frac{\beta}{\sqrt{\gamma}}\int_{t_1}^{t_2} X e^{X^2}\, dX + \frac{\beta^2}{4\gamma}\int_{t_1}^{t_2} e^{X^2}\, dX\right] =$$
$$\frac{e^{-\beta^2/4\gamma}}{2\gamma\sqrt{\gamma}}\,[e^{(\beta^2/4\gamma)+\beta}\{\sqrt{\gamma}(e^{\beta} + e^{-\beta}) - (\beta/2\sqrt{\gamma})(e^{\beta} - e^{-\beta})\} + (\beta^2/2\gamma - 1)\,\{E(t_2) - E(t_1)\}] \quad (13)$$

where we used the formulas

$$\int X^2 e^{X^2}\, dX = \frac{1}{2}Xe^{X^2} - \frac{1}{2}\int e^{X^2}\, dX$$
$$\int X e^{X^2}\, dX = \frac{1}{2}e^{X^2}$$

From eq. 12, 10 and 13 one obtains

(13) Lord Rayleigh, *Phil. Mag.*, [5] **44**, 28 (1897).
(14) C. T. O'Konski and S. Krause, THIS JOURNAL, in preparation.
(15) H. M. Terrill and L. Sweeny, *J. Franklin Inst.*, **237**, 495 (1944); **238**, 220 (1944).

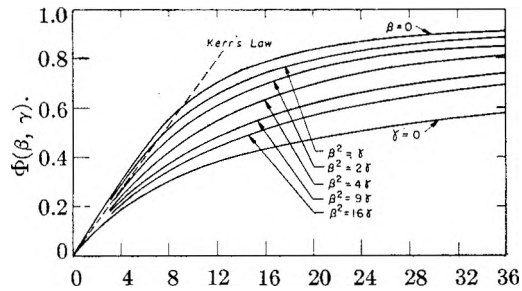


Fig. 1.—Degree of orientation, $\Phi(\beta, \gamma)$, *vs.* $\beta^2 + 2\gamma$ for $\beta = 0$, $\beta^2 = \gamma$, $\beta^2 = 2\gamma$, $\beta^2 = 4\gamma$, $\beta^2 = 9\gamma$, $\beta^2 = 16\gamma$, and $\gamma = 0$.

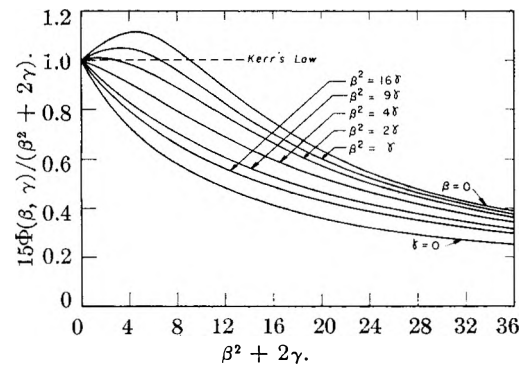


Fig. 2.—$15\Phi(\beta, \gamma)/(\beta^2 + 2\gamma)$ *vs.* $\beta^2 + 2\gamma$.

$$\Phi(\beta,\gamma) = \frac{3}{4\gamma}\times \left[\frac{e^{(\beta^2/4\gamma)+\gamma}\{\sqrt{\gamma}(e^{\beta}+e^{-\beta}) - (\beta/2\sqrt{\gamma})(e^{\beta}-e^{-\beta})\}}{E(\beta/2\sqrt{\gamma}+\sqrt{\gamma}) - E(\beta/2\sqrt{\gamma}-\sqrt{\gamma})} + \beta^2/2\gamma - 1\right] - 1/2 \quad (14)$$

$\Phi(\beta,\gamma)$ is a useful function to consider because as $E \to \infty$, $\Phi \to 1$. If the steady-state birefringence at infinite field strength is denoted by $\Delta n_s$, then

$$\frac{1}{C_v}\frac{\Delta n_s}{n} = \frac{2\pi}{n^2}(g_1 - g_2) \quad (15)$$

Using $\Delta n_s$, eq. 11 can be put in the form

$$\Delta n/\Delta n_s = \Phi(\beta,\gamma) \quad (16)$$

$\Phi(\beta,\gamma)$ is an orientation factor, which may be called the degree of orientation.

Three special cases of eq. 14 are of interest.

(a) **Weak Fields.**—$\beta,\gamma \ll 1$.—In this case eq. 14 can be expanded in the series

$$\Phi(\beta,\gamma) = \frac{2}{15}\gamma + \frac{1}{15}\beta^2 + \frac{4}{315}\gamma^2 + \frac{4}{315}\beta^2\gamma - \frac{2}{315}\beta^4 \ldots \quad (17)$$

There are small discrepancies between the coefficients of the last two terms and Benoit's values.

From eq. 17 there is obtained the limiting formula

$$\lim_{E\to 0}\frac{\Phi(\beta,\gamma)}{\beta^2+2\gamma} = \frac{1}{15} \quad (18)$$

Therefore

$$\left(\frac{\Delta n}{E^2}\right)_{E\to 0} = \frac{\Delta n_s}{15}(b^2 + 2c) \quad (19a)$$

where we have introduced the quantities $b$ and $c$, related to the dipole moment and polarizabilities

$$b = \beta/E = \mu B_1/kT \quad (19b)$$

$$c = \gamma/E^2 = (\alpha_1 - \alpha_2)/2kT \quad (19c)$$

The specific Kerr constant, as defined by Peterlin and Stuart,[10] and employed in this Laboratory,[6] is

$$K_{sp} = \frac{1}{C_v n}\left(\frac{\Delta n}{E^2}\right)_{E\to 0}$$

Introducing eq. 19a and 15

$$K_{sp} = \frac{2\pi(g_1 - g_2)}{15n^2}(b^2 + 2c) \quad (20)$$

(b) **Pure Permanent Moment Orientation.** $\beta \gg \gamma$.—Then

$$\Phi(\beta,0) = \Phi_\beta = 1 - 3(\coth\beta - 1/\beta)/\beta \quad (21)$$

The limiting form for low fields may be obtained from eq. 17. For limiting high fields

$$\Phi_\beta = 1 - 3/\beta + 3/\beta^2 \quad (22)$$

(c) **Pure Induced Moment Orientation.** $\gamma \gg \beta$.—Then

$$\Phi(0,\gamma) = \Phi_\gamma = \frac{3}{4}\left(\frac{e\gamma}{\sqrt{\gamma}E(\sqrt{\gamma})} - \frac{1}{\gamma}\right) - \frac{1}{2} \quad (23)$$

This function may be computed from a table of $e^{-t^2}E(t)$ given by Miller and Gordon.[16] Equation 17 gives the form for small values of $\gamma$. For large values of $\gamma$ ($\gamma > 10$)

$$\Phi_\gamma = 1 - 3/(2\gamma - 1) \quad (24)$$

Equation 24 was obtained from the work of Schwarz[17] who has investigated the anisotropy of conductance of solutions produced by electric fields.

The limiting form of eq. 14 for high fields is

$$\Phi(\beta,\gamma) = 1 - 3/(\beta + 2\gamma) \quad (25)$$

Values of $\Phi_\beta$ and $15\,\Phi_\beta/\beta^2$ as functions of $\beta$ are given in Table I, and those of $\Phi_\gamma$ and $15\Phi_\gamma/2\gamma$ as functions of $\sqrt{\gamma}$ are given in Table II. $\Phi(\beta,\gamma)$ and $15\Phi(\beta,\gamma)/(\beta^2 + 2\gamma)$ are plotted against $\beta^2 + 2\gamma$ (which is equal to $(b^2 + 2c)E^2$) in Fig. 1 and Fig. 2, respectively, for some special cases. $15\Phi(\beta,\gamma)/(\beta^2 + 2\gamma)$ is a useful function because of the relationship to the experimental quantity

$$(\Delta n/E^2)/(\Delta n/E^2)_{E\to 0} = 15\Phi(\beta,\gamma)/(\beta^2 + 2\gamma) \quad (26)$$

**B. Rise of the Birefringence in a Saturating Field.**—The equation for the rise of the birefringence under the action of a rectangular pulse was obtained for limiting low field strength by Benoit,[3] who solved the diffusion equation for axially symmetric molecules. It is quite difficult to solve the diffusion equation for arbitrary field strength. However, at sufficiently high field strength, the effect of rotational diffusion can be neglected as a first approximation, as was pointed out by Schwarz.[17] Equations for the buildup of the birefringence are given below for two special cases.

(a) **Permanent Dipole Orientation.**—The torque exerted on the axially symmetric dipole molecule in an electric field is

$$M = -\mu E B_1 \sin\theta \quad (27)$$

where $\theta$ is the angle which the axis of the dipole

(16) W. L. Miller and A. R. Gordon, THIS JOURNAL, **35**, 2785 (1931).

(17) Schwarz, *Z. Physik*, **145**, 563 (1956).

makes with the applied field. Under the influence of the torque the molecule will be rotated with an angular velocity given by the equation

$$\frac{d\theta}{dt} = \frac{\Theta}{kT} M = -\frac{\mu E B_1}{kT} \Theta \sin\theta = -\beta\Theta \sin\theta \quad (28)$$

where $\Theta$ is the rotational diffusion constant. Thus, the time $t$ which is required for the dipole axis to move from the initial angle $\theta'$ to $\theta$ after applying a rectangular pulse is given by

$$t = -\frac{1}{\beta\Theta}\int_{\theta'}^{\theta}\frac{d\theta}{\sin\theta} = -\frac{1}{\beta\Theta}\ln\frac{\tan\frac{\theta}{2}}{\tan\frac{\theta'}{2}}$$

Therefore

$$\tan\frac{\theta'}{2} = e^{\beta\Theta t}\tan\frac{\theta}{2} \quad (29)$$

The molecules having a direction of the dipole axis between $\theta'$ and $\theta' + d\theta'$ at the time $t = 0$ will turn to the direction between $\theta$ and $\theta + d\theta$ after the lapse of time $t$. Since all directions of the dipole have the same probability in the absence of an electric field, one has

$$N(1/4\pi)\, 2\pi \sin\theta' d\theta' = Nf(\theta,t)\, 2\pi \sin\theta\, d\theta \quad (30)$$

where $f(\theta,t)$ is the angular distribution function at the time $t$. From eq. 29 and eq. 30

$$f(\theta,t) = \frac{e^{2\beta\Theta t}}{\pi[1 + e^{2\beta\Theta t} + (1 - e^{2\beta\Theta t})\cos\theta]^2} \quad (31)$$

Introducing eq. 31 into eq. 1 the equation for the rise of the birefringence is

$$\frac{\Delta n}{\Delta n_s} = 1 + \frac{12e^x}{(e^x - 1)^2} - \frac{6xe^x(e^x + 1)}{(e^x - 1)^3} \quad (32)$$

where

$$x = 2\beta\Theta t = 2(\mu E B_1/kT)\,\Theta t \quad (33)$$

Here $\Delta n_s$ is the limiting value of $\Delta n$ as $t \to \infty$ and $E \to \infty$ and it is given by eq. 15.

Figure 3 represents the right-hand side of eq. 32 as a function of $x$. As is seen from the graph, the initial slope of the rise curve is zero. For small values of $x$, eq. 32 can be expanded in the series

$$\frac{\Delta n}{\Delta n_s} = \frac{1}{10}x^2 - \frac{1}{168}x^4 \cdots \quad (34)$$

**(b) Induced Dipole Orientation.**—This case was treated by Schwarz[17] in the analogous problem of the anisotropy of electric conductance. For the present model, the torque is equal to

$$M = -(\alpha_1 - \alpha_2)E^2 \sin\theta\cos\theta \quad (35)$$

The angular distribution function is

$$f(\theta,t) = \frac{e^{-2\gamma\Theta t}}{4\pi\sqrt{(e^{-4\gamma\Theta t}\cos^2\theta + \sin^2\theta)^3}} \quad (36)$$

The equation for the rise of the birefringence is

$$\frac{\Delta n}{\Delta n_s} = \frac{1}{1 - e^{-y}}\left(1 + \frac{1}{2}e^{-y} - \frac{3\tan^{-1}\sqrt{e^y - 1}}{2\sqrt{e^y - 1}}\right) \quad (37)$$

where

$$y = 4\gamma\Theta t = \frac{2(\alpha_1 - \alpha_2)E^2}{kT}\Theta t \quad (38)$$

Figure 4 represents the right-hand side of eq. 37 as a function of $y$. For small values of $y$, eq. 37 can be expanded in the series

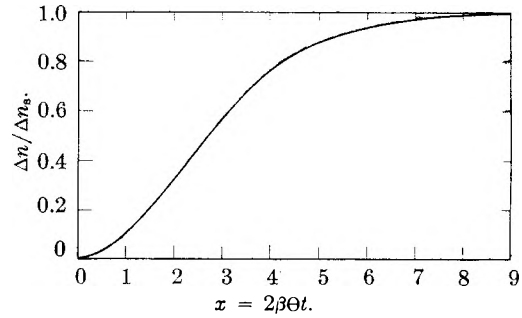


Fig. 3.—Theoretical rise curve of birefringence in a saturating field for the case of permanent dipole orientation.

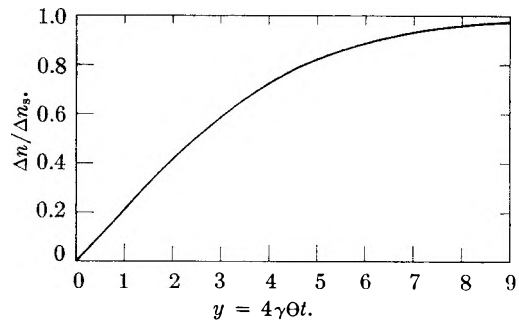


Fig. 4.—Theoretical rise curve of birefringence in a saturating field for the case of induced dipole orientation.

$$\frac{\Delta n}{\Delta n_s} = \frac{1}{5}y + \frac{1}{70}y^2 \cdots \quad (39)$$

Therefore

$$\left(\frac{d\Delta n}{dt}\right)_{t\to 0} = \frac{4}{5}\frac{(\alpha_1 - \alpha_2)E^2}{2kT}\Theta\Delta n_s \quad (40)$$

On the other hand, Benoit[2] deduced a limiting equation for low fields

$$\left(\frac{d\Delta n}{dt}\right)_{t\to 0} = \frac{12c}{b^2 + 2c}\Theta\Delta n_\infty \quad (41)$$

where $\Delta n_\infty$ is the value of $\Delta n$ as $t \to \infty$, *i.e.*, the steady-state value. Introducing eq. 19a into eq. 41, one obtains the same relation as eq. 40. Therefore, eq. 40 is expected to hold for arbitrary field strength.

**C. Decay of the Birefringence from Saturating Fields.**—Benoit[2] has shown that the field-free decay of birefringence in a dilute monodisperse system is given by the simple exponential law

$$\Delta n = \Delta n_0 e^{-6\Theta t} \quad (42)$$

where $\Delta n_0$ is the initial value of the birefringence. He stated that this law is general, depending only upon the validity of the diffusion equation. We have verified this result by direct use of the diffusion equation and eq. 1, without recourse to expansion of the distribution function in terms of Legendre polynomials.

If the system is polydisperse, the decay is not exponential and depends on the field strength (the larger the field strength, the faster the decay). Summing contributions of the various species, the following equation is obtained if a steady state was reached before the field was removed

$$\frac{\Delta n}{\Delta n_0} = \frac{\sum_i \phi_i (g_1 - g_2)_i \Phi(\beta_i, \gamma_i) e^{-6\Theta_i t}}{\sum \phi_i (g_1 - g_2)_i \Phi(\beta_i, \gamma_i)} \quad (43)$$

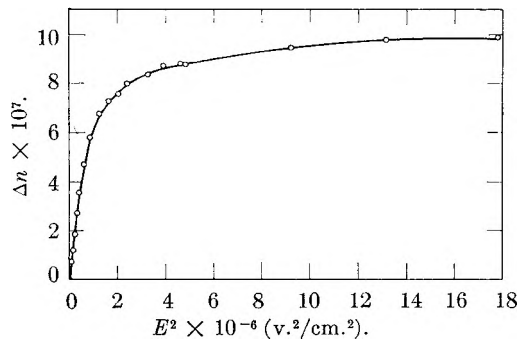


Fig. 5.—$\Delta n$ *vs.* $E^2$ for an aqueous solution of TMV at 0.049 g./l.

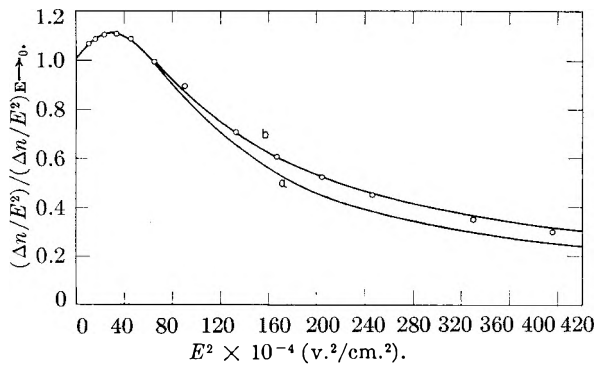


Fig. 6.—$(\Delta n/E^2)/(\Delta n/E^2)_{E\to 0}$ *vs.* $E^2$ for the TMV solution: circles, experimental values; curve a, theoretical curve for $\sqrt{c} = 27 \times 10^{-4}$ volt$^{-1}$ cm.; curve b, theoretical curve for $\sqrt{c_1} = 27 \times 10^{-4}$ volt$^{-1}$ cm., $\sqrt{c_2} = 14 \times 10^{-4}$ volt$^{-1}$ cm., $\phi_1 = 0.65$, $\phi_2 = 0.35$.

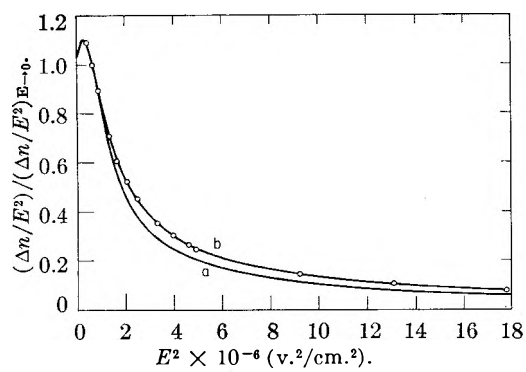


Fig. 7.—The same as Fig. 6 except that the range of field strength is wider.

where $\phi_i$ is the volume fraction of component i in the pure macromolecular phase. In the limit of infinitely high field $\Phi(\beta_i,\gamma_i)$ will tend to 1. Therefore, eq. 43 will reduce to

$$\frac{\Delta n}{\Delta n_0} = \frac{\sum_i \phi_i (g_1 - g_2)_i e^{-6\Theta_i t}}{\sum_i \phi_i (g_1 - g_2)_i} \qquad (44)$$

If the optical factor is the same for each component which is the case when the system is composed of macromolecules differing only in length and the axial ratio of each component is large, one obtains

$$\frac{\Delta n}{\Delta n_0} = \sum_i \phi_i e^{-6\Theta_i t} \qquad (45)$$

That is, the coefficient of the exponential function gives directly the value of volume fraction. Thus, the analysis of birefringence decay from the saturated state will yield the weight distribution of polydisperse systems if the density is constant.

## Experimental

**Materials.**—The sample TMV was a preparation of the common strain of October 1, 1958, contributed by Professor C. A. Knight. The stock solution contained 20 g./l. in distilled water.

The PBLG was a preparation of Dr. E. R. Blout. The weight average molecular weight determined in his laboratory was 195,000. The solvent was dichloroethane.

The sodium polyethylene sulfonate was supplied by Dr. D. S. Breslow of Hercules Powder Company (Preparation No. X9070-56). A fractionation was carried out by fractional precipitation of the polymer from aqueous solution, dioxane being used as a precipitant.[12] Four fractions were obtained from the original sample. Conductivity water was used to dissolve the polymer.

**Apparatus.**—The electric birefringence of the solutions was measured over a wide range of field strength with the pulse technique. Rectangular pulses were generated by the Tektronix Type 161 or 163 pulse generators, amplified by a linear amplifier and a power amplifier, and applied to the liquid in a Kerr cell. The apparatus and procedures for electric birefringence measurements are described elsewhere.[4,6,11,18]

## Results and Discussion

**Tobacco Mosaic Virus.**—The steady-state birefringence $\Delta n$ of the TMV solution, diluted to 0.049 g./l. with distilled water, is plotted against the square of the field strength $E$ in Fig. 5. The temperature was 25.5°. At the highest field strength, 4.2 kv./cm., $\Delta n$ is very close to complete saturation. By extrapolating a plot of $\Delta n/E^2$ *vs.* $E^2$, we obtained $(\Delta n/E^2)_{E\to 0} = 7.2 \times 10^{-13}$ volt$^{-2}$ cm.$^2$ = $6.5 \times 10^{-8}$ e.s.u. Taking the specific volume of TMV as 0.73 cc./g.[19] and expressing the concentration as volume fraction, the specific Kerr constant is

$$K_{sp} = \frac{1}{C_{vn}} \left(\frac{\Delta n}{E^2}\right)_{E\to 0} = 1.36 \times 10^{-3} \text{ e.s.u.}$$

In previous studies,[6] it was shown that the value of the specific Kerr constant depended upon the electrolyte concentration. A monodisperse preparation, in $1.5 \times 10^{-4}$ *M* phosphate buffer at *p*H 7, gave a specific Kerr constant of $8.5 \times 10^{-4}$ e.s.u.; the present higher value can be explained by the fact that the solvent in the present case was distilled water.

Figures 6 and 7 show the experimental data plotted as $(\Delta n/E^2)/(\Delta n/E^2)_{E\to 0}$ *versus* $E^2$. Curve *a* is a theoretical one computed for pure induced dipole orientation ($\sqrt{c} = 27 \times 10^{-4}$ v.$^{-1}$ cm.) because it had been found[6] that the permanent dipole moment contribution was negligible in the case of the common strain of TMV. Experimental points fall on curve *a* only at low field strengths. This and the analysis of the birefringence decay curves showed that this sample of TMV was not monodisperse. The log $\Delta n$ *vs.* $t$ curve was not linear, and the decay was faster, the higher the field strength. As a first approximation we assumed that the TMV was composed of two components and that the optical factor was the same for each component. Then the birefringence will be given by the equation

(18) S. Krause and C. T. O'Konski, *J. Am. Chem. Soc.*, **81**, 5082 (1959).

(19) M. A. Lauffer, *ibid.*, **66**, 1188 (1944).

$$\frac{1}{C_v}\frac{\Delta n}{n} = \frac{2\pi}{n^2}(g_1 - g_2)\sum_{i=1,2}\phi_i\Phi_\gamma(c_iE^2) \quad (46)$$

instead of eq. 11, where $c_i$ is the value of $(\alpha_1 - \alpha_2)/2kT$ for component i and $C_v$ and $\phi_i$ were defined above. Instead of eq. 26 one obtains

$$\frac{(\Delta n/E^2)}{(\Delta n/E^2)_{E\to 0}} = \frac{15}{2}\frac{\sum_i \phi_i\Phi_\gamma(c_iE^2)}{\sum_i \phi_i c_i E^2} \quad (47)$$

Curve *b* is a theoretical fit obtained with the values $\sqrt{c_1} = 27 \times 10^{-4}$ volt$^{-1}$ cm., $\phi_1 = 0.65$ and $\sqrt{c_2} = 14 \times 10^{-4}$ volt$^{-1}$ cm., $\phi_2 = 0.35$. An analysis of the decay curve at very high field strength showed that $\phi_1$ was about 0.65, and various $c_1$ and $c_2$ were tried. Curve b represents the experimental behavior fairly well. From $c_1$ and $c_2$, $\alpha_1 - \alpha_2$ of components 1 and 2 were calculated to be $5.4 \times 10^{-14}$ cm.$^3$ and $1.4 \times 10^{-14}$ cm.$^3$, respectively.

Extending eq. 20 to a multi-component system in which $b = 0$ (induced moment orientation)

$$K_{sp} = \frac{4\pi(g_1 - g_2)}{15n^2}\sum_i \phi_i c_i \quad (48)$$

From this relation, with the above values of $\phi_i$, $c_i$ and $K_{sp}$, the optical anisotropy, $g_1 - g_2 = 5.9 \times 10^{-3}$. Alternatively, the value of $\Delta n$ may be extrapolated in a $\Delta n$ *vs.* $1/E^2$ plot to $E = \infty$. This gave $\Delta n_s = 1.03 \times 10^{-6}$; inserting this in eq. 15 gave $g_1 - g_2 = 6.1 \times 10^{-3}$. It is evident that if a good fit of the birefringence data is made in the strongly oriented region, the value of $g_1 - g_2$ is relatively independent of the exact choice of $\phi_i$ and $c_i$.

We may now compute the polarizability of the monomeric TMV from the earlier result for the Kerr constant of a monodisperse preparation. Taking $K_{sp} = 8.5 \times 10^{-4}$, $g_1 - g_2 = 6.0 \times 10^{-3}$, we find $\alpha_1 - \alpha_2 = 3.3 \times 10^{-14}$ cm.$^3$ at *p*H 7 in $1.5 \times 10^{-4}$ *M* phosphate buffer. Wippler[20] studied the variations of the intensity of scattered light produced by an electric field and calculated the electrical anisotropy of TMV in distilled water. He reported $(\alpha_1 - \alpha_2)/kT = 1.08$ cm.$^3$/erg. which gives $\alpha_1 - \alpha_2 = 4.4 \times 10^{-14}$ cm.$^3$. This value represents an average over the components of his polydisperse preparation. A curve of $\Delta n$ *vs.* $E^2$ given by Benoit[2] for his TMV preparation exhibits some saturation which enabled us to make the rough estimate $\alpha_1 - \alpha_2 = 3 \times 10^{-14}$ cm.$^3$. All of the values of $\alpha_1 - \alpha_2$ are below the upper limit $\alpha_1 - \alpha_2 = 7 \times 10^{-14}$ cm.$^3$ which would be expected on the basis of a perfectly conducting model[6,21] to represent the contribution of ion atmosphere polarization. The differences easily can be due to polydispersity, and variations of *p*H and conductivity[14] of the preparations.

The value of optical factor calculated earlier[6] from the Peterlin–Stuart equation[10] is $8.9 \times 10^{-3}$ and the experimental value from flow birefringence is $7.5 \times 10^{-3}$ (Donnet[22]). The later flow birefringence value of Rowen and Ginoza[23] appears to be in error.

(20) C. Wippler, *J. chim. phys.*, **53**, 328 (1956).

(21) M. Eigen and G. Schwarz, *Z. physik. Chem.* [*N.F.*], **4**, 380 (1955); *J. Colloid Sci.*, **12**, 181 (1957).

(22) J. B. Donnet, *J. chim. phys.*, **50**, 377 (1953).

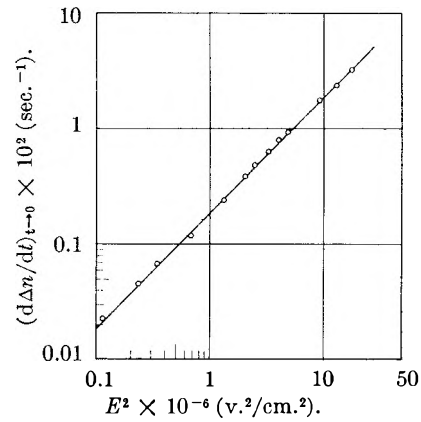


Fig. 8.—$(d\Delta n/dt)_{t\to 0}$ *vs.* $E^2$ for the TMV solution, logarithmic scale.

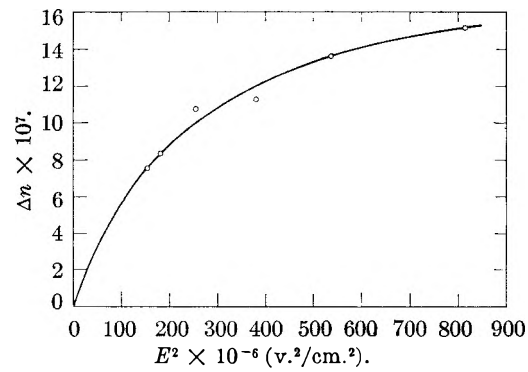


Fig. 9.—$\Delta n$ *vs.* $E^2$ for a dichloroethane solution of PBLG (mol. wt. $1.95 \times 10^5$) at 0.20 g./l.

The initial slopes of the build-up curves $(d\Delta n/dt)_{t\to 0}$ are plotted against $E^2$ in Fig. 8. The data can be correlated by the relation

$$(d\ \Delta n/dt)_{t\to 0} = 1.9 \times 10^{-9}\ E^2$$

where $t$ is in sec. and $E$ in volt/cm. Under the assumption of the same optical anisotropy of various species, eq. 40 may be extended to a multicomponent system

$$(d\ \Delta n/dt)_{t\to 0} = \frac{4}{5}\Delta n_s \cdot \sum_i \phi_i c_i \theta_i \cdot E^2 \quad (49)$$

The rotational diffusion constant of each component was estimated from the decay curve[4] and found to be $2.9 \times 10^2$ sec.$^{-1}$ and $12 \times 10^2$ sec.$^{-1}$. Introducing the values of $\Delta n_s$, $\phi_i$, $c_i$ and $\theta_i$ into the theoretical equation

$$(d\ \Delta n/dt)_{t\to 0} = 1.8 \times 10^{-9} E^2$$

The agreement with the experimental value above is satisfactory.

**Poly-γ-benzyl-L-glutamate.**—Details of the electric birefringence experiments will be described in another paper[11] together with dielectric dispersion measurements. One typical example is analyzed here to illustrate the saturation behavior.

The steady-state birefringence of a dichloroethane solution of a sample of PBLG is plotted against $E^2$ in Fig. 9. The concentration was 0.20 g./l. and the temperature was 28.5°. The solvent contribution was subtracted. It was found that the data could be fitted to a function of the form

(23) J. W. Rowen and W. Ginoza, *Biochim. Biophys. Acta*, **21**, 416 (1956).

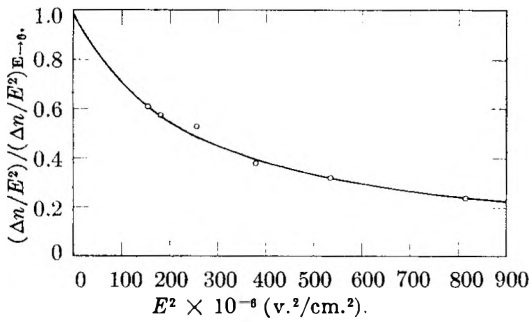


Fig. 10.—$(\Delta n/E^2)/(\Delta n/E^2)_{E\to 0}$ *vs.* $E^2$ for the PBLG solution: circles, experimental values; solid curve, theoretical curve for $b = 2.13 \times 10^{-4}$ volt$^{-1}$ cm.

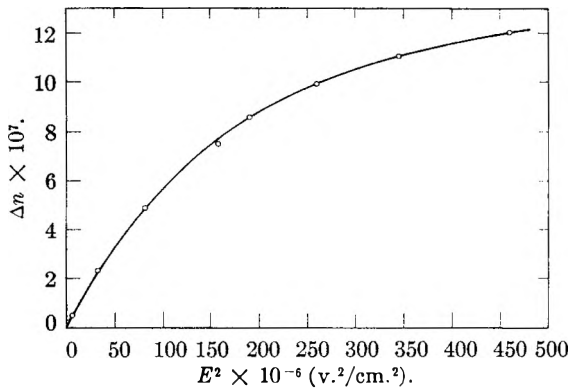


Fig. 11.—$\Delta n$ *vs.* $E^2$ for an aqueous solution of NaPES at 0.14 g./l.

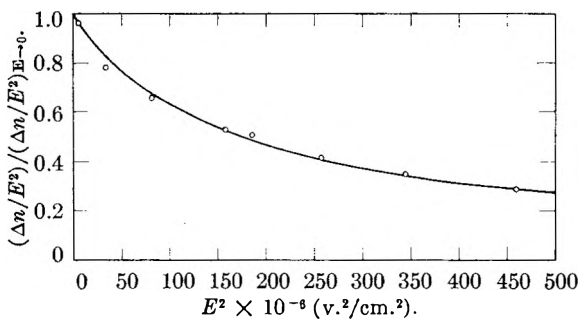


Fig. 12.—$(\Delta n/E^2)/(\Delta n/E^2)_{E\to 0}$ *vs.* $E^2$ for the NaPES solution: circles, experimental values; solid curve, theoretical curve for $b = 2.5 \times 10^{-4}$ volt$^{-1}$ cm.

$$\Delta n = A + B(1/E) + C(1/E)^2$$

at high field strength. This equation has the same form as the theoretical limiting equation in the case of pure permanent dipole orientation, that is, eq. 22. The constants $A$, $B$ and $C$ were determined by the least squares method and the parameters $b$ and $\Delta n_s$ were calculated from them. The values were

$$b = 2.13 \times 10^{-4} \text{ volt}^{-1} \text{ cm.}, \quad \Delta n_s = 26 \times 10^{-7}$$

From these values, taking c = 0 in eq. 19a, $(\Delta n/E^2)_{E\to 0} = 8.0 \times 10^{-15}$ volt$^{-2}$ cm.$^2$. Taking the density of PBLG as 1.32 g./cc.,[24] $K_{sp} = 3.3 \times 10^{-6}$ e.s.u. Figure 10 shows experimental values of $(\Delta n/E^2)/(\Delta n/E^2)_{E\to 0}$ *vs.* $E^2$. The solid curve is a theoretical fit with $b = 2.13 \times 10^{-4}$ volt$^{-1}$ cm.

For long thin particles with dipole moment along the symmetry axis, the internal field function $B_1$ equals unity,[25] irrespective of the dielectric constants inside and outside the rod. Hence, from eq. 19b, $\mu = 2.7 \times 10^3$ debye. The dipole moment estimated from a dielectric dispersion study was 3000 to 4000 d.[11] The optical factor computed from $\Delta n_s$ with eq. 15 was $4.0 \times 10^{-3}$. This is in agreement with the value $4.1 \times 10^{-3}$ obtained from flow birefringence.[26] Employing a value for the specific refractive index increment, the optical anisotropy factor can be estimated from the Peterlin–Stuart equation[10] on the assumption the macromolecule is optically isotropic. In solvents of similar refractive index,[24] $dn/dc$ is 0.12 cc./g. and $g_1 - g_2$ is thus estimated to be $4 \times 10^{-3}$.

The electrical anisotropy factor was estimated from the same equation, employing the known dielectric constant of the solvent (10.4 at 25°) and assuming the dielectric constant of PBLG to be of the order of $n^2$, *i.e.*, 2.5 to 3. This gave $\alpha_1 - \alpha_2 \lesssim 10^{-19}$ cm.$^3$. This corresponds to $b^2/2c \lesssim 10^3$, indicating again that the induced moment contribution is negligible for PBLG.

**Sodium Polyethylene Sulfonate.**—The steady-state birefringence of an aqueous solution of the highest molecular weight fraction of the sodium polyethylene sulfonate is plotted against $E^2$ in Fig. 11. The concentration was 0.14 g./l. and the temperature was 30°. By extrapolation of a $\Delta n/E^2$ *vs.* $E^2$ plot we obtained $(\Delta n/E^2)_{E\to 0} = 9.1 \times 10^{-15}$ volt$^{-2}$ cm.$^2$. Taking the partial specific volume of sodium polyethylene sulfonate as 0.42 cc./g.[27] we obtained the specific Kerr constant, $K_{sp} = 1.0 \times 10^{-5}$ e.s.u.

Figure 12 shows the experimental data plotted as $(\Delta n/E^2)/(\Delta n/E^2)_{E\to 0}$ *versus* $E^2$. The solid curve on the graph represents the theoretical equation for pure permanent dipole orientation with $b = 2.5 \times 10^{-4}$ volt$^{-1}$ cm. The discrepancy between the theory and experiment found in the region of low field strength may be due to the polydispersity of the sample. The dipole moment $\mu$ was calculated from eq. 19b by assuming that the internal field was equal to the external field, that is, $B_1 = 1$. The value thus obtained was $\mu = 3.1 \times 10^3$ d. From eq. 20, and the values of $b$ and $K_{sp}$, with $c = 0$, the optical anisotropy factor was found to be $8 \times 10^{-3}$.

In a more comprehensive study,[12] it has been found that the specific Kerr constant and the dipole moment decreased with increasing NaPES concentration and with increasing concentration of added salts. This behavior resembles other properties of dilute solutions of linear polyelectrolytes such as reduced viscosity and specific dielectric increment.

The occurrence of a saturation behavior most closely resembling pure permanent dipole orientation was not expected, in view of the polyelectrolyte nature of this system and the large electrical polarizabilities associated with other polyelectrolyte macromolecules. There are two mechanisms we are considering to explain the large dipole moment. (a) It may arise from vector addition of monomer permanent moments of the macromole-

(24) P. Doty, J. H. Bradbury and A. M. Holtzer, *J. Am. Chem. Soc.*, **78**, 947 (1956).

(25) J. A. Stratton, "Electromagnetic Theory," McGraw-Hill Book Co., New York, N. Y., 1941, Ch. 3.

(26) P. Doty, unpublished results, see ref. 7.

(27) K. Dialer and R. Kerber, *Makromol. Chem.*, **17**, 56 (1956).

cule in a rather extended configuration, or (b) it may be associated with a statistical displacement of the center of charge from the hydrodynamic center, if the macromolecule can be regarded as a relatively stiff kinked chain.

**Acknowledgments.**—We are pleased to acknowledge financial support of this work by the National Science Foundation. Additional support during the summer of 1958 was provided by the Petroleum Research Fund administered by the American Chemical Society.

## Appendix

TABLE I

$\Phi_\beta$ AND $15\Phi_\beta/\beta^2$ AS FUNCTIONS OF $\beta$

$$\Phi_\beta = 1 - \frac{3}{\beta}\left(\coth\beta - \frac{1}{\beta}\right)$$

| $\beta$ | $\Phi_\beta$ | $15\Phi_\beta/\beta^2$ | $\beta$ | $\Phi_\beta$ | $15\Phi_\beta/\beta^2$ |
|---|---|---|---|---|---|
| 0 | 0 | 1 | 2.0 | .1940 | .7276 |
| .05 | 0.000167 | 0.9998 | 2.2 | .2223 | .6889 |
| .1 | .000661 | .9991 | 2.5 | .2637 | .6329 |
| .2 | .002656 | .9960 | 3.0 | .3284 | .5473 |
| .3 | .005949 | .9915 | 3.5 | .3862 | .4729 |
| .4 | .01051 | .9850 | 4.0 | .4370 | .4097 |
| .5 | .01628 | .9768 | 4.5 | .4813 | .3565 |
| .6 | .02321 | .9669 | 5.0 | .5199 | .3120 |
| .7 | .03121 | .9555 | 5.5 | .5537 | .2746 |
| .8 | .04022 | .9427 | 6.0 | .5833 | .2430 |
| .9 | .05018 | .9292 | 6.5 | .6095 | .2164 |
| 1.0 | .06089 | .9134 | 7.0 | .6327 | .1937 |
| 1.1 | .07237 | .8972 | 7.5 | .6533 | .1742 |
| 1.2 | .08449 | .8801 | 8.0 | .6719 | .1575 |
| 1.3 | .09715 | .8623 | 9.0 | .7037 | .1303 |
| 1.4 | .1103 | .8439 | 10 | .7300 | .1095 |
| 1.5 | .1238 | .8250 | 11 | .7521 | .0932 |
| 1.6 | .1375 | .8058 | 20 | .8575 | .0322 |
| 1.7 | .1515 | .7863 | 50 | .9412 | .00565 |
| 1.8 | .1656 | .7668 | 100 | .9703 | .00146 |
| 1.9 | .1798 | .7472 | $\infty$ | 1 | 0 |

## DISCUSSION

K. E. VAN HOLDE (University of Illinois).—Did you have measurements on the polybenzylglutamate in solvent where you had expected it to be a random coil?

C. T. O'KONSKI.—No. We did not study it in dichloroacetic acid. I think it would be interesting. Dielectric measurements are extremely difficult at low frequencies in the more conducting solvents, because the currents due to electrical conduction at low frequencies become large with respect to the displacement current, and reliable data on dielectric constant frequently are hard to get. We have measured (Orttung and O'Konski, Abstracts of the San Francisco Meeting, 1958) and we plan to report in greater detail dielectric dispersion and electric birefringence measurements on various preparations of PBLG.

UNKNOWN.—Do these three systems extend through the critical degree of polymerization?

C. T. O'KONSKI.—The range of molecular weight we studied is from 84,000 to 350,000. The critical size for the $\alpha$-helix has been shown by Applequist and Doty to be very small, probably too small for convenient measurements. By means of viscosity measurements,[27] the molecular weight of the NaPES fraction studied here was found to be 24,000. Specific conductivities of the TMV and NaPES solutions were $9 \times 10^{-6}$ and $4.8 \times 10^{-5}$ ohm$^{-1}$ cm.$^{-1}$, respectively.

TABLE II

$\Phi_\gamma$ AND $15\Phi_\gamma/2\gamma$ AS FUNCTIONS OF $\sqrt{\gamma}$

$$\Phi_\gamma = \frac{3}{4}\left(\frac{e^\gamma}{\sqrt{\gamma}E(\sqrt{\gamma})} - \frac{1}{\gamma}\right) - \frac{1}{2}$$

| $\sqrt{\gamma}$ | $\Phi_\gamma$ | $15\Phi_\gamma/2\gamma$ | $\sqrt{\gamma}$ | $\Phi_\gamma$ | $15\Phi_\gamma/2\gamma$ |
|---|---|---|---|---|---|
| 0 | 0 | 1 | 2.5 | .7248 | .8697 |
| .1 | 0.00133 | 1.00095 | 2.6 | .7487 | .8306 |
| .2 | .00535 | 1.0038 | 2.7 | .7697 | .7919 |
| .3 | .0121 | 1.0085 | 2.8 | .7882 | .7541 |
| .4 | .0217 | 1.015 | 2.9 | .8046 | .7175 |
| .5 | .0341 | 1.023 | 3.0 | .8190 | .6825 |
| .6 | .0496 | 1.033 | 3.5 | .8710 | .5332 |
| .7 | .0682 | 1.043 | 4.0 | .9027 | .4231 |
| .8 | .0900 | 1.055 | 4.5 | .9238 | .3422 |
| .9 | .1152 | 1.067 | 5.0 | .9387 | .2816 |
| 1.0 | .1438 | 1.0788 | 5.5 | .9495 | .2354 |
| 1.1 | .1759 | 1.0902 | 6.0 | .9577 | .1995 |
| 1.2 | .2113 | 1.1003 | 6.5 | .9641 | .1711 |
| 1.3 | .2497 | 1.1081 | 7.0 | .9691 | .1483 |
| 1.4 | .2909 | 1.1130 | 7.5 | .9731 | .1297 |
| 1.5 | .3342 | 1.1140 | 8.0 | .9764 | .1144 |
| 1.6 | .3791 | 1.1106 | 8.5 | .9791 | .1016 |
| 1.7 | .4247 | 1.1021 | 9.0 | .9814 | .0909 |
| 1.8 | .4701 | 1.0881 | 9.5 | .9833 | .0817 |
| 1.9 | .5144 | 1.0688 | 10 | .9849 | .0739 |
| 2.0 | .5569 | 1.0443 | 11 | .9876 | .0612 |
| 2.1 | .5969 | 1.0152 | 12 | .9896 | .0515 |
| 2.2 | .6339 | 0.9822 | 20 | .9963 | .0187 |
| 2.3 | .6675 | .9464 | $\infty$ | 1 | 0 |
| 2.4 | .6978 | .9086 | | | |

# EFFECT OF PARTIAL COAGULATION UPON THE SIZE DISTRIBUTION CURVE IN HETERODISPERSE COLLOIDAL SYSTEMS

BY WILFRIED HELLER, ENGLEBERT ROWE, ROBERT BERG AND

*Chemistry Department, Wayne State University, Detroit, Michigan*

JOHN H. L. WATSON

*Physics Department, The Edsel B. Ford Institute for Medical Research, Detroit, Michigan*

*Received March 6, 1959*

The size distribution of the unaggregated particles remaining after partial coagulation of a colloidal solution of spheres is found to be altered in favor of the large particles as compared to the distribution in uncoagulated control specimens. The results obtained in a di-disperse latex of polystyrene were quantitatively compared with the ones expected on the basis of Müller's theory. The order of magnitude of the effect observed agrees with that expected from the difference in probability of collisions between unequal sized particles as compared to equal sized particles. The same type of shift is found for a heterodisperse polystyrene latex. All results can be explained satisfactorily without the assumption that the collision number (the "stability") varies with particle size within the colloidal range.

## Introduction

The coagulation of colloidal solutions differs from an ordinary bimolecular reaction by the fact that the reaction product of a successful collision between two particles represents again a reactant: a "secondary particle" formed may again undergo a successful collision with another single or secondary particle to form a still larger unit. Consesequently, an originally monodisperse colloidal system will, during partial coagulation, become polydisperse, and an originally polydisperse system will become still more polydisperse. In the latter instance, the theoretically intriguing and practically significant question arises as to whether or not the unreacted portion of the colloidal solution shows, after partial coagulation, a shift in its distribution curve. No conclusive experimental evidence is available for typical colloidal systems. The present exploratory investigation is concerned with this problem.

## Survey of the Problem

Two factors may determine the size distribution of the unreacted portion of an originally polydisperse system: (1) the relative probability of collisions between particles of unequal size and between particles of equal size; (2) the hypothetical variation, with particle size, of the relative collision number (the average number of collisions necessary in order to obtain one successful collision). The first factor has been treated theoretically by Müller.[1] He arrived at the equation

$$W_2 = \frac{(R + r)^2}{4Rr} W_1 = \gamma W_1 \qquad (1)$$

where $W_1$ is the probability of collision of two equal-sized particles, $W_2$ is the probability of collision of two unequal-sized particles, and $R$ and $r$ are the respective radii in the latter instance. When the radii are not equal, $\gamma$ is seen to be always greater than unity, meaning that collisions between unequal sized particles are more likely than those between equal sized particles. If factor 2 could be neglected, one would therefore expect a shift of the maximum and of the skewness of the size distribution curve in the unreacted portion of a colloidal solution in favor of large particle sizes.

A variation in the collision number with particle size would require that the height of the maximum of the potential energy curve between two colloidal particles varies with their size. No simple answer is possible. Verwey and Overbeek[2] find on the basis of their computations of potential energy curves that "when the particles are small relative to the dimensions of the double layer, stability always increases with increasing particle dimensions." This would work in the same direction as the "Mueller effect" just described. On the other hand, it appears conceivable—as shown by the same authors—that very large particles (diameter $> 1\ \mu$) might give rise to a sufficiently deep potential energy minimum (second minimum) so as to produce a "long range" aggregation. This would produce a result opposite to that due to the Mueller effect, *viz.*, preferential coagulation of large particles.

In the earliest work pertinent to factor 1 Wiegner[3] and Galecki[4] showed that during the progressive coagulation of gold sols, the apparent size of the gold particles visible in the ultramicroscope increased while their number remained fairly constant[5] until it decreased sharply near the end of the coagulation. Wiegner concluded that the large visible particles acted as nuclei for the aggregation of very small particles invisible in the ultramicroscope. This observation is in qualitative agreement with the theory of Mueller developed later. However, the use of the ultramicroscope limits the conclusiveness of the observations very much. For, a constancy in number and an increase in average size of the visible particles would result also if aggregation of ultramicroscopically visible particles were compensated by the growth of originally invisible aggregates to ultramicroscopic dimensions. Later, very extensive investigations by Tuorila,[6] again conducted with the ultramicroscope, showed that the rate of rapid coagulation in polydisperse systems was faster than in monodisperse systems just as predicted by the Müller theory. During the slow coagulation of gold sols,

(1) H. Müller, *Kolloid-Z.*, **38**, 1 (1926).

(2) E. J. W. Verwey and J. Th. G. Overbeek, "Theory of the Stability of Lyophobic Colloids," Elsevier Publishing Co., New York, N. Y., 1948, p. 177.

(3) G. Wiegner, *Kolloid-Z.*, **8**, 227 (1911).

(4) A. Galecki, *Z. anorg. Chem.*, **74**, 174 (1912).

(5) Actually when the electrolyte concentration was low, the number increased slightly at first.

(6) P. Tuorila, *Kolloidchem. Beih.*, **22**, 191 (1926).

on the other hand, Tuorila believed he had found that the particles too small to be visible in the ultramicroscope coagulated more slowly than the larger particles. Particularly noteworthy among the more recent work is that by Figurovskii and Seregin.[7] These authors actually studied the effect of coagulating agents upon the size distribution curves in suspensions as obtained by sedimentation analysis. Some of the results definitely indicate a shift of the distribution curve toward large particles. Unfortunately the systems studied were coarse suspensions with the particle diameter varying between 4 and 10 $\mu$. In addition, it is not certain that the shape of the non-spherical particles, an important factor in the coagulation rates, was a constant.

Factor 2 has, experimentally, found considerable attention particularly during the earlier periods when no theoretical argument of any kind was available as yet as to the possible effect of size on the stability of colloidal solutions. Probably the first investigation of consequence is that by Oden[8] who succeeded in fractionating sulfur sols by a combination of partial coagulation, centrifugation and peptization. On investigating moderately monodisperse sulfur sols thus obtained, he concluded that colloid stability was larger the smaller the particle size.[9] Westgren,[10] on the other hand, found no difference in the stability of monodisperse gold sols whose particle sizes differed by a factor of about two. More recent work also is contradictory. Thiessen, Thater and Kandelaky,[11] and, more recently, Holliday[12] reported a decrease in the stability of gold sols with increasing particle size. Utzino[13] and Monterumici,[14] on the other hand, indicated for Se-sols and polymethyl methacrylate latices, respectively, that larger particle systems are more stable.

In the present investigation—which is merely exploratory in nature—an attempt was made to study the size distribution in the residual sols that remain after a sufficiently slow partial coagulation of di-disperse or hetero-disperse colloidal solutions and to compare it with the distribution prior to coagulation. Electron microscopy was used since it does not have the weakness inherent in ultramicroscopy and, to a lesser extent, in sedimentation analysis, that the smallest particles fail to play a role in the analysis. In addition, systems were selected in which all particles were strictly spherical irrespective of size. This identity of shapes is difficult to control particularly in microscopic suspensions of inorganic materials, but it is important since the rate of coagulation is larger the more particles deviate from spherical shape.

## III. Experimental Procedure

Polystyrene latices obtained from the Dow Chemical Co.[15] (original solids content: 30–40 weight %) were diluted and partially coagulated, primarily by addition of electrolyte. The bulk of the aggregated particles was removed by centrifuging and the size distribution curve of the remaining colloidal solution was obtained by electron microscopy. It was compared with the distribution curve of an aliquot portion of diluted latex to which no electrolyte had been added but which otherwise had been treated in the same manner including centrifugation. Two types of latices were investigated: (1) a "didisperse latex," that is, a latex obtained by mixing two monodisperse latices of which one contained particles 557 m$\mu$ in diameter and the other particles 814 m$\mu$ in diameter; (2) a polydisperse latex which had a continuous size distribution curve, the smallest and largest particle diameter being 30 and 1800 m$\mu$, respectively. All particles were rigid enough to exclude coalescence and to avoid the disturbing effect of flattening out in electron microscopy.

**A. Treatment of Latex Prior to Coagulation.**—Prior to preparing the di-disperse latex, the 557 and 814 m$\mu$ latices were individually diluted with doubly distilled watert o a solids content of 0.0430 and 0.0305 g. per 100 g. latex, respectively.[16] The diluted latices were centrifuged for 15 minutes at 320 *g*. About 90% of the supernatant liquid was removed. Centrifugation and decantation were repeated in a quantitatively identical manner. The finally obtained samples were mixed in a volume proportion of 18.1% small particle latex to 81.9% large particle latex. Thus, the didisperse latex obtained contained practically equal numbers of large and small particles. Its concentration was 0.0327 g. per 100 g. of colloidal solution and the total number of particles per milliliter was $1.65 \times 10^9$. This di-disperse system represented the stock latex for all the respective experiments. It was kept at about 5° for seven days before the first coagulation experiments were started. This guaranteed reestablishment of equilibrium of the stabilizer adsorption.

The polydisperse latex was treated in the same manner except for reducing the total time of centrifugation to 20 minutes. Its final solids content was 0.034 g. per 100 g. of latex. This was the stock latex used for all respective experiments.

**B. Partial Coagulation of the Latex.**—Partial coagulation was brought about by addition of suitable amounts of KCl solution to samples of the stock latices. A concentration of 134 mmoles of KCl per liter of latex was necessary to produce in 6 days, a coagulation of about 90% in the di-disperse latex. The polydisperse latex was more sensitive to electrolyte. It required a concentration of 32.4 mmoles of KCl per liter of latex for a 90% coagulation within 2 days. The KCl concentrations used in the actual experiments were generally smaller. They varied, for the di-disperse system, between 101 and 134 mmoles per liter mixture (latex including added electrolyte solution); and for the heterodisperse system between 1.4 and 13.1 mmoles per liter. In all instances, the degree of coagulation was estimated from the turbidity of the residual sol. Following addition of electrolyte, the respective samples of the didisperse system, kept at room temperature, and those of the heterodisperse system, kept at 25.00°, were allowed to coagulate slowly for at least 2 days, and at the most, 3 months. After the desired degree of coagulation had been reached (minimum, 20%; maximum, 95%), the samples were centrifuged at 245 *g* for 5 or 10 minutes. In the case of the di-disperse system, shaking of the samples for 1 hr., with a frequency of 8.5 sec.$^{-1}$ preceded centrifugation. The residual colloidal solution was decanted and centrifuged again in the same manner. This twofold centrifugation removed practically all the aggregated particles. In addition, a certain fraction of the unaggregated primary particles also settled out. To neglect this fact would have falsified the size distribution curves in favor of the small particles. In order to exclude this possible major source of error, control samples, taken from the stock latices, brought to an identical polymer concentration, and stored and aged identically, were centrifuged simultaneously with the coagulating samples and were decanted identically.

**C. Electron Microscopy and Treatment of Electron Microscopic Data.**—Immediately after centrifugation, electron microscope specimens were prepared from the residual

(7) N. A. Figurovskii and A. V. Seregin, *Kolloid. Zhur.*, **17**, 140 (1955).

(8) S. Oden, *Koll. Z.*, **8**, 186 (1911).

(9) S. Oden, *Z. physik. Chem.*, **78**, 682 (1913).

(10) A. Westgren, *Arkiv. Kemi Mineral. Geol.*, **7**, 6 (1917–1918).

(11) P. A. Thiessen, K. L. Thater and B. Kandelaky, *Z. anorg. allgem. Chem.*, **180**, 11 (1929).

(12) A. K. Holliday, *Trans. Faraday Soc.*, **46**, 447 (1953).

(13) S. Utzino, *Kolloid Z.*, **32**, 149 (1923).

(14) R. Monterumici, *Materie plastiche*, **15**, 129 (1949).

(15) Courtesy of Dr. J. W. Vanderhoff, The Dow Chemical Co., Midland, Mich.

(16) The solids content was determined gravimetrically on aliquot portions of the centrifuged samples by drying specimens of known weight in a vacuum.

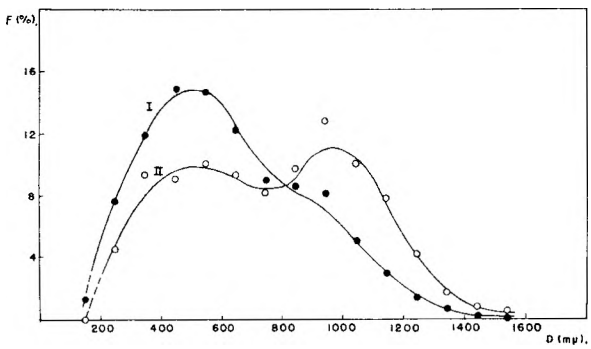


Fig. 1.—Particle size distribution in original polydisperse polystyrene latex (I) and in residual latex (II) remaining after partial coagulation by electrolyte: ●, 2464 particles counted; O, 758 particles counted; $D$ is diameter.

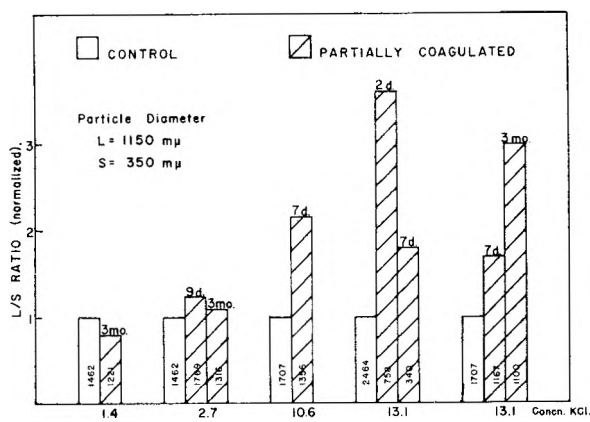


Fig. 2.—Relative frequency of two particle diameters differing by a factor of 3.0, in the original polydisperse polystyrene latex and in the residual latex remaining after partial coagulation. Numbers on top of rectangles, days (d) or months (mo) after addition of electrolyte; numbers within rectangles, numbers of particles considered in analysis of electron micrographs.

colloidal solutions and from the controls using Formvar films as a substrate. The electron micrographs, taken with an RCA electron microscope (model EMU-2B) were projected onto a large screen so as to obtain an over-all magnification of exactly 100,000. In the case of the di-disperse system, analysis was relatively simple because it was sufficient to count the number of large and small particles. A minimum of 670 particles was counted. Extensive tests showed that measurements of the diameter of a minimum of about 1000 particles were desirable in the polydisperse system. Except for two instances of rather highly coagulated samples, this desirable minimum was adhered to.

## Results

**A. Di-disperse System.**—Table I summarizes the results. Column 6 shows that the number ratio of large ($L$) and small ($S$) particles was always larger in the residual sol ($L/S$) than prior to coagulation, $(L/S)_0$. The smallest excess of $(L/S)$ over $(L/S)_0$ was 2%, the largest 36%. This indicates that the coagulum contained always an excess of small particles.

The individual $(L/S)_0$ and $(L/S)$-values, given in columns four and five, are only of secondary interest, but they give an approximate idea on the precision of the results in column 6. $(L/S)_0$ should be expected to be $\leq 1.0$, values $< 1.0$ being likely on account of the partial settling of unaggregated particles during centrifugation. The average $(L/S)_0$-value is 0.97. The only significant deviation in the direction of $(L/S)_0$-values $> 1.0$ is represented by the value of 1.08. The value of 8–10% may therefore be considered as a measure of the over-all uncertainty inherent in the results. The major cause of this uncertainty is the occasional formation of hexagonal patterns, in electron microscopy, of one size group only. A series of special experiments showed that this phenomenon introduced an average uncertainty of 7.5% into the statistical analysis of electronmicroscopic data. (This complication did not arise with the polydisperse systems discussed below.)

TABLE I

EFFECT OF PARTIAL COAGULATION, BY ELECTROLYTE, ON THE SIZE DISTRIBUTION OF PRIMARY PARTICLES IN DI-DISPERSE POLYSTYRENE LATEX

(Diameter of particles: $L$ = 814 mμ; $S$ = 557 mμ) 25°

| Expt. | Mmoles KCl per l. latex | $t^a$ | $(L/S)_0$ | $(L/S)$ | $(L/S)/(L/S)_0$ |
|---|---|---|---|---|---|
| 1 | 101 | 30 | 0.93 (1552)[b] | 1.11 (1355)[b] | 1.19 |
| 2 | 101 | 88 | 1.08 (1448) | 1.26 (927) | 1.16 |
| 3 | 122 | 53 | 1.04 (670) | 1.06 (2095) | 1.02 |
| 4 | 134 | 14 | 0.86 (1353) | 1.17 (1268) | 1.36 |
| 4a | 101 | 14 | 0.86 (1353) | 0.97 (808) | 1.13 |

[a] Days elapsed since addition of electrolyte. [b] Number of particles considered in the analysis.

**B. Polydisperse System.**—Five experimental series were carried out on the effect of partial coagulation on size distribution in the polydisperse latex. In four of the series, the size distribution curve in the residual sols changed decidedly in favor of the large particles. (In the single series which showed the opposite trend, the change was within the range of experimental error.) The most pronounced change found in the distribution curve is illustrated by Figure 1 (KCl, 13.1 mmoles per liter of mixture; status two days after addition of electrolyte). In order to express the results of all series graphically in a simple fashion, an $L/S$ ratio was calculated, representing the number ratio of 1150 mμ diameter particles to 350 mμ diameter particles. The results are thus summarized in Fig. 2, where $(L/S)_0$, after centrifuging, is normalized throughout.

Shaking the electrolyte containing samples prior to centrifuging did not have any clear cut effect.[17] In the two instances investigated, the effect, if any, seemed to be opposite to that produced by electrolyte coagulation alone.

## Discussion

The results obtained on the di-disperse and polydisperse system show that during slow coagulation, by electrolyte addition, the small particles participate preferentially in the process of aggregation. This effect, though modest, is definite. A quantitative comparison between theory and experimental results is possible only for the di-disperse system since eq. 1 applies to such a system. The

(17) It should be noted, however, that shaking in the absence of electrolyte produced no coagulation in these systems.

probability of a large and small particle colliding should be here 4% larger than that for a collision between equal-sized particles. The actually observed values of $(L/S)/(L/S)_0$ (Table I) are of the proper order of magnitude. Since, therefore, the "Müller effect" can account for the effects observed it is unnecessary to assume that the collision-number (stability) of colloidal particles varies, in a given system, with particle size within the limits used in the di-disperse system. Müller's theory being limited to di-disperse systems, no definite quantitative comparison between theory and experiment is possible for the polydisperse system. In a di-disperse system containing particles with a diameter of 30 and 1800 m$\mu$, respectively, in equal numbers, the probability of a small particle colliding with a large particle would be 1750% larger than the probability of collision between equal-sized particles. These are the extreme sizes in the polydisperse system investigated. In a di-disperse system containing particles with a diameter of 350 and 1150 m$\mu$, the result would be 40%. These are the sizes taken as a reference in Fig. 2. In view of the actual presence in the polydisperse system of sizes considerably smaller and somewhat larger, the effect observed for the 2 reference sizes should be within the two limiting values. The maximal effect actually observed (Fig. 2) is 260%. This at least suggests that the Müller effect alone might be sufficient here also to account for the observations.[18]

(18) It should be noted that the actual shift in the size distribution curve in the residual sols of the polydisperse system in favor of the large particles is bound to be slightly larger than that observed. The reason is that a certain portion of small particle aggregates which are formed, although statistically less often, must have remained in the residual sol after centrifugation. This must have altered, to some modest extent, the electron microscopic evidence in favor of the small particles.

# BOUNDARY SPREADING IN SEDIMENTATION VELOCITY EXPERIMENTS. VI. A BETTER METHOD FOR FINDING DISTRIBUTIONS OF SEDIMENTATION COEFFICIENT WHEN THE EFFECTS OF DIFFUSION ARE LARGE

BY ROBERT L. BALDWIN[1,2]

*Contribution from the Chemical Department of the Carlsberg Laboratory and from the Departments of Biochemistry and Dairy and Food Industries, The University of Wisconsin, Madison, Wisconsin*

*Received March 16, 1959*

Three additional procedures for obtaining distributions of sedimentation coefficient by extrapolation to infinite time have been studied theoretically. One of these has marked advantages over methods now in use, if the effects of diffusion are large. This method was used to study the homogeneity of the main peak in the sedimentation patterns of hog thyroglobulin, since an earlier extrapolation procedure was known to exaggerate the estimate of its heterogeneity. Other than a small amount of a faster-sedimenting component, no heterogeneity was found by this method.

## Introduction

The boundary curves observed in sedimentation velocity experiments reflect sensitively the heterogeneity in sedimentation behavior of the material being studied. In favorable cases, one can determine the sample's entire distribution of sedimentation coefficient ($s$). However, the boundary curves are also affected markedly by diffusion and by the dependence of $s$ on concentration.[3] In order to measure the distribution of $s$, extrapolation procedures have been devised for taking into account the effects of diffusion and of concentration dependence. First an "apparent distribution of $s$" ($g^*(S)$) is extrapolated to infinite time to remove the effects of diffusion.[4-6] Next this can be extrapolated to zero concentration[7] or a calculated correction[8] can be made for the effects of concentration dependence. For synthetic polymers[9] or naturally occurring polysaccharides[7,10] the chief problem is to take account of the concentration dependence. For globular proteins the correction for diffusion is equally, or more, important.

In principle[5] one can find a region of time in which $g^*(S)$ is a linear function of $(1/t)$, or a closely related variable.[5] In practice the length of the cell limits $s\omega^2 t$ ($s\omega^2 t < 0.2$) and this linear region is very rarely reached[6] ($\omega$ is angular velocity and $t$ is time). Study of the analytic expression for $g^*(S)$ when $g(s)$ is Gaussian[6] showed that there is an approximately linear region in which useful results can be obtained for many systems. However, in order to use this procedure, the boundary spreading from heterogeneity should be roughly three times that from diffusion, by the end of the experiment. This is rarely the case with globular proteins.

Recently Eriksson[9] introduced some new methods of extrapolation to infinite time. He was studying a synthetic polymer (polymethyl methacrylate) so that the effects of diffusion were relatively moderate; he concluded that the different methods of extrapolation were equally acceptable. When the effects of diffusion are large, different methods of extrapolation should give different results and so the analytical expression[6] for $g^*(S)$ when $g(s)$ is Gaussian was used to study the two methods used by Eriksson[9] and also another method suggested, but not used, by him. This last method was found to have definite advantages when the effects of diffusion are large.

## Theory

We wish to consider the simple case in which the sedimentation coefficients are constant, independent of concentration, all solutes have the same diffusion coefficient ($D$) and the distribution of $s$ is Gaussian.

$$g(s) = \frac{1}{p\sqrt{2\pi}} e^{-(s-\bar{s})^2/2p^2} \qquad (1)$$

Here $p$ is the standard deviation and $\bar{s}$ the mean, of the distribution of $s$.

**The Rectangular Approximation.**—The theoretical basis for the new extrapolation method can be seen most directly in the case of sedimentation in a rectangular cell and constant field (the "rectangular approximation").

$$g^*(S) = \frac{1}{p\sqrt{2\pi}\left(1+\frac{K}{t}\right)^{1/2}} e^{-(S-\bar{s})^2/2p^2\left(1+\frac{K}{t}\right)} \qquad (2)$$

$$K = 2D/p^2\omega^4 r_0^2 \qquad (2a)$$

This equation (with, of course, different notation) was derived by Alberty[11] in his study of boundary spreading in electrophoresis. The apparent distribution is denoted by $g^*(S)$, $S$ being a reduced coördinate with the units of sedimentation coefficient; $t$ is time, $\omega$ is angular velocity, $r_0$ is the distance from the center of rotation to the meniscus and $\omega^2 r_0$ is taken to be the (constant) centrifugal field strength.

One can see that, like $g(s)$, $g^*(S)$ is also Gaussian in form. Comparison with the usual form of the normalized Gaussian function

$$\Phi(x) = \frac{1}{\sqrt{2\pi}} e^{-x^2/2} \qquad (3)$$

shows that, by measuring any property of the

(1) Dept. of Biochemistry, Stanford University, Stanford, California.

(2) John Simon Guggenheim Memorial Fellow, 1958-1959. This research was supported in part by a grant from The National Institutes of Health (RG 4196).

(3) In non-aqueous solvents, dependence of sedimentation coefficients on pressure may also be important.

(4) R. L. Baldwin and J. W. Williams, *J. Am. Chem. Soc.*, **72**, 4325 (1950).

(5) L. J. Gosting, *ibid.*, **74**, 1548 (1952).

(6) R. L. Baldwin, THIS JOURNAL, **58**, 1081 (1954).

(7) J. W. Williams and W. M. Saunders, *ibid.*, **58**, 854 (1954).

(8) R. L. Baldwin, *J. Am. Chem. Soc.*, **76**, 402 (1954).

(9) A. F. V. Eriksson, *Acta Chem. Scand.*, **10**, 360 (1956).

(10) J. Larner, B. R. Ray and H. F. Crandall, *J. Am. Chem. Soc.*, **78**, 5890 (1956).

(11) R. A. Alberty, *J. Am. Chem. Soc.*, **70**, 1675 (1948).

curve which fixes $x^2$, one can find $(S - \bar{s})^2/(1 + \frac{K}{t})p^2$ and for a Gaussian curve there are several quantities which are functions of $x$ only. Eriksson[9] used fixed values of the area under the curve of $g^*(S)$ *vs.* S. Another, and perhaps simpler, method is to use fixed values of $g^*(S)/g^*(S)_{max}$ and to determine the values of S at which these occur.

$$\frac{g^*(S)}{g^*(S)_{max}} = e^{-(S-\bar{s})^2/2p^2\left(1+\frac{K}{t}\right)} = e^{-x^2/2} \quad (4)$$

It follows from equation 4 that

$$(S - \bar{s})^2 = p^2x^2\left(1 + \frac{K}{t}\right) \quad (5)$$

Thus at fixed values of $g^*(S)/g^*(S)_{max}$ the plot of $(S - \bar{s})^2$ *vs.* $1/t$ should be linear and one can use the intercepts at $(1/t) = 0$ to construct the curve of $g(s)$ *vs.* $s$, the actual distribution of $s$. This procedure was suggested, but not used, by Eriksson.[9] Instead he used the graphs of $S/\bar{s}$ and $(S/\bar{s})^2$ *vs.* $1/t$; as equation 5 shows, neither of these is linear.

When the material under study is homogeneous ($p = 0$), equation 2 becomes

$$g^*(S) = \frac{\omega^2 r_0 t}{\sqrt{4\pi Dt}}\, e^{-(S-\bar{s})^2\left(\frac{\omega^4 r_0^2 t}{4D}\right)} \quad (6)$$

and equation 5 becomes

$$(S - \bar{s})^2 = \left(\frac{2x^2D}{\omega^4 r_0^2}\right)\left(\frac{1}{t}\right) \quad (6a)$$

Thus the plot of $(S - \bar{s})^2$ *vs.* $1/t$ is still linear and all lines pass through 0, 0. The extrapolation procedure shows correctly that the material is homogeneous.

**The Actual Sedimentation Case.**—A slightly more complicated expression for $g^*(S)$ is obtained[6] when account is taken of the sector-shaped cell and varying field strength[12]

$$g^*(S) = \frac{e^{-(S-\bar{s})^2/2p^2(1+K/te^{S\omega^2t})}}{p\sqrt{2\pi}\,(1 + K/te^{S\omega^2t})^{1/2}}\left(\frac{3}{2}e^{2b} - \frac{1}{2}e^{3b} + \dots\right) \quad (7)$$

$$b = (\omega^2 t)(S - \bar{s})/(1 + te^{S\omega^2t}/K) \quad (7a)$$

$$K = 2D/p^2\omega^4 r_0^2 \quad (7b)$$

One obtains S and $g^*(S)$ from experimentally measured quantities by the defining relations

$$S \equiv [\ln (r/r_0)]/\omega^2 t \quad (8a)$$

$$g^*(S) \equiv \frac{\partial \tilde{n}}{\partial r}\,\omega^2 t r^3/\tilde{n}^0 r_0^2 \quad (8b)$$

The symbol $\tilde{n}$ refers to the refractive increment, or difference in refractive index between solution and solvent; $\tilde{n}^0$ is the refractive increment of the initial solution. When effects of diffusion and concentration dependence are negligible, equations 8a and 8b give directly the curve of $g(s)$ *vs.* $s$.[13]

In order to find a linear extrapolation from equation 7, one would have to resort to rather complicated variables and this is probably not worthwhile, since the case of a Gaussian $g(s)$ is a special case. However one can infer from equation 7 that the plot, at fixed values of $g^*(S)/g^*(S)_{max}$, of $(S - \bar{s})^2$ *vs.* $1/te^{S\omega^2t}$ should be approximately linear. Some results obtained by this procedure are discussed later on.

(12) This expression is approximate and is intended for use only when $s\omega^2 t < 0.2$. When first printed there was a misprint which is corrected here: $\sqrt{2\pi}$ was written $2\sqrt{\pi}$.

(13) R. Signer and H. Gross, *Helv. Chim. Acta*, **17**, 726 (1934).

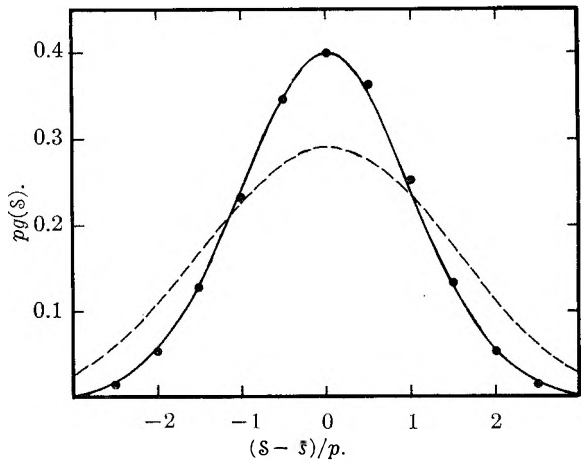


Fig. 1.—Comparison of the known distribution with results obtained by extrapolation to infinite time under extreme conditions. The solid line is the known distribution, discs show results obtained by the new extrapolation procedure and the dashed line shows the result of using the former extrapolation procedure. All values were calculated from the analytic expression for $g^*(S)$ when $g(s)$ is Gaussian (equation 7).

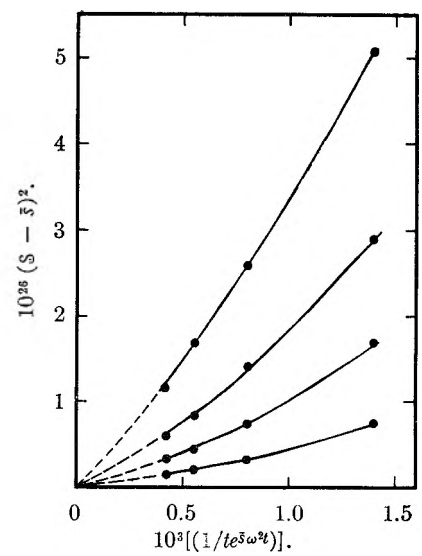


Fig. 2.—Use of the new extrapolation procedure in studying thyroglobulin. The points show $(S - \bar{s})^2$ as a function of $(1/te^{\bar{s}\omega^2 t})$, at fixed values of $g^*(S)/g^*(S)_{max}$ (0.2, 0.4, 0.6, 0.8) on the trailing side of the boundary. The concentration in this experiment was $0.55_3$ g./dl.

## Experimental

Sedimentation studies were made with a Spinco Model E ultracentrifuge, equipped with schlieren optics (a phase-plate schlieren diaphragm), and temperature control (the "RTIC" unit). All experiments were performed at 52,640 r.p.m., within 0.2 of 20°.

The hog thyroglobulin, a gift from J. J. Butzow, was prepared by the method of Derrien, Michel and Roche.[14] It was studied in an ($M$/15) phosphate buffer (0.033 $M$ $KH_2PO_4$, 0.033 $M$ $Na_2HPO_4$) of *p*H $6.8_5$ at 20°.

A comparator with a two-way movement, designed by Dr. M. Ottesen, was used to read the photographic plates. Readings were taken where the concentration gradient is 0.2, 0.4, 0.6, 0.8 and 1.0 times its maximum value. These do not quite coincide with the points where $g^*(S)/g^*(S)_{max}$

(14) Y. Derrien, R. Michel and J. Roche, *Biochim. Biophys. Acta*, **2**, 454 (1948).

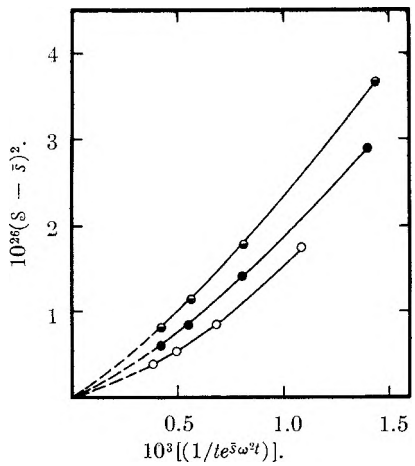


Fig. 3.—The new extrapolation plot at varying concentrations of thyroglobulin: open circles, c = 0.77$_0$ g./dl.; filled circles, $c$ = 0.55$_3$ g./dl.; half-filled circles, $c$ = 0.45$_1$ g./dl. The value of $g^*(S)/g^*(S)_{max}$ is 0.4.

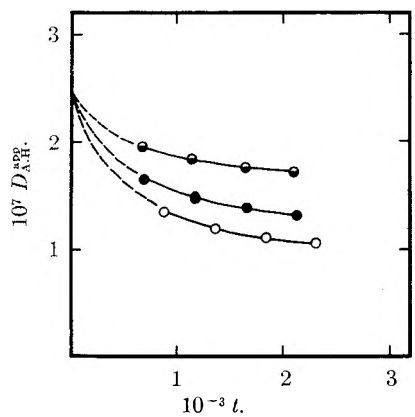


Fig. 4.—The apparent, height-area diffusion coefficients (not corrected for the dependence of $s$ on $c$) from the same three experiments: open circles, $c$ = 0.77$_0$ g./dl.; filled circles, $c$ = 0.55$_3$ g./dl.; half-filled circles, $c$ = 0.45$_1$ g./dl. These results were computed by equation 9.

= 0.2, ..., because of the $r^3$ factor in equation 8b. However they are sufficiently close to allow reliable numerical interpolation in the plot of $(S - \bar{s})^2$ *vs.* log $[g^*(S)/g^*(S)_{max}]$. Reference baselines were obtained in separate experiments, since a double cell was not available.

## Results and Discussion

**Calculations for the Case of a Gaussian $g(s)$.**—The former procedure of extrapolating $g^*(S)$ *vs.* $1/t$ is known[6] to give unsatisfactory results when the ratio of boundary spreading from heterogeneity to that from diffusion is less than about 3 by the end of the experiment. (This ratio is given by $te^{5\omega^2 t}/K$, in the notation of equation 7.) Consequently calculations were made for a case in which this procedure was known to be unsatisfactory: $(te^{5\omega^2 t}/K) = 0.7$ at the end of the experiment. The results are shown in Fig. 1 plotted as a curve of $pg(S)$ *vs.* $(S - \bar{s})/p$.[15] One can see that the results obtained by the new procedure (plotting $(S - \bar{s})^2$ *vs.* $(1/te^{5\omega^2 t})$ at fixed values of $g^*(S)/g^*(S)_{max}$) are much better than those obtained by the former procedure (plotting $g^*(S)$ *vs.* $(1/te^{5\omega^2 t})$ at fixed values of $S$). The graph of $(S - \bar{s})^2$ *vs.* $1/t$ gave less satisfactory results than that of $(S - \bar{s})^2$ *vs.* $(1/te^{5\omega^2 t})$.

The two methods of extrapolation used by Eriksson[9] also were tried: $S$ and $S^2$ were each graphed *vs.* $(1/te^{5\omega^2 t})$ at fixed values of $g^*(S)/g^*(S)_{max}$. Results from these two methods were quite similar; they were slightly better than the results of graphing $g^*(S)$, but not nearly as good as the results of graphing $(S - \bar{s})^2$.

The case of a Gaussian $g(s)$ is, of course, a special case and in general one can expect curvature in the plot of $(S - \bar{s})^2$ *vs.* $(1/te^{5\omega^2 t})$. Even so, the fact that this procedure works so well for the case of a Gaussian $g(s)$ makes it probable that it is more reliable in the general case than is the former procedure, when the effects of diffusion are large.

**Results with Thyroglobulin.**—In the course of some studies[16] on the enzymatic breakdown of thyroglobulin, it was noticed that a curving plot of $g^*(S)$ *vs.* $1/t$ was obtained for the main peak of the thyroglobulin preparation. When this happens, the values of $g(s)$ obtained by extrapolation are likely to exaggerate the heterogeneity of the sample: *cf.* the dashed line of Fig. 1. Consequently thyroglobulin appeared to be a good choice for studying the usefulness of the new extrapolation procedure. Only the main peak was examined; all preparations seem also to contain both faster and slower sedimenting material. Measurements were made at different concentrations in order to investigate the effects of concentration dependence.

The new extrapolation plot, applied to thyroglobulin, is shown in Fig. 2. Two conclusions are evident: the lines are slightly curved and, as far as one can tell, they all pass through the point 0,0. Thus by this procedure the main peak of thyroglobulin does not show measurable heterogeneity. One can see from Fig. 2 that heterogeneity would be detected if the standard deviation of the distribution were 0.4 $S$ or greater. On the leading side of the peak there appears to be 8% of a faster-sedimenting component.[17] Once allowance has been made for this, the results from the leading side of the boundary curve support the same conclusions.

Effects of varying the protein concentration are shown in Fig. 3. Other results, which are not shown, are of this same type. The curves are displaced downwards with increasing concentration, but the curvature is not strikingly different. Again, as far as one can tell, all curves pass through the point 0,0.

There is additional evidence that the new extrapolation procedure is giving a reliable answer. Figure 4 shows the apparent height-area diffusion coefficients, calculated from the equation of Faxén[19]

(15) In the rectangular approximation (see equation 2), the curve of $pg^*(\ )$ *vs.* $(S - \bar{s})/p$ is a function only of $(K/t)$, and so this is a convenient graph with which to represent the behavior of all systems with a Gaussian $g(s)$. In the actual sedimentation case (see equation 7) this curve is chiefly a function of $(K/t)$ but values must be given to other parameters as well. Here $\omega^2 = 4 \times 10^7$ sec.$^{-2}$, $\bar{s} = 4 \times 10^{-13}$ sec.$^{1}$, $r_0 = 6$ cm.$^{1}$, $p = 0.4 \times 10^{-13}$ sec.$^{1}$, and $D = 7.37 \times 10^{-7}$ cm.$^2$ sec.$^{-1}$ A linear extrapolation was made from the values at the two times $0.25 \times 10^4$ and $1.00 \times 10^4$ sec.$^{1}$.

(16) I. J. O'Donnell, R. L. Baldwin and J. W. Williams, *Biochim. Biophys. Acta*, **28**, 294 (1958).

(17) This was found by doubling the area on the trailing side and subtracting this from the total area,[18] after correction for the radial dilution.

(18) R. L. Baldwin, *Biochem. J.*, **65**, 503 (1957).

(19) H. Faxén, *Arkiv. Mat. Astron. Fysik*, **21B**, No. 3 (1929).

which does not take account of the dependence $s$ on $c$.

$$D^{app}_{A/H} = \left(\frac{A}{H}\right)^2\left(\frac{s\omega^2}{2\pi}\right)/[(r_H/r_0)^2 - 1] + \ldots \quad (9)$$

In this equation $r_H$ is the position of the maximum gradient $H$ and $A$ is the area under the boundary gradient curve.[20] At all concentrations studied, the boundary is sharper than expected from diffusion alone; thus any heterogeneity present must be outweighed by effects of concentration dependence. In these circumstances, a procedure for extrapolating the results to infinite time would not be expected to show measurable heterogeneity.

The limitations of this new extrapolation procedure are not yet clearly defined. Even for the case of a Gaussian $g(s)$ with negligible concentration dependence, the plot is not strictly linear; small differences between the known and extrapolated values of $g(s)$ can be discerned in Fig. 1. It is not as sensitive for the detection of heterogeneity as a method[18] based on the use of Fujita's equation[21] for the sedimentation of a solute whose sedimentation coefficient depends linearly on $c$. However, since Fujita's equation was derived for the case of a single solute, it is suitable for detecting but not for measuring heterogeneity. A rather general procedure[22] is available for finding $p$, the standard deviation of the distribution of $s$, when the sedimentation coefficients depend on concentration. However, the equations must be applied to the entire boundary gradient curve, and the method is not useful for studying the homogeneity of one peak when the sedimentation patterns also show minor components. Thus there is a need for the type of extrapolation procedure introduced here, which can give information about the homogeneity of particular components in a sedimentation pattern, when the effects of diffusion are large.

(20) The height of the gradient curve can be left in arbitrary units, since these cancel in the ratio $A/H$, but the abscissa must be in units of cm. in the cell.

(21) H. Fujita, *J. Chem. Phys.*, **24**, 1084 (1956).

(22) R. L. Baldwin, *Biochem. J.*, **65** 490 (1957).

**Acknowledgment.**—During much of this work the author enjoyed the hospitality of the Carlsberg Laboratory for which he would like to thank the Director of the Chemical Department, Professor K. Linderstrøm-Lang.

## DISCUSSION

H. K. SCHACHMAN (University of California at Berkeley).—How does the use of this method compare with that of Fujita's equation for studying the heterogeneity of proteins?

R. L. BALDWIN.—The method based on Fujita's equation is more sensitive, because it makes an explicit correction for the dependence of s on $c$ and because it uses the maximum height of the boundary curve, which can be measured precisely. However the calculations are simpler in the method given here and it can be used to study the homogeneity of the main component when minor components are present, as in this thyroglobin preparation.

H. K. SCHACHMAN.—Can this method be used if there is a large dependence of sedimentation coefficient on concentration?

R. L. BALDWIN.—One has to be able to measure the boundary curves when the concentration is low enough that the sedimentation coefficient is within 10% of its value at infinite dilution. Until the method has been tested more thoroughly one should accept only with caution the demonstration that a particular protein is homogeneous by this approach. If the heterogeneity is slight the efiects of concentration dependence may mask those of heterogeneity at each concentration studied. However, the method should work well when one does find heterogeneity, and the measurements are extrapolated to zero concentration.

RUFUS W. LUMRY (University of Minnesota).—Can one use this approach to study chemically reacting systems?

R. L. BALDWIN.—Yes, the shape of the boundary curve gives information about the reaction as Gilbert has shown for the case of rapid equilibria. Dr. Wake and I are working on this now, from a slightly different point of view.

RUFUS W. LUMRY.—Can one study systems in which the reaction is not rapid?

R. L. BALDWIN.—Except for the case of an isomerization reaction, which has been worked out by Cann, Kirkwood and Brown, the mathematical difficulties are formidable.

# THE SEDIMENTATION VELOCITY OF OSMIUM TETROXIDE IN AQUEOUS SOLUTION

BY K. E. VAN HOLDE

*Department of Chemistry and Chemical Engineering, University of Illinois, Urbana, Ill.*

*Received March 2, 1959*

The sedimentation velocity of osmium tetroxide ($OsO_4$) has been measured at a number of concentrations in aqueous solution. The results indicate that the sedimentation coefficient at infinite dilution is about $0.97 \times 10^{-13}$ sec. and increases slowly with increasing concentration. Use of this value of $s_0$ together with Stokes' law leads to a value for the molecular radius in surprisingly good agreement with that obtained from known molecular dimensions. The implications of this and similar instances of agreement of the sedimentation and diffusion of very small neutral molecules with Stokes' law are discussed briefly.

## Introduction

Sedimentation velocity measurements, while commonly used in the study of macromolecules, have but rarely been carried out with small molecules. There are a number of reasons why such investigations should be of interest. In the first place, many low molecular weight substances can be obtained in a high degree of purity and with accurately known molecular weights. Thus critical tests of the phenomenological equations proposed to relate such transport processes as sedimentation and diffusion should be possible. Also, such data should provide evidence concerning the applicability of hydrodynamic theories such as Stokes' law to molecules whose dimensions are comparable to those of the solvent molecules.

The ideal material for such a study would be readily purified, of accurately known composition, molecular weight and molecular dimensions, soluble in water, but non-ionized. The heteropoly acids which have been investigated in this way by Baker, Lyons and Singer[1,2] satisfy many of these requirements. However, their acidic nature requires that either the ionization be taken into account or that excess salt be added to the system. In the latter case, one is dealing with a three component system, and the questions of possible interaction of flows should be examined.

Osmium tetroxide ($OsO_4$) satisfies all of the requirements mentioned above. Although it is technically an acid, its ionization in aqueous solutions is very slight; the ionization constant ($K_a = 8 \times 10^{-13}$) determined by Yost and White[3] indicates that in a 1% solution the fraction ionized is less than $5 \times 10^{-6}$. While the molecular weight is rather low (254.20), the high density of the solid (4.91 g./ml. at 22°) and the small molecular radius would suggest that the sedimentation coefficient, while not large, should be readily measurable.

This paper describes the determination of the sedimentation coefficient of $OsO_4$ in aqueous solutions at a number of concentrations. Diffusion coefficient and activity coefficient measurements will be described in a later communication.

## Experimental

**Materials and Preparation of Solutions.**—Reagent grade osmium tetroxide was further purified by sublimation *in vacuo* in the presence of calcium chloride. The sample was held at 35–40°, and sublimed onto a surface kept at about 18°. In order to avoid handling large quantities of this very toxic material, small amounts were purified as needed. A sample as obtained melted at 40.50°, the product of a single sublimation at 40.55°, and twice sublimed material also at 40.55°. The latter two values compare favorably with the melting points quoted by Sidgwick[4] (40.6°, 39.5°, 40.6°). Since the second sublimation resulted in no change in melting point, all samples after the first were purified by a single sublimation.

Solutions were prepared using doubly distilled water. The volatility of solid $OsO_4$ makes the accurate preparation of solutions by weight rather difficult, for if the solid is first weighed into a dry flask, saturation of the air in the flask with $OsO_4$ vapor will lead to an appreciable loss of solute, unless most of this $OsO_4$ vapor dissolves in the water which is subsequently added. To avoid this difficulty, the following procedure finally was adopted. The approximate required amount of water was first added to a weighed flask, keeping the neck dry and using a flask of suitable volume to be nearly filled. After the water was weighed, the approximate amount of $OsO_4$ was added and weighed. Additions of $OsO_4$ or water could then be made to yield the desired concentration. All weighings were corrected for air buoyancy.

It was found difficult to store these solutions (even in flasks with glass stoppers greased with fluorocarbon grease) without loss of $OsO_4$. For this reason solutions were always used as soon as possible after preparation.

**Density Measurements.**—The densities of three solutions were measured in duplicate, and a single determination was made with a fourth. All measurements were performed at 25.000 ± 0.002°, using pycnometers fashioned from 25-ml. erlenmeyer flasks. The pycnometer necks were formed from 1 mm. (i.d.) capillary tubing; the cross-sectional area of these necks had been determined by measuring the length of a weighed mercury thread in each. This area together with the height of the meniscus above a reference mark was used in the determination of the solution volume. The pycnometers were calibrated with doubly distilled water, and densities quoted are based upon the assumed density of this water (0.997044 g./cm.$^3$). The results of the density measurements can be expressed by the equation

$$\rho = 0.99704 + 0.00800c \qquad c \leq 4.20$$

where $\rho$ is the density in g./cm.$^3$ and $c$ is the concentration in g./100 cm.$^3$. The above equation represents the data with an average deviation of ±0.003%, which is of the order of magnitude of the reproducibility of duplicate measurements (0.002%).

The solutions used in these measurements were prepared by placing a weighed portion of $OsO_4$ in an empty flask, and then adding water. Hence, it is probable that some loss of $OsO_4$ had occurred. In the unlikely event that all of the $OsO_4$ vapor was lost, the concentrations would average about 1% too high.

**Sedimentation Experiments.**—The sedimentation velocities were determined in a Spinco Model E ultracentrifuge, using a phase plate at the schlieren diaphragm. The tem-

(1) M. C. Baker, P. A. Lyons and S. J. Singer, *J. Am. Chem. Soc.*, **77**, 2011 (1955).

(2) M. C. Baker, P. A. Lyons and S. J. Singer, THIS JOURNAL, **59**, 1074 (1955).

(3) D. M. Yost and R. J. White, *J. Am. Chem. Soc.*, **50**, 81 (1928).

(4) N. V. Sidgwick, "Chemical Elements and Their Compounds," Vol. II, Clarendon Press, 1950, p. 1504.

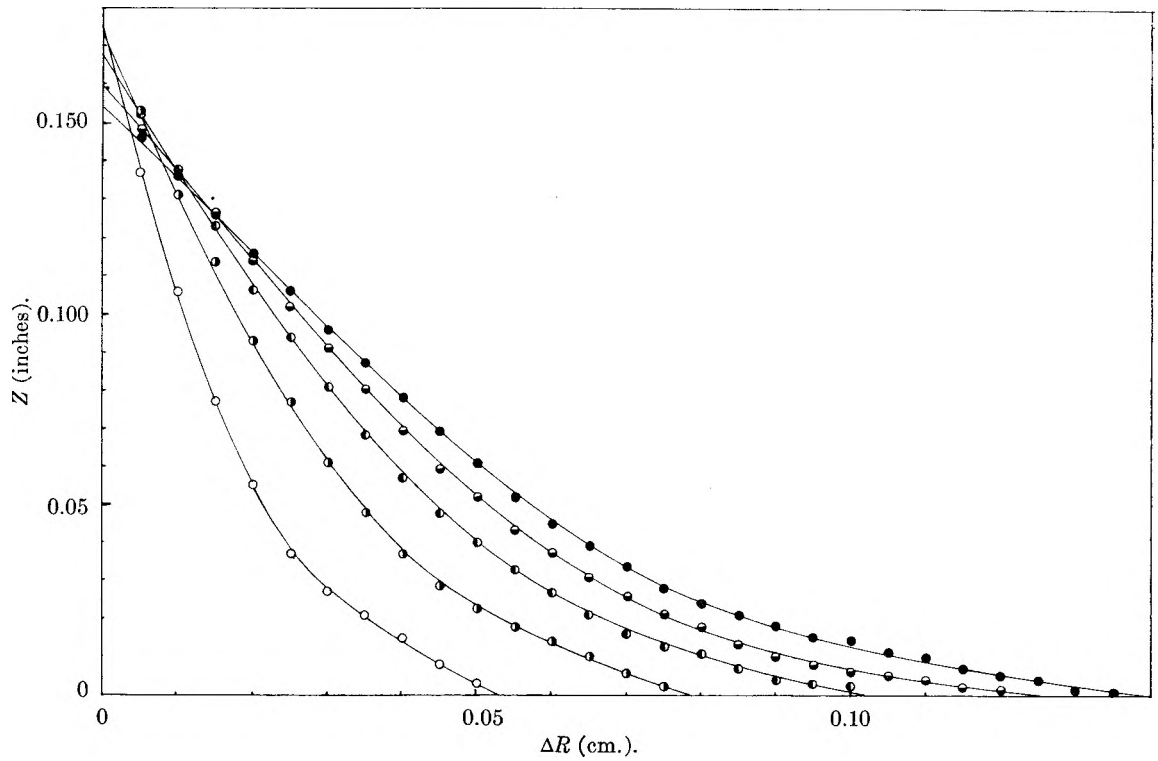


Fig. 1.—$Z$ *vs.* $\Delta R$ curves for the experiment with solution I. The first photograph (○) was taken approximately 2 minutes after the rotor reached full speed. Successive photographs were taken at the following times (taking the time of the first picture as zero): ◑, 360 sec.; ◐, 730 sec.; ◒, 1080 sec.; ●, 1440 sec.

peratures of all experiments were between 24.5 and 25.1°. Results were corrected to 25.0° by means of the relation $s_{25}/s_T = \eta_T/\eta_{25}$. Density corrections were negligible.

Two experiments were required for the determination of the sedimentation coefficient at each concentration: a sedimentation velocity experiment and a synthetic boundary cell experiment. Because of the difficulty in storing solutions, these were always carried out on the same day. The sedimentation velocity experiments were carried out at a rotor speed of about 59,200 r.p.m. (determined for each experiment by the revolution counter) and the synthetic boundary experiments at about 13,400 r.p.m.

In the sedimentation velocity experiments, the correct determination of the solvent base line proved to be of utmost importance. The ideal solution would have been the use of a double sector cell, but the only such cell available had an epoxy-resin centerpiece. It was feared that this material would be attacked by the $OsO_4$ solutions, since $OsO_4$ catalyzes the oxidation of organic materials. For this reason a pair of aluminum centerpiece cells were used, one containing water, the other solution. The base line was thus obtained on the same photograph as the refractive index gradient curve. It was found that this base line was accurately parallel to the gradient curve in the zero gradient region of the cell, and only slightly displaced from it. This displacement could be measured to ±0.001 inch. Since this procedure avoids the problems of the accurate alignment of two separate photographic plates during measurement, it is felt to be superior to the use of separate solution and solvent experiments, though inferior to the use of a double sector cell.

The photographic plates were measured with a two-way comparator. It was found possible to reproduce measurements of the phase boundary image to within ±0.0005 inches on the best plates, and ±0.001 inch on the worst.

## Results

A small molecule like osmium tetroxide has a relatively large diffusion coefficient and small sedimentation coefficient. Consequently a sedimenting boundary will not be formed even at the highest rotor speeds obtainable with the ultracentrifuge used. It has been shown, however, that it is possible to calculate the sedimentation coefficient from the change of the refractive index gradient curve with time. As long as there exists in the cell a point $r_\beta$ where $(\partial c(r_\beta)/\partial r)_t = 0$, we can calculate the sedimentation coefficients from the equation of Baldwin[5]

$$s\omega^2 t = -2.303 \log [1 - Q] \quad (1)$$

$$Q = \frac{\int_{r_a}^{r\beta} (r - r_a)^2 \frac{dc}{dr} dr + 2r_a \int_{r_a}^{r\beta} (r - r_a) \frac{dc}{dr} dr}{c^0 r_a^2} \quad (2)$$

where $r_a$ is the distance of the meniscus from the center of rotation, $c$ is the concentration at the point $r$ and $\omega$ is the angular velocity of the rotor. The integrals can be expressed in terms of the observed deflection $Z$ of the phase boundary image on photographs of the sedimenting solution. If the specific refractive index increment $(\partial n/\partial c)_{T,P}$ is a constant, the integrals in equation 2 become

$$\int_{r_a}^{r\beta} (r - r_a)^2 \frac{dc}{dr} dr = \frac{1}{f^3 \left(\frac{\partial n}{\partial c}\right) Gab \cot \psi} \int_{R_a}^{R\beta} (\Delta R)^2 Z \, dR \quad (3a)$$

$$\int_{r_a}^{r\beta} (r - r_a) \frac{dc}{dr} dr = \frac{1}{f^2 \left(\frac{\partial n}{\partial c}\right) Gab \cot \psi} \int_{R_a}^{R\beta} \Delta R Z \, dR \quad (3b)$$

In these equations $\Delta R = f\Delta r$, where $R$ is the distance along the cell on the photographic plate, and $f$ is the cell magnification factor. $G$ is the cylinder lens magnification factor, $a$ is the cell thickness, $b$

(5) R. L. Baldwin, *Biochem. J.*, **53**, 644 (1953).

the optical lever arm and $\psi$ the phase plate angle. The initial concentration $c^0$ can be expressed in terms of similar measurements of photographs of a boundary obtained in the synthetic boundary cell

$$c^0 = \frac{1}{f\left(\frac{\partial n}{\partial c}\right) Ga'b \cot \psi'} \int_{R_1}^{R_2} Z' \, dR \qquad (4)$$

where $R_1$ and $R_2$ are positions in the zero gradient region on either side of the boundary, and $a'$, $\psi'$ and $Z'$ the values of $a$, $\psi$ and $Z$ for the synthetic boundary experiment. The quantity $Q$ then becomes

$$Q = \frac{\int_{R_a}^{R\beta} (\Delta R)^2 Z \, dR + 2fr_a \int_{R_a}^{R\beta} \Delta R Z \, dR}{f^2(a \cot \psi / a' \cot \psi') \int_{R_1}^{R_2} Z' \, dR} \qquad (5)$$

The integrals are evaluated readily by numerical integration, using 10–20 points and the trapezoidal rule. After $Q$ has been calculated in this way, the sedimentation coefficient can be determined from the slope of a graph of $(-\log [1 - Q])$ *vs.* $t$.

In Fig. 1, the $Z$ *vs.* $\Delta R$ curves for experiment with solution I are shown. Figure 2 represents the $(-\log [1 - Q])$ *vs.* $t$ graph obtained from the data. The time of the first photograph has arbitrarily been taken as zero. The sensitivity of the result to the position of the base line is shown by the dotted line in Fig. 2, which was obtained by arbitrarily moving the base line 0.001 inch in a direction parallel to the meniscus trace. An error of 3% in $s$ results from this. Thus, although it is felt that the base line position could be estimated to within 0.001 inch, this remains the single largest source of error in these experiments. The % error does not increase proportionately at lower concentrations, for it was found that with the higher phase plate angles used at these lower concentrations, the displacement could be measured nearly as well as in the example above.

The area under the synthetic boundary cell curves has been used to replace the quantity $c^0$ in the calculations. This will be strictly justified only if $(\partial n/\partial c)$ is a constant, independent of concentration. In order to test this, three of the synthetic boundary cell experiments were performed immediately after preparation of the solutions. The results of these experiments are summarized in Table I.

TABLE I

TEST OF CONSTANCY OF $(\partial n/\partial c)$

| Soln. | $c^0$ (g./100 cm.$^3$) | $A^a$ | $\psi^b$ | $A/c \times \cot \psi$ |
|---|---|---|---|---|
| IV | 1.464 | 2.543 | 59.7$_0$ | 2.972 |
| V | 3.344 | 4.705 | 64.7$_0$ | 2.976 |
| I | 4.76$_0$ | 5.241 | 69.7$_0$ | 2.977 |
| | | | Av. | 2.975 |

[a] Area under synthetic boundary cell curve in arbitrary units. [b] Corrected for true 90° position of phase plate.

The quantity $A/c \cot \psi$ should be constant if $(\partial n/\partial c)$ is constant. The results indicate that this is so, within experimental error.[6] Solutions II and III were prepared by dilution of solution I. Because of the possibility of evaporation of $OsO_4$ during the handling of the small quantities of solution, the concentrations of these solutions were calculated from the synthetic boundary runs, using the average value of $A/c \cot \psi$.

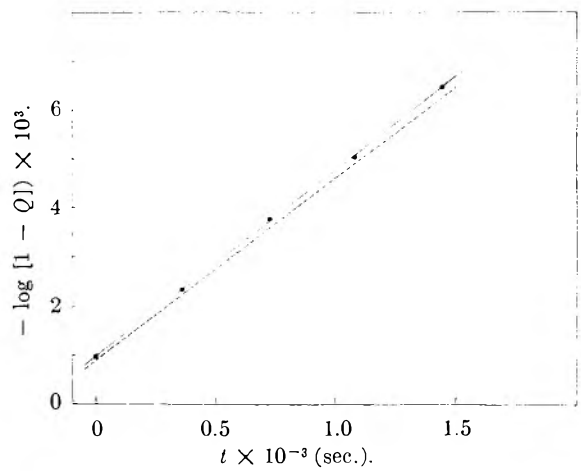


Fig. 2.—The graph of $(-\log [1 - Q])$ *vs.* $t$ for the experiment with solution I. The dotted line indicates the effect of arbitrarily shifting the base lines in the photographs so as to decrease each $Z$ value by 0.001 inch.

The results of the sedimentation experiments are summarized in Table II. A relation between $s$ and $c^0$ was obtained by least squares, using the $s$ values before rounding off to 2 decimals, and weighting the data according to the estimated error.

$$s_{25} \times 10^{13} = 0.97 - 0.041c + 0.017c^2$$

The data fit this equation with a standard deviation of 0.8%. The value of $s_{25,0}$ is thus about $0.97 \times 10^{-13}$ sec. The concentration dependence of $s$ is rather unusual, at least in terms of what has generally been observed with macromolecules, in that $s$ increases with $c^0$ at high concentrations. Preliminary measurements of the diffusion coefficients and activity coefficients of aqueous $OsO_4$ yield results which are consistent with the form of this observed concentration dependence of $s$.

TABLE II

SEDIMENTATION VELOCITY MEASUREMENTS

| Soln. | $c^0$ (g./100 cm.$^3$) | $T$ (°C.) | $sT \times 10^{13}$ (sec.) | $s_{25} \times 10^{13}$ (sec.) |
|---|---|---|---|---|
| IV | 1.464 | 24.5 | 0.95 | 0.96 |
| II | 2.003 | 24.6 | .94 | .94 |
| III | 2.870 | 24.7 | .99 | .99 |
| V | 3.344 | 25.1 | 1.03 | 1.03 |
| I | 4.760 | 24.6 | 1.15 | 1.16 |

The dimensions and shape of the $OsO_4$ molecule are quite accurately known. The oxygen atoms are tetrahedrally placed about the osmium atom; the Os–O bond distance, from electron diffraction measurements[7] is 1.66 Å., which may be taken as a

(6) Another possible source of error is a small "shoulder" sometimes observed near the meniscus at the beginning of a sedimentation velocity experiment (at rotor speed of about 8,000 r.p.m.). This did not appear to be a high molecular weight impurity, since it always flattened out into the base line before full speed was reached. If, however, it was such, the sedimentation coefficients will be in error to the extent that this material was "counted" in the synthetic boundary cell experiment and not in the sedimentation velocity experiment. The area under this "shoulder" was never more than about 3% of the area under the synthetic boundary curve. It seems more likely, from the behavior of this "shoulder," that it arose from a small temperature difference in the solution near the meniscus.

(7) L. O. Brockway, *Rev. Mod. Phys.*, **8**, 260 (1936).

minimum for the "effective" radius of the molecule. Assuming that the radius of the oxygen is 0.55 Å. (that of a doubly-bonded oxygen in organic compounds), we obtain a maximum radius of about 2.2 Å. It is of interest to attempt to calculate this same quantity from the sedimentation data. According to Stokes' law, the sedimentation coefficient of a spherical molecule at infinite dilution will be given by

$$s_0 = \frac{M(1 - \bar{v}_0\rho_0)}{N6\pi\eta_0 R} \qquad (6)$$

where $M$ and $R$ are, respectively, the molecular weight and radius of the solute, $\bar{v}_0$ is the solute partial specific volume at infinite dilution, and $\rho_0$ and $\eta_0$, respectively, the density and viscosity of solvent. The value of $\bar{v}_0$ is 0.201 cm.$^3$/g., according to the density measurements. Inserting the known values in equation 6, we obtain for the radius the value of 2.1 Å.

It is rather surprising to obtain from Stokes' law a result in such good agreement with the theoretical value. Stokes' law is derived for the transport of a spherical particle in a continuous medium, and it is certain that water cannot be considered a continuous medium for a molecule of 2 Å. radius.

Closer examination reveals that the situation is more complex than is indicated above. Stokes' law assumes that the layer of solvent adjacent to a solute molecule moves with it. If this is to be interpreted at all for a real medium, a solvation shell of water molecules is indicated. On the other hand, another form of Stokes' law has been obtained by postulating "slip" of the solvent past the moving particle. In this case, the coefficient 6 in the denominator of equation 6 is replaced by 4. This would lead to a radius for the sedimenting molecule of about 3.2 Å., which again represents the approximate radius of an $OsO_4$ molecule surrounded by a solvation shell of thickness equal to one water molecule. Evidently, the *assumption* of either form of Stokes' law leads to the picture of the sedimenting entity being a solvated $OsO_4$ molecule.

This is not the only case in which the transport of very small molecules has shown surprising agreement with Stokes' law. Baker, Lyons and Singer[1] found this to be true for silicotungstic acid ($R \cong 6$ Å.), and Müller and Stokes[8] for undissociated citric acid ($R = 3.7$ Å.). The suggestion that solvation plays an important role is supported by the observation of Stokes[9] that the "no slip" Stokes' law is fairly well obeyed by a number of substances in aqueous solution, whereas the diffusion of carbon tetrachloride in organic solvents is in better agreement with the theory postulating free slip at the molecular surface.

## DISCUSSION

R. L. BALDWIN (Stanford University).—Would you care to comment on the use of such measurements to test the Svedberg equation at finite concentrations?

K. E. VAN HOLDE.—The equation referred to is

$$\frac{D}{s} = \frac{RT\left(1 + c\frac{\partial \ln y}{\partial c}\right)}{M(1 - v\rho)}$$

which can be obtained for a binary system from the thermodynamics of irreversible processes. We have some of the data to test this equation, namely, $D$ and $s$ as functions of concentration. Activity coefficient data are still needed; I had hoped to obtain these from sedimentation equilibrium measurements, but it turns out that the base-line problems which caused difficulty in the determination of $S$ are even more bothersome here. A double-sector cell is needed.

W. HELLER (Wayne State University).—If the unexpected concentration dependence of the sedimentation coefficient is due to aggregation, this should be checked easily by light scattering, since the specific refractive index increment should be large.

K. E. VAN HOLDE.—I would hesitate to cite specifically aggregation as the cause of this concentration dependence. However, light scattering studies would be informative.

(8) G. T. A. Müller and R. H. Stokes, *Trans. Faraday Soc.*, **53**, 642 (1957).

(9) R. H. Stokes, *Australian J. Sci.*, **19**, 35 (1957).

# ULTRACENTRIFUGE STUDIES WITH RAYLEIGH INTERFERENCE OPTICS. I. GENERAL APPLICATIONS[1,2]

BY E. GLEN RICHARDS[3] AND HOWARD K. SCHACHMAN

*Contribution from the Department of Biochemistry and Virus Laboratory, University of California, Berkeley, California*

*Received June 30, 1959*

As a result of studies of some of the problems inherent in the adaptation of the Rayleigh interferometer to the ultracentrifuge several components of the existing optical system have been modified and procedures have been devised for their precise alignment. Though optical problems still remain, the interferograms possess remarkable clarity; the resolution is comparable to that commonly obtained in diffusion studies. Measurements can be made to ±0.02 fringe, which for a 0.5 g./100 ml. solution corresponds to 0.1% accuracy in the determination of concentration. In a test of the radial dilution equation for sedimentation velocity experiments it was found that a plot of log c *versus* log $x$ gave a straight line with a slope equal to 2.00 ± 0.02. In performing these studies it was necessary to evaluate the equivalent of the second moment of the gradient curve and the Rayleigh system proved more convenient than the schlieren system for such measurements. The interferometer was also employed in determinations of molecular weights by the Archibald method, and it was found that the labor ordinarily involved in the evaluation of the solute concentrations at the ends of the liquid column was virtually eliminated. Examination of several procedures for the evaluation of the concentration gradient from the interferograms showed that differentiation of these patterns leads to certainly no greater precision than that given directly by schlieren optics. As a consequence it seems that molecular weight determinations by the Archibald method are best performed using schlieren optics for the evaluation of the concentration gradient and interference optics for the concentration. Several experimental techniques were used for the analysis of the concentration distribution in sedimentation equilibrium experiments. One of these consists of the location of the zeroth order fringe in the pattern by the addition to the reference liquid of a low molecular weight material which increases the refractive index of the solvent. 1,3-Butanediol serves ideally as such a substance, and no redistribution of it in aqueous solutions was detectable since its density is close to that of water. Sedimentation equilibrium experiments were made on sucrose, raffinose, ribonuclease and β-lactoglobulin. Plots of log c *versus* $x^2$ gave straight lines for the small molecules, whereas the data for the proteins showed an upward curvature indicating heterogeneity of the solute molecules. With sucrose in dilute solutions the molecular weight was in excellent agreement with the known value and the accuracy was about 0.3%; similar results were obtained with raffinose. The results indicate that interference optics should be used in preference to other optical methods when high accuracy is desired. Finally the optical system was used for the development of a technique for comparing directly two similar substances and measuring the small difference in sedimentation coefficients in a single experiment. The theory for this differential method is presented along with experimental data obtained as a test of the method. Although the results are encouraging and the precision is excellent, some aspects of the problem are still unclear and further work is required before the potential of the differential method can be fully assessed.

## Introduction

In view of the progress resulting from the application of interferometric optical methods to the study of diffusion,[4] workers interested in ultracentrifugation have been eagerly awaiting the adaptation of these optical principles to the ultracentrifuge. Two such optical systems, the Jamin and Rayleigh interferometers, have been incorporated in modified form into ultracentrifuges,[5,6] but thus far there have been no detailed investigations as to their utility, accuracy and limitations.

It is of historic interest to record here that Philpot and Cook[7] were concerned principally with the ultracentrifuge at the time they first considered adapting the principles of the Rayleigh interferometer for the construction of a self-plotting optical system. Despite this, the optical method they proposed until very recently found no application in ultracentrifugation; yet during the same time interval it has been used extensively for diffusion and electrophoretic investigations.[8,9]

Although enhanced accuracy has been the goal of many workers who adopted interferometric methods for routine diffusion studies, there is an additional motivation for workers interested in ultracentrifugation. Schlieren optical methods furnish a measure of the total refractive index gradient as a function of distance; and no distinction is made (without recourse to special procedures) between the gradients arising from the sedimentation of the macromolecules, on the one hand, and those stemming, on the other, from the redistribution of buffer salts and the compressibility of the liquid. Also cell distortion at high centrifugal fields is manifested as an apparent refractive index gradient, and the contribution of this to the observed schlieren pattern is not detected readily. With interference methods these latter effects are eliminated directly. Only the residual refractive index gradients arising from the migration (or redistribution) of the principal solute molecules are recorded, and no corrections are necessary. Finally, the interferometric methods reduce substantially the tedious calculations that are required in the translation of the photographic patterns to meaningful data.

This communication presents the results of investigations into some of the problems inherent in adapting the Rayleigh interferometer to the ultracentrifuge. Then we will report on the application of the interferometer for investigations of a variety of ultracentrifugal problems. These studies include (1) location of the second moment of

(1) These studies were aided by a contract between the Office of Naval Research, Department of the Navy, and the University of California, NR-121-175; and by a grant from the National Science Foundation.

(2) Presented at the 33rd National Colloid Symposium, June 18–20, 1959.

(3) Submitted in partial fulfillment of the requirements for the Ph.D. degree in Biochemistry at the University of California.

(4) For review see L. J. Gosting, *Advances in Protein Chem.*, **11**, 429 (1956).

(5) J. W. Beams, N. Snidow, A. Robeson and H. M. Dixon III, *Rev. Sci. Instr.*, **25**, 295 (1954).

(6) Spinco Division, Beckman Instruments, Inc., Tech. Bull. No. 6001-B; see also Technical Manual, Part IX.

(7) J. St. L. Philpot and G. H. Cook, *Research*, **1**, 234 (1948).

(8) L. G. Longsworth, *J. Am. Chem. Soc.*, **74**, 4155 (1952).

(9) L. G. Longsworth, *Anal. Chem.*, **23**, 346 (1951).

boundaries for the measurement of sedimentation coefficients, (2) analysis of radial dilution during sedimentation velocity experiments, (3) evaluation of concentration and concentration gradients for use in the Archibald method for the determination of molecular weights, (4) concentration measurements for the determination of molecular weights by the technique of sedimentation equilibrium, and (5) measurement of small differences in sedimentation coefficients by a differential technique which permits the direct measurement in a single experiment.

## Materials and Methods

Bushy stunt virus (BSV) was used as the sedimenting material in the alignment of the optical system. It was also used in the sedimentation velocity experiments and in the differential sedimentation studies. Tobacco mosaic virus (TMV) also was used in some experiments. The authors are indebted to Drs. C. A. Knight and G. Rushizky for the virus preparations. To decrease the sedimentation rate of the virus, $D_2O$ (99.5% purity) was added in known amount. Sedimentation equilibrium experiments were made with solutions of sucrose (Merck) or raffinose (Pfanstiehl). Equilibrium studies also were made on ribonuclease (Armour, Lot No. 381-059) and $\beta$-lactoglobulin (Armour, Lot No. 128-210).

Sedimentation experiments were conducted in a Spinco Model E ultracentrifuge equipped with a phase plate as the schlieren diaphragm and a rotatable light source for Rayleigh optics. Double sector cells were made of epoxy resin filled with either metal or graphite and the optical path was 12 mm. Some experiments were conducted in 30 mm. cells. To provide additional support for the quartz windows special vinylite gaskets containing a central rib were used in place of the annular gaskets commonly used between the window and its holder. When it was important that the menisci be at the same distance from the axis of rotation two alternative procedures were used: (1) if communication between the two liquids was permissible (as in the alignment of the cylinder lens) a connecting groove was impressed into the partition between the two compartments at a distance just above the cell bottom and (2) when the solutions differed in composition an inert, insoluble liquid (Dow Corning No. 555 silicone fluid,[10] KEL-F No. 1 oil,[11] or fluorochemical FC43[12]) was added to both compartments to a height above the communicating channel; then the solution and solvent were placed in the separate sections of the cell. For certain other experiments requiring reproducible filling of the cell compartments a micrometer syringe was used. Concentrations of solutions were measured directly in fringes through the use of a double sector synthetic boundary cell.[6] A Kodak Wratten filter, No. 77A, was used for the Rayleigh optical system. All measurements of ultracentrifuge patterns were made in a Gaertner two dimensional microcomparator. Bright fringes (constructive interference) were used for all measurements because of the "fogged" background. The procedures suggested by Trautman[13] were employed for reading the plates, and a considerable saving of labor was effected thereby.

In order to permit sufficient diffusion so that the fringes were completely resolved while the boundary was still near the meniscus, the following procedure was used in most of the sedimentation experiments with BSV. First the rotor was accelerated to 14,290 r.p.m. and maintained there for about 5 minutes. This was followed by a deceleration to 5563 r.p.m. at which speed it was maintained for about 60 minutes. Finally the speed was adjusted to and maintained at 14,290 r.p.m. for the duration of the experiment. In the sedimentation equilibrium experiments with proteins a sequence of speeds was used which permitted the establishment of a base line and a more rapid attainment of equilibrium throughout the cell. This will be described in detail in a subsequent publication.

(10) A. Ginsburg, P. Appel and H. K. Schachman, *Arch. Biochem. Biophys.*, **65**, 545 (1956).

(11) K. E. Van Holde and R. L. Baldwin, THIS JOURNAL, **62**, 734 (1958).

(12) D. A. Yphantis, *ibid.*, **63**, 1742 (1959).

(13) R. Trautman, *ibid.*, **60**, 1211 (1956).

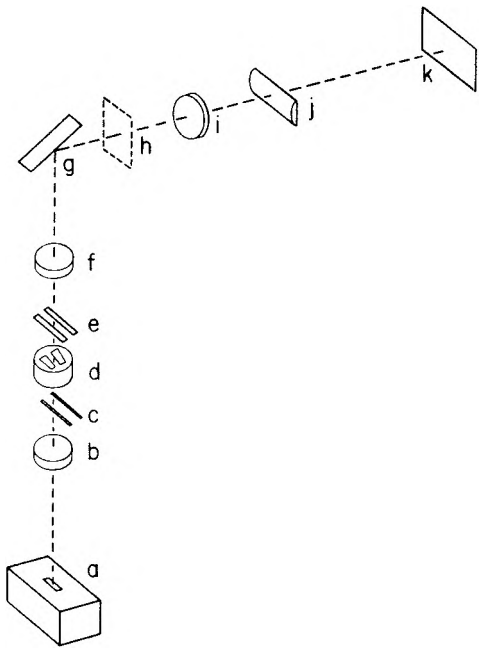


Fig. 1.—Schematic drawing of the Rayleigh interference optical system used in the Spinco ultracentrifuge. This optical system can be used alternately with the schlieren optical system, a few minor changes being required. Light from the mercury arc (a), which is oriented so that the slit is at 90° relative to its normal position for schlieren optics, is filtered (filter not shown) and then rendered parallel by the lower schlieren or collimating lens (b) situated at the base of the vacuum chamber. The parallel light then passes through a pair of fine slits (c) which divide the single beam into two beams, which then traverse the double sector cell (d). The slits at (c) are incorporated into the holder for the lower quartz window, and the whole unit is a special assembly for the interference optical system. The two slits are parallel even though the paths of sedimentation are not. After the light passes through the rotating cell, it enters a pair of wider slits (e) which acts as a diaphragm to limit the angle through which the rotor can turn while conditions for interference are still observed. The light is then focused by the lens (f), which is the upper schlieren or condensing lens. For convenience the mirror (g) is used to bend the light path. The plane (h) is the focal plane of the upper schlieren lens, and it is there that the schlieren diaphragm (phase plate or bar, for example) is located. This schlieren diaphragm can be adjusted so as to avoid the path of light for the interference optical system. The lens (i) is the camera lens which forms an image of the cell on the photographic plate (k), and (j) is the cylinder lens in its normal position and orientation for the schlieren optical system.

## Modification and Alignment of the Rayleigh Optical System

**Description of the Optical System.**—Beams and co-workers[6,14] have employed a modified Jamin interferometer in conjunction with a light chopper for measuring the differences in refractive index between a solution and a solvent as a function of the level in the ultracentrifuge cell. In this instrument the single light beam is split into two parallel beams by the Jamin interferometer plates. Recombination of the two beams is achieved through the use of a second pair of Jamin plates. The beam splitting in the Rayleigh interferometer is effected simply by the insertion of a special mask (the Rayleigh mask) into the optical path. This mask contains two parallel, narrow slits separated by a known distance. The coherent beams of light emerging from these slits interfere constructively and destructively to give an interference pattern consisting of a series of parallel fringes. For the fringes to be straight, the optical paths for the two

(14) J. W. Beams, H. M. Dixon III, A. Robeson and N. Snidow, *ibid.*, **59**, 915 (1955).

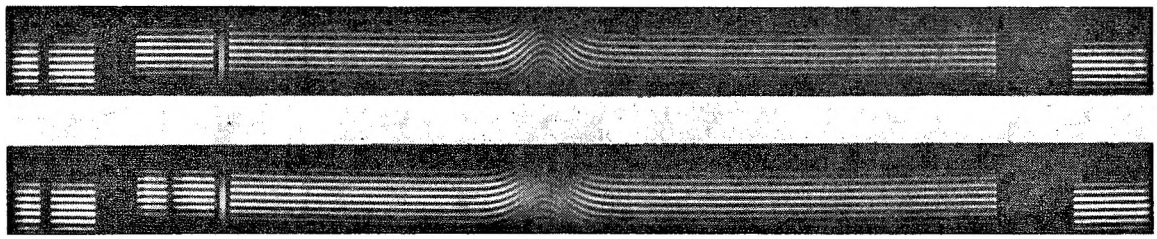

Fig. 2.—Effect of the aperture slit width. For the upper pattern the slit width was 0.75 mm. and for the lower pattern it was 1.58 mm. Both compartments of the cell were filled to different levels in order to produce a differential boundary. The sedimenting material was BSV at a concentration of 0.5 g./100 ml. in 0.1 *M* sodium phosphate buffer, *p*H 6.8.

beams of light must either be equal or differ by a constant amount independent of position in the cell. When there is a concentration gradient (more properly a refractive index gradient) in one of the cells behind the slits in the Rayleigh mask the fringes will be warped in a manner which describes the change in refractive index with distance. The Rayleigh interferometer in its most simple form prevents the utilization of the cylindrical lens schlieren method unless substantial alterations are made each time one or the other optical system is used. But Svensson[15] showed that the cylindrical lens optical system can be used as a Rayleigh interferometer by the simple expedient of changing the slit at the light source from horizontal to vertical, employing monochromatic light and having a double cell with its appropriate mask.

Figure 1 is a schematic diagram of the Rayleigh optical system as used in the ultracentrifuge. Here we will concentrate our discussion on (1) the cell and the Rayleigh mask, (2) the design and accurate positioning of the upper aperture, (3) the positioning and orientation of the light source, and (4) the orientation of the cylindrical lens.

**Orientation of the Cell and the Rayleigh Mask.**—The double sector cell first visualized by workers[7,16] interested in adapting interferometric optical principles to the ultracentrifuge has been used routinely even for schlieren optics.[17,18] In order to adapt it for the Rayleigh system a special mask (the Rayleigh mask) is incorporated into the metal cup (disc holder) for the lower quartz window of the ultracentrifuge cell. This mask contains two parallel slits (0.510 mm. wide) which allow light to pass through only a small segment of each sector of the double cell. It should be noted that neither of these slits is along radii from the axis of rotation. The double sector cell was oriented in the rotor by optical means through the use of the cell aligning tool described by Hersh and Schachman.[19] For the utilization of this tool it is necessary that the sector walls of the centerpiece be visible. Since the light passing through the interference cell is limited by the slits in the lower window holder, the alignment tool must be used in an indirect fashion. The window holders are replaced by special holders so constructed that all four sectorial walls of the centerpiece are visible, and the cell is rotated within the rotor until the walls of the sector openings lie along radii from the center of the rotor. The rotor is then removed from the aligning fixture and the relative positions of the outer scribe lines on the cell and the rotor are carefully noted with the aid of a ten power ocular. When the normal window holders are replaced the cell is aligned correctly and reproducibly by adjusting the scribe lines to the same relative positions (using magnification to position the cell in terms of distinguishing marks within the scribe lines).

**Design and Positioning of Limiting (Upper) Aperture.**—A basic feature of the optical system developed by Beams and co-workers[6] is the light chopper used in conjunction with the interferometer so that the fringes are not obscured due to the movement of the double sector cell past the optical bench. A thin slit is cut into the rotor at a position 90° ahead of the cell. Only when this slit is over the light beam can light pass through the optical system; thus the rotor acts as a light chopper and viewing occurs while the cell turns through an angle of only 0.003 radian. This system is complicated both mechanically and optically but the results reported thus far[14] are very promising. In the instrument used here a simpler arrangement is employed.[6] Above the rotating cell, on the condensing lens at the top of the vacuum chamber, is placed a special mask which acts as an aperture, allowing light to pass through the cell during only a small angle of its rotation. This aperture, like the mask in the cell, is composed of two parallel slits of the same separation as those in the cell. Thus the light rays traversing the double sector cell can form an interference pattern only when the cell is located so that light passes through both sectors simultaneously. To be sure, some light reaches the photographic plate during the rotation of the rotor even while both cells are not in the proper orientation for the conditions of interference. This light creates a background on the photographic plate and the fringe pattern is superimposed on this "fogged" plate. With photographic plates of high contrast this does not cause much difficulty, although the quality of the fringe pattern is not as good as that obtained with stationary cells. As the slits in the upper aperture are narrowed, the fringe pattern for differential sedimentation experiments becomes much more distinct as shown in Fig. 2. Of course an increase in the exposure time is required as the slit width is decreased. For the work reported here the slit width was reduced from 1.58 mm. (in the aperture supplied by the manufacturer) to 0.750 mm. With Kodak Spectroscopic plates, Type II-G, exposures of 5 to 10 seconds were required. Some gain in light intensity was achieved by inserting a metal foil around the water jacket which surrounds the light source. A small gap was left in the foil so that the reflected light passed through the normal single slit used for the schlieren and Rayleigh optical systems. A multiple slit source[20] would likely be an improvement.

There are two alternative arrangements for the upper aperture. On the one hand, the aperture slits can be arranged symmetrically about and parallel to a radius from the center of rotation; on the other hand[6] one of the slits can be directly above a radius from the center of rotation with the second displaced from but still parallel to it. Each of these arrangements possesses certain advantages while at the same time suffering from some limitations. The former, termed here a symmetrical aperture, was used for all of the work unless specified otherwise. For experiments in which there are large refractive index gradients in both compartments of the double sector cell it is preferable since conjugate levels in the cell are being compared. With the second arrangement (the offset aperture) conjugate levels are not compared; here laborious and even uncertain corrections must be applied if buffer salts are redistributed during an experiment. When there are refractive index gradients in only one cell this complication with the offset aperture is avoided, but it should be noted that the images of the reference edges and the menisci are recorded twice on the photographic plate. Moreover, these images appear at different levels thereby making measurements difficult. This disadvantage is even greater when the schlieren system is employed since two overlapping patterns are obtained. When the symmetrical upper aperture is used this difficulty is avoided with both optical systems. The offset aperture has the advantage that distances on the photographic plate are directly proportional to radial distances in the cell for that compartment beneath the radial slit at the time interference conditions are met. With the symmetrical aperture, however, corrections are required since distances on the plate do not correspond simply to radial distances in the cell (it should be noted that the corrections are almost negligible). Moreover, with the offset

(15) H. Svensson, *Acta Chem. Scand.*, **4**, 399 (1950).

(16) J. W. Beams and H. M. Dixon III, *Rev. Sci. Instr.*, **24**, 228 (1953).

(17) L. J. Milch, *Lab. Invest.*, **2**, 441 (1953).

(18) R. Trautman, THIS JOURNAL, **60**, 1211 (1956).

(19) R. T. Hersh and H. K. Schachman, *ibid.*, **62**, 170 (1958).

(20) H. Svensson, *Acta Chem. Scand.*, **5**, 1301 (1951).

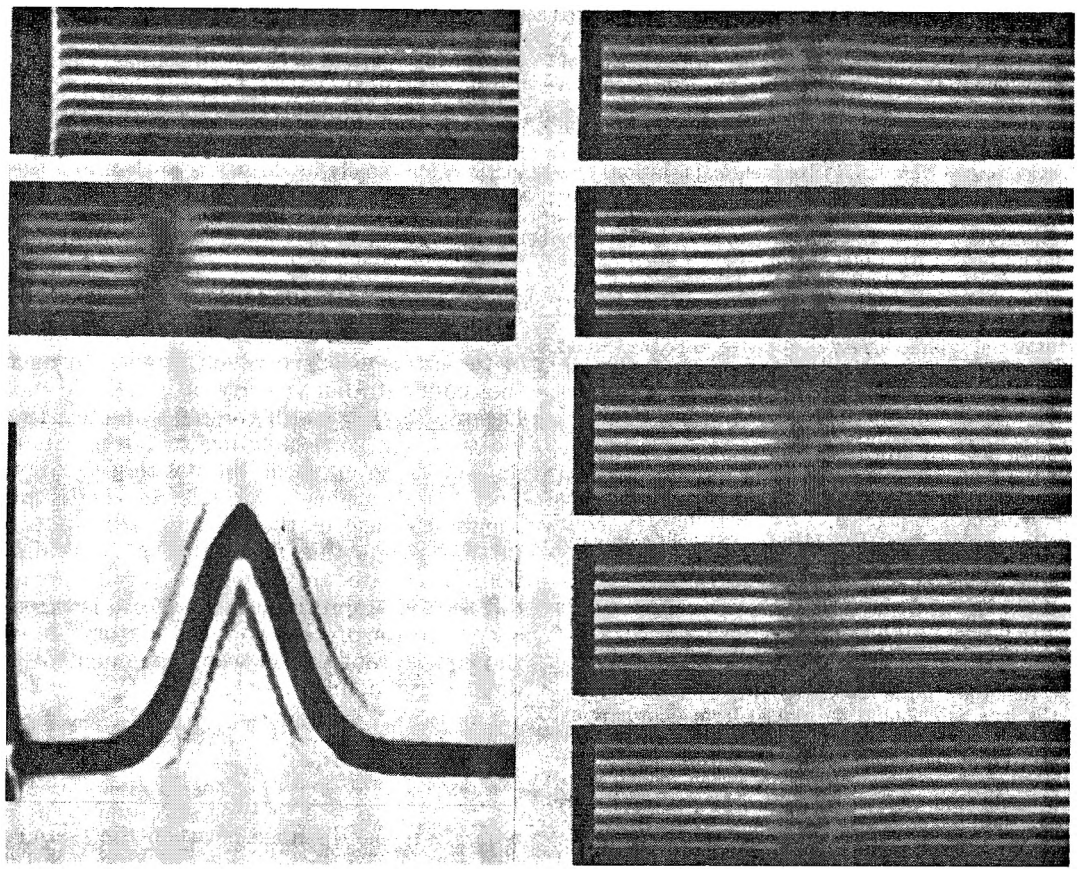

Fig. 3.—Effect of the orientation of the cylinder lens. Both compartments of the cell were filled to the same level with a solution of BSV at a concentration of 0.5 g./100 ml. in 0.1 *M* sodium phosphate buffer at *p*H 6.8. After 4 minutes at 14,290 r.p.m. the rotor was decelerated to 5563 r.p.m. and maintained at that speed for the duration of the experiment. The times corresponding to the pictures are (a), 0 min.; (b), 27 min.; (c)-(h), 50–58 min. Pictures (d)-(h) correspond to different positions of the adjustment screw for the tilt of the cylinder lens, each picture representing a change of $^1/_{20}$ turn of the screw. For (c) the angle of the schlieren diaphragm was set at 80°.

slit aperture and the cell filled correctly[6] the gradients in the solution cell would be parallel to the axis of the cylinder lens. With gradients in the comparison (or reference cell) distortion of the pattern would result as a consequence of lack of orientation of the cylinder lens relative to the refractive index gradient.

Another important factor dictating the offset arrangement of slits is the requirement that the light deviated because of refractive index gradients in the solution (under the radial slit) not be intercepted by the upper aperture. Nor should those light rays suffer any displacement by the cylinder lens due to lack of alignment of the axis of the lens parallel to the refractive index gradient. The difficulties due to the concentration gradients are observed readily with the symmetrical aperture. When two identical solutions are placed in the cell and the speed of the rotor is such that large refractive index gradients are produced, the light beams are deviated so much that they cannot pass through the upper aperture simultaneously. As a result the fringes in the region of the pattern conjugate to the boundaries are blurred. After the gradients are decreased due to diffusion, the fringe pattern becomes distinct. Even at this stage, however, an interesting effect is observed as illustrated by Fig. 3b. Owing to the deviation of light along radii there is an apparent widening in the distance between the slits in the Rayleigh mask. According to the theory for fringe formation an increase in the separation of the slits leads to a crowding together of the Rayleigh fringes. This is shown clearly in Fig. 3b. The central fringe (corresponding to the zeroth fringe since the solutions in the two compartments of the cell are identical) is straight but all of the fringes on either side bend in slightly in the region corresponding to the boundary. That the fringes are straight initially is shown in Fig. 3a, the pattern obtained shortly after the rotor obtained the desired speed. The schlieren pattern in Fig. 3c shows that the boundaries in the two halves of the cell occur at exactly the same position to give the appearance of a pattern obtained in a single sector cell.

In order to position the upper aperture reproducibily several changes were made in the existing arrangement. First, the support fork which holds the rotor before it is coupled to the drive was machined carefully so that its edges were parallel and symmetrically placed about the center of the lens mount. Then a new aperture assembly, machined from solid brass, was made to slide onto the support fork. This assembly could hold various inserts made of brass and constructed in such a way that they could be located precisely. One insert contained the two slits arranged symmetrically, a second had the offset arrangement, and the third had a single, narrow sector shaped slit for use with schlieren optics. Finally, to ensure reproducibility in locating the upper aperture relative to the rotating cell a spacing tool was constructed for locating the fork whenever the condensing lens mount was removed. With this tool in place the screws holding the lens mount are tightened and the fork is thereby centered about the stationary rotor. This operation must be performed each time a new drive is placed in the ultracentrifuge or whenever the condensing lens is removed for cleaning. By this combination of procedures the slits in the upper aperture can be reproducibly and accurately aligned relative to a radius from the center of the rotor.

**Location and Orientation of the Light Source.**—The light source was positioned both horizontally and vertically by a reflection technique similar to the procedure used by Trautman[21] for schlieren optics. After the light source had been rotated through 90° and the slit was narrowed to its limiting position (0.038 mm.) blurred fringes are observed in the telescope assembly. Adjustment of the lateral stop on the light source housing leads to a sharpening of the fringes. Limiting the length of the slit by means of a special mask which pro-

(21) R. Trautman, *Biochim. et Biophys. Acta*, **14**, 26 (1958).

duces a length of 4.8 mm. leads to a sharpening of the pattern in a radial direction.

Orientation of the Cylinder Lens.—Due to the design of the optical system in the ultracentrifuge a mechanical means of orienting the cylinder lens was not feasible. Therefore recourse was made to an optical procedure based upon the rotating cell as a prime reference. Both compartments of the double sector cell were filled with identical solutions of a sedimenting substance. By simple modification of the conventional double cell (impressing a communicating channel into the central rib near the bottom) a U-tube was created so that the liquid flowed from one channel to the other as the rotor was accelerated.[22] As a result the menisci in the two columns were at the same distance from the axis of rotation. After the boundaries had migrated part-way through the cell, the tilt of the cylinder lens was adjusted until the fringes on the photographic plate were straight throughout the cell, as if no concentration gradients were present. For this test it is mandatory that the symmetrical upper aperture be used. A very slight error in the orientation of the cylinder lens produced warped fringes in the boundary region as shown by the sequence of pictures Figs. 3d-3h. Straight fringes are obtained readily as in Fig. 3f if the cylinder lens is oriented with its axis parallel to the aperture slits. Only in this position are conjugate levels in the two cells compared by the interferometer. When the axis of the cylinder lens is tilted slightly a pattern resembling a Gaussian curve is produced as if two identical concentration *versus* distance curves were slightly displaced from each other and one curve was subtracted from the other. In this test, it is important that the light source orientation be altered as the cylinder lens is rotated so that the fringes remain sharp. The final adjustment of the lens axis should be judged from photographs. To facilitate the orientation of the cylinder lens, the mount was altered so that the adjustment was controlled by a calibrated thumbscrew working against a spring loaded stop. With this scale and pointer reproducible positions were readily obtained.

General Remarks.—Considerable simplification of the optical system would be effected by incorporating the Rayleigh mask into the mount for the lower collimating lens. In this manner only a single mask would be required. As in the system described above, the pair of parallel slits could be arranged either symmetrically or one of the pair could be offset and parallel to the conjugate slit which is on a radius. This arrangement would permit a considerable reduction in exposure times since light would reach the photographic plate during the entire movement of the cell across the two light beams. The "fogging" of the plate due to light traversing the cell when interference conditions are not met would be comparable to that observed when an upper aperture is used. This alternative approach was not exploited in the work described here because of our tentative conclusion that distortion of the cell was presently the most serious limitation in the optical system. If the slits are removed from the cell and placed below it on a stationary component of the optical system, the entire cross section of each compartment of the cell would contribute to the Rayleigh pattern and any distortion of the quartz windows would cause deterioration in the quality of the fringes. At high centrifugal fields the distortion is so great, at present, that the beams from the two compartments in the cell (even with an incorporated Rayleigh mask) do not unite sufficiently to give a resolvable fringe pattern. This is particularly noticeable near the cell bottom where the pressure may be several hundred atmospheres. Preliminary experiments with sapphire windows have indicated that the cell assembly need not be a deterrent to good interference optics; excellent fringe patterns were obtained even at 60,000 r.p.m. with a filled cell. When these windows become available for routine work the arrangement with the Rayleigh mask on the collimating lens may prove to be the method of choice.

As yet, no facilities have been devised for incorporating a compensating cell into the optical path in the manner suggested by Beams, *et al.*[5] Thus the observation of a white light fringe is not feasible unless the concentration of the sedimenting material is very low. This difficulty was circumvented in many of our experiments by the addition to the reference liquid of a substance which increases the refractive index of the solvent to a value essentially equal to that of the solution. By this means a white light fringe is detected and photographed with ease. Moreover the quality of the whole fringe pattern is enhanced considerably through the use of fringes of low order. For this purpose we have found 1,3-butanediol (Eastman Organic Chemicals) to be almost ideal. It is readily available in pure form, it is soluble in water, its refractive index increment is neither too high nor too low, and finally its density is so close to that of dilute buffer solutions that no redistribution of it has been detected. Although this device works well for many types of experiments, the development of a holder for a compensating cell would be of value.

(22) The double sector synthetic boundary cell supplied by the manufacturer could be used for this purpose.[6]

## Measurement of Boundary Position

Goldberg[23] has shown that it is the second moment of the gradient curve which provides a measure of the sedimentation velocity of individual molecules. Despite this, it is still common practice to use the location, $x_H$, corresponding to the maximum ordinate of the gradient as the position of a boundary. For homogeneous materials of high molecular weight the use of the maximum ordinate can be justified; but this procedure is not valid if the boundaries are unsymmetrical or if spreading by diffusion is appreciable. Hence it is often necessary (and for precise work mandatory) to evaluate the square root of the second moment of the gradient curve defined as

$$\bar{x}^2 = \frac{\int_{x_m}^{x_p} x^2(\partial c/\partial x)\,dx}{\int_{x_m}^{x_p} (\partial c/\partial x)\,dx} \qquad (1)$$

where $\bar{x}$ is the distance between the boundary and the center of rotation, $x$ and $(\partial c/\partial x)$ are the distance and the concentration gradient and the subscripts, m and p, correspond to the meniscus and a surface in the plateau region. Equation 1 is written in a form suitable for application to schlieren optics, but the reading of the plates and the subsequent calculations are very laborious. With interference optics which give $c$ as a function of $x$ the evaluation of the patterns is less tedious; $\bar{x}$ can be written in the alternative form

$$\bar{x}^2 = \frac{\int_{x_m}^{x_p} x^2\,dc}{\int_{x_m}^{x_p} dc} \qquad (1a)$$

Since each fringe traversed in crossing the boundary from solvent to solution presents a constant increment in concentration, the integral in the numerator of eq. 1a is evaluated as $\Delta c \sum_i x_i^2$ while that in the denominator becomes the total number of fringes across the boundary at some specific time.

Typical Rayleigh patterns from a sedimentation velocity experiment with BSV are shown in Fig. 4. Also included is one schlieren pattern obtained shortly after the last fringe pattern was recorded. Evaluating the positions of the fringes and calculating $\bar{x}$ according to eq. 1a require substantially less time than the comparable procedures when only schlieren patterns are available. Moreover, there is less subjectivity in reading the interference patterns than in the measurement of the net refractive index gradients from the schlieren patterns. Table I summarizes the data from an experiment with BSV. Although the agreement

(23) R. J. Goldberg, THIS JOURNAL, **57**, 194 (1953).

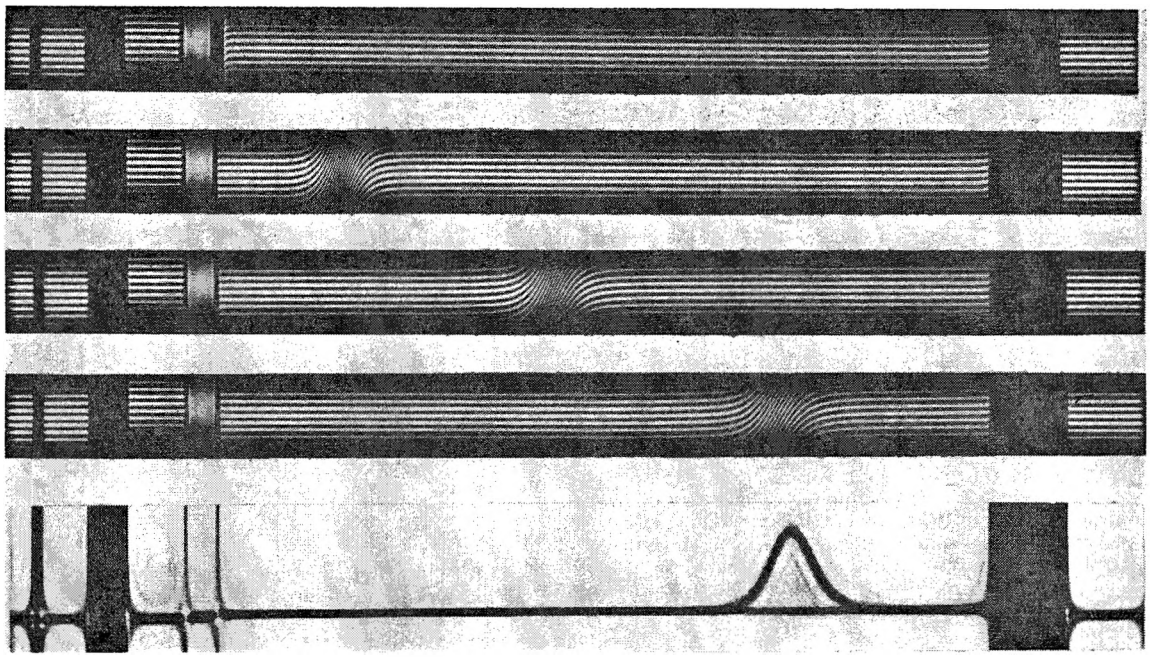

Fig. 4.—Interference patterns from a sedimentation velocity experiment. The sedimenting material was BSV at a concentration of 0.5 g./100 ml. in a solvent containing 0.1 *M* potassium chloride and 0.01 sodium acetate at *p*H 4.1. The reference liquid contained sufficient 1,3-butanediol to give a refractive index intermediate between those of the solvent and the solution. The pictures from top to bottom correspond to 0, 64, 96, 128 and 130 min. For the bottom picture the schlieren diaphragm was set at an angle of 80°.

among the three procedures is excellent in this case, other experiments with TMV showed that $x_H$ is not a satisfactory measure of the boundary position and that the Rayleigh patterns are to be preferred over schlieren patterns for the accurate evaluation of $\bar{x}$ when the boundaries are sharp and not symmetrical.

TABLE I

MEASUREMENT OF BOUNDARY POSITION[a]

| *t* min. | $\bar{x}_H$ schlieren, cm. | $\bar{x}$ schlieren, cm. | $\bar{x}$ interference,[b] cm. |
|---|---|---|---|
| 62 | 6.101 | 6.103 | 6.102 |
| 82 | 6.312 | 6.313 | 6.313 |
| 98 | 6.486 | 6.487 | 6.486 |
| 114 | 6.665 | 6.667 | 6.666 |
| 130 | 6 851 | 6 853 | 6 851 |

[a] The sedimenting material was BSV at 0.5 g./100 ml. in a solution containing 0.1 *M* potassium chloride and 0.01 *M* sodium acetate at *p*H 4.1. The speed of the rotor was 14,290 r.p.m. [b] Actually the Rayleigh patterns were obtained at slightly different times from the schlieren photographs. Therefore the values recorded here were evaluated by interpolation of data derived at other times. The reference liquid contained 1,3-butanediol.

Even if a complete boundary is not formed because of the low sedimentation rate and high diffusion coefficient of the solute molecules, the Rayleigh patterns should prove ideal for the measurement of sedimentation coefficients. In that case eq. 1 takes the form

$$\bar{x}^2 = \frac{c_m x_m^2 + \int_{x_m}^{x_p} x^2\,dc}{\int_{x_m}^{x_p} dc} \qquad (1b)$$

Calculations according to eq. 1b' require knowledge of $c_m$, the concentration at the meniscus. The evaluation of this will be discussed in a subsequent section.

### Radial Dilution During Sedimentation

Owing to the sector shape of ultracentrifuge cells and the radial inhomogeneity of the centrifugal field, there is a progressive dilution of the contents of the cell during a sedimentation velocity experiment. The description of this phenomenon was given first by Svedberg and Rinde[24] in the form of an equation relating the concentration in the plateau region as a function of the boundary position. Since then Trautman and Schumaker[25] treated this problem in a more general way arriving at the same conclusion, *viz.*

$$\frac{c_t}{c_0} = \frac{x_m^2}{\bar{x}_t^2} \qquad (2)$$

where $c_0$ is the initial concentration and $c_t$ and $\bar{x}_t$ are the concentration in the plateau region and the boundary position at time *t*. With ultracentrifuge cells of present design the maximum dilution of the cell contents is only about 30%. Thus a critical test of the validity of eq. 2 is dependent on the existence of techniques with which concentrations can be measured with great accuracy. Although studies by a variety of workers using different materials have given results in accord with eq. 2 the concentration data were probably accurate to only ±2%. To be sure greater precision is now possible through the introduction of the phase plate as the schlieren diaphragm, but it seems likely that no technique can rival interferometric methods for this purpose. Accordingly a series of individual experiments like

(24) T. Svedberg and H. Rinde, *J. Am. Chem. Soc.*, **46**, 2677 (1924).

(25) R. Trautman and V. N. Schumaker, *J. Chem. Phys.*, **22**, 551 (1954).

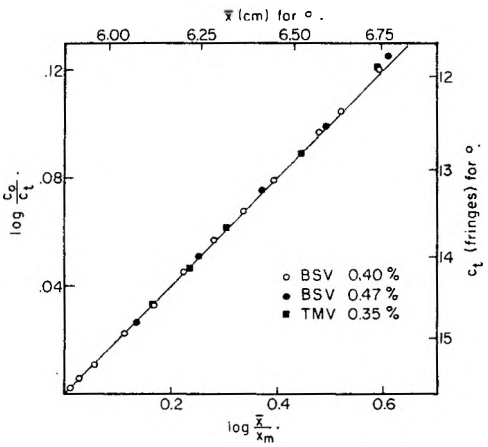


Fig. 5.—Test of the radial dilution equation: (○) BSV at 0.40 g./100 ml. in 0.1 *M* sodium phosphate buffer, *p*H 6.8; ● BSV at 0.47 g./100 ml. in 0.2 *M* potassium chloride, 0.01 *M* potassium phosphate buffer, *p*H 6.7. The offset aperture is used for this experiment. ■ TMV at 0.35 g./100 ml. in 0.01 *M* sodium phosphate buffer, *p*H 6.8. The speed of the rotor was 9,945 r.p.m.

that illustrated by Fig. 4 were analyzed in terms of the concentration changes during the experiment.

Figure 5 presents the results of three separate experiments. In order that all of the data can be represented by a single plot the ordinate is given as log $(c_0/c_t)$ and the abscissa as log $(\bar{x}_t/x_m)$. The least squares line through the data has a slope of 2.00 ± 0.02. Thus the agreement with theory is excellent. It should be noted that the concentrations were relatively low; moreover the boundary of TMV was noticeably skewed and the position of the maximum ordinate of the gradient curve was much greater than that evaluated from the fringe patterns according to eq. 1a. In most of these experiments there were about 15 fringes across the boundary and their number is estimated readily to ±0.02 fringe. Thus high accuracy is obtained merely by counting the number of fringes.

The radial dilution equation was tested in another way and the details are presented in Table II. Columns 1 and 2 record the time after attaining the desired speed and the position of the boundary. Column 3 gives the direct count of fringes across the boundary ($c_t$) and column 4 gives the change in concentration ($\Delta c_t$) in the plateau region as measured by the lateral shift in fringes in the plateau region.[26] The sum of the values in columns 3 and 4 is remarkably constant as shown in column 5. Since a slight change in concentration had occurred before the first pattern was obtained the values in column 5 were corrected to give the initial concentration $c_0$ shown in column 6. In making this correction a factor was included to account for the sedimentation occurring during the acceleration of the rotor. Finally $c_0$ is calculated (column 7) by means of eq. 2. The agreement is excellent; moreover these results show that dilution in the plateau region is measured easily from the lateral movement of the fringes across the pattern. A comparable measurement with schlieren optics is not possible.

TABLE II

RADIAL DILUTION[a]

| $t$, min. | $x_H$, cm. | $ct$ fringes | $\Delta ct$ fringes | $ct + \Delta ct$ fringes | $c_0$ fringes | $ct(\bar{x}_t/x_m)^2$ fringes |
|---|---|---|---|---|---|---|
| 2 | 5.905 | 15.63 | ... | 15.63 | 15.73 | 15.73 |
| 4 | 5.924 | 15.51 | 0.11 | 15.62 | 15.72 | 15.71 |
| 8 | 5.962 | 15.35 | 0.28 | 15.63 | 15.73 | 15.75 |
| 16 | 6.039 | 14.94 | 0.70 | 15.64 | 15.74 | 15.73 |
| 24 | 6.118 | 14.58 | 1.04 | 15.62 | 15.72 | 15.76 |
| 32 | 6.198 | 14.17 | 1.46 | 15.63 | 15.73 | 15.71 |
| 40 | 6.278 | 13.80 | 1.82 | 15.62 | 15.72 | 15.70 |
| 48 | 6.360 | 13.46 | 2.17 | 15.63 | 15.73 | 15.72 |
| 56 | 6.442 | 13.11 | 2.50 | 15.61 | 15.71 | 15.71 |
| 68 | 6.569 | 12.58 | 3.04 | 15.62 | 15.72 | 15.67 |
| 74 | 6.633 | 12.36 | 3.27 | 15.63 | 15.73 | 15.70 |
| 84 | 6.741 | 11.92 | 3.72 | 15.64 | 15.74 | 15.64 |

[a] The sedimenting material was BSV at a concentration of 0.4 g./100 ml. in 0.1 *M* phosphate buffer at *p*H 6.8. The speed was 14,290 r.p.m. The reference liquid contained 1,3-butanediol.

### The Archibald Method

The determination of molecular weights by the Archibald method[10, 27–29] is dependent on knowledge of both the concentration gradient and the concentration at the upper and lower surfaces of the liquid column. Although the gradient of concentration with distance can, in principle, be measured directly and rapidly through the use of schlieren optics, the evaluation of the concentrations from the schlieren patterns is tedious and time consuming. With interference optics the converse is true. Concentrations can be determined merely by a counting procedure. No integration is required. But the evaluation of the concentration gradient from the interferograms requires a laborious differentiation procedure. Nonetheless, in view of the sensitivity and accuracy of the Rayleigh system as compared to schlieren optics it is profitable to consider the evaluation of $\partial c/\partial x$ by differentiating the data derived from the interferograms. Certain aspects of these problems have been considered by Mommaerts and Aldrich[30] in studies of the molecular weight of myosin. However, no mention was made in their work of the optical problems discussed above nor were any photographs presented. Our procedures and conclusions as to the use of interference optics for the Archibald method differ markedly from those of Mommaerts and Aldrich.[30]

Following the practice initiated by Klainer and Kegeles[28] most workers now use a synthetic boundary cell as a refractometer for the evaluation of the initial concentration $c_0$ of the solution. With the Rayleigh system a double sector synthetic boundary cell[6] is required and patterns like that

(26) It should be noted that there was a slight slope of the fringes on the centrifugal side of the boundary, as if the sample contained some aggregated material; consequently all measurements were made at a level just above the bottom of the cell. Some experiments were conducted in an effort to detect the influence of convection caused by sedimentation against the wall of the cell, but these studies were inconclusive.

(27) W. J. Archibald, THIS JOURNAL, **51**, 1204 (1947).

(28) S. M. Klainer and G. Kegeles, *ibid.*, **59**, 952 (1955).

(29) H. K. Schachman, "Methods in Enzymology," Ed. S. P. Colowick and N. O. Kaplan, Vol. 4, Academic Press, New York, N. Y., 1957, p. 32.

(30) W. F. H. M. Mommaerts and B. B. Aldrich, *Biochim. et Biophys. Acta*, **28**, 627 (1958).

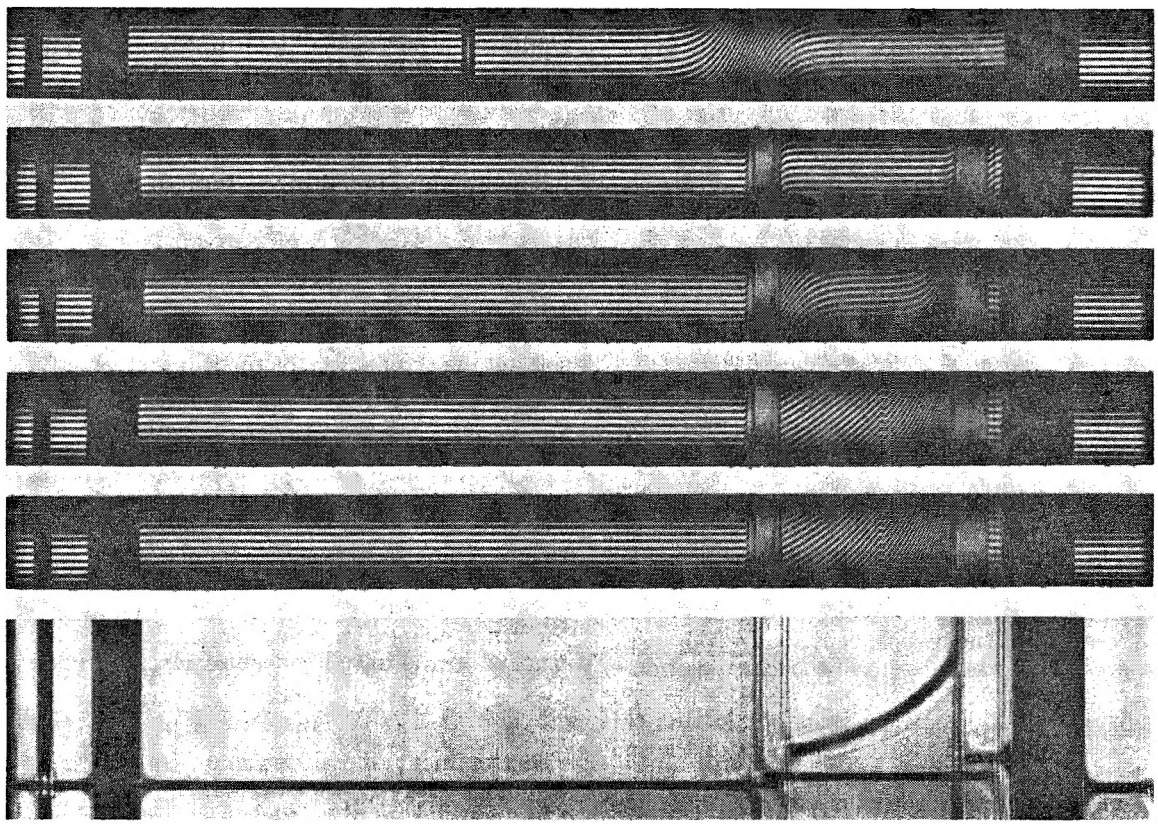

Fig. 6.—Interference patterns obtained from a combined Archibald and equilibrium experiment. One compartment contained ribonuclease at 0.5 g./100 ml. in 0.2 *M* potassium chloride and 0.01 *M* potassium phosphate, *p*H 6.8. The other contained solvent to which was added sufficient 1,3-butanediol to raise its refractive index to that of the solution. Kel-F No. 1 oil was added to both compartments. The first picture was taken from the companion experiment in which the synthetic boundary cell was used to determine $c_0$. The remaining pictures were taken from the equilibrium experiment and correspond to 20,410 r.p.m., 0 min.; 29,500 r.p.m., 15 min.; and 20,410 r.p.m., 84 and 496 min. The offset aperture was used for this experiment.

in Fig. 6a are obtained. A count of the number of fringes across the boundary gives $c_0$ (in fringes) with an accuracy of about 0.1%. The value of $c_0$ then is used with other data for the determination of the concentrations at the meniscus $c_m$ and bottom of the solution $c_b$ in the experiment for the molecular weight determination. With schlieren optics different procedures are available for the calculation of $c_m$ and $c_b$ (see 31 for a summary), but common to all of them is an integration procedure. In one method the radial dilution in the plateau region must be evaluated either by a correction involving the sedimentation coefficient or by a careful experiment with a synthetic boundary cell.[32] Alternatively, expressions can be used which implicitly account for the effect. The Rayleigh system affords the simplest and most direct means for evaluating $c_m$ and $c_b$. Mere counting of the fringes from the plateau region to either the meniscus or the bottom of the liquid column (in patterns like those of Fig. 6c) gives $c_m$ and $c_b$ in terms of the concentration in the plateau region, $c_p$. Since dilution in the plateau region is accompanied by the lateral movement of the fringes across the pattern (see Table II) the difference between $c_p$ and $c_0$ is given directly. Hence, $c_m$ and $c_b$ are evaluated accurately in three steps, each of which is simply and rapidly performed.

Two alternatives are available for the evaluation of the concentration gradients, $(\partial c/\partial x)_m$ and $(\partial c/\partial x)_b$. They can be obtained directly, albeit with some subjectivity, by the use of schlieren optics; or the interferograms can be differentiated, as done by Mommaerts and Aldrich.[30] Our own experience with several graphical differentiation procedures indicates that $\partial c/\partial x$ can be obtained from the Rayleigh system with certainly no greater precision than that afforded directly by the schlieren system. Since the labor involved in converting the interferograms into data of $\partial c/\partial x$ *versus* $x$ is so excessive, this procedure has little to recommend it. If reliable data for $\partial c/\partial x$ close to the upper and lower surfaces could be obtained from the interference patterns the extra labor would be worthwhile. At present, this does not appear to be the case.

Consequently, it appears preferable to utilize schlieren and interference optics in conjunction with each other for molecular weight determinations by the Archibald method. This has been done in experiments with both ribonuclease (Fig. 6) and β-lactoglobulin. Some typical data for the latter protein are presented in Table III. For this experiment the ultracentrifuge was operated at a relatively high speed so that the refractive index gradient curve at the meniscus became almost hori-

(31) H. K. Schachman, "Ultracentrifugation in Biochemistry," Academic Press, New York, N. Y., 1959, pp. 182-194.

(32) A. Ehrenberg, *Acta Chem. Scand.*, **11**, 1257 (1957).

TABLE III

MOLECULAR WEIGHT OF β-LACTOGLOBULIN BY THE ARCHIBALD METHOD[a]

| $t$, min. | Molecular weight: Schlieren and interference[b] × $10^{-4}$ | Interference: Method 1[c] × $10^{-4}$ | Interference: Method 2[d] × $10^{-4}$ |
|---|---|---|---|
| 6 | 3.40 | ... | ... |
| 14 | 3.45 | 3.41 | 3.59 |
| 25[e] | 3.55 | 3.46 | 3.59 |
| 32 | 3.52 | 3.38 | 3.69 |

[a] β-lactoglobulin at 0.5 g./100 ml. in 0.2 $M$ sodium chloride, 0.02 $M$ sodium acetate, $p$H 5.2; rotor velocity, 31,410 r.p.m.; temperature 23.5°. [b] Corresponding interference and schlieren pictures were taken 1 minute apart; therefore values of $c_m$ corresponding to the times for the schlieren pictures were obtained by graphical interpolation. [c] These values were obtained from the extrapolation to the meniscus of a plot of $(\Delta c/\Delta x)/cx$ *versus* $x$, where $\Delta x$ is the separation between successive fringes. The values for $c$ and $x$ correspond to the mid-point of the increment. [d] These values were obtained from $(\Delta c/\Delta x_{ext})/c_m x_m$. The value for $\Delta x_{ext}$ was obtained from the extrapolation to the meniscus of a plot of the fringe separation $\Delta x$ *versus* the position of the mid-point of the increment. [e] At this time the gradient curve at the meniscus was nearly horizontal.

zontal early in the experiment.[32] In this way, some of the hazards inherent in the extrapolation of the gradient curve to the level of the meniscus were avoided. Molecular weights obtained in this way correspond to the weight average of the material present there when the pattern was photographed. When the rotor is operated at high speeds, the data at the bottom of the solution are unreliable. It should be noted that the optical constants for the schlieren system must be related to those for the interference system. This is achieved readily in an experiment with a synthetic boundary cell by measuring the area under the curve produced by the schlieren system and comparing it with the number of fringes given by the Rayleigh pattern. Column 2 in Table III gives the molecular weights obtained from a combination of the schlieren and interference data while columns 3 and 4 give the results of molecular weight determinations involving alternative procedures for differentiating the interferograms.

Since data at the bottom of the column are valuable for investigations of the homogeneity of the sedimenting substance, low speed operation is frequently desirable. However, the errors in evaluating $\partial c/\partial x$ at both ends of the liquid column in such experiments are of the order of 3 to 5%. In an effort to reduce this source of error, experiments are now in progress in which the rotor is first overspeeded for a brief period and then decelerated to a lower operating speed. The adjustment of the concentration gradients at the ends of the column is extremely rapid and accurate measurements of $\partial c/\partial x$ and c may be feasible.

## Sedimentation Equilibrium

Despite the long standing and sound theoretical foundation of the sedimentation equilibrium method, it has been used relatively infrequently as a technique for the study of large and small molecules. The last few years, however, have witnessed a renewed interest in the method along with vigorous activity both on theoretical and experimental lines.[10,11,33-36] With the adaptation of interference optics the use of the sedimentation equilibrium method is likely to become even more widespread.[37,38]

For an ideal solution containing two components the molecular weight $M$ can be obtained from the slope of the plot of ln $c$ *versus* $x^2$ according to the following equation derived both from thermodynamics and from a kinetic treatment[39]

$$M = \frac{2RT}{(1 - \bar{V}\rho)\omega^2} \frac{\mathrm{d} \ln c}{\mathrm{d}x^2} \qquad (3)$$

In eq. 3, $R$ is the gas constant, $T$ is the absolute temperature, $\bar{V}$ is the partial specific volume of the solute, $\rho$ is the density of the solution, $\omega$ is the angular velocity in radians/sec. and $c$ is the concentration at different distances, $x$, from the axis of rotation. Plots which are concave upward indicate polydispersity while downward curvature is an indication of the non-ideality of the solution. There is still another equation for the molecular weight which is well suited for use with interferometric data. Lansing and Kraemer[40,41] showed that the molecular weight can be evaluated from the total change in concentration across the cell relative to the initial concentration according to

$$M = \frac{2RT}{(1 - \bar{V}\rho)\omega^2(x_b^2 - x_m^2)} \frac{c_b - c_m}{c_0} \qquad (4)$$

The treatment of Lansing and Kraemer has been extended recently by Van Holde and Baldwin[11] who considered non-ideal solutions. For these solutions eq. 4 takes the form

$$M = \frac{2RT(1 + c\partial \ln \gamma/\partial c)}{(1 - \bar{V}\rho)\omega^2(x_b^2 - x_m^2)} \frac{c_b - c_m}{c_0} \qquad (4a)$$

where the concentration dependent terms correspond to $(c_b + c_m)/2$.

As a test of the utility and accuracy of interference optics, sedimentation equilibrium experiments were made with sucrose, raffinose and ribonuclease at different concentrations. Typical interferograms are shown in Figs. 6 and 7; also present for comparison is one schlieren pattern from each experiment.

Merely counting the number of fringes between the meniscus and bottom of the solution gives $c_b - c_m$. Combining this with $c_0$ and the other terms in eq. 4 leads to the molecular weights shown in Table IV. Included in the calculations for sucrose was a correction for the non-ideality of the solution made with the data compiled by Gosting and Morris.[42] Although this method of handling

(33) T. F. Young, K. A. Kraus and J. S. Johnson, *J. Chem. Phys.*, **22**, 878 (1954).

(34) J. S. Johnson, K. A. Kraus and G. Scatchard, THIS JOURNAL, **58**, 1034 (1954).

(35) J. S. Johnson, K. A. Kraus and T. F. Young, *J. Am. Chem. Soc.*, **76**, 1436 (1954).

(36) L. Mandelkern, L. C. Williams and S. G. Weissberg, THIS JOURNAL, **61**, 271 (1957).

(37) J. S. Johnson and K. A. Kraus, *J. Am. Chem. Soc.*, **81**, 1569 (1959).

(38) J. S. Johnson, G. Scatchard and K. A. Kraus, THIS JOURNAL, **63**, 787 (1959).

(39) T. Svedberg and K. O. Pedersen, "The Ultracentrifuge," Oxford University Press, London and New York, N. Y., 1940, p. 8-9.

(40) W. D. Lansing and E. O. Kraemer, *J. Am. Chem. Soc.*, **57**, 1369 (1935).

(41) See eq. 239 in Svedberg and Pedersen (ref. 39).

(42) L. J. Gosting and M. S. Morris, *J. Am. Chem. Soc.*, **71**, 1998 (1949).

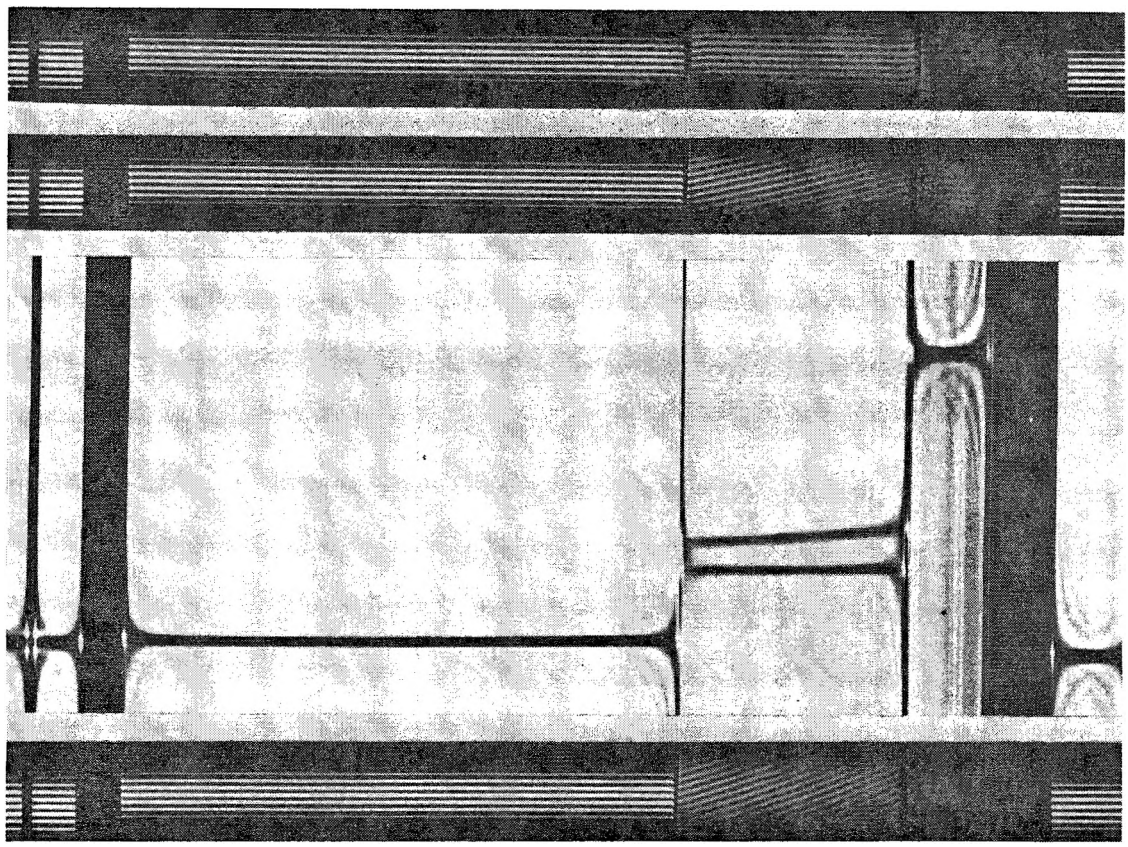

Fig. 7.—Interference patterns from a sedimentation equilibrium experiment. One compartment contained sucrose at 1 g./100 ml. The other contained water with sufficient 1,3-butanediol to elevate the refractive index to that of the solution. Kel-F No. 1 oil was added to both compartments. A channeled centerpiece was used to reduce the possibility of leakage between the two compartments. The upper two patterns correspond to 0 and 256 min. at 42,040 r.p.m. The lower pair correspond to equilibrium at 50,740 r.p.m. The schlieren pattern was obtained with the schlieren diaphragm set at an angle of 70°.

the data is simple it does not exploit all of the information available in the interferograms. For polydisperse systems, eq. 4 gives a weight average molecular weight, which by itself provides no evidence about homogeneity. Moreover, some extrapolation is required to evaluate the fractional fringe between the meniscus and the first observed fringe (a similar extrapolation is needed for the bottom of the column). In order to make use of all of the data, plots of ln $c$ *versus* $x^2$ were constructed (see eq. 3). As seen in Fig. 8 the data fall on a straight line, as expected for a homogeneous material. The variation of the activity coefficient with concentration (in the range involved here) is so slight that downward curvature is not expected. The internal precision of the data is illustrated by the deviation graph[37] in Fig. 8 where $\Delta \log c$ is the difference between the experimental points and the values calculated from the least mean squares straight line.

TABLE IV

MOLECULAR WEIGHT BY SEDIMENTATION EQUILIBRIUM[a]

| Material | Column height, mm. | Molecular weight Eq. 3 | Eq. 4 | Formula |
|---|---|---|---|---|
| Sucrose | 3.7 | 343.4[b] | 341.8[b] | 342.3 |
| | 6.0 | 341.1[b] | 341.6[b] | 342.3 |
| Raffinose | 5.9 | 501.5 | 501.0 | 504.4 |

[a] Concentration of solute, 1 g./100 ml.; rotor velocity, 42,040 r.p.m.; temperature, 25°. [b] These values have been corrected for the non-ideality of the solution.

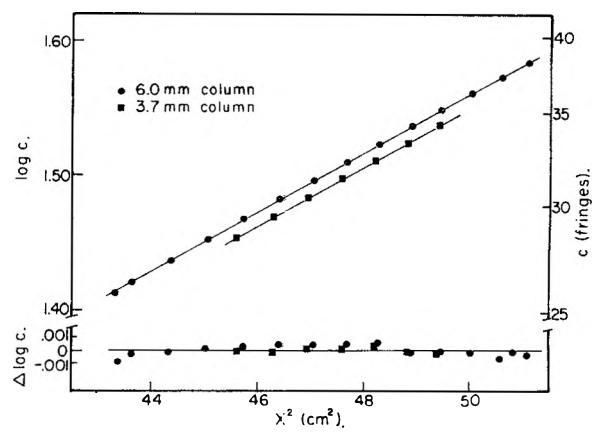


Fig. 8.—Plot of log $c$ *versus* $x^2$ for sedimentation equilibrium experiments with sucrose. The concentration of sucrose was 1 g./100 ml. and the speed of the rotor was 42,040 r.p.m.; ● 6.0 mm. column of solution, ■ 3.7 mm. column of solution. Δ log c is the difference at a given values of $x^2$ between the least mean squares straight line and the experimental points.

Two different procedures were used for the translation of the fringe patterns into data expressing concentration as a function of distance. This cannot be done directly until the concentration corre-

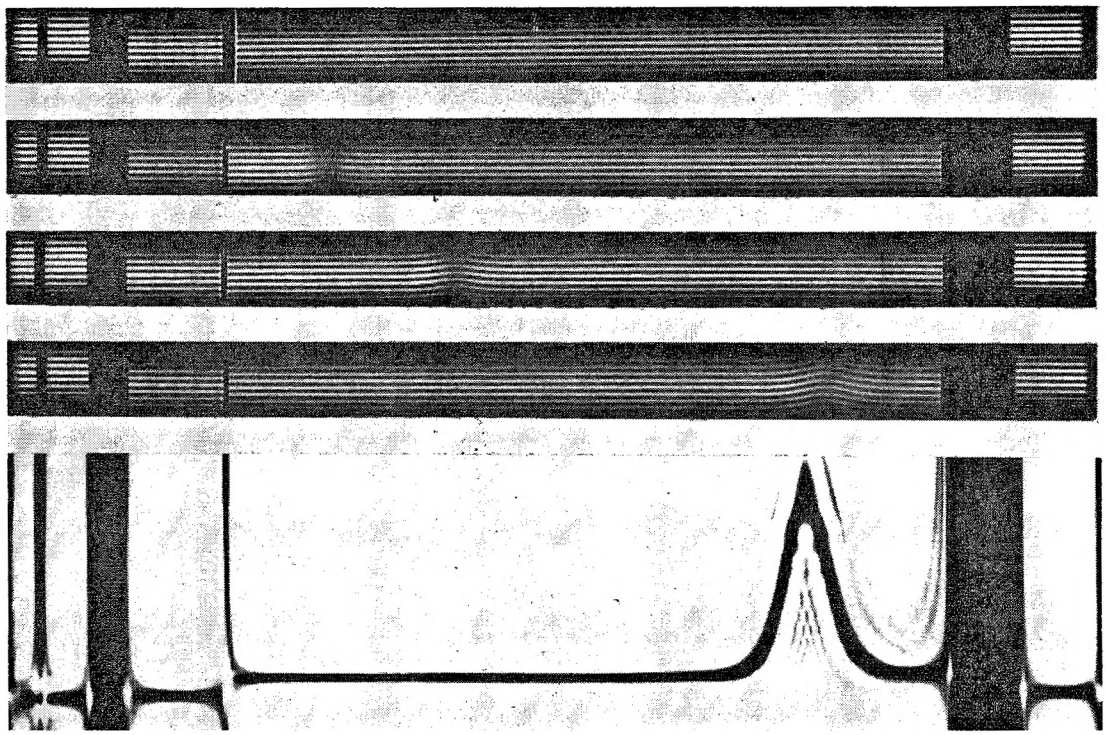

Fig. 9.—Interference patterns obtained from a differential sedimentation experiment. Both compartments in the cell contained BSV at 0.4 g./100 ml. in 0.1 *M* sodium phosphate buffer at *p*H 6.8, but one also contained $D_2O$ at a concentration of 2.5 ml./100 ml. The compartments were filled by means of a micrometer syringe so that the menisci would be at the same level. The patterns from top to bottom correspond to 0, 65, 88, 148 and 144 min. The schlieren pattern was obtained with the schlieren diaphragm set at an angle of 65°.

sponding to one of the fringes is determined. From a statement of the conservation of mass the concentration at the meniscus can be described by

$$c_m = c_0 - \frac{x_b^2(c_b - c_m) - \int_{x_m}^{x_b} x^2\,dc}{x_b^2 - x_m^2} \qquad (5)$$

Once $c_m$ is evaluated from eq. 5, the concentration throughout the cell follows directly. In addition, it was determined which fringe in the equilibrium interferogram corresponds to the initial concentration. This is referred to frequently as the hinge point.[10, 27] For this purpose the filter was removed from the optical system and the white light fringe was photographed.[43] The intersection of the white light fringe on the equilibrium pattern with the corresponding fringe observed and photographed immediately after the rotor attained the desired speed gave $c_0$. The two methods complement each other and thereby reduce the possibility of errors.

The results of the experiments with sucrose and raffinose, using both eq. 3 and 4 are summarized in Table IV. For sucrose the agreement is excellent whereas the results with raffinose indicate the need for a correction due to the non-ideality of the solution. Many experiments were performed with ribonuclease but the data are not given here because of the observation of polydispersity in the preparation. This was evident in the thickening of the interface at the bottom of the column of solution and from the upward curvature in plots of ln *c versus* $x^2$. Work is now in progress to characterize different preparations in terms of the weight average molecular weight $M_w$ and the *z* average molecular weight, $M_z$. Both of these can be evaluated from the interferograms, the former through the use of eq. 4 and the latter from the equation derived by Lansing and Kraemer[40]

$$M_z = \frac{M_{wb}c_b - M_{wm}c_m}{c_b - c_m} \qquad (6)$$

where $M_{wb}$ and $M_{wm}$ are evaluated from the limiting slopes of ln *c versus* $x^2$.

Although more studies, especially with proteins, are needed it seems already that interferometric optics afford a means for determining molecular weights with accuracy greater than heretofore anticipated.

## Direct Measurement of Small Differences in Sedimentation Coefficients

Frequently, the sedimentation coefficient of a substance may be altered so little as a result of a specific treatment or by the addition of a third component that the effect cannot be described quantitatively because of present limitations in experimental precision. With the adaptation of interferometric optics to the ultracentrifuge it has become possible to devise a differential method whereby the sedimentation coefficients in two solutions can be compared directly and the difference measured accurately.[44] This technique makes use of the property of the Rayleigh interferometer which permits the measurement, at each level

(43) In order to observe this fringe it is necessary that a compensating cell be available or that the refractive index of the solvent be increased to that of the solution by the addition of a material which does not redistribute, *e.g.*, 1,3-butanediol.

(44) E. G. Richards and H. K. Schachman, *J. Am. Chem. Soc.*, **79**, 5324 (1957).

within the cell, of the difference in refractive index between the solutions in the two compartments. If both solutions are identical, despite the presence of boundaries, the Rayleigh pattern consists of a series of parallel, straight interference fringes. For the fringes to be straight, the boundaries must migrate and spread at the same rate so that the refractive index difference at conjugate levels throughout the cell is constant. When one boundary moves faster than the other, the fringe pattern at the boundaries is warped to produce curved fringes whose shape resembles the tracings produced by schlieren optical systems. Depending upon which compartment contains the faster moving species, the pattern will show a maximum or a minimum. A sequence of typical patterns is shown in Fig. 9. Also included is a schlieren pattern observed just prior to the last fringe photograph. Since the sedimentation rates of the BSV in the two compartments are so similar, differing by only 1%, the schlieren optical system shows only a single boundary. In that experiment special precautions were taken to be certain that the menisci in the two compartments were at the same distance from the axis of rotation. Although this is convenient experimentally, it is not a requisite of the technique for the appropriate theoretical treatment can account for variations not only in sedimentation coefficient but also in concentration and meniscus position.

In order to relate the difference in sedimentation coefficient to parameters which can be evaluated from the fringe patterns, the sedimentation is considered in terms of the transport method. The transport equation, resulting from a statement of the conservation of mass, can be written

$$\frac{1}{2}c_0(x_p^2 - x_m^2) - \int_{x_m}^{x_p} cx\,dx = \frac{1}{2}c_0x_p^2(1 - e^{-2\omega^2 st}) \tag{7}$$

where the first term expresses the total mass of solute present initially between the surfaces, $x_m$ and $x_p$, the second term describes the mass behind $x_p$ at some time, $t$, and the last term represents the total mass of material transported across the surface in the plateau region at $x_p$ during the time $t$. It is implicitly assumed in this presentation that the sedimentation coefficient $s$ is constant throughout the experiment. This equation can be written for each of the two solutions designated by the subscripts, 1 and 2, the slower and faster moving components, respectively. Rearrangement of these equations and subtraction of the second from the first gives

$$\int_{x_m}^{x_p} \Delta c\, x\, dx = \frac{1}{2}c_0x_p^2(e^{-2\omega^2 s_1 t} - e^{-2\omega^2 s_2 t}) \tag{8}$$

where

$$\int_{x_m}^{x_p} \Delta c\, x\, dx$$

is written for

$$\int_{x_m}^{x_p} c_1\, x\, dx - \int_{x_m}^{x_p} c_2\, x\, dx$$

It should be noted that $\Delta c$, the difference in concentration at any level, $x$, is evaluated directly by means of the interferometer. Simplification of eq. 8 is achieved by the substitutions, $s_1 = s_{av} - \Delta s/2$ and $s_2 = s_{av} + \Delta s/2$, to give

$$2\int_{x_m}^{x_p} \Delta c\, x\, dx = x_p^2 c_0 e^{-2\omega^2 s_{av} t}(e^{\omega^2 \Delta s t} - e^{-\omega^2 \Delta s t}) \tag{9}$$

Since $\omega^2 \Delta s t$ is very small (less than 0.02), only the first three terms need be retained in the expansion and eq. 10 results directly.

$$\int_{x_m}^{x_p} \Delta c\, x\, dx = x_p^2 c_0 \omega^2 \Delta s t e^{-2\omega^2 s_{av} t} \tag{10}$$

Further simplification is achieved by the substitutions of $(x_m/x_{av})^2$ for $e^{-2\omega^2 s_{av} t}$ and $(1/s_{av})$ ln $(x_{av}/x_m)$ for $\omega^2 t$ to give

$$\frac{1}{c_0 x_m^2}\int_{x_m}^{x_p} \Delta c\, x\, dx = (\Delta s/s_{av})\frac{x_p^2}{x_{av}^2}\ln\frac{x_{av}}{x_m} \tag{11}$$

Thus $\Delta s/s_{av}$ is evaluated from the appropriate plot of the data according to eq. 11. A more general treatment allowing for differences in menisci positions $\Delta x_m$, and initial concentrations $\Delta c_0$ yields

$$\frac{1}{c_{0,av}\, x_{m,av}^2}\int_{x_m}^{x_p} \Delta c\, x\, dx = (\Delta s/s_{av})\frac{x_p^2}{x_{av}^2}\ln\frac{x_{av}}{x_{m,av}} + \frac{\Delta x_m}{x_{m,av}} + \frac{\Delta c_0}{2c_{0,av}}\left(\frac{x_p^2}{x_{av}^2} - 1\right) + \ldots \tag{12}$$

Two types of experiments were performed as a test of the method and the equations presented above. In the first, the same solutions were placed in each of the two compartments of the double sector cell but more liquid was added to one than the other. As a result the menisci were offset. Independent sedimentation in the two compartments gives boundaries which, though moving at identical rates, originate at different levels and traverse the cell slightly displaced from one another. This leads to interference patterns like those shown in Fig. 2. Since both solutions become diluted progressively the area under the curved fringes should decrease with time; but, ac-

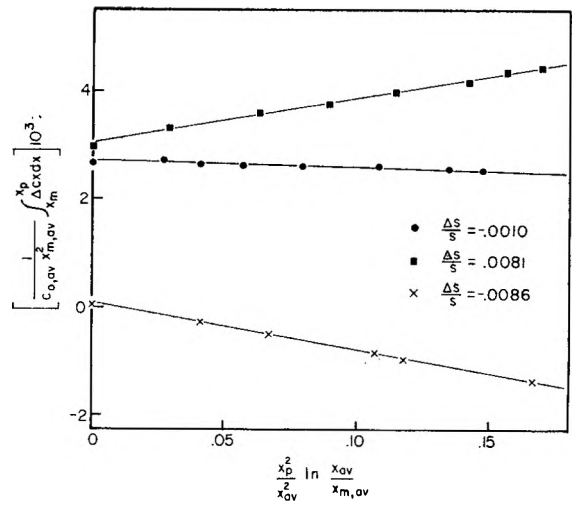


Fig. 10.—Differential sedimentation.—The experiments correspond to: ● BSV *versus* BSV; ■ BSV in 2.5% $D_2O$ *versus* BSV; × BSV *versus* BSV in 2.5% $D_2O$ (solutions reversed in cell). BSV concentration, 0.4 g./100 ml. in 0.1 *M* sodium phosphate, *p*H 6.8. The points on the vertical axis were obtained from the $\Delta x_m/x_{m,av}$ term of eq. 12. The sign of the slope indicates merely the relative placement of the solutions in the cell; the sign of $\Delta s/s_{av}$ should be determined by the sense of the experiment.

cording to the theory, the first moment of the fringe pattern should remain constant as the two boundaries move through the cell. In the second type of experiment a known difference in sedimentation coefficient was produced by sedimenting the same substance in solvents which were identical except for the fact that a small amount of $D_2O$ was added to one of the two solutions. The presence of the $D_2O$ led to a decrease in the sedimentation rate of the macromolecules because of the increase in the density and viscosity of the solution. This change in sedimentation rate caused by the $D_2O$ was evaluated independently from experiments performed in a conventional manner with schlieren optics and using high concentrations of $D_2O$. By interpolation from these data the effect of low concentrations of $D_2O$ was determined accurately and the results then were compared with those derived from the differential technique.

In both types of experiments precise data were obtained readily; the area under a curve such as those shown in Fig. 9 could be measured reproducibly with a deviation no greater than 2%. However, the area under the interference curves was not in accord with the theory presented above; and therefore, the accuracy of the differential technique cannot as yet be considered satisfactory. Typical results from different experiments are represented by the plots in Fig. 10. The central curve was obtained in a differential experiment involving identical solutions in the two compartments but with different amounts of liquid so that the menisci were not at the same level. Although $\Delta s/s_{av}$ was zero for this experiment the differential technique indicated a value of $-0.0010$. This can be stated in an alternative fashion: the first moment of curve under the fringes, instead of being constant throughout the experiment, decreased by 6%. In a second experiment the cell was filled in the opposite manner (the solutions were interchanged relative to the two compartments). Although the patterns showed minima instead of maxima (as in Fig. 9) the effect was not eliminated; again there was a slight slope of the plot according to eq. 12. When $D_2O$ was added to one of two solutions of BSV in an amount sufficient to reduce the sedimentation coefficient making $\Delta s/s_{av}$ equal to $-0.0103$, the first moment of the area which was zero initially increased with time yielding a value of $-0.0086$ for $\Delta s/s_{av}$. About the same result ($\Delta s/s_{av} = -0.0081$) was obtained in another experiment in which the menisci were offset and the two solutions were interchanged relative to the cell. The experiments with the identical solutions can be used for the calculation of a correction factor which makes the first moment of the area independent of time. If this factor is used in the treatment of all of the data from experiments of different types, the values of $\Delta s/s_{av}$ deduced from the interferograms are found to be in accord with the values expected on the basis of independent measurements of the effect of $D_2O$. It is clear, however, that further investigations are required as to the effect of aggregates in the solution, convection in the cells, and the optical system itself before the full potential of the differential technique can be assessed.

**Acknowledgment.**—The authors wish to express their thanks to E. G. Pickels for valuable suggestions during the course of this work. Also they are indebted to D. A. Yphantis and K. A. Kraus and J. S. Johnson for details of their work prior to publications.

## DISCUSSION

R. TRAUTMAN (U. S. Department of Agriculture).—I would like to comment on your method of aligning the cylindrical lens by tilting it until the fringe pattern is straight in the boundary region for the cell filled with identical solutions in both channels. I have found that by opening the chamber while the rotor is spinning and adjusting the mask on the upper condensing lens the fringe pattern could be straightened either by shifting the mask laterally parallel to itself or by tilting the cylindrical lens.

E. G. RICHARDS.—We have discovered that it is very important indeed that the upper aperture be positioned accurately and reproducibly. To this end we have constructed a mechanical device which permits us to locate the slits in the upper aperture so that they are both parallel to and symetrically arranged about a radius from the center of the rotor. It is mandatory, of course, that this special aligning tool which is described in the manuscript be used every time the drive is changed or whenever the upper condensing lens is removed for cleaning.

R. TRAUTMAN.—I have tried to devise an optical method for the adjustment of the upper mask so that it is symmetrical to the center of rotation rather than use an elaborate mechanical scheme. By taking out the cylindrical lens and moving the camera lens toward the photographic plate the upper mask can be brought into focus. Then with a water–benzene mixture in a cell two menisci can be found, one near the bottom of the cell and one near the top. With the light source in the schlieren position very sharp flanking fringes can be seen at these menisci with the rotor spinning, chamber closed. By direct observation, or more precisely by comparation, one can see whether the arcs these menisci have are symmetrical in the image of the mask and then the mask can be shifted appropriately.

E. G. RICHARDS.—This seems like an interesting addition to our technique and it will certainly bear close inspection. Offhand it would seem that a combination of both the mechanical and optical procedures would be worthwhile. The rigid construction which we have achieved certainly leads to a reproducible system and it may prove advisable to use the optical technique as an added precaution in the alignment of the upper aperture relative to the rotating cell.

R. TRAUTMAN.—As a further comment on the alignment by opening the chamber with no rotor, the cylindrical lens can be tilted so that its axis is consistent with that at the upper mask. Now there appear two bands of light on the screen with diffraction images from the edges of the mask. By moving the full surface mirror to the left the pattern can be moved down on the screen to the neighborhood of the 90° phase plate shadow. The cylindrical lens can now be tilted to align the fringes with the phase plate shadow. After using these optical methods, it was verified by your method that there was no "hump."

E. G. RICHARDS.—It is apparent that further research along this line will lead to a more precise procedure for the alignment of the different optical components for the Rayleigh interference system as applied to the ultracentrifuge. It may even turn out that the system of choice will be one in which the Rayleigh mask is incorporated onto the lens mount in the lower part of the vacuum chamber. In that case the upper aperture can be eliminated completely and the problem then will be one of the precise alignment of the Rayleigh mask at the base of the vacuum chamber. It is our feeling at present that the major deterrent to using this alternative scheme is the inadequacy of the cells themselves since with this arrangement interference fringes would be formed during the passage of the cells past the optical beams. Thus the effect of distortion in the quartz windows would be more serious than is presently the case in which the

Rayleigh mask is built into the cell itself. We are certainly looking forward to further experimental results with the different systems.

M. CREETH (University of Wisconsin).—At least formally there are some pressure effects which one should consider in the experiments of the type you have described and I wonder whether you have given any thought to these. These would be manifest in the experiment in which you have offset the menisci and they would also appear in those experiments in which you have added a small amount of heavy water to produce a difference in sedimentation coefficient. These effects may very well prove to be negligible.

E. G. RICHARDS.—We have indeed been worried about the effect of pressure and it was for this reason in part that we have chosen to do most of our experiments with bushy stunt virus. In view of its very large sedimentation rate most of the ultracentrifuge experiments were conducted at low speeds so that it is likely that the pressure effects are negligible. However this will bear further inspection as the accuracy of the methods increases.

F. M. FOWKES (Shell Development Co.).—I would like to have an estimate of the accuracy in the determination of concentrations.

E. G. RICHARDS.—A solution containing 1 g./100 ml. corresponds to about 40 fringes with the existing arrangement of the optics. At the present time we have no difficulty in reading reproducibly the fringe patterns with the precision of 0.02 fringe. Thus our precision in the determination of concentrations is of the order of 1 part in 2000.

R. L. BALDWIN (Stanford University).—I wonder if you would comment on the use of the Archibald method as compared with measurements by sedimentation equilibrium.

E. G. RICHARDS.—It would appear that much greater precision can be obtained by the sedimentation equilibrium technique since there is still considerable subjectivity involved in the determination of the concentration gradient at the ends of the liquid column when using the Archibald method. With short columns of liquid, sedimentation equilibrium throughout the whole solution can be achieved in such a relatively short period of time that for many experiments which have heretofore been conducted by the Archibald technique it would seem that the sedimentation equilibrium method with interference optics would be preferable. There may, however, be special reasons which dictate the use of the Archibald technique.

# MOVING BOUNDARY THEORY APPLIED TO PREPARATIVE ULTRACENTRIFUGATION[1]

BY RODES TRAUTMAN AND SYDNEY S. BREESE, JR.

*Plum Island Animal Disease Laboratory, Agricultural Research Service, U. S. Department of Agriculture, Greenport, Long Island, New York*

*Received March 6, 1959*

The moving boundary method is formulated for five arrangements of cells and fields: a cell of uniform cross-sectional area in a uniform gravitational field, a sector-shaped cell in a centrifugal field, a cylindrical tube in a horizontal rotor, a cylindrical tube in an angle rotor and a hypothetical hyperbola-shaped cell. The first two have no complications due to the collision of sedimenting particles with the sides of the cell; the others require some simplifying assumptions. The law of the conservation of mass and the specification that the boundary move at the same sedimentation rate as do the particles ahead in the bulk solution can be put into a general form applicable to all these geometrical cases. This involves (a) change of variable from the radius $r$ to the volume $v$ of the cell contained between the level in question and the starting level of the boundary and (b) introducing, as a parameter, the volume $V$ that the cell would have between the center of rotation and the starting level, if the sides were extrapolated. The basic differential equations are $d[c_p(1 + \bar{v}/V)]/dt = 0$ and $d[c_p(v' - \bar{v})]/dt = 0$, in which $c_p$ is the concentration of the region at $v = v'$ somewhere in the bulk solution ahead of the boundary at $v = \bar{v}$ and $t$ is the time. The case of a uniform cell in a uniform field is specified by infinite $V$. The general solution of these equations for $\bar{v}$ is considered and expressed for the three types of data possibly available: concn. gradient, $\partial c/\partial r$ (eq. 23); concn., $c$ (eq. 15); and recovered quantity, $\int (c/c^0)dv$ (eq. 17) where $c^0$ is the initial concentration. If the volume is expressed in terms of the radius for the uniform and the sector cell a first moment and a second moment, respectively, will be required in calculating $\bar{v}$ from concentration gradient measurements. When optical methods are not appropriate, as with impure active agents for which there is a specific biological assay, the quantity is measured which is contained between the meniscus and some level $v$ where a cut is made. For this preparative ultracentrifugation the expression for $\bar{v}$ is generalized to a function $v^*$ (eq. 33). Considering the following properties of $v^*$, it is called the "apparent boundary position" function: (a) it is a continuous distribution as a function of $v$; (b) the boundary position $\bar{v}$ is the constant value that $v^*$ attains for a short region somewhere in the lower part of the tube in the moving boundary experiment which moves the boundary from the meniscus only partly down the length of the tube; (c) with heterogeneity and/or diffusion, $v^*$ varies as the sampling level passes through the boundary region in such a way that the integral of the concentration distribution can be obtained as a simple difference between $v^*$ and $v$, corrected for the effect of $V$. It is confirmed that the error in $s$-rate is much less than the assay error provided that there are cuts near the level of the boundary position. The facilitating functions are considered for the case in which only a two-compartment cell is used. Here there must be several experiments at different speeds and times to obtain reliable data about the $s$-rate. Experimental studies to illustrate the procedures recommended are reported for bovine plasma albumin, $\gamma$-globulin and hemocyanin solutions. Two methods were used to fractionate the contents of a cylindrical tube after centrifugation. The first was successive removal of samples from the top with a Pasteur pipet. The second method, while not physically removing samples, enabled light absorption to be measured in successive 1-mm. layers down the tube. This was effected with an attachment to a standard spectrophotometer. The sedimentation coefficient could be determined from a preparative ultracentrifuge experiment with an error of $\pm 10\%$ in the range of 4-100 $S$ tested. Heterogeneity information also could be estimated, provided extreme care was exercised in the fractionation.

The application of physical methods to biological problems involves the development of techniques for the characterization of physical entities associated with biological activity. In particular, techniques leading to a knowledge of the sedimentation coefficient ($s$-rate) have enabled (a) design of centrifugal methods for concentrating the active agent in biological fluids, (b) good estimates of the molecular size of the active particle, and (c) proper identification and interpretation of optical patterns obtained during analytical ultracentrifugation of concentrates from chemical and other procedures for purification.

Moving boundary preparative ultracentrifugation is one of the physical techniques which has permitted measurement of the $s$-rate of substances that can only be followed by biological assay. The term "moving boundary method" is well established in the free electrophoresis literature.[2] It is also applicable to sedimentation (or flotation) in a tube or cell which is initially uniformly filled and in which the particles of each type move only in one direction. In such a system the movement of the particles in the region of uniform concentration is to be inferred from measurements made on the "boundary region" between this "plateau" and the supernatant fluid which develops. Two functions related to the mass concentration distribution in the tube at various times have theoretical as well as practical properties. One is the derivative and the other the integral of the concentration distribution with respect to the coördinate along the field. The former is called the "concentration gradient" and the latter the "quantity." In terms of the concentration gradient distribution a "plateau" is a region of limited radial extent for which the gradient vanishes, thus ensuring that the concentration is independent of radius, although it may be a function of time. Use of the concept of the "quantity" permits the expression of the law of conservation of mass and leads to the functions described here for locating the boundary from biological assay of preparative fractions. One can think in terms of gradient curves or concentration curves in the particular form some instrument displays them, or in terms of the modified quantity distributions calculated from assay data which are proposed here. Each of these distributions when separately known permits evaluation of the sedimentation coefficient, the homogeneity and the relative composition of heterogeneous mixtures.

Moving boundary or "differential centrifugation" experiments have been performed in at least five situations—(a) a tube of constant cross-sectional

(1) This paper was presented at the 33rd National Colloid Symposium, Minneapolis, Minn., June, 1959.

(2) L. G. Longsworth, in "Electrophoresis," M. Bier, ed., Academic Press, New York, N. Y., 1959.

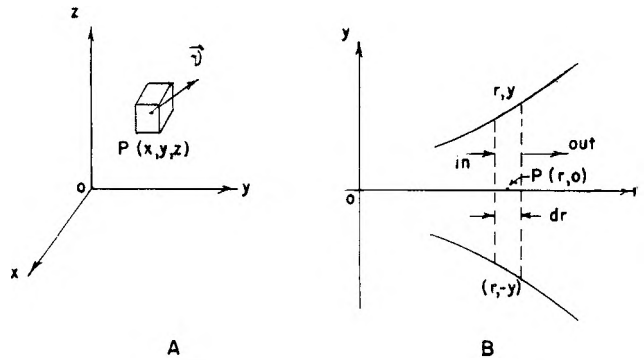


Fig. 1.—Coördinate system for expressing the law of conservation of mass: A, general rectangular coördinates; velocity of moving particles $\vec{\nu}$ and their concentration $c$ are functions of the coördinates of each point P($x,y,z$). B, two-dimensional force field; cell has thickness $h$ perpendicular to the ($r,y$)-plane, cell boundaries given by $y(r)$ and $-y(r)$; lamina of width d$r$ at P($r$,0) extends from wall to wall of cell; particles enter from the left and leave to the right.

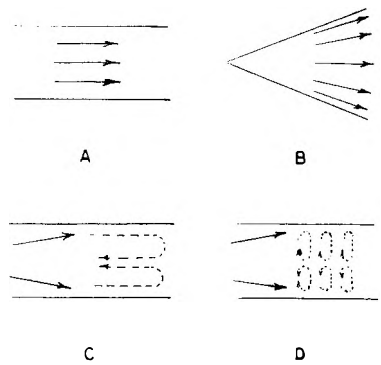


Fig. 2.—Convection caused by cells not conforming to the force field: A,B, ideal geometry—no collision with the walls; A, uniform cell in uniform field; B, sector-shaped cell in radial field. C, convection along the field—increased density region at wall slides to bottom; solution in center rises. D, convection across the field—increased density region exchanges with solution at center of cell at the same level. Solid arrows indicate the direction of the force field on particles; broken arrows indicate the direction of hydrodynamic forces on elements of fluid.

areas in a uniform field (*e.g.*, acceleration due to gravity); (b) a cylindrical centrifuge tube in either an angle rotor or (c) a swinging bucket rotor; (d) a sector shaped centrifuge cell; or (e) a cell which "toes in" with increasing radius as does a reversed sector cell or a conical tube. An effort has been made here to select a general starting concept which is applicable to all these cases. In so doing, some of the well known relations for analytical ultracentrifugation are reformulated. No attempt is made to consider the approach to sedimentation equilibrium as has been done by Yphantis and Waugh,[3] the analysis here being strictly applicable to the sedimentation velocity classification.

This paper is presented in three parts. Part I deals with the general considerations which show the influence of cell shape and form of the field on the expressions for locating the position of the boundary and calculating the initial concentration; Part II, with the theory as applied to the preparative ultracentrifuge; and Part III, with an experimental check of some of the relations for a horizontal, uniform cross-section tube.

(3) D. A. Yphantis and D. F. Waugh, THIS JOURNAL, **60**, 623 (1956).

## Part I. Introduction to Moving Boundary Theory

**Expression of the Law of the Conservation of Mass.**—The law of the conservation of mass applied to any element of volume d$v$ as in Fig. 1A in which particles move with velocity $\vec{\nu}$ in a field of force requires that in a time d$t$ the mass entering less the mass leaving must equal the mass increase inside the element. This has been expressed[4,5] for the sector shaped centrifuge cell as a particular case of the general vector analysis expression[6]

$$-\frac{\partial c}{\partial t} = \nabla . c\vec{\nu} \qquad (1)$$

where $c$ is the mass concentration. In order to employ such a general relationship for the several types of geometrical cells in a radial or a uniform field, it is necessary to investigate the velocity $\vec{\nu}$ in a little detail. Unless the sides of the cell are parallel to the field vector (Fig. 2A and B), particles will either collide with or be depleted at the wall. The resulting hydrodynamic circulation may extend an appreciable distance along the direction of the field, as in Fig. 2C. Alternatively, convection across the field, as in Fig. 2D, may take place. The solid arrows indicate the direction of the field on the particles when moving relative to solvent. The dotted arrows indicate movement of fluid and particles together. In the convective cases, like Fig. 2D, we prefer to consider only the average component of $\vec{\nu}$ of equation 1 which is along the field vector in the center of the cell, denoted by $\vec{\nu}_c$. A practical method for making $\vec{\nu}_c$ represent only systematic relative motion of particles with respect to fluid has been to use a slight density gradient of solvent[7,8] so that the region of increased density at the wall cannot sink along the field but is turned in toward the center (where the density tends to drop in the radial field cases) by the magnified hydrostatic leveling forces. Such a convection will be assumed for the cases other than the ideal of Fig. 2A and B.

We find it advantageous to use the classical definition of sedimentation coefficient $s$ as the velocity of particles divided by the force per unit mass, provided sedimentation is the only process producing the systematic relative motion.[4] This will require that there be no such net movement either by electrokinetics or by Brownian motion, for example. Since the former can be suppressed it will be neglected, but the latter vanishes only in the absence of concentration gradients. The moving boundary method, by nature, has such gradients and hence all particles of a given type do not move at the same velocity per unit field. This does not mean that

(4) T. Svedberg and K. O. Pedersen, "The Ultracentrifuge," Clarendon Press, Oxford, 1940.

(5) J. W. Williams, K. E. Van Holde, R. L. Baldwin and H. Fujita, *Chem. Revs.*, **58**, 715 (1958).

(6) L. Page, "Introduction to Theoretical Physics," D. Van Nostrand Co., Inc., New York, N. Y., 1935, p. 26.

(7) E. G. Pickels, *J. Gen. Physiol.*, **26**, 341 (1943).

(8) H. Kahler and B. J. Lloyd, Jr., THIS JOURNAL, **55**, 1344 (1951).

the definition of $s$ is not applicable, for in a great many practical applications, a plateau region of limited radial extent will remain in which the concentration, even though different from the initial, is independent of the radius. It is not difficult to set up moving boundary situations for which this is not the case,[9,10] but these will not be considered here. The moving boundary method requires a plateau and, in effect, represents the technique used to make the definition of $s$ operational.

With these two qualifications as to the convection and the existence of a plateau, we now express the equation of continuity in a form suitable for the different cells and fields to be studied.[11] Consider the element of volume indicated in two dimensions in Fig. 1B with a constant thickness $h$ perpendicular to the paper. The mass per unit time entering the left-hand face is the (velocity)·(area)·(concentration) or $(sg)(2yh)c$, where the force per unit mass is $g = \omega^2 r$ for the centrifugal field, but constant for the uniform field. The mass per unit time leaving the right-hand face is then $2cghsy + [\partial(2cghsy)/\partial r]dr$, where $r$ is the coördinate along the centerline of the cell. The rate of increase of mass is the difference between these and can also be expressed as the rate determined from the (change in concentration per unit time)·(volume) or $(\partial c/\partial t)(2hydr)$. Therefore

$$\frac{\partial c}{\partial t} = -\left(\frac{1}{y}\right)\frac{\partial(cgsy)}{\partial r} \qquad (2)$$

In a plateau region the concentration is independent of $r$, by definition, and $s$ is also independent of $r$ since it depends only on the composition (except in those cases for which $s$ is pressure dependent[10]). Therefore equation 2 can be written

$$\frac{dc_p}{dt} = -(c_p s)\left[\frac{d\,(gy)}{y\,dr}\right] \qquad (3)$$

where $c_p$ is the plateau concentration. We shall now apply equation 3 to the four cases depicted in Fig. 3, using the letter of this figure corresponding to each case for identification of the appropriate equation

$$dc_p/dt = 0 \qquad (3A, D)$$

$$dc_p/dt = -2\omega^2 c_p s \qquad (3B)$$

$$dc_p/dt = -\omega^2 c_p s \qquad (3C)$$

The fact that the dimensions of the cells do not appear means that sections perpendicular to the axis of rotation in any particular cell or tube need be only of the same shape but not necessarily the same size. Rigorously, equation 3B is better derived from equation 1 by expression in cylindrical coördinates. The derivation from equation 3 implicitly treats the sector cell as a summation of small angle sector cells for which $y$ is perpendicular to the central radius.

In these four cases, as well as in a slightly more general cell in which $y$ is proportional to any power of the radius, $dc_p/dt$ is not a function of $r$ and thus the original plateau will not be destroyed, even though its magnitude and extent are time dependent.

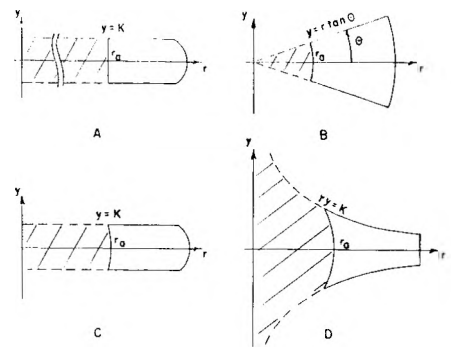


Fig. 3.—Cells and fields considered: A, uniform cell in uniform field; B,C,D, sector, uniform and hyperbolic cells, respectively, in a centrifugal field. Cross-sectional area in A and C is $A$; thickness of cell perpendicular to the $(r,y)$-plane in B and D is $h$; $r_a$ is the position of the meniscus; cross-hatching indicates region extending from $r_a$ to the center of rotation, which is denoted as the extended cell volume $V$.

**Expression of the Moving Boundary Condition.**—In the preceding we thought of $s$ as being the velocity divided by the force per unit mass of the particles that moved through the fixed element of volume at a point P in Fig. 1A. Now we need to select a group of particles which will remain in the plateau region during the centrifugation. This means that they could not have been near the top or bottom of the cell initially for then they would either be involved in the boundary region or be sedimented into the bottom. Let the particles selected be all those in a lamina extending from side to side of the cell as in Fig. 1B. Since the $s$-rate at all levels in the plateau has been assumed the same, it is convenient to use the same symbol $s$ for the velocity divided by the force per unit mass of these marked particles and to let $r'$ be the moving coördinate which measures their distance from the center of rotation. Even though there are processes other than sedimentation taking place in the boundary region, the moving boundary method relies on the specification of a boundary which, starting at the meniscus, in this case, moves at the same $s$-rate as do the particles far ahead of it in the plateau.[12] Since this is the only sense in which "boundary" is meant when used alone, the modifiers "equivalent," "hypothetical" or "true"[11-17] will not be used. Let $\bar{r}$, a function of time, be the distance of the boundary from the center of rotation. Then, the basic specification of the moving boundary method is

$$\frac{1}{\omega^2\bar{r}}\left(\frac{d\bar{r}}{dt}\right) = \frac{1}{\omega^2 r'}\left(\frac{dr'}{dt}\right) = s \qquad (4)$$

(9) R. T. Hersh and H. K. Schachman, THIS JOURNAL, **62**, 170 (1958).

(10) H. Fujita, *J. Am. Chem. Soc.*, **78**, 3598 (1956).

(11) Part of the discussion on convection, the equation of continuity (equation 3), and the hyperbolic cell of Fig. 3D are modified from Univ. of Calif. Radiation Lab. Report No. UCRL 1869 by R. Trautman (July 8, 1952).

(12) An animated motion picture depicting this concept was prepared by R. Trautman, E. H. Myers and V. N. Schumaker, Univ. of Calif. Rad. Lab., and shown by R. Trautman and V. N. Schumaker at the 130th National Meeting of the American Chemical Society, New York, N. Y., Sept., 1954.

(13) R. Goldberg, THIS JOURNAL, **57**, 194 (1953).

(14) L. G. Longsworth, *J. Am. Chem. Soc.*, **65**, 1755 (1943).

(15) V. P. Dole, *ibid.*, **67**, 1119 (1945).

(16) R. Trautman and V. N. Schumaker, *J. Chem. Phys.*, **22**, 551 (1954).

(17) R. Trautman, THIS JOURNAL, **60**, 1211 (1956).

Equations 3A, B, C, D and 4 are the two differential equations applicable to the cases we wish to consider. The purpose is to solve them for $\bar{r}$ in terms of the concentration distribution or its derivative or integral forms in the boundary region. This will be done after first generalizing them in the next section.

Goldberg[13] also observed that a property of the particle distribution which moved at the same $s$-rate as particles in the plateau was desired. He and others[5,14-17] defined the boundary position $\bar{r}$ as the location the boundary would have had if it had remained infinitely sharp. Several workers have realized that it is not obvious that the equivalent, infinitely sharp boundary meets the $s$-rate requirement and have given proofs.[5,16] Here, we choose to go the other way around: specify that the boundary moves at the $s$-rate of the particles in the plateau and then deduce, among other properties, that it is located at the equivalent, infinitely sharp position.

**Generalization of the Two Differential Equations Using Volume Coördinates.**—For the sector cell case, $s$ can be eliminated between equations 3B and the outer members of equation 4. The result can then be multiplied by $\bar{r}^2$ and arranged to give

$$\bar{r}^2 \frac{dc_p}{dt} + 2\bar{r}\frac{d\bar{r}}{dt} c_p = 0 \qquad (5B)$$

This is the perfect differential

$$d(\bar{r}^2 c_p)/dt = 0 \qquad (6B)$$

On the other hand, $s$ could have been eliminated between equations 3B and the middle member of equation 4 to yield an equation identical to equation 6B with $\bar{r}$ replaced with $r'$. Subtraction of these two equations gives

$$d[c_p(r'^2 - \bar{r}^2)]/dt = 0 \qquad (7B)$$

Similarly for the uniform cell in the centrifuge (Fig. 3C), we obtain

$$d(\bar{r}c_p)/dt = 0 \qquad (6C)$$
$$d[c_p(r' - \bar{r})]/dt = 0 \qquad (7C)$$

A different approach is used for the hyperbolic cell of Fig. 3D, since equation 3D indicates that $c_p$ is a constant. First put equation 4 into logarithmic form as $d(\ln r' - \ln r)/dt = 0$ and multiply $c_p$ inside the derivative. Thus

$$d[c_p(\ln r' - \ln r)]/dt = 0 \qquad (7D)$$

covers the case of Fig. 3D.

Comparison of these three forms (B, C, D) of equation 7, realizing that the volume of the respective cells varies as $r^2$, $r$ and $\ln r$, provides the clue to the desired generalization. We choose to change the variable from $r$ to the volume $v$ of the cell between the starting level at $r_a$ and the level at $r$. We also introduce as a parameter the volume $V$ that the cell would have between the starting level and the axis of rotation, if the sides were extrapolated. $V$, shown as the shaded area in Fig. 3, can be called the "extended cell volume." It should be noted that $V$ is infinite for the cell of Fig. 3A because a uniform gravitational field requires the center of mass to be a great distance away. The following are the volume expressions for the four cases of Fig. 3

$$v = A(r - r_a) \qquad V = \infty \qquad (8A)$$
$$v = \theta h(r^2 - r_a^2) \qquad V = \theta h r_a^2 \qquad (8B)$$
$$v = A(r - r_a) \qquad V = Ar_a \qquad (8C)$$
$$v = 2hK(\ln r - \ln r_a) \qquad V = \infty \qquad (8D)$$

With this change of variable the second differential equation (7B,C,D) can be written

$$d[c_p(v' - \bar{v})]/dt = 0 \qquad (9)$$

This is also applicable to the uniform cell in the uniform field (Fig. 3A) as can be seen by expanding the derivative.

The first differential equation (3A,D and 6B,C) for the four cases becomes

$$d[c_p(1 + \bar{v}/V)]/dt = 0 \qquad (10)$$

In equations 9 and 10, $\bar{v}$ and $v'$ are obtained when $r$ takes the values $\bar{r}$ and $r'$, respectively. These two equations are the general expressions of the conservation of mass (equation 3), and the moving boundary condition (equation 4) almost inextricably intermeshed. The fact that there are two equations means that two things can be determined. In the analytical ultracentrifuge, these are usually the boundary position and the initial concentration, as will be seen in the last section of this part.

The parameter $V$ encompasses variable filling and the radial location of the cell, terms which unfortunately are frequently not specified in reporting centrifuge conditions. In the angle centrifuge, $V$ is the volume obtained by extrapolating the inclined tube back to the axis of rotation, provided there are suitable density gradients to promote convection across the field for both the particles hitting the side walls, because of the radial field, and those hitting the upper wall, because of the inclination of the tube. Since the only difference in the calculations, in volume coördinates, for two tubes, one from an angle and the other from a horizontal rotor is in the size of $V$, no further explicit reference to the angle case need be made. It should be pointed out that Ray and Deason[18] have considered the various cases of radial convection not treated here. For flotation, $V$ is still positive, being the volume from the center of rotation to the bottom of the cell, but $v$ is negative.

**Integration of Basic Differential Equations.**—Integrate equation 9 to

$$c_p(v' - \bar{v}) = Q \qquad (11)$$

where the constant of integration $Q$ is independent of the time. We now determine the physical meaning of $Q$ by noting that initially the concentration is $c$ and $\bar{v}$ is zero. Thus, from equation 11

$$c^0(v')_{t=0} = Q \qquad (12)$$

Equation 12 shows that $Q$ represents all the particles initially between the meniscus and the peripheral limit of $(v')_{t=0}$. Since no particles pass through the group of moving marked particles at this limit the number in $v'$ must remain constant. Hence at any time $t$, $Q$ of equations 11 and 12 can also be obtained as the summation of the particles in $v'$

$$Q = \int_0^{v'} c\, dv \qquad (13)$$

(18) B. R. Ray and W. R. Deason, THIS JOURNAL, 59, 956 (1955).

The solution to equation 9 is obtained by combining equations 11 and 13

$$\bar{v} = v' - \int_0^{v'} c\, dv/c_p \qquad (14)$$

Physically, equation 14 states that $\bar{v}$ is less than $v'$ by a volume calculated from the quantity of particles recovered in $v'$ divided by the plateau concentration. It is proof of the statement that the boundary position is the location of the step in concentration obtained by rearranging the particles to extend the plateau concentration in the region between $\bar{v}$ and $v'$. Equation 14 can be expressed differently using integration by parts

$$\bar{v} = \int_{c_a}^{c_p} v\, dc/c_p \qquad (15)$$

where $c_a$ is the concentration at $v = 0$ and $c_p$ is the plateau concentration at $v = v'$.

In the general case an additional relationship between $\bar{v}$ and $c_p$ can be obtained from the other basic differential equation 10. Note that the constant of integration is $c^0$, thus

$$c_p(1 + \bar{v}/V) = c^0 \qquad (16)$$

The equations 14 and 16 represent the general solutions to equations 9 and 10. All the relations used to calculate boundary position or initial concentration from schlieren, interferometric or absorption optical representations or from assay of preparative fractions follow as deductions. Of particular interest are the set formed by the simultaneous solution between equations 16 and 14, and then 16 and 15. First solving for $\bar{v}$

$$\bar{v} = \left[v' - \int_0^{v'} (c/c^0)\, dv\right] \Big/ \left[1 + \left(\int_0^{v'} (c/c^0)\, dv\right)\Big/V\right] \qquad (17)$$

$$\bar{v} = \left[\int_{c_a}^{c_p} v\, dc\right] \Big/ \left[c^0 - \left(\int_{c_a}^{c_p} v\, dc\right)\Big/V\right] \qquad (18)$$

and then for $c^0$

$$c^0 = c_p(1 + v'/V) - \left(\int_0^{v'} c\, dv/V\right) \qquad (19)$$

$$c^0 = c_p + \left(\int_{c_a}^{c_p} v\, dc\right)\Big/V \qquad (20)$$

**Boundary Location and Initial Concentration from Concentration and Concentration Gradient Distributions.**[19]—Equation 15 is already in a suitable form for determining $\bar{v}$ when the concentration distribution of particles is known, as in Fig. 4C. If $V$ is not infinite and the difference between the plateau concentration and the initial concentration can be measured, then an alternative relationship is obtained by rearranging equation 16

$$\bar{v} = (c^0 - c_p)V/c_p \qquad (21)$$

In order to determine $c^0$, equation 20 can be used, or it can be rewritten as

$$c^0 = c_a + \int_{c_a}^{c_p} (1 + v/V)\, dc \qquad (22)$$

To express the equations for $\bar{v}$ and $c^0$ in terms of concentration gradients (Fig. 4B), observe that $dc = (\partial c/\partial r)\, dr$, and $c_p = c_a + \int_{r_a}^{r_p} (\partial c/\partial r)\, dr$, in which $r_p$ is some level in the plateau region. Consider first the cases for which $c_a = 0$. Then from equation 15

$$\bar{v} = \frac{\int_{r_a}^{r_p} v(\partial c/\partial r)\, dr}{\int_{r_a}^{r_p} (\partial c/\partial r)\, dr} \qquad (23)$$

It is thus seen that, if $c_a = 0$, the boundary location is the first volume moment of the concentration gradient distribution. In actual calculation for the cases in which $V$ is not infinite (and $c_a = 0$), it is more convenient to write equation 23 as

$$V + \bar{v} = \frac{\int_{r_a}^{r_p} (V + v)(\partial c/\partial r)\, dr}{\int_{r_a}^{r_p} (\partial c/\partial r)\, dr} \qquad (24)$$

When equation 24 is expressed in terms of radius, a first moment will result for a uniform tube and a second moment for a sector cell. Williams, *et al.*,[5] have discussed the relationship between the moments and the familiar approximations as the location of the maximum ordinate and/or the half concentration point.

When $c_a \neq 0$ more calculation is needed to extract $\bar{v}$ from gradient measurements. Either $c^0$ must be known or the gradient distribution determined for several times during the centrifugation. First consider equation 22 rewritten as

$$c^0 - c_a = \int_{r_a}^{r_p} (1 + v/V)(\partial c/\partial r)\, dr \qquad (25)$$

This has been derived recently for the sector cell by Kegeles, *et al.*[20] Of course if $c_a = 0$, this equation enables determination of $c^0$. Otherwise the right-hand side can be plotted as a function of the value of the gradient at $r_a$, denoted by $(\partial c/\partial r)_{r_a}$. The intercept at $(\partial c/\partial r)_{r_a} = 0$ is $c^0$. Incidentally, the slope of such a plot is related to the molecular weight by the Archibald method.[17,20,21] With this value of $c^0$, equation 18 can be used for $\bar{v}$

$$\bar{v} = \frac{\int_{r_a}^{r_p} v(\partial c/\partial r)\, dr}{c^0 - \left(\int_{r_a}^{r_p} v(\partial c/\partial r)\, dr\right)\Big/V} \qquad (26)$$

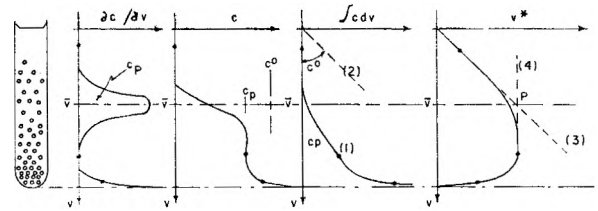


Fig. 4.—Boundary location in the ultracentrifuge: A, schematic representation of particle distribution after partial centrifugation; B, concentration $\partial c/\partial v$ distribution; C, concentration $c$ distribution; D, quantity $\int c\, dv$ distribution; E, apparent boundary position distribution $v^*$. Refer to text for explanation of symbols in the figures.

(19) When converted from $v$ back to the radius $r$, the equations of this section lead to the relationships used without derivation in the summary of sector cell equations for the calculation of schlieren optical patterns given elsewhere.[17] It has not been necessary to assume that there are no concentration gradients at the meniscus nor that the sedimentation coefficients are constant. Also, here the cell geometry need not be sector shaped.

(20) G. Kegeles, S. M. Klainer and W. J. Salem, THIS JOURNAL, **61**, 1286 (1957).

(21) R. Trautman and C. F. Crampton, *J. Am. Chem. Soc.*, **81**, 4036 (1959).

Again, for the cases in which $V$ is not infinite this can be rearranged to

$$V + \bar{v} = \frac{c^0 V}{c^0 - \int_{r_a}^{r_p} [(V + v)/V](\partial c/\partial r)\, dr + \int_{r_a}^{r_p} (\partial c/\partial r)\, dr} \quad (27)$$

## Part II. Theoretical Distribution Functions for the Analysis of Preparative Centrifugation

**Centrifugation and Assay.**—Initially, the tube is filled with the solution containing the particles of interest, oftentimes as a crude extract. The centrifugation is empirically terminated before all the particles have sedimented to the bottom, as in the hypothetical distribution of the particles indicated in Fig. 4A. Imagine an apparatus which will determine the concentration gradient, the concentration and the integral of the concentration as in Fig. 4B, C and D, respectively. These distributions represent point-by-point values plotted as a function of $v$, the volume between the meniscus and the level in question. Both $\bar{v}$ and $c^0$, the position of the boundary and the initial concentration of the corresponding component, respectively, can be determined from each of these curves. The appropriate equations for $\bar{v}$ are equations 23 and 15 for Fig. 4B and C, respectively. For the calculations involving quantity measurements (Fig. 4D), it will be advantageous to rearrange equation 14 as

$$\int_0^{v'} c\, dv = c_p v' - c_p \bar{v} \quad (28)$$

Here $v'$ represents values of $v$ in the (*a priori* unknown) plateau region of the tube. The integral $\int_0^v c\, dv$ for all values of $v$ is plotted in Fig. 4D. Equation 28 shows that the straight portion, indicated as line (1), locates the plateau region of the tube, and has $c_p$ for its slope and $\bar{v}$ for its intercept. The initial concentration $c^0$ is calculated from equation 16, after $c_p$ and $\bar{v}$ are obtained from the graphs, which are indicated in Fig. 4. The quantity representation is the only one for which it is practical to calculate the average concentration from the entire recovery

$$c_{avg} = \int_0^{v_b} c\, dv/v_b \quad (29)$$

where $v_b$ is the volume between the meniscus and the bottom of the tube. This value is shown in Fig. 4D as the slope of the dotted line (2) which passes through the data curve, marked (1), at $v_b$.

The initial concentration has special significance, for, by definition, the active agent can be assayed in the presence of other solutes. It should always be possible, then, for an aliquot of the starting material to be assayed in replicate at the same time the fractions are assayed. There are several reasons why the calculated value of $c^0$ from $c_p$ and $\bar{v}$ (equation 16) might be significantly less than the known starting value. (a) In the gradient method, there might be slower sedimenting material for which the boundary has not cleared the meniscus and so is not detected in Fig. 4B. (b) There might be faster sedimenting material which has completely sedimented into the bottom region of the tube. The gradient and concentration representations of Fig. 4 show sharp upturns at the bottom, in which such faster material would be undetected. Conceivably, the quantity distribution of Fig. 4D would reveal this if the average concentration of equation 29 equaled the known initial concentration. (c) There could have been inactivation of the agent during the experiment. (d) The conversion factor between the method used to measure the initial concentration and the gradient, concentration or quantity distribution of Fig. 4B, C, and D is in error. Since these limitations are important for any particular biophysical application, various ways of incorporating the known value of the initial concentration into the calculation of the data were considered. To do this the quantity distribution of Fig. 4D can be replaced by another distribution, which, by sacrificing the ability to calculate $c^0$ yields $\bar{v}$ and does portray limitations on the experiment listed above (a-d). This will be considered in the next section, in which equation 17 rather than 14 is used, since it contains $c^0$ as well as the concentration integral.

**Definition of the "Apparent Boundary Position" Distribution Function.**—Let the volume $v$ between the meniscus and the level in question be divided into $n$ not necessarily equal fractions, each of volume $\Delta v_i$. Let $q$ be the recovery of active agent calculated as the quantity recovered divided by the quantity initially present in the volume $v$. Thus

$$v = \sum_{i=1}^{n} \Delta v_i \quad (30)$$

$$q \equiv \sum_{i=1}^{n} c_i \Delta v_i / c^0 v \quad (31)$$

where $c^0$ and $c_i$ are the initial and recovered concentrations, respectively, in each of the fractions. The expression for $q$ can also be written as an integral if the point-by-point distribution of $c$ is known

$$qv = \int_0^v (c/c^0)\, dv \quad (32)$$

In the assay of the fractions it is not known, *a priori*, whether or not $v$ for a particular cut extends to the plateau and should be considered as $v'$. However, the right-hand side of equation 17 could be calculated for successive values of $v$ to determine the limiting value approached when $v$ reaches the plateau region. Prior to reaching this value the calculated values could be considered as apparent boundary positions. Thus define $v^*$ as the "apparent boundary position" distribution, valid for all the geometries of Fig. 3, and generalized from equation 17 as

$$v^* \equiv (v - qv)/(1 + qv/V) \quad (33)$$

with $q$ to be obtained from either equation 31 or 32.

If the fractionation level is in the supernatant fluid, $c = 0$, which makes $q = 0$ and $v^* = v$. This line, marked (3), is shown in Fig. 4E. For fractionation levels in the plateau, $v^* = \bar{v}$, which is the line marked (4) in Fig. 4E. The intersection of these two lines locates the same $\bar{v}$ determined from the concentration gradient, concentration or quantity distributions of Fig. 4B, C and D, respec-

tively. The $v^*$ curve is shown turned back to zero as the bottom of the tube is reached since, with all the material recovered, $q = 1$ and $v^* = 0$ from equation 33.

The apparent boundary position function will be especially useful when only a few fractions can be taken. Suppose that the dots indicated in Fig. 4 represent the data for just three fractions. Then, the $v^*$ plot (4E) locates $\bar{v}$, but the concentration plot (4C) does not.

An alternate form of equation 33 with $qv$ appearing only in one term, but not useful when $V$ is infinite, is

$$V + v^* = (V + v)/(1 + qv/V) \quad (33B, C)$$

This is the reciprocal of the antilog of the expression introduced by Tiselius, *et al.*,[22] for the two-compartment cell when expressed in volume coördinates, if $v$ is the volume of the upper compartment. Other forms have been reviewed by Ray and Deason.[18]

**Effect of the Error of the Assay.**—In sharp contrast to optical methods for determining concentration distributions, the biological assay of fractions involves large errors. Consider now the error in $v^*$ contributed by an error in the measurement of the concentration in each fraction. First differentiating $q$ with respect to $c$ in equation 32 gives $\mathrm{d}qv = (\mathrm{d}c/c)\int_0^v (c/c^0)\,\mathrm{d}v$ where it is assumed that $\mathrm{d}(c/c^0)/(c/c^0) = \mathrm{d}c/c$, a constant. Thus

$$\mathrm{d}q/q = \mathrm{d}c/c \quad (34)$$

Secondly, differentiating $v^*$ with respect to $q$ in equation 33 and substituting equation 34 yields

$$-\mathrm{d}v^* = (v - v^*)(\mathrm{d}c/c)[(1 + v^*/V)/(1 + v/V)] \quad (35)$$

The error $\mathrm{d}v^*$ will vanish when $v^* = v$, which occurs, as indicated above, when $q = 0$. On the other hand, after $v$ extends to the plateau region, the error increases proportionately to $(v - v^*)$, if $V$ is infinite. The limits $\pm\ \mathrm{d}v^*$ are shown in the shaded area of Fig. 5B for $\mathrm{d}c/c = 0.25$. The corresponding influence of this error in the concentration distribution is shown in Fig. 5A. It is important to observe that the error in the $s$-rate depends upon the range of values of $v^*$ for the best line in the plateau region. The greater the boundary spreading, the greater will be the influence of the assay error in locating the point P. The consequent error in $s$ is nevertheless smaller than if only one value of $q$ were known in the plateau region, say at point T, Fig. 5B. These considerations support the well known conclusion[23,24] that large assay errors do not mean that there is a commensurate error in the $s$-rate, provided one can find the centrifugal conditions for which a compartment is just emptied. A formula (equation 47) is derived from equation 33 in a later section for the error in $s$ for data from a single point in the concentration plateau.

**Two Components without Diffusion.**—In order to see the effects of heterogeneity on the $v^*$ plot,

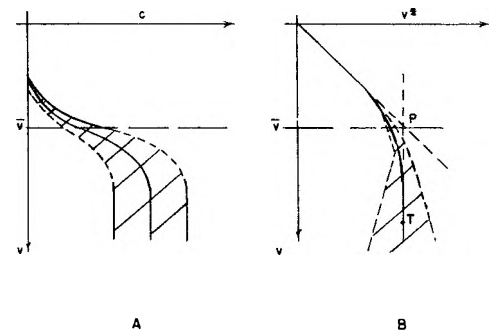


Fig. 5.—Effect of a 25% error in the assay on the $c$ and $v^*$ representations: A, concentration distribution; B, apparent boundary position distribution. Cross-hatching shows the limits for $\mathrm{d}c/c = 0.25$. Refer to text for explanation of symbols in the figures.

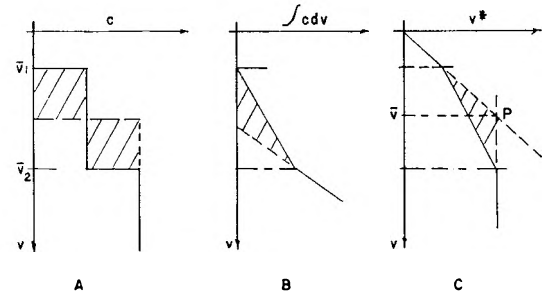


Fig. 6.—Two components without diffusion: A, total concentration $c$ after partial centrifugation moving slower component boundary to $\bar{v}_1$ and faster component boundary to $\bar{v}_2$; B, quantity distribution $\int c\,\mathrm{d}v$ corresponding to A; C, apparent boundary position $v^*$ corresponding to A. Cross-hatched region is the result of having two components not distinguished in the assay. P locates the weight average boundary position $\bar{v}$.

consider two components of $c_1^0$ and $c_2^0$ initial concentrations with their boundaries at $\bar{v}_1$ and $\bar{v}_2$, respectively, as indicated in Fig. 6A. Assume that there is no diffusion broadening each boundary region. In the supernatant, $v < \bar{v}_1$, $q = 0$, and $v^* = v$. The value of $v^*$ in the plateau region of the slower component, and then in the plateau containing both components will now be deduced, using the moving boundary theory of Part I.

When $\bar{v}_1 \leq v \leq \bar{v}_2$, $c_p = c_1^0/(1 + \bar{v}_1/V)$ from equation 16. In equation 31 $c^0 = (c_1^0 + c_2^0)$ since both components are considered indistinguishable in the assay. Thus equation 31 yields

$$qv = \int_{\bar{v}_1}^{v} \frac{c_1^0\,\mathrm{d}v}{(c_1^0 + c_2^0)(1 + \bar{v}_1/V)} = \frac{c_1^0(v - \bar{v}_1)}{(c_1^0 + c_2^0)(1 + \bar{v}_1/V)} \quad (36)$$

In equation 33 this gives

$$v^* = \frac{c_1^0\bar{v}_1/(1 + \bar{v}_1/V) + c_2^0 v/(1 + v/V)}{c_1^0/(1 + \bar{v}_1/V) + c_2^0/(1 + v/V)} \quad (37)$$

which is a continuously increasing function of $v$. For infinite $V$ it is a linear relationship.

Now in the plateau region containing both components, $c_p = c_1^0/(1 + \bar{v}_1/V) + c_2^0/(1 + \bar{v}_2/V)$, where $v \geq \bar{v}_2$, with the first term present from $\bar{v}_1$ to $v$ and the second from $\bar{v}_2$ to $v$; hence

$$(c_1^0 + c_2^0)qv = \int_{\bar{v}_1}^{v} [c_1^0/(1 + \bar{v}_1/V)]\mathrm{d}v + \int_{\bar{v}_2}^{v} [c_2^0/(1 + \bar{v}_2/V)]\,\mathrm{d}v \quad (38)$$

(22) A. Tiselius, K. O. Pedersen and T. Svedberg, *Nature*, **140**, 848 (1937).

(23) H. T. Epstein and M. A. Lauffer, *Arch. Biochem. Biophys.*, **36**, 371 (1952).

(24) S. S. Breese, Jr., and A. Briefs, *Proc. Soc. Exptl. Biol. Med.*, **83**, 119 (1953).

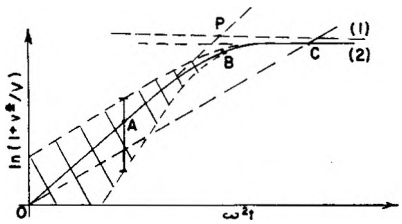


Fig. 7.—Determination of $s$-rate from data obtained with a two-compartment cell. $\omega$ is the angular velocity; $t$ is the time; $\ln (1 + v^*/V)$ is calculated from the quantity recovered in the upper compartment; P locates the maximum value of $\ln (1 + v^*/V)$ which is obtained when the upper compartment is just emptied, if the boundary remained infinitely sharp; slope of $\overline{OP}$ is the correct $s$-rate; cross-hatching shows the band the data would fall in if the assay error were ±25%; point A corresponds to stopping the centrifuge before the upper compartment is emptied; point B corresponds to just emptying the upper compartment; point C corresponds to centrifuging too long.

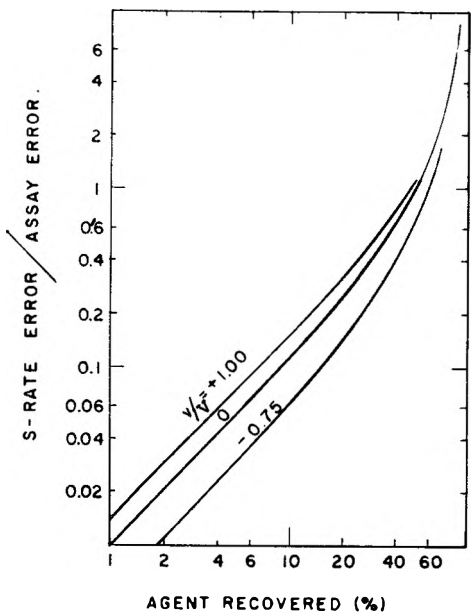


Fig. 8.—The error in the $s$-rate from a two-compartment experiment. $v/V$ is the ratio of the fluid volume in the supernatant compartment to the extended cell volume between the starting level and the axis of rotation; $v$ is negative for flotation; $V$ is infinite for a uniform cell in a uniform field. The error ratio is $ds/s/dq/q$ of equation 46, and the per cent. recovered is $q$ for the volume $v$.

and the corresponding expression for $v^*$ becomes

$$v^* = \frac{c_1^0\bar{v}_1/(1 + \bar{v}_1/V) + c_2^0\bar{v}_2/(1 + \bar{v}_2/V)}{c_1^0/(1 + \bar{v}_1/V) + c_2^0/(1 + \bar{v}_2/V)} = \frac{(c_p)_1\bar{v}_1 + (c_p)_2\bar{v}_2}{(c_p)_1 + (c_p)_2} \equiv \bar{v} \quad (39)$$

This is the value that $v^*$ of equation 37 reached when $v = \bar{v}_2$. It remains constant since equation 39 is independent of $v$, which canceled out in the derivation. A sketch of equations 37 and 39 is shown in Fig. 6C. The intersection of the only plateau line with the $v^* = v$ line determines the single value $\bar{v}$ for the experiment. In the case of infinite $V$, equation 39 indicates that this $\bar{v}$ will be a simple weight average of $\bar{v}_1$ and $\bar{v}_2$. In other cases equation 39 can be rearranged to a form similar to equations 33B and 33C as

$$V + \bar{v} = \frac{c_1^0 + c_2^0}{c_1^0/(V - \bar{v}_1) + c_2^0/(V + \bar{v}_2)} \quad (40)$$

which is slightly less than the simple weight average.

In principle the curve extending from $\bar{v}_1$ to $\bar{v}_2$ can be differentiated to obtain the concentration plot in order to determine whether the shaded area in Fig. 6C is a result of heterogeneity or diffusion. The procedure is to draw a smooth curve through the data on the $v^*$ plot to calculate the right-hand side of equation (41), rearranged from equations 32 and 33

$$\int_0^v (c/c^0)\, dv = (v - v^*)/(1 + v^*/V) \quad (41)$$

and then graphically to differentiate in order to get the concentration distribution

$$\frac{c}{c^0} = \frac{d}{dv}\left(\frac{v - v^*}{1 + v^*/V}\right) \quad (42)$$

**Conversion to $s$-Rate.**—The preceding sections indicate how to determine the boundary position $\bar{v}$ for any particular cell that is fractionated at several levels. The conversion of $\bar{v}$ to $s$-rate will depend upon the speed, time and temperature of the run and the geometry of the cell. Using equation 4 with the change in variable (equation 8), it follows for the four geometrical cases of Fig. 3, respectively, if $s$ is constant during the run, that

$$s = \bar{v}/(Agt) \quad (43A)$$
$$s = [\ln (V + \bar{v}) - \ln V]/(2\omega^2 t) \quad (43B)$$
$$s = [\ln (V + \bar{v}) - \ln V]/(\omega^2 t) \quad (43C)$$
$$s = \bar{v}/(2\omega^2 hKt) \quad (43D)$$

For both the uniform and sector cells in the centrifugal field, equations 43B and 43C indicate that $\ln (1 + \bar{v}/V)$ should be plotted against $\omega^2 t$ for all the experiments with possible differences in $V$ and/or $\omega^2$. The slope of the least squares line through the data is used to calculate the $s$-rate. (Corrections for any temperature variation during the run have been reviewed recently by Williams, *et al.*[5]).

Since the quantity $V$ appears in the calculations, it is important to know how accurately it must be determined. At the point P of Figs. 4, 5, 6, $q = 0$ and $v^*$ is independent of $V$ by equation 33. The influence of an error in $V$ comes then in the $s$-rate conversion. From equations 43B and/or 43C

$$\frac{-ds/s}{dV/V} = \left(\frac{1}{1 + \bar{v}/V}\right)\left[\frac{\bar{v}/V}{\ln (1 + \bar{v}/V)}\right] \quad (44)$$

The maximum value of the right-hand side is unity, for which the percentage error in $s$ equals the percentage error in $V$.

**Two-compartment Cell.**—If the experiment is conducted so that only two fractions are taken, an upper and a lower one, it will be denoted here as a two-compartment cell case. This situation would arise for (a) the partition cell of Tiselius, *et al.*,[22] (b) the separation cell of Yphantis and Waugh,[25] (c) the sheared capillary cell of Bradish, *et al.*,[26] (d) a centrifuge tube in which the component is just pelleted and the supernatant decanted, or (e) a plastic centrifuge tube which is sliced into two parts.[27] With only a two-compartment cell it is

(25) D. A. Yphantis and D. F. Waugh, THIS JOURNAL, **60**, 630 (1956).

(26) C. J. Bradish, J. B. Brooksby, J. F. Dillon and M. Norambuena, *Proc. Roy. Soc.* (*London*), **B140**, 107 (1952).

not possible to make a $v^*$ *vs.* $v$ plot (Fig. 4E), nor is it possible to make an $\int c\,dv$ plot (Fig. 4D). However, the concepts of the quantity type measurement still apply, and instead of varying $v$ as in fractionation, several runs can be made varying $V$, $\omega^2$ or $t$. Here it is essential to know $c^0$.

The function $v^*$ of equation 33 should be calculated, using the volume of the upper compartment for the only value of $v$. Then, plot ln $(1 + v^*/V)$ *vs.* $\omega^2 t$. For illustration, consider the case depicted in Fig. 7 for which $v/V$ is constant and hence the maximum value of the ordinate is ln $(1 + v/V)$, the line marked (1). The plot depends on several conditions: *i.e.*, only partial emptying of the upper compartment (A); diffusion of the boundary region or convection on fractionation (B); or residual contamination (C) leading to the constant line (2).

The correct $s$-rate is given by the slope of $\overline{OP}$. Evidently, several runs must be made in order to establish the curve through B, near P. Data obtained near C will yield too small an $s$-rate, slope $\overline{OC}$, because of centrifuging too long. On the other hand, the error in the $s$-rate, when only data near A are available depends on the assay error, denoted by the cross-hatching. This error can be derived from equations 35 and 43B or 43C for the uniform or sector cells in the centrifugal field

$$\frac{-ds}{s} = \frac{(v - v^*)(dc/c)}{(V + v)\ln(1 + v^*/V)} \qquad (45)$$

In terms of $q$ this can be written

$$\frac{-ds/s}{dc/c} = \frac{v/V}{(1 + qv/V)\ln(1 + v/V)}\left[\frac{q}{1 - [\ln(1 + qv/V)]/[\ln 1 + v/V]}\right] \qquad (46)$$

Equation 46 for infinite $V$ reduces to

$$\frac{-ds}{s} = \left(\frac{q}{1 - q}\right)\left(\frac{dc}{c}\right) \qquad (47)$$

an expression derived by Bradish, *et al.*[26] Equation 46 is shown plotted in Fig. 8 for various values of $v/V$. The range of values from 1.00 to $-0.75$ has been chosen to cover commonly used two-compartment cells, the negative values applying to flotation. It is seen that for any of the cell-field combinations in this range of $v/V$, the $s$-rate error is less than the assay error (*i.e.*, the ordinate is less than unity) if there is less than roughly 50% of the solute remaining.

## Part III. Experimental

The experiments to be described were chosen to simulate those situations for which numerous samples cannot be taken. There are several reasons why this might be encountered in biological experiments. First of all, the level of concentration of the agent may be such that a large volume, say 0.5–1.0 ml., is necessary for the assay. Secondly, the equipment may not be available to permit the collection of the numerous, small volume fractions. Thirdly, detailed experiments already may have established the optimum speed, time and cutting level for a particular agent, and it is desired to study, in a survey fashion, a large number of different starting samples. Fourthly, a sector-shaped cell is to be used, for other reasons, and the only ones presently available for high-speed runs are the two-compartment type. It should be emphasized[23] that the $s$-rate must be determined using the biological assay whether or not the agent is sufficiently concentrated to view with the optical systems of the analytical ultracentrifuge.

(27) Tube slicer of the E. C. Boyle type is available from Spinco (37).

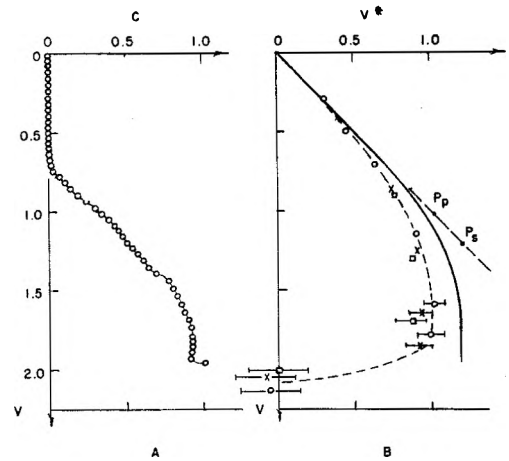


Fig. 9.—Preparative centrifugation of albumin; 35,600 r.p.m., 944 min., SW 39 rotor, 2-ml. quartz tubes, 18°. A, concentration $c$ scanned as optical density at 280 m$\mu$, as a function of the volume $v$ in ml. below the meniscus; B, apparent boundary position $v^*$ (ml.); circles, crosses and squares represent data from pipetted samples from 3 separate tubes, respectively; solid curve is obtained from the integral of the curve in A. Weight average $s$-rate calculated from $P_p$ is 3.7 $S$, from $P_s$, 4.2 $S$ (expected, 4.1 $S$).

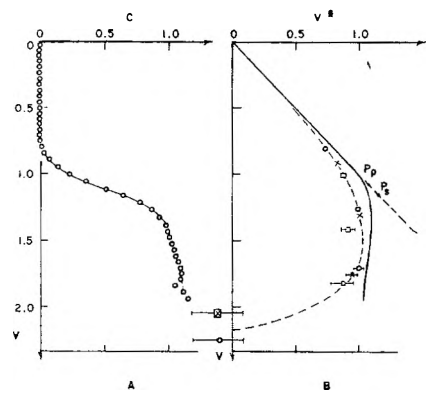


Fig. 10.—Preparative centrifugation of albumin–globulin mixture; 35,600 r.p.m., 757 min., SW 39 rotor, 2-ml. quartz tubes, 20°. A, B, see legend of Fig. 9. Weight average $s$-rate calculated from $P_p$ is 4.7 $S$; from $P_s$, 5.5 $S$ (expected, 5.4 $S$).

This section does not in any sense provide a verification of the theoretical relationships presented in Part I, and it provides only a limited check for Part II. Other workers have developed fractionation devices and established that a density gradient is required in order for the distribution to be an accurate representation of the sedimentation process.[7,8,28–32]

Two practical applications to $s$-rate determination of agents encountered in the foot-and-mouth disease virus system, the 140S virus and the 14S smaller complement-fixing particle, have appeared elsewhere.[33,34]

**Materials and Methods.**—Commercial preparations of bovine plasma albumin and $\gamma$-globulin were used as models in the 4S and 7S class, respectively. These proteins have

(28) A. Polson and A. M. Linder, *Biochim. et Biophys. Acta*, **11**, 199 (1953).

(29) G. W. Hogeboom and E. L. Kuff, *J. Biol. Chem.*, **210**, 733 (1954).

(30) N. G. Anderson, *Exptl. Cell Res.*, **9**, 446 (1955).

(31) E. L. Kuff, G. H. Hogeboom and A. J. Dalton, *J. Biophys. Chem. Cyt.*, **2**, 33 (1956).

(32) A. Polson, A. Ehrenberg and R. Cramer, *Biochim. et Biophys. Acta*, **29**, 612 (1958).

(33) R. Trautman, M. Savan and S. S. Breese, Jr., *J. Am. Chem. Soc.*, **81**, 4040 (1959).

(34) S. S. Breese, Jr., R. Trautman and H. L. Bachrach, *Arch. Biochim. Biophys.*, in press.

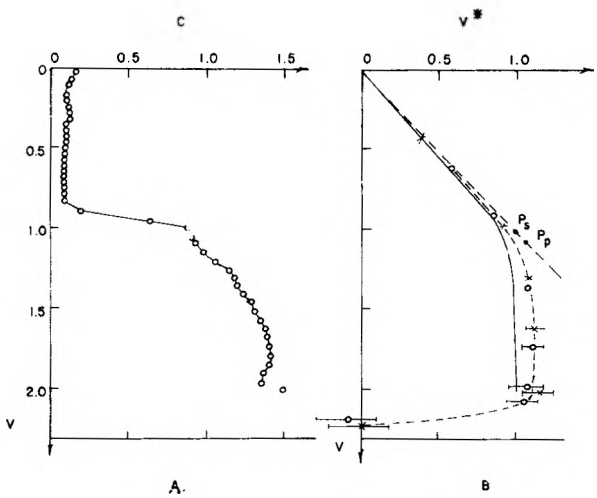

Fig. 11.—Preparative centrifugation of hemocyanin solutions; 25, 980 r.p.m., 77.2 min., SW 39 rotor, 2-ml. quartz tubes, 19°. A, B, see legend of Fig. 9, except optical density at 346 mμ. Weight average s-rate calculated from $P_p$ is 98 $S$; from $P_s$, 92 $S$ (expected, 90 $S$).

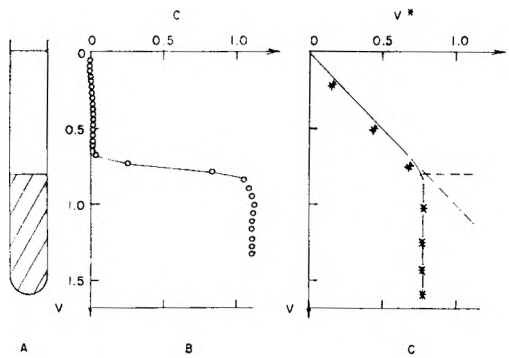

Fig. 12.—Fractionation of sharp boundary system without centrifugation. Initial boundary of 2 mg./ml. albumin at $v$ = 0.80 ml., as marked by cross-hatching; tube scanned and pipetted within 30 min. of careful layering, 2-ml. quartz tube. B, C, see legend of Fig. 9, except * represents data from pipetted samples.

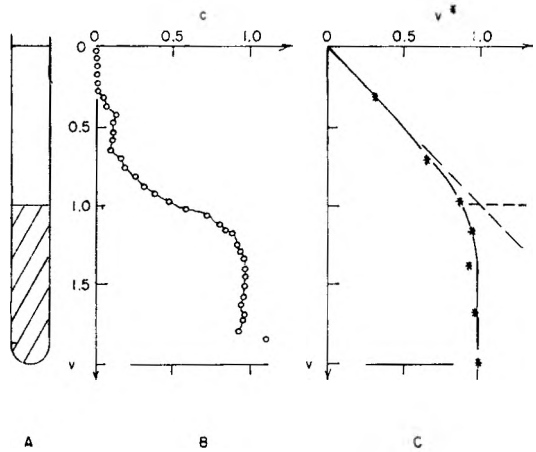

Fig. 13.—Fractionation of diffuse boundary system in the presence of a strong sucrose gradient without centrifugation. Initial boundary of 2 mg./ml. albumin layered at $v$ = 1.00 ml., as marked by cross-hatching, with sucrose gradient ranging from 0 to 18% concentration at the bottom of the tube; boundary broadened by twirling a saw-toothed wire paddle; 2-ml. quartz tube. B, C, see legend of Fig. 9, except * represents data from pipetted samples.

an absorption maximum at 280 mμ, and were made in and dialyzed against 0.1 *M* KCl. Blood from the sea snail *Busycon canaliculatum* was obtained from the Marine Biological Laboratory, Woods Hole, Mass. This contains hemocyanin molecules of 130S which dissociate easily into components of 80S and 100S.[35] Whole blood shows these components with a specific absorption at 346 mμ, characteristic of the oxidized form.[36] Such blood provides a convenient model system in the 80–130S range. Phosphate buffer of 0.1 ionic strength, *p*H 6.9 was used as diluent. These materials were chosen so that the concentration distribution, after preparative centrifugation, and the s-rate could be determined by optical methods.

The Beckman model DU spectrophotometer was used to measure the optical density at 280 or 346 mμ in a 1-ml., 1.0-cm. path, rectangular cuvette. Such measurements correspond to a specific assay for the biologically active agent since the buffer, salts and added sucrose have negligible absorptions at these wave lengths.

Centrifugation was done in a Spinco SW 39 rotor in a model E ultracentrifuge equipped with a thermistor temperature indicating and controlling device.[37] Both 5-ml. Lusteroid and 2-ml. quartz centrifuge tubes were used. These are of uniform cross-sectional area, and so correspond to the case of Fig. 3A, if not centrifuged, and of Fig. 3C, if centrifuged. In all centrifugation experiments, a sucrose gradient from 0–5% was used. This was obtained by adding crystalline sucrose to two aliquots of the protein solution and then layering these and one containing no sucrose in the centrifuge tube. The volumes were chosen so that the center layer was twice the volume of the bottom and top layers which were equal. A continuous gradient was made by twirling a saw-toothed wire inserted in the tube. Various solvent gradients were not tried as this matter has been carefully explored.[8,29,31] Corrections for the viscosity, density and osmotic pressure gradients have been given by others.[31,38,39]

Fractionation was accomplished with a Pasteur pipet of 1-mm. bore at the tip. Gentle suction from a firm rubber bulb was used to withdraw a mixture of solution and air bubbles from the meniscus.[40] The contents after each withdrawal were transferred to McNaught centrifuge tubes[41] marked in 0.01-ml. divisions up to 0.4 ml. and then wider divisions of 6.5 ml. After the volume of the fraction was recorded, appropriate dilution for the optical density measurement was made in the same tube.

To compare the results from the pipetted samples with the distribution before fractionation, a special adapter for the spectrophotometer was obtained from Spinco.[37] This permitted scanning the quartz centrifuge tubes at 1-mm. intervals along their length without disturbing the contents. Scanning was done at 280 mμ for the albumin–globulin mixtures and 346 mμ for the hemocyanin solutions.

The sedimentation data of the model systems used here were checked by analytical ultracentrifugation of identical solutions employing a double sector 12- or 30-mm. cell and phase-plate schlieren optics. The s-rate was calculated by standard methods from the photographic plates.

**Results.**—Typical results of experiments on the centrifugation and fractionation of albumin, albumin–globulin mixture and two hemocyanin components are shown in the figures. Figs. 9–11 deal with centrifugation and Figs. 12 and 13 just with fractionation.

Three comparisons are to be made in Figs. 9–11. The first comparison is between the s-rate obtained from pipetted fractions and the s-rate determined

(35) I.-B. Erikson-Quensel and T. Svedberg, *Biol. Bull.*, **71**, 498 (1936).

(36) J. Roche and P. Dubouloz, *Acad. Sci., Paris. Compt. rend.*, **196**, 646 (1933).

(37) Spinco Division, Beckman Instruments, Inc., Palo Alto, Calif.

(38) J. F. Thomson and E. T. Mikuta, *Arch. Biochem. Biophys.*, **51**, 487 (1954).

(39) J. F. Thomson and F. J. Klipfel, *ibid.*, **70**, 224 (1957).

(40) O. deLalla and J. W. Gofman, in "Methods of Biochemical Analysis," D. Glick, ed., Interscience Publishers, New York, N. Y., 1954.

(41) Kimble Glass Co., Toledo 1, Ohio, KIMAX #46800.

in the analytical ultracentrifuge. Figures 9B-11B show the function $v^*$, the apparent position of the boundary in the tube, as calculated from the recovered solute in the volume $v$ using equation 33. This function behaves as follows: if there were no solute, then the boundary position would be at least at the bottom of the volume at $v$, and $v^*$ would follow the dashed diagonal line. If fractions were made in the plateau solution, $v^*$ would be the boundary position $\bar{v}$, a constant value for the whole plateau region. The $v^*$ function returns to zero when all the contents of the tube are removed and indicates complete recovery of the solute. Since the dotted curve (Figs. 9B-11B) does become constant, it demonstrates the existence of a plateau of concentration. The value of $\bar{v}$ is obtained on the $v$ scale at the intersection of the line through the plateau data with the dashed diagonal line $v = v^*$. This value of $\bar{v}$ was converted to an $s$-rate with the speed and time data using equation 43C. In the case of two components (Figs. 10 and 11) a weight average value is obtained. The $s$-rate in the three cases illustrated is within 10% of that obtained from the analytical ultracentrifuge, as indicated in the legends.

The second comparison is made between the scanned concentration curve (Figs. 9A-11A) and that expected from an analytical experiment. It can be seen that the preparative ultracentrifuge does resolve the 4S and 7S components (Fig. 10A) and also the 80 $S$ and 100 $S$ components (Fig. 11A) when the concentration points can be plotted sufficiently close together.

The third comparison is between the solid curve from scanned data and the dotted curve from the pipetted data on the $v^*$ plot (Figs. 9B-11B). The data from several tubes fractionated at different levels were used to increase the number of points. The dotted and the solid curves do not coincide, but they are sufficiently similar to show that the pipetting procedure results in an $s$-rate which is comparable to that from data with a large number of points.

In order to determine what errors were introduced by the mixing involved in the pipetting procedure, several experiments were performed in which artificial distributions were made with albumin solutions layered in the 2-ml. quartz centrifuge tubes. The initial layers of two typical experiments are shown in Figs. 12A and 13A. The concentration c obtained by scanning the tube is indicated in Figs. 12B and 13B. The integral of the concentration and $v^*$ were calculated for both the scanned and pipetted data using infinite $V$ in equation 33. This $v^*$ is shown as the solid line and the asterisks in Figs. 12C and 13C. In both Figs. 12 and 13, the agreement is good. Comparing these results with Figs. 9–11, it would appear that a diffuse boundary in the lower sucrose gradient of 0–5% used in the centrifugation experiments was minimal, and that some stirring of the tube contents during fractionation may have occurred.

## Discussion

The inductive approach was used to obtain the two basic differential equations in volume coördinates. Our attempts to arrive at these as deductions from the general equation of continuity have failed. Perhaps others can supply such a derivation from general considerations of differential equations. In this connection, note that the true boundary position $\bar{r}$ (or $\bar{v}$), instead of being defined, appears automatically (with a different symbol) in the solution of special cases of the partial differential equation 1 by the method of characteristics by Fujita.[5,10] The approach here has been to focus attention on the existence of a plateau solution, and hence be able to work with total derivatives rather than the partials. Note also that the definition of $\bar{v}$ (the property which moves at the same $s$-rate as particles ahead of it), circumvents the early controversy in the electrophoresis literature as to which phase the mobility referred.[15,42] Evidently, the electrophoresis case can be similarly treated, with equations identical to those of the uniform field in a uniform cell, and with the result that the first moment of the gradient curve of an appearing species moves at the mobility of that species ahead of the boundary. The basic concepts of the moving boundary method are independent of the geometry of the cell or the nature of the force field. It is because centrifugation is done in a different, more complex situation that the moving boundary electrophoresis theory has not been adapted readily to the centrifuge. The volume generalization of such theory was never needed, since the experimenter was only confronted with the simplest case of a uniform field in a cylindrical tube or rectangular channel.

The hyperbolic cell, not seriously proposed as practical, was first considered when *changes* in the Johnston–Ogston effect[43] due to radial dilution during the experiment were being investigated.[11,44] Its use here is theoretically advantageous since it provides a situation in the centrifuge similar to the uniform cell in a uniform field. Here the volume between the center of rotation and some level is infinite and so would not be a suitable change in variable for $r$. Thus the hyperbolic cell serves to emphasize that the displacement from the starting level is important, not the location of a boundary with respect to the center of rotation. (Students frequently turn off the centrifuge as soon as the boundary clears the meniscus, and report that the material is homogeneous!) Cells that do not have sides conforming to the field are useful in non-optical applications since stabilizing density gradients can be employed which do not interfere with the concentration assay. Sector-shaped preparative tubes[30] may still require a density gradient to break the radial circulation, caused by the deceleration, into eddies across the cell.

It is important to stress that the several equations for $\bar{v}$ are not alternative methods of calculation for the same data. They are all the same equation with merely a change of variable. The appropriate equation depends upon the terms which are measured. Thus if a great many frac-

(42) H. Svensson, *Archiv. Kemi, Mineral. Geol.*, **22A**, No. 10, 1 (1946).

(43) J. P. Johnston and A. G. Ogston, *Trans. Faraday Soc.*, **42**, 789 (1946).

(44) R. Trautman, V. N. Schumaker, W. F. Harrington and H. K. Schachman, *J. Chem. Phys.*, **22**, 555 (1954).

tions are collected,[28-32] then it is the concentration distribution that is determined. But with only a few fractions, it is instead the quantity distribution. For this case the apparent boundary position representation $v^*$, in effect, treats the tube as a series of two-compartment cells with the level of the separation or partition varying. Of course, if the initial concentration is unknown, then one of the other formulas would be used. As one gets further into the study of the specific agent, certain short-cut procedures are possible (such as using the $\int c\,dv$ directly or using just a two-compartment cell). Eventually, the agent may be isolated in pure form and possibly studied optically in the analytical ultracentrifuge.

The comparison made in the experimental section between the optically scanned curve and the assay of pipetted fractions could be made here on the model systems because of the absence of any contaminants. However, the scanning technique could be used to locate known $s$-rate markers or to determine whether there were contaminants of similar $s$-rate to the unknown. Furthermore, the combination of the scanning device and quartz tubes in a swinging bucket rotor offers the possibility of converting a preparative ultracentrifuge into an absorption optics analytical ultracentrifuge for those laboratories not so equipped, or for those who choose to use several different wave lengths on the same sample.

## DISCUSSION

VERNE N. SCHUMAKER (University of Pennsylvania, Philadelphia) (communicated).—In reference to your comment that the development of the two generalized differential equations 9 and 10 depended on induction, I wonder if you have considered substituting $dv/dr = hy/2$ and $s = (dr/dt)/g$ into equation 3 and rearranging to $g(dv/dr)dc_p/dt + c_p d(gdv/dr)/dt = 0$ which is the perfect differential $d(c_p g dv/dr)dt = 0$. Then consider two general classes of cells and fields such that either $gdv/dr \propto v$ or a constant.

R. TRAUTMAN.—No, we have not made that substitution. Since you substituted for the $s$ in the plateau region, primes should appear on your terms to give $d(c_p g' dv'/dr'))/dt = 0$. (Primes really should be used in equation 3, but note that only the cases were considered for which the term in the square brackets is independent of $r'$). It is not immediately apparent how to go from your equation to equations 9 and 10 which involve v. But perhaps this can be done and thus provide a deductive derivation. Thank you for the suggestion.

# THE INTERPRETATION OF ABNORMALITIES IN THE LOG-NORMAL DISTRIBUTION OF PARTICLE SIZE

BY RIYAD R. IRANI

*Research Department, Inorganic Chemicals Division, Monsanto Chemical Company, St. Louis 66, Missouri*

*Received April 8, 1959*

It is well accepted that the distribution of particle size, in many processes of growth or breakage, obeys the log-normal law. In the present paper, basal cases where "non-ideal" log-normal distributions prevail are treated, and simple methods are presented for their resolution into the "parent" distributions. The cases of limited formation, multiple formation rates and boundary conditions, and artificial separation are discussed. Depending on whether the size distribution is on a number, surface or weight basis is it shown that abnormal log-normal distributions may or may not be detected.

## Introduction

The log-normal distribution law has been applied by several authors[1-8] to the distribution of sizes of particles obtained by crystallization and/or crushing. Hatch[9] and later Ames, *et al.*,[8] showed that if the particle size distribution gives a straight line on a number basis when plotted on log-probability graph paper, then the size distribution by weight or surface area is a parallel straight line on the same coördinates.

Kottler[10] has published an excellent discussion on "the goodness of fit and the distribution of particle sizes." Kottler[11] also showed how to handle algebraically the size distribution encountered by Loveland and Trivelli[12] during the study of photographic emulsions, where it was found that the simple log-normal distribution does not fit the data. This article presents an interpretation and discussion of possible basal cases whereby a *modified* log-normal distribution is obeyed. The interpretations are particularly useful for powders obtained through fractionation, spray drying and/or controlled formation. They are also useful in the measurement of particle size through the use of the Tyndall spectra (the variation of scattered light with wave length) where Heller and others[13-15] have shown that the tool is powerful for monodisperse systems and would be more generally applicable if the distribution function of the particles had been known *a priori*.

## Experimental

The particle size distribution measurements were made according to previously described techniques.[8]

**Limited and Unlimited Formation.**—Kottler[5] was the first to treat size distribution from a kinetic

(1) P. Drinker, *J. Ind. Hyg. Tox.*, **7**, 305 (1925).
(2) J. B. Austin, *Ind. Eng. Chem., Anal. Ed.*, **11**, 334 (1939).
(3) T. Hatch and S. Choate, *J. Franklin Inst.*, **207**, 369 (1933).
(4) B. Epstein, *ibid.*, **244**, 471 (1947); *J. Appl. Phys.*, **19**, 140 (1948); *Ind. Eng. Chem.*, **40**, 2289 (1948).
(5) F. Kottler, *J. Franklin Inst.*, **250**, 339 (1950); **250**, 419 (1950).
(6) G. W. Phelps and S. G. Maguire, *J. Am. Ceram. Soc.*, **40**, 403 (1957).
(7) O. Menis, H. P. House and C. M. Boyd, ORNL 2345, Chemistry-General, Oak Ridge, Tenn., Atomic Energy Commission Unclassified Report.
(8) D. P. Ames, R. R. Irani and C. F. Callis, THIS JOURNAL, **63**, 531 (1959).
(9) T. Hatch, *J. Franklin Inst.*, **215**, 27 (1933).
(10) F. Kottler, *ibid.*, **251**, 499 (1951); **251**, 617 (1951).
(11) F. Kottler, THIS JOURNAL, **56**, 442 (1952).
(12) R. P. Loveland and A. P. H. Trivelli, *J. Franklin Inst.*, **204**, 193 (1927); **204**, 377 (1927); THIS JOURNAL, **51**, 1004 (1947).
(13) W. Heller and E. Vassy, *Phys. Rev.*, **63**, 65 (1943).
(14) W. Heller and E. Vassy, *J. Chem. Phys.*, **14**, 565 (1946).
(15) A. B. Loebel, *Ind. Eng. Chem.*, **51**, 118 (1959).

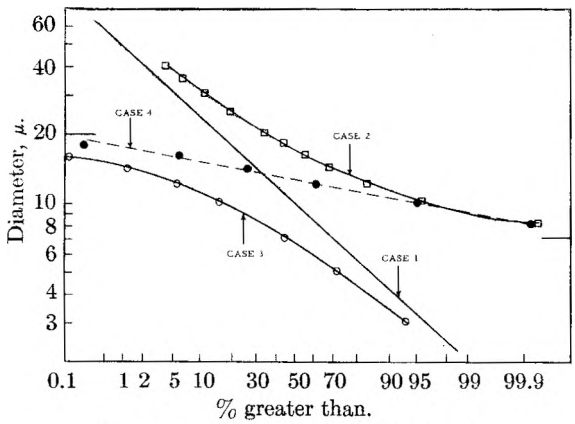


Fig. 1.—Limited and unlimited growth.

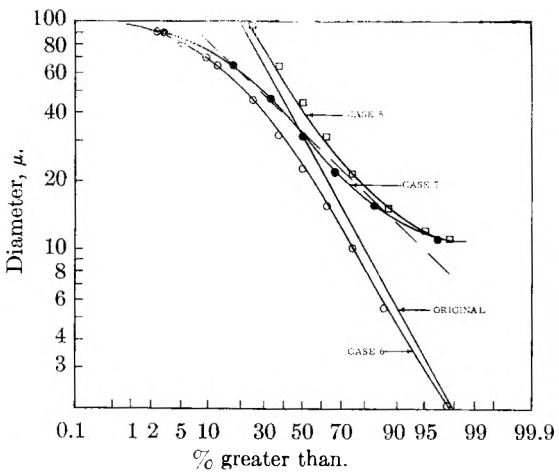


Fig. 2.—Artificial separation: case 7, if $10\ \mu > x > 100\ \mu$ removed; case 5, if $x < 10\ \mu$ removed; case 6, if $x > 100\ \mu$ removed.

point of view. In general, it can be assumed that the size $x$ of a particle grows or diminishes according to the equation

$$\frac{dx}{dt} = \phi(x) \qquad (1)$$

where $t$, the time of growth or disappearance is normally distributed

$$f(t) = 1/\sqrt{2\pi}\exp(-t^2/2) \qquad (2)$$

where $f(t)$ is the probability of a particle growing or diminishing for a time interval $t$. The function $\phi(x)$ can be expressed as

$$\phi(x) = K\frac{(x - x_0)(x_\infty - x)}{(x_\infty - x_0)} \qquad (3)$$

where $x_0$ and $x_\infty$ are the minimum and maximum sizes formed, respectively, while $K$ is a velocity constant of formation. It is significant to note that when $x$ is equal to either $x_0$ or $x_\infty$ then $x$ becomes time independent. If equation 3 is combined with equation 1 and integrated then

$$t = a + b\ln\frac{(x - x_0)(x_\infty - x_0)}{(x_\infty - x)} \qquad (4)$$

where $a$ and $b$ are constants.

If equation 4 is substituted into equation 2, then it can be shown that

$$f(x) = \frac{1}{\sqrt{2\pi}\ln\sigma}\exp\left[-\left(\frac{\ln\left\{\frac{(x - x_0)(x_\infty - x_0)}{(x_\infty - x)}\right\} - \ln M}{\sqrt{2}\ln\sigma}\right)^2\right] \qquad (5)$$

where $f(x)$ is the probability of occurrence of size $x$, and $M$ and $\sigma$ are the geometric mean diameter and geometric standard deviation,[8] respectively. From equation 5 we note that $f(x) \to 0$ as $x$ approaches either $x_0$ or $x_\infty$. Equation 5 can be integrated to yield $P$ the per cent. greater than diameter $x$

$$P = 100\int_{x=x}^{x=\infty} f(x)\,d\ln[(x - x_0)/(x_\infty - x)] = 50 - 100\,\mathrm{erf}\left[\frac{\ln\frac{(x - x_0)(x_\infty - x_0)}{M(x_\infty - x)}}{\ln\sigma}\right] \qquad (6)$$

The special cases of equation 6 are as follows:

**Case 1.**—If $x_0 = 0$ and $x_\infty \to \infty$, then equation 6 reduces to the *simple* log-normal distribution that gives a straight line on log probability axis as shown in Fig. 1 for $M = 10\mu$ and $\sigma = 2$. This case corresponds to *unlimited formation.*

**Case 2.**—Figure 1 also illustrates the case when $M = 10\mu$, $\sigma = 2$, $x_\infty \to \infty$ but with $x_0 = 7\mu$. The curve is shown to be asymptotic to $7\mu$; the points are calculated from equation 6. Here if $(x - x_0)$ rather than $x$ had been plotted on log probability paper, a straight line would have been obtained. The case with $x_0 > 0$ has been used by several authors of whom we can mention Sheppard, *et al.*,[16] and Gaddum.[17]

**Case 3.**—When $x_\infty \neq \infty$ a plot similar to the one shown as case 3 in Fig. 1 is obtained. The curve is always asymptotic toward the upper limit diameter, as illustrated in Fig. 1 for $x_\infty = 20\ \mu$, $M = 10\mu$ and $\sigma = 2$. If $(xx_\infty/(x_\infty - x))$ rather than $x$ had been plotted on log-probability paper, a straight line would have been obtained.

**Case 4.**—If $x_0 = 7\mu$, $x_\infty = 20\mu$, $M = 10\mu$ and $\sigma = 2$ the plot shown in Fig. 1 is obtained. The interesting point here is that similar plots do not deviate significantly from a straight line (shown dotted) and when the data are obtained experimentally it is not justifiable to use the 4-parameter fit indicated above, but rather *two* new parameters, namely, $M' = 12.6\mu$ and $\sigma' = 1.18$. The importance of this conclusion is that although most powders are formed according to the kinetic equation describing case 4, the evaluation of experimental data indicates simple unlimited-growth type log normal distribution. Thus, although a particular substance under specified conditions has a specific rate constant $K$ the values of $M'$ and $\sigma'$ can be varied by changing $x_0$, *e.g.*, nucleation or finer grinding, and $x_\infty$, *e.g.*, changing the time function by shortening or prolonging the particle formation period.

For cases 2 and 3 $x_0$ and $x_\infty$ are located easily from the asymptotical character of the curve.

**Artificial Distributions.**—Cases 2 through 4 cover the modifications in the log-normal distribution

(16) S. E. Sheppard, E. D. Wightman and A. P. H. Trivelli, *Phot. J.*, **49**, 134 (1925).

(17) J. H. Gaddum, *Nature*, **156**, 463 (1945).

due to variables controlling the formation of the particles. However, after formation, powders are generally tampered with, either through dust separation by cyclones or removal of coarse particles (or combinations of these and similar operations) as described in cases 5–7 below and illustrated in Fig. 2.

**Case 5.**—If particles below a certain diameter $x_1$ are removed, *e.g.*, cyclone dust removal, a curve asymptoting toward $x_1$ is obtained. In Fig. 2, $x_1 = 10\mu$, $M = 32\mu$, $\sigma = 4$.

**Case 6.**—If particles above a certain diameter $x_m$ are removed, *e.g.*, precise sieving or collecting the fines in a cyclone, a curve asymptoting toward $x_m$ is obtained. In Fig. 2, $x_m = 100\mu$, $M = 32\mu$, $\sigma = 4$.

**Case 7.**—This is a combination of cases 5 and 6. In Fig. 2, $x_m = 100\mu$, $x_1 = 10\mu$, $M = 32\mu$ and $\sigma = 4$. Case 7 is similar to case 4 in that a straight line, shown dashed in Fig. 2, can adequately represent the data.

The original distribution can be obtained for case 6 by first estimating the "per cent. finer than" $(100 - P°)$ that would have been observed had there been no removal of particles bigger than the diameter exhibiting an asymptote, and then dividing the "per cent. finer than" by $100/P°$ at various diameters to get the original distribution exhibiting log normal behavior. The value of $P°$ can be estimated within 10% by extrapolating the straight line observed at low diameters to the diameter exhibiting an asymptote. If the chosen value of $P°$ does not render a straight line the fit can be improved either by increasing or decreasing $P°$ as illustrated in Fig. 3. The data shown in Fig. 3 are for a sample of clay that had been treated to remove large particles; it is shown that by making only two approximations one can obtain the *parent* size distribution curve and also the amount of clay that had been removed above $45\mu$.

Case 5 can be treated in the same manner as Case 6 except that $P°$ is used in place of $(100 - P°)$.

A question that arises at this point is whether Cases 5, 6 and 7 are significantly different from those of 2, 3 and 4. It turns out to be that they are different and that they can be distinguished easily from a histogram plot. For cases 2, 3 and 4 the size-frequency plot has a definite slope at $x_0$ and $x_\infty$ as compared with cases 5, 6 and 7 where a discontinuity in the size-frequency curve is obtained at $x_1$ and $x_m$. This phenomenon is illustrated in Fig. 4 for cases 2 and 5, where it can be easily seen that although $x_1$ and $x_0$ were identical for a particular distribution, the two cases gave histograms exceedingly different near $x_1$ nd $x_0$.

**Heterogeneous Distributions.**—Kottler[11] has discussed the problem of homogeneous *vs.* bi-modal heterogeneous particle size distributions from an algebraic-statistical point of view. Although the approach is rigorous, it is time consuming; and, due to the unavoidable experimental error in size determination, it becomes less advantageous as compared to the semi-graphical approach given below.

Heterogeneous particle size distributions generally arise either due to mixing of powders or due to

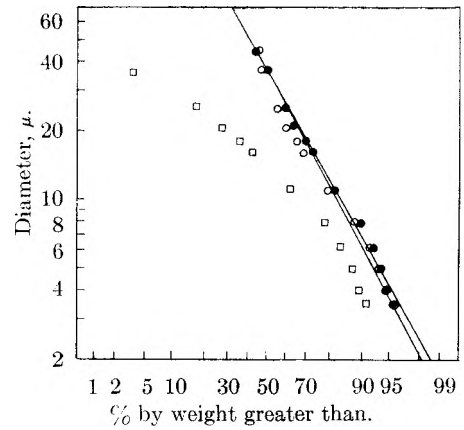


Fig. 3.—○, for $P° = 55\%$; ●, for $P° = 50\%$; □, experimental points.

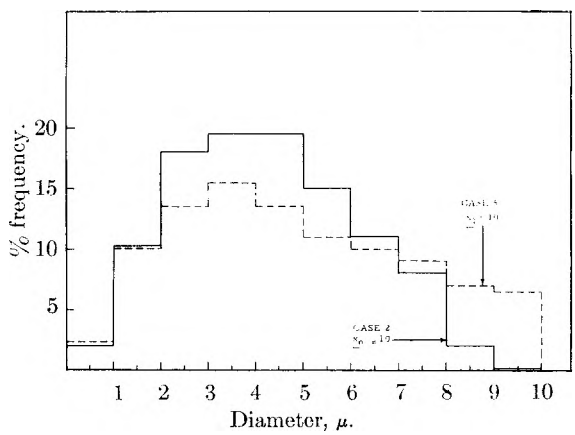


Fig. 4.—Histograms for cases 2 and 5 with $M = 6.5$ and $\sigma = 2.31$.

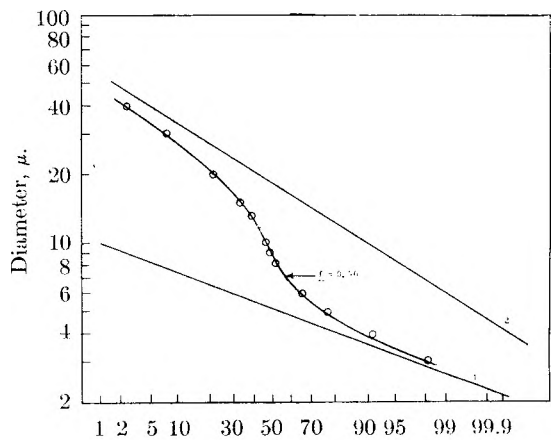


Fig. 5.—Heterogeneous distribution case 8a.

different rates and boundary conditions existing during the formation of the particles, *e.g.*, different shape particles and/or crystal habits. Thus, if one had an *nth-modal* distribution, meaning $n$ populations, then $P$ can be expressed as

$$P = 50 - 100 \sum_{i=1}^{i=n} f_i \operatorname{erf} \left[ \frac{\ln \left\{ \frac{(x - x_{0i})(x_{\infty i} - x_{0i})}{M_i (x_{\infty i} - x)} \right\}}{\ln \sigma_i} \right] \quad (7)$$

where the subscript i refers to a particular popula-

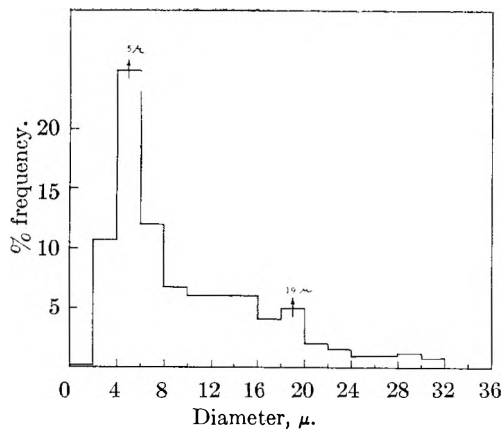


Fig. 6.—Histogram of heterogeneous distribution case 8a.

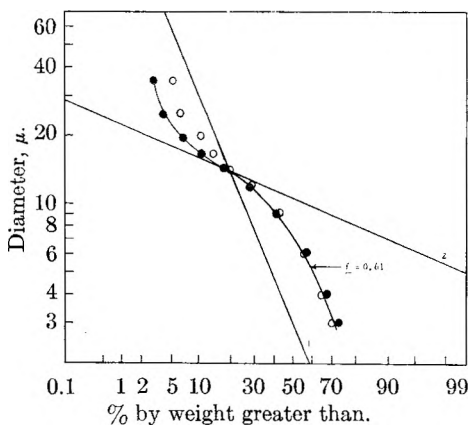


Fig. 7.—Heterogeneous distribution case 8b: ●, measured; ○, calculated.

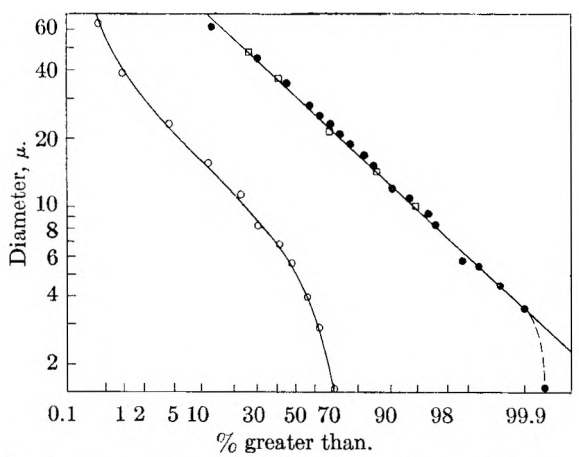


Fig. 8.—●, weight convert of number data; ○, number data (cintel); □, weight data (sedimentation).

tion. However, in most practical cases $n = 2$ and in the following special cases it will be also assumed that $x_{0i} = 0$ and $x_{\infty i} \rightarrow \infty$. In both cases a good estimate of $M_1$ and $M_2$ can be made from the size-frequency histogram as illustrated by Whitby[18] for a sample of flour.

**Case 8a.**—If the parent distribution curves do not intersect on a log probability plot, a curve similar to that shown in Fig. 5 is obtained. The characteristic of the plot is that it asymptotes at its upper and lower levels to two non-horizontal lines, these lines being the parent distributions (equation 7).

As an example the experimental points shown in Fig. 5 are treated as follows to obtain the parent distributions. The data are plotted on a size-frequency histogram as shown in Fig. 6 to obtain $M_1 = 5\mu$ and $M_2 = 19\mu$. Equation 7 becomes

$$P = 50 - 100f \operatorname{erf}\left(\frac{\ln x/5}{\ln \sigma_1}\right) - 100(1 - f) \operatorname{erf}\left(\frac{\ln x/19}{\ln \sigma_2}\right) \quad (8)$$

where $f$ is the fraction $f_1$. The next step is to get a first approximation of $\sigma_1$ and $\sigma_2$ from the asymptotes of the experimental points and compute the value of $f$ at various values of $P$. If the value of $f$ turns out to be independent of $P$ and $x$, then the estimated values of $\sigma_1$ and $\sigma_2$ are accurate. Otherwise successive approximations are necessary. Table I demonstrates the relative constancy of $f$ for the data in Figs. 5 and 6 after only two successive approximations to obtain $\sigma_1$ and $\sigma_2$. The calculated $f$ values at the lowest values of $x$ tend to be off due to the high dependence upon $(100 - P)$ shown in equation 8; at low values of $x$, the value of $P$ usually cannot be determined with enough accuracy, so that the calculated $f$ can be ignored in that region.

**Case 8b.**—If the parent distribution curves intersect on a log probability plot, a curve similar to that shown in Fig. 7 is obtained. However, in this case the experimental points asymptote at both ends of the distribution toward the original parent distribution with the higher $\sigma$. The asymptotes do not approach specific diameter values as was observed in case 8a. However, the point of inflection turns out to be an important point since both parent curves must go through it. Therefore, to resolve the example given in Fig. 7, the data are first plotted on a histogram (as was done in Fig. 6) to obtain $M_1$ and $M_2$ which in this case turns out to be 3.0 and 10.5$\mu$, respectively. The point of inflection can then be located very accurately by drawing the tangents to the curve and locating the point of maximum change of slope, 14$\mu$ in this example. $M_1$ and $M_2$ are located on 50% probability and connected to the point of inflection by

TABLE I

HETEROGENEOUS DISTRIBUTION EXAMPLE FOR CASE 8a

| $x$ | $P_{(meas.)}$ | $f_{calcd.}$[a] |
|---|---|---|
| 3 | 98.3 | 0.85 |
| 4 | 91 | .51 |
| 5 | 77 | .46 |
| 6 | 65 | .45 |
| 8 | 52 | .48 |
| 9 | 49 | .48 |
| 10 | 46 | .51 |
| 13 | 39 | .51 |
| 15 | 33 | .52 |
| 20 | 21 | .54 |
| 30 | 7.5 | 53 |
| 40 | 2.5 | 46 |
| Av.[b] | | 0.50 ± 0.03 |

[a] Assuming $M_1 = 5\ \mu$, $M_2 = 19\ \mu$, $\sigma_1 = 1.28$, $\sigma_2 = 1.56$. [b] Ignoring the value at $x = 3$.

(18) K. T. Whitby, *Heating, Piping, Air Conditioning*, **27**, No. 6, 139 (1955).

straight lines to obtain $\sigma_1 = 6.0$ and $\sigma_2 = 1.47$. The values of $f$ are then computed from equation 9 at various measured values of $P$ and $x$

$$P = 50 - 100f \operatorname{erf}\left(\frac{\ln x/3}{\ln 6}\right) - 100(1 - f) \operatorname{erf}\left(\frac{\ln x/10.5}{\ln 1.47}\right) \quad (9)$$

The calculated values of $f$ are shown in Table II, and are erratic for the low values of $P$ due to the high dependence of $f$ on the measured values of $P$; unavoidable experimental errors in $P$ can cause variations in $f$ as shown for $x = 14\mu$ and $x = 17\mu$. However, if the average value of $f$ is taken and $P_{\text{calcd}}$ compared with $P_{\text{measd}}$ the average difference is only ± 2 which is definitely within the ± 5 for the experimental error. Thus, from only one estimate an excellent resolution was obtained. For all the resolutions we have done it was not necessary in any situation to do more than three approximations. Table III shows the agreement between calculated $f$ and known values of $f$ for synthetic powdered mixtures.

TABLE II

HETEROGENEOUS DISTRIBUTION EXAMPLE FOR CASE 8b

| $x(\mu)$ | $P_{(\text{measd.})}$ | $f_{(\text{calcd.})}$[a] | $P_{(\text{calcd.})}$[b] | $\Delta$[c] |
|---|---|---|---|---|
| 3.0 | 71 | 0.58 | 69.0 | 2.0 |
| 4.0 | 66 | .60 | 65.3 | 0.7 |
| 6.0 | 56 | .63 | 57.6 | 1.6 |
| 9.0 | 42 | .62 | 42.3 | 0.3 |
| 12.0 | 28 | .63 | 28.3 | 0.3 |
| 14.0 | 20 | ( .77) | 20.4 | 0.4 |
| 17.0 | 10 | ( .06) | 14.1 | 4.1 |
| 20 | 6.5 | .... | 10.8 | 4.3 |
| 25 | 4.0 | .... | 8.5 | 4.5 |
| 35 | 3.0 | .... | 5.1 | 2.1 |
| | | Av.[d] 0.61 ± 0.02 | | |

[a] Assuming $M_1 = 3.0\ \mu$, $M_2 = 10.5\ \mu$, $\sigma_1 = 6.0$, $\sigma_2 = 1.47$. [b] Assuming $a$ and $f = 0.61$. [c] $P_{\text{calcd}} - P_{\text{measd.}}$ [d] For $14\ \mu > x > 3\ \mu$.

TABLE III

HETEROGENEOUS DISTRIBUTION

| $f_{\text{calcd.}}$ | $f_{\text{known}}$[a] | $f_{\text{calcd.}}$ | $f_{\text{known}}$[a] |
|---|---|---|---|
| 0.50 | 0.50 | 0.18 | 0.20 |
| .61 | .67 | .72 | .75 |
| .30 | .33 | .66 | .67 |
| .85 | .80 | | |

[a] From synthetically mixing known weights of two powders.

In some rare cases where *limited growth* distributions are combined, the treatments presented for cases 8a and 8b do not apply directly and the complexity of the problem of resolution increases "exponentially."

**Number–Surface–Weight Distributions.**—As was shown previously[8] the value of $P$ depends to a large extent on whether it is referred to a number, surface or weight basis. Thus, if one had the hypothetical case of equal numbers of spherical particles having 1 and 10$\mu$ diameters then the contribution of the small particles to the mixture is ($^1/_2$) on a number basis, ($^1/_{101}$) on an external surface basis and ($^1/_{1001}$) on a weight basis. When abnormal distributions are encountered they may be important on a number basis and not on a surface or weight basis, and *vice versa*. Figure 8 illustrates this point clearly. The number–size distribution shows definite bi-modality while the weight convert of the data and the measured weight size distribution agree with one another and show log normal behavior in all practical regions. The dotted line shown in Fig. 8 is where the weight-size distribution starts deviating from a straight line. Many other similar examples have been observed for cases 2–8.

**Acknowledgment.**—The author wishes to thank Dr. D. P. Ames and Dr. C. F. Callis for helpful discussions and Mr. W. W. Morgenthaler for making some of the measurements.

## DISCUSSION

M. J. VOLD (University of Southern California).—To what extent does the log normal distribution depend critically on the assumed form of $\phi(x)$? And have you found any instances in which departure from the log normal distribution could be due to $\phi(x)$ having a different form?

R. R. IRANI.—The dependence of the log normal distribution law on the assumed form of $\phi(x)$ lies only in the proper choice of $X_0$ and $X_\infty$. During our investigations which covered hundreds of powdered materials we have found that the particle size distribution can be very well represented by one of the cases described in this article.

W. HELLER (Wayne State University).—How sensitive are the $f$ values to choice of the parameters needed for their calculation?

R. R. IRANI.—In the worst case we have had to make three approximations to arrive at $f$ values that do not deviate by more than 2 per cent. and are random in character.

W. HELLER.—Do you think there is any chance of applying your method of analysis to systems with three components?

R. R. IRANI.—Yes, but adding three new parameters complicates matters.

# SEDIMENT VOLUME AND STRUCTURE IN DISPERSIONS OF ANISOMETRIC PARTICLES[1]

BY MARJORIE J. VOLD

*Department of Chemistry, University of Southern California, Los Angeles 7, California*

*Received March 6, 1959*

The sedimentation of dilute dispersions of randomly oriented rod-like particles has been simulated by a numerical model employing a high speed digital computer. For a model in which the particles cohere to each other on initial contact the volume per cent. solids in the sediment decreases uniformly from 12.8% for a length/width ratio of unity to 1.46% for a length/width ratio of 18. End-to-end and end-to-center contacts predominate over crossed structures in the sediment. The proportion of particles making more than two contacts with other particles and hence helping to develop rigidity in the sediment increases slightly as the length to width ratio increases. Suspensions of lithium stearate in benzene appear to conform to the model used in calculations so far as cohesion on contact is concerned, but exhibit preferred end-to-end contacts in 7-fold excess of that predicted for random orientation during settling.

The volume occupied by the sediment resulting from complete settling of a suspension is commonly regarded as related to its tendency toward flocculation but is not yet a useful measure of the dominant factor, particle interaction, which controls flocculation behavior. In previous work[2] it has been shown that the sediment volume of moist glass spheres in toluene, 13% solids, can be derived from a theoretical model based on the hypothesis that each sphere coheres rigidly to each other sphere that it contacts as it falls. The present work extends this calculation to rigid rod-like particles with the same hypothesis of strong interaction, and compares the results with the observed sediment volume of lithium stearate in benzene.

A large mass of data exists concerning the sediment volumes of various powdered and colloidal materials in various liquids, with and without additives. Shur[3] has given an extensive review which serves to emphasize many of the important ideas involved in establishing a basis for utilizing such measurements. Flocculation and sedimentation of both flocs and primary particles occur simultaneously without pronounced stratification of particle or floc sizes in the sediment. Large sediment volumes, *i.e.*, small concentrations of solids in the sediment, result from sedimentation of suspensions of anisometric particles and from suspensions in which flocculation builds a loose scaffold type structure. The volume fraction of solids in the sediment tends to be large for isometric particles and also at the two extremes of little floc formation and compact floc formation. The observed values vary between wide limits, from a few tenths of a per cent. to as much as 65% volume fraction of solids.

The process of floc or sediment formation can be simulated by an iterated calculation in which one particle at a time is placed at an arbitrary location within the range of the field of force emanating from the growing floc, initially a single particle, and its subsequent fate determined according to the characteristics ascribed to this field. For sedimentation the interparticle forces act in conjunction with the vertical fall of the particles while for pure flocculation they are superposed on thermal motions. The goal of the program, of which the work here reported is a part, is to evaluate the magnitude of particle interactions in comparison with thermal and gravitational (or centrifugal) forces. However, the present calculation is concerned primarily with the role of particle shape for the case of unstable suspensions in which the effect of motion under gravity is only to bring the particles into mutual proximity.

**Theoretical Calculation.**—Rod-like particles of varying length to width ratio are simulated by linear assemblies of mutually tangent spheres. The particles are initially positioned in random orientation and random location above a rectangular container. The particles are numbered consecutively from one to $K$ and the member spheres of each particle are also numbered from one to $J$ with the lowest lying member assigned to $J = 1$. Each particle in turn is then permitted to drop into the container (*i.e.*, its $z$-coördinate is reduced) until its fall is arrested either by contact with a previously dropped particle or by the bottom of the container. After the arrest, the final $x$, $y$ and $z$ coördinates of each member sphere of the aggregate, the identification number (1) of the particle causing the arrest, and the identification numbers ($J$) of the member spheres which contact each other to produce the arrest are all recorded. After a predetermined number of particles has been processed in this way the number of member spheres whose centers lie within each of twenty-four equal successive ranges of $Z$ extending from $Z = 0$ to the largest $Z$ recorded are counted, first for all spheres and then for those whose $x$ and $y$ coördinates lie in various ranges.

Figure 1 is a schematic flow sheet for performance of this calculation which was carried out on an IBM 709 computer. Table V is a sample of the out-put from the computer for a length/width ratio of 3, *i.e.*, three member spheres per particle. The procedure employed to determine the sediment volume and sediment structure for each complete set of results can be illustrated by considering the sample given in Table I.

The layer population is constant, apart from fluctuations, up to layer 13, but beyond that exhibits a downward trend. This means that the 400 particles dropped were sufficient to fill up 13 levels, but that higher levels still contain holes which would be filled were the computation continued.

(1) This work was supported in part by the Office of Ordnance Research, U. S. Army. Computer facilities were provided by the Western Data Processing Center, University of California at Los Angeles.

(2) M. J. Vold, *J. Coll. Sci.*, **14**, 168 (1959).

(3) E. G. Shur, *Paint and Varnish Prod.*, **45**, No. 5, 30 (1955).

TABLE I

PARTIAL RESULTS OUTPUT FROM COMPUTATION OF THE SEDIMENT VOLUME AND SEDIMENT STRUCTURE OF ROD-LIKE PARTICLES WITH LENGTH/WIDTH = 3 SEDIMENT STRUCTURE[a]

| $K$ | $I$ | $J_K$ | $J_I$ | $X_{0K}$ | $Y_{0K}$ | $Z_{0K}$ | $X_{TK}$ | $Y_{TK}$ | $Z_{TK}$ |
|---|---|---|---|---|---|---|---|---|---|
| 29 | 7 | 3 | 3 | 42.5 | 16.2 | 20.0 | 33.4 | 16.6 | 30.7 |
| 30 | 24 | 3 | 2 | 23.5 | 78.3 | 28.2 | 15.8 | 67.4 | 32.4 |
| 31 | 0 | 1 | 0 | 4.5 | 52.5 | 3.5 | 13.8 | 51.1 | 13.9 |
| 32 | 0 | 1 | 0 | 0.5 | 95.1 | 3.5 | 1.5 | 97.7 | 17.2 |
| 33 | 29 | 1 | 3 | 35.9 | 15.3 | 37.1 | 35.8 | 16.3 | 51.0 |
| 34 | 19 | 3 | 3 | 59.8 | 8.4 | 30.2 | 61.6 | 22.1 | 32.1 |
| 35 | 23 | 1 | 1 | 46.1 | 85.2 | 9.4 | 48.4 | 98.0 | 14.7 |
| 36 | 2 | 1 | 1 | 32.2 | 1.4 | 6.5 | 33.4 | 0.6 | 20.4 |
| 37 | 0 | 1 | 0 | 69.2 | 61.4 | 3.5 | 73.2 | 74.0 | 8.3 |
| 38 | 27 | 1 | 1 | 19.6 | 41.4 | 7.7 | 19.5 | 41.7 | 21.7 |
| 39 | 29 | 1 | 1 | 45.2 | 14.9 | 26.4 | 54.5 | 21.7 | 34.4 |
| 40 | 28 | 3 | 3 | 94.9 | 31.9 | 37.3 | 95.4 | 18.2 | 39.3 |

Layer height = 13.42

LAYER POPULATIONS

| Layer No. | 5 | 7 | 9 | 11 | 13 | 16 | 19 | 24 |
|---|---|---|---|---|---|---|---|---|
| $0 \leq x, y < 100$ | 62 | 70 | 59 | 68 | 62 | 37 | 13 | 5 |
| $10 \leq x, y < 90$ | 39 | 43 | 32 | 51 | 40 | 29 | 9 | 4 |
| $20 \leq x, y < 80$ | 19 | 23 | 14 | 34 | 26 | 16 | 4 | 2 |
| $30 \leq x, y < 70$ | 11 | 8 | 6 | 19 | 13 | 6 | 0 | 0 |

[a] $K$ and $I$ are order numbers of the falling particle and contacted particle. $J_K$ and $J_I$ are the order numbers of the member spheres in each which establish the contact. $X_{0K}$, $Y_{0K}$, $Z_{0K}$ and $X_{TK}$, $Y_{TK}$ and $Z_{TK}$ are the coördinates of the centers of the initial (lowest) and terminal (highest) member spheres of the $K$th particle. For this table they have been rounded off to one decimal place.

TABLE II

SEDIMENT VOLUME AND SEDIMENT STRUCTURE FOR ROD-LIKE PARTICLES

| Length/Width ratio | 2 | 3 | 4 | 7 | 12 | 18 |
|---|---|---|---|---|---|---|
| Vol. % solids, excluding boundary region | (10.8)[a] | 8.7 | (7.7)[a] | 4.9 | 2.8 | 1.46 |
| Mean contact no. | 1.99 | 2.05 | 2.06 | 2.12 | 2.18 | 2.17 |
| Contact frequencies, % | | | | | | |
| 1 | 26 | 25 | 29 | 28 | 25 | 35 |
| 2 | 49 | 47 | 41 | 42 | 43 | 26 |
| 3 | 25 | 27 | 24 | 15 | 21 | 31 |
| 4 | .. | 1 | 6 | 15 | 11 | 4 |
| 5 | .. | .. | .. | .. | .. | 4 |
| Contact types, % | | | | | | |
| End-to end | 100 | 69 | 45 | 22 | 12 | 7 |
| End-to-center | .. | 29 | 47 | 54 | 52 | 48 |
| Crossed structures | .. | 2 | 8 | 24 | 36 | 45 |
| Falling particle, leading end arrests, % | 78 | 66 | 56 | 45 | 37 | 33 |
| Contacted particle, terminal end contacts, % | 78 | 65 | 54 | 39 | 30 | 21 |

[a] When these runs were made the program had not yet been arranged to permit exclusion of the boundary region in calculating the sediment volume.

Accordingly the mean layer population is calculated from the first 13 levels and the total volume of solids per layer obtained from this and the volume of the member spheres. This volume of material occupies a container volume equal to the layer cross section times the layer height. Generally the concentration of material near the walls of the container (*i.e.*, that counted in the first but not in subsequent $x,y$-ranges) was markedly greater or markedly less than that in the interior and was discounted in selecting the best value. Occasionally the inhomogeneity extended into the second range as well. Results for sediment volume as a function of length/width ratio obtained in this manner are shown in Fig. 2 and Table II.

Of the nine particles in Table I which do not fall to the bottom of the container ($I \neq 0$), five make contact with others through their leading member ($J_k = 1$) and four are caught by their terminal member ($J_k = 3$). They strike the arresting particle at either end five and three times, respectively, and once at the central member. Of nine interparticle contacts eight are end-to-end, one is end-to-center and none involve crossed particles. Results from this kind of counting for all interparticle contacts are summarized in Table II.

While all particles are considered in determining contact type except those which fall to the bottom of the container, only a restricted number can properly be included in counting the frequency with

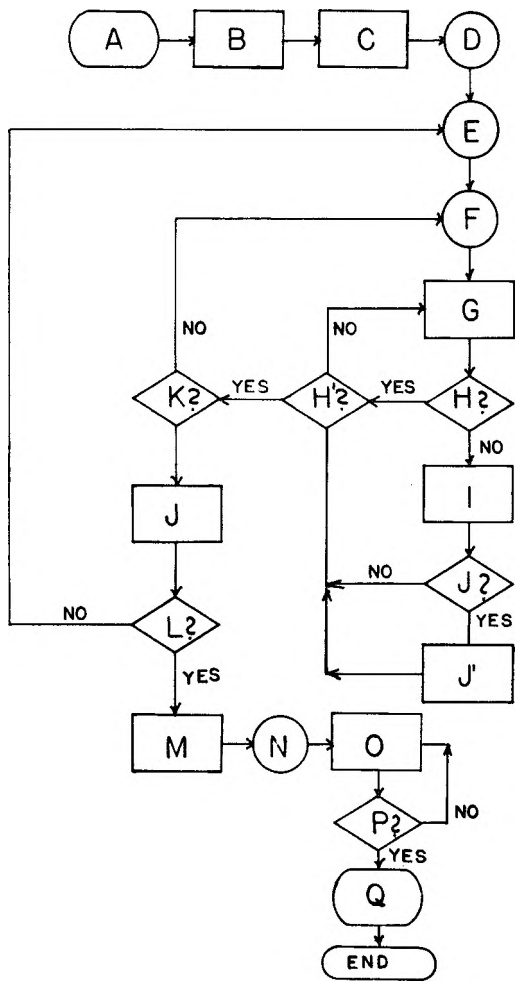


Fig. 1.—Schematic flow sheet for computation of sediment volume and sediment structure of rod-like particles.[a] A. Data input. Copy random digits[b] in K sets of four groups of five digits each, pointing off three decimal places and treating the four groups as the $x$- and $y$-coördinates of the center of the lowest lying member sphere of the $K$th particle, and the azimuthal angle $\theta$ and polar angle $\phi$ (restricted to $\theta \leq \phi \leq \pi/2$) determining its orientation. B. Compute the $x$- and $y$-coördinates of each of the remaining (J − 1) member spheres of each of the K particles. If any $x$ or $y$ so computed falls outside the range $0 \leq x,y < 100$, apply a suitable translation to all member spheres of that particle so that all its $x$- and $y$-values are included in the range (*i.e.*, choose particles which will not "miss" the "container" when "dropped"). Retain the quantities $\Delta Z(k) = 2R|\cos\phi|$ as well as the $x,y$-values which are numbered consecutively from 1 to KJ. C. For the first particle (K = 1), set $Z(1) = R$, $Z(2) = R + \Delta Z(1)$, etc., up to $Z(J)$. D. Carry out steps E to L for each of the K particles in turn beginning with the second. E. Carry out steps F to K for each of the J members of the Kth particle. F. Carry out steps G to H′ for each of the (K − 1)J member spheres of previously "dropped" particles. G. Compute the test quantity $DSQ = (x_n - x_m)^2 + (y_n - y_m)^2$ where n and m identify the spheres being examined. H. Test if $DSQ > 4R^2$? If so, repeat step G unless the test at H′ shows that m is the last of the (K − 1)J spheres to be tested. If not, proceed to step I. I. Since $DSQ \leq 4R^2$ the mth sphere arrests the particle containing the nth sphere in its fall. Compute the corresponding $Z$-value for the Jth member (highest) of the Kth particle. This is $ZT(n)$, a tentative $Z$-value pending determination as to whether this arrest is the *first* that would occur. J. Test if $ZT(n)$ is larger than the largest $ZT'(n)$ previously found for an arrest of the same sphere n. If so, record it (step J′), proceed to H′. If not, discard it and proceed to H′ directly. K. Test if n is the last of the J member spheres belonging to the Kth particle. If not repeat steps F to K. If so, proceed to step J. J. Find the largest of the $ZT(n)$ values recorded for each of the J members of the Kth particle. It is this sphere (n) which was first arrested in the fall of the Kth particle. Compute the corresponding $Z$-values of the remaining members of the particle, record the order numbers of the contacting members of the two particles, and the order numbers of the particles themselves and proceed to L. L. Test if K is the last of the K particles. If not, repeat steps E–L. If so proceed to step M. M. Identify the largest $Z$-value recorded and divide it by 24. This is the height of the layers into which the container is to be divided for the purpose of counting the density of the sediment. N. Carry out step O for all KJ member spheres four times with the ranges of $x(n)$ and $Y(n)$ $0 \leq x, y < 100$, $10 \leq x, y < 90$, $20 \leq x, y < 90$, $20 \leq x, y < 80$ and $30 \leq x, y < 70$, respectively. O. For all spheres whose $x$- and $y$-values lie in the appropriate range, count and record the number whose $Z$-values fall in each of the 24 layers established by step M. P. Test if step O has been completed four times. If so, proceed to Q. Q. Results output. Report for each particle, the order number of the particle arresting its fall, the order numbers within each particle of the contacting members, the $x$-, $y$- and $z$-coördinates of the initial and terminal members of each particle, the layer height, and the numbers of individual member spheres located in each layer for the four ranges of $x$ and $y$. (a) Numerous short cuts and details are omitted from this schematic presentation. (b) The sequence of random digits was obtained from "the Rand Table," The Free Press, Glencoe, Ill., 1955. Provision was made to begin copying at an arbitrary point in the sequence.

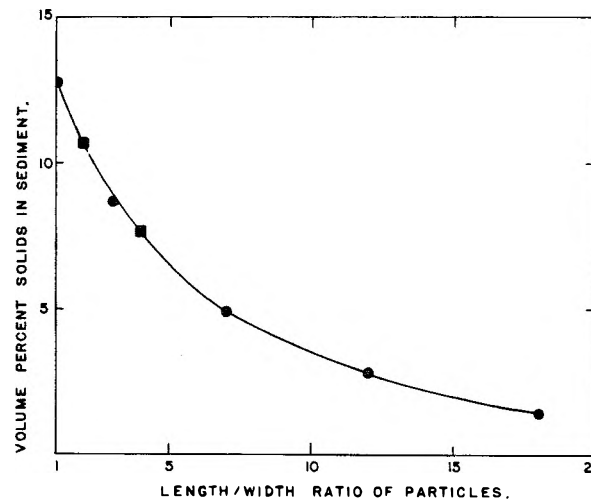


Fig. 2.—Calculated sedimentation volume for rod-like particles with strong interaction.

which particles make one, two, three, etc., contacts with other particles in the sediment. They must be embedded in the sediment deeply enough so that the particle concentration immediately above them is uniform; this criterion is satisfied by requiring the $Z$-coördinate of the terminal member to be less than the layer height times $^2/_3$ of the number of full levels. They must be particles dropped early enough in the calculation to give them adequate opportunity to intercept subsequently dropped particles; this criterion is satisfied by specifying that they must be among the first 60% of the particles dropped. Finally they must be sufficiently removed from the walls of the container so that they can arrest subsequent particles falling on all sides; this criterion is satisfied by requiring that no member sphere be within 5 units (out of a container width of 100) from any wall. Of the twelve particles in the sample of Table I only six (numbers 29, 30, 33, 34, 38 and 39) satisfy all three criteria. The number of particles resting against

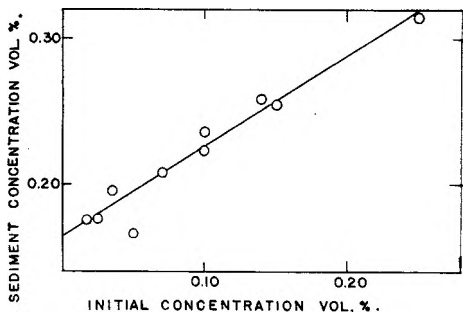


Fig. 3.—Sediment volume of lithium stearate in benzene.

each of these is one more than the number of times that order number appears anywhere in the column of $I$ values for the entire run. For example, just in the short section given in Table I, particle 29 appears twice in the $I$ column, showing that it caused the arrest of particles 33 and 39, and once in the $K$ column, showing that its own fall was arrested by particle 7. It happens that particle 29 is absent from the balance of the complete run of 400 particles. Hence this particle is resting against three others in the sediment. Similar examination of the complete run for the six "eligible" particles of Table I shows that they make 3, 3, 2, 1, 2 and 1 contact with other particles, respectively. For just these six the mean contact number is 2.0 with $33^1/_3\%$ of the particles making 1, 2 and 3 contacts. Results for the complete group of eligible particles for various values of $L/W$ are shown in Table II.

The computed results were shown to be independent of "trivial" variables, including radius of the member spheres, number of particles processed, and particular choice of sets of "random" coördinates and orientations by multiple runs at $L/W = 3$. Duplicate runs were made also at $L/W = 4$ and 7. The remaining results are from single runs. This procedure, partially dictated by the large amount of machine time required for the larger $L/W$ ratios, is justified by the concordance obtained between multiple runs at $L/W = 3$.

## Experimental Part[4]

Lithium stearate was prepared from a technical stearic acid and obtained as a fine dispersion by rapid crystallization from mineral white oil, followed by elution of the oil with benzene. The particle size distribution was obtained by electron microscopy as described elsewhere.[5] Fifty per cent. of the particles had lengths between 0.4 and 0.6 $\mu$ with a mean length to width ratio of 10 and a thickness estimated from shadow lengths as not over 600 Å. Accordingly the comparisons between theoretical and experimental results are based on particle dimensions of $0.6 \times 0.06 \times 0.006$ $\mu$.

Sediment volumes for these dispersions, measured after three weeks settling time at room temperature (*ca.* 25°) in cylindrical tubes 3 cm. in diameter, are shown as a function of the initial concentration of the suspension in Fig. 3.

## Discussion

The most significant question to be asked from a comparison of the experimental and theoretical results is "In what ways does the experimental system conform to or diverge from the model employed?" The model supposes rigid cohesion between particles at first contact. If the cohesion is weak enough to permit occasional rupture of contacts due to thermal motions (or accidental thermal gradients or mechanical jarring) the particles released can settle further, leading to a sediment concentration higher than that predicted. The model supposes random orientation of the particles during settling. Preferred orientation of the particles with respect to the direction of fall should lead to more nearly regular packing in the sediment and hence also to a higher sediment concentration. The same result would be achieved if the particles line up parallel to each other. However, if the particles tend to assume end-to-end configurations with random orientations of such structures with respect to the container, the resulting concentration in the sediment would be reduced corresponding to a larger mean length to width ratio for actual structural unit than for the primary particle.

In order to effect comparison between the experimental data and the theoretical result it is first necessary to correct the experimental data for the effect of initial concentration of the suspension, which is assumed in the model to be infinitely dilute, since each particle is made to fall freely until it contacts some particle already embedded in the sediment. The concentration in the sediment from an infinitely dilute suspension is seen from Fig. 3 to be 0.16 volume %. Presumably the source of the concentration dependence lies in the fact that all initial orientations cannot be equally probable in concentrated suspensions. The volume of the average particle, *ca.* $2.2 \times 10^{-4}$ cubic micron, is only *ca.* 0.2% of the 0.11 cubic micron that a particle of that length would sweep out in assuming all possible orientations, so that the initial concentration must be rather less than this if random initial orientation is to be guaranteed.

Secondly, it is necessary to make some choice of effective length to width ratio for the experimental particles which are thin laths rather than rods of uniform cross section. As the lath-like object falls, it will present its width $W$ or its thickness $T$, or more generally a dimension of $W \cos\theta + T \sin\theta$, to the deposited sediment. The effective width for a lath-shaped particle assuming all orientations $\theta$ about its long axis with equal probability is then the average value of this quantity which is $2W/\pi(1 + T/W)$. Since $T/W$ is *ca.* 0.1 for the present particles, the effective width is 0.7 times the true width and the effective length/width ratio is 14.

Figure 2 indicates that a model system with a length to width ratio of 14 would be expected to form a sediment in which the volume per cent. solids is 2.3%. The model particle, however, has a total volume of $\pi L^3 \div 6(L/W)^2$, being composed of $L/W$ spheres of radius $W/2$; or $5.76 \times 10^{-4}$ cubic microns per particle while the actual particle has a volume of only $2.2 \times 10^{-4}$ cubic microns. Accordingly the sediment volume to be taken as the theoretical prediction for the system of lithium stearate in benzene if it conformed to the model is $2.3 \times 2.2/5.76$ or *ca.* 0.9%. The experimental value is 0.16%.

According to the reasoning given above an observed volume fraction of solids in the sediment which is less than the model value means that the particles do cohere on contact, but that the end-to-

(4) Results obtained in collaboration with D. V. Rathnamma, The Indian Institute of Science, Bangalore 3, India.

(5) M. J. Vold, D. L. Bhattacharya and D. V. Rathnamma, *J. Ind. Inst. Sci.*, XL, No. 3, 97 (1958).

end configurations of the particles are preferred over any others. This result is in agreement with a prediction made earlier[6] that elongated particles able to become oriented in accord with their net van der Waals attraction should tend toward an end-to-end approach.

Analysis of the model results for contact type presented in Table II shows that even random orientation of particles during fall does not result in an equal distribution of contact types among the several possibilities. For example for $L/W$ = 3 there are four chances for end-to-end contact (1–1, 1–3, 3–3, 3–1), four for end-to-center contacts (2–3, 3–2, 1–2 and 2–1) and only one for crossed structures (2–2). Adherence to these combinatory possibilities would give 44.5% end-to-end contacts, 44.5% end-to-center contacts and 11% crossed structures whereas the observed results are 69, 29 and 2%. Similarly the leading end of the three member aggregate is first arrested by contact with previous particles in 65% of the contacts rather than 33⅓%. The reason for these results is that the leading portion of the falling particle has first opportunity to effect contact with others below it and following portions can effect contact only over the fraction of their surface which is not in the wake of preceding portions.

Presumably it is the existence of cross linked structures which leads to development of rigidity in the sediment. The proportion of particles in the sediment which participate in such cross links increases with the frequency of multiple contacts. As seen in Table II the proportion of contacts involving more than two particles increases only very slightly as the length to width ratio increases. Since the volume fraction of solids in the sediment is simultaneously decreasing markedly, the resulting decrease in number of cross links per unit volume might be expected to lead to less rigid sediments from elongated than from isometric particles. This prediction is not in conflict with the well known increase in consistency that occurs for lubricating greases of constant solids concentration as the anisometry of the particles increases.[7] A different model is needed to derive the expected distribution of contact types and hence to explore a theoretical basis for the rheology of systems of constant composition as a function of particle shape.

Finally, it is possible to contort the results of the model calculation in an admittedly dubious manner to obtain a crude estimate of the extent to which the proportion of end-to-end contacts is increased in the lithium stearate system over that which would be expected from the given model. While the principal value of the estimate is for guidance in constructing a better model for the real system, it is presented here as a matter of interest. The dubious assumption which is made is that the given proportion of end-to-end contacts represents a sediment structure leading to the indicated volume per cent. solids times the factor 0.4 for conversion from linear aggregates of spheres to lath shaped particles with the indicated length to width ratio. The volume per cent. solids that would be found instead, if the particles were pared down to a length to width ratio of 14 without disturbing the structure, is then calculated. The results of this procedure are shown in Table III. Interpolation in columns one and five of the table leads to 70% end to end contacts for the observed fraction of 0.16% in place of the model expectation of 10% derived by interpolating in columns one and four for the effective length to width ratio of 14.

(6) M. J. Vold, *Proc. Ind. Acad. Sci.*, XLVI, 152 (1957).

(7) R. H. Leet, *N. L. G. I. Spokesman*, *XIX*, No. 1, 20 (1955), note accompanying bibliography.

TABLE III

ESTIMATE OF THE VOLUME PER CENT. SOLIDS IN THE SEDIMENT FOR PARTICLES OF $L/W$ = 14 FOR VARIOUS PROPORTIONS OF END-TO-END CONTACTS

| End-to-end contacts, % | Vol. % solids, aggs. of spheres | Vol. % solids laths | $L/W$ | Vol. % solids for $L/W$ = 14 |
|---|---|---|---|---|
| 100 | 10.8 | 4.2 | 2 | 0.086 |
| 69 | 8.7 | 3.4 | 3 | .156 |
| 45 | 7.7 | 3.0 | 4 | .245 |
| 22 | 4.9 | 1.92 | 7 | .480 |
| 12 | 2.8 | 1.10 | 12 | .81 |
| 7 | 1.46 | 0.57 | 18 | .94 |

## DISCUSSION

J. J. BIKERMAN (Massachusetts Institute of Technology).—Do you find that sediment volumes are constant with time?

M. J. VOLD.—In the case of lithium stearate in benzene they seem to be. The suspensions settle down rapidly at first and then compact slowly over a period of three or four days, but there is virtually no change from the volume at three weeks to that at 8.5 months. Part of the reason for this is that the sediment is a weak gel. You can turn the cylinder on its side and the interface between sediment and medium remains vertical for at least 24 hours.

H. K. SCHACHMAN (University of California at Berkeley).—We have plenty of rather precise data on the equilibrium volumes occupied by various materials thrown down at different field strengths in the ultracentrifuge. For example, we have this for TMV. Can your model help to interpret these data?

M. J. VOLD.—The present model which is based on permanent cohesion on contact would not predict any dependence of the volume on the centrifugal field but we are working on a model which will take this into account by introducing a variable cohesion probability. This will be easier to do for spheres than for anisometric particles. If you have similar data on some globulin particles it could be very useful to us.

F. M. FOWKES (Shell Development Company).—The lithium stearate gels used as experimental models are characterized not only by a lath-like shape but by an uneven distribution of polar surfaces. The flat faces of the lath present a surface of methyl groups whereas the edges and ends have polar groups exposed to a certain degree. I should expect edge-to-edge contacts in addition to end-to-end contacts.

M. J. VOLD.—Our model assumes that all contacts, whether end-to-end or end-to-center or any other, are strong enough to form bonds. Then we observe that the observed sediment volume is larger than that calculated. This deviation cannot be lessened by assuming that the contacts form bonds only when they occur between polar surfaces. What is meant is that contacts between polar surfaces at the ends of the laths is a more frequent occurrence than one would predict from probability alone. I would not expect this to be the case for edge-to-edge contacts.

# A RADIOTRACER STUDY OF ADSORPTION OF AN ETHYLENE OXIDE–PROPYLENE OXIDE CONDENSATE ON QUARTZ POWDERS

BY H. R. HEYDEGGER AND H. N. DUNNING

*Surface Chemistry Laboratory, Petroleum Experiment Station, Bureau of Mines, U. S. Department of the Interior, Bartlesville, Okla.*

*Received March 2, 1959*

The adsorption isotherm of a non-ionic detergent, a ethylene oxide–propylene oxide condensate, on a standard quartz powder has been determined by radiotracer methods. Because of the high specific activity of the labeled detergent, it was possible to extend the measurements to equilibrium concentrations as low as one p.p.m. The extent of adsorption is considerably less than that of other non-ionic detergents tested on the same quartz sample. Adsorption is reversible and can be described by a Langmuir-type equation $X/M = C/(60.06C + 850.2)$, where $X/M$ = μgrams detergent adsorbed per cm.², and $C$ = equilibrium concentration, μgrams per gram (p.p.m.).

## Introduction

The problem of detergency in petroleum production has been explored extensively in this Laboratory. A major deterrent to the use of detergents in stimulating oil production is their adsorption on the extensive surfaces of reservoir rocks. Therefore, a general study was made[1] of the adsorption of series of polyoxyethylated alkyl phenols. A comparative study of non-ionic detergents adsorption also was made by radiotracer, spectrophotometric and surface tension methods.[2]

These studies showed that many non-ionic detergents were strongly, but reversibly, adsorbed at the quartz–water interface. Also, detergents of higher molecular weight were less extensively adsorbed. However, in the detergent series studied, the higher molecular weight members depart from the hydrophilic–lipophilic balance of maximum detersive effectiveness. Accordingly, the adsorption of Pluronic L-64,[3] a detergent of good hydrophilic–lipophilic balance but of very high molecular weight, was investigated with the standard quartz sample used previously.

Unlike the alkyl phenols, the Pluronics have no groups that absorb energy in the visible or ultraviolet regions. The availability of a sample labeled with carbon-14, therefore, offered the first opportunity for precise analysis and hence for studying the adsorption characteristics of this type of detergent.

## Experimental

**Materials.**—The Pluronics are a series of non-ionic detergents having the general formula[4]

$$HO(C_2H_4O)_m(C_3H_6O)_n(C_2H_4O)_pH$$

The specific detergent studied, Pluronic L-64, is a member of this series with a molecular weight of about 2,850 and a hydrophobic base material of about 1,750 molecular weight.

A stock solution of 8.092 g. of Pluronic L-64 (100% active agent) in 20 ml. of ethanol was furnished by the manufacturer. This concentration was verified in this Laboratory. The detergent molecules were labeled with C-14 in the condensed ethylene oxide portion and had a specific activity of about 0.32 mc./g. according to the manufacturer's assay.

The quartz powders used in this study have been described previously.[1] The powder used in most of the experiments had a nitrogen B.E.T. surface area of $3.9 \times 10^4$ cm.²/g. A second powder had a surface area of $1.2 \times 10^4$ cm.²/g.

All samples for radioactivity measurement were prepared as follows. A 100-lambda aliquot of the solution was carefully evaporated to dryness under an infrared lamp as a drop on a cleaned aluminum planchet (about 3.1 cm. diameter). The micropipet was washed twice with distilled water and the wash liquid also evaporated on the drop. Control experiments showed that no detectable activity remained in the micropipet after this treatment. Considerable care was required to avoid splattering and spreading of the very low surface-tension solutions to the edge of the planchet. Concentration data are based on at least three replicate samples. Standard statistical tests were applied before discarding anomalous results.

**Counting Procedure.**—All radioactivity measurements were made with a thin end-window (1.7 mg./cm.²) Geiger–Mueller tube mounted on a vertically adjustable sample stage and attached to a scaling unit. The planchet containing a sample was located at a fixed small distance (1.5 mm.) from the G–M tube window by use of a precision micrometer screw mounting of the sample stage, thus achieving very nearly $2\pi$ geometry.

"Dead-time" corrections were made as required by use of a standard formula.[5] The "dead-time" of the G–M tube was found to be 150 ± 20 microseconds by an oscilloscopic method described by Stever.[6]

Since the fraction of detergent adsorbed was small at the higher concentrations studied, the significance of self-absorption and scattering phenomena were considered. Self-absorption corrections were made by use of Henriques' formula.[7] Gora and Hickey's[8] value of the mass adsorption coefficient for $C^{14}$ in organic samples (0.25 ± 0.01 cm.²/mg.) was employed for these calculations.

The backing provided by the planchet (about 27 mg./cm.²) and the sample stage ensured saturation backscattering for all samples.[5,9,10] Because of the masking effect of the backscattered radiation and the thinness (less than 0.2 mg./cm.²) of the carrier-free samples, self-scattering corrections were not made and should be negligible.[5,10,11] Background readings were taken frequently and, if a difference was noted between the background before and after a series of sample determinations, the average value was used in correcting the radioactivity data of that series for background. Standard deviations for all radioactivity data were calculated from standard formulas already given by Jarrett.[12]

**Adsorption Measurements.**—Aliquot parts of the detergent–ethanol stock solution were diluted with distilled water to prepare a series of solutions of concentration varying approximately from 10 to 1,800 p.p.m. Radioactivity measurements were made on 100-lambda aliquot parts of these solutions, and a calibration curve was constructed from these data. The data yielded a straight line, which was calculated by the method of least squares. The stand-

(1) H. N. Dunning, *Ind. Eng. Chem.*, **2**, No. 1, 88 (1957).
(2) Lun Hsiao and H. N. Dunning, THIS JOURNAL, **59**, 362 (1955).
(3) Trademark, Wyandotte Chemical Corp., Wyandotte, Mich.
(4) "Pluronics, A New Series of Non-ionic Surface Active Agents," Wyandotte Chemical Corp., Wyandotte, Mich.
(5) G. Friedlander and J. W. Kennedy, "Nuclear and Radiochemistry," John Wiley and Sons, New York, 1955.
(6) H. G. Stever, *Phys. Rev.*, **61**, 38 (1942).
(7) F. C. Henriques, Jr., G. B. Kistiakowsky, C. Margnetti and W. G. Schneider, *Ind. Eng. Chem., Anal. Ed.*, **18**, 349 (1946).
(8) E. K. Gora and F. C. Hickey, *Anal. Chem.*, **26**, 1159 (1954).
(9) G. W. Reed, Jr., ANL-5608, U. S. A.E.C., 1956.
(10) L. E. Glendenin and A. K. Solomon, *Science*, **112**, 623 (1950).
(11) R. G. Baker and L. Katz, *Nucleonics*, **11**, No. 2, 14 (1953).
(12) A. A. Jarrett, AECU-262, U. S. A.E.C., 1956.

ard deviation of the data from the least squares line was 3.5%. All later concentrations were calculated from this calibration curve.

The adsorption experiments were performed by adding an aliquot part (usually 10.0 ml.) of the prepared solution to a weighed amount of powder in a glass-stoppered Pyrex bottle. The bottle and contents were then shaken for varying periods on a "wrist-action" shaker. The concentration of the added solution was determined before and after it was shaken with the powder. The latter was determined by removing an aliquot part (usually 2.0 ml.) of the supernatant liquid after about 18 hours of sedimentation and centrifugation of the sample for 2 hours. Then the sample was evaporated and counted as above. The extent of adsorption was calculated from the observed change in concentration.

Desorption experiments were performed by decanting the supernatant liquid after completion of the adsorption studies and reweighing the bottle and contents to determine the amount of solution remaining. A known volume of distilled water was added, the sample agitated as before, and concentration determinations carried out as above. The extent of desorption was calculated from the observed concentration change after shaking, corrections being made for the original detergent solution remaining. The temperature during all experiments was maintained at 23.5 ± 2.0° in the air-conditioned laboratory.

**Control Experiments.**—The adsorption of detergent by the walls of the glass bottles used in these experiments was found to be undetectable by following the usual procedure of an adsorption experiment without quartz powder present. This would be expected since the area of the container was less than 0.05% of the area of the powder samples.

A 1-day shaking period was found to be sufficient to achieve equilibrium adsorption for solutions up to about 1,100 p.p.m. Redetermination of several of the solutions after longer shaking periods showed negligible changes. This was also corroborated by agreement (within the experimental error) of adsorption values calculated for samples with widely varying shaking periods and weights of powder. The period of centrifugation was established by repeated determinations on the same liquid after varying centrifugation periods. No change in specific radioactivity was found after 1 hour or longer of centrifugation.

The effect of the small amounts (maximum 2.5% by volume) of ethanol in the solutions was evaluated by evaporating an aliquot of the stock solution to dryness and redissolving in distilled water. Experiments with this alcohol-free solution gave results which agreed within the experimental error with those of similar concentration prepared from alcoholic stock solution. Standards were checked from time to time to assure constancy in the performance of the tube.

## Results and Discussion

The adsorption isotherm of Pluronic L-64 on the fine quartz powder is presented in Fig. 1. The slope of this isotherm is very steep at the lowest concentrations, decreasing gradually until it is nearly zero at equilibrium concentrations above 300 p.p.m. Above this concentration the extent of adsorption is essentially constant (at 640 μgrams of detergent adsorbed per gram of quartz) until a concentration of about 1,000 p.p.m. is reached. At concentrations above 1,000 p.p.m. the experimental error is quite large because of the small amount of detergent adsorbed. However, the data indicate an increase in adsorption at higher concentrations.

Because of the relatively high specific activity of the detergent, it was possible to determine low concentrations more accurately than in previous work.[1,2] Accordingly, the low concentration portion of the isotherm is more clearly defined.

The location of the plateau portion of the isotherm has been calculated by the method of least squares for the data at concentrations between 300 and 1,000 p.p.m. This straight line has a value of $x/m$ equal to 640 and 641 μgrams per gram at 300 and 1,000 p.p.m., respectively, and a slope of 0.002 between these points. The average standard deviation of the data points in this region is 35.

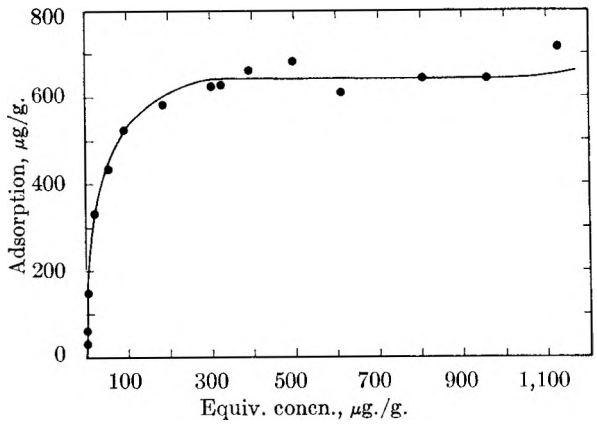


Fig. 1.—Adsorption isotherm of detergent on quartz (wt. basis).

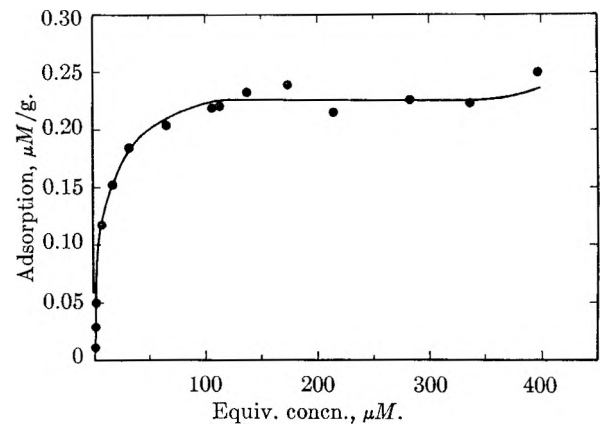


Fig. 2.—Adsorption isotherm of detergent on quartz (molar basis).

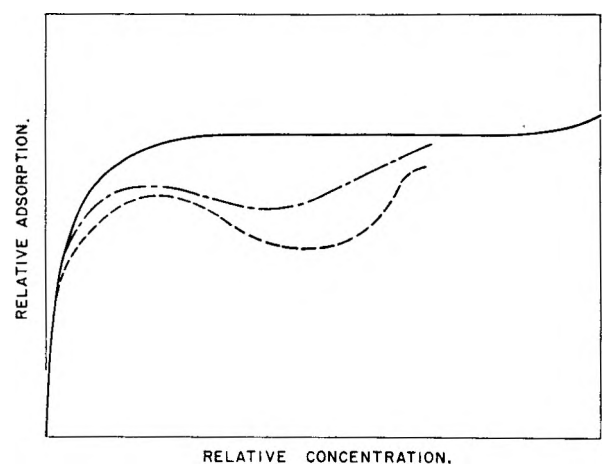


Fig. 3.—Relative adsorption isotherms showing kinetic effect; ———, equilibrium data, (2–10 days shaking, 1 day sedimentation); — - —, (4 hours shaking, 10 day sedimentation); — — —, (4 hours shaking, 1 day sedimentation).

The adsorption data are plotted on a micromolar basis in Fig. 2. Although the molar quantities have more theoretical significance, the actual value of detergent adsorbed probably is best shown by calculations on a weight basis.

The adsorption of this detergent also was determined on the coarser powder used previously.[1] The determinations made indicated a slightly higher extent of adsorption, based on surface area, for the coarser powder.

A Langmuir plot [$C/(x/m)$ *versus* $C$] of the data is linear to an equilibrium concentration of 1,125 $\mu$g./g. Earlier data[1,2] departed from such a plot at concentrations below about 40 $\mu$g./g. As mentioned above, the low concentration portion of this isotherm was more clearly defined. Therefore, the deviations in the earlier work probably can be accounted for by the larger experimental error at very low concentrations.

The location of the Langmuir plot was established by the method of least squares with values of 0.00154 for the slope and 0.0218 for the intercept. The average standard deviation of the data points from the calculated line was 0.0479.

Values of the Langmuir function [$C/(x/m)$] determined by desorption measurements lie within this deviation. Therefore, the adsorption is reversible and may be described by the equation

$$x/m = C/(0.00154C + 0.0218)$$

on a weight basis, or by the equation

$$X/M = C/(60.06C + 850.2)$$

on a surface area basis where

$x/m$ = $\mu$g. detergent adsorbed per g. of quartz
$C$ = equilibrium concn., $\mu$g. per g. (p.p.m.)
$X/M$ = $\mu$g. detergent adsorbed per cm.$^2$ of surface

Another series of experiments was conducted in which the powder and solution were shaken for only 4 hours. The relative adsorption isotherm is shown above in Fig. 3. The preliminary data generally indicated lower specific adsorption than that for longer shaking periods as might be expected. However, there was a definite minimum in the isotherm at a concentration of about 600 p.p.m. Upon redetermination after about 10 days of standing, the minimum was considerably less pronounced, as shown in Fig. 3, indicating a kinetic effect in the region from 370 to 770 p.p.m. A similar minimum in the equilibrium adsorption of Igepal CO-710 on Tip Top sand in approximately the same concentration range was reported previously[2] but refuted by later data.[1] The present study indicates that this minimum is a kinetic effect rather than an equilibrium condition.

The extent of maximum adsorption (640 $\mu$g./g. or 0.225 $\mu M$/g.) is unusually low in comparison to the non-ionic detergents studied previously. The adherence to the Langmuir formula indicates that the plateau of the isotherm represents a monomolecular layer. The area per molecule for this layer is 2,880 Å.$^2$. Similar areas calculated for polyoxyethylated alkyl phenols range from about 35 to 200 Å.$^2$. The unusually low adsorption of this detergent may be due to the large size of the hydrophobic polypropylene group located in the center of the molecule compared to the terminal hydrophobic alkyl phenol of the detergents already studied.

Because non-ionic detergents are reversibly adsorbed at the quartz–water interface, they would be expected to move through porous media in the form of a chromatographic zone. Such behavior has been observed in the laboratory in similar systems.[13] Adsorption isotherms provide the basic data for calculations of such zone movement according to chromatographic theories. The shapes of the adsorption isotherms of non-ionic detergents indicate that, according to DeVault,[14] the front boundary of their chromatographic zone will exhibit "self-sharpening" tendencies. That is, the front boundary will resist concentration decreases due to channeling, diffusion and non-attainment of equilibrium. Also, the rear boundary will become spontaneously diffuse. Qualitatively, the low adsorption of Pluronics will lead to a much more rapid zone movement than that attained by the non-ionic detergents studied previously. For this reason, detergents of this type appear promising for use in systems where adsorption on solid surfaces is an economical deterrent to detergent use.

**Acknowledgments.**—The authors thank J. W. Hensley, Wyandotte Chemicals Corp., for supplying the labeled detergent sample and data on its properties. The assistance of R. T. Johansen and F. E. Armstrong, of this Station, in measurements of surface area and G–M dead-time, respectively, is also acknowledged.

## DISCUSSION

P. BECHER (Atlas Powder Company).—I wish to make a comment on the shapes of these curves. We were working with this identical Pluronic a short time ago. We found that the critical micelle concentration was about 260 gamma per gram. This is the concentration at which your isotherm flattens out. Now, if detergent monomer is the species which is being absorbed, you will initially get a strong dependence on concentration. However, above the CMC there is no increase in monomer concentration. Thus, you get something that looks like a Langmuir isotherm, but in which the mechanism is quite different.

H. N. DUNNING.—Some of our previous work with polyoxyethylated detergents has shown that their critical micelle concentrations and critical adsorption concentrations are rather directly related. In fact, one can be calculated from the other. Therefore, I would expect a relationship for these properties with this detergent. The data here, below the critical micelle concentration, fit the Langmuir equation closely. This leads to the conclusion that the adsorption is reversible. I would agree that adsorption of such detergents is influenced by the micellar phenomenon. This would cause a relatively constant adsorption above the critical micelle concentration, not too different from the Langmuir shape since such adsorption increases very slowly in the higher concentration ranges.

A. C. ZETTLEMOYER (Lehigh University).—I'd like to comment about your slow rate of attainment of adsorption equilibrium. Some work we did on alkyl aryl sufonates showed the rate of breakdown of the micelles was slowed by the presence of small amounts of hydrocarbon produced by hydrolysis. The rate of de-micellization is usually extremely rapid, but could it be that the slow approach to equilibrium you observed was due to a similar cause?

H. N. DUNNING.—We did have some alcohol present from the original stock solution. This we would have preferred to avoid but felt that the solution could be more accurately prepared this way. The detergent probably also contained hydrocarbons, such as those you mentioned, and your observations may be a good explanation. The difference in attainment of equilibrium results from shaking for four hours as opposed to one day. In the finely divided powder, and with the very large molecular weight adsorbate, diffusion of course would be slow anyway.

(13) H. N. Dunning and Lun Hsiao, *Producers Monthly*, **18**, No. 1, 24 (1953).

(14) Don DeVault, *J. Am. Chem. Soc.*, **65**, 532 (1943).

# INFRARED SPECTRA OF HYDROCARBONS ADSORBED ON SILICA SUPPORTED METAL OXIDES

BY L. H. LITTLE[1]

*Department of Colloid Science, University of Cambridge, England*

*Received March 2, 1959*

Infrared studies have been made of surface species formed by the adsorption of ethylene on the oxides of nickel, copper and palladium supported in optically transparent porous Vycor silica glass. Quantitative adsorption measurements showed that polymerization of ethylene occurred on the metal oxides. Concurrent measurements of the spectra of the gas phase and the adsorbed phase have been made to study the equilibrium between these phases. *trans*-Butene-2 was formed in the gas phase for ethylene admitted to nickel oxide samples. The surface species on these samples were composed of methyl, methylene and unsaturated groups. However, the surface species formed by ethylene on copper oxide contained only methylene groups, while that on oxidized palladium contained methyl and methylene groups. In the latter systems the gas phases remained ethylene. The integrated absorption intensities of the surface species were measured and compared to hydrocarbons in normal liquid environments. This comparison provided knowledge about the perturbations of molecular vibrations due to adsorption of molecules on to surfaces. For the following hydrocarbon-supported metal oxide systems only physically adsorbed molecules were detected and no bands characteristic of new chemisorbed species were found: acetylene on silica supported nickel, copper, palladium and silver oxides; ethylene on silica supported silver oxide and ethane on silica supported nickel oxide. Quantitative measurements showed physical adsorption occurred largely on the silica support.

The application of infrared spectroscopy to the study of molecules adsorbed on solid surfaces has been reviewed recently by Eischens[2] and by Sheppard.[3] The value of this technique for investigation of adsorption problems lies in the direct evidence that it may provide for the structure of adsorbed surface species. This knowledge is of the greatest importance in the understanding of mechanisms involved in heterogeneous catalysis.

Difficulties in the use of this technique arise largely from scattering and absorption of energy from the infrared beam by the sample. In the case of supported catalysts this occurs at both the adsorbent and its support. The sensitivity may be enhanced by decreasing the catalyst particle size which reduces scattering and also increases the surface area and hence the amount of adsorbed material in the sample. Finely divided metal catalysts supported on high area silica powder have been used extensively by Eischens.[2] In the present work Vycor porous silica glass was used to support the finely divided oxides in the manner described previously.[4] This material has the advantage that it scatters less infrared radiation than does silica powder, although the available thicknesses of porous glass restrict the usable region of the spectrum to frequencies above 1500 cm.$^{-1}$ (>2000 cm.$^{-1}$ for samples 1 mm. thick) because of the strength of silica absorption bands.

The present study extends the results for the chemisorption of ethylene on supported nickel oxide that have been reported earlier.[4] Additional infrared spectra are reported for ethylene chemisorbed on copper and palladium oxides and for the gas phase in equilibrium with the adsorbents. No chemisorption was detected on supported silver oxide, and in this case, as in the cases of ethane and acetylene on the other oxide–glass systems, only physical adsorption was detected. These results are reported more briefly.

(1) Division of Applied Chemistry, National Research Council, Ottawa, Canada.

(2) R. P. Eischens, *Z. Elektrochem.*, **60**, 782 (1956). R. P. Eischens and W. A. Pliskin, "Advances in Catalysis and Related Subjects," Vol. X, Academic Press Inc., New York, N. Y., 1958, p. 1.

(3) N. Sheppard, "Molecular Spectroscopy," Hydrocarbon Research Group Conference on Molecular Spectroscopy, London, February 1958 (to be published by Pergamon Press, London).

(4) L. H. Little, N. Sheppard and D. J. C. Yates, to be published.

## Experimental

The samples were tubular specimens of porous Vycor glass, 1 mm. wall thickness, 20 mm. diameter and 5 cm. long. These were cleaned by heating to 400° in oxygen, evacuated, cooled and weighed quickly before water was adsorbed from the atmosphere. The sample then was immersed in a nitrate solution suitable to give 2% by weight of metal oxide.

The metal nitrate was decomposed to oxide by heating under vacuum and the sample was then cooled, reweighed to find the amount of metal oxide and then transferred to a glass infrared-adsorption cell having a furnace wound on one portion. The sample was free to slide in this cell between the furnace section and a section fitted with sodium chloride windows for measuring the spectrum.

After heating and evacuating at 300°, the sample was cooled and the background spectrum recorded. Then a dose of gas was admitted and the amount of adsorption measured. The spectrum was again recorded and the absorption of the surface species found. The infrared cell permitted the measurement of the spectrum of the gas phase in contact with the sample, and throughout this work simultaneous study was made of the spectra of the adsorbed species and the gas with which it was in equilibrium.

Unfortunately it was necessary to detach the cell from the adsorption system in order to measure the spectra. Therefore intermediate pressures during slow adsorption processes had to be obtained from intensities and optical densities of the gas phase *via* previously determined calibration curves. At the end of the series of infrared measurements the cell was replaced on the adsorption system and the final equilibrium gas pressure was found.

Finally the amount of adsorption on the metal oxide was obtained from the difference between the total adsorption and the physical adsorption on the glass without oxide present.

The infrared spectra were recorded on a Perkin–Elmer Model 21 Spectrophotometer fitted with either a sodium chloride or a calcium fluoride prism. The following spectral parameters were measured for absorption bands of surface species: frequency $\nu$ (cm.$^{-1}$); band half width $\Delta\nu_{1/2}$ (cm.$^{-1}$); optical density $D = \log (I_0/I)$; extinction coefficient $\epsilon = 1/Cl \log (I_0/I)$ (mole$^{-1}$ l. cm.$^{-1}$); integrated intensity $T = T \log (I_0/I) d\nu$ (cm.$^{-1}$); molar integrated intensity $M = 1/Cl\, T \log (I_0/I)\, d\nu$ (mole$^{-1}$ l. cm.$^{-2}$).

Here $I_0$ and $I$ are the incident and transmitted radiation intensities at a particular frequency; $C$ is the concentration of adsorbed material in terms of moles of adsorbate per liter of sample, where the sample volume is defined by the external dimensions of the porous Vycor support; $l$ is the total path length traversed in the sample in cm. The extinction coefficients were not corrected for the effect of finite spectrometer resolving power[5] because of the overlapping nature of the bands.

The integrated intensities are probably within 10% of the true values. The two greatest sources of error in the quan-

(5) D. A. Ramsay, *J. Am. Chem. Soc.*, **74**, 72 (1952).

titative results were (1) the measurement of the amount of material adsorbed on the surface of the metal oxide and (2) the construction of the background spectrum relative to which the spectrum of the adsorbed molecules was measured. Estimated errors in integrated intensities are given in the tables of results.

Throughout this work the band intensities of the adsorbed species have been measured to investigate the effect of perturbation of molecular vibrations by the solid surfaces. The intensities of a number of halogenated hydrocarbons were measured (Table VI) and previously published gas and liquid intensities have been converted into the units employed here (Table VII) for comparison with those of the surface species.

At the completion of the infrared investigations the metal oxides were reduced with hydrogen to metals on which hydrogen, carbon monoxide and oxygen adsorption measurements were made to determine the surface areas of the dispersed materials (Table VIII).

## Results

(i) **Ethylene Adsorption on Nickel Oxide in Porous Glass. (a) Adsorption on Non-stoichiometric Nickel Oxide.**—The nickel oxide samples prepared as described above were black and were presumed to be the non-stoichiometric oxide.[6] Under certain conditions this could be partially reduced to the greenish stoichiometric oxide, which will be referred to below. Oxygen admitted to the latter sample returned it to the original black colour.

When ethylene was admitted at 20° to a non-stoichiometric nickel oxide sample, absorption bands appeared at 3020, 2970, 2940 and 2885 cm.$^{-1}$. In Fig. 1a the bands are shown 80 minutes after admitting ethylene.

Arising from the porous Vycor support an intense absorption band was observed between 3800 and 3400 cm.$^{-1}$; this was due to the $\nu_{OH}$ vibration of the hydroxyl groups on the surface of the glass. The bands at 2760 and 2540 cm.$^{-1}$ belong to the skeletal silica vibrations.[7] Quantitative results for the spectrum in Fig. 1a are given in Table I.

TABLE I

$C_2H_4$ ON NICKEL OXIDE IN POROUS GLASS

NaCl prism, 16 cm.$^{-1}$ slit width, % nickel oxide 2.7, sample thickness 0.28 cm.

| Gas pressure (cm.) | | $C_2H_4$ adsorbed (cc./g. glass) | | |
|---|---|---|---|---|
| $C_2H_4$ | *trans*-butene-2 | Total | − Physical | = Chemisorbed |
| 1.90 | 0.48 | 4.85 | 0.55 | 4.30 |

| | Absorption bands | | | | Total intensity | |
|---|---|---|---|---|---|---|
| $\nu$ | 3020 | 2970 | 2940 | 2885 | $T$ | $M$ |
| $\epsilon$ | 6 | 12 | 12 | 7 | 146 | 1800 |

The pressure in the cell decreased continuously over a period of five days when the ethylene was allowed to stand at 20° in contact with the sample. The intensity of the bands increased as adsorption proceeded. At the same time the relative intensity of the bands changed, probably indicating that more than one adsorbed species was present on the surface.

By comparing the spectra with those obtained by Sheppard and Yates[7] it may be seen that no bands were attributable to physically adsorbed ethylene. Physical adsorption of ethylene on the glass surface during the adsorption process led to the perturbation of the $\nu_{OH}$ band of the surface hydroxyl groups on the glass, as seen by the difference between the two dashed curves in Fig. 1a.

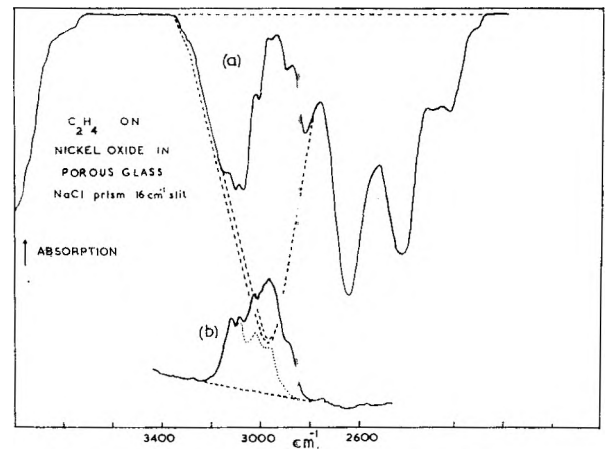


Fig. 1.—(a) spectrum of the ethylene surface species formed on non-stoichiometric nickel oxide in porous silica glass; ———, background spectrum of sample without adsorbate. (b) gas phase (ethylene and *trans*-butene-2) in equilibrium with (a); . . . . ., spectrum of ethylene component of gas phase.

**Composition of the Gas Phase.**—As described above the intensity of the surface species increased with increasing adsorption. Concurrently the gas phase was found to change from ethylene to *trans*-butene-2. These aspects of the adsorption process are shown in Table II. The ethylene component of the gas spectrum has been shown dotted in Fig. 1b and the intense maximum superimposed at 2960 cm.$^{-1}$ was due to *trans*-butene-2.

TABLE II

$C_2H_4$ ON NICKEL OXIDE IN POROUS GLASS

| Time after admitting $C_2H_4$ | Pressure (cm.) $C_2H_4$ | *trans*-butene-2 | $C_2H_4$ adsorbed (cc./g. glass) Physical | Chemisorbed | Total intensity $T$ | $M$ |
|---|---|---|---|---|---|---|
| | | (a) 1st Series | | | | |
| 80 min. | 1.90 | 0.48 | 0.55 | 4.30 | 146 | 1800 |
| 130 min. | 1.55 | 0.64 | 0.40 | 4.80 | 187 | 2040 |
| 14 hr. | 0.20 | 0.68 | 0 | 5.99 | 238 | 2100 |
| | | (b) 2nd Series | | | | |
| 40 min. | 5.20 | 0 | 1.15 | 1.34 | 72 | 2900 |
| 70 min. | 3.6 | 0.31 | 0.85 | 2.44 | 113 | 2400 |
| 105 min. | 2.6 | .44 | .65 | 3.36 | 168 | 2600 |
| 235 min. | 1.1 | .68 | .35 | 4.27 | 200 | 2450 |
| 475 min. | 0.2 | .59 | .05 | 5.47 | 233 | 2200 |
| 48 hr. | 0 | .43 | 0 | 5.89 | 270 | 2400 |

To confirm the presence of *trans*-butene-2 in the gas phase, the gas had been compressed and the more intense spectrum so obtained permitted a comparison of all absorption bands between 4000 and 650 cm.$^{-1}$ to be made with known standard spectra. No *cis*-butene-2 was found, but the maximum concentration of this isomer that could have escaped detection was approximately 20%, as shown by the absence of the characteristic C–H out of plane deformation band at about 680 cm.$^{-1}$.

When *trans*-butene-2 in the gas phase was re-

(6) S. J. Teichner and J. A. Morrison, *Trans. Faraday Soc.*, **51**, 961 (1955).

(7) N. Sheppard and D. J. C. Yates, *Proc. Roy. Soc.*, (London), **A238**, 69 (1956).

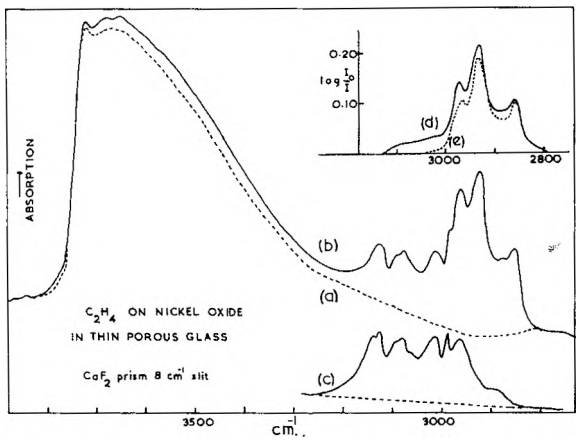


Fig. 2.—Ethylene admitted to nickel oxide in thin porous silica glass: (a) background spectrum of sample of porous silica glass containing nickel oxide and without adsorbate; (b) combined spectrum of sample, surface species and gas phase; (c) gas phase spectrum; (d) obtained by subtracting (c) from (b); (e) obtained after evacuating gas phase.

moved from the cell, more was desorbed from the sample showing that this gas was involved in a physical adsorption equilibrium. Indications are that this was most probably physical adsorption on the hydroxyl groups of the silica glass. Stepwise out-gassing of the *trans*-butene-2 from the adsorption cell resulted in the disappearance of the absorption band at 3020 cm.$^{-1}$ as well as some reduction of the 2970 and 2940 cm.$^{-1}$ bands. The former band was thus ascribed to physically adsorbed *trans*-butene-2.

**Ethylene Adsorption on Nickel Oxide in Thin Glass Samples.**—In Fig. 2 the spectrum is shown of the species formed by ethylene on a sample of non-stoichiometric nickel oxide in 0.1 mm. thick porous silica glass. Bands appeared at 2960, 2920 and 2860 cm.$^{-1}$. Weak absorption occurred above 3000 cm.$^{-1}$ which disappeared on evacuation. This probably was due to a species weakly adsorbed on the sample. The molar integrated intensity of the surface species on this sample was slightly smaller than that shown in Table I.

The adsorption process ceased after 18 days even though a considerable amount of ethylene still remained in the system.

Hydrogen added to the system after the completion of the adsorption led to the hydrogenation of the remaining ethylene. The spectrum of the surface species was unaffected by the hydrogen.

Samples of 0.1 mm. thickness were transparent down to but not below 1475 cm.$^{-1}$. Thus it was not possible to detect C–H deformation bands of the adsorbed hydrocarbon. With the present samples no absorption bands appeared between 1500 and 1700 cm.$^{-1}$ in the region characteristic of the absorption of unsymmetrically substituted carbon–carbon double bonds.

Figure 2 shows the $\nu_{OH}$ absorption of the surface hydroxyl groups of the glass. The sharp band at 3735 cm.$^{-1}$ corresponds to absorption by free hydroxyl groups on the glass surface and the broad band at lower frequency to hydrogen bonded hydroxyl groups. It may be seen that due to physical adsorption of ethylene on the hydroxyl groups, the $\nu_{OH}$ vibration was perturbed (spectrum a to b) with an increase of intensity of the lower frequency hydrogen bonded component.

**Reproducibility of Catalyst for Adsorption.**—It was possible to remove the species from the surface of the nickel oxide by heating at 350° for 12 hours with oxygen. A fresh dose of ethylene was then admitted and, apart from a small decrease in rate, the adsorption process occurred as before, with *trans*-butene-2 formed in the gas phase and the spectrum of the surface species was the same as that in Fig. 1a. Table IIa shows the rate of formation of the surface species on a fresh nickel oxide sample and Table IIb the rate after cleaning and admitting more ethylene.

The sample then was reduced completely by hydrogen at 320° to nickel metal. Ethylene standing for two weeks over this sample did not produce absorption bands due to surface species on the nickel. After reoxidizing by heating with oxygen at 300° for 12 hours it was possible to repeat the process with ethylene. However, there was a great decrease in the rate of formation of the surface species after reduction and reoxidation, possibly due to loss of surface area of the nickel oxide.

**(b) Adsorption of Ethylene on Stoichiometric Nickel Oxide.**—Non-stoichiometric samples were normally prepared by decomposing nickel nitrate in the pores of the silica glass. It was possible partially to reduce these to give light green samples which were presumably the stoichiometric oxide.[6]

A premixed dose of hydrogen and ethylene (Table III) was admitted to the sample at 20° and allowed to stand to investigate (1) whether the adsorption was the same on this sample as on the previous ones and (2) whether ethylene would be hydrogenated over nickel oxide.

TABLE III

PREMIXED $C_2H_4 + H_2$ ON STOICHIOMETRIC NICKEL OXIDE IN POROUS GLASS

$CaF_2$ prism 8 cm.$^{-1}$ slit width, % nickel oxide 2.3, sample thickness 0.22 cm., original gas mixture $H_2$ 9.41 cm. and $C_2H_4$ 4.71 cm.

| Time after admission | Pressure (cm.) $C_2H_4$ | *trans*-Butene-2 | $C_2H_6$ | $C_2H_4$ adsorbed (cc./g. glass) Physical | Chemisorbed | Absorption bands $\epsilon$ (2970 cm.$^{-1}$) | Total intensity $T$ | $M$[a] |
|---|---|---|---|---|---|---|---|---|
| 20 min. | 4.2 | 0 | 0 | 0.85 | 0 | .. | .. | [b] |
| 80 min. | 3.5 | 0.29 | 0 | .70 | 0.47 | 40 | 30 | 4900 |
| 130 min. | 3.0 | .34 | 0 | .65 | 0.94 | 27 | 50 | 4100 |
| 5 hr. | 2.1 | .35 | 0.40 | .55 | 1.56 | 25 | 88 | 4300 |
| 20.5 hr. | 0.5 | .35 | 1.3 | .15 | 2.70 | 21 | 129 | 3700 |

[a] Accuracy ± 20%. [b] Only physical adsorption on glass.

The early stages of the adsorption proceeded in a similar manner to that on the non-stoichiometric samples and *trans*-butene-2 was produced. Later, however, the reaction $C_2H_4 + H_2 \rightarrow C_2H_6$ commenced and the rate of production of ethane was soon faster than that of *trans*-butene-2. Eventually all the ethylene was consumed by hydrogenation and by adsorption. The final gas phase contained *trans*-butene-2, ethane and excess hydrogen and possibly butane.

The spectrum of the adsorbed species on this sample showed a strong band at 3020 cm.$^{-1}$, which persisted even after evacuation at room temperature for 3 hours at a vacuum of $10^{-5}$ mm. This was unlike the 3020 cm.$^{-1}$ band in the non-stoichio-

metric samples which was easily removable by pumping and which was demonstrated to be due to physically adsorbed *trans*-butene-2.

Throughout the course of the adsorption measurements the sample remained green. When air was admitted at 20° the sample rapidly became black indicating non-stoichiometric nickel oxide. The absorption intensity of the surface species was unaltered by this process.

(ii) **Ethylene Adsorption on Copper Oxide in Porous Glass.**—A surface species having absorption bands at 2920 and 2860 cm.$^{-1}$ was produced when ethylene was allowed to stand over a sample containing copper oxide prepared in the same manner as the nickel oxide samples. The intensity of these bands increased with time as more ethylene was adsorbed. In Fig. 3 the spectrum of the adsorbed species has been measured and replotted on an optical density scale. The quantitative results are shown in Table IV.

TABLE IV

$C_2H_4$ ON COPPER OXIDE IN POROUS GLASS

NaCl prism 13 cm.$^{-1}$ slit width, % copper oxide 2.1, sample thickness 0.20 cm.

| Fig. 3 | Time | $C_2H_4$ pressure (cm.) | Vol. adsorbed (cc./g. glass) Physical | Chemisorbed | Concn. (mole/l.) |
|---|---|---|---|---|---|
| a | 45 min. | 6.1 | 1.30[a] | 0.37 | 0.026 |
| b | 19 hr. | 5.8 | 1.25 | .67 | .047 |
| c | 43 hr. | 5.7 | 1.20 | .99 | .069 |
| d | 43 days | 4.4 | 1.00 | 2.73 | .19 |
| e | 67 days | 3.9 | 0.90 | 3.49 | .24 |

Absorption bands

| | 2920 cm.$^{-1}$ $D$ | ($\Delta\nu_{1/2}$ = 50 cm.$^{-1}$) $\epsilon$ | 2860 cm.$^{-1}$ $D$ | ($\Delta\nu_{1/2}$ = 45 cm.$^{-1}$) $\epsilon$ | Total intensity $T$ | $M$ |
|---|---|---|---|---|---|---|
| a | 0.050 | 10 | 0.03 | 5 | 5 | 1200 |
| b | .11 | 12 | .05 | 5 | 11 | 1200 |
| c | .16 | 11 | .08 | 6 | 18 | 1300 |
| d | .74 | 19 | .39 | 10 | 72 | 1900 |
| e | .99 | 20 | .54 | 11 | 100 | 2000[b] |

[a] Physically adsorbed $C_2H_4$ on glass (concn. 0.091 mole/l.). Absorption bands:

| 3090 cm.$^{-1}$ | 3000 cm.$^{-1}$ | Total intensity | |
|---|---|---|---|
| $\epsilon$ = 3.5 | $\epsilon$ = 3.5 | $T$ | $M$ |
| | | 11 | 600(±50%) |

[b] Accuracy ±20%.

In addition to the bands at 2920 and 2860 cm.$^{-1}$, weak bands appeared at 3090 and 2990 cm.$^{-1}$ due to ethylene physically adsorbed on the glass.[7] The gas phase remained ethylene during the adsorption process.

Electron diffraction and X-ray studies on the porous glass containing copper oxide failed to reveal the oxidation state of the copper. It was presumed that the sample contained cuprous oxide as this material is usually more active in catalysis than cupric oxide. For example ethylene is readily adsorbed by cuprous oxide.[8]

(iii) **Ethylene Adsorption on Oxidized Palladium in Porous Glass.**—Bands appeared at 2960, 2940 and 2870 cm.$^{-1}$ and the molar integrated intensity was about 1500 mole$^{-1}$ l. cm.$^{-2}$ when ethylene was admitted to a porous glass supported sample of palladium, oxidized by heating in

(8) W. E. Garner, F. S. Stone and P. F. Tiley, *Proc. Roy. Soc.* (*London*), **A211**, 472 (1952).

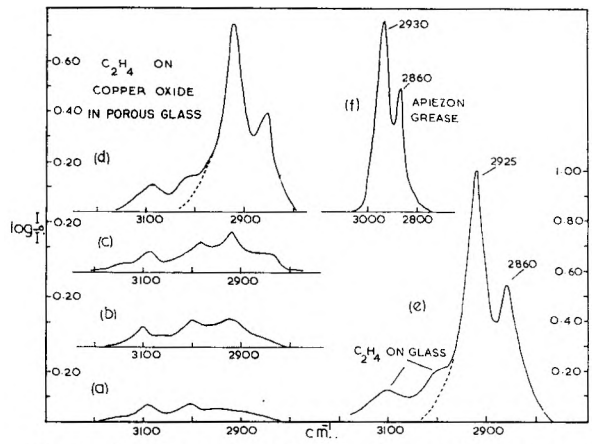


Fig. 3.—Spectrum of ethylene surface species on copper oxide in porous silica glass at the following times after admission: (a) 45 minutes; (b) 19 hours; (c) 43 hours; (d) 43 days; (e) 67 days; (f) comparison spectrum of long chain hydrocarbon $-CH_2CH_2-$...

air. The intensity of the bands increased with time over a period of several days as adsorption proceeded.

(iv) **Ethylene Adsorption on Silver Oxide in Porous Glass.**—The amount of ethylene adsorbed on the silver oxide sample (prepared by decomposing silver nitrate impregnated in porous glass) was equal to that adsorbed on a clean glass sample at the same pressure. Absorption bands appeared at 3090 and 2990 cm.$^{-1}$ corresponding to physically adsorbed ethylene on the glass of the sample. The intensity of the bands was similar to that shown at the foot of Table IV for ethylene on the copper oxide sample. No other bands appeared in the spectrum even after standing for two weeks.

(v) **Ethane Adsorption on Nickel Oxide in Porous Glass.**—Only physical adsorption occurred when ethane was admitted at 20° to a non-stoichiometric sample of nickel oxide in porous glass. The amount of adsorption on the sample was equal to that on a clean glass sample at the same pressure. No absorption bands persisted when the gas phase was evacuated or when the sample was heated to 150° with ethane. The intensity of the physically adsorbed ethane is given in Table V.

TABLE V

PHYSICAL ADSORPTION ON NICKEL OXIDE-POROUS SILICA GLASS

NaCl prism 15 cm.$^{-1}$ slit width, sample thickness 0.28 cm.

| Gas | Pressure (cm.) | Vol. adsorbed (cc./g. glass) | Concn. (mole/l.) |
|---|---|---|---|
| $C_2H_2$ | 3.68 | 1.16 | 0.079 |
| $C_2H_6$ | 4.80 | 0.51 | 0.035 |

Absorption bands

| | $\nu$ | $\Delta\nu_{1/2}$ | $D$ | $\epsilon$ | Total intensity $T$ | $M$[a] |
|---|---|---|---|---|---|---|
| $C_2H_2$ | 3240 | 48 | 1.20 | 50 | 77 | 3500 |
| $C_2H_6$ | 2950 | .. | 0.50 | 52 | 58 | 6000 |

[a] Accuracy ±25%.

(vi) **Acetylene Adsorption on Porous Glass Containing Oxides of Nickel, Copper, Palladium or Silver.**—Acetylene was admitted to porous glass samples containing the above metal oxides and in each case a well resolved intense band appeared at 3240 cm.$^{-1}$ due to acetylene physically adsorbed

on the glass of the sample.[7] No bands were found at lower frequencies.

The $\nu_{OH}$ vibration of the surface hydroxyl groups of the glass was perturbed by this adsorption and the low frequency hydrogen bonded component of the hydroxyl absorption band was increased. The gas phase remained acetylene even after prolonged standing.

Quantitative results of the band of physically adsorbed acetylene on a non-stoichiometric nickel oxide sample are given in Table V. When this sample was evacuated at $10^{-5}$ mm. and 20° for 45 minutes the spectrum showed a considerable amount of acetylene remaining. Intensity measurements of the 3240 cm.$^{-1}$ band of acetylene on the samples containing other metal oxides were in good agreement with that given in Table V.

No other absorption bands appeared when hydrogen was added to the oxide systems containing acetylene. The acetylene in the gas phase was also unaffected by adding hydrogen. Hydrogen at 20° reduced the very transparent silver oxide samples to silver which was opaque to visible light.

## Discussion

**Ethylene Adsorption on Metal Oxides in Porous Silica Glass; Assignment of Vibrational Bands.**—The bands at 2970 and 2885 cm.$^{-1}$ in the spectrum of the ethylene surface species on nickel oxide samples (see Results ia) have been assigned to C–H stretching vibrations of methyl groups and the band at 2940 cm.$^{-1}$ to the asymmetric methylene C–H stretching vibration by comparison to normal hydrocarbon spectra.[9] These assignments also agree within narrow frequency limits with the spectra of halogen substituted hydrocarbons (Table VI). The methylene vibrational band at 2850 cm.$^{-1}$ did not appear in the spectrum of the ethylene–nickel oxide system and this band is indeed weak or poorly resolved in the spectra of the halogenated hydrocarbons such as 1,2-dichloroethane, 1,2-dibromoethane and the *n*-propyl halides.

Absorption bands above 3000 cm.$^{-1}$ are characteristic of C–H stretching modes of normal unsaturated hydrocarbons.[9] However in certain circumstances the presence of polar substituents in a saturated hydrocarbon may raise the frequency of a C–H stretching mode above the normal limits. In such cases frequencies above 3000 cm.$^{-1}$ may not indicate unsaturation. For example methyl iodide (Table VI) has an absorption band at 3053 cm.$^{-1}$.

The absorption band at 3020 cm.$^{-1}$ in the spectrum of the ethylene on non-stoichiometric nickel oxide (see Results ia) has been shown to belong to physically adsorbed *trans*-butene-2. In view of this and the correspondence of bands below 3000 cm.$^{-1}$ with those of normal hydrocarbons it seems likely that the 3020 cm.$^{-1}$ band on the stoichiometric nickel oxide (Results ib) was due to an unsaturated species.

The frequencies of the ethylene species on oxidized palladium suggest the presence of methyl and methylene groups (Results iii).

In contrast to the spectrum of the surface species on the palladium and nickel oxide samples the spectrum of the ethylene surface species on copper oxide (Results ii) corresponds to the structure $-CH_2-CH_2-$ . . . The frequencies and contour of the bands on the copper oxide sample may be compared to the spectrum of Apiezon grease, shown in Fig. 3f, which contains a large proportion of long unbranched chains $-CH_2-CH_2-$ . . .

TABLE VI

INTENSITIES OF C–H STRETCHING MODES—HALOGENATED HYDROCARBONS

$CaF_2$ prism 8 cm.$^{-1}$ slit width

| Compound | $\nu$ | $\epsilon$ | Total intensity $M$ |
|---|---|---|---|
| Methyl iodide | 3053 | 1.1 | 554 |
| | 2951 | 13.1 | |
| | 2814 | 1.3 | |
| Ethyl bromide | 2980 | 16.8 | 1660 |
| | 2927 | 12.8 | |
| | 2870 | 7.8 | |
| 1,2-Dichloroethane | 2960 | 13.1 | 814 |
| | 2880 | 2.2 | |
| | 2846 | 1.9 | |
| *n*-Propyl chloride | 2973 | 71 | 4840 |
| | 2945 | Shoulder | |
| | 2885 | 25 | |
| | 2855 | Shoulder | |
| *n*-Propyl iodide | 2970 | 81 | 4530 |
| | 2938 | 36 | |
| | 2880 | 24 | |
| | 2849 | 13 | |

**The Adsorption Process and Nature of the Surface Species.**—The ratio of the number of ethylene molecules adsorbed to the total number of nickel atoms in the catalyst in the later stages of the adsorption process (Results ia and b) exceeded 1:1, so that even assuming maximum surface area of the nickel oxide it would not be possible to accommodate the ethylene in a single adsorbed layer. However, it would be possible to accommodate the ethylene as a polymeric species extending outward from the surface of the nickel oxide.

The formation of one type of dimer in the nickel oxide system was shown conclusively by the presence of *trans*-butene-2. Measurement of the surface area of the nickel, after reduction from nickel oxide, confirmed the occurrence of polymerization. Thus from Table II the maximum amount of ethylene adsorbed on the nickel oxide was 6 cc. per gram of glass, while from Table VIII the hydrogen adsorption on the sample, after reduction to nickel, was 0.37 cc. per gram of glass. The hydrogen molecule adsorbs as atoms on two surface metal atoms[10] and assuming that two metal sites were covered by the hydrocarbon chain it was probable that the surface species was comprised of fifteen ethylene molecules.

The amounts of hydrogen and carbon monoxide adsorbed on the copper oxide sample, and also on the sample after reduction to copper, were very small (Table VIII). It has been shown that the adsorption of hydrogen on clean copper surfaces is very small[15] and therefore it is probable that the

(9) R. N. Jones and C. Sandorfy in "Chemical Applications of Spectroscopy," Vol. IX, Interscience Publishers, New York, N. Y., 1956.

(10) B. M. W. Trapnell, "Catalysis," Vol. 3, Reinhold Publ. Corp., New York, N. Y., 1955, p. 1.

TABLE VII

INTENSITIES OF C–H STRETCHING MODES—GASES AND LIQUID HYDROCARBONS

| Gas | Ref. | Total intensity $M$ |
|---|---|---|
| Acetylene | 11 | 3000 |
| Ethylene | 12 | 1670 |
| Ethane | 13 | 7370 |
| Liquid | | |
| $CH_3$–$CH_3$ | 14 | 7680 |
| $CH_3$–$CH_2$– | 14 | 7160 |

surface area of the copper in the present sample was greater than indicated in Table VIII. In view of this, an estimate of 0.3 to 0.4 cc. (per gram of glass) of hydrogen to completely cover the copper surface was made by comparison to the amount of hydrogen adsorbed on a nickel sample with a similar concentration of metal. Since the amount of ethylene adsorbed on the sample was much greater than this figure, polymerization of ethylene must have occurred on the sample. If the polymer chain was assumed to cover two surface metal atoms in the oxide, then the chain length of the $-CH_2-CH_2-$ . . . surface species for maximum coverage (Table IV) was about ten ethylene molecules long. Similarly adsorption measurements showed that ethylene was also polymerized on oxidized palladium samples.

TABLE VIII

ADSORPTION ON METAL OXIDES AND METALS IN POROUS GLASS

Surface area of total sample (B.E.T. method using argon at 79°K.)

| Surface area ($m.^2/g.$) | Nickel oxide sample 195 | Copper oxide sample 179 |
|---|---|---|
| | Chemisorption studies (17°) | |
| | Nickel oxide sample | Copper oxide sample |
| Gas | Vol. chemisorbed (cc./g. glass) | Vol. chemisorbed (cc./g. glass) |
| CO | 0.13 | 0.09 |
| $H_2$ | 0.04 | 0.02 |
| | Samples reduced to metals | |
| $H_2$ | 0.37 | 0.03 |
| CO | .. | .07 |
| $O_2$ | 0.89 | .69 |

**Absorption Intensity of Surface Species.**—Polymerization of ethylene has been shown to occur on the oxides of nickel, copper and palladium with the formation of surface species, which are for the greater part saturated and composed of methyl and methylene groups. This assignment of structure was made on the basis of the band frequencies and contours as described above. From these observations it is apparent that in the adsorption process the ethylene molecules have been perturbed and reacted to give new chemical species.

It is of interest to see whether the C–H stretching modes of the new polymeric surface species, through adsorption on to the surface, have been greatly perturbed. This has been done by comparing the absorption intensities with those of molecules of similar basic structure, but in normal liquid on gas environments.

Before making this comparison some idea of the intensity variations of the C–H stretching vibrations of liquid hydrocarbons may be obtained by comparing the intensity of the C–H stretching mode of chloroform in dilute solution in carbon tetrachloride (174 $mole^{-1}$ l. $cm.^{-2}$)[16] with that found for liquid chloroform (407 $mole^{-1}$ l. $cm.^{-2}$). This twofold intensity increase illustrates the effect of changing the polar nature of the solvent environment.

Francis[14] has measured the intensity of the stretching vibration of tertiary C–H groups in aliphatic hydrocarbons and a value of 1210 $mole^{-1}$ l. $cm.^{-2}$ has been calculated from his results. It may be seen that the intensity of a tertiary C–H group is considerably decreased by the presence of adjacent polar substituents. Similar conclusions may be drawn from Tables VI and VII where the intensities of halogen substituted molecules are one-fifth to one-tenth as large as those of unsubstituted molecules with similar basic structure. It is probable from these considerations that great variations of C–H intensities may be caused by varying the environment of the C–H groups.

The intensities of the ethylene surface polymers (Tables I, II, III and IV) were intermediate between those of the halogen substituted hydrocarbons (Table VI) and those of the unsubstituted molecules shown in Table VII. In view of this it was concluded that the adsorption of the polymer on to the metal oxide surface introduced no greater perturbation of C–H stretching modes than that produced by substitution of halogen atoms into similar molecules.

In the examples where acetylene and ethane were admitted to porous glass samples containing metal oxides, the intensities of these molecules, physically adsorbed on the samples (Table V), were in good agreement with the intensities of the corresponding molecules in the gaseous state (Table VII). Any chemisorption of acetylene and ethane on to the metal oxides, and also of ethylene on to silver oxide, must have occurred to less than monolayer coverages. A monolayer of material with intensity comparable with those reported in Tables I–IV would have been detected readily by the spectrum.

**Acknowledgments.**—The author wishes to thank Dr. N. Sheppard for suggesting and supervising this research and Dr. D. J. C. Yates for advice. Awards of a Hackett Postgraduate Studentship and a Consolidated Zinc Corporation Bursary are gratefully acknowledged.

## DISCUSSION

A. C. ZETTLEMOYER (Lehigh University).—Is it possible you have water present in the nickel oxide sample?

L. H. LITTLE.—Only adsorbed water which is unaffected by evacuation for several hours at 300° could be present on the sample.

The spectrum of the porous silica support shows an intense hydroxyl absorption band even after prolonged evacuation. With samples of 0.1 mm. thickness it is possible to resolve

(11) D. F. Eggers, I. C. Hisatsune and L. Van Alten, THIS JOURNAL, **59**, 1124 (1955).

(12) R. C. Golike, I. M. Mills, W. B. Person and B. Crawford, *J. Chem. Phys.*, **25**, 1266 (1956).

(13) I. M. Nyquist, I. M. Mills, W. B. Person and B. Crawford, *ibid.*, **26**, 552 (1957).

(14) S. A. Francis, *ibid.*, **18**, 861 (1950).

(15) G. L. Kington and J. M. Holmes, *Trans. Faraday Soc.*, **49**, 417 (1953).

(16) N. S. Bayliss, A. R. H. Cole and L. H. Little, *Australian J. Chem.*, **8**, 26 (1955).

this band into a high frequency component due to free hydroxyl groups on the surface and a broad low frequency component due to hydrogen bonded surface hydroxyl groups. Strongly adsorbed water which remains after evacuation would be hydrogen bonded and it would not be possible from the infrared spectrum to distinguish between this water and the surface hydroxyl groups which are involved in hydrogen bonding.

# SORPTION AND MAGNETIC SUSCEPTIBILITY STUDIES ON NITRIC OXIDE–SILICA GEL SYSTEMS AT A NUMBER OF TEMPERATURES

BY AAGE SOLBAKKEN[1] AND LLOYD H. REYERSON

*Contribution from the School of Chemistry, University of Minnesota, Minneapolis, Minnesota*

*Received March 2, 1959*

Sorptions of nitric oxide by silica gel were determined at 181, 193, 273 and 293°K. A movable magnet made it possible to measure the magnetic susceptibility of the sorbed nitric oxide at each point on the sorption isotherm. The results showed that the nitric oxide was sorbed in the same average magnetic state at 273 and 293°K. as it existed in the gas phase. However, at 181 and 193°K., the nitric oxide, up to nearly monolayer coverage, was sorbed entirely in a state with a magnetic moment equal to the excited $^2\pi_{3/2}$ state. Additional sorbed nitric oxide had the same susceptibility as the gas at the same temperature. This seems to be positive evidence that the first molecules sorbed at these lower temperatures were all present on the surface in an excited state.

In an earlier study in this Laboratory,[2] the magnetic susceptibility of $NO_2$ sorbed on silica gel was determined at two temperatures over a considerable sorption range. The results showed the $NO_2$ was physically adsorbed but that it existed on the surface of the silica gel almost entirely as the nitrogen tetroxide dimer. During July, 1958, in a private communication to one of us, Professor J. H. deBoer reported that, in studies on the sorption of NO on silica gel at the Laboratories of the States Mines in Holland,[3] the sorbed system turned a greenish color at 0° and that this color intensified as sorptions were carried out at lower and lower temperatures. A lighter color was observed when NO was sorbed on alumina gel. This suggested that the sorption surfaces might have catalytically changed the sorbed nitric oxide. If so, then by following the magnetic susceptibility of the strongly paramagnetic nitric oxide, as it was sorbed by the silica gel, it should be possible to determine whether or not any change had taken place. The following experiments record a number of very interesting results obtained by such a study at temperatures ranging from 181 to 293°K.

## Experimental Procedure

The general schematic layout of the equipment used in these experiments is shown in Fig. 1 and it was much like that reported in the previous work[2] except that a new, better-designed and better-cooled electromagnet had been built and installed in the travelling magnet frame. The field strength of this magnet was about 9000 oersteds when operating at full current strength and the pole pieces, as constructed, gave a very inhomogeneous field. A spherical glass bucket, containing 0.1732 g. of very pure silica gel, was suspended on a quartz fiber from the quartz spiral spring. A glass jacket surrounded the tube containing the spiral spring as well as the mercury manometer. This jacket was kept at a constant temperature of 30° by circulating water from a thermostat maintained at this temperature. The diagram shows how the sample was maintained at a constant temperature by moving large quantities of air through a thermostat, then up a large insulated tube to a jacket surrounding the tube containing the sample, and then down through an outer jacket and out. Calibrated thermometers determined the thermostat temperatures, and thermocouple junctions placed in the thermostat and in the jacket surrounding the sample made it possible to maintain the sample at a constant temperature. Using solid $CO_2$ in acetone, together with a bimetallic control to an immersion heater, permitted measurements to be made at 181 and 193°K., while the use of ice in water made possible the determinations at 273°K. At 293°K., the air was blown through water thermostated to the desired temperature. A sample of the same silica gel that was used in the previous study[2] was carefully dried and weighed into the sample bulb. It was thoroughly outgassed before each run and its magnetic susceptibility showed it to be free of paramagnetic impurities. The NO, that was transferred to the large flask, had been prepared for spectroscopic studies and proved to be free of other oxides of nitrogen by all the tests that were made on it. By surrounding the tip of the large flask with liquid nitrogen, the gaseous NO could be frozen and thus handled easily during its transfer and use in the sorption process.

The sorption system was thoroughly outgassed while the flask of NO was shut off from it. The isotherm at a given temperature was obtained by measuring the extension of the calibrated quartz spring as the NO reached equilibrium with the silica gel, following the addition of successive increments of gas from the flask. Once sorption equilibrium was established for each increment or decrement of gas, the magnetic field was turned on and the precision lift raised or lowered the magnet until it exerted its maximum force on the sample with the sorbed NO. This permitted the determination of the magnetic susceptibility of the sorbed NO. The magnetic field had been calibrated by using 173.2 mg. of CuO in a Pyrex bulb weighing 62.5 mg. The calibration was carried out in an atmosphere of argon at 50 mm. and the results are given in Table I.

TABLE I

CALIBRATION OF MAGNETIC FIELD

| Temp., °K. | Force on CuO, dyne | $(H\partial H/\partial s)^a$ |
|---|---|---|
| 181 | 2.0338 | $5.486 \times 10^6$ |
| 193 | 2.1711 | $5.466 \times 10^6$ |
| 273 | 2.6171 | $5.378 \times 10^6$ |
| 293 | 2.6732 | $5.340 \times 10^6$ |

[a] Calculated using magnetic susceptibility of Pyrex = $-0.337 \times 10^{-6}$ [4] and interpolated values of magnetic susceptibilities of CuO from reference 5.

## Results and Discussion

The equilibrium sorption values for NO sorbed by 0.1732 g. of silica gel are given for the four tempera-

(1) Graduate Norwegian Fellow at the University of Minnesota from the Norwegian Institute of Technology, Trondheim, Norway.

(2) L. H. Reyerson and John Wertz, THIS JOURNAL, **53**, 234 (1949).

(3) door C. Bokhoven and P. Zwietering, *Chem. Weekblad*, **52**, 83 (1956).

(4) J. M. Honig, Thesis, Univ. of Minn., 1952.

(5) N. Perakis, A. Serres and T. Karantassis, *J. phys. radium*, **17**, 134 (1956).

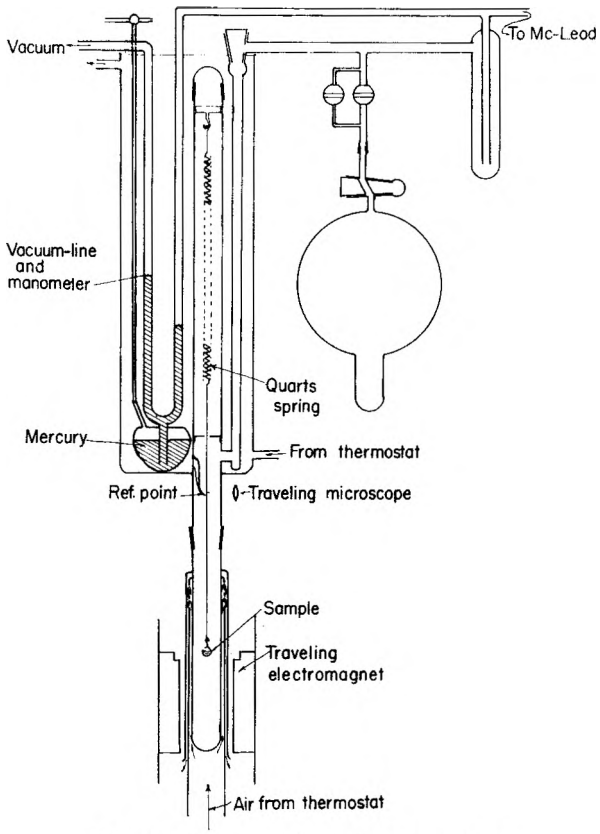


Fig. 1.—Diagram of sorption apparatus.

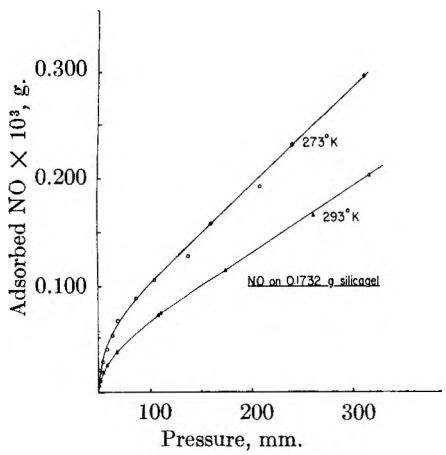


Fig. 2.—Sorption isotherms at 273 and 293°K.

tures in Figs. 2 and 3. These results showed that NO is more weakly adsorbed on silica gel than was nitrogen dioxide.[2] At none of these temperatures, nor at about 83°K., was any color detected as was reported by Professor de Boer. It seems likely that traces of impurities in the silica gel or in the NO, together with the possibility of trace residues of oxygen, may have been the cause of the color. In the present investigation, the system was outgassed for eight days while infrared lamps heated the whole system. The results, using such a high purity sorbent and sorbate, strongly indicated that the silica gel surface did not catalytically decompose any of the NO. In Figs. 4, 5 and 6, the magnetic force acting on the sorbed NO is plotted against the amounts taken up by the silica gel. From these

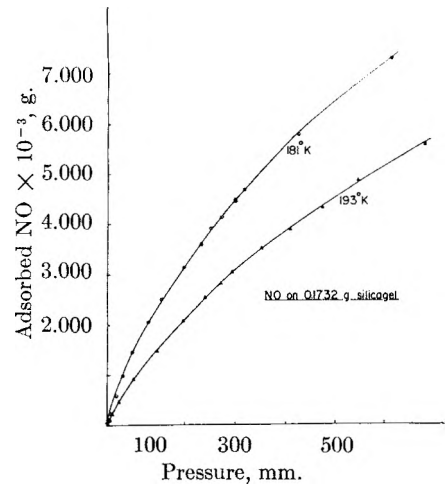


Fig. 3.—Sorption isotherms at 181 and 193°K.

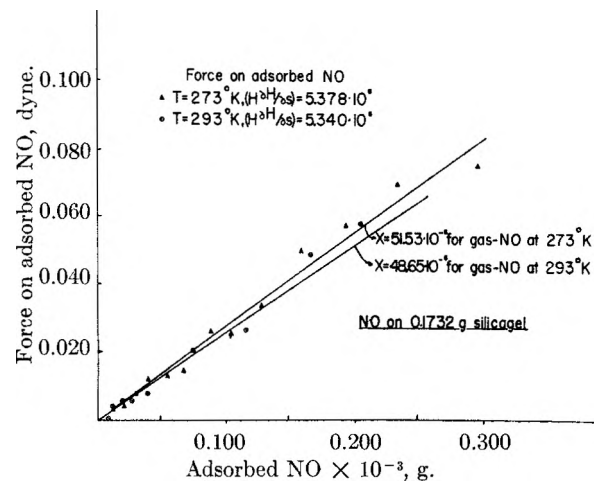


Fig. 4.—Magnetic force *vs.* amount of NO sorbed at 273 and 293°K.

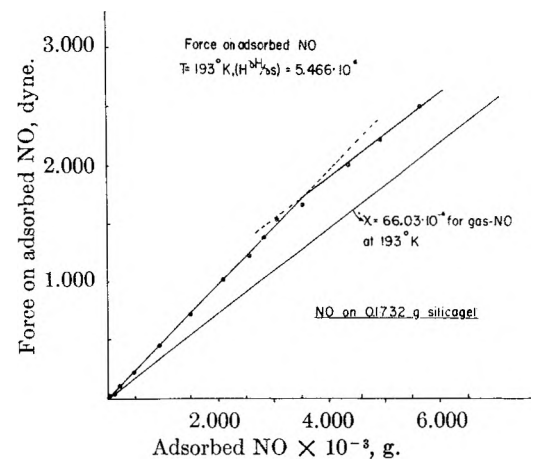


Fig. 5.—Magnetic force *vs.* amount of NO sorbed at 193°K.

values the magnetic susceptibility of the sorbed NO is calculated readily.

Examination of the magnetic data showed that the NO, sorbed at 273 and 293°K., had the same magnetic susceptibility on the surface as it had in the gas phase at the same temperature. Figure 4 shows the plot of the magnetic force against the amounts sorbed at these two temperatures. The

TABLE II

MAGNETIC STATE OF GASEOUS AND ADSORBED NO

| Temp., °K. | Gaseous NO[a] Magn. susc. $\chi \times 10^6$[b] | Gaseous NO[a] Bohr magn. number = $\mu$ | Gaseous NO[a] % $^2\pi_{3/2}$ state | Adsorbed NO[c] Magn. susc. $\chi \times 10^6$ | Adsorbed NO[c] Bohr magn. number = $\mu$ | Adsorbed NO[c] % $^2\pi_{3/2}$ state |
|---|---|---|---|---|---|---|
| 181 | 68.95 | 1.717 | *ca.* 33 | 92.23 | 1.98 | *ca.* 100 |
| 193 | 66.03 | 1.735 | *ca.* 36 | 87.80 | 1.99 | *ca.* 100 |
| 273 | 51.53 | 1.823 | *ca.* 59 | *ca.* 51.5 | 1.83 | *ca.* 59 |
| 293 | 48.65 | 1.835 | *ca.* 64 | *ca.* 48.6 | 1.83 | *ca.* 64 |

[a] Data interpolated and calculated from ref. 7, 8 and 9. [b] Calculated, using $\chi_{293} = 48.65 \times 10^{-6}$[6] and the formula (ref. 9, p. 22)

$$\mu = (3\chi RT/N_0^2)^{1/2}$$

where $\mu$ = Bohr magneton number, $\chi$ = magnetic susceptibility, $N_0$ = Avogadro's number. [c] Before the breaking point in the magnetic susceptibility curve, Figs. 5 and 6.

points give the experimental data and the straight lines are calculated from the susceptibility values of gaseous NO at these temperatures. Considering the small amounts of NO sorbed, the results are well within experimental limits and the agreement seems excellent. However, at the two lower temperatures, 193 and 181°K., Figs. 5 and 6, the force curve for sorbed NO departs from the calculated curve for gaseous NO at the same temperature. This departure continues until the silica gel is covered by something less than a monolayer of NO. Here a break occurs in the force curve and with further sorption of NO the points fall on a line that parallels the curve for gaseous NO. The break in the force curve seems less sharp at 181°K. than it is at 193°K. The force curves before the break fit the calculated curves for the magnetic susceptibility of NO, assuming that all of the molecules are in the excited $^2\pi_{3/2}$ state. Thus all of the molecules of NO that are sorbed before the break point are sorbed in the excited $^2\pi_{3/2}$ state. After that, the molecules seem to be sorbed in a state having the same susceptibility as the gas phase.[6]

Except at absolute zero, molecules of gaseous NO should exist as a mixture of molecules in the ground state, $^2\pi_{1/2}$, and in the excited state, $^2\pi_{3/2}$. As the temperature rises, the percentage of NO in the $^2\pi_{3/2}$ state increases. The energy difference between the two states is small, being about 352 cal. per mole.[7] The Bohr magneton number for NO in the $^2\pi_{1/2}$ state is zero and for the $^2\pi_{3/2}$ state is 2. Table II gives a calculated comparison of the magnetic susceptibility, the Bohr magneton number and the percentage of the NO in the $^2\pi_{3/2}$ state for the gaseous and adsorbed molecules at the four temperatures at which measurements were made. From these results, it is evident that at the two lower temperatures and up to nearly monolayer coverage, the silica gel surface sorbs only the excited molecules of NO or that all molecules sorbed in the $^2\pi_{1/2}$ state are converted to molecules in the $^2\pi_{3/2}$ state. The results definitely show that the shift in the equilibrium to higher concentrations of NO in the $^2\pi_{1/2}$ state as the temperature is lowered is reversed completely on the surface of the silica gel. Calculating the Bohr magneton numbers of NO on the silica gel for the two lower temperatures gave values of 1.98 and 1.99, which is a round number of 2 within the limits of experimental error. These results suggested a sorption study at still lower temperatures. One such experiment was carried out at about 83°K. using liquid nitrogen as the cooling agent. Since NO liquefies above this temperature, a gas pressure of 0.20 mm. of Hg was used. At this pressure, 8.0255 mg. of NO was sorbed on the 0.1732 g. of silica gel. One might expect that the NO would become diamagnetic due to dimerization at this temperature but the magnetic force was still 1.0094 dynes, which indicates that considerable paramagnetism remained in the sorbed NO.

Since sorption appears to be of the same type at the two lower temperatures and at the two higher temperatures, it was felt that heats of adsorption as

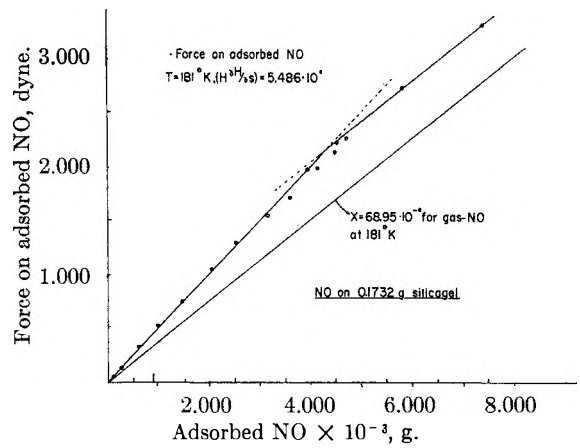


Fig. 6.—Magnetic force *vs.* amount of NO sorbed at 181°K.

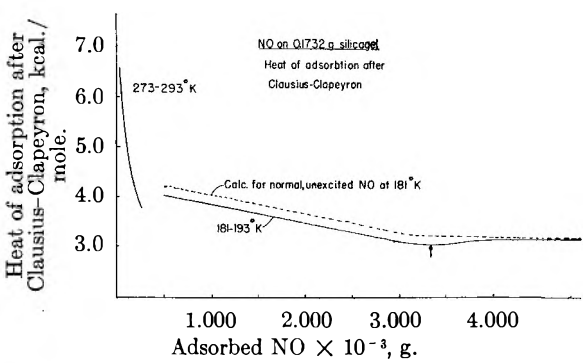


Fig. 7.—Differential heat of adsorption *vs.* amount of NO sorbed.

(6) In this paper, whenever the adsorbed gas is said to be in the $2\pi_{3/2}$ excited state, it is to be understood that the molecules of NO on the surface are in a magnetic state equivalent to that of the gas molecules in the $2\pi_{3/2}$ state.

(7) E. Bauer and A. Picard, *J. physik.*, **1**, 97 (1920).

(8) J. H. Van Vleck, "The Theory of Electric and Magnetic Susceptibilities," Oxford Press, New York, N. Y., 1932.

(9) D. M. Yost and H. Russell, "Systematic Inorganic Chemistry," Prentice-Hall, Inc., New York, N. Y., 1944.

obtained by Clausius–Clapeyron calculations might show something about the character of the sorption process.

The calculations for the two pairs of temperatures are presented graphically in Fig. 7. The sorption points are taken directly from the smooth isotherms giving values within experimental limits One notes that the largest $\Delta H$ values are found for the first small amounts sorbed. These calculated values fall as more NO is taken up by the silica gel. The solid lines represent the calculated points for the 273–293°K. and 181–193°K. data. The dashed curve represents the results to be expected if the gas had been sorbed in the same ratio of the two states as exists in the gas phase at this temperature. The arrow points to the spot in the magnetic curves where deviation from the first straight line begins. The slow rise in $\Delta H$ following this point seems to be a second proof that the additional sorbed gas goes on the gel in the same ratio of composition as in the gas phase. It should be noted that the solid curves for the two temperature pairs cover essentially the same pressure range of NO.

The magnetic studies, as well as the calculations of the heats of adsorption, seem to be positive proof that the NO sorbed up to nearly monolayer coverage at the lower temperatures is all in a state equivalent to that of $^2\pi_{3/2}$. In the gaseous state at the same temperature, only about one-third of the molecules exist in this excited state. It seems more than likely that surface forces have uncoupled the magnetic coupling between the spin $S$ and the orbital $\Delta$ of the odd electron of the NO adsorbed on the surface.

## DISCUSSION

F. H. HEALY (Lever Bros. Research Center).—Is it possible for the magnetic field to influence adsorption?

L. H. REYERSON.—We don't turn the magnetic field on until we reach equilibrium for the adsorption. With the old magnet we did have some heat effect. But this new magnet is kept at such a constant temperature that we do not observe any loss of gas from the surface at all during the magnetic measurement.

J. L. SHERESHEFSKY (Howard University).—Is the adsorption of nitric oxide reversible?

L. H. REYERSON.—Completely.

A. C. ZETTLEMOYER (Lehigh University).—I would like to ask whether it is known whether the water content of Professor Reyerson's silica gel was the same as Dr. de Boer's? A difference could account for the different results attained.

L. H. REYERSON.—It was about the same as far as we know. Our silica gel had less than 5% water of constitution. It is more probable that de Boer's material had small amounts of extraneous gases such as oxygen present.

# ADSORPTION STUDIES ON METALS. VIII. MONOFUNCTIONAL ORGANIC MOLECULES ON REDUCED AND OXIDE-COATED NICKEL AND COPPER

BY YUNG-FANG YU, J. J. CHESSICK AND A. C. ZETTLEMOYER

*Surface Chemistry Laboratory, Lehigh University, Bethlehem, Penna.*

*Received March 9, 1959*

Monolayer coverage, reversibilities and heats of adsorption of monofunctional organics were studied at 0 to 35° on reduced nickel and copper powders. More extensive and intensive chemisorption of 1-propanol, *n*-propylamine and benzene occurred on the electron-deficient d-metal, nickel, than on the electron-rich s,p metal, copper. Evidence for considerable surface reaction developed in the case of *n*-butyraldehyde on nickel. Exponentially decreasing heats of adsorption with increasing coverage were usually found for chemisorption. Only for the system propanol on nickel did the heats of adsorption remain constant up to essentially monolayer coverage; a dissociative adsorption mechanism is used to explain this phenomenon. The presence of biographical heterogeneities need not be considered to explain the heat curves. The relatively low heats of adsorption for benzene on nickel are explained on the basis of energy absorption needed to destroy the resonance of the aromatic ring. Comparisons were made with adsorption on thinly coated oxide films on the metals where the interactions were much less energetic and the packing of the adsorbate molecules less dense.

## Introduction

The nature of the adsorption of organic vapors by metal surfaces is of vital interest in catalysis, in lubrication and in corrosion inhibition. While some by-product information has been developed mostly from catalytic studies, very few direct studies of interactions of organic molecules possessing polar functional groups with bare metal surfaces are available. Chief among these was the development of an activity series for metal films by Trapnell[1] based on a semi-quantitative rating of their tendency to chemisorb a number of gases including ethane and ethylene. In a later more detailed study, Trapnell[2] ascribed the low activity of Fe, Co and Ni films for the chemisorption of methane and ethane to the ferromagnetic alignment of some of their unpaired electrons. Trapnell[3] also reported that one ethylene molecule takes up four tungsten sites; this ratio can be explained if hydrogens split off from each of the carbons to occupy two additional tungsten atoms *or* if each of the unsaturated carbons interacts with two tungsten atoms. Whether ethylene adsorption is associative or dissociative in character on supported nickel has been resolved by Eischens and co-workers[4] by means of infrared spectroscopy; on freshly reduced nickel films there is clear evidence for dissociative chemisorption which is eliminated when the surface is satisfied by the addition of small amounts of hydrogen.

Contrary to the low activity of nickel films found by Trapnell, Selwood[5] showed by changes in magnetic susceptibility that nickel supported on kieselguhr readily chemisorbs ethane. Furthermore, the greater effectiveness of ethane over ethylene in lowering magnetic susceptibility can be ascribed to the greater dissociative adsorption of the saturated molecule. In addition, Selwood showed that the initial rate of decrease of magnetic susceptibility with coverage for hydrogen, benzene and cyclohexane on supported nickel is in the ratio of 2:6:8. This relationship is to be expected if the hydrogen splits to become adsorbed as atoms, if no hydrogens split off the planar benzene ring and if one hydrogen splits off each of the four carbons in cyclohexane which contacts the surface in the "boat" form.

When aromatic compounds chemisorb on metals, the $\pi$-electrons of the ring often add to the electron-deficient energy levels of the so-called d-metals to reduce the electrical resistance. Suhrmann,[6] the chief proponent of this technique, showed the effectiveness of benzene and naphthalene adsorbed on nickel films. One of the few previous measurements of heats of adsorption of organic vapors onto metals is of interest here. Maxted and Josephs[7] showed that the initial heat of adsorption of thiophene on platinum black is lower than its aliphatic counterpart ethyl sulfide; the difference is just the resonance energy of the thiophene which the system absorbs as the $\pi$-electrons add to the metal.

Because of the paucity of data on the adsorption of organic molecules onto metals, it has not been possible to relate the electron donor tendency of various functional groups to the electronic configuration of metals. The present work was initiated to attempt to fill in some of this needed information by adsorption and calorimetric techniques. There is evidence[8] that the state of the metal, whether deposited film, single crystal, supported crystallites or polycrystalline powder, considerably affects the surface states and hence the adsorption properties. The early work in this series was begun with metal powders[9] and these substrates were used here with the realization that comparisons should be made with other forms. Nickel powder was chosen as a typical d-metal and copper as a typical s,p-metal.

## Experimental

**Materials.**—The nickel and copper powders were prepared by thermal decomposition of C.P. nickel carbonate and basic copper carbonate, respectively. These powders were decomposed to oxides at 400° under reduced pressure and the

(1) B. M. W. Trapnell, *Proc. Roy. Soc. (London)*, **A218**, 566 (1953).
(2) B. M. W. Trapnell, *Trans. Faraday Soc.*, **52**, 1619 (1956).
(3) B. M. W. Trapnell, *ibid.*, **48**, 160 (1952).
(4) R. P. Eischens and W. A. Pliskin, "Advances in Catalysis," Vol. IX, Academic Press, Inc., New York, N. Y., 1957, p. 662.
(5) P. W. Selwood, *J. Am. Chem. Soc.*, **79**, 4637 (1957).
(6) R. Suhrmann, "Advances in Catalysis," Vol. VII, Academic Press, Inc., New York, N. Y., 1955, p. 320; R. Suhrmann and K. Schulz, *J. Colloid Sci.*, Sup. 1, 55 (1954).
(7) E. B. Maxted and M. Josephs, *J. Chem. Soc.*, 2635 (1956).
(8) See for example J. H. deBoer, "Advances in Catalysis," Vol. VIII, Academic Press, Inc., New York, N. Y., 1956, p. 109.
(9) Y. F. Yu, J. J. Chessick and A. C. Zettlemoyer, "Advances in Catalysis," **IX**, 415 (1957) (no. VI of this series); A. C. Zettlemoyer, J. J. Chessick, Y. F. Yu and F. H. Healey, THIS JOURNAL, **61**, 1319 (1957).

outgassing was continued 12 hours beyond the point of no apparent gas evolution. The oxides were reduced with dry hydrogen at 400 and 300°, respectively; these temperatures used previously are the lowest feasible so that sintering could be minimized. After reduction, the metal powders were degassed at $10^{-5}$ mm. at 450 and 350°, respectively, just prior to the adsorption studies.

The organic liquids used to provide the adsorption vapors were reagent grade. They were dried with anhydrous magnesium sulfate and then frozen and pumped through several cycles so that only the middle portion was taken for the adsorption measurements.

**Adsorption Apparatus.**—The basic feature of the adsorption apparatus is the Teflon stopcocks. Besides the simplification these stopcocks made possible, they eliminated possible contamination of the metal samples with mercury from the cut-offs usually employed. These stopcocks would not hold a good vacuum at the outset, but they steadily improved when operated frequently during the first ten days of use. A liquid nitrogen trap was employed between the adsorption system and the pumps.

The adsorption system includes a sample tube, glass break-seal, organic vapor reservoir and a calibrated doser, and it is terminated with a glass Bourdon spoon gage. The gage is balanced with helium pressure which is measured by an Apiezon B oil manometer; small deflections of the gage from zero are determined by a microscope eyepiece. The equilibrium pressures can be determined to ±0.02 mm. and the range of the oil manometer is from 0–10 cm. A side arm is attached to the gage and immersed in silicone oil to damp the vibrations.

The reduced samples were sealed off and transferred to the adsorption apparatus. The seal was broken by a magnetically operated plunger just prior to each run. For studies on oxide-coated surfaces, the reduced powders were first exposed to dry oxygen at 25° and 1 cm. for 10 minutes so that the oxide films resulting were from 10 to 15 Å. thick.

**Calorimeter.**—The basic calorimeter design was that used previously for heats of chemisorption of oxygen on these same metals.[10] Modification includes a glass break-seal so the sample could be transferred from the apparatus on which it was reduced and a twenty-five junction copper–constantan thermocouple with the reference junctions held within 0.1° of the adsorption temperature to minimize heat loss through the thermocouple wires. The e.m.f. is amplified then recorded on a Brown Recorder. The sensitivity of the calorimeter is 0.001° or about 0.01 cal.; the heat capacity of the filled calorimeter ranged from 10 to 15 cal. per degree.

It was estimated for the calorimetric heats recorded here that over 90% of the heat evolution occurred within the first two minutes after the introduction of each portion of organic vapor.

## Results

A series of monofunctional compounds, both donor and acceptor types, were chosen for adsorption studies on nickel. Table I shows that 1-propanol, *n*-propyl bromide, *n*-propylamine, *n*-nitropropane, *n*-butyraldehyde and benzene were included. Four of the more interesting of these, namely, *n*-propyl alcohol, *n*-propylamine, *n*-nitropropane and benzene, were chosen for adsorption studies on copper. The isotherms as indicated in Table I were measured at temperatures ranging from 0 to 35° depending upon the vapor pressures of the adsorbates. The BET plots were linear except for butyraldehyde-on-nickel. This system gave indication of polymerization occurring on the surface; the apparent isotherm was almost linear and a $v_m$ could not be estimated from the BET plot.

Table I lists the BET $v_m$'s for the other adsorbates on the freshly reduced powders as $v_m$I's. These values are compared to the corresponding argon $v_m$ rather than assigning doubtful area values to each adsorbate molecule. The doubt arises particularly because the packing may be different in the portion of the first layer where chemisorption occurs and those portions physically adsorbed.

(10) J. J. Chessick, Y. F. Yu and A. C. Zettlemoyer, "Proceedings of the Second International Congress on Surface Activity," Vol. II, Academic Press, New York, N. Y. (no. VII of this series), p. 269.

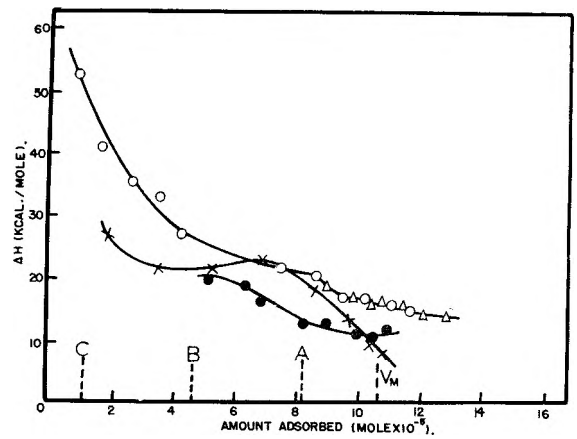


Fig. 1.—Heats of adsorption of *n*-propylamine on nickel: O, reduced surface, run 1; △, reduced surface, run 2, degassed at 25°, $\theta$ = 0 at A; X, reduced surface, run 3, degassed at 25° and 100°, $\theta$ = ) at C; ●, oxidized surface, $\theta$ = 0 at B.

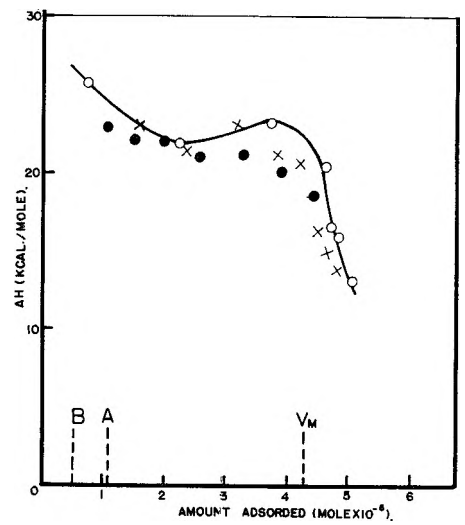


Fig. 2.—Heats of adsorption of *n*-propylamine on copper: O, reduced surface, run 1; X, reduced surface, run 2, $\theta$ = 0 at A; ●, oxidized surface, $\theta$ = 0 at B.

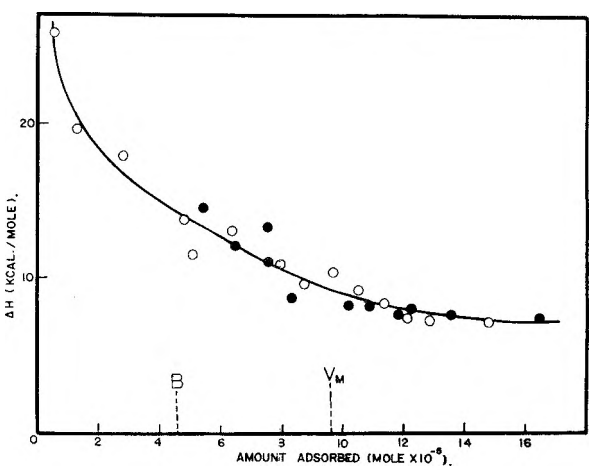


Fig. 3.—Heats of adsorption of benzene on nickel: O, reduced surface; ●, oxidized surface, $\theta$ = 0 at B.

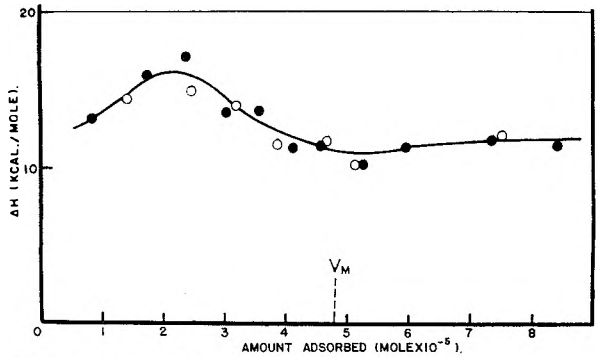


Fig. 4.—Heats of adsorption of benzene on copper: ○ reduced surface; ●, oxidized surface.

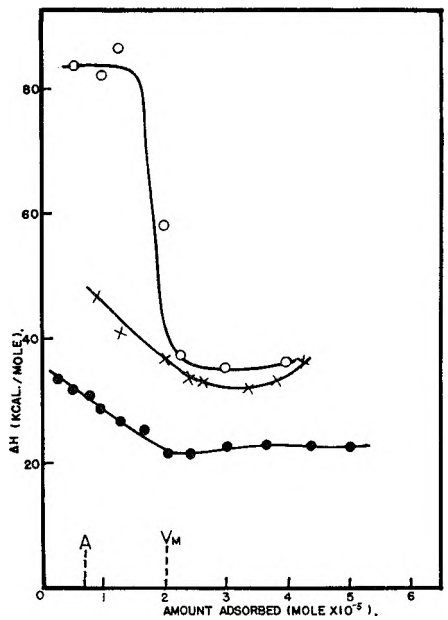


Fig. 5.—Heats of adsorption of *n*-propyl alcohol on nickel: O, reduced surface, run 1; X, reduced surface, run 2, $\theta = 0$ at A; ●, oxidized surface.

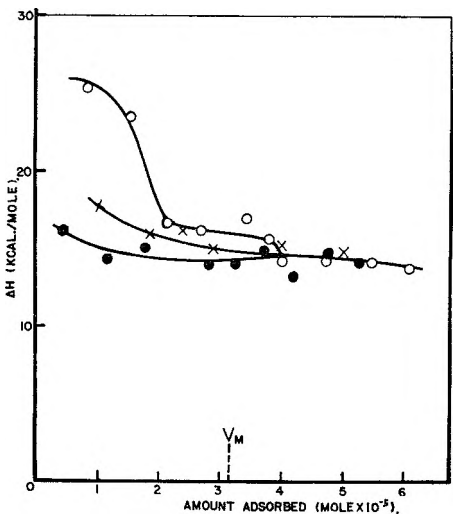


Fig. 6.—Heats of adsorption of *n*-propyl alcohol on copper: O, reduced surface, run 1; X, reduced surface, run 2; ●, oxidized surface.

In each case, the residual vapor after completion of the isotherm was condensed in a liquid nitrogen trap. Only in the case of the propyl alcohol was any permanent gas detected, and this amount was quite small. Hence, dissociated fragments in the gas phase did not invalidate the pressure measurements.

TABLE I

ADSORPTION OF MONOFUNCTIONAL ORGANICS ON METALS

| Adsorbate | Temp., °C. | $v_m^I/v_m^A$ | $v_m^{II}/v_m^A$ | $R_r$, % | $v_m^{III}/v_m^A$ | $v_m^{IV}/v_m^A$ | $R_o$, % |
|---|---|---|---|---|---|---|---|
| Nickel (1.2–1.3 m.²/g.) | | | | | | | |
| 1-Propanol | 25 | 0.57 | 0.44 | .. | 0.45 | 0.29 | 64 |
| *n*-Propyl bromide | 0 | .75 | .58 | 79 | .57 | .37 | 65 |
| *n*-Propylamine | 0 | .89 | .37 | 41 | .42 | .44 | 105 |
| *n*-Nitropropane | 35 | .59 | .30 | 50 | .28 | .25 | 89 |
| *n*-Butyraldehyde | 25 | .. | .. | .. | .86 | .68 | 79 |
| Benzene | 0 | .68 | .51 | 76 | .38 | .36 | 94 |
| Copper (0.4–0.5 m.²/g.) | | | | | | | |
| 1-Propanol | 25 | 0.31 | 0.29 | 94 | 0.31 | 0.25 | 80 |
| *n*-Propylamine | 0 | .64 | .51 | 81 | .57 | .41 | 72 |
| *n*-Nitropropane | 35 | .37 | .18 | 50 | .23 | .22 | 96 |
| Benzene | 0 | .34 | .34 | 100 | .38 | .38 | 100 |

After each initial isotherm on the reduced surface was completed, the systems were degassed at 25°, employing a liquid nitrogen trap and high vacuum system, for about 16 hours to a vacuum of better than $10^{-5}$ mm. A good vacuum was usually attained after 4 hours. The isotherms were then repeated to give new BET $v_m^{II}$'s. The ratio 100 $v_m^{II}/v_m^I$ is designated reversibility on the reduced surface, $R_r$; differences of a few per cent. between these values are no doubt meaningless. The reversible fraction of a monolayer is regarded to a first approximation as the physically adsorbed portion. Further detailed evidence emerges from the measurements of heats of adsorption.

Similar repeat adsorption isotherms were measured on the oxidized metal surfaces. The respective $v_m$ values are listed in Table I as $v_m^{III}$ and $v_m^{IV}$. The ratio 100 $v_m^{IV}/v_m^{III}$ is designated reversibility on the oxidized surface, $R_o$. On the oxidized surfaces it was expected that a complete monolayer would form mostly by physical adsorption; a comparison of these amounts adsorbed with the reversible portions (at 25°) adsorbed on the reduced metals would then help to reveal differences in orientation and packing.

The direct determinations of calorimetric heats of adsorption of the 1-propanol, *n*-propylamine and benzene on both reduced and oxidized nickel and copper powders are plotted against amount adsorbed in Figs. 1 to 6. These measurements were made at 22° at which temperature the calorimeter functions best.

Each set of runs is plotted so that the $v_m$ values are superimposed. For example, in Fig. 1, the zero point represents the start of the first run on the reduced surface; the BET $v_m$ value from this first run is indicated at the appropriate amount adsorbed by a vertical dashed line. After degassing for 16 hours at 25°, a second run gave a much smaller $v_m$ and the heat measurements made on this partially covered surface were plotted as though the

zero point for the new coverage was at ($v_m^I - v_m^{II}$), point A. Using this scheme, the heat values were found to coincide with the original values. If the amine–nickel system was degassed after this second run, first at 25° for 16 hours followed by one hour at 100°, a greater amount of adsorbate was removed. The isotherm on this surface revealed a much larger $v_m$; subtracting this value from $v_m^I$ gave point C for the zero point of the heat determinations on this more stringently outgassed surface. This heat of adsorption curve fell on a somewhat different curve than the first ones. Since the system was irreversibly altered by outgassing at 100°, this procedure was not followed for the other systems.

On the oxidized nickel surface, the measured $v_m^{III}$ is represented by the difference between $v_m^I$ and point B. These heats of adsorption fell somewhat lower than those on the reduced or outgassed surfaces.

## Discussion

It is valuable to consider the heats of adsorption first. The initial values on the reduced metal surfaces are much higher for nickel than for copper; in accord with this finding, the reversibilities are less for nickel than for copper. The high initial heats for the alcohol and amine on nickel suggest electron transfer to the unfilled d-band. The electron-rich copper cannot participate in such transfer.

The low initial heat for benzene on nickel at first appears to be an anomaly since portions of the amine adsorbed with such low energies could be desorbed at 25°. In accord with an earlier suggestion,[7] however, it is reasonable to conclude that transfer of the $\pi$-electrons of benzene only occurs at the cost of the resonance energy. Thus, about 40 kcal./mole would be added to the heats of adsorption if this energy had not been absorbed. The possibility that some dissociative adsorption of benzene may also occur,[11] cannot be discounted on the basis of the measurements made here. The complete reversibility and lower heats for benzene on copper, on the other hand, suggest no strong interactions of any kind.

The initial constant high heat values for the alcohol on nickel *versus* the immediate gradual decrease for the amine on nickel deserves further examination. The unshared pair of nitrogen electrons in the amine no doubt add in coördinate covalent bond fashion to the d-band. Hence, dipoles with the positive end directed outward are developed. The addition of electrons to the metal gradually decreases the work function. Coupled with the dipole–dipole repulsion, these two factors cause the decrease in the heats of adsorption. If it were not for the discrete location of the dipoles and their mutual depolarization on near approach,[12] the decrease with coverage would be even more rapid. On the other hand, the initial constant high heats for the alcohol on nickel up to coverages approaching one layer can only be explained if dipole–dipole repulsion and more significantly, the decrease in the work functions are not large. Dissociative adsorption appears to be the likely factor; this interpretation is supported, as mentioned previously, by the evidence of uncondensed product on desorption. For this reason, Table I does not list the reversibility for the *n*-propyl alcohol although it was nominally 78%. In addition, the heats from the second run after degassing at 25° did not coincide in this case with those from the first run at superimposed $v_m$ values. It appears likely that the propoxy radical adds its electron pair to the nickel as the proton from the hydroxyl group adsorbs separately.[13] The tendency for decrease in the work function due to the electron donating capacity of the propoxy group is thus countered by the electron attracting capacity of the proton. The latter probably resides within the boundary of the top layer of metal atoms. Then mutual depolarization of the dipoles created would lessen repulsion as coverage increases. An approximate calculation of the heat of dissociative adsorption of the alcohol on nickel according to the method of Eley[14] gave a value about 20 kcal./mole less than that measured.

The heat curves for the amine and for benzene on the reduced metals for the second run after degassing at 25° coincided well with those from the first run at superimposed $v_m$ values. For these systems the adsorption and desorption steps do not alter the reversible portions of the surface.

The low vapor pressure of nitropropane prevented valid determination of heats of adsorption. This adsorbate differs from the others in that it irreversibly adsorbs to the same extent on both nickel and copper. The electron donating capacity of the tautomeric form together with the electron accepting capacity of the nitro group may explain its dual activity on both the electron-poor nickel and the electron-rich copper.

In contrast to the initial high heats obtained on the base metal surfaces, those for the oxidized surfaces are all much lower. There seems to be no doubt that here physical adsorption predominates. The generally lower reversibilities on oxide-coated nickel than on oxide-coated copper, and the higher heats of adsorption of the alcohol, may be ascribed to the larger concentration of $O^-$ field-creating ions on the former.[10] At first glance at the $v_m$ ratios against argon, the good agreement between the values for the amounts physically adsorbed on the reduced surfaces, $v_m^{II}/v_m^A$, and those for the adsorption on the oxidized surfaces, $v_m^{III}/v_m^A$, is striking. On further reflection, this agreement seems to be more fortuitous than meaningful. Apparent molecular areas of organic molecules on polar surfaces have often been reported to be larger than on graphitic or metal surfaces.[15] The oriented chemisorption on the reduced surfaces aids in the development of the larger values for the $v_m^I/v_m^A$ ratios.

**Acknowledgment.**—The authors wish to express their appreciation for the financial support provided by the Office of Ordnance Research.

(11) J. R. Anderson and C. Kemball, "Advances in Catalysis," IV, Academic Press, New York, N. Y., 1957, p. 51.

(12) J. H. de Boer, in "Advances in Catalysis," VIII, Academic Press, New York, N. Y., 1956, p. 107 ff.

(13) M. Ingram and R. Gomer, *Z. Naturforschung*, **10a**, 876 (1955).

(14) D. D. Eley, *Disc. Faraday Soc.*, **8**, 105 (1950).

(15) J. J. Van Voorhis, R. G. Craig and F. E. Bartell, THIS JOURNAL, **61**, 1513 (1957); see also ref. 11, p. 82.

## DISCUSSION

F. M. FOWKES (Shell Development Company).—The direct heats of interaction of these metals with the amine and alcohol are very much greater than expected for electron donation to ions of these metals (perhaps 15 kcal./mole). Doesn't this indicate that bonds in the organic molecules are broken and new species are formed?

A. C. ZETTLEMOYER.—In the case of the alcohol, we do indeed believe that the alcohol molecule breaks up, and to a large extent the hydrogen from the hydroxyl group and the propoxy radical are separately adsorbed. The amine, on the other hand, is very energetically adsorbed through a coordinate covalent or dative bond created by the originally unshared nitrogen electrons. In solution, water molecules must be separated from the metal ions as such bonds are formed; the cost of this water displacement apparently accounts for the lower exothermic heats in such cases.

# THE ADSORPTION OF SOME GASES ON EVAPORATED METAL FILMS AND ON OXIDIZED FILMS OF NICKEL[1]

BY J. L. SHERESHEFSKY AND BIBHUTI R. MAZUMDER

*Contribution from the Chemistry Department, Howard University, Washington, D. C.*

*Received May 11, 1959*

Low pressure adsorption isotherms at 76.8 and 90.2°K. are reported for krypton, methane and ethane on copper and oriented nickel evaporated films, and on an oriented oxidized film of nickel. The krypton and methane isotherms on nickel oxide and the krypton isotherms on nickel follow the Langmuir equation. The methane isotherm at 76.8°K. on nickel is s-shaped, the low pressure region following the Langmuir equation. The ethane isotherms on copper, nickel and nickel oxide are all s-shaped. The ethane isotherm on nickel oxide shows a first-order phase change. The nature of the adsorbed phase, the variation of the calculated heat of adsorption is discussed from the point of view of the van der Waals two-dimensional equation, the entropy of adsorption and the effect of the polarizing field of the adsorbent on the van der Waals attraction. Proof is given for the orientation of ethane in the adsorbed phase, and a method for the preparation of oriented films of nickel oxide is described.

### Introduction

Two-dimensional condensations in monolayers spread on liquid substrates has been known and understood for a long time. The similar phenomenon in gases adsorbed on solid surfaces has only recently attracted attention and is the subject of a number of investigations. It was first observed and recognized in this Laboratory in a study on the adsorption of nitrogen[2] and oxygen[3] on glass spheres; it was confirmed and some of its properties studed by Ross and coworkers.[4] These studies showed that the critical temperature and pressure of the transition, and the shape of the transition curve depend not only on the nature of the adsorbate but also on the adsorbent and the purity of the surface. Condensation was observed to take place on surfaces of sublimed sodium and potassium chloride, graphitized carbon and mixed surfaces of glass and minerals.

To the present, two-dimensional condensation has not been observed on metal surfaces. The technique developed in recent years of producing evaporated metal films, the high purity of such surfaces and the homogeneous surface of the oriented metal film induced us to undertake the present study. In the course of the investigation it was found that also oriented films of nickel oxide can be produced, and the investigation was extended to include adsorption on this type of surface.

### Experimental

The apparatus in which the determinations of the adsorption isotherms were made was of the conventional volumetric type, except that mercury cut-offs were used instead of stopcocks, and that it included a multi-range McLeod gauge. A double gas trap in the shape of an inverted u, between the adsorption vessel and the rest of the system, cooled by liquid air, kept mercury vapor out of the adsorption vessel. The latter, after being cleaned with chromic acid and distilled water, was baked at 400° in high vacuum for five hours, so that a vacuum of about 0.001 $\mu$ could be maintained for several hours.

The vessel consisted of a Pyrex glass tube 6 cm. long and 2 cm. in diameter. It was connected to the apparatus through a narrower tube carrying two tungsten electrodes, one mm. in diameter, to which the metal filaments were attached. The films were deposited on the inner surface of the tube by subliming part of the filament.

The temperature of the films was maintained with liquid nitrogen or oxygen, kept in a liter Dewar flask constant to 0.1°. The temperature was measured with a Leeds and Northrup platinum resistance thermometer.

The nickel films were prepared from nickel filaments 0.5 mm. in diameter. The filament was heated to a temperature of 1100°, by passing a current of 6.8 amp. The sublimation was carried out in an argon atmosphere of 0.85 mm. of pressure, and the temperature of the filament was measured with a micro-optical pyrometer made by the Pyrometer Instrument Company. The temperature of the adsorption vessel during sublimation was kept at 23°. The weight of the film was determined by the difference in the weight of the filament before and after deposition. The films were on the average 55 mg. in weight and 1.6 $\mu$ in thickness. The films resulting from this manner of deposition were found to be oriented with the 110 plane in the surface, as determined at the National Bureau of Standards by X-ray and electron diffraction methods.

The nickel oxide film was prepared from a nickel film deposited in the above manner, by oxidation in air at 275° for one hour. The air was purified by passing it over sodium

(1) Presented at the Oolloid Symposium, University of Minnesota, June 18–20, 1959. This paper is based on a thesis submitted by Bibhuti R. Mazumder, in partial fulfillment of the requirements for the degree of Doctor of Philosophy, to the Graduate School of Howard University, June, 1958. The experimental observations are reported in full in the original Thesis, copies of which may be obtained from University Microfilms, Ann Arbor, Michigan.

(2) J. L. Shereshefsky and C. E. Weir, *J. Am. Chem. Soc.*, **58**, 2022 (1936).

(3) J. L. Shereshefsky and C. E. Weir, THIS JOURNAL, **60**, 1162 (1956).

(4) S. Ross, *J. Am. Chem. Soc.*, **70**, 3830 (1948); S. Ross and C. H. Secoy, THIS JOURNAL, **53**, 308 (1949); S. Ross, *ibid.*, **53**, 383 (1949); S. Ross and W. Winkler, *J. Am. Chem. Soc.*, **76**, 2637 (1954); S. Ross and H. Clark, *ibid.*, **76**, 4291, 4297 (1954); S. Ross and C. Sanford, THIS JOURNAL, **58**, 288 (1954); S. Ross and W. Winkler, *J. Colloid Sci.*, **10**, 319, 330 (1955).

hydroxide and through a trap cooled in liquid air. Electron diffraction studies showed the top layers of the film to be oriented with the 111 plane parallel to the substrate, and the deeper lying layers the original unoxidized nickel.

The copper films were prepared from electrolytic copper which was electro-deposited on a molybdenum filament. The filament was heated in a high vacuum to 830°, by passing a current of 4.6 amp. During the deposition of the metal, the walls of the vessel were kept at the ice-water temperature. The films thus prepared were unoriented, weighed about 10 mg. and were 0.29 $\mu$ in thickness, calculated from bulk density.

The materials used in the determination of the isotherms of krypton, methane and ethane on films of copper, nickel and nickel oxide were of the following purity.

Argon and krypton obtained from Matheson Co., Inc., were 99.9% pure; the methane and ethane gases obtained from the same source were, respectively, 99 and 95% pure. The latter were further purified by passing through traps cooled in liquid air, or in a Dry Ice and ether mixture.

The nickel which was supplied by the courtesy of the Washington, D. C., office of the International Nickel Co. was nickel A, 99.45% pure. The filament was further purified by degassing at 880° in a high vacuum for five hours.

The copper was obtained from J. T. Baker Chemical Co., as electrolytic copper foil. It was free of iron, antimony, tin or lead.

## Experimental Results

The results obtained on the adsorption isotherms are reported on the basis of 100 mg. of film.

**Krypton Isotherms.**—The adsorption isotherms of krypton at 76.8 and 90.2° K. on an evaporated nickel film, oriented with the 110 plane parallel to the substrate, extend from about 0.005 to 100 $\mu$ at 76.8°K. and from 0.05 to 500 $\mu$ at 90.2°K. The lower pressure regions up to 0.06 $\mu$ for the former and 0.6 $\mu$ for the latter are shown in Fig. 1, curves A and B; the higher pressure regions up to 10 or 100 $\mu$ are shown in Fig. 2. The application of the Langmuir equation to these isotherms is shown in Fig. 3. Adsorption at pressures higher than those shown in Fig. 2 follows the straight lines of the Langmuir plots. Each isotherm forms two straight lines, intersecting at about 40 and 45% coverage, as based on the monolayer constant, $V_m$, determined by the BET method. The constants determined by the Langmuir and BET methods are given in Table II.

The isotherms of krypton on the 111 plane of nickel oxide films extend from 0.002 to 200 $\mu$ at 76.8°K., and from 0.05 to 100 $\mu$ at 90.2°K. The low pressure regions up to 0.65 $\mu$ are shown in Fig. 1, curves C and D; the higher pressure regions up to 90 $\mu$ are shown in Fig. 4. The Langmuir and BET monolayer constants are given in columns 2 and 3 of Table II.

**Methane Isotherms.**—The methane isotherms on the 110 plane of evaporated nickel films extend from 0.002 to 1800 $\mu$ at 76.8°K. and from 0.012 to 750 $\mu$ at 90.1°K. The isotherms up to a monolayer coverage are shown in Fig. 5, and those at higher pressures in Fig. 6. The application of the BET equation, including the parameter $N$, to the 76.8°K. isotherm, in accordance with the procedure of Joyner, Weinberger and Montgomery,[5] is shown in Fig. 7. It is seen that one and one-half layers were built up within a relative pressure of two-tenth. The Langmuir and BET monolayer constants are given in Table II. The low pressure regions of these isotherms are shown in Fig. 8, curves A and B.

The methane isotherms on the 111 plane of nickel oxide extend from 0.05 to 100 $\mu$ at 76.8°K. and from 1.2 to 680 $\mu$ at 90.2°K. The low pressure regions of these isotherms are shown in Fig. 8, curves C and D, where the maximum pressures are 0.6 and 5.7 $\mu$, respectively. In Fig. 9 are shown the isotherms up to a pressure of 120 $\mu$.

**Ethane Isotherms.**—The adsorption of ethane was measured only at one temperature, at 90.2°K., on films of copper, nickel and nickel oxide. The copper film was unoriented, and the adsorption on it extends from 0.1 to 8.7 $\mu$. The adsorption on oriented nickel film extends from 0.016 to 6.2 $\mu$.

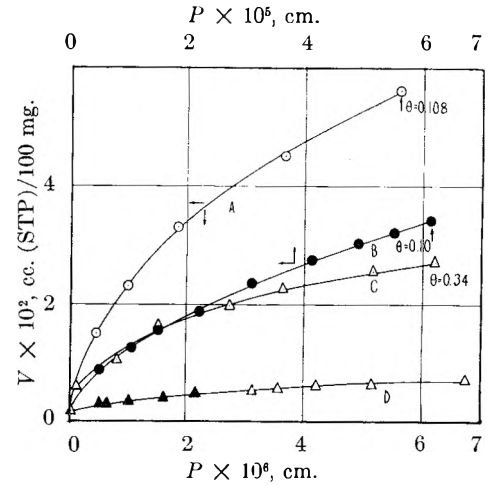


Fig. 1.—Adsorption of krypton on the 110 plane of nickel and the 111 plane of nickel oxide: A, nickel at 76.8°K.; B, nickel at 90.2°K.; C, nickel oxide at 76.8°K.; D, nickel oxide at 90.2°K.

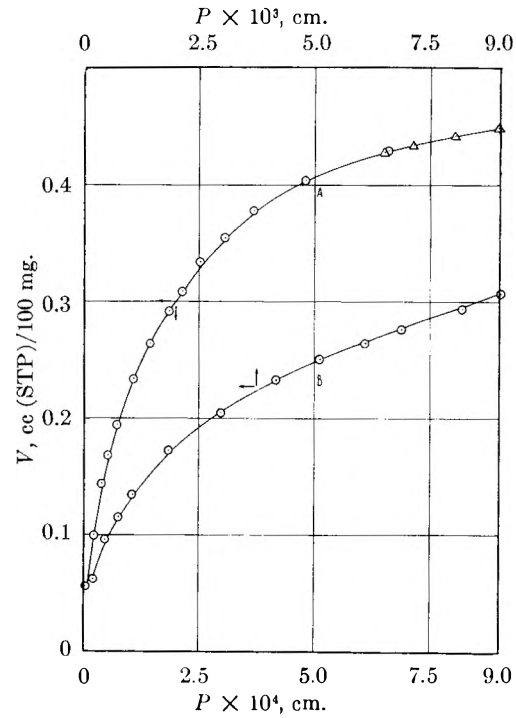


Fig. 2.—Adsorption of krypton on the 110 plane of nickel: A, 76.8°K.; B, 90.2°K.; ⊙, adsorption; △, desorption.

(5) L. G. Joyner, E. E. Weinberger and C. W. Montgomery, *J. Am. Chem. Soc.*, **67**, 2182 (1945).

TABLE I

ENTROPY OF ADSORPTION OF KRYPTON, METHANE AND ETHANE ON ORIENTED FILMS OF NICKEL AND NICKEL OXIDE AT THE STANDARD STATE OF $\theta = 0.5$

| | °K. | $p \times 10^{-4}$, cm. | $-\Delta F$, kcal. mole$^{-1}$ | $-\Delta H$, kcal. mole$^{-1}$ | $\Delta S$, e.u. | $_2S_t$, e.u. | $_3S_t$, e.u. |
|---|---|---|---|---|---|---|---|
| Krypton on nickel | 76.8 | 3.24 | 1.89 | 3.57 | −20.0 | 32.9 | 17.0 |
| | 90.2 | 18.4 | 1.91 | | | | |
| Krypton on nickel oxide | 76.8 | 2.06 | 1.96 | 3.53 | −17.7 | | 17.0 |
| | 90.2 | 5.01 | 2.14 | | | | |
| Methane on nickel | 76.8 | 0.543 | 2.17 | 1.64 | + 7.7 | 27.9 | 13.8 |
| | 90.1 | 12.16 | 2.39 | | | | |
| Methane on nickel oxide | 76.8 | 1.70 | 1.99 | 2.27 | − 2.2 | | 13.8 |
| | 90.2 | 3.80 | 2.19 | | | | |
| Ethane on copper | 90.2 | 0.30 | 2.64 | 4.45[a] | −20.0 | 30.2 | 15.8 |
| Ethane on nickel | 90.2 | 0.0767 | 2.89 | 4.60[a] | −19.0 | | 14.3 |
| Ethane on nickel oxide | 90.2 | 0.977 | 2.43 | 4.45[a] | −22.4 | | 15.8 |

[a] Calculated from BET equation, taking the heat of vaporization as 3860 cal./mole.

TABLE II

SOME PHYSICAL PROPERTIES OF ADSORBED KRYPTON, METHANE AND ETHANE ON EVAPORATED FILMS OF COPPER, NICKEL AND NICKEL OXIDE

| 1 | 2 °K. | 3 $V_m$(L), cc. | 4 $V_m$(BET), cc. | 5 $\mu$, Debye: $\theta = 0.1$ | 5 $\mu$, Debye: $\theta = 0.5$ | 6 $\mu^2/2\alpha$, kcal. mole: $(\theta = 0.1)$ | 6 $\mu^2/2\alpha$, kcal. mole: $(\theta = 0.5)$ | 7 $T_{c2}$ $(\theta = 0.5)$ |
|---|---|---|---|---|---|---|---|---|
| Krypton on nickel | 76.8 | 0.35; 0.52 | 0.52 | 1.24 | 0.73 | 4.43 | 1.51 | 32 |
| | 90.2 | 0.18; 0.34 | .34 | 1.25 | .70 | 4.46 | 1.40 | 38 |
| Krypton on nickel oxide | 76.8 | 0.080 | .078 | 1.32 | .69 | 4.93 | 1.32 | 39 |
| | 90.2 | 0.034 | .034 | 1.41 | .71 | 5.7 | 1.43 | 36 |
| Methane on nickel | 76.8 | 0.50; 0.60 | .497 | 1.39 | .71 | 5.36 | 1.40 | 38 |
| | 90.1 | 0.342 | .348 | 1.40 | .85 | 5.45 | 2.03 | 7 |
| Methane on nickel oxide | 76.8 | 0.0795 | .0795 | 1.02[a] | .84 | 2.81[a] | 1.98 | 9 |
| | 90.2 | 0.0495 | .050 | 0.72 | .72 | 1.43 | 1.43 | 35 |
| Ethane on copper | 90.2 | | .050 | 1.13 | 1.13 | 2.04 | 2.04 | 42 |
| Ethane on nickel | 90.0 | | .56 | 1.27 | 1.27 | 2.58 | 2.58 | 16 |
| Ethane on nickel oxide | 90.2 | | .0765 | 1.33 | 0.74 | 2.83 | 0.845 | 105 |
| | | | | 1.57[b] | 1.29[b] | 4.47[b] | 3.02[b] | 104[b] |

[a] At $\theta = 0.25$. [b] Oriented with long diameter normal to surface.

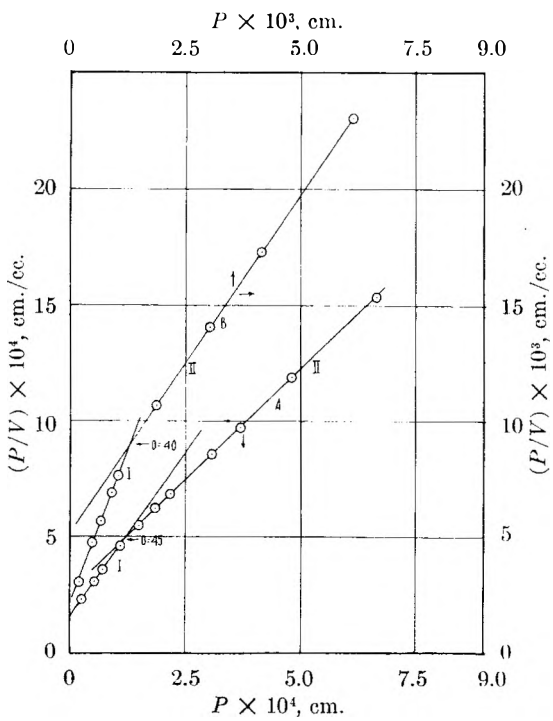


Fig. 3.—The application of Langmuir's equation to the krypton isotherms on the 110 plane of nickel: A, 76.8°K.; B, 90.2°K.

Both isotherms are s-shaped and are shown in Fig. 10. The low pressure regions are shown in Fig. 8, curves E and F. The BET $V_m$ values are given in Table II. On nickel, the monolayer is complete at a relative pressure of 0.1, and on copper at a relative pressure of 0.17.

Figure 11 shows the adsorption of ethane on the 111 plane of nickel oxide. The isotherm extends from 0.08 to 6.7 $\mu$. In the first run, at low pressures, adsorption increases almost linearly with pressure; the isotherm then turns first convex and then concave to the pressure axis, and on further adsorption the pressure falls to a lower value, as shown by the broken line and the numbered sequence of open circle points. After this pressure drop, adsorption continues to increase linearly with pressure.

It is of interest to note that the point preceding the pressure drop, the open circle point 2 remained constant for about 12 hours, and the drop in pressure to point 3 occurred only after the addition of more gas. In the second run, the points designated with triangles follow the first run in the linear, low pressure region of the isotherm. At about 1.1 $\mu$, on further addition of gas made in small increments, the adsorption continues to rise from 0.05 cc. to about 0.078 cc. at a constant pressure of 1.15 $\mu$. Point 5, which follows the constant pressure interval, seems to fall on the higher pressure linear part

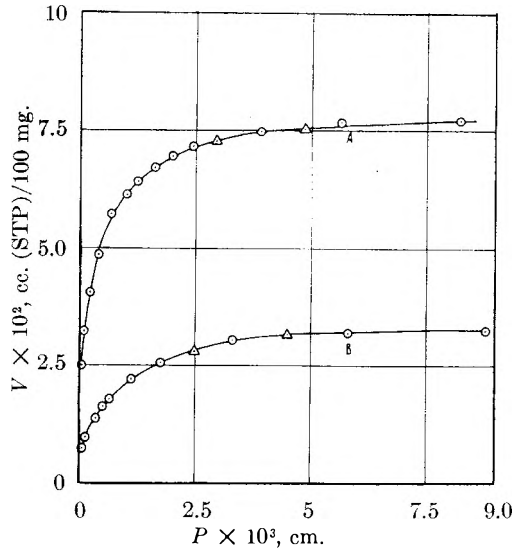


Fig. 4.—Adsorption of krypton on the 111 plane of nickel oxide: A, 76.8°K.; B, 90.2°K.; ⊙, adsorption; △, desorption.

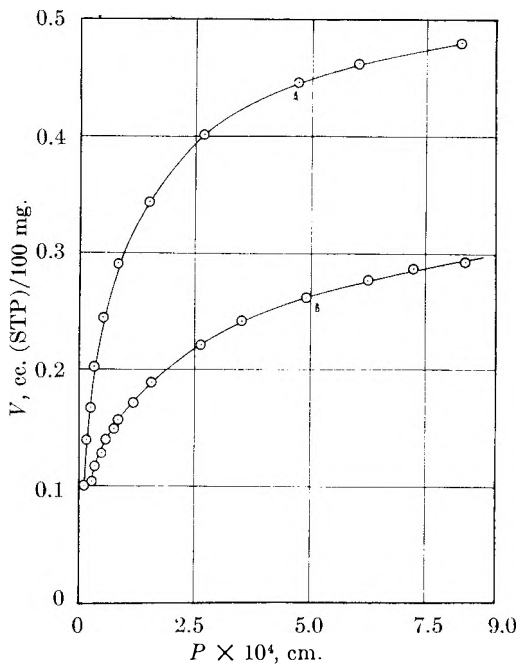


Fig. 5.—Adsorption of methane on the 110 plane of nickel to a monolayer coverage: A, 76.8°K.; B, 90.1°K.

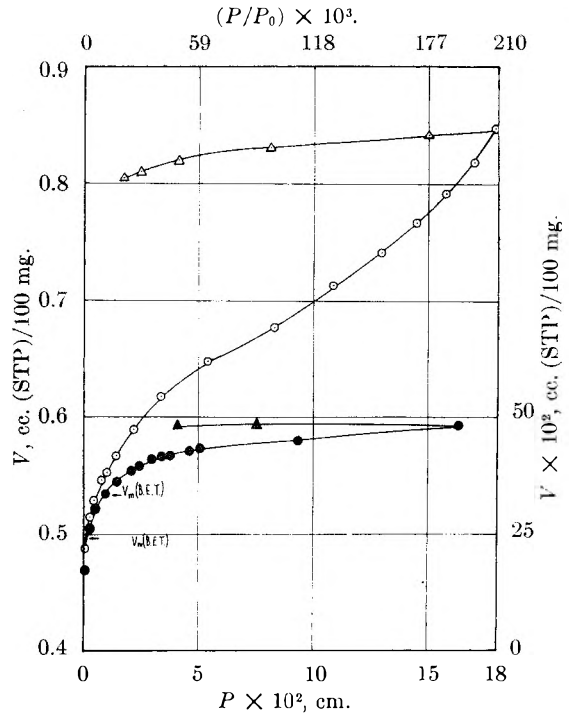


Fig. 6.—Adsorption of methane on the 110 plane of nickel: A, 76.8°K.; B, 90.2°K., pressure = $P \times 5 \times 10^2$; ⊙, adsorption; △, desorption at 76.8°K.; ●, adsorption; ▲, desorption at 98.2°K.

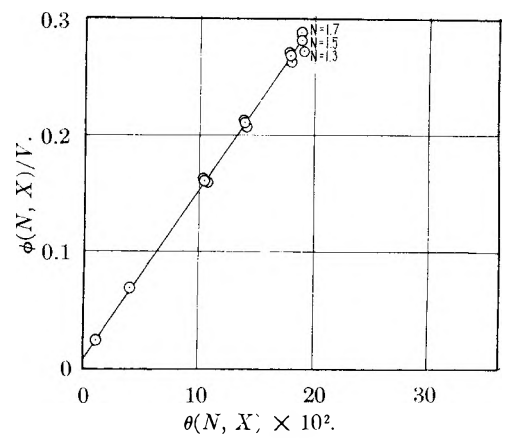


Fig. 7.—Application of the full BET equation to the methane isotherm at 76.8°K. on nickel.

of the isotherm. The third run further confirms the linearity of the low pressure region of the isotherm. The application of the BET equation gives three different values for $V_m$, corresponding to three different regions. The values and the corresponding relative pressures are given in Table II, shown by the sequences of points 16 to 20, E to H.

**Irreversible Isotherms.**—To test the reversibility of the isotherms, partial desorption was carried out. In the ethane isotherm on nickel oxide desorption experiments in the three different regions show strong hysteresis as indicated by the numbered or lettered sequences of points in Fig. 11, points 7 to 15; B, C, D; I to N; and A′, B′, C′, D′. Adsorption following partial desorption, does not fall on or tend to join the original curve, as shown by the sequence of points 16 to 20, E to H, and E′ to L′. However, it should be pointed out that in the latter sequence, the segment J′ to L′, contrary to the usual behavior, and the other runs, is below the original curve. In this segment the pressure at a given amount adsorbed is higher than in the original curve, which, perhaps, indicates that segment J′ to L′ is not in stable equilibrium.

Hysteresis is shown also by the ethane isotherms on nickel and copper at 90.2°K., and by the methane isotherms on nickel at 76.8 and 90.1°K. The isotherms of krypton on nickel and nickel oxide, and the isotherm of methane at 76.8°K. on nickel oxide are reversible, as shown by the partial desorption in Figs. 2, 4 and 9. The isotherm of methane on nickel oxide at 90.2°K. was not tested for hysteresis. However, its behavior at high pressure would seem to indicate irreversibility

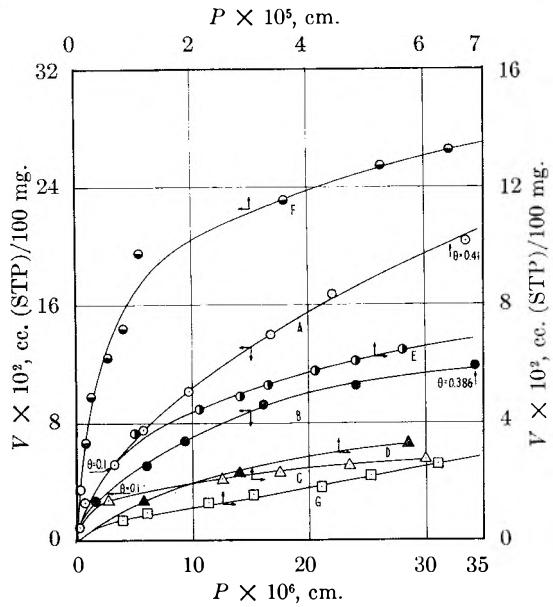


Fig. 8.—Low pressure isotherms of methane and ethane: A, methane at 76.8°K. on nickel; B, methane at 90.1°K. on nickel; C, methane at 76.8°K. on nickel oxide; D, methane at 90.2°K. on nickel oxide; pressure, $P \times 10^4$ cm.; E, ethane at 90.2°K. on copper, volume, $V \times 2 \times 10^2$ cc.; F, ethane at 90°K. on nickel, volume, $V \times 0.5 \times 10^2$ cc.; G, ethane at 90.2°K. on nickel oxide.

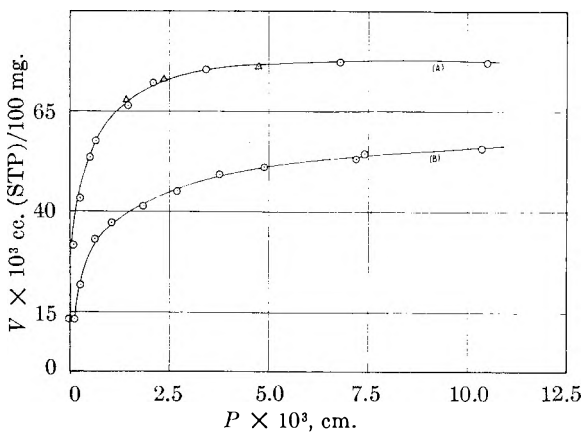


Fig. 9.—Adsorption of methane on the 111 plane of nickel oxide: A, 76.8°K.; B, 90.2°K.; ⊙, adsorption; △, desorption.

**Transpiration.**—Low pressure measurements were corrected for transpiration in accordance with Liang.[6] The pressure shifting factor for methane was calculated from the collision diameter of 4.0 Å. The constants for ethane were not known, and the results with this gas are reported without corrections.

**Reproducibility.**—The reproducibility of the evaporated nickel films may be illustrated with the following example. The isotherms of krypton and methane at 76.8°K. on nickel were obtained on different film preparations. The ratio of $V_m(CH_4)/V_m(Kr)$ was found to be 0.960, and the ratio $d^2(Kr)/d^2(CH_4)$, where $d$ is the molecular diameter given in Table III, was found to be 0.958.

**Heat of Adsorption.**—The isosteric heats of adsorption of krypton and methane on nickel and nickel oxide films were calculated from the isotherms at 76.8 and 90.2°K. by the Clausius-Clapeyron equation

$$\Delta H = 2.303R(T_1T_2/(T_2 - T_1))(\log p_2 - \log p_1)$$

where $p_2$ and $p_1$ refer to the equilibrium pressures at the same value of $V$ in cc. adsorbed at the temperatures $T_1$ and $T_2$.

The variation of the isosteric heats with coverage is shown in Fig. 12. It is seen that the shape of the curves, with the exception of that for methane on nickel oxide, is essentially the same. The heat of

(6) S. Chu Liang, THIS JOURNAL, **57**, 910 (1953).

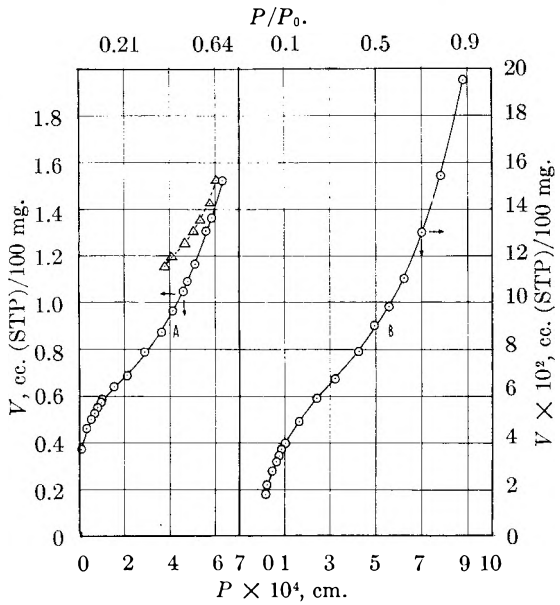


Fig. 10.—Adsorption of ethane at 90.2°K. on the 110 plane of nickel (A) and unoriented copper (B); ⊙, adsorption; △, desorption.

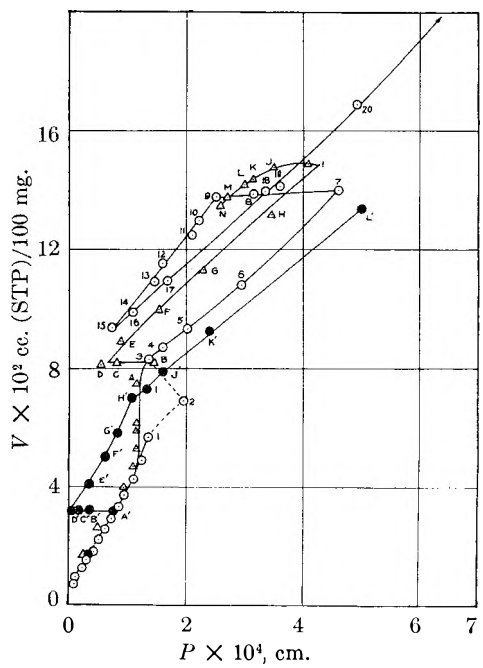


Fig. 11.—Adsorption of ethane at 90.2°K. on the 111 plane of nickel oxide: ⊙, run 1; △, run 2; ●, run 3. Phase change is shown by sequence 1, 2, 3 and vertical sequence of triangle points. Desorption and readsorption is shown by sequences 7, 8, 9...B C D...E F G...I J K...A′ B′ C′ ... and E′ F′ G′ ...

TABLE III

MOLECULAR CONSTANTS USED IN CALCULATING THE VALUES GIVEN IN TABLES I AND II

| | $a \times 10^{-12}$, ergs. cm.$^3$ per mole | $b$, cm.$^3$ per mole | $a_2 \times 10^{32}$, ergs. cm.$^2$ per molecule | $b \times 10^{16}$, cm.$^2$ per molecule | $d$, Å. | $\alpha \times 10^{24}$ | $\alpha_1 \times 10^{24}$ cc. per molecule | $\alpha_2 \times 10^{24}$ |
|---|---|---|---|---|---|---|---|---|
| Krypton | 2.33 | 39.8 | 7600 | 15.7 | 3.17 | 2.54 | 2.54 | 2.54 |
| Methane | 2.26 | 42.8 | 7500 | 16.4 | 3.24 | 2.61 | 2.61 | 2.61 |
| Ethane | 5.46 | 64.2 | 15,100 | 21.6 | 3.71 | 4.53 | | |
| | | | | 10.3 | 2.56[a] | | 5.6 | |
| Ethane oriented | | | | 39.8 | 5.12[b] | | | 4.0 |

[a] Normal to surface. [b] Parallel to surface.

adsorption starts out with a high value, decreases with increase of coverage, reaching a minimum at a coverage less than 0.5, and increases with further increase of adsorption. In the case of methane on nickel oxide, the minimum value of the heat is approximately equal to the heat of bulk condensation in the same temperature range, and is about 2.3 kcal.

The isosteric heat of methane on nickel behaves in a way similar to that of krypton on nickel, from about 30% to complete coverage. However, for methane, at low values of $\theta$, the heat remains constant and lower than the heat of bulk condensation. A similar curve was observed for argon adsorbed on zinc.[7]

## Discussion

**The Adsorbed State of Krypton on Nickel and Nickel Oxide Films.**—Ross and Winkler[4] found that krypton undergoes two-dimensional condensation on graphitized carbon black at a pressure of about 1.7 $\mu$ at 77.1°K. Furthermore, the two-dimensional critical temperature of krypton as calculated from the equation

$$T_{c2} = 0.5T_c$$

given by de Boer,[8] is about 105°K. The conditions of the present experiment were therefore favorable for a two-dimensional transition at 76.8 and 90.2°K.

The reason for the absence of this phase transition is to be found in the partially hindered mobility and the weak lateral attraction of the adsorbate. The applicability of the Langmuir equation at the low pressures shown in Fig. 1 indicates a localized type of adsorption, which is borne out by the entropy calculation shown in Table I.

In this table ${}_3S_t$ gives the translational entropy of the ideal gas in the standard state of 1 atm. pressure; $\Delta S$ gives the difference in entropy between the standard adsorbed state of $\theta = 0.5$ and the former; ${}_2S_t$ gives the entropy of the ideal gas when restricted to two degrees of translation. The free energy of adsorption, $\Delta F$, was calculated from the equation

$$\Delta F = -2.3RT(\log 76 - \log p)$$

where $p$ is the equilibrium pressure at $\theta = 0.5$ given in the third column. The values for $\Delta H$ were obtained from Fig. 12, and $\Delta S$ was calculated for the mean temperature of 83.5°K. from the equation

$$\Delta F = \Delta H - T\Delta S$$

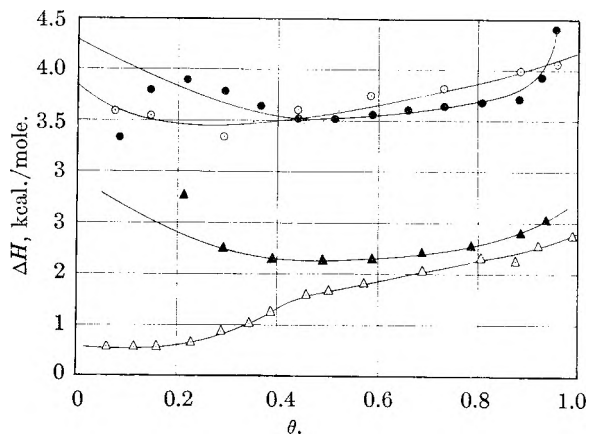


Fig. 12.—The heat of adsorption of krypton and methane on films of nickel and nickel oxide: ⊙, krypton on nickel; ●, krypton on nickel oxide; △, methane on nickel; ▲, methane on nickel oxide.

The values for ${}_3S_t$ were calculated from the Sackur–Tetrode equation

$${}_3S_t = 2.3R \log (T^{5/2}M^{3/2}) - 2.3$$

and those for ${}_2S_t$ from the equation of Kemball[9]

$${}_2S_t = 2.3R \log (TMa) + 65.80$$

where $a$ is the area per molecule, available at $\theta = 0.5$, and taken as twice the value of 15.7 Å.$^2$ for krypton, and twice the value of 16.8 Å.$^2$ for methane.

It will be observed that the entropy of the adsorbed phase of krypton on nickel is 12.9 e.u., and for krypton on nickel oxide 15.2 e.u. In the former, the entropy is 4.1 e.u. lower than for a mobile two-dimensional film, showing some hindrance to complete freedom of translation. The entropy of vibration normal to surface, as it will be seen later, is likely to be small. On nickel oxide, the hindrance is much smaller, as the entropy difference is only 1.8 e.u.

The two-dimensional van der Waals equation derived by de Boer[10] and Hill[11] to account for the behavior of real gases in a two-dimensional state implies complete freedom of mobility along the surface by the adsorbed molecules in the film. The adsorbed phases of krypton on nickel and nickel oxide were shown to be hindered in mobility in different degrees. Nevertheless, it is permissible to apply this equation of state to these isotherms, in view of the presence of a molecular equilibrium distribution

(7) T. N. Rhodin, THIS JOURNAL, **57**, 143 (1953).

(8) J. H. de Boer, "The Dynamical Character of Adsorption," The Clarendon Press, Oxford, 1953, p. 147.

(9) C. Kemball, "Advances in Catalysis," Vol. II, Academic Press, Inc., New York, N. Y., 1950, p. 233; J. H. de Boer, ref. 8, p. 113.

(10) J. H. de Boer, ref. 8, p. 179.

(11) T. L. Hill, *J. Chem. Phys.*, **14**, 441 (1946).

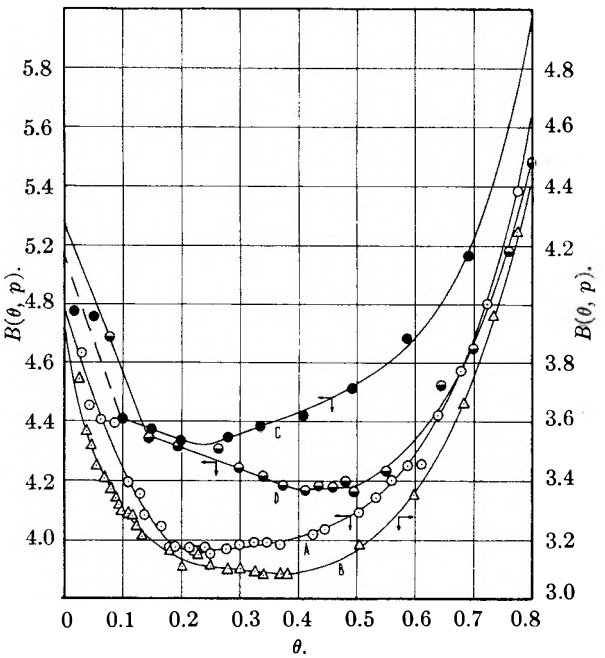


Fig. 13.—The application of the two-dimensional van der Waals equation to krypton and methane isotherms on nickel films: A, krypton at 76.8°K.; B, krypton at 90.2°K.; C, methane at 76.8°K.; D, methane at 90.2°K.

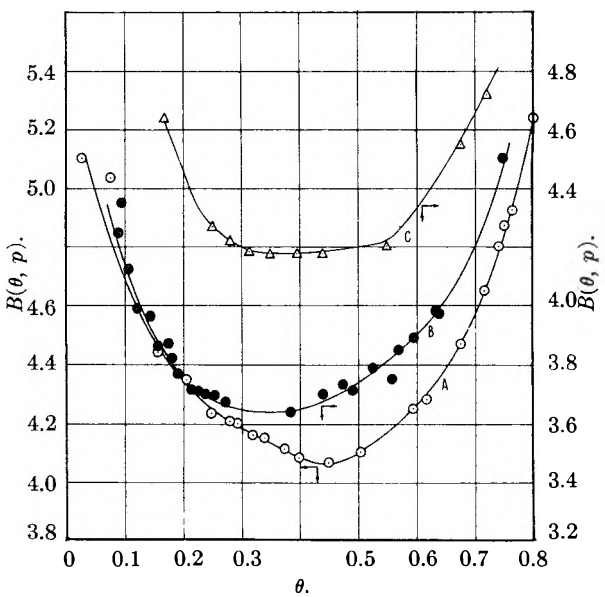


Fig. 14.—The application of the two-dimensional van der Waals equation to the krypton and methane isotherms on nickel oxide films: A, krypton at 76.8°K.; B, krypton at 90.2°K.; C, methane at 76.8°K.

by virtue of the exchanges between the adsorbed and gas phases.

In the reduced form of this equation given by de Boer[10]

$$p = k_2 \frac{\theta}{1-\theta} e^{\frac{\theta}{1-\theta}} e^{-k_1\theta}$$

$p$ is the equilibrium gas pressure, $\theta$ is the fraction covered, and $k_2$ and $k_1$ are constants, the latter given by

$$k_1 = 2a_2/b_2kT$$

where $a_2$ and $b_2$ are the two-dimensional constants, analogous to $a$ and $b$ in the van der Waals equation of state.

Figures 13, 14 and 15 show the application of this equation to the several adsorption isotherms. The function $B(\theta,\mathrm{p})$ plotted against $\theta$ is given by

$$B(\theta,\mathrm{p}) = \log \frac{\theta}{1-\theta} + \frac{\theta}{2.3(1-\theta)} - \log p$$

The slope of this plot is equal to $k_1$, which is a constant and positive.

The plots for the krypton isotherms, except for a short range of $\theta$, have continuously changing slopes, which are initially negative, and which increase with increasing $\theta$ to positive. This behavior can be explained on the basis of the assumption, for which there is substantial evidence, that the krypton molecules were polarized by the strong electric field at the surfaces of nickel and nickel oxide, and that the dipoles thus induced were adsorbed parallel oriented.

Mignolet[12] found that the surface potential of evaporated nickel films became positive, when nitrogen, argon and xenon were adsorbed, which means that these gases, under the influence of the electrical double layer at the metal surface, have become polar.

de Boer,[13] in discussing the effect of parallel oriented permanent dipoles on the two-dimensional attraction constant $a_2$, suggests the introduction of a factor $a^1$ into the equation to correct for this effect. In accordance with this, the expression for $k_1$ is

$$k_1 = 2(a_2 - a^1)/b_2kT$$

It is seen easily that when the dipole moment is large the repulsion factor $a^1$ may be greater than the attraction $a_2$, and make the effective van der Waals correction negative. However, as the molecular population increases, the induced dipoles give rise to an electric field which counteracts the polarizing field of the adsorbent. In this connection, it is of interest to point out that for nickel films the same number of molecules is required to depolarize the field at the metal surface, to the same extent irrespective of the value of $V_m$. Thus, the $\theta$'s for krypton on nickel at which the slopes are zero are, approximately, 0.22 at 76.8°K. and 0.38 at 90.2°K., which correspond, respectively, to 0.12 and 0.13 cc. of gas. This relation holds also for the methane isotherms on nickel.

From the slope and the values of $a_2$ and $b_2$ one can obtain the dipole moment and the critical temperature of the adsorbate. de Boer[13] has shown that the correction $a^1$ to the van der Waals attraction due to the repulsion of the dipoles of moment $\mu$ is equal to $-\pi\mu^2/d$, where $d$ is the diameter of the molecule. The critical temperature was calculated from the equation $T_{c2} = (8/27)(a_2 - a^1)/b_2k$, where $k$ is the Boltzmann constant.

The $\mu$ and $T_{c2}$ values for krypton thus calculated are given in columns 5 and 7 of Table II. The values of $\mu$ decrease with coverage. At $B(\theta,\mathrm{p})$ minimum the values of $\mu$ at 76.8 and 90.2°K. are the same and equal to 0.88 $D$, since at these surface densities the repulsion factor $a^1$ equals $a_2$, the two-

(12) J. C. P. Mignolet, *Trans. Faraday Soc., Disc.*, **8**, 104 (1950).
(13) J. H. de Boer, ref. 8, p. 155.

dimensional van der Waals attraction. The values for $T_{c2}$ account for the absence of a first-order transition, since the experimental temperatures were above these values. The dipole repulsion forces are sufficiently great to lower the critical temperature below the experimental also at surface coverages higher than 0.5.

The variation of the heat of adsorption of krypton on nickel and nickel oxide and of methane on nickel oxide with coverage is parallel to the variation of the effective van der Waals attraction ($a_2 - a^1$) with coverage. This behavior is in agreement with the relation $(d\Delta H/d\theta)_T = 2(a_2 - a^1)/b_2$ which can be derived from the de Boer and Hill equation, upon including the term $a^1$. Evidently, the heats of adsorption include, in addition to the van der Waals energy of attraction, also the energy of electrostatic attraction, $\mu^2/2\alpha$, between the adsorbent and the polarized adsorbate molecules. At low coverage the latter heat represents the major contribution to the total heat, and at 0.50 it is from 40 to 70% of the isosteric heat. The electrostatic energy is given in column 6 of Table II.

The heat of adsorption values for krypton on nickel and nickel oxide at low coverage approach the calorimetric value[14] of krypton on graphitized carbon black. At coverages between 0.2 and 0.6 the values are higher from 200 cal. to 600 cal./mole than those obtained by Ross and Winkler[4] on graphitized carbon black.

**The Adsorbed State of Methane.**—The plots of function $B(\theta,p)$ *vs.* $\theta$ for methane on nickel at 76.8° and 90.2°K. are similar to those for krypton. However, they have greater ranges of coverage with constant negative slopes. The induced dipole moments are approximately of the same magnitude as those for krypton, which is to be expected, since the polarizibilities, $\alpha$, of these two molecules are approximately equal. The lowering effect that this has on the two-dimensional critical temperature is shown in column 7 of Table II. The temperatures of the experiments were below the normal value of $0.5T_c$ where $T_c$, the three-dimensional temperature, is 190.6°K.; but considerably above the calculated values, which explains the fact that no two-dimensional condensation was observed. Stepwise adsorption of methane on graphite at −195° and at relative pressures of 0.35 and 0.75 observed by Bonnetain, Duval and Letort[15] is likely not a first-order phase transition, in view of the polymolecular thickness of the adsorbed phase.

The plots of function $B(\theta,p)$ for methane on nickel oxide are different from those on nickel. At 76.8°K., the plot shows a constant negative slope at low coverage, a constant positive slope at high coverage, and a zero slope for intermediate coverages. At 90.2°K., the plot has no negative slope, as it shows a constant positive slope up to $\theta = 0.7$. However, the polarization is considerable, and its effect on lowering the effective van der Waals attraction and the two-dimensional critical temperature is about the same as for the adsorbed phase on nickel. Pace, Heric and Dennis[16] report that no first-order phase changes were observed in methane on rutile, between 80 and 140°K.

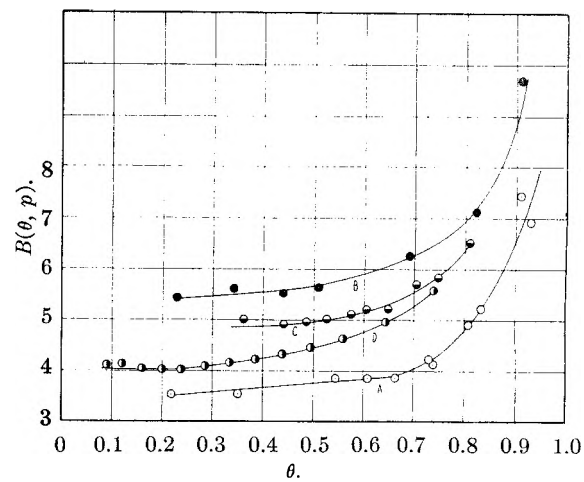


Fig. 15.—The application of two-dimensional van der Waals equation to the methane and ethane isotherms at 90.2°K.: A, methane on films of nickel oxide; B, ethane on films of nickel; C, ethane on films of copper; D, ethane on films of nickel oxide.

The dependence of the heat of adsorption of methane on nickel oxide on coverage seems to be normal, in the sense that it varies in proportion with $(a_2 - a^1)$. The value of $-\Delta H$ from $0.3 < \theta < 0.9$ corresponds approximately to the value of methane on rutile[16] at $\theta = 1$. The entropy of adsorption, shown in Table I, in agreement with the function $B(\theta,p)$ plot indicates a supermobile adsorbed phase with a low frequency of vibration normal to the surface of about $2 \times 10^{10}$ per second.

The entropy of adsorption of methane on nickel at $\theta = 0.5$, according to the calculation shown in Table I is positive, which may indicate that the adsorbate molecules vibrate normal to the surface with a very low frequency, the entropy of vibration being approximately equal to the loss of translational entropy, and that the increase is due to the combinatory entropy. However, in view of the high energy of electrostatic binding indicated by the function $B(\theta,p)$, it would seem that a dissociative process may be involved in the adsorption of methane on nickel, in which case the combinatory term in the entropy is even greater than in the former.

**The Ethane Adsorbed Phase.**—The variation of the function $B(\theta,p)$ with $\theta$ of the ethane isotherms is shown in Fig. 15. Although none of the plots has a negative slope, the polarizing field of the several surfaces greatly affects the lateral attraction of the adsorbate molecule. This is due to the high polarizibility of ethane. The effect is reflected in the magnitude of the dipole moments given in Table II, and accounts for the fact that no first-order phase change was observed in the isotherms on copper and nickel.

The polarizibility of ethane is greatest along the length of the molecule, and the molecule tends to orient parallel to the surface. However, the at-

(14) C. H. Amberg, W. B. Spencer and R. A. Beebe, *Can. J. Chem.*, **33**, 305 (1955).

(15) L. Bonnetain, X. Duval and M. Letort, *Comp. rend.*, **234**, 1363 (1952).

(16) E. L. Pace, E. L. Heric and Kent S. Dennis, *J. Chem. Phys.*, **21**, 1225 (1953).

traction of the adsorbate molecules for each other, which is greatest when they are parallel to each other, causes an orientation perpendicular to the surface. The mode of the orientation can be tested by the relation $V_m/V_m^1 = d_1^2/d^2$, where $V_m$ and $d$ are, respectively, the BET molecular layer constant and the molecular diameter of methane and $V_m^1$ and $d_1$ are the equivalent values for ethane. The values for the diameters were calculated from the three-dimensional van der Waals constant $b$, on the assumption that the methane molecule is a sphere and the ethane molecule is a cylinder with a height equal to twice the diameter. This makes the ratio of the square of the diameters equal to 0.624, and the ratio of the $V_m$ values on nickel as adsorbent equal to 0.622, and 0.69 on copper as adsorbent. For the isotherm on nickel oxide the $V_m$ ratio is 0.65. The ratio of the square of the diameters, using for ethane the diameter of a spherical molecule, is 1.31.

The ethane isotherms were measured only at 90.2°K., and the heats of adsorption were calculated from the BET equation. The different values for the entropy of the two-dimensional gas, ${}_aS_t$, are due to the different values of $a$, the molecular area, assigned to the molecule in the standard state, on the assumption of different orientations. The value of ${}_aS_t$ for the ethane molecule oriented flat on the surface is the highest and is equal to 17 e.u. The adsorbed phases of ethane seem to be films with limited freedom of mobility, provided the BET value for the heat of adsorption is correct.

The polarizing field of nickel oxide had a lesser effect on the ethane molecules than that of copper or nickel. This is evident from the greater slope the function $B(\theta,p)$ gives with $\theta$, and the smaller values of $\mu$ displayed by ethane at 0.5 coverage, as computed for the average value of $b_2$. On nickel oxide the value of $\mu$ is 0.74 $D$ as compared with 1.13 $D$ on copper and 1.27 $D$ on nickel. The calculated value for the critical temperature does not depend on the orientation. The value of 104.5°K. given in Table II is still 50 degrees below the normal two-dimensional critical temperature. However, it could not be very much lower, as evidenced by the first-order phase change observed. For the other isotherms in which no phase change was observed, the calculated critical temperatures were below the experimental. The phase change seems to have begun at about 63% coverage, and was completed at about the formation of a saturated monolayer.

## DISCUSSION

M. J. VOLD (University of Southern California).—Do you have any explanation why the van der Waals interaction of the adsorbed molecules, which is modified by their polarization on the surface, should depend upon the extent of surface coverage?

J. L. SHERESHEFSKY.—The correction factor to the two-dimensional van der Waals constant which is opposite in sign may be so large as to cause repulsion between the adsorbate molecules. However, as the molecular surface density increases, the electric field produced by the polarized molecules counteracts the field of the metallic surface, and thereby decreases the magnitude of the induced dipole moment and the correction factor.

SYDNEY ROSS (Rensselaer Polytechnic Institute).—The two dimensional van der Waals equation as derived by Hill and de Boer is restricted to an ideally uniform (homotattic) substrate. The deviation from a constant slope of the function $B(\theta,p)$, which I have designated $W$ in my papers to honor van der Waals, is interpreted by Dr. Shereshefsky as entirely caused by variations with $\theta$ of the two-dimensional $a$ and $b$ constants. I want to draw his attention to an alternative interpretation: let us suppose that the substrate is not ideally uniform but presents a distribution of adsorptive energies to an adsorbate molecule; with this model it is equally possible to predict variations of $W$ with $\theta$ corresponding to those determined experimentally, *without* postulating any variation with $\theta$ of the two-dimensional $a$ and $b$ constants. In other words, two extreme interpretations are equally good at describing the facts. We may suppose either the surface is ideally uniform but the adsorbate–adsorbate interactions are subject to marked variation of *type* (*i.e.*, $a/b$ varies) as the surface concentration increases; or we may suppose, alternatively, that the surface is heterogeneous but no qualitative differences in the adsorbate–adsorbate interactions occur as adsorption proceeds. We have no means of telling, at our present state of knowledge, which of the two interpretations is valid as a description of the observed behavior of physically adsorbed mobile monolayers. But I suggest that the second approach contains the seeds of fruitful application. By ascribing all deviations of the behavior of mobile adsorbed films from the two-dimensional van der Waals equation to surface heterogeneity, we have potentially a tool for the characterization of solid surfaces in terms of their adsorptive energy distribution (AED).

We can minimize any possible effects due to polarization of the adsorbate by selecting, as our standard for measurement of AED, a gas that is least likely to be subject to this effect, say argon or neon. In a forthcoming publication my collaborator, Mr. J. P. Olivier, and I plan to show how far and how usefully this concept can be carried.

With an adsorbate such as ethane, the complete description of its behavior cannot properly overlook qualitative changes of van der Waals interaction with surface concentration. I agree with Dr. Shereshefsky in this respect, though I would still deprecate his neglect of substrate heterogeneity. In one respect, however, and that still a controversial one, we are in perfect accord, namely, the change in the orientation of ethane molecules from flat to upright in the course of a two-dimensional phase transition. I first suggested this interpretation in 1948 (S. Ross, *J. Am. Chem. Soc.*, 70, 3830 (1948)) for the two-dimensional phase change of adsorbed ethane on sodium chloride, and I am pleased to see Dr. Shereshefsky has come to the same conclusion for adsorbed ethane on yet another substrate.

J. L. SHERESHEFSKY.—In general, I agree with Professor Ross that the variation of the $B(\theta, p)$ function with $\theta$ may be interpreted also in terms of the heterogeneity of the substrate. However, in the present instance, because of the nature of the substrate, the conditions of its preparation, and, particularly, the constancy of the pressure at which the phase change in ethane occurs, it is quite evident that the substrate ishig hly homogeneous, and Professor Ross' interpretation would not be permissible. Furthermore, the "heterogeneity-of-surface" approach would not have proved very fruitful in explaining the differences between isotherms of krypton and methane on the same surfaces. May I add that the explanation given is based on the assumption of the variation of the two-dimensional van der Waals constant $a$ only.

I am grateful for the information that Professor Ross has come to the same conclusion as we with regard to the orientation of the ethane molecule in the condensed phase of the monolayer.

# HEATS OF IMMERSION. II. CALCITE AND KAOLINITE—THE EFFECT OF PRETREATMENT

BY WILLIAM H. WADE AND NORMAN HACKERMAN

*Department of Chemistry, University of Texas, Austin, Texas*

*Received May 11, 1959*

The heat of immersion in water per unit area ($\Delta H_i$) of calcite is independent of the calcining temperature over the range 110 to 300°, whereas the $\Delta H_i$ for kaolinite gradually increases over this temperature range and at 380° discontinuously falls coincident with loss of bulk lattice water.

## Introduction

Kaolinite crystallizes in a layered lattice of the mica type. As first outlined by Pauling[1] and later considered in more detail by Brindley[2] and Gruner,[3] its structure consists of stacked silica tetrahedra and alumina octahedra. The alumina oxygen atoms not common to the silica tetrahedra exist as (–OH groups. The molecular structural unit is $Al_2O_3 \cdot 2SiO_2 \cdot 2H_2O$. The *c*-axis bonding is probably due to van der Waals interactions or hydrogen bonding and is relatively weak compared to either the *a*- or *b*-axis bonding.

Both differential thermal analysis[4] and weight loss studies[5] on kaolinite show a loss of bulk lattice water at 500–550° with subsequent loss of crystallinity. Previous heats of immersion studies of kaolinite in water have not been correlated with surface area but rather with either sample weights[6,7] or particle size distribution.[8] These measurements do show trends indicative of changes in surface structure. Water adsorption isotherms on this material shown B.E.T. Type II behavior at relative pressures 0.6–0.8.[9]

Apparently there are no reported studies on the surface structure or the heat of immersion of calcite in water; however, water adsorption isotherms for calcite also show Type II behavior with complete absence of hysteresis effects.[10]

## Experimental

The calorimeter and its operational procedure have been characterized previously.[11] It is of the differential, adiabatic type with thermistor temperature sensing elements. The calorimeter was thermostated at 25.0 ± 0.1° for all measurements. Random bath temperature excursions were less than 0.001° during runs. The samples, which weighed approximately 4 g., were contained in annealed thin-walled cylindrical Pyrex glass holders 1.6 cm. in diameter and 3-4 cm. in length. Pretreatment consisted of outgassing the samples at the desired temperature (± 5°) for 24 hours under a pressure of less than $5 \times 10^{-4}$ mm. The water used in all measurements was doubly distilled from dilute sulfuric acid and alkaline potassium permanganate. The kaolinite clay was supplied by Whittaker, Clark and Daniels, Inc. The composition as furnished by the supplier was: 44.94% $SiO_2$, 38.2% $Al_2O_3$, 13.6% combined water, 1.25% $TiO_2$, 0.28% MgO, and 0.21% NaO. The calcite, also from the same supplier, consisted of 98.2% $CaCO_3$, 1.2% $MgCO_3$ and 0.45% $SiO_2$. Tamms, Inc., supplied a second sample of calcite designated by the manufacturer as "ultra pure" which was used for several spot checks of the $\Delta H_i$ for calcite.

Surface areas of these samples were measured by the B.E.T. method using krypton as the adsorbate. The area of the krypton molecule was taken to be 20.8 A.$^2$. The specific surface areas in m.$^2$/g. obtained were: Whittaker kaolinite, 13.30 ± 0.05; Whittaker calcite, 2.78 ± 0.03; and Tamms calcite, 0.705 ± 0.010. The limits of error are assigned from three determinations on each sample.

Two electric calibrations were run before and after the sample immersion, and the average deviation of these sets of four determinations averaged approximately 1%. The heat of bulb breaking corrections were the same as described previously[11] with the exception that the smaller sample bulbs used in the present investigation liberated only 0.2 ± 0.1 joule when broken. The experimentally observed sample heats were on the order of 10 joules. For the heat capacity of the system, this corresponded to a temperature rise of approximately 0.02°.

Table I gives the experimental $\Delta H_i$ values in ergs/cm.$^2$ corresponding to various outgassing temperatures. The values given are the average of two determinations—one from each calorimeter. Reproducibility for the two measurements was always better than ±2% which is consistent with the limits of error from the calibrations and the heat of bulb breaking measurements. The absolute accuracy is probably no better than 5 to 10%, limited entirely by the accuracy inherent in the B.E.T. theory.

## Results and Discussion

**A. Kaolinite.**—Figure 1 shows that with increasing temperature, $\Delta H_i$ rises, levels off, falls discontinuously and once again levels off at the highest temperature used. To attempt an interpretation of these data, a knowledge of the surface structure of kaolinite is necessary.

The *surface* structures of kaolinite and especially any of the more complex clay minerals are not known, but the following picture seems reasonable from analogies with simpler systems. Regardless of the layers stacked in the *c*-axis direction, one side of the microscopic kaolinite platelets has exposed oxygen atoms from the silica tetrahedra while the other side has exposed hydroxyl groups from the alumina octahedra, since it is now well known that the surface[12] of pure silica exposed to a moist atmosphere is hydrated, *i.e.*, there exist stable surface hydroxyl groups. By comparison, it is reasonable to expect analogous existence of such groups on the outermost silica tetrahedra of kaolinite particles. Thus both sides of the basal cleavage plane can function as possible sites for cation exchange, instead of just the alumina side as is ordinarily assumed.[13] The hydroxylated silica

(1) L. Pauling, *Proc. Natl. Acad. Sci. U.S.*, **16**, 578 (1930).

(2) G. W. Brindley and K. Robinson, *Mineralog. Mag.*, **27**, 242 (1946).

(3) J. W. Gruner, *Z. Krist.*, **83**, 75 (1932).

(4) S. Spiel, L. H. Berkelheimer, J. A. Pask and B. Davies, U. S. Bur. Mines Tech. Paper 664, 1945.

(5) S. J. Gregg and M. J. Stephens, *J. Chem. Soc.*, 3951 (1953).

(6) H. Janert, *J. Agr. Sci.*, **24**, 136 (1934).

(7) C. W. Parmelee and D. Frechette, *J. Am. Ceram. Soc.*, **25**, 108 (1942).

(8) C. G. Harmon and F. Fraulini, *ibid.*, **23**, 252 (1940).

(9) A. C. Hall and N. Hackerman, The University of Texas, unpublished data.

(10) A. C. Hall and N. Hackerman, THIS JOURNAL, **62**, 1212 (1958).

(11) A. C. Makrides and N. Hackerman, *ibid.*, **63**, 594 (1959).

(12) R. K. Iler, "The Colloid Chemistry of Silica and Silicates," Chap. VIII, Cornell University Press, Ithaca, N. Y., 1955.

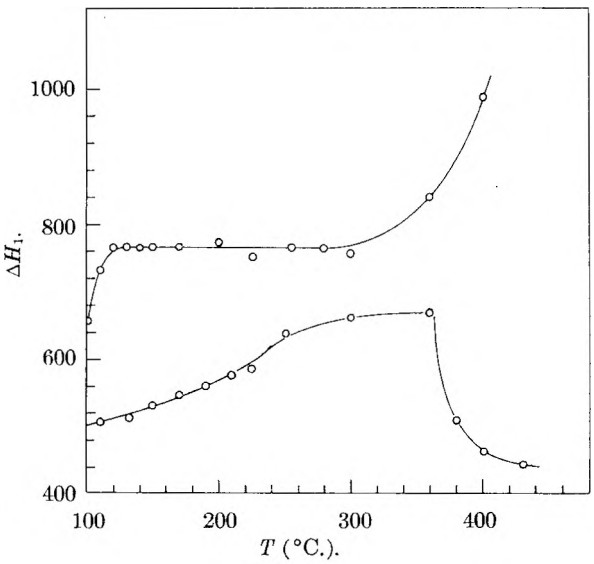


Fig. 1.

surface has been shown by previous studies to be hydrophilic compared to the completely dehydrated surface.[11] The present heat of immersion studies suggest that the discontinuity in $\Delta H_i$ at 370° arises primarily from the *surface* dehydration of both the exposed alumina and silica surfaces. Previous measurements have shown that the surface dehydration of pure silica occurs at approximately this temperature.[11] It is suggested here that the loss of bulk lattice water at the temperature in question is only incidental to the surface wetting process. Weight loss studies in the early phases of this investigation showed that bulk lattice water is lost irreversibly at 380°. If such were not the case the measured heats of immersion at temperatures greater than 370° would have been orders of magnitude higher owing to exothermic lattice rehydration. D.T.A. studies being of non-equilibrium character exhibit this loss of bulk lattice water at somewhat more elevated temperatures (500–550°).[4] In practice, the lattice dehydration was quite explosive during the outgassing routine unless the temperature was taken through the transition temperature very slowly.

Surface areas (see Table II and ref. 5) were found to be independent of outgassing temperature over the entire range studied. Thus the interlayer bonds must remain intact although there is interlayer loss of water. Complete breakdown of crystallinity during the loss of interlayer water might be expected to occur. X-Ray studies verify this.[5]

The initial rise of $\Delta H_i$ with outgassing temperature probably is due to the removal of the last traces of water physically adsorbed on the most energetic sites. The values of 650 to 670 ergs/cm.$^2$ correspond to the heat of immersion for the clean, fully hydroxylated kaolinite surface. The highest temperature attainable with the Pyrex sample holders was 460°. At this temperature, the heat of immersion of completely dehydrated kaolinite (sometimes referred to as meta-kaolinite) approaches 400 ergs/cm.$^2$. This last value may be an upper limit because of the possible existence of pores smaller than the krypton dimensions but larger than the water molecule dimensions.[5]

(13) R. E. Grim, "Clay Mineralogy," McGraw-Hill Book Co., New York, N. Y., 1953, p. 133.

TABLE I

HEATS OF IMMERSION IN ERGS/CM.$^2$

| Outgassed at temp., °C. | Whittaker calcite | Whittaker kaolinite | Tamms calcite |
|---|---|---|---|
| 100 | 653 | .. | .. |
| 110 | 730 | 508 | 767 |
| 120 | 762 | .. | .. |
| 130 | 762 | 511 | 780 |
| 140 | 761 | .. | .. |
| 150 | 762 | 530 | 769 |
| 170 | 763 | 547 | 782 |
| 190 | .. | 561 | 780 |
| 200 | 774 | .. | .. |
| 210 | .. | 574 | .. |
| 225 | 750 | 585 | .. |
| 250 | 762 | 638 | .. |
| 280 | 762 | .. | .. |
| 300 | 756 | 661 | .. |
| 360 | 840 | 668 | .. |
| 380 | .. | 508 | .. |
| 400 | 986 | 463 | .. |
| 430 | .. | 442 | .. |
| 460 | .. | 431 | .. |

TABLE II

AREA RELATIVE TO THAT OUTGASSED AT 110°

| Outgassed at | Relative area 110° | 250° | 290° | 370° | 400° | 440° C. |
|---|---|---|---|---|---|---|
| Whittaker kaolinite | 1.00 | ... | 1.01 | 1.00 | 0.99 | 1.00 |
| Whittaker calcite | 1.00 | 1.00 | ... | 1.00 | ... | ... |

**B. Calcite.**—The upper curve of Fig. 1 is for Whittaker calcite. The heat of immersion between 120 and 300° is constant at 762 ± 2 ergs/cm.$^2$ The last traces of physically adsorbed water are removed below 120° as shown by the initial rise of the curve. The increased heats of immersion between 300 and 400° are due to a partial conversion of calcium carbonate to calcium oxide. Applying measured thermodynamic data to the Clausius–Clapeyron equation gives a dissociation pressure of $1 \times 10^{-5}$ mm. at 350° for the reaction $CaCO_3 \rightleftarrows CaO + CO_2$. Using the experimentally measured heat of reaction-solution of CaO, the enhanced "heat of immersion" at 400° of about 200 ergs/cm.$^2$ corresponds to 0.07% conversion of $CaCO_3$ to CaO. There was no attempt to measure degassing pressures accurately and above 300° the measured heat of immersion is dependent on the kinetics of the decomposition process. Additional data are given in Table I for Tamms calcite. The agreement with the Whittaker calcite data is good considering the inherent uncertainties of the surface area measurements. Moreover independent measurements confirmed that the surface areas of the calcites used were independent of the outgassing temperature (Table II).

There has been no work on the surface structure of calcite but it would be supposed that plastic deformations introduced in the grinding process destroy most of the surface crystallinity. The

present measurements show that the surface structure of calcite is unaffected by the outgassing temperature.

## Conclusions

The heat of immersion of kaolinite exhibits a discontinuity corresponding to dehydration between surface hydroxyl groups. This occurs concurrently with the loss of bulk lattice water. The heat of immersion of the kaolinite surface free of physically adsorbed water is 660 ± 5 ergs/cm.$^2$ and that of the high temperature phase (metakaolinite) is approximately 400 ergs/cm.$^2$.

The heat of immersion of calcite is 762 ± 2 ergs/cm.$^2$ and is independent of the outgassing temperature from 120 to 300°. Noticeable conversion of $CaCO_3$ to CaO occurred only at the highest outgassing temperatures investigated.

**Acknowledgment.**—This work is a contribution from Project 47d of the American Petroleum Institute and the Department of Chemistry, The University of Texas. The authors wish to express their appreciation to the American Petroleum Institute for their unfailing support. They also wish to express their appreciation to Mr. Richard Every for his continued assistance throughout the investigation and to Mr. Clarence Williams, the departmental glassblower, for his effective help in building the apparatus.

## DISCUSSION

A. C. ZETTLEMOYER (Lehigh University).—Couldn't the water lost from the kaolinite be from the exchange ions rather than from silanol groups?

N. HACKERMAN.—Not completely. The discontinuity in the kaolinite data comes where the lattice loses its bulk water. This was seen in the outgassing procedure where unless the temperature was raised slowly through this point the samples exploded.

L. A. ROMO (du Pont Company).—In addition to the adsorbed water which varies from 1 to 5%, there is the water from dehydroxylation. For this infrared data would be useful. It is a well known fact that dehydroxylation takes place between 500 and 600° as shown by D.T.A. curves. Thus the dehydroxylation which may have taken place at 300° must be very small. With reference to edge effects, English workers have shown that the edges of silica tetrahedra contribute about 5% of the total cation exchange capacity of kaolinite.

N. HACKERMAN.—D.T.A. curves are definitely nonequilibrium in character (see Ref. 4) and are generally not carried out in evacuated samples. Our samples were outgassed at $10^{-6}$ mm. and this lowers the temperature at which bulk lattice water is lost.

A. C. ZETTLEMOYER.—I should like to comment that the bulb breaking correction depends upon the liquid in the calorimeter. Your reported value, it should be emphasized, is for water; for some organics we now believe the correction is negligible.

N. HACKERMAN.—Our correction for bulb breaking is based on water. Corrections based on heats of vaporization of approximately 8 kcal./mole, such as for a typical non-polar hydrocarbon, are negligible.

---

# CHROMATOGRAPHIC FRONTAL ADVANCE OF AN ADSORBATE THAT HAS AN ADSORPTION MAXIMUM

BY IRVING FATT AND MOHAMED A. SELIM

*Department of Mineral Technology, University of California, Berkeley 4, California*

*Received June 30, 1959*

Laboratory studies of surfactants of potential use as aids in waterflood recovery of petroleum often have showed these surfactants to have a maximum in the adsorption isotherm. Recently Vold and Sivaramakrishnan have given a plausible explanation of such adsorption behavior. This paper shows the effect of an adsorption maximum on the frontal advance of an adsorbate through a chromatographic column. Using an initial concentration distribution it is shown that the adsorption maximum leads to a concentration front that is stepped rather than a single vertical line on a concentration *versus* distance plot as would be obtained from a Langmuir type isotherm. Continued injection of a solution more concentrated than that at the adsorption maximum may lead to a concentration front that moves backward. The effect on frontal movement of a discontinuity in the slope of the adsorption isotherm at the c.m.c., as shown by Vold and Sivaramakrishnan, is also demonstrated. Frontal advance in a system in which the input concentration increases with time also is shown.

## Introduction

Movement of the adsorbate concentration front when a single solute solution is flowed through a chromatographic column can, in most cases, be calculated using methods given by De Vault.[1] Difficulties arise, however, when De Vault's treatment is applied to a solute that has an adsorption maximum. Laboratory studies of surfactants of potential use as aids in water-flood recovery of petroleum often have showed these surfactants to have an adsorption maximum. Recently Vold and Sivaramakrishnan[2] have given a plausible explanation of such adsorption behavior. The purpose of this paper is to show that the shape and position of the concentration front in a system with an adsorption maximum can be obtained by using a method of solving differential equations known as the method of characteristics.

**De Vault's Equation.**—De Vault has shown that in a linear column with instantaneous adsorption equilibrium and no diffusional effects, the position of any concentration at the front will be given by

$$x = S(c) + [V/(\alpha + Mf'(C))] \qquad (1)$$

where

$X$ = the distance of any point in the column
$S(c)$ = the initial distribution of solute concentration in the column
$V$ = volume of solution that has been pumped into the column
$\alpha$ = pore volume per unit length of column
$M$ = amount of adsorbing material per unit length of column
$f'(C)$ = first derivative of the adsorption isotherm
$C$ = concentration of solution

(1) D. De Vault, *J. Am. Chem. Soc.*, **65**, 532 (1943).

(2) R. D. Vold and N. H. Sivaramakrishnan, THIS JOURNAL, **62**, 984 (1958).

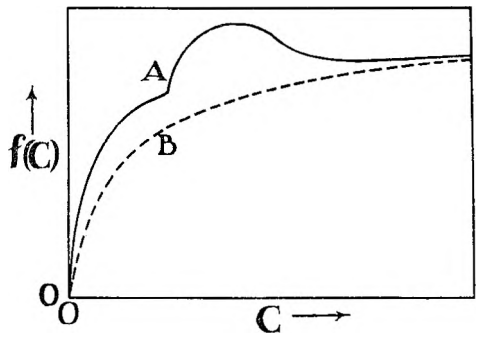


Fig. 1.—Isotherms: A, idealized Vold and Sivaramakrishnan isotherm; B, typical Langmuir isotherm.

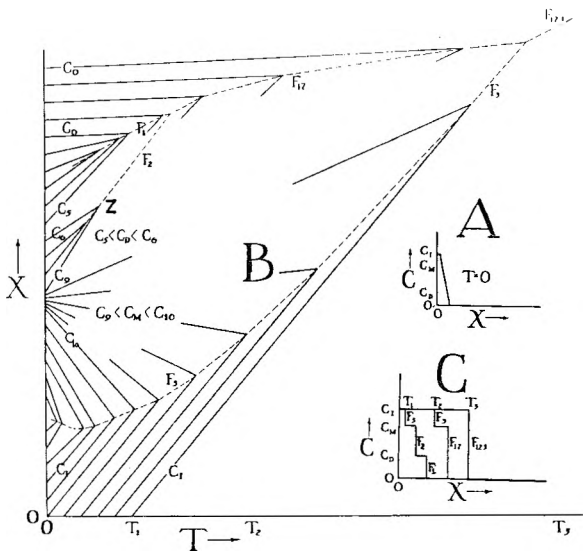


Fig. 2.—Characteristic plot for isotherm of Fig. 1A: A, initial concentration profile; B, characteristics; C, concentration profile as a function of time.

When equation (1) is applied to an isotherm of the Langmuir type the plot of $C$ *versus* $X$ may become double valued at the front and therefore physically unreal. To circumvent this difficulty, De Vault presents what he calls a discontinuous solution. This is simply a method whereby a material balance is used to obtain the position of the vertical line on the $C$ *versus* $X$ plot behind which must be all of the solute pumped in up to that time. The position of this line is given by

$$X_d = \frac{V(C_b - C_a) + \int_{C_a}^{C_b} [\alpha + Mf'(C)]S(c)dC)}{\alpha(C_b - C_a) + M[f(C_b) - f(C_a)]} \quad (2)$$

where $C_a$ is the concentration in the column ahead of the front and $C_b$ is the concentration of the injected solution.

**Method of Characteristics.**—Recently Fayers and Perrine[3] have shown that the rate of frontal advance in a chromatographic column can be obtained by the method of characteristics from the same basic equations used by De Vault.

When applied to the usual Langmuir type isotherm the method of characteristics leads to the time derivatives of equations (1) and (2). If the injection rate is constant, then the equations from the method of characteristics can be integrated to give equations (1) and (2).

An important difference between the methods of De Vault and of Fayers and Perrine arises when the adsorption isotherm has a maximum, an inflection point, a discontinuity in the first derivative or any combination of these. For such systems the method of characteristics predicts a stepped front during the early part of the injection history whereas De Vault's equation, equation (2) above, if used without caution, may lead to a single front.

To demonstrate the application of the method of characteristics an idealized form of one of the isotherms given by Vold and Sivaramakrishnan was used. This isotherm is shown as curve A in Fig. 1. Curve B in Fig. 1 shows a Langmuir type isotherm.

The rate of advance of any concentration is given by

$$\left(\frac{dx}{dt}\right)_c = \frac{q}{\alpha + Mf'(C)} \quad (3)$$

where $q = V/t$. Equation (3) is the time derivative of equation (2) for $q$ = constant. A plot in the $X,t$ plane will be a series of lines of constant concentration, known as the characteristics, with slope equal to the rate of advance of that concentration. The initial concentration distribution is arbitrary and, for reasons to be discussed later, will be taken as shown in Fig. 2A.

Figure 2B shows the constant concentration lines in the $X,t$ plane based on the isotherm of Fig. 1A. This isotherm has a discontinuity in the first derivative at $C_D$ and a maximum at $C_M$. All characteristic and front profile diagrams in this paper are for demonstration only and are not intended to show quantitative behavior of any particular system.

When two characteristics intersect, the physically impossible situation of two concentrations at the same point and same time is predicted. This situation is interpreted to mean that a concentration shock is formed. At the shock front the concentration rises abruptly. Fayers and Perrine show that the velocity of propagation of the shock front is given by

$$\frac{dx_d}{dt} = \frac{q(C_b - C_a)}{\alpha(C_b - C_a) + M[f(C_b) - f(C_a)]} \quad (4)$$

Equation (4) gives the slope of the line that passes through the intersection of the characteristics for $C_a$ and $C_b$. If the concentration increments are small, then the characteristics are close together and there is no problem in determining the shock front path from the slope of the path at the intersections.

Note that as $C_b - C_a$, the "strength" of the shock front, vanishes then equation (4) goes over into the characteristic equation (3).

Equation (4) can be used to trace the development and movement of a shock. Shock formation occurs at that instant on the time axis when two infinitely close characteristics cross. For example, this may be the point Z in Fig. 2B. The slope of the shock path at Z is the same as the slope of the characteristic through Z.

When the shock path is curved, step by step methods must be used to trace it. Given the known

(3) F. J. Fayers and R. L. Perrine, *Trans. Am. Inst. Mining, Met. and Pet. Engrs.*, in press.

location and slope of a shock path, at Z for example, the path can be continued as a straight line for a small time interval $\Delta t$ to determine its position at $t + \Delta t$. The characteristics which meet the shock at $t + \Delta t$ can be found by trial and error. These characteristics carry the concentrations $C_a$ and $C_b$ and the slope of the shock path at $t + \Delta t$ is then given by equation (4). If the time intervals are chosen small enough, this method allows the shock path to be traced as accurately as desired.

The use of a finite number of characteristics in the $X,t$ plane is equivalent to replacing the continuous front of Fig. 2A by a number of steps equal to the number of characteristics. At this point the reason caution is needed in using equation (2) can be seen. If $S(c)$, the initial concentration, is not zero then the integral in equation (2) must be evaluated. Also, for an isotherm that has a maximum the quantity $[f(C_b) - f(C_a)]$ will be negative in certain regions. To use equation (2) the region from zero concentration to $C_b$ must be divided into several increments. If these increments are sufficiently small, then equation (2) will show the development of several fronts just as the method of characteristics does. In fact, the method of characteristics is simply a convenient way of solving equation (2) in increments of concentration.

To avoid the possibility that a shock front will form at negative values of the $x$ coördinate the initial concentration distribution was taken as shown in Fig. 2A. This causes no difficulty because the $x = 0$ point can be put at any point on the $x$ coördinate.

An interpretation of the frontal advance from Fig. 2B is presented. Given the initial concentration profile of Fig. 2A, all characteristics for concentrations less than $C_D$ will collide to form the front marked $F_1$ in Fig. 2B. The position of this front at any time is read directly from the $F_1$ trajectory. Characteristics of concentrations between $C_D$ and $C_M$ will collide to form the front marked $F_2$. From time $T_1$ to time $T_2$ there are two fronts advancing. After time $T_2$ fronts $F_1$ and $F_2$ advance as the single front $F_{12}$ with concentration limits of zero and $C_M$. These concentration profiles are shown in Fig. 2C.

To avoid confusing the characteristic diagram several characteristics in the range from $C_9$ to $C_{10}$ are shown only partially. It is to be understood that the trajectory of fronts $F_{12}$ and $F_3$ is composed of collision between characteristics for $C_0$ and $C_I$ and those eminating from $T = 0$ in the region on the $x$ axis between $C_9$ and $C_{10}$.

During the time the aforementioned two fronts were forming and coalescing, another front, $F_3$, was forming between the injection concentration, $C_I$, and $C_M$. This front is formed by the intersection of the characteristic for $C_I$ and a characteristic for a lower concentration, which has a negative slope. The negative slope arises from the portion of the isotherm which has negative slope. The trajectory of the front, as shown in Fig. 2B, is such that for a time the front is moving counter to the direction of injected solution. Depending upon the isotherm, this front may move to $x = 0$ and temporarily disappear from the column. Continued injection at concentration $C_I$ will bring the $F_3$ front back into the column and it will eventually merge with front $F_{12}$ to form front $F_{123}$ which has the concentration limits zero and $C_I$.

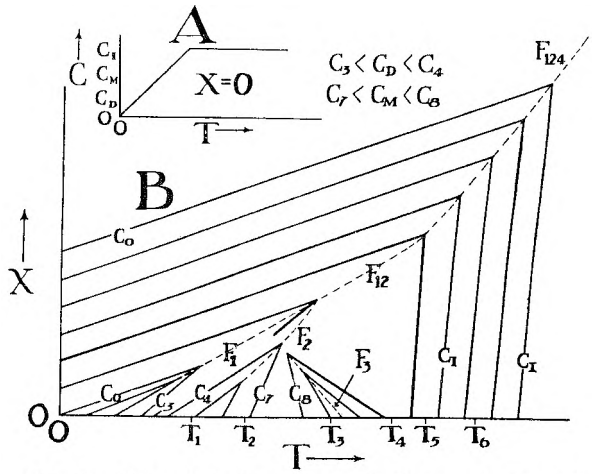


Fig. 3.—Characteristic plot for isotherm of Fig. 1A: A, input concentration as a function of time; B, characteristics.

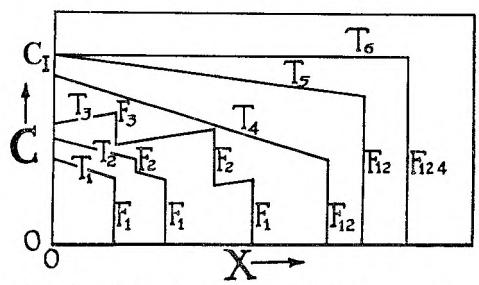


Fig. 4.—Concentration profiles obtained from Fig. 3B.

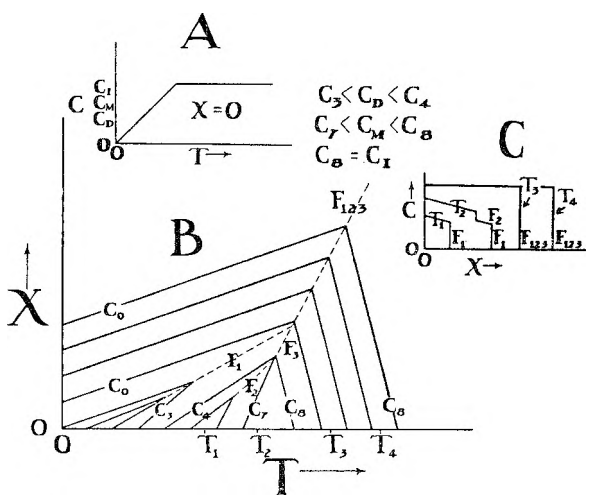


Fig. 5.—Characteristic plot for isotherm of Fig. 1A: A, input concentration as a function of time; B, characteristics; C, concentration profiles.

The method of characteristics can be used to show frontal advance for a system in which the injected concentration increases with time. At the input concentration the characteristics have positive slope. The isotherm of Fig. 1A and the input concentration *versus* time curves of Fig. 3A are used. Figure 3B shows the development of the two forward moving fronts $F_1$ and $F_2$ and the backward moving front $F_3$.

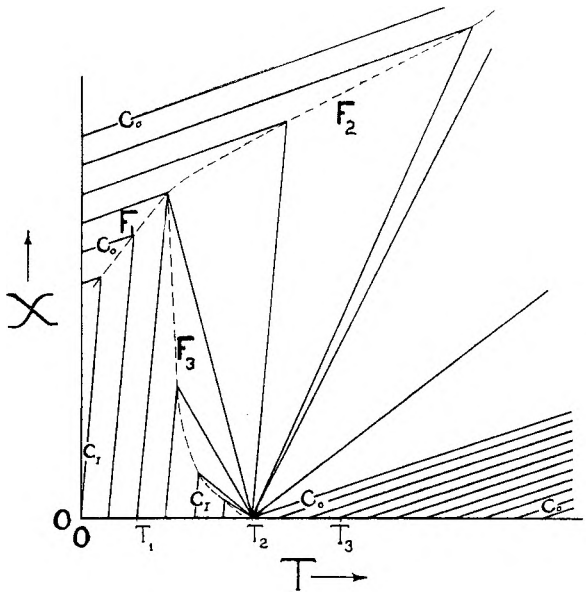


Fig. 6.—Characteristic plot for isotherm of Fig. 1A: input switched from solution to pure solvent.

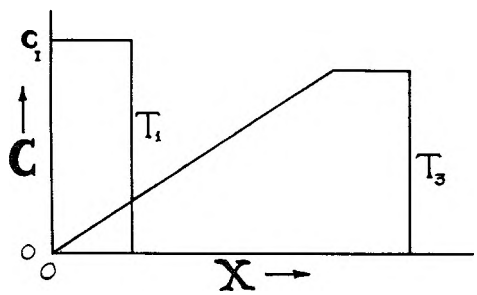


Fig. 7.—Concentration profiles obtained from Fig. 6.

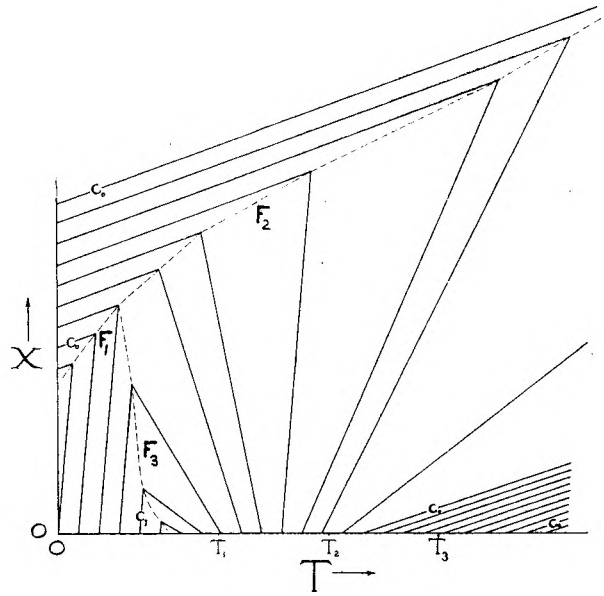


Fig. 8.—Characteristic plot for isotherm of Fig. 1A: input slowly changed from solution to pure solvent.

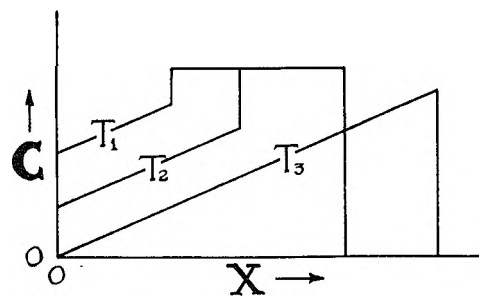


Fig. 9.—Concentration profiles obtained from Fig. 8.

The two forward moving fronts collide after a time and proceed as one front. The backward moving front, $F_3$, forms between concentration characteristics for which the slope is negative. This front moves out of the column entrance. Front $F_{12}$ now begins to collide with positive slope characteristics of saturations above $C_M$ and begins to form front $F_{124}$ which extends between zero concentration and $C_I$. The front then advances at a constant rate with concentration limits of zero and $C_I$.

Concentration profiles resulting from the characteristics in Fig. 3B are shown in Fig. 4.

Figure 5 shows the characteristics solution for a system in which the input concentration is on the negative slope of the isotherm.

On cursory examination the formation of front $F_3$ in Fig. 3B seems to violate the law of physics which states that no event of the future can influence present behavior. That this law is not violated can be shown. The negative slope of concentration characteristics above $C_M$ seems to indicate that these concentrations appear before they are injected. This is actually true because solutions of concentration greater than $C_M$ cause desorption and thereby carry forward a more concentrated solution than was injected. In this connection it should be pointed out that concentration $C_M$ moves at the velocity of injection and this is the maximum possible velocity. This is true despite the fact that equation (2) predicts an infinite velocity for the concentration $C_M$ when $\alpha = Mf'(C)$ in the region where $f'(C)$ is negative.

The method of characteristics also can be used to determine the profile of the trailing edge when injection of solution is discontinued and pure solvent injection begins. At $T_2$ in Fig. 6 solution injection ended and solvent injection began. This means that characteristics for all concentrations from $C_I$ to $C_M$ must radiate from $X = 0$, $T = T_2$. Concentration $C_M$ will move at maximum velocity and build up a concentration bank ahead of itself. This causes concentrations between $C_I$ and $C_M$ to move backward. The resultant trailing edge profile is shown in Fig. 7. As the distance on the time coördinate between the last $C_I$ characteristic and the first $C_0$ characteristic is brought to zero, it is seen that front $F_3$ becomes more vertical until the characteristic plot shows that $F_3$ has only an instantaneous existence. Figure 7 shows the concentration profiles resulting from the characteristic plot of Fig. 6.

In practice the transition from $C_I$ to $C_0$ cannot be made instantaneously, therefore $F_2$ may exist as shown in Fig. 8. The concentration profiles are shown in Fig. 9.

One problem that may arise when using the

method of characteristics in chromatography is scaling of the characteristic plots. Some isotherm and column properties require that different scales be used for the several parts of the characteristic plot. For example, in Fig. 2B the characteristics that develop front $F_2$ may have, if plotted on the same scale as those that develop front $F_1$, such high slope as to make the point of their intersection difficult to determine. In such case the $F_1$ and $F_2$ fronts can be developed on different plots and only their trajectory transferred to a common plot.

**Summary.**—Solutions which have an adsorption maximum or discontinuities in the first derivative of the isotherm will have a stepped concentration profile in a chromatographic column. The method of characteristics provides a convenient graphical procedure for obtaining the concentration profiles.

**Acknowledgment.**—The authors wish to thank R. L. Perrine, J. F. Fayers, and W. T. Cardwell of California Research Corporation, and J. W. Sheldon and B. Zondek of Computer Usage Company for providing manuscripts of unpublished papers on the method of characteristics.

## DISCUSSION

M. J. VOLD (University of Southern California).—Dr. Fatt's paper is very interesting and important since it offers a means of verifying the existence of an adsorption maximum. Dr. Robert Vold and his students have verified their experimental results repeatedly with carefully purified materials and many similar isotherms have been obtained by others. But Dr. K. J. Mysels has devised a perpetual motion machine based on an adsorption isotherm having a maximum in it! Also we are painfully aware of the many years of effort that went into explaining the "minimum" in surface tension–concentration curves which turned out to be due to impurities after all. Dr. Fatt's method can be used to show that a distinctive pattern of concentration of effluent from a column of given length results from this type of isotherm. Do you have in mind undertaking experiments to verify this?

I. FATT.—We do plan some experiments to verify the predictions from the method of characteristics. There are, however, several complicating features. If the adsorption isotherm with a maximum is a non-equilibrium situation but is reversible then an experiment carried out over a period that is short, relative to the time needed for complete equilibrium, will verify the existence of the maximum. If, however, the maximum is part of the irreversible behavior of the system then a chromatographic experiment will not clarify the situation. The method I have proposed for determining frontal advance requires that the isotherm be completely reversible. This is also the requirement of DeVault's method.

# EVALUATION OF MONTE CARLO METHODS IN STUDYING FLUID-FLUID DISPLACEMENT AND WETTABILITY IN POROUS ROCKS[1]

BY CHARLES G. DODD AND O. GERALD KIEL

*The University of Oklahoma, Norman, Oklahoma*

*Received March 6, 1959*

Network models have been used to determine the roles of various parameters on the quasi-static capillary pressure desaturation of a wetting liquid from a porous solid matrix. We have modified the network model suggested by Fatt to permit wetting fluid to be trapped during a desaturation process; and we have studied the effects of pore size distribution, network distribution, number of connections per pore, and network size on calculated capillary pressure desaturation curves. The results indicate that network models involving random distributions of selected properties are a valuable tool for investigating these parameters. Of more significance, however, is the indication that a still more valuable application of the network models may be made in the characterization of the wettability of porous media with respect to specified pairs of immiscible fluids saturating the solid. In the initial work reported herein the wettability concept was equated to the probability of entrance of displacing fluid into a pore filled with the fluid being displaced. Further considerations, and a review of recent experimental work, indicate a need for a more sophisticated approach to the problem which would include an assigned distribution of wettability to internal pores and the application of Monte Carlo methods to the study.

## Introduction

The description of single and multiphase fluid flow through capillary pores in solid porous media has been unsatisfactory because the pore geometry generally is too complex to be described adequately by analytical expressions. Physical models, such as bundles of parallel capillary tubes, heretofore used to develop analytical expressions, have been overly simplified. A new approach to this problem was suggested by Fatt[2] who set up a network model incorporating random assignments of parameters such as pore size distribution and number of connections between pores, within which fluid flow could be followed as one pore after another, or one set of pores after another, was desaturated according to the rules set up to describe a quasi-static or a dynamic desaturation process. A network model such as that devised by Fatt is but one of many discussed by Scheidegger[3] in his comprehensive review of the problem. Rose[4] has criticized Fatt's model because it did not describe rock pore geometry and orientation more exactly, but we have found a modification of Fatt's model accurate enough to simulate actual capillary pressure curves of sandstone rocks. We have chosen to explore the potentialities of the network model further and have found it a promising means of applying stochastic processes such as Monte Carlo methods to a study of the complex and subtle problem of wettability in porous media.

Fatt devised a network model in which he replaced each pore in a sphere-packed model with a cylinder. To facilitate calculations, the model was reduced to two dimensions. Each cylinder was viewed on end in the network where it was connected with other cylinders in a regular geometric pattern. The effects of pore-size distribution, network distribution and number of connections per pore on the model were studied. Four regular geometrical patterns were used to show the effects of number of connections per pore. Different random number tables were used to define network distribution. Three pore-size distributions were used to study that effect upon the desaturation process. In order to determine the effect of varying the size of the individual cylinders, Fatt assumed the length of each cylinder was proportional to its radius raised to the power, alpha. He tried different values for alpha and selected a value of $-1$. All of Fatt's calculations were performed assuming a continuous wetting phase. As a consequence, no wetting phase fluid could be trapped in a desaturation process.

We have extended the work of Fatt by employing desaturation steps such that wetting fluid can be trapped, and we have studied parameters similar to those he studied in the desaturation process. More important, however, we have attempted to consider the elusive factor of wettability by treating the probability of entrance of displacing fluid into a wetting fluid-filled pore as a stochastic process.

## Experimental

**The Network Model.**—We have defined a probabilistic model representing the pore geometry of porous media and have carried through an operation on the model analogous to the capillary-pressure desaturation process employed in the "restored state" laboratory testing of petroleum reservoir rock core samples.[5] The system employed consisted of two fluids, analogous to an oil–water system, in which the contact angle measured through the fluid initially found in the network was less than 90 degrees. The cylinders representing the pores were assumed to contain only one fluid at a time; this allowed the displaced fluid to be trapped if no continuous path to the effluent end was available. Variations in the parameters of pore-size distribution, network distribution and number of connections per pore were studied to indicate their effects on the desaturation process.

A modification of Fatt's network model was employed in order to make calculations more convenient when studying the trapping of displaced fluid. Rather than showing a series of basic geometrical designs with an end view of the cylinders connected

(1) This paper was based in part on work done by O. G. Kiel and reported in a M. Petroleum Engr. Thesis submitted in partial fulfillment of the requirements for the M.P.E. Degree to the Graduate College of the University of Oklahoma, 1957.

(2) I. Fatt, *Trans. Am. Inst. Mining Met. Engrs.*, **207**, 144, 160, 164 (1956).

(3) A. E. Scheidegger, "The Physics of Flow Through Porous Media," Toronto Univ. Press, Toronto, Canada, 1957.

(4) W. Rose, "Studies of Waterflood Performance. III. Use of Network Models," Illinois State Geol. Survey, Circ. No. 237, Urbana, Ill., 1957.

(5) W. Rose and W. A. Bruce, *Trans. Am. Inst. Mining Met. Engrs.*, **186**, 127 (1949).

by lines to common junction points, the lines in the geometrical designs were replaced with side views of the cylinders. In this manner a certain number of cylinders were shown to terminate at a given point according to the number of connections per pore. This alteration facilitated keeping track of the possible paths of fluid movement in the desaturation process. Three such regular networks, shown in Fig. 1, were used as models, one having four connections per pore, one having six connections per pore, and one having ten connections per pore. An effort to distribute the number of connections per pore in a random manner was tried, but the manner of allocating the various connections proved inadequate for the size of model studied.

The graphical representations of pores, such as those in Fig. 1, show a distinct orientation for each pore with respect to the other pores, but this orientation was not effective in the desaturation process. For any pressure gradient applied across the network, displacement was equally likely in all pores contiguous to the displacing phase having radius size corresponding to the imposed pressure gradient. Additional assumptions required for this model were that both fluids in the system were incompressible, the viscosity of each phase was constant and played no role in the quasi-static capillary pressure desaturation process under study, the displacement was piston-like with only one fluid occupying a pore at a given time, and there was no interaction between fluid and solid matrix.

In order that the wetting fluid might be trapped during the displacement process, it was necessary to devise a suitable method of entry for the displacing fluid and exit for the displaced fluid. The model used represented a vertical section of a core sample in a restored state capillary pressure desaturation apparatus. The displacing fluid was allowed to enter on three sides and the displaced fluid to exit on the fourth side. Further, it was assumed that a membrane containing pores, the largest size of which was less than the smallest pore in the network model, was placed at the effluent end. This membrane was assumed to be preferentially wet by the wetting fluid which was displaced from the network model. The effects of gravity in the systems were neglected to simplify the problem. The interfacial tension at fluid–fluid interfaces within the network was assumed constant. The wettability of the solid matrix, as measured by the fluid–fluid interfacial contact angle, was considered constant except in those modifications of the network where this parameter was specifically varied or otherwise investigated.

Using the assumptions and simplifications discussed above, it was possible to express capillary pressure in the classical manner as a function of the inverse value of the cylindrical pore radius, and, further, to define a scaled capillary pressure equal to the inverse of pore radius, using Fatt's alpha of $-1$.

In carrying out a desaturation operation with the network model, a stepwise process was employed. The first increment of pressure to be selected for application to a model was infinitesimally greater than that necessary to displace wetting

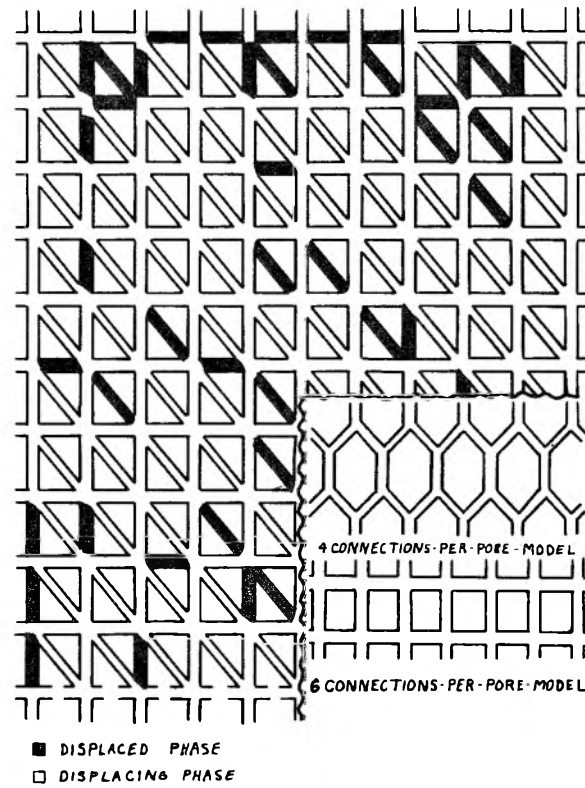


Fig. 1.—Network models having four, six and ten connections per pore. The distribution of displaced fluid that was trapped upon complete desaturation is shown for the model having ten connections per pore, and using pore size distribution one and random number table two.

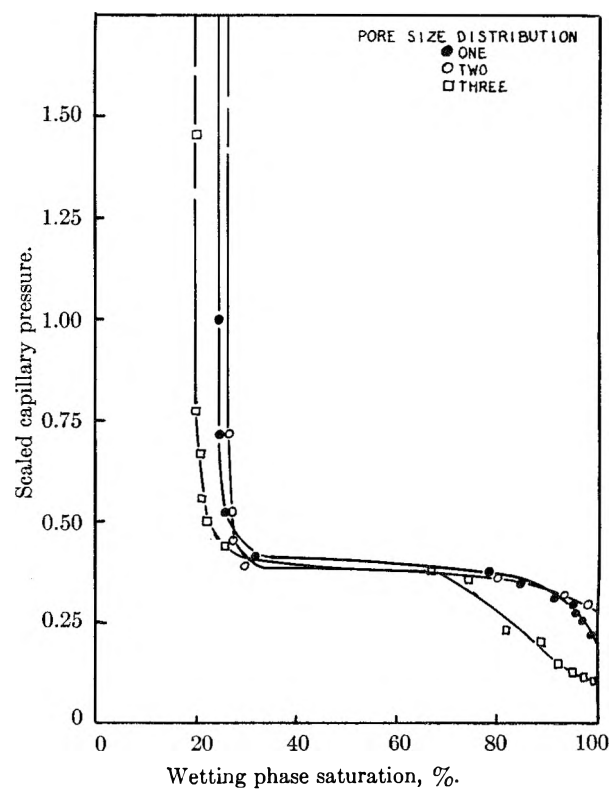


Fig. 2.—Capillary pressure curves showing the effect of pore size distribution for a model having six connections per pore and using random number table one.

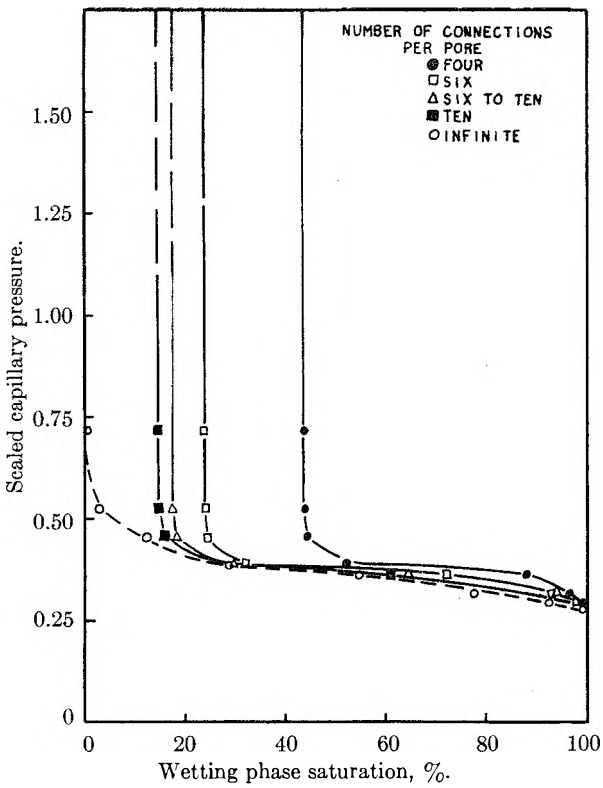


Fig. 3.—Capillary pressure curves showing the effect of number of connections per pore for pore size distribution two and random number table two.

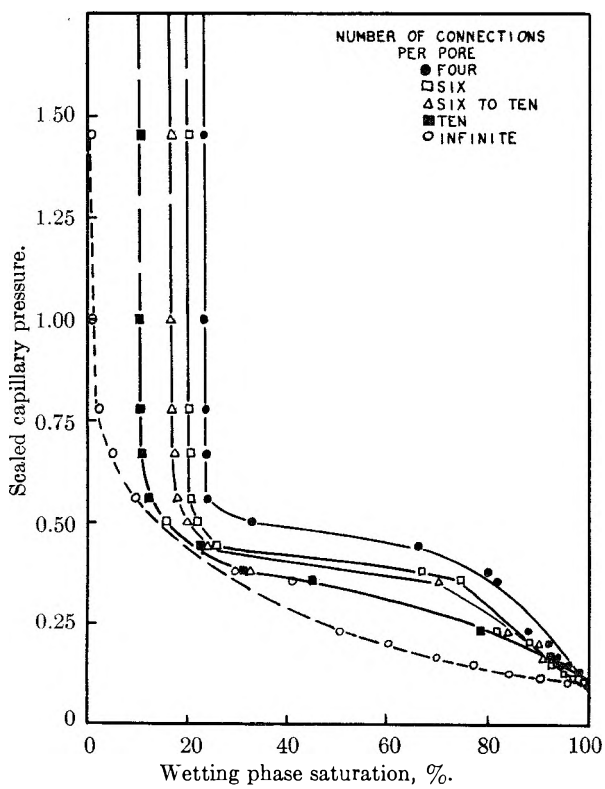


Fig. 4.—Capillary pressure curves showing the effect of number of connections per pore for pore size distribution three and random number table one.

fluid from the largest pores in the network contiguous to the upper three sides of the network. The pressure gradient at the second step was selected to be just greater than the capillary pressure required to desaturate the next smaller group of pores contiguous to those pores now filled with displacing fluid. This stepwise process was continued for the number of steps required to complete the desaturation process.

The various pore-size distributions assumed were distributed in a random manner throughout the model. Sequences of unique random numbers were obtained from two sources,[6] by copying a sequence selected at a random place in one of the tables and deleting any duplicates. After obtaining the desired sequence of random numbers, a one-to-one correspondence between these numbers and the ordered sequence of network position numbers was constructed. This gave each position a unique identification. The one-to-one correspondence was then re-ordered with respect to the random numbers.

The pore-size distributions used were those cited by Fatt as being representative of a narrow distribution, an intermediate distribution, and a wide distribution, referred to herein as pore-size distributions one, two and three, respectively. The number of pores to be associated with each radius size was determined by multiplying the percentage times the total number of pores in the network and adjusting to the nearest whole number. A final check was made to assure that the sum of the number of pores equalled the total number of pores. If $n_1$ was the number of pores having a radius $r_1$, then the first $n_1$ ordered random numbers were assigned the relative radius size $r_1$. The next $n_2$ pores were assigned $r_2$, and the process was repeated until the entire group had been assigned. Having obtained a one-to-one relation between network location, its corresponding random number and its assigned pore radius, the groups were re-ordered so the position numbers formed a sequence from smallest to largest.

The stepwise desaturation process was carried out in the manner indicated above by repeatedly imposing a capillary pressure gradient required to displace wetting fluid from the next smaller set of pores, checking to determine whether any pores containing displaced fluid were isolated so there was no continuous path for movement of displaced fluid, considering wetting fluid in such pores to be trapped and to remain in that condition for the entire desaturation process, and, finally, checking pores contiguous to those displaced by the displacing phase to ascertain if any additional pores would be displaced at the existing pressure gradient. This sequence of steps of displacing, checking for trapping and checking for further displacement was repeated for each pore size in the network. The number of displaced pores resulting from each successive sequence of steps was then tallied and assembled in an appropriate table outlining the results of the process. Allowance was made for those cases when pores having radii corresponding to pressure gradients smaller than that imposed at the step under

(6) (a) G. W. Snecdor, "Statistical Methods," Iowa State College Press, Ames, Ia., 1946, p. 11–12. (b) The Rand Corporation, "A Million Random Digits with 100,000 Normal Deviates," The Free Press, Glencoe, Ill., 1955, p. 191–192.

study were found contiguous to the displacing phase. The over-all process was repeated until desaturation was complete. The results then were tabulated. Finally, the capillary pressure–fluid saturation curve was plotted using the functional relationship developed by Fatt. Representative capillary pressure desaturation curves obtained in this manner are shown in Fig. 2 for the three pore-size distributions.

**Results Obtained with the Model.**—The effect of the number of connections per pore was not separated easily from those of the other parameters. This was due to the slight variation necessary in the size and arrangement required to obtain a geometric configuration corresponding to a given number of connections. The predominant effect shown in Figs. 3 and 4 is believed to result from changes in the number of connections.

The effects of network distribution were determined by the use of two ordered random number tables to define the distribution of pore sizes. Examples of the resulting capillary pressure curves are shown in Fig. 5.

The selection of the number of cylinders to be included in the various network models, *i.e.*, the network size, was a compromise between the large number of pores required to represent adequately the physical prototype and justify the use of a stochastic process, and the limitations imposed by the task of accounting manually for each step in the desaturation process. This first study was done without the help of a digital computer, and it was limited to two-dimensional models containing from 310 to 480 pores in order to permit several sets of parameters to be evaluated in the time available. The capillary pressure curves obtained from this work, however, were sufficiently like those obtained from rock core samples to give confidence in the significance of the results. Extensions of the work now are being programmed for digital computers employing larger models of varying geometry. Comparisons of three of the curves obtained with 310- and 480-pore models are shown in Fig. 6.

**Characterization of Wettability.**—During the last few steps of the desaturation process where simultaneous movement in pores of equal size was assumed, the possible continuous paths for desaturation were observed to be few in number. As few as one continuous path to the effluent end was found to exist for several of the desaturation calculations. This made it necessary for numerous pores having the same radius to empty through the existing path. As a result, the movement was not simultaneous but rather one in which the more remote pores were desaturated first followed by successively less remote pores. This problem made it necessary to consider the necessity of modifying one of the basic premises upon which the network study had been based up to this time, *i.e.*, the concept of simultaneous desaturation of all pores contiguous to the displacing fluid and having a pore size such that displacement could occur.

Further reflection upon this development led to the conclusion that the problem presented was very similar to that of characterizing the "wettability" of the internal surfaces of a porous rock sample. Intuitive considerations based on such commonplace observations as the jerky, irregular movements of liquid droplets moving over heterogeneous solid surfaces, the intermittent advance of fluid–fluid interfaces in glass tubes not uniformly clean, and the displacements of microscopic interfaces in porous bead packs[7] support the plausibility of the proposition that fluid–fluid interfacial movement and displacement in a porous solid is a random process. The unsolved problem of contact angle hysteresis supports the stochastic concept, but it also leads to the thought that the statistics involved in the process should be biased in terms of surface energies, or some related physical factor, when assigning probabilities of interfacial movement in a given situation. This line of reasoning has led to an examination of the possibility of applying stochastic processes such as Monte Carlo methods[8] to the determination or characterization of the effective wettability of a given sample of porous solid with respect to the displacement of one fluid by another within its pores.

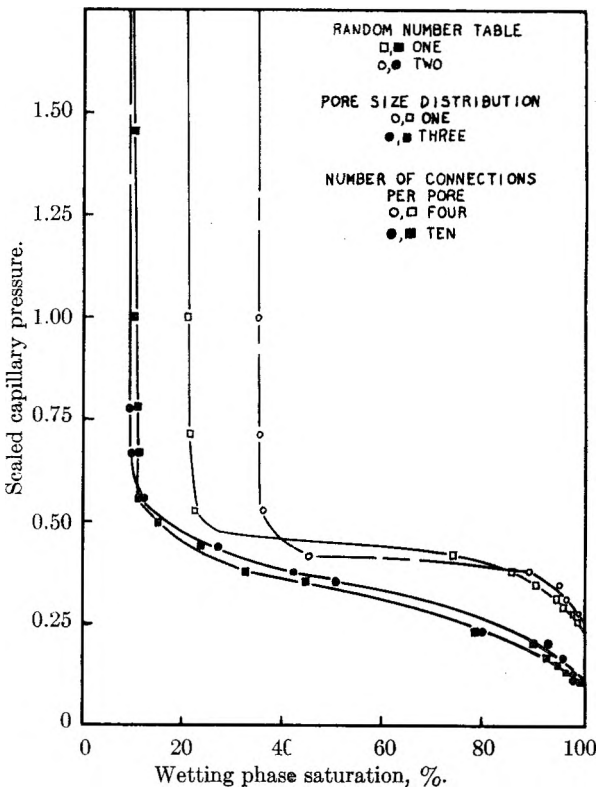


Fig. 5.—Capillary pressure curves showing the effect of network distribution in two models.

The balance of the work with the first simple network model described above was based on the assumption of a zero pore-size distribution network, *i.e.*, a network containing equal-sized pores. Since the problem of direction between pores did not exist, this problem was approached in a manner analogous to that of a random walk problem in one dimension having no reflection barriers.[9] For exemplary purposes, the network model having four connections per pore was used for these calculations.

(7) A. Chatenever and J. C. Calhoun, Jr., *Trans. Am. Inst. Mining Met. Engrs.*, **195**, 149 (1952).

(8) H. A. Meyer, Ed., "Symposium on Monte Carlo Methods," John Wiley and Sons, New York, N. Y., 1956.

(9) S. Chandrasekhar, *Rev. Mod. Phys.*, **15**, 1 (1943).

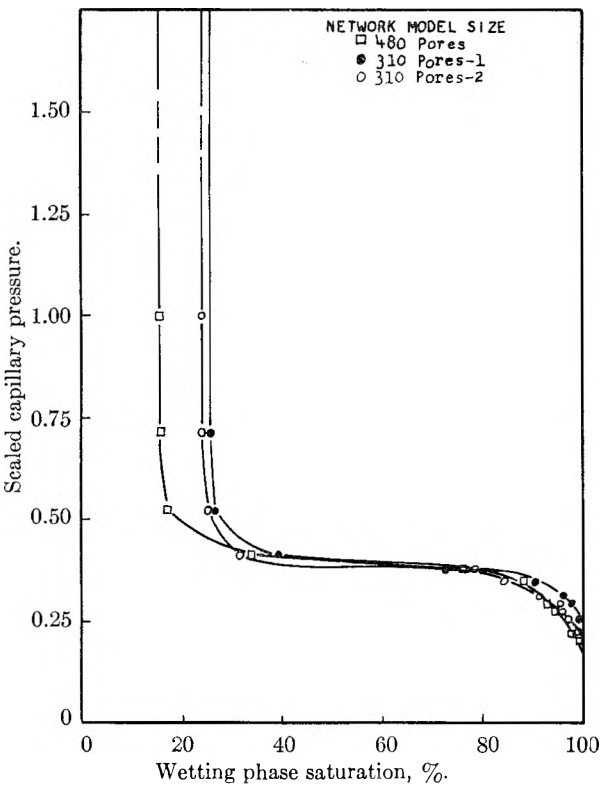


Fig. 6.—Capillary pressure curves showing the effect of model size for pore size distribution one in a model having six connections per pore.

If one considers a zero pore-size distribution network model in its initial state, totally saturated with the fluid to be displaced, and with $n$ pores contiguous to the displacing phase, one would expect all $n$ pores to be desaturated when the (scaled) capillary-pressure gradient exceeded the displacement pressure of the individual pores. Under the conditions set up for these models, displacement would occur over an infinite period of time, and each set of pores contiguous to the displacing phase would be desaturated before desaturation of the next set would begin. To express the probability of displacement in a pore, it was assumed that, of the $n$ possible positions of entry for the displacing fluid, a certain number would occur. This number of identical events which was most probable was obtained from the binomial expansion

$$(M + S)^n = M^n + nM^{n-1}S + \ldots + \frac{n(n-1)\ldots(n-r+2)M^{n-r+1}S^{r-1}}{(r-1)!} + \ldots + nMS^{n-1} + S^n$$

where

$M$ = probability of success for instantaneous movement,
$S$ = probability of failure for instantaneous movement,
$M + S = 1$

The first case considered was that for which $M = 1$ and $S = 0$, *i.e.*, it was certain that the displacing fluid would enter the pore and displace the fluid on contact. Under this assumption the most probable number of events occurring simultaneously would be $n$. The calculations for this case were made according to the procedure used for the desaturation process described above. Under this most extreme condition there was not total desaturation.

The second case considered was that the probability of movement or no movement was equal, *i.e.*, $M = S = 1/2$. Again, by substituting these values along with the value for $n$, each of the terms was evaluated. Since $M = S$, it was necessary to evaluate only the coefficients of the terms. The general $r$th coefficient is

$$\frac{n(n-1)(n-2)\ldots(n-r+2)}{(r-1)!}$$

If this coefficient has the maximum numerical value, the most probable number of simultaneous occurrences would be $n - r + 1$. In terms of $n$, this value is $n/2$ or $1/2(n \pm 1)$, according to whether $n$ is even or odd.

After determining the number of pores into which the displacing phase would enter simultaneously, a means had to be devised to differentiate among the $n$ possible locations to select the network locations where displacement would occur. The uniqueness was defined by the random numbers associated with each network position number. The method devised to determine the positions was to extract from a table of one-to-one correspondence between the random numbers and network locations the $n$ network locations contiguous to the displacing fluid. This set of $n$ random numbers was ordered sequentially with the first pair having the smallest random number and the last pair the largest. In the first step of the desaturation process the first $n/2$ or $1/2(n + 1)$ pairs from the ordered group were selected starting with the pair having the smallest random number having zero as the hundreds digit. The displacing fluid was allowed to desaturate these pores. A check was made to determine whether any pores containing the displaced phase were cut off from a continuous path for desaturation. Again, the process of ordering the set of $n$ pairs of numbers corresponding to all network positions contiguous to the displacing phase was carried out. Then the $n/2$ or $1/2(n + 1)$ pairs were taken in sequential order starting with the smallest random number having a three in the hundreds position. The starting point for the next step was the smallest number having a six in the hundreds position. Each succeeding starting point was advanced by adding three to the hundreds position, modulus ten, until the desaturation process was completed. The results indicated a larger residual than when the probability of movement was one.

For the final case the displacement process was considered as a series of displacements where one pore was displaced before another displacement began. This was equivalent to considering the term $nMS^{n-1}$ as the term having the maximum value. The reason for not considering the case where $S = 1$ was that no displacement would occur under these conditions. The procedure of ordering the random numbers and selecting the starting positions was the same as that described above. The resulting residual saturation was the largest.

If oil were the displacing fluid and water the displaced fluid, it seems reasonable to interpret these results as indicating a greater probability of displacement for the least water-wet system. The case where the probability of movement is in the neighborhood of one would correspond to an oil-wet sys-

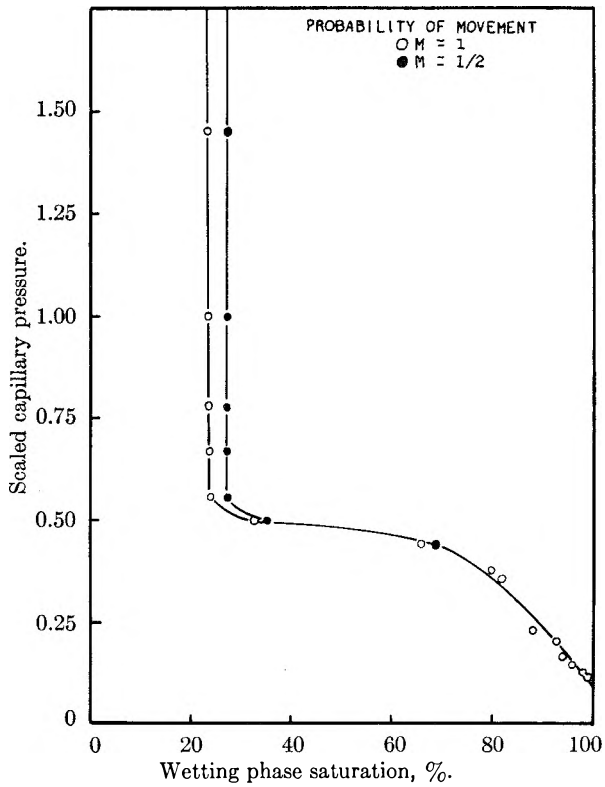


Fig. 7.—Capillary pressure curves showing the effect of change in probability of movement for a model having four connections per pore, using pore size distribution three and random number table one.

tem. The case where the probability of movement is in the neighborhood of $1/n$ would correspond to a water-wet model. Values between these two extremes, such as the case where the probability of movement is one-half, would define the degree of wettability of the solid for the fluid-fluid system.

The residual saturations, calculated for a model having four connections per pore, were 46, 16 and 2%, respectively, for $M$ values of $1/n$, $1/2$, and 1. The residual saturations determined by assuming a value of $M = 1/2$ for network models having four, six, ten and an infinite number of connections per pore were 16, 12, 9 and 0%, respectively.

Finally, the probability of displacement principle was applied to a simple network model having four connections per pore and a wide distribution of pore sizes. Capillary desaturation curves were calculated for values of $M = 1$ and $M = 1/2$. These curves are shown in Fig. 7. It is seen that the assumed variations in wettability affected only the residual fluid saturation.

## Discussion

The results of the work described in this paper confirm and extend the developments of Fatt.[2] In general, our results indicate the wider the pore size distribution of the model, the lower is the residual displaced fluid saturation. In comparing the two random number tables used in constructing the network models it was found that, for a model of the size studied, there was a greater sensitivity to network distribution in models having a smaller number of connections per pore. In particular, for the models incorporating pore-size distribution one, a narrow distribution, there was a considerable difference in the curves for the models obtained with different random number tables. The residual saturations were most sensitive to changes in the number of connections per pore.

The distributions of trapped residual fluid, such as that shown in Fig. 1, when correlated with pore size, indicated that the displaced fluid was trapped largely in the smaller pores within the network, and this was emphasized in the models having the larger number of connections per pore. In general, it appeared that the models having ten connections per pore appeared to be more representative of the properties of relatively homogeneous sandstone rocks. The network model, when constructed with due consideration of the properties of the rock prototype it represents, appears to be a valid means of studying quasi-static fluid–fluid displacements such as those involved in the determination of capillary pressure desaturation curves, particularly when the object of the investigation is to study the interrelationships between the parameters that control capillary pressure equilibrium. Applications of the model to dynamic systems have been made by Fatt[2] and Rose.[4]

The subject of greater interest to the writers is the study of the complex problem of fluid–fluid wettability within porous media. The ideas concerning wettability discussed in this paper are of an elementary nature compared to the apparent potentialities for applying stochastic processes, such as the Monte Carlo method, to the problem of defining and determining wettability. The concept of equating the probability of entrance of displacing fluid to the wettability at each step in the desaturation process is a simple one, but it does involve a more or less random determination of the pores to be displaced. The fraction of the total number of contiguous pores at any step is determined by the assigned probability, or wettability, but the selection of the actual pores on the model for displacement is done in a pseudo-random manner.

A more sophisticated approach to the problem might involve an assignment of an assumed distribution of wettabilities to each pore in the model initially. If the wettability of a pore were considered to be determined by the more conventional concept of the cosine of the interfacial contact angle, it would be logical to determine which pores were displaced at each step by the quotient of the cosine divided by the pore radius (or by the product of interfacial curvature times the cosine), rather than by the reciprocal of the pore radius alone. The assumed distribution of wettabilities might take the form of a normal Gaussian distribution or it might be selectively biased in accordance with some sampling scheme determined by the perceptive intuition or experience of the investigator. Such an approach may be described as a Monte Carlo method.

Brown and Fatt[10] have advocated the use of the concept of fractional wettability which they defined in terms of the fractional internal surface area in contact with a single fluid phase. To determine fractional water wettability they utilized nuclear

(10) R. J. S. Brown and I. Fatt, *Trans. Am. Inst. Mining Met. Engrs.*, **207**, 262 (1956).

magnetic resonance experiments to estimate the fraction of internal rock surface in contact with water. Holbrook and Bernard[11] used a simple dye adsorption test to measure the same quantity. Iwankow[12] prepared unconsolidated sand packs containing known fractions of water-wet grains and silane-treated, oil-wet grains. The sands were mixed well before packing, the packs were saturated with water, and the water-saturated packs were flooded with four pore volumes of oil. Holding other parameters constant, he found that the residual water saturations varied systematically with the fraction of oil-wet sand in the pack. In these experiments a normal distribution of oil-wet sand grains, and hence oil-wet surface area, was assumed throughout the sand packs.

Fatt and Klikoff[13] packed similar mixtures of water-wet and oil-wet sand grains for use in capillary pressure drainage experiments in which water was displaced by oil. In their experiments with a sand pack composed of uniformly sized grains, the capillary pressure curves were lowered and the residual saturations were reduced as the fractional oil-wettability increased. The decrease in residual water saturation is in agreement with our calculations referred to above. The decrease in the "plateau" of the capillary pressure curve with increasing oil-wettability is normal, but it was not found in the only pertinent calculation made with our network model, shown on Fig. 7, because the assumption of a wettability number did not result in trapping any additional fluid in this pore size region. We did not assume a distribution of wettability such as characterized the Fatt and Klikoff experiment. Their experiments and Iwankow's work show the need for the use of some kind of wettability distribution in the network models.

In other experiments Fatt and Klikoff found that the shape of the capillary pressure curves was changed when a wide sand-grain-size distribution was used to make the sand packs and the fractional oil wettability was increased in the same experiment. In one case they treated only the finest grains with silane and found a much higher residual water saturation as well as a change in shape of the curve. This work shows the need for considering the quotient of wettability divided by pore size in determining displacement of a given set of pores when desaturating the network models.

(11) O. C. Holbrook and G. G. Bernard, Paper No. 896-G, Society of Petroleum Engineers-A.I.M.E. Meeting, Dallas, Texas, Oct. 6-9, 1957.

(12) E. N. Iwankow, "A Correlation of Interstitial Water Saturation and Heterogeneous Wettability," M. Petroleum Engr. Thesis, University of Oklahoma, Norman, 1958.

(13) I. Fatt and W. A. Klikoff, Jr., "Effect of Fractional Wettability on Multiphase Flow Through Porous Media," paper presented at Amer. Inst. Chem. Eng. Meeting, Kansas City, Mo., May 17, 1959.

## DISCUSSION

I. FATT (University of California at Berkeley).—I am keenly aware of the amount of time put into this work. I believe that this type of approach is applicable to many important unsolved problems. Your model is a static one in which the pressure in the network is constant at each instant. It would be useful to make a dynamic model which takes the pressure gradient into account and shows how the system behaves while fluids are actually moving through it.

C. G. DODD.—This is certainly worthy of further effort but it would require a faster computer and a very large machine memory in comparison with the quasi-static problem.

M. J. VOLD (University of Southern California).—You have used Fatt's relationship between pore diameter and pore length. Might it not be more realistic to use a random distribution of pore lengths? Doing this would enable you to calculate the pressure drop through each pore and would facilitate converting the static model into a dynamic one.

C. G. DODD.—This is an interesting suggestion. There is no analytical or procedural problem involved in distributing the pore lengths randomly throughout the model or in making the saturation calculations. The difficulty is to find a machine big enough to permit all of the data to be included in memory locations corresponding to each pore location.

I. FATT.—I made use of a random combination of lengths and radii in one calculation and discussed it in my AIME paper in 1956. The results are surprisingly close to those obtained with the inverse relation Dr. Dodd has used. I have no explanation as to why this should be so.

M. J. VOLD.—Do you have any guess as to how many pores will have to be included in a model network to get a statistically valid result?

I. FATT.—A sandstone cube $1/4''$ on a side has about 10,000 pores. We made capillary pressure curves on a cube 2″ on a side and got reliable results. Then we began slicing it up into smaller and smaller bodies. We began to get serious fluctuations when the cube was only $1/4''$ on a side, but this probably was due to mechanical inhomogeneity in the block. The computer model would be a homogeneous network and it may be that many less than 10,000 pores are required.

C. G. DODD.—We may be helped in this problem of determining network size and assigning pore lengths and wettability distributions if we have insight concerning the most applicable statistics for the problem. In other words, if we know beforehand how the sampling scheme should be biased we can select the appropriate distribution. This is the Monte Carlo Approach. We need essentially to know part of our answer ahead of time to minimize the parameters that must be varied and, hence, the machine time required.

# THE SORPTION OF $H_2O$ AND $D_2O$ BY LYOPHILIZED LYSOZYME[1]

BY WASYL S. HNOJEWYJ[2] AND LLOYD H. REYERSON

*The School of Chemistry, University of Minnesota, Minneapolis 14, Minnesota*

*Received March 6, 1959*

Isotherm data for the sorption of $H_2O$ and $D_2O$ on lyophilized lysozyme are reported. The heats of sorption are calculated. Not only is $D_2O$ more sorbed than $H_2O$, but the differential heats of sorption show interesting differences.

Earlier work from this Laboratory[3] presented data for the sorption of $H_2O$ by lyophilized ribonuclease. Calculated heats of sorption gave rather large values for the first percentages of water taken up but these values fell rapidly until about 5.5% of water had been sorbed. Evidence indicated that the break in the heat curve occurred roughly at monolayer coverage, which meant, as suggested by Pauling,[4] that the polar side groups on the protein had been saturated by water molecules It was felt desirable that this type of work be extended to other lyophilized proteins and that isotherms for $H_2O$ be compared with those of $D_2O$. This work presents results obtained for the sorption of $H_2O$ and $D_2O$ by lyophilized lysozyme at 17 and 27°.

## Experimental

Sorption isotherms were measured gravimetrically using a quartz spring helix having a sensitivity of 12.580 mg./cm. Displacements were measured with a traveling microscope to ±0.003 mm. 169.8 mg. of the protein was used for the $H_2O$ sorptions and 176.7 mg. for the $D_2O$ study. The lysozyme was obtained from the Armour Research Division of the Armour Company (Lot D-638040) and was lyophilized from about a 3% solution in triply distilled, deionized water at a *p*H of 6.8 to 7. It was frozen dried on a fine glass rod using an alcohol–$CO_2$ mixture. The glass rod containing the protein was attached to the hook at the lower end of the quartz spring balance. After careful outgassing at a pressure of $10^{-6}$ mm., the isotherms were determined in the same manner as previously described,[3] except that in this case the measurements were carried out at 17 and 27°. The purified $H_2O$ and $D_2O$ (99.5%) were outgassed by a series of freezings, thawings and evacuations.

## Results and Discussion

Since comparisons between $H_2O$ and $D_2O$ were being made, the isotherms for the sorptions of both vapors are given in Figs. 1 and 2. In the case of the isotherm of $H_2O$ at 27°, the vapor was sorbed up to 18.7% of the weight of the dry protein. The desorption that followed was slow but it was found possible to finally return to the original zero point in spite of the marked hysteresis, as shown in Fig. 1. At 17° the sorption was carried to a much higher vapor pressure and, as a result, to a much higher uptake by the protein. Even at an adsorption of 58% of the protein's weight of $H_2O$, the shape of the protein on the glass rod remained essentially unchanged except that a slight swelling was observed. The ribonuclease used in the previous study formed a solution in the water when it had taken up about this amount of the vapor. In the case of the lysozyme, when the uptake of $H_2O$ reached about 70%, the fluffy white protein on the rod collapsed. The desorption hysteresis shows a difference from that at 27° but it was found possible to finally reach the same zero point in spite of the longer time needed.

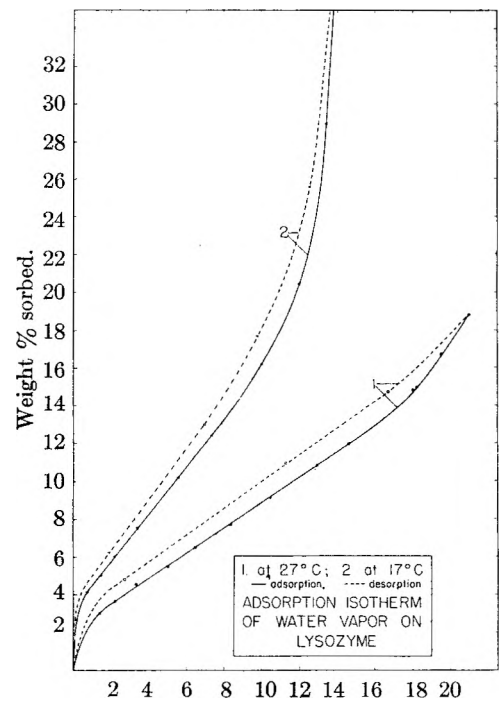


Fig. 1.

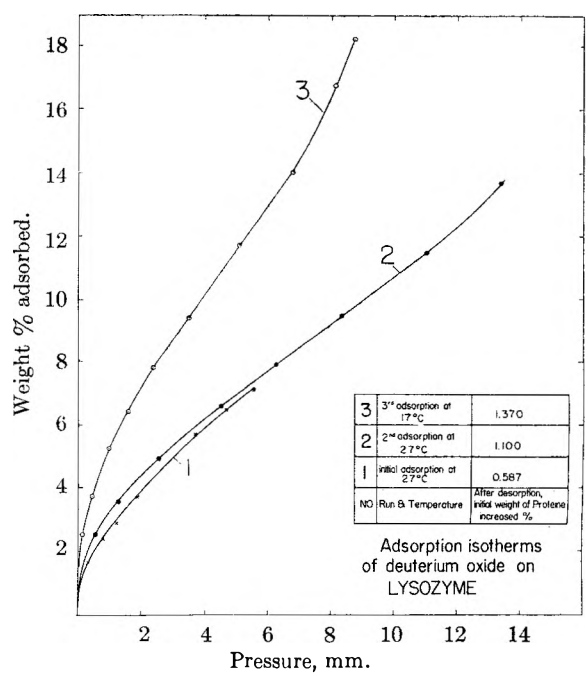


Fig. 2.

(1) This work was supported by a Research Grant from the National Institutes of Health.

(2) Research Associate, University of Minnesota.

(3) J. G. Foss and L. H. Reyerson, THIS JOURNAL, **62**, 1214 (1958).

(4) L. Pauling, *J. Am. Chem. Soc.*, **65**, 555 (1945).

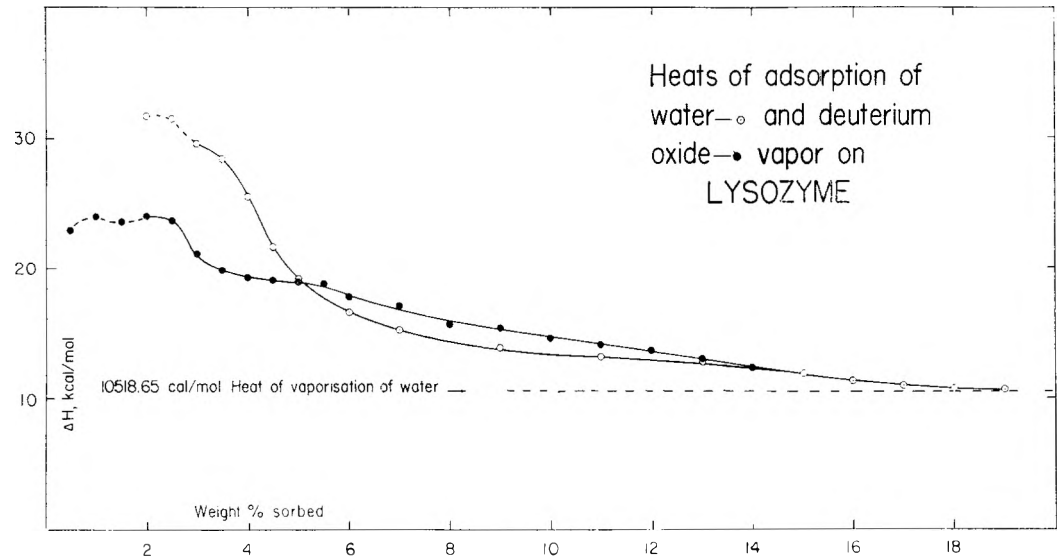


Fig. 3.

The collapse of the protein certainly altered the porous structure of the protein and there could have been some internal changes, but the desorption isotherm does not show too significant a difference.

It was apparent, almost immediately after beginning the studies using $D_2O$, that the protein sorbed more $D_2O$ at the same vapor pressure than it did $H_2O$. The second sample may have had a different surface, even though the two were prepared alike. The first isotherm at 27° carried the increase in weight to about 7.0% of the weight of the protein. Upon desorption, under the same conditions as for $H_2O$, it was found that the weight of the protein did not return to the same zero point. In this first case, the permanent addition of weight amounted to 0.587% of the initial weight. A second sorption then was determined, with the amount of added $D_2O$ reaching approximately 14% of the weight of the protein. Upon desorption, the protein retained $D_2O$ equal to 1.10% of its original weight. The final isotherm at 17° was carried up to about 18% of added $D_2O$. Upon desorption, the protein retained $D_2O$ equal to 1.37% of its initial weight. Since the protein sample was the same for all three isotherms, this meant that an increase in weight occurred during each adsorption–desorption cycle. This strongly suggests that deuterium exchange took place on the surface of the lyophilized protein, between certain of the hydrogen atoms of the protein and the deuterium of the adsorbed $D_2O$.

Using the data from the isotherms for $H_2O$ and $D_2O$ at 17 and 27°, the differential heats of sorption were calculated and the values plotted, as shown in Fig. 3. The dashed sections of the curves were used to indicate that the precision attained in the initial adsorption values at low vapor pressures was not quite good enough to make the heat value calculations exact. The solid lines in Fig. 3 are considered to be reasonably good. The heats for the initial uptake of $H_2O$ are higher than for $D_2O$. There is an initial maximum for each vapor and this is nearly twice as great for $H_2O$ on the lysozyme as was found for $H_2O$ on ribonuclease. The maximum for the $H_2O$ calculates to be about 30 kcal. per mole, while for $D_2O$ the value turns out to be about 24 kcal. The heat values fall for both as more vapor is adsorbed, but the rate of fall is much greater for $H_2O$ and the two heat curves cross at an uptake of 5% where the heat value is 19 kcal. Beyond this point the differential heat is higher for $D_2O$ than for $H_2O$ until the two curves meet at between 13 and 14% uptake. Here the heat value is 12.5 kcal. There are no values beyond this point for $D_2O$, but those for $H_2O$ continue to fall slowly until 19% uptake where the heat is close to that of the heat of vaporization of $H_2O$. Studies are being continued over a wider temperature range in the hope that a reasonable explanation may be arrived at for the differences between the sorption of $D_2O$ and $H_2O$.

In conclusion, one may say that $H_2O$ is more strongly sorbed by lysozyme at the low vapor pressures than is $D_2O$. The differential heat calculations show that in the initial uptake of vapor the heat of sorption of $H_2O$ is greater than that of $D_2O$. However, the heat curves cross at 5% uptake and that of $D_2O$ remains above that of $H_2O$ until the values approach the heat of vaporization of $H_2O$. A reasonable explanation of these results is being sought by additional studies.

## DISCUSSION

W. HELLER (Wayne State University).—How long did it take to reach equilibrium?

L. H. Reyerson.—From 4 to 6 hours and in some cases as much as a day was required.

W. HELLER.—How thin was the layer of protein?

L. H. REYERSON.—It was a rather loose, cotton-like porous mass hanging on a glass rod.

# CONFLICTS BETWEEN GIBBSIAN THERMODYNAMICS AND RECENT TREATMENTS OF INTERFACIAL ENERGIES IN SOLID–LIQUID–VAPOR SYSTEMS

BY RULON E. JOHNSON, JR.

*Contribution No. 284, Jackson Laboratory, Organic Chemicals Department, E. I. du Pont de Nemours and Company, Inc. Wilmington, Delaware*

*Received May 11, 1959*

Many recent papers on the thermodynamics of solid–liquid–vapor systems are in conflict with J. Willard Gibbs' treatment of the subject. The nature of these differences is discussed. Using the techniques of Gibbs, Young's equation is derived for a sessile drop on a solid. Adsorption and gravity are explicitly considered. It is shown that Young's equation is valid in all situations studied, provided it is understood to be a relationship among surface tensions rather than surface free energies.

In recent years, Young's equation (equation (31) or (32)) has generated considerable discussion and controversy. Bikerman,[1] for example, denies the validity of Young's equation both on theoretical and experimental grounds. In discussing this equation at the Second International Congress of Surface Activity he states, "perhaps it is not too much to hope that this Congress will mark the downfall of this relation."[2] Pethica and Pethica[3] deny the validity of the equation in a gravitational field. Others[4,5] deny its validity for zero contact angle. Moreover it is widely assumed that the equation should be written in terms of surface free energies.

Gibbs[6] developed the thermodynamics of solid–liquid–vapor systems very completely and elegantly. He derived Young's equation for the non-gravitational case and outlined its derivation for a system in a gravitational field. A derivation of the equation using the methods of Gibbs is given below. Adsorption and gravity are explicitly considered. It is shown that the equation is generally valid.

Four reasons can be advanced for the confusion that exists concerning this subject.

1. It is assumed by many (*e.g.*, reference 3) that the surface tension $\gamma$ of an interface defined by equation (1) is numerically equal to the specific surface free energy $f$ defined by equation (2). The two in fact are related by equation (3).

$$(\partial F/\partial \Omega)_{T,V,n_i} = \gamma \qquad (1)$$

where $F$ = Helmholtz free energy of the system
$\Omega$ = surface area of interface
$T$ = temperature
$V$ = volume
$n_i$ = number of moles of component i

$$f = (F - F^{\alpha} - F^{\beta})/\Omega \qquad (2)$$

where $F^{\alpha}$ = Helmholtz free energy of a unit of volume in the homogeneous part of $\alpha$ multiplied by the volume of $\alpha$
$F^{\beta}$ = Helmholtz free energy of $\beta$ defined analogously to $F^{\alpha}$

$$f = \gamma + \sum_{i=1}^{K} \Gamma_i \mu_i \qquad (3)$$

where $\Gamma_i$ = surface excess of component i per unit area
$\mu_i$ = $(\partial F/\partial n_i)_{T,V,\Omega,n_j}$ *i.e.*, the chemical potential of component i
$K$ = number of components in the system

Often the adsorption of a solvent can be considered to be zero so that for a one-component system $\gamma$ does equal $f$. For those systems in which adsorption phenomena are important, the two are definitely not equal. As shown below, Young's equation is valid in terms of $\gamma$ not $f$.

2. It has been assumed (*e.g.*, by Harkins[7]) that for systems containing surfaces the necessary and sufficient condition for equilibrium is that the free surface energy of the system be a minimum. Actually, the total free energy of the system, at constant $T$, $V$, and mass must be a minimum. This misconception has allowed derivations to be made such that specific surface free energies appear for the terms in Young's equation.[3,8]

3. A general lack of rigor in discussing surface energetics has contributed immeasurably to the confusion. For example, the quantities in Young's equations have been variously identified as surface tensions, surface free energies, specific surface free energies and surface energies. While it is permissible (although sometimes confusing) for an author to name physical quantities as he desires, the quantities in question should be unambiguously defined. Unfortunately, in most discussions of surface free energy, the name itself is the only definition given for the quantity. It is only when the quantities are relatively well defined, as in the paper of Pethica and Pethica, that errors in physical meaning become obvious.[9]

4. The physical interpretation of $\gamma$ has created

(1) J. J. Bikerman, "Solid Surfaces," in "Second International Congress of Surface Activity," Vol. III, Academic Press, New York, N. Y., 1957, p. 131.

(2) *Ibid.*, p. 191.

(3) B. A. Pethica and T. J. P. Pethica, "The Contact Angle Equilibrium," in "Second International Congress of Surface Activity," Vol. III, Academic Press, New York, N. Y., 1957, p. 131.

(4) S. Baxter and A. B. D. Cassie, *J. Text. Inst.*, 36, T67 (1945).

(5) J. L. Moilliet and B. Collie, "Surface Activity," D. Van Nostrand Co., New York, N. Y., 1951, pp. 98–99.

(6) J. Willard Gibbs, "The Collected Works of J. Willard Gibbs Volume I. Thermodynamics," Yale University Press, New Haven, Conn., 1928, pp. 314–331.

(7) W. D. Harkins, "The Physical Chemistry of Surface Films," Reinhold Publishing Corp., New York 36, N. Y., 1952, pp. 80–82.

(8) C. G. Sumner in "Symposium on Wetting and Detergency," Chem. Publ. Co., New York, N. Y., 1937, p. 15.

(9) Examples of the type of confusion discussed here are given in the writings of Adam and Harkins. Adam[10] rigorously defines surface free energy as a surface excess in the manner of Gibbs. But he also says, "It is always possible mathematically, to replace a free energy per unit area of a surface by a tension acting parallel to the surface" (*ibid.* pp. 2–3 and p. 178). In a later paper[11] he says he has simply used the name surface free energy for surface tension. Harkins[7] says that he too defines the surface free energy as Gibbs, yet the equations he develops can only be reconciled with the definition for $\gamma$ given above.

(10) N. K. Adam, "The Physics and Chemistry of Surfaces," 3rd ed., Oxford University Press, London, 1941, pp. 107–110 and pp. 404–407.

(11) N. K. Adam, *Disc. Faraday Soc.*, 3, 5 (1948).

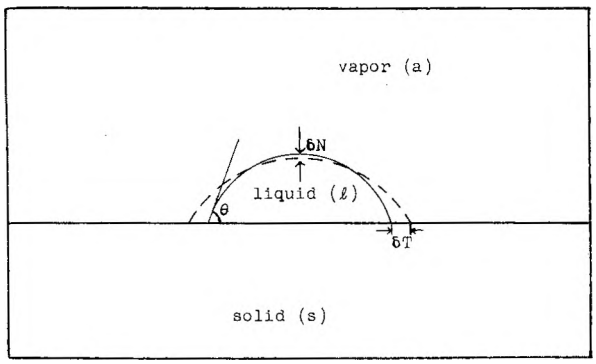


Fig. 1.

many problems for the understanding of Young's equation. While it is rather generally recognized that for solids in a state of strain, $\gamma$ cannot be interpreted as a "compressive force" in the surface, it is not so generally recognized that $\gamma$ cannot be interpreted as the specific surface free energy of the system. Gibbs himself did not give $\gamma$ a name when applied to solid surfaces. He did however call $\zeta^{(sl)}$ which is defined by equation (4) "the superficial tension of a liquid in contact with a solid."

$$\zeta^{(sl)} = \gamma^{(sl)} - \gamma^{(so)} \qquad (4)$$

Where: $\gamma^{(so)}$ = the surface tension of a solid against a vacuum

As his discussion indicates,[12] he considers that $\zeta^{(sl)}$ measures the ability of the solid to modify the tendency of the liquid to contract. That is, the liquid in contact with the solid is constrained to contract along the solid with a force measured by $\zeta^{(sl)}$. As shown below (equations 31 to 34) Young's equation is equally valid when written in terms of $\zeta^{(sa)} - \zeta^{(sl)}$. When this viewpoint is accepted the abstract and difficult concepts associated with a solid surface tension do not interfere with an understanding of the spreading of liquids on solids. Moreover, while the solid surface tensions are most difficult to measure experimentally, the quantities $\zeta$ are susceptible to direct measurement. An analysis based on these concepts[13] also shows that Young's equation is indeed valid for zero contact angle. Apparently the concept that the equation is invalid for zero contact angle has resulted from a confusion of $f$ with $\gamma$.

**The Derivation of Young's Equation Including Adsorption and Gravity.**—In what follows the term free energy will always refer to the Helmholtz free energy

$$F = U - TS \qquad (5)$$

where $U$ = energy
$T$ = absolute temperature
$S$ = entropy

Gibbs made his analysis using the equilibrium condition that the variation of the energy of a system at constant entropy, volume, and mass be zero, *i.e.*

$$(\partial U)_{S,V,n_i} = 0 \qquad (6)$$

We will use the equivalent condition that the variation of the free energy of the system at constant temperature, volume, and mass be zero, *i.e.*

$$(\delta F)_{T,V,n_i} = 0 \qquad (7)$$

In our notation the symbol $\delta$ refers to a variation of the system in the sense of a virtual work variation. The symbol d refers to an element or differential of a quantity.

Consider the system of Fig. 1. The solid is insoluble in the liquid. Its surface is homogeneous, continuous, and isotropic. The superscripts s, l, and a refer to the solid, liquid, and vapor respectively. The superscripts (sl), (sa) and (la) refer to the solid–liquid, solid–vapor and liquid–vapor interfaces, respectively. Some or all of the components in the liquid may exist in the vapor. Any summation of components is understood to be a summation of the components in the specified phase or interface.

Since we cannot consider the pressures and surface tensions to be uniform throughout the phases and surfaces of a system in a gravitational field, we must consider elements small enough that the pressure or surface tension is uniform in each. The intrinsic energy of an element in $\alpha$ is given by

$$dU^\alpha = Tds^\alpha - PdV^\alpha + \sum_i \mu_i dn_i^\alpha \qquad (8)$$

and the total intrinsic energy of $\alpha$ is then

$$U^\alpha = \int_{x_1}^{x_2}\int_{y_1}^{y_2}\int_{z_1}^{z_2}\left(\frac{\partial U}{\partial x} + \frac{\partial U}{\partial y} + \frac{\partial U}{\partial z}\right)dxdydz = \int_{V^\alpha} dU^\alpha \qquad (9)$$

The limits of integration are chosen to define the volume of $\alpha$. Similar equations can be written for other phases and for surfaces. In order to prevent the equations from becoming too cumbersome the symbols $\int_V$ and $\int_\Omega$ will indicate integrations over all the volumes and surfaces, respectively. The symbol $\delta dF^l$ indicates the variation of the intrinsic free energy in an element of volume in the liquid phase. Similar notation is used for the other quantities. The intrinsic free energy of an element is that free energy not explicitly dependent on gravity.

The total free energy of the system is given by

$$F = \int_V dF^V + \int_\Omega dF^\Omega + \int_V gzdm^V + \int_\Omega gzdm^\Omega \qquad (10)$$

where $g$ = acceleration of gravity
$dm^V$ = the mass of an element $dV$
$dm^\Omega$ = the mass of an element $d\Omega$
$z$ = the height of the element above a horizontal plane

$$\delta F = \delta\int_V dF^V + \delta\int_\Omega \partial F^\Omega + \delta\int_V gzdm^V + \delta\int_\Omega gzdm^\Omega = 0 \qquad (11)$$

Because we are dealing with reversible variations

$$\delta F = \int_V \delta dF^V + \int_\Omega \delta dF^\Omega + \int_V g\delta zdm^V + \int_V gz\delta dm^V + \int_\Omega g\delta zdm^\Omega + \int_\Omega gz\delta dm^\Omega = 0 \qquad (12)$$

Now

$$dF^V = -PdV + \sum_i \mu_i dn_i^V \qquad (13)$$

and

(12) Gibbs, *op. cit.*, pp. 328–329.
(13) Gibbs, *op. cit.*, pp. 330–331.

$$dF^{\Omega} = \gamma d\Omega + \sum_i \mu_i dn_i^{\Omega} \quad (14)$$

Therefore

$$\delta F = \int_V -P\delta dV + \sum_i \int_V \mu_i \delta dn_i^V + \int_\Omega \gamma \delta d\Omega + \sum_i \int_\Omega \mu_i \delta dn_i^\Omega + \int_V g\delta z dm^V + \int_V gz\delta dm^V + \int_\Omega g\delta z dm^\Omega + \int_\Omega gz\delta m = 0 \quad (15)$$

Note: $n_i = m_i/M_i$, where $M_i$ is the molecular weight of component i.

Because the variations of mass are independent of variations of $V$ and $\Omega$ equation (15) can be separated into two independent equations

$$\int_V -P\delta dV + \int_\Omega \gamma\delta d\Omega + \int_V g\delta z dm^V + \int_\Omega g\delta z dm^\Omega = 0 \quad (16)$$

and

$$\sum_i \int_V \mu_i \delta dn_i^V + \sum_i \int_\Omega \mu_i \delta dn_i^\Omega + \int_V gz\delta dm^V + \int_\Omega gz\delta m^\Omega = 0 \quad (17)$$

Equation (17) contains the conditions for chemical equilibrium in a gravitational field and (16) the conditions for mechanical equilibrium. Now

$$dm^V = \rho dV \quad (18)$$

and

$$dm^\Omega = \lambda d\Omega \quad (19)$$

where: $\rho$ = density of the volume element in units of mass/volume
$\lambda$ = surface density of the surface element in units of mass/area

Furthermore

$$\int_{V^1} P\delta dV^1 = \delta \int_{V^1} PdV^1 - \int_{V^1} \delta P dV^1 \quad (20)$$

and

$$\delta \int_{V^1} PdV^1 = \int_{\Omega^{(1a)}} P^1 \delta N^{(1a)} d\Omega^{(1a)} \quad (21)$$

where $\delta N^{(1a)}$ = the normal component of motion of the element of surface into the vapor
$P^1$ = the pressure on the element measured in the liquid

Equation (21) is valid since each side represents the virtual work done by the liquid phase in the variation. The integral is only over the liquid–vapor interface since the solid surface is not considered to vary normal to itself.

Similarly

$$\int_{V^a} P\delta dV^a = \delta \int_{V^a} PdV^a - \int_{V^a} \delta P dV^a \quad (22)$$

$$\delta \int_{V^a} PdV^a = -\int_{\Omega^{(1a)}} P^a \delta N^{(1a)} d\Omega^{(1a)} \quad (23)$$

where: $P^a$ = the pressure on the element of surface measured in the vapor

$$\int_{\Omega^{(1a)}} \gamma^{(1a)} \delta d\Omega^{(1a)} = \delta \int_{\Omega^{(1a)}} \gamma^{(1a)} d\Omega^{(1a)} - \int_{\Omega^{(1a)}} \delta\gamma^{(1a)} d\Omega^{(1a)} \quad (24)$$

and

$$\delta \int_{\Omega^{(1a)}} \gamma^{(1a)} d\Omega^{(1a)} = \int_L \gamma^{(1a)} \cos\theta\, \delta T dL + \int_{\Omega^{(1a)}} \gamma^{(1a)} \left[\frac{1}{r_1} + \frac{1}{r_2}\right] \delta N^{(1a)}\, \delta\Omega^{(1a)} \quad (25)$$

where $dL$ is the element of length of the line formed by the intersection of the three surfaces and $\delta T$ is the virtual motion of this line normal to $dL$ along the solid and in a direction which increases $\Omega^{(1s)}$. $\theta$ is the contact angle and $r_1$ and $r_2$ are the principal radii of curvature of $d\Omega$. The final term of equation (25) comes from the change of area of the liquid–vapor interface due to the change of shape of the drop in the variation. The geometrical significance of this term is discussed by J. Rice.[14]

$$\int_{\Omega^{(sl)}} \gamma^{(sl)} \delta d\Omega^{(sl)} = \delta \int_{\Omega^{(sl)}} \gamma^{(sl)} d\Omega^{(sl)} - \int_{\Omega^{(sl)}} \delta\gamma^{(sl)} d\Omega^{(sl)} \quad (26)$$

and

$$\delta \int_{\Omega^{(sl)}} \gamma^{(sl)} d\Omega^{(sl)} = \int_L \gamma^{(sl)} \delta T dL \quad (27)$$

$$\int_{\Omega^{(sa)}} \gamma^{(sa)} \delta d\Omega^{(sa)} = \delta \int_{\Omega^{(sa)}} \gamma^{(sa)} d\Omega^{(sa)} - \int_{\Omega^{(sa)}} \delta\gamma^{(sa)} d\Omega^{(sa)} \quad (28)$$

and

$$\delta \int_{\Omega^{(sa)}} \gamma^{(sa)} d\Omega^{(sa)} = -\int_L \gamma^{(sa)} \delta T dL \quad (29)$$

Substituting equations (18) to (29) into equation (16) and collecting terms gives

$$\int_{\Omega^{(1a)}} \left[(P^a - P^1)\delta N + \left(\frac{1}{r_1} + \frac{1}{r_2}\right) \gamma^{(1a)}\, \delta N + g\lambda^{(1a)}\, \delta z - \delta\gamma^{(1a)}\right] d\Omega^{(1a)} + \int_{V^1} [\delta P + g\rho\delta z] dV^1 + \int_L [\gamma^{(sl)} + \gamma^{(1a)} \cos\theta - \gamma^{(sa)}]\delta T dL + \int_{\Omega^{(sl)}} [g\lambda^{(sl)}\, \delta z - \delta\gamma^{(sl)}] d\Omega^{(sl)} + \int_{\Omega^{(sa)}} [g\lambda^{(sa)}\, \delta z - \delta\gamma^{(sa)}] d\Omega^{(sa)} = 0 \quad (30)$$

Since the variations are arbitrary it is necessary and sufficient that each integrand be zero. The last two integrals are zero if the solid surface is level and flat. The coefficient of $dV$ gives the distribution of pressure within the liquid. The coefficient of $d\Omega^{(1a)}$ gives the effect of surface tension and curvature on the pressure within the liquid. The coefficient of $dL$ yields Young's equation

$$\gamma^{(1a)} \cos\theta = \gamma^{(sa)} - \gamma^{(sl)} \quad (31)$$

If we repeat the analysis using $\zeta^{(sa)}$ and $\zeta^{(sl)}$ (defined by equation (4)) then it is found that

$$\gamma^{(1a)} \cos\theta = \zeta^{(sa)} - \zeta^{(sl)} \quad (32)$$

For a solid in contact with a pure liquid and its vapor, the Gibbs adsorption equation yields

$$\zeta^{(sa)} = \int_{P=0}^{P=P_0} \Gamma d\mu \quad (33)$$

where: $P_0$ = vapor pressure of the liquid. Combining with equation (32)

$$\zeta^{(sl)} = \int_{P=0}^{P=P_0} \Gamma d\mu - \gamma^{(1a)} \cos\theta \quad (34)$$

(14) J. Rice in "Commentary on the Scientific Writings of J. Willard Gibbs. Volume I, Thermodynamics," F. G. Donnan and A. Haas, editors, Yale University Press, New Haven, Conn., 1936, p. 13.

These last two equations have been discussed by Bangham and Razouk,[15] and Boyd and Livingston.[16] When reading these authors and others, it should be understood clearly that the Gibbs adsorption equation (*e.g.*, equation (33)) gives a change in surface tensions (equation (1)), not specific surface free energies (equation (2)).

## DISCUSSION

J. J. BIKERMAN (Massachusetts Institute of Technology).—I shall not speak of semantics or nomenclature because in my opinion these questions are really not important for deciding whether Young's equation is or isn't correct. There are two types of proofs of Young's equation—one using surface energy and the other using surface tension. Since Dr. Johnson agrees that the proofs of the first type are incorrect, we have a 50% agreement because I believe that also the proof based on tensions is unsatisfactory. As given by Gibbs it was fundamentally not different from the treatment given by Young who considered the result evident. It is clear that the force pushing the three-phase line of contact to the right must be equal to that pushing it to the left, if equilibrium is present; thus, $\gamma_{12}\cos\theta + \gamma_{23} = \gamma_{13}$.

However, this condition is not sufficient for equilibrium as follows, for instance, from Gibbs' discussion of the liquid-liquid-gas system. For this system, *i.e.*, for the case of a liquid drop floating on another liquid in a gas, Gibbs writes $\Sigma\gamma\delta l = 0$. In this equation $\gamma$ represents the various surface and interfacial tensions, and $\delta l$ is the virtual displacement of the three-phase line. In fluids, this equation can be satisfied. It is not essentially different from the rule of the parallelogram of forces. It also has been confirmed by experiments. However, this equation cannot be satisfied in solids, at least as long as the solid surface is treated as a plane, *i.e.*, as long as the two tensions $\gamma_{13}$ and $\gamma_{23}$ are supposed to act along one straight line. If we substitute $\gamma_{13} - \gamma_{23}$ for two separate tensions, we are left with two forces acting in two different directions. They cannot compensate each other. The resultant of these tensions is $\gamma_{12}\sin\theta$. As long as this force is not balanced, no equilibrium can exist. Presumably, the tension $\gamma_{12}\sin\theta$ has a real existence and causes effects which I hope to measure. Miss Bailey has mentioned that she observed curling of a mica sheet on which a drop of water was deposited. I hope to show that the force $\gamma_{12}\sin\theta$ raised a ridge and is compensated by stresses. We hope to detect it on gels. If we succeed, Young's equation would be disproved, first of all because $\gamma_{13}$ and $\gamma_{23}$ would have to act along different directions and, consequently, the difference $\gamma_{13} - \gamma_{23}$ would be meaningless. The main thing, however, is that if this ridge exists, another form of energy, namely, the strain energy of the solid, must be considered when writing down the equilibrium conditions. This would be true also when displacement of the 3-phase, *i.e.*, a dynamic process, is considered. When this line moves along the solid, not only the surface areas and, consequently, the surface energies vary but also the shape of the solid and the work of deformation must be taken into account.

I should like to stress the statement made by Dr. Johnson that equilibrium is determined by the free energy of the whole system, not by the capillary part of this energy. If a drop on a solid deforms the solid, the strain energy is a part of the free energy of the system. Gibbs didn't consider it because Gibbs restricted himself to "unchangeable" solids, but real solids are not "unchangeable."

R. E. JOHNSON.—It is not claimed, nor is it true, that Young's equation is the only requirement for total mechanical equilibrium for solid-liquid-vapor systems. In fact equation (30) will yield six separate equations which must be satisfied. What Gibbs has shown is that no matter what other conditions must be fulfilled, the respective surface tensions must obey Young's equation at equilibrium. If the component "$\gamma_{12}\sin\theta$" mentioned by Dr. Bikerman is discussed in terms of equation (30) as a whole, the apparent anomaly of an unbalanced force will disappear.

While I have indeed considered the solid to be rigid (but not necessarily plane) the proof would have to be modified only slightly for mobile surfaces (*e.g.*, gelatin). Equation (30) would then contain an additional term depending on the curvature of the solid, but Young's equation would still appear in the form given. Similarly, equations describing the internal stresses in a solid would appear separate from Young's equation. This is physically reasonable since stresses in the interior of a solid should not influence the spreading of a liquid over the solid.

W. A. ZISMAN (U. S. Naval Research Laboratory).—I wish to congratulate Dr. Johnson for his illuminating and well presented paper. As I understand it, the basic problem of concern here goes back to the recognition over a 100 years ago that a purely mechanistic explanation of surface tension and surface energy was out of the question until such time as a precise knowledge would be available of the field of force between neighboring molecules in liquids and solids. Since a detailed mechanism was not possible, and still is not known sufficiently precisely, refuge had to be sought in a thermodynamic approach. The problem before us is how to apply thermodynamics correctly to surface behavior.

Dr. Johnson's paper does much to clear up the unfavorable situation now existing widely in the literature which has been caused by frequent and continued carelessness in the application of thermodynamics to surface systems. Unquestionably, there is much confusion in the literature because of the use of the Gibbs free energy instead of the Helmholtz free energy, or the work function as physicists often call it. Especially helpful is Dr. Johnson's discussion of the incorrectness of identifying the surface tension of a *solution* with the free energy per unit area.

I agree with the author's treatment of the Young equation. It would be a backward step, indeed, to derive the Young equation by treating the problem as a static equilibrium of a group of vector tensions acting as a point. It is more logical, more general, and more teachable to discriminating students to show that the Young equation follows necessarily from thermodynamics. Johnson's point is usually missed that at equilibrium an infinitesimal virtual displacement of the disposable parameters must cause a negligible change in the free energy of the *entire* system. Almost invariably the condition for equilibrium is expressed in terms of the virtual change in the free energy resident in the *surfaces* of the system.

Although Johnson's discussion can be derived from material to be found in Gibbs' papers, it is a valuable contribution because it will do much to eliminate errors and confusion which have arisen because these aspects of Gibbs' presentation were much too condensed and sketchy.

(15) D. H. Bangham and R. I. Razouk, *Trans. Faraday Soc.*, **33**, 1459 (1937).

(16) G. E. Boyd and H. K. Livingston, *J. Am. Chem. Soc.*, **64**, 2383 (1942).

# AN INTERPRETATION OF ELECTROCHEMICAL MEASUREMENTS ON A MONTMORILLONITE CLAY[1]

BY K. B. DESHPANDE AND C. E. MARSHALL

*Department of Soils, University of Missouri, Columbia, Missouri*

*Received March 2, 1959*

Changes in (1) conductivity, (2) *p*H, (3) cation activity, (4) migration velocity of clay particles and (5) cation–halide ion pair activities during the titration of an acid-montmorillonite clay were studied. An attempt has been made to interpret these by considering charge distribution around clay particles and by the application of the double layer theory. The agreement between the charge densities on the clay particles and the total of the charge densities on the various "planes" is striking.

## Introduction

The interfacial properties of clay suspensions are determined partly by the atomic structures of clays and partly by the nature of the ionic surroundings in the suspension. The correct interpretation of the phenomena involved would greatly benefit colloid chemistry and clay technology. The study of such systems requires, in the ultimate analysis, the consideration of single ion activities by both experimental and theoretical approaches.

Such systems have so far been studied by thermodynamic, quasi-thermodynamic and conductometric methods. Davis[2] employed the cell Ag. AgCl/Clay suspension ||XCl/Ag.AgCl which effectively measured the chemical potential of the Na-, K- or other chloride in the clay system. Using the same proportions of clay, water, salt and varying the nature of the salt to correspond to the cation on the clay, the chemical potential of KCl was found to be significantly different from that of NaCl. The use of tertiary electrodes operating through the ionic equilibrium set up by two sparingly soluble salts with a common ion[3] also gives a measure of the chemical potential of the molecular species involved. Both of these methods lead to an indirect determination of the surface properties through their effect on the chemical potential of a soluble molecular species. What is needed for the structural interpretation is the relation between the silicate surface and the individual ions which balance its charge. This can be obtained by a quasi-thermodynamic route which involves certain plausible but not strictly proved assumptions.

The quasi-thermodynamic method, like conductivity, affords data which can be interpreted directly in terms of single ions. In such an interpretation the activity which is a geometric average is treated like concentration in its conversion to conductivity. This is permissible in the case of very dilute systems where the activity and concentration are about the same. As one of the authors[4] has pointed out, a combination of transport number, conductivity and activity determinations for a series of clay suspensions should lead to a more accurate evaluation of the electrochemical properties of cations in the clay systems. Use of silver halide electrodes in addition to calomel electrodes will throw further light on the ionic distribution in such systems.

In the present investigation an attempt has been made to study the titration of a dilute acid–clay suspension in a limited *p*H range by measurement of (a) conductivity, (b) *p*H, (c) cation-activity, (d) migration velocity of clay particles, and (e) cation–halide ion pair activity with the corresponding Ag–Ag halide electrodes. The results obtained in these last determinations will be discussed separately since they show a number of features at low salt concentration, quite different from those of Davis.[2] In this paper we shall offer an interpretation of conductance in bentonite clay, based on a combination of conductometric, quasi-thermodynamic and cataphoretic measurements. In this clay, Bloksma's diffusion experiments[5] indicate a value for the mean activity coefficient of the sodium ion in close agreement with membrane electrode results.

## Experimental

(1) Preparation of the Acid Clay.—The clay, Wyoming bentonite (Belle Fourche, American Colloid Company) was similar to the material used by previous workers in this Laboratory.[6] A 1% suspension was prepared and the fraction less than 0.2 $\mu$ in equivalent spherical diameter was separated using a Sharples supercentrifuge. This fine suspension was then electrodialyzed using a cell of the type reported earlier,[6] until it reached the *p*H of about 2.5. This stock suspension, about 2%, was diluted from time to time as required for the titrations. The *p*H of the suspension was checked at frequent intervals and showed very little variation.

(2) The exchange capacity of the clay was determined by the batch method[7] and was found to be 80.0 meq. per 100 g. of dry clay.

(3) The titration was set up by weighing out accurately the same amount of suspension in a series of flasks and adding to each the requisite amounts of water, alkali and dilute K-halide solution. In all the systems the final volume was maintained the same. Systems with 5, 10 and 20 ml. of 0.00065 *N* halide solution were investigated. After about 48 hours of standing, the following measurements were made on each system. (a) Conductivity was measured at 10,000 cycles/sec. (b) *p*H and K ion activities were measured in the same way as reported previously.[6] (c) The cation–halide ion pair activity: This was measured by use of Ag–Ag halide electrodes. Each of these electrodes Ag–AgCl, Ag–AgBr, Ag–AgI was tested at frequent intervals, with solutions of known concentrations of the corresponding K-halides on the two sides of a clay membrane. (d) Mi-

(1) Contribution from the Missouri Agricultural Experiment Station, Journal Series No. 1976. Approved by the Director.

(2) L. E. Davis, *Natl. Acad. Sci. Natl. Res. Council*, **395**, 290 (1955).

(3) E. W. Russell and G. A. Cox, *Fourth Internatl. Cong. Soil Sci., Amsterdam, Trans.*, **1**, 138 (1950).

(4) C. E. Marshall, *Natl. Acad. Sci. Natl. Res. Council*, **456**, 288 (1956).

(5) A. H. Bloksma, *J. Colloid Sci.*, **12**, 40 (1957).

(6) E. O. McLean and C. E. Marshall, *Soil Sci. Soc. Amer. Proc.*, **13**, 179 (1949).

(7) D. R. Lewis, *Prelim. Rep. No. 7, Am. Petr. Inst., Pro.*, **49**, 91 (1950).

TABLE I

Weight of clay = 0.3867 g., final volume = 100 ml.

| Meq. KOH added/g. clay | pH | $Q_K \times 10^4$ | $Q_{(H+K)Cl} \times 10^4$ | Specific conductivity Measured $\lambda m \times 10^5$ | Specific conductivity Calcd. $\lambda c \times 10^5$ | $(\lambda m - \lambda c) \times 10^5$ |
|---|---|---|---|---|---|---|
| | | | Series 1 | | | |
| | | | Ml. of 0.00065 *N* KCl added = 5.0 | | | |
| 0.13 | 5.38 | 2.738 | 1.413 | 3.95 | 3.11 | 0.84 |
| .26 | 6.00 | 3.018 | 1.555 | 4.53 | 3.29 | 1.24 |
| .39 | 6.28 | 3.419 | 1.760 | 5.18 | 3.66 | 1.52 |
| .52 | 6.51 | 4.322 | 2.099 | 6.66 | 4.48 | 2.18 |
| .65 | 7.52 | 5.678 | 2.655 | 9.89 | 5.96 | 3.93 |
| .78 | 8.69 | 10.980 | 3.473 | 13.88 | 11.46 | 2.42 |
| | | | Series 2 | | | |
| | | | Ml. of 0.00065 *N* KCl added = 10.0 | | | |
| 0.13 | 5.20 | 2.869 | 1.419 | 4.43 | 3.48 | 0.95 |
| .26 | 5.92 | 3.200 | 1.645 | 4.85 | 3.62 | 1.23 |
| .39 | 6.20 | 3.727 | 1.860 | 5.55 | 4.14 | 1.41 |
| .53 | 6.52 | 4.859 | 2.293 | 6.91 | 5.28 | 1.63 |
| .66 | 7.32 | 6.955 | 2.617 | 10.44 | 6.42 | 4.02 |
| .79 | 8.91 | 10.900 | 3.480 | 16.38 | 11.58 | 4.80 |
| | | | Series 3 | | | |
| | | | Ml. of 0.00065 *N* KCl added = 20.0 | | | |
| 0.13 | 5.02 | 3.329 | 1.900 | 5.72 | 4.39 | 1.33 |
| .27 | 5.91 | 3.770 | 1.920 | 5.94 | 4.52 | 1.42 |
| .40 | 6.23 | 4.092 | 2.070 | 6.35 | 4.82 | 1.53 |
| .53 | 6.60 | 4.934 | 2.239 | 7.38 | 5.66 | 1.72 |
| .66 | 7.67 | 7.233 | 2.689 | 11.00 | 8.02 | 2.98 |
| .80 | 8.60 | 10.850 | 3.321 | 16.16 | 11.77 | 4.39 |

gration velocity of the clay particles. This was measured by using Engel and Pauli's method.[8]

The results obtained are reported in tabular form in Table I.

## Discussion of Results

The conductivity measurements bring out an important fact. If the various ions are attributed their mobilities at infinite dilution, the corresponding conductivities can be calculated from their respective activities. This requires evaluation of conductivity due to the clay particles which can be done using the fact that the algebraic sum of the charges on the positive and negative ions per unit volume of suspension is equal to the sum of the charges on all the clay particles in it. The migration velocities for all systems were found to be very close to 3 $\mu$ per sec. per volt per cm. The values for conductivities of suspension obtained from such calculations are given in Table I.[9] It is observed that the measured conductivities are higher than those calculated in all systems.

One possible cause can lie in the fact that the migration velocities at infinite dilution used for the various ions and that for the clay are those obtained by application of a direct current, whereas the measured conductivities are obtained by using a high frequency a.c. According to Debye–Falkenhagen[11] the latter should give higher values as the relaxation effect disappears more or less completely depending on the frequency of the a.c. The frequency above which this happens is given by $\nu$ thus:

$$\nu = CZ\lambda/71.3 \times 10^{10} \text{ for a binary electrolyte}$$

where

$C$ = g. moles of the electrolyte/per l.
$Z$ = valency of the ions
$\lambda$ = equivalent conductance

In the case of clay particles all the corresponding terms cannot be defined under given conditions. Hence, one has to consider other related aspects of the situation. The clay particle is much larger than an ion and hence will have a much larger volume for its ionic atmosphere. The low clay concentration contributes further to the extension of the latter. The charge required to decay during the relaxation time is much larger than that for a monovalent negative ion in a solution of the same concentration as the clay. The conductivity of a clay particle is much less than that of an ordinary ion. This implies that the delay time for the ionic atmosphere of a clay particle is much longer than that for the ionic atmosphere of a monovalent negative ion. Hence, the abnormality appears at a much lower frequency than for ordinary electrolytes. The cause of this abnormality or difference in conductivity from the expected value is attributable to those double layer ions which are physically adsorbed to the surface. Those adsorbed chemically will form a part of the surface (as far as conductivity is concerned), reduce its charge density, and will not contribute to the process of building and decay of ionic at-

(8) W. Pauli and E. Valko, "Elektrochemie der Kolloide," Vienna, 1929, p. 165.

(9) It is assumed that the activity of K measured represents its concentration and that the chloride is negatively adsorbed.[10]

(10) S. Mattson, *Soil Sci.*, **28**, 179 (1929).

(11) P. Debye and Falkenhagen, *Physik. Z.*, **29**, 121, 401 (1928).

TABLE II

All charges described are coulombs/cc.

| Moles/l. K in Stern layer × $10^4$ | Moles/l. K chemisorbed × $10^4$ | Charge/cc. in Stern layer $X$ | Charge/cc. in Gouy layer $Y$ | $X + Y$ | Charge/cc. on clay after neutn. $X_1$ | Charge/cc. due to sorbed K $Y_1$ | $X_1 - Y_1$ |
|---|---|---|---|---|---|---|---|
| 1.15 | 1.48 | 0.011 | 0.024 | 0.035 | 0.048 | 0.014 | 0.034 |
| 1.69 | 5.70 | .017 | .026 | .043 | .097 | .055 | .042 |
| 2.07 | 9.96 | .021 | .030 | .051 | .145 | .096 | .049 |
| 2.97 | 13.20 | .030 | .039 | .069 | .194 | .127 | .067 |
| 5.37 | 14.50 | .054 | .052 | .106 | .242 | .140 | .102 |
| 3.30 | 19.30 | .034 | .102 | .136 | .291 | .186 | .105 |
| 1.30 | 1.57 | 0.013 | 0.022 | 0.035 | 0.049 | 0.015 | 0.034 |
| 1.68 | 5.94 | .017 | .025 | .042 | .098 | .057 | .041 |
| 1.92 | 10.25 | .019 | .030 | .049 | .147 | .099 | .048 |
| 2.21 | 13.92 | .022 | .041 | .063 | .186 | .134 | .052 |
| 5.48 | 13.63 | .056 | .061 | .117 | .244 | .131 | .113 |
| 6.54 | 13.71 | .067 | .098 | .165 | .283 | .132 | .151 |
| 1.81 | 1.30 | 0.018 | 0.021 | 0.039 | 0.050 | 0.013 | 0.037 |
| 1.93 | 5.88 | .019 | .024 | .043 | .099 | .057 | .042 |
| 2.08 | 10.55 | .021 | .027 | .048 | .148 | .102 | .046 |
| 2.34 | 14.58 | .024 | .035 | .059 | .198 | .141 | .057 |
| 4.06 | 15.71 | .041 | .057 | .098 | .247 | .151 | .096 |
| 5.98 | 15.32 | .061 | .092 | .153 | .297 | .148 | .149 |

mosphere. This means that the $K^+$ ions equivalent to the defect in conductivity are situated in the physically adsorbed layer (Stern layer), whereas the rest are in the chemisorbed state.

The above consideration leads to an approximation as to the nature and extent of distribution of the ions around the clay particles. Table II gives the values of ionic concentrations for each of these layers. The figures given in this table are the relative concentrations of the ions in a unit volume of the suspension and not in terms of the actual concentration in each layer. The latter can be obtained by taking into account the surface area of the particles and by considering that the depth of the adsorbed layer is about twice the ionic diameter, *i.e.*, about 5 Å.

The validity of such an ionic distribution can be tested by examining the charge distribution in each system. The surface charge density and the number of clay particles in a unit volume of the suspension can be found as described by Olphen.[12] The entire surface area of a gram of clay is 750 m.$^2$. The exchange capacity, showing the charge on 1 gram, is 0.8 meq. Hence, the charge density is about 10.32 $\mu$coulombs (= $10^{-6}$ coulomb) per cm.$^2$. The number of particles is given by

$$N = 0.01 \times c + \frac{1}{Adps}$$

where

$A$ = surface area of the flat side of a clay plate (cm.)
$p$ = no. of unit layers per particle
$s$ = density of dry clay (g./cc.)
$c$ = g. clay per 100 ml. of suspension
$d$ = thickness of a unit layer of bentonite (cm.)

In calculating the surface charge on the clay particles, account has been taken of the hydrogen neutralized by hydroxyl ions added and also the H in the ionized form as shown by the $p$H measured.

The charge on the clay surface is partly neutralized by the chemisorbed ions and the rest is balanced by the ions in the Stern layer and the diffuse part of the double layer, to be called "Gouy layer" in what follows. Table II gives the charge densities in various parts, the charges mentioned being coulombs in respective parts per ml. of suspension. The application of the Donnan principle to the Gouy and the Stern layers will give the relative amounts of K and H in each. However, the $p$H in each system is high enough to render this discrimination unimportant.

It can be seen that in most cases the surface charge is balanced by the layer-wise charges which is, in part, a test of the validity of the distribution arrived at.

Application of the theories of charge distribution around a colloid particle can now be considered. The Gouy–Chapman theory would lead to an abnormally high concentration of ions in the proximity of the surface of clay particles. Also it does not consider the possibility of adsorption. The Stern theory with its modification by Grahame[13] takes into account such a possibility and could well be applied to the case in point.

The potential at the outer surface of the Stern layer ("outer Helmholtz plane") is given by $\psi_\sigma$. Thus

$$N = N_{oi} e^{-Ze_1\psi\sigma/kT}$$

Where

$N$ = no. of ions adsorbed per ml. in Stern layer
$N_{oi}$ = no. of ions per ml. away from clay surface
$z$ = valency of the ion concerned
$K$ = Boltzmann constant
$T$ = absolute temperature
$e_1$ = electronic charge

The surface charge density of the Gouy layer[14] is given by $\sigma_2$, thus

$$\sigma_2 = \sqrt{\frac{\epsilon kT n_{oi}}{2\pi}} \sin h \frac{Ze_1\psi\sigma}{2kT}$$

Where

(12) H. Van Olphen and M. H. Waxman, *Natl. Acad. Sci., Natl. Res. Council* **566**, 61 (1958).

(13) D. C. Grahame, *Chem. Revs.*, **41**, 441 (1947).

(14) E. J. W. Verwey and J. Th. G. Overbeek, "Theory of the Stability of the Lyophobic Colloids," Elsevier Pub. Co., New York, N. Y., 1948, p. 144.

$\epsilon$ = dielectric constant of medium and other symbols have the same meaning as before

The charge density in the adsorbed part is given by $\sigma_1$, thus

$$\sigma_1 = 2Ze_1 r n_{oi} e^{-(Ze_1\psi_i+\varphi)/kT}$$

$$n_i = 2r n_{oi} e^{-Ze_1\psi_i+\varphi/kT}$$

$n_i$ = concn. of adsorbed ions per sq. cm.
$r$ = ionic radius
$\varphi$ = adsorption potential
$\psi_i$ = potential in the inner part of Stern layer ("inner Helmholtz plane")

The quantities $\psi_i$ and $\varphi$ are inaccessible with the measurements made. However, $n_i$ is known from the balance of K between that added to the acid-clay and the concentration of K in Gouy layer;

TABLE III

All charges described are $\mu$coulombs/cm.$^2$

| Moles/l. K adsorbed $\times 10^4$ | $\sigma_1$ | $\sigma_2$ | $\sigma_1 + \sigma_2$ | $\sigma$ |
|---|---|---|---|---|
| 2.63 | 0.880 | 0.842 | 1.722 | 1.669 |
| 7.40 | 2.473 | 1.029 | 3.502 | 3.360 |
| 12.04 | 4.026 | 1.124 | 5.150 | 5.044 |
| 16.18 | 5.378 | 1.376 | 6.754 | 6.732 |
| 19.87 | 6.645 | 1.849 | 8.494 | 8.418 |
| 22.61 | 7.558 | 2.044 | 9.602 | 10.090 |
| 2.87 | 0.958 | 0.899 | 1.867 | 1.708 |
| 7.62 | 2.548 | 1.047 | 3.595 | 3.391 |
| 12.18 | 4.070 | 1.102 | 5.172 | 5.087 |
| 16.13 | 5.393 | 1.187 | 6.580 | 6.527 |
| 19.12 | 6.392 | 1.862 | 8.254 | 8.484 |
| 20.25 | 6.774 | 2.081 | 8.855 | 9.987 |
| 3.11 | 1.040 | 0.838 | 1.878 | 1.730 |
| 7.81 | 2.611 | 1.100 | 3.711 | 3.420 |
| 12.63 | 4.228 | 1.147 | 5.365 | 5.150 |
| 16.93 | 5.651 | 1.219 | 6.870 | 6.860 |
| 19.77 | 6.612 | 1.609 | 8.321 | 8.570 |
| 21.29 | 7.129 | 1.952 | 9.081 | 10.310 |

$\sigma_1$ can, therefore, be calculated. The values of $\sigma_1$ and $\sigma_2$ obtained thus are given in Table III. In comparing the total of these figures in each system with $\sigma$, the surface charge density of clay (taking into account the H presumably still on it), it should be noted that the theories applied give approximation of the magnitude of the surface charge distribution in each of the three layers. The agreement between the $\sigma$ and $\sigma_1 + \sigma_2$ values is striking.

Since acidic clays are commonly hydrogen–aluminum systems, possible errors caused by disregarding the $Al^{+++}$ ion should be mentioned. Table I indicates that no systems under study had $p$H values below 5.0, even in presence of salt. The $pK_s$ value for aluminum hydroxide is 32.7 at 20°. Thus at $p$H 5, $p$Al would be at least 5.7, and at $p$H 6 at least 8.7. Hence dissociated aluminum ions would not contribute measurably to the conductivity nor to the activity measurements. Any exchangeable aluminum present must thus be either in the Stern layer or the solid. The high bonding energy of trivalent aluminum would be equivalent to chemisorption, that is, to association with the solid surface. In view of the likelihood of its reincorporation in the octahedral layer of the silicate structure with increasing $p$H, we believe that our interpretation is not materially affected by disregarding the exchangeable aluminum.

**Cation–Halide Ion-Pair Activities.**—It was observed that the use of silver bromide and iodide electrodes yielded results very close to those given by silver chloride electrodes. The figures given in Table I are, therefore, the mean of such readings obtained by the use of all three electrodes. The measurements show the measure of the product of (H + K) ion activity and halide ion activity in each suspension. The fact that the substitution of bromide and iodide for chloride electrode does not change the results shows that the solubility differences between the three silver halides do not have appreciable effect on these measurements. The interpretation of these results appears to require further experimental data, particularly regarding the possibility of halide ion adsorption by the clay. This is being further investigated.

## DISCUSSION

C. T. O'KONSKI (University of California at Berkeley).—What concentration of electrolyte did you have in your system?

K. B. DESHPANDE.—Around $10^{-4}$ molar.

C. T. O'KONSKI.—Then I agree that the counterion relaxation, or polarization of the ion atmosphere, will be an important effect. But the Debye–Falkenhagen theory is not adequate to treat it in the present case because particle size and shape are clearly very important factors and the theory treats only point charges. In a polyelectrolyte, the counterions are restrained in their motion by the high central charge of the charged particle, but they may move relatively freely in the vicinity of a surface; therefore, it appears that an appropriate model to employ is one in which the conductivity of the solvent and the high localized conductivity at the interface are both taken into account. I have treated the complex dielectric constant of polyelectrolyte systems, *i.e.*, the frequency-dependent dielectric constant and conductivities on the basis of a model incorporating a surface conductivity, $\lambda$, which may be evaluated from the ion distributions and mobilities. Arbitrary internal and external dielectric constants and bulk conductivities also are taken into account. The resulting equations resemble the Maxwell–Wagner equations, although the latter do not allow for an interfacial conductivity. For spherical particles with a thin ion atmosphere, the effective conductivity turns out to be the internal volume conductivity of the sphere, $\kappa_2$, plus $2\lambda/a$, where $a$ is the radius. As a result of this localized conductivity, an induced dipole is set up, the field in the sphere and its vicinity is decreased and, thus, the contribution of the counterions to the conductivity is reduced at low frequencies. At high frequencies, where the induced polarization does not have time to build up completely, the local field is greater and the counterions contribute more fully to the conductivity. Thus the conductivity undergoes a dispersion characteristic of any lossy dielectric, including simple electrolytes. This is the effect you observed. If the particles are not spherical, the effect of shape upon the effective conductivities along the various axes must be considered, and the appropriate depolarization factors must be introduced to take into account the effect of shape on the internal field, in the treatment of the electric field problem. This is a rather intricate problem, but fortunately it can be solved by introduction of some simplifying approximations which seem reasonable. The magnitudes of the conductivity and the dielectric dispersions turn out to be shape dependent, so that with your system, which I believe consists of platelike particles, this must be taken into account. A manuscript describing this contribution to the theory is in preparation for publication in THIS JOURNAL.

# EXCHANGE EQUILIBRIA IN A CARBOXYLIC RESIN AND IN ATTAPULGITE CLAY[1,2]

BY C. E. MARSHALL AND G. GARCIA

*Departments of Soils and Agricultural Chemistry, University of Missouri, Columbia, Missouri*

*Received March 2, 1959*

Cation-exchange equilibria were determined for the carboxylic exchange resin IRC 50 and for Attapulgite clay using Na–K, Na–Rb, Na–Cs, Mg–Ca, Mg–Sr and Mg–Ba. Curves showing variations in selectivity number with composition of the solid phase were obtained at low ionic strength of the outer solutions. The resin showed small variations in $K_s$ with monovalent cations but very large variations with divalent. This is ascribed to partial blocking of sites by $MgOH^+$ ions. With attapulgite, very large variations in $K_s$ are found, suggesting a polyfunctional character with fixation of K, Rb and Cs by one mechanism, and of Mg by a different mechanism.

## Introduction

Numerous electrochemical studies of clay minerals have, without exception, shown a polyfunctional character with respect to the dissociation of monovalent and divalent cations.[3] Cation-exchange studies with synthetic resins usually have been formulated as though the resin phase were monofunctional, and exchange reaction "constants" have been widely employed under such terms as "relative affinity coefficients," "selectivity coefficients," "concentration equilibrium quotients," "apparent equilibrium constants," and "selectivity constants." In recent publications and in technical application the terms "selectivity constant" and "selectivity coefficient" have come into widespread use. At the same time their variability has become more generally recognized. To avoid any false impression of constancy we shall here employ the term "selectivity number," defined purely in terms of the analytical results. For cations of the same valency, the selectivity number

$$K_S = (C_1/C_2)_E/(C_1'/C_2')_S$$

where $C_1$ and $C_2$ refer to analytically determined concentrations in the external solution at equilibrium, and $C_1'$ and $C_2'$ are similarly determined for the total cations completely displaced by suitable solutions from the substrate phase. The ratio $C_1'/C_2'$ is thus equal to $M_1'/M_2'$, the molar ratio of the cations at equilibrium on the substrate.

To determine the relative behavior of the substrate phase with respect to two exchange cations it is desirable to eliminate ionic interactions in the external solution. When the latter is sufficiently dilute and selected cations of the same valency are employed, the concentration ratio $C_1/C_2$ equals the activity ratio $a_1/a_2$ to a good approximation. We shall here assume this to be true for solutions of chlorides below $M/100$ of the pairs $Na^+/K^+$, $Na^+/Rb^+$, Na/Cs and $Mg^{++}/Ca^{++}$, $Mg^{++}/Sr^{++}$ and $Mg^{++}/Ba^{++}$.

This brings a further advantage. Donnan theory indicates that when the effective cation concentration in the solution phase is much below that in the substrate phase the salt concentration in the latter will be negligible and the activity ratio $a_1/a_2$ in the external solution will equal the activity ratio of the two cations of the substrate phase. Thus

$$(C_1/C_2)_E = (a_1/a_2)_E = (a_1'/a_2')_s$$

Hence

$$K_s = (a_1'/a_2')_s/(M_1'/M_2']_s = (f_1'/f_2')_s$$

But $M_2'/M_1'$ can be taken as equal to the corresponding ratio of cationic concentrations in the substrate phase. Then $K_s$ becomes the ratio of the two cationic activity coefficients $f_1'/f_2'$ in the substrate phase. Provided the external solution is sufficiently dilute Donnan theory indicates that the value of $K_s$ should be independent of actual concentration.

The present work provides a comparison of two dissimilar exchangers in their behavior toward the same pairs of cations, namely, Na–K, Na–Rb, Na–Cs and Mg–Ca, Mg–Sr, Mg–Ba. The organic exchange resin chosen was a copolymer of methacrylic acid with divinylbenzene, 5–6% cross linked (Amberlite IRC 50, Rohm and Haas). Carboxyl groups occur on alternate carbon atoms of the chains except where the latter are cross linked by the benzenoid members. Hence the exchange capacity is high and chelation of cations is possible. The resin volume appeared to vary little with the nature and amount of the cations employed, although no exact measurements were made.

The clay employed for comparison was the lath-like attapulgite, which has a rigid structure with pores about 6.3 × 3.8 Å. in cross section running parallel to the fiber axis. Its cation exchange capacity is caused by atomic proxying of Al for Si in the silica sheets and is commonly about 20–30 meq. per 100 g. This corresponds to one effective exchange site per 50 silicon atoms. Presumably, therefore, the sites are well separated. In comparison with other clays, attapulgite shows the greater dissociation of cations, both monovalent (potassium) and divalent (calcium).[4]

## Experimental Procedures

(a) **Exchange Resin IRC 50.**—The H form of the resin was thoroughly washed with hot doubly distilled water and air-dried. A 1:1 suspension gave a *p*H of 4.8. Samples of 1 g. of air dry resin were weighed into calibrated plastic centrifuge tubes. Each was brought to neutrality with 4 ml. of 0.4728 *N* sodium hydroxide, *i.e.*, 1.891 meq. This represents only about 20% of the exchange capacity of the resin as defined by the total carboxyl content. Normal sodium and potassium chloride solutions then were added in twelve different proportions so that the total cation content

(1) Contribution from the Missouri Agricultural Experiment Station, Journal Series No. 1977. Approved by the Director.

(2) Experimental results from M.S. Thesis of G. Garcia, University of Missouri, January, 1959.

(3) C. E. Marshall, *2nd Nat. Conf. Clays, Natl. Acad. Sci.*, **327**, 364 (1954).

(4) S. A. Barber and C. E. Marshall, *Soil Sci.*, **72**, 373 (1951).

remained the same, namely, 100 meq. per tube. The systems were mixed and after 24 hours the clear supernatant liquid was carefully decanted. Doubly distilled water was then added to the mark, the systems were mixed and again decanted after 24 hours. This process was repeated. The equilibrium then attained was defined by analysis as follows. The liquid decanted was analyzed for chloride by the Mohr titration and for sodium and potassium by the flame photometer using air–acetylene. Working curves were obtained using standard solutions and no interference was found between sodium and potassium, rubidium or cesium.

After removal of the outer solution the moist resin sample was treated with about 10 ml. of 1 *N* ammonium nitrate solution and transferred to a filter funnel. Further portions of 10–15 ml. ammonium nitrate solution were added until about 75 ml. of filtrate was collected. The latter was then made up to 100-ml. volume and analyzed for Na and K as described above. The chloride concentration was about $10^{-5}$ *M*, whereas in the equilibrium solution it was $10^{-3}$ to $10^{-2}$ *M*. The complete series of 12 samples was run in duplicate and good agreement was obtained.

The sodium–rubidium and sodium–cesium equilibria were conducted similarly except that 0.5-g. samples of resin were used, and correspondingly lower concentrations of sodium hydroxide, sodium chloride, rubidium chloride and cesium chloride. Single series only were employed.

Under the experimental conditions used, concentrations measured by the flame photometer are believed reliable to 1 p.p.m.

In the divalent series 0.5-g. samples were initially titrated with 0.979 meq. sodium hydroxide; then 25 meq. of $Mg^{++}$ + $Ca^{++}$ as chlorides were added. With so large an excess of divalent ions relatively little sodium remained on the exchanger and it was reduced to entirely negligible amounts by the subsequent dilutions of the outer liquid. (Since the ratio(Monovalent)/$\sqrt{\text{Divalent}}$ tends, by Donnan theory, to remain constant upon dilution, it is necessary for the Ca/Na ratio on the exchanger to increase). The same decantation procedure was used as before, 24 hours being allowed for the final equilibrium.

In the external liquid, chloride was determined by mercuric nitrate titration and the sum of the divalent cations was obtained by Versenate titration as described by Metson[5] with the addition of a known amount of magnesium chloride solution which improves the end-point (Martell and Calvin[6]). The details were the same for the Mg/Ca and Mg/Sr systems but in order to obtain a good end-point with barium, Cook and Yardley's modification was used. In this case an excess of standard magnesium chloride solution was added to the samples to be titrated.

Calcium, strontium and barium were determined using the flame photometer. Suitable dilutions of the samples were made where necessary (notably at high Ba concentrations). The results appear reliable to 1 p.p.m.

Displacement of divalent cations from the resin substrate followed the procedure for monovalent cations, and subsequent analyses were as described above. Thus in all cases the magnesium estimation was the difference between total divalent cations by Versenate titration and calcium, strontium or barium by flame photometer.

All systems comprised twelve different proportions of divalent cations and all were carried through in duplicate. Good agreement was found.

(b) **Attapulgite Clay.**—The sample used was A.P.I. sample H-43 supplied by Wards Natural Science Establishment. It contains 1–3% of quartz, as the major impurity. The chief exchangeable cations on the natural clay are calcium and magnesium.

A 1:2 clay–water suspension of the sample gave a *p*H of 7.4. The crude clay was ground in a ball mill, then passed through a 40-mesh sieve.

The exchange capacity of attapulgite is much lower than that of IRC-50; around 0.30 meq. per gram; 25 meq. of Na plus K as chlorides were added first to 1-gram samples of the clay in centrifuge tubes. After 24 hours the supernatant liquid was decanted and the treatment was repeated. Again the supernatant liquid was removed and the tubes were made up to the mark with doubly distilled water. After 24 hours the liquid was removed and tested for Ca and Mg. Tests were negative. Water was added to the mark and after 24 hours the tubes were centrifuged, and the top liquid was decanted as completely as possible.

The chloride concentration was then about $1.4 \times 10^{-2}$ molar. Analyses for Na and K by the flame photometer followed the procedure used with IRC 50. The clay phase was leached with 1 *N* ammonium nitrate in the same manner as the resin. The combined leachates were made up to 100 ml. and analyzed for Na and K as before.

Similar techniques were used for the Na–Rb and Na–Cs systems, except that single series only were set up, whereas the Na–K series were duplicated.

Divalent cations were determined using the Versenate–flame photometer combination as described for the resin system. Because of the low exchange capacity, the concentrations in the ammonium nitrate leachate were lower than in the resin series.

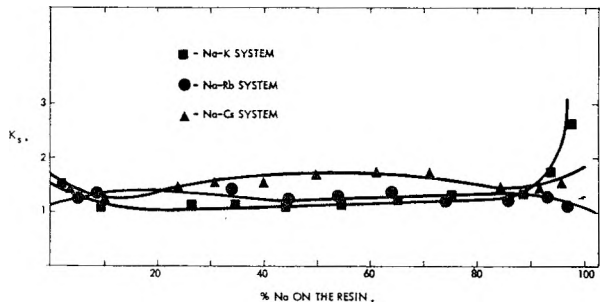


Fig. 1.—Selectivity numbers of IRC 50 in Na–K, Na–Rb and Na–Cs systems of varying composition.

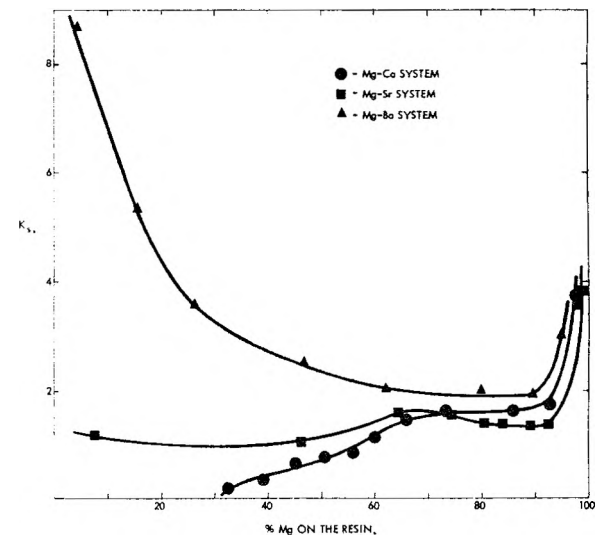


Fig. 2.—Selectivity numbers of IRC 50 in Mg–Ca, Mg–Sr and Mg–Ba systems of varying composition.

## Results

(a) **Exchange Resin IRC 50.**—The Na–K, Na–Rb and Na–Cs equilibria are represented in Fig. 1, in which the selectivity number is plotted vertically and the percentage saturation with sodium of the solid phase horizontally. Values of $K_s$ higher than unity indicate that the cation other than sodium has the lower activity coefficient, *i.e.*, is more firmly held by the resin substrate.

Variations in selectivity number with composition were least for the Na–Rb system (about 15% variation, irregular). The Na–Cs system showed about 30% variation with a flat maximum in the middle range. The Na–K system showed good con-

(5) A. J. Metson, "Methods of Chemical Analysis for Soil Survey Samples," Govt. Printer, New Zealand. 1956.

(6) A. E. Martell and M. Calvin, "Chemistry of the Metal Chelate Compounds," New York, N. Y., 1953.

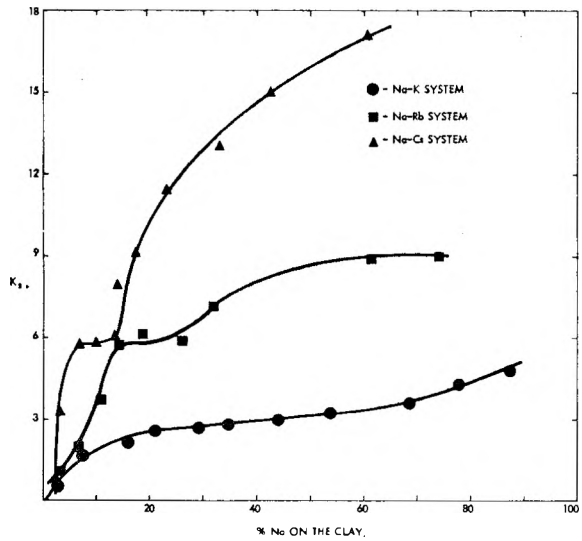


Fig. 3.—Selectivity numbers for attapulgite in Na–K, Na–Rb and Na–Cs systems of varying composition.

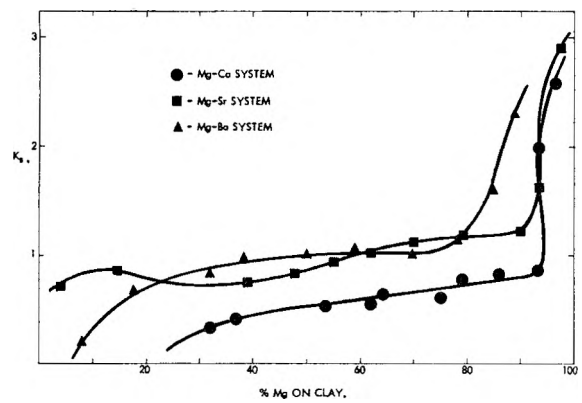


Fig. 4.—Selectivity numbers for attapulgite in Mg–Ca, Mg–Sr and Mg–Ba systems of varying composition.

stancy from about 65% Na to 10% Na, but rising values of $K_s$ at both ends of the curve.

Over the middle range the order was definitely ${}^{Na}_{Cs}K_s > {}^{Na}_{Rb}K_s > {}^{Na}_{K}K_s$ as might be expected from the properties of these ions in surface reactions generally. The curves cross for small and more strikingly for large percentages of sodium. Except for the extreme value 2.7 in the K–Na system, the variations might well correspond to activity coefficient variations caused by interionic forces in the interior of the resin, where concentrations are over 1 molar. Kitchener curves[7] showing activity coefficient variations of acetates and *p*-toluenesulfonates indicate that the order depends on the anion. Thus acetates show $\gamma_{NaAc} < \gamma_{KAc} < \gamma_{RbAc} < \gamma_{CsAc}$ whereas for sulfonates $\gamma_{KS} < \gamma_{NaS} < \gamma_{LiS}$. Glueckauf's[7] osmotic coefficient curves for a weakly cross-linked resin indicate Li > Na > K as the order of dissociation, which agrees with the sulfonate series above and with the order found here.

The distinct upward turn of $K_s$ for compositions involving a high proportion of sodium shows itself even more strongly in the divalent cation curves (see below) and strongly suggests that a small proportion of the exchange sites falls into a separate category. The other more gradual variations of $K_s$ with composition in the monovalent series are not of sufficient magnitude definitely to establish a polyfunctional character.

The Mg–Ca, Mg–Sr and Mg–Ba curves (Fig. 2) show an entirely different type of behavior. The selectivity numbers are very small for small proportions of magnesium; that is, up to 55% magnesium saturation this ion is held more strongly than calcium. The curve turns up sharply at about 90% saturation with magnesium and the last point recorded (3% Ca, 97% Mg) corresponds to a selectivity number 3.71. The Sr–Mg curve does not dip below unity but shows a flat maximum at about 70% saturation with magnesium and a sharp upturn beyond 90% saturation. The Mg–Ca and Mg–Sr curves cross at about 73% saturation. The barium curve shows very high values of $K_s$ for small proportions of Mg, a fairly flat region from about 60 to 90% Mg and a rapid increase beyond 90% Mg.

These complex results indicate the presence of competing factors. All curves show the strong upturn in $K_s$ for high proportions of magnesium. Differences due to polyfunctional characteristics are known to be much accentuated for divalent cations as compared with monovalent,[3] so it is not surprising that the right-hand portions of the curves show this.

Great differences in the three curves are shown for compositions between 0 and 60% magnesium. In the methacrylate chains there is choice of two structural sites for divalent cations. (a) They act as links joining two carboxyl groups. In this way 8-membered rings would be formed. The strength of bonding would be Ba > Sr > Ca > Mg but it is difficult to explain the tremendous differences from calcium to barium on this basis alone. (b) The monovalent ion $MgOH^+$, which from Bower and Truog's work[8] takes part in exchange reactions, might form a six-membered ring with a single carboxyl group and the hydrogen atom of the carbon. Here magnesium would be more tightly held than calcium, as shown by the low values of $K_s$ up to 55% Mg. Sites occupied in this way by magnesium would seriously interfere with the distribution of (a) type sites, especially if, as seems likely, the former occurred on alternate carboxyls. There would be competition involving $MgOH^+ > CaOH$ ($SrOH^+ > BaOH^+$) with its very sharp decrease in bonding from magnesium to calcium, and $Ba^{++} > Sr^{++} > Ca^{++} > Mg^{++}$ which is the normal order.

Hence what appears at first sight as an extreme manifestation of polyfunctional character may largely be explained on the basis of competing mechanisms. However, there is clear evidence that some 5% of sites differ from the rest.

**(b) Attapulgite Clay.**—The Na–K, Na–Rb and Na–Cs curves are shown in Fig. 3. The sodium–potassium equilibria indicate that potassium is normally more tightly held than sodium, but there exists a narrow region at high potassium contents where the reverse is true. The sodium–rubidium and sodium–cesium curves are complex. In both

(7) J. A. Kitchener, *Ion Exchange Conference, Soc. Chem. Ind.*, 24 (1955).

(8) C. A. Bower and E. Truog, *Soil Sci. Soc. Amer. Proc.*, **5**, 86 (1940).

cases small amounts of sodium give selectivity numbers close to unity. Then a steep rise occurs, followed by a narrow zone in which the selectivity number is around 6 and changes little with increasing proportions of Na. From about 26% Na in the Na–Rb case and from about 14% Na in the Na–Cs curve another sharp rise occurs. Finally the Na–Rb system shows only slight changes between 45 and 75% Na whereas the Na–Cs system gives increasing values of the selectivity number. Cesium shows such high bonding that in the present series no system with less than 40% cesium resulted.

Potentiometric titration curves of attapulgite with potassium hydroxide[4] indicate that although this clay holds potassium somewhat less strongly than other clays, a certain proportion of the exchange sites have a much higher bonding energy than the rest. The polyfunctional character comes out even more strongly in the $K_s$ curves. The extremely high values for cesium indicate that special geometrical factors are important. Silicate exchangers with exposed silica sheets generally seem to have very high selectivity toward cesium, as shown by recent studies of the uptake of radioactive cesium by soils.[9] The mechanism is probably a fixation similar to that of potassium on micas.

The Mg–Ca, Mg–Sr and Mg–Ba curves reproduced in Fig. 4 show other remarkable properties of attapulgite clay. In all cases the values of $K_s$ are below unity up to about 70% saturation with magnesium. Hence magnesium is held more firmly than calcium, strontium or barium over a wide range of compositions. In the middle range the $K_s$ values for Mg–Sr and Mg–Ba systems are close together; the curve for the Mg–Ca system lies considerably lower. The polyfunctional character of the clay is much less strikingly shown by the divalent series as compared with the monovalent. Nevertheless the downward course of the $K_s$ curves between 0 and 20% Mg, and their strongly upward turn between 85 and 100% Mg show a polyfunctional character.

Structurally, the strongly preferential bonding of magnesium can be ascribed to the free access (by the fixed channels), to the octahedral layer, which is composed of magnesium and aluminum bonded to oxygen and hydroxyl. These octahedral units are in narrow strips which form two parallel walls of the roughly rectangular channels. Thus equilibrium between structural magnesium ions and exchangeable magnesium ions would be facilitated, the general effect being enhanced bonding energy for magnesium as compared with the larger ions calcium, strontium and barium which do not enter the octahedral structure. This fixation mechanism does not produce such exaggerated effects as does chelation in the carboxylic resin for reasons evident from the discussion. It is quite different also from fixation of Cs, Rb, K and $NH_4$ at mica-like surfaces composed of $Si_2O_3$ sheets, in which the cation is accommodated in hexagonal rings of oxygen ions.

An alternative explanation, namely, that small fixed channels in exchangers favor the bonding order for dehydrated ions rather than hydrated[3] seems improbable, because in the monovalent series with attapulgite we have so clearly the order Cs > Rb > K > Na, characteristic of the hydrated series. In the divalent case magnesium alone is exceptional. Calcium, strontium and barium fall in their normal order.

9) H. Nishita, *et al.*, *Soil Sci.*, **81**, 317 (1956).

# THE SURFACE TENSION OF PERFLUORO SULFONATES IN STRONG AND OXIDIZING ACID MEDIA

BY E. L. TALBOT

*Contribution No. 154 from Minnesota Mining and Manufacturing Company, St. Paul, Minnesota*

*Received March 6, 1959*

The surface tension of a saturated solution of $n$-$C_8F_{17}SO_3K$ in water may be lowered from a value of 40 dynes to 17 dynes by the addition of a strong acid such as sulfuric, nitric or hydrochloric. The surface tension lowering is proportional to the log of the increase in the hydrogen ion over the concentration range $(H^+) = 10^{-3}$ $M$ to 10 $M$. At concentrations above 10 $M$ for sulfuric and nitric acid the surface tension increases again. Hydrochloric acid continues to lower the surface tension even above 10 $M$. Acetic acid also falls on the same curve when plotted according to the available hydrogen ion. Sodium chloride and potassium chloride also decrease the surface tension of solutions of $C_8H_{17}SO_3K$ to a lesser degree than do the strong acids.

## Introduction

The chemical stability of the perfluoro acids and salts under extreme reducing and oxidizing conditions has been established by several workers.[1,2,3]

Hydrocarbon surfactants have little utility in concentrated solutions of sulfuric and nitric acids because they are quickly decomposed, but the perfluoro surfactants remain stable under these conditions and lower the surface tension of these acids in a very effective manner.

Alkyl perfluorocarboxylic acids are relatively strong acids and at low concentrations exhibit a $p$H nearly equivalent to that of hydrochloric acid at the same concentrations.[3] In previous studies[4,5]

(1) E. A. Kauck and A. R. Diesslin, *Ind. Eng. Chem.*, **43**, 2332 (1951).

(2) J. O. Hendricks, *ibid.*, **45**, 99 (1953).

(3) D. R. Husted and A. H. Ahlbrecht, "Chemistry of the Perfluoro Acids and Their Derivatives," 122nd Meeting American Chemical Society, Atlantic City, N. J., 1952, Abstracts, p. 29-K.

(4) E. L. Talbot, "The Effects of $p$H and Ionic Strength Upon the Surface Tension of Certain Perfluoro Alkyl Acids and Their Salts," 124th meeting of American Chemical Society, Chicago, Ill., 1953, Abstracts 4-I.

(5) S. R. B. Cooke and E. L. Talbot, *Mining Engineering*, **7**, 1149 (1955).

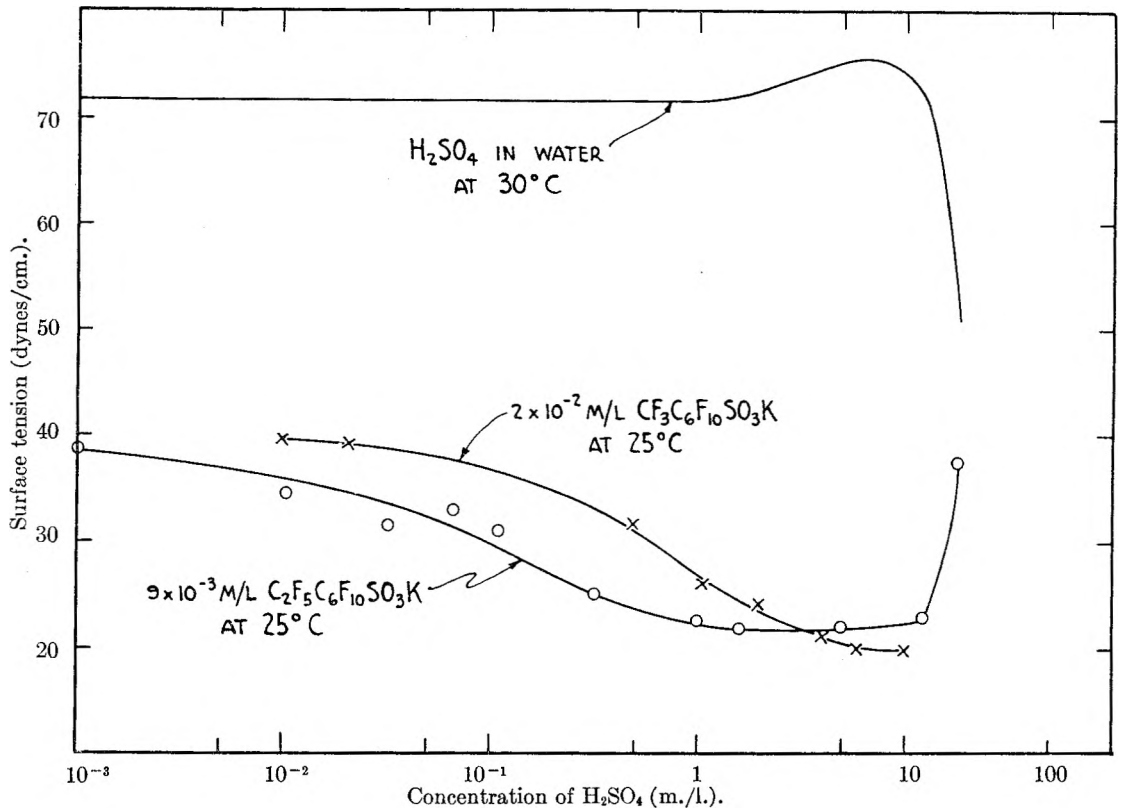


Fig. 1.—The effect of sulfuric acid upon the surface tension of cyclic perfluoro sulfonate solutions.

the surface tension of a $3.27 \times 10^{-3}$ m./l. solution of $C_7F_{15}COOH$ was shown to decrease rapidly as hydrochloric acid was added. Twenty times more sodium chloride than hydrochloric acid was required to effect the same lowering of the surface tension. The surface tension of a $C_7F_{15}COONa$ solution also was lowered by 15 dynes between *p*H values of 4 and 1 as hydrochloric acid was added. The phenomenon was explained on the basis of formation of free acid[6,7,8] by the reaction $H^+ + X_f^- = HX_f$ where $H^+$ is the available hydrogen ion, $X_f^-$ is a perfluoro anion and $HX_f$ is the corresponding free or undissociated acid form. The free acid form is more strongly adsorbed[9] than the ionic form and results in a lower surface tension. Because of low solubility and salting-out effects, the perfluorocarboxylics have limited utility in more concentrated solutions of acids.

The perfluoro alkane sulfonic acids and derivatives[10] being more soluble and stronger than the perfluorocarboxylic acids will have more utility in the concentrated acids. The surface tension of more concentrated inorganic acids may be lowered effectively by the addition of perfluoro sulfonic materials. Since perfluoro sulfonic acids are stronger acids than the perfluoro carboxylic acids, higher concentrations of inorganic acid would be required to achieve the same degree of lowering of the surface tension. Since ionic materials also depress the surface tension, sodium and potassium chloride would be expected to have an influence on the surface tension of the perfluoro sulfonic acids but to a lesser degree than does hydrochloric acid.

(6) M. A. Cook, *Engineering and Mining Journal*, **150**, No. 2, 110 (1949).

(7) M. A. Cook and J. C. Nixon, THIS JOURNAL, **54**, 445 (1950).

(8) M. A. Cook and E. L. Talbot, *ibid.*, **56**, 412 (1952).

(9) N. K. Adam, "The Physics and Chemistry of Surfaces," Oxford University Press, New York, N. Y., 1946. p. 140.

(10) P. W. Trott, *et al.*, "Perfluoro Alkanesulfonic Acids and Derivatives," 126th meeting American Chemical Society, New York, N. Y., 1954, Abstracts, p. 42-M.

## Experimental

The fluorinated materials used in these experiments were specially prepared in the laboratories of the Minnesota Mining and Manufacturing Company. The $C_7F_{15}COOH$ had a neutral equivalence of 415 (theoretical 414), a free fluoride ion of 0.019 mg./g. and a total hydrolyzable fluoride of 0.19 mg./g. The $C_7F_{15}COONa$ contained 5.29% Na (theoretical 5.28%), 65.1% F (theoretical 65.5%, hydrolyzable fluoride 0.2 mg./g. Both of the cyclic perfluoro sulfonates $CF_3C_6F_{10}SO_3K$ and $C_2F_5C_6F_{10}SO_3K$ were prepared from repurified starting materials. The $C_2F_5C_6F_{10}SO_3K$ was further purified by a triple water extraction method until no lowering of the surface tension in water was observed after saturation was obtained. The $n$-$C_8F_{17}SO_3K$ had 7.57% K (theoretical 7.24), 5.78% S (theoretical 5.94), 58.2% F (theoretical 60.0) and 0.5 mg./g. of hydrolyzable fluoride.

The inorganic acids were reagent grade. The distilled water was prepared in a block tin still and stored in Pyrex. Glassware was cleaned in a warm detergent solution, rinsed, then cleaned in a hot concentrated sulfuric:nitric acid (10:1) mixture and rinsed in distilled water. All samples except those containing sodium or potassium chloride were stored at 25 ± 0.1° for at least 24 hours before measuring to insure equilibrium conditions. The solutions containing varying concentrations of sodium or potassium chloride were made up in distilled deionized water and stored at 23 ± 3° for only a short time. Equilibrium probably was not established because a slight to considerable flock of white material was floating in most of these solutions.

Surface tension measurements were made by maximum bubble or du Nouy tensiometer methods with good agreement between the two methods. Ring measurements were corrected using Harkins and Jordan[11] or Fox and Chrisman[12] corrections.

The surface tensions of the inorganic acids were obtained

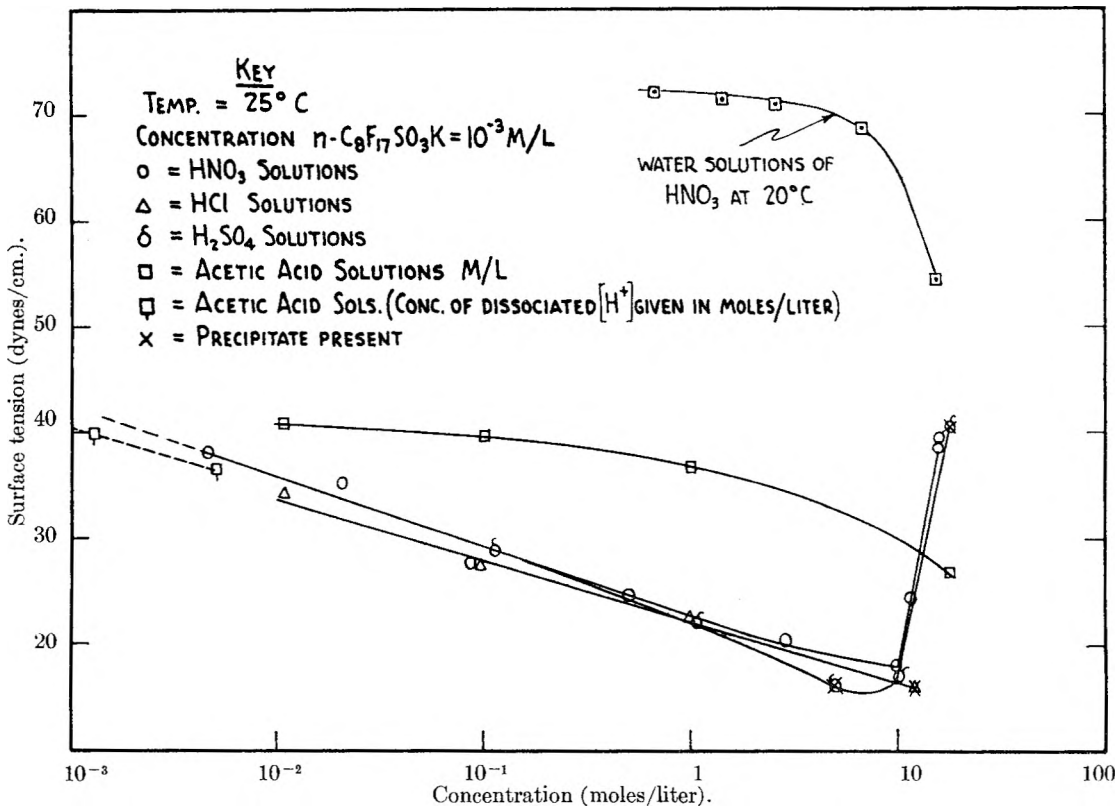


Fig. 2.—The effect of various acid media upon the surface tension of $n$-$C_8F_{17}SO_3K$ solutions.

from "International Critical Tables"[13] or determined by the ring method where no data existed.

## Results and Discussions

The concentration at the knee of the surface tension *vs.* concentration curve was chosen in each case for continued study. Since the surface is already saturated with the surfactant, the only way the surface tension could be decreased would be by changing the nature of the adsorbing constituents.

Figure 1 shows the effect of sulfuric acid upon the surface tension of two cyclic perfluoro sulfonic acids. Since the $C_2F_5C_6F_{10}SO_3K$ was considered to be the better sample, more extensive work was done on it. The surface tension was lowered gradually as the acid content was increased to 1 $M$. Above 10 $M$, sulfuric acid was not as effective at lowering the surface tension of the sulfonate solution even though over this concentration range the surface tension of sulfuric acid itself was decreasing. The work on $CF_3C_6F_{10}SO_3K$ was not carried out sufficiently to determine the effect at higher acid concentrations.

In Fig. 2 the effect of several acids is shown. Hydrochloric, nitric and sulfuric acids all gave the same curve over the region $10^{-3}$ to 10 $M$. Hydrochloric acid continued to lower the surface tension until its saturation concentration of 12 $M$ was reached. Sulfuric and nitric acids both showed less of an effect on lowering the surface tension at acid concentrations above 10 $M$ even though the surface tension of both nitric and sulfuric acid was decreasing.

The addition of a weak acid such as acetic had a decidedly less effect on the surface tension than the stronger acids. If the ionization of acetic acid is considered, however, the curves come into coincidence when the hydrogen ion is used as a basis for the plot. According to classical discussions in Fritz Ephraim's "Inorganic Chemistry,"[14] the hydrogen ions in concentrated nitric and sulfuric acids are tightly held in the acid molecule and are unavailable for ionic reactions. Hydrogen is not evolved when iron is placed in either concentrated acid. Hydrochloric acid, however, is only 37% by weight in concentrated acid and the hydrogen ion is available for reaction with iron or combinations with anions.

A qualitative explanation of the observed phenomena is offered here on the basis of free acid formation and adsorption. At a concentration of about $10^{-3}$ m./l. of $C_8F_{17}SO_3K$, which falls near the knee of the surface tension–concentration curve, the surface is essentially saturated with the perfluoro anions. The presence of hydrogen ions in the solution forces the equilibrium toward the free acid form which adsorbs more strongly at the interface and displaces some of the ionic form, thus producing a lower surface tension.

In the more concentrated acid region for nitric and sulfuric acids, the hydrogen ion is not as readily available and the equilibrium is not shifted as far toward the free acid form. Since the hydrogen ions

(11) W. D. Harkins and H. F. Jordan, *J. Am. Chem. Soc.*, **52**, 1751 (1930).

(12) H. W. Fox and C. H. Chrisman, Jr., THIS JOURNAL, **56**, 284 (1952).

(13) "International Critical Tables," McGraw-Hill Book Co., New York, N. Y., 1926–30.

(14) "Inorganic Chemistry," Edited by P. C. L. Thorne and E. R. Roberts, Interscience Publishers, Inc., New York, N. Y., 1946.

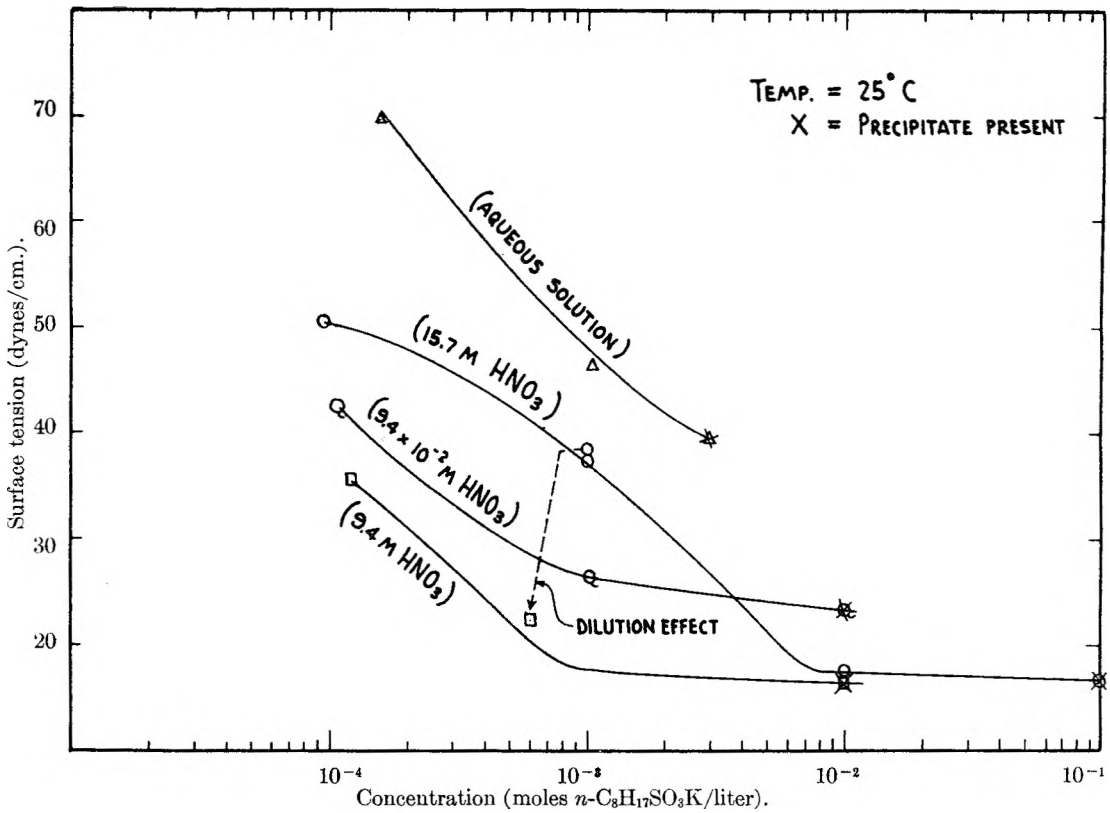


Fig. 3.—The effect of $n$-$C_8F_{17}SO_3K$ upon the surface tension of nitric acid solutions.

are available in hydrochloric acid, the same phenomenon is not exhibited at the maximum concentration of 12 $M$. Acetic acid completes this picture of free acid formation by the curves being coincidental when the available hydrogen ion is considered as the basis for plotting instead of molar concentration.

A second qualitative explanation for the concentrated region and for acetic acid would be the possibility of formation of a complex of the acids with the perfluoro anion to move the reaction toward the ionic form. This would be a possibility only if one were to make up the solutions in concentrated acid and then dilute them. This, however, was not the method of preparation.

If a complex were to be formed which was more surface active than the original sulfonate, this could account for the initial decrease in surface tension at low acid concentration except that a complex formation would be more likely to form in concentrated acids then in dilute solutions. The experimental evidence shows this not to be the case. In addition, a less surface active complex would have to be postulated to account for the region between 10 $M$ and concentrated acid.

In Fig. 3 the effect of concentration of $n$-$C_8F_{17}SO_3K$ in various nitric acid solutions was studied. The surface tension was decidedly depressed by using approximately 0.1 $M$ nitric acid as the solvent instead of water. Using 10 $M$ nitric acid reduced the surface tension even more. These curves fell as expected from the data of Fig. 2. Accordingly the curve for concentrated nitric acid was higher than either 0.1 $M$ or 10 $M$ solutions.

In the case of $C_7F_{15}COONa$, salting out occurred above a hydrochloric acid concentration of 0.1$M$[4]; however, $n$-$C_8F_{17}SO_3K$ is actually 10-fold more soluble in concentrated nitric acid than in 10 $M$. The minimum surface tension is also lower for the more concentrated acids.

Two other experiments were conducted to attempt to show that complexes were not being formed at high acid concentrations. Dilution of a surfactant ordinarily results in an increase in surface tension. However, the surface tension of a $10^{-3}$ $M$ solution of $n$-$C_8F_{17}SO_3K$ in concentrated nitric acid did not increase when diluted to 9.4 $M$ but rather decreased by 16 dynes and fell onto the curve for this new concentration of sulfonate in 9.4 $M$ nitric acid. If a complex existed, the reaction was completely reversible on diluting the acid.

The second experiment consisted of dissolving some of the purified $C_8F_{17}SO_3H$ in concentrated acid and evaporating it slowly at room temperature until the liquid just disappeared. The infrared curve for the pure perfluoro sulfonic acid and the nitric acid treated material were identical, again indicating that no stable complex had been formed.

The effect of ionic materials upon the surface tension of solutions of $C_8F_{17}SO_3K$ was studied briefly. The data for the effect of potassium and sodium chloride are not considered to be as reliable as those of the inorganic acids because of the shorter storage time and because in most solutions a slight scum was observed. This was especially noticeable in the sodium chloride solutions. In solutions above 1 $M$ in potassium chloride, a definite flock occurred which gathered at the sur-

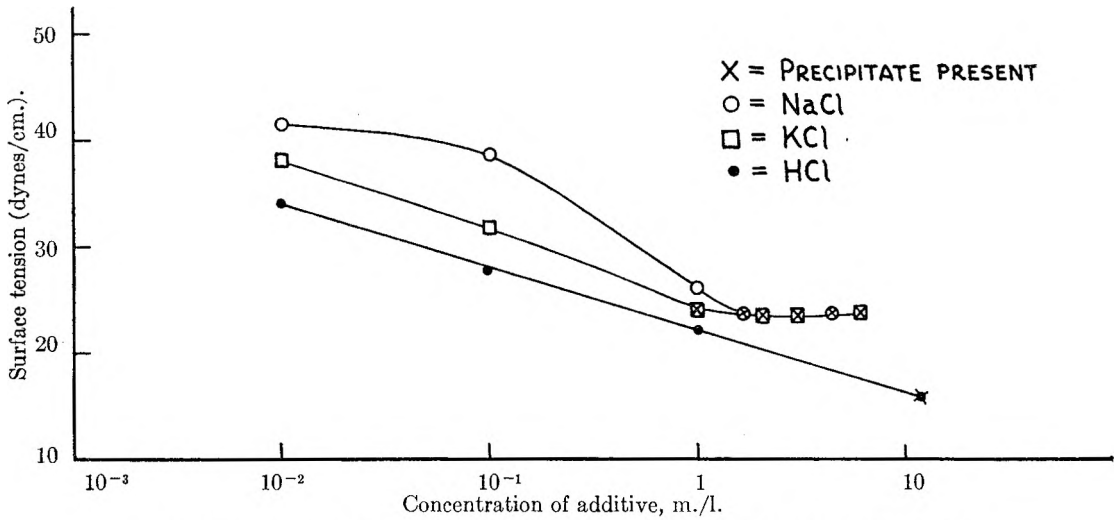


Fig. 4.—The effect of ionic strength upon the surface tension of $C_8F_{17}SO_3K$ solutions.

face. At higher concentrations for sodium chloride, the flocking was even more pronounced. In spite of the flocking conditions, Fig. 4 shows that the ionic effect cannot be neglected in considering surface tension depression by the addition of highly ionized acids.

In the case of the perfluoro carboxylic acid study[4,5] a concentration more dilute than the knee of the surface tension curve was chosen. The difference between the effect of ionic salt and hydrochloric acid was clearly shown as a 20-to-1 ratio. In the present studies, the salts and acids were more nearly equal in their effect because the sulfonate solution chosen was much nearer to the surface saturation point. No explanation is offered as to why potassium and sodium chloride do not give results closer to each other. Since additions of acids resulted in a larger depression of the surface tension than when the neutral ionic materials were added, hydrogen ion was shown to have an additional effect which qualitatively can be interpreted as free acid absorption.

## Summary and Conclusions

The effect of strong and oxidizing acids upon the surface tension of solutions of $C_2F_5C_6F_{10}SO_3K$ and $n$-$C_8F_{17}SO_3K$ was explained qualitatively by postulating the formation of free acid molecules. The free acid molecules are generated by the reaction of the perfluoro anion with the available hydrogen ions in the solution. They are then preferentially adsorbed at the surface to cause a depression of the surface tension proportional to the available hydrogen ion. This concept was used to explain these observations:

(1) The same surface tension curve was obtained by adding hydrochloric, nitric, or sulfuric acid to a $10^{-3}$ $M$ solution of $n$-$C_8F_{17}SO_3K$ at concentration of acid below 10 $M$.

(2) Acetic acid additions also fell onto the same curve as the other acids if the available hydrogen ion was calculated and used as a basis for plotting.

(3) Nitric and sulfuric acids more concentrated than 10 $M$ showed less lowering of the surface than did 10 $M$ acid.

(4) Hydrochloric acid continued to lower the surface tension of $n$-$C_8F_{17}SO_3K$ solutions as the acid concentration was increased to 12 $M$.

(5) No evidence was substantiated for the formation of a complex in the presence of concentrated nitric or sulfuric acid.

The effect of neutral ionic materials also was noted as being significant in lowering the surface tension of solutions of $n$-$C_8F_{17}SO_3K$.

## DISCUSSION

M. J. VOLD (University of Southern California).—Did you measure the interfacial tension between organic solvents and these strong oxidizing acids in the presence of the perfluorosulfonates? Was the interfacial tension lowered between the two systems which had their surface tensions lowered?

E. L. TALBOT.—Data were reported by J. W. Shepard and J. A. Mann at the 129th meeting of the American Chemical Society, Dallas, April, 1956. Interfacial tensions between concentrated acids and organic solvents are lowered by these materials. This has a direct connection with the present research and will be the subject of another paper.

M. J. VOLD.—It is not surprising that sodium and potassium chloride have a considerable effect. At the surface tension of 40 dynes, corresponding to the knee of the surface tension–concentration curve, the surface already was saturated with adsorbed additive. The addition of charged ions would neutralize the surface and alter the amount which can be associated in the ionic form. It is quite a common experience to find that surface tension is lowered as the ionic strength increases.

E. L. TALBOT.—Perhaps my choice of concentration in the experiments using perfluorocarboxylic acids was more fortuitous than in the case of the perfluorosulfonics. For the carboxylics I picked a point which was about half way to saturation. The perfluorosulfonate was already at the saturation point and would not be as sensitive to hydrogen ion.

# A NEW METHOD FOR THE DETERMINATION OF CRITICAL MICELLE CONCENTRATIONS OF UN-IONIZED ASSOCIATION COLLOIDS IN AQUEOUS OR IN NON-AQUEOUS SOLUTION

BY SYDNEY ROSS AND J. P. OLIVIER

*Department of Chemistry, Rensselaer Polytechnic Institute, Troy, New York*

*Received March 6, 1959*

A new method for the determination of critical micelle concentration (CMC) of un-ionized surface-active agents is developed, and shown to be applicable in a number of different solvents. The method depends on the formation of a colored iodine-micelle complex. The absorption maximum of the complex is always at 360 mμ for different agents and for different solvents. Critical micelle concentrations in water, benzene, carbon tetrachloride and petroleum ether solutions have been determined. The results by the new method are found to agree with those obtained by independent methods, namely, measurements of static surface tension and relative differential refractive index. Colored impurities in the agent are not troublesome except at high concentrations, and even there an empirical correction can be applied. An isosbestic point in the absorption spectra is evidence that dissolved iodine is in equilibrium with the iodine in the micelle and that only one type of iodine–micelle complex is present in the solution.

## Introduction

The spontaneous molecular association of ionic surface-active agents in aqueous solution can be detected readily by measurements of electrical conductivity. The two chief advantages of this method lie in the availability of suitable instruments and the absence of any need to add additional substances to the solutions being measured. No experimental technique of comparable ease has yet been discovered for the study of the association of non-ionic surface-active agents, and methods based on solubilization or color changes of dyes are all suspect when the associated micelle is formed at concentrations of agent that are close to the concentration of the added solubilizate or indicator. The latter objection is frequently valid with non-ionic surface-active agents, whose tendency to associate may be expected to be stronger than that of ionic agents, because molecules of the former have little or no electrical force to resist aggregation. A new method that is even relatively free from these objections is therefore important for the further study of the non-ionic association colloids.

In organic solvents the distinction between ionic and non-ionic agents disappears, and we have no convenient method of detecting the association of the solute. Oil-soluble detergents, such as the petroleum mahogany sulfonates and petroleum naphthenates, are extensively used as additives in lubricating oils and as rust inhibitors both in lubricants and in preservative coatings. These practical applications are handicapped because so little is known about the state of dispersion, and the factors that affect it, of soap dispersions in oil. A method that could be adapted for the investigation of these systems would find a wide range of application.

The method that we report is based on the color change of iodine that takes place when non-ionic association micelles are added to an iodine solution.[1]

The absorption spectrum that results always shows a development of a new maximum absorption peak at a shorter wave length; the position of this maximum does not vary from one solvent to another. The method is equally applicable, therefore, to the determination of critical micelle concentration (CMC) in aqueous or in non-aqueous solutions. Iodine also has the advantage of small molecular size compared to the molecule of the surface-active agent; it is less likely, therefore, to affect micelle formation as much as do the large dye molecules customarily used for CMC determination by spectral shift. This supposition has been found to be true in the few cases where the results of an independent determination of CMC of non-ionic agents have been available for comparison. Unfortunately, the large body of information about colloidal electrolytes in aqueous solution cannot be used for this comparison; no interaction takes place between iodine and negatively charged micelles, and a precipitate is formed with positively charged micelles. The method is restricted, therefore, to un-ionized surface-active agents, although agents that are colloidal electrolytes in aqueous solution are brought within the scope of the method when dissolved in non-ionizing solvents.

(1) N. A. Allawala and S. Riegelman, *J. Am. Pharm. Assoc., Sci. Ed.*, 42, 267, 396 (1953).

## Apparatus and Materials

Most of the measurements for this study were made with a Beckman Model B spectrophotometer; a few sets of solutions were measured with the Perkin–Elmer Spectracord. The surface-active agents were all commercial samples of non-ionics; no attempt was made to purify them, or to remove water. The non-aqueous solvents were dried before use; benzene was distilled over sodium; carbon tetrachloride was distilled. Measurements of static surface tension were made with a Cenco–du Nouy tensiometer. Differential refractive index was measured with a Brice–Phoenix laboratory differential refractometer, Model 1890, at 546 mμ.

The stock solution of iodine (A) was selected to transmit 80% of the light transmitted by the pure solvent; the concentrations required for this purpose are: for water, 30 mg./l.; for benzene 25 mg./l.; for carbon tetrachloride, 21 mg./l. The stock solution of the surface-active agent (B) contained a known concentration of agent well above its CMC and the same concentration of iodine as in solution A. By diluting solution B with solution A, a series of concentrations of the surface-active agent could be obtained, each with the same concentration of iodine. This series had to include concentrations above and below the CMC to be determined, which usually made necessary a crude preliminary titration of B with A in order to fix an appropriate range of concentrations with which to work.

The spectrophotometer readings are best made with solution A as the standard for 100% transmittance, although sometimes the pure solvent can be used. The failure of the reported curves to show 100% transmission in the absence of surface-active agent is caused by imperfect matching of the cells used; this effect, however, can have no influence on the determination of the CMC.

TABLE I

MATERIALS USED (DESCRIPTION AND SOURCE) AND RESULTS

| Trade name | Description | Source | Solvent | CMC in g./dl. |
|---|---|---|---|---|
| Brij 30 | 4 Oxyethylene lauryl ether | Atlas Powder Co. | $C_6H_6$ | 0.70 |
| Brij 35 | 23 Oxyethylene lauryl ether | Atlas Powder Co. | $H_2O$ | 0.0058 |
| G-3701 | 1 Oxyethylene lauryl ether | Atlas Powder Co. | $CCl_4$ | 0.036 |
| Pluronic L62 | $HO(C_2H_4O)_a(C_3H_6O)_b(C_2H_4O)_cH$ | Wyandotte Chemicals Corp. | $H_2O$ | 2.40 |
| Renex 36 | Polyoxyethylene tridecyl alcohol | Atlas Powder Co. | $C_6H_6$ | 0.078 |
| Renex 698 | Polyoxyethylene alkyl aryl ether | Atlas Powder Co. | $H_2O$ | 0.0047 |
| Siponic BC | Ethoxylated branched chain alcohol | American Alcolac Corp. | $H_2O$ | 0.011 |
| Span 40 | Sorbitan monopalmitate | Atlas Powder Co. | $C_6H_6$ | 0.66 |
| Span 40 | Sorbitan monopalmitate | Atlas Powder Co. | $CCl_4$ | 0.045 |
| Span 80 | Sorbitan monoöleate | Atlas Powder Co. | $C_6H_6$ | 3.5 |
| Triton X-100 | $C_8H_{17}C_6H_4O(C_2H_4O)_{10}H$, etc.[4] | Rohm and Haas Co. | $H_2O$ | 0.016 |

The absorption maxima of iodine in different environments[2,3] are given:

| | mμ | Color transmitted |
|---|---|---|
| $I_2$ vapor | 512 | Violet |
| $I_2$ in carbon tetrachloride | 510 | Violet |
| $I_2$ in benzene | 300, 490 | Red |
| $I_2$ in water | 450 | Brown |
| $I_2$–micelle complex | 360 | Yellow |
| $I_2$–KI complex in water[3] | 288, 353 | Yellow |

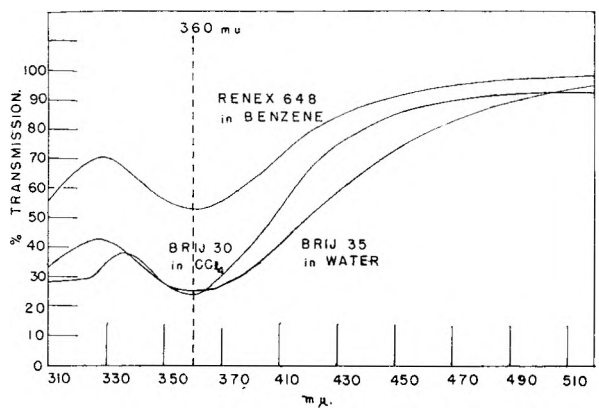


Fig. 1.—Absorption spectra of Renex 648 + iodine in benzene; Brij 30 + iodine in carbon tetrachloride; and Brij 35 + iodine in water. All these spectra have a characteristic maximum at 360 mμ.

The value of 360 mμ for the iodine–micelle complex was found to hold constant with the different agents here tested, and in different solvents. All the spectrophotometer readings, therefore, were taken at a wave length of 360 mμ. In Fig. 1 we report the absorption spectra of three different agents, each above the CMC, and each in a different solvent, to illustrate the constancy of the absorption maximum of the iodine–micelle complex under different conditions of formation.

The materials used and their commercial sources are given in Table I, which also reports the results of CMC determinations in various solvents by the present method.

## Results

In Fig. 2 we report the spectrophotometer readings of the intensity of transmitted light at 360 mμ for three non-ionic agents as a function of their concentration in aqueous solution. We interpret the break in the curve as caused by the presence of micelles in appreciable amounts, and the CMC values thus determined are reported in the diagram. No particular difficulties were encountered with these agents in the application of the present method. The readings should be taken within an hour of the preparation of the solutions because of a slow fading of the color of the iodine–micelle complex. At high concentrations of agent (3 to 4 times CMC) the equilibrium is reached more slowly, but errors due to non-equilibrium in this range of concentration do not affect the determination of the CMC.

The CMC of Siponic BC, determined by the present method (Fig. 2), is 0.0110 g./dl. Measurements of static surface tension provide an independent method of finding CMC. The ensuing description[5] refers to the determination of CMC by this method: "The static surface tension data when plotted against the log of the concentration give two straight lines whose point of intersection can be located accurately. The CMC from this method is 0.0120 ± 0.0005 g./dl. This value is based on two independent series of determinations. Fresh solutions were prepared for each series. Each series of determinations gave the same CMC."

The CMC of Triton X-100, determined by the present method, is reported in Fig. 2 as 0.0158 g./deciliter. This value can be compared with the CMC determined by the surface tension method by Hsiao, Dunning and Lorenz,[6] who reported, for a condensate product of octylphenol with a mole ratio of 8.5 ethylene oxide, a CMC of 180–230 μM. If we take a molecular weight of 646 (see formula in Table I) for Triton X-100, the CMC by the present determination is 245 μM, which gives us a reasonably good agreement with the results of the surface tension method.

The CMC of Brij 35 has been determined in this laboratory by Mr. R. C. Little from measurements of static surface tension, and found to be 0.006 g./dl., which agrees with the value 0.0058 g./dl. obtained by the present method (Fig. 2).

The method failed to give a CMC value when applied to aqueous solutions of Myrj 59 and Myrj 52. The characteristic absorption color was visible, but measurements did not disclose the expected discontinuity in the curve for transmitted intensity at 360 mμ *vs.* concentration; instead the development of

(2) H. A. Benesi and J. H. Hildebrand, *J. Am. Chem. Soc.*, **70**, 2832 (1948); **71**, 2703 (1949).

(3) A. D. Awtrey and R. E. Connick, *ibid.*, **73**, 1842 (1951).

(4) L. M. Kushner and W. D. Hubbard, THIS JOURNAL, **58**, 1163 (1954).

(5) W. G. Cutler, Whirlpool Corporation Research Labs., private communication.

(6) L. Hsiao, H. N. Dunning and P. B. Lorenz, THIS JOURNAL, **60**, 657 (1956).

the color seemed to take place gradually and continuously. We have traced this effect *in these agents* to a shift of the maximum absorption wave length, which is 360 mμ only for high concentrations of agent (*i.e.*, about 5%); on dilution with stock solution A, the absorption peak shifts gradually to 380 mμ. A probable explanation is the presence of free polyethylene glycol in the sample. We find that polyethylene glycol alone in aqueous solution forms a complex with iodine, shown by the presence of a new broad and weak absorption maximum in the vicinity of 350 mμ. This alone would not interfere with the determination of CMC, but in the presence of the non-ionic agent the effect is greatly enhanced. On adding polyethylene glycol to one of the agents reported in Fig. 2, namely, Brij 35, the same perturbing effect that had been encountered with Myrj 52 and Myrj 59 is reproduced. Apparently an interaction occurs between all three solutes when appreciable amounts of uncombined polyethylene glycol are present with the agent.

In Fig. 3 we report the application of the iodine method to two agents dissolved in benzene. For comparison of CMC determinations by an independent method we have used relative differential measurements of the refractive index. For Renex 36 the iodine method gives 0.075 g./dl. compared with 0.10 g./dl. by differential refractive index; for Span 40 the two methods are in closer agreement, *viz.*, 0.66 g./dl. and 0.65 g./dl., respectively. As measurements of the relative differential refractive index are seldom used for this purpose, especially in non-aqueous solution, we include (Fig. 4) the application of the method to Span 40 in benzene solution.

It is important with benzene solutions that the comparison solution used in the spectrophotometer also contain iodine, because of a maximum absorption peak of iodine in benzene at 318 mμ. The absorption peak at 318 mμ becomes confused with the 360 mμ absorption of the iodine–micelle complex, unless it is eliminated by a proper comparison. For aqueous and carbon tetrachloride solutions this factor does not arise, and it would then be permissible to use the pure solvent without iodine as the comparison solution.

Another complication arises if the original agent is itself colored. Our work with Span 80 (sorbitan monoöleate) introduced us to this difficulty. The original data failed to give the expected discontinuity. It then was necessary to measure the transmittance at 360 mμ of Span 80 solutions in benzene in the absence of iodine, as a function of concentration of the agent. These data provided a correction curve for the light absorption due to the colored constituents in the Span 80; by means of this curve the readings for the iodine-micelle complex were corrected

$$\text{Corrected \% transmission} = \frac{\text{Total \% transmission}}{\text{\% Transmission of agent}} \times 100$$

the discontinuity then became apparent.

We have applied the method to agents dissolved in carbon tetrachloride. This solvent displays the greatest change in absorption spectrum, and the method is correspondingly easier and less complex with carbon tetrachloride solutions than with either water or benzene.

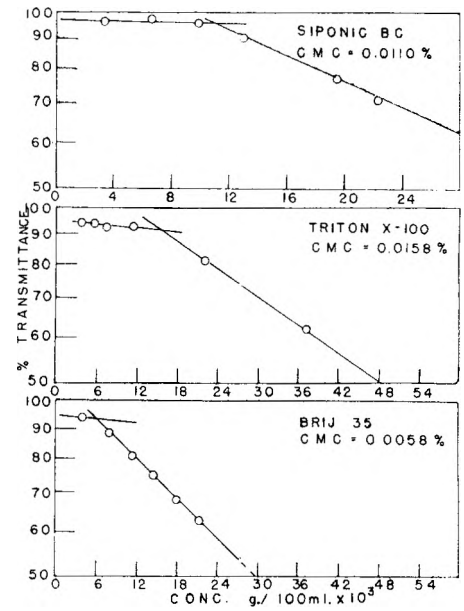


Fig. 2.—Log per cent. transmittance at 360 mμ of aqueous solutions of Siponic BC with iodine, Triton X-100 with iodine, and Brij 35 with iodine, as a function of concentration.

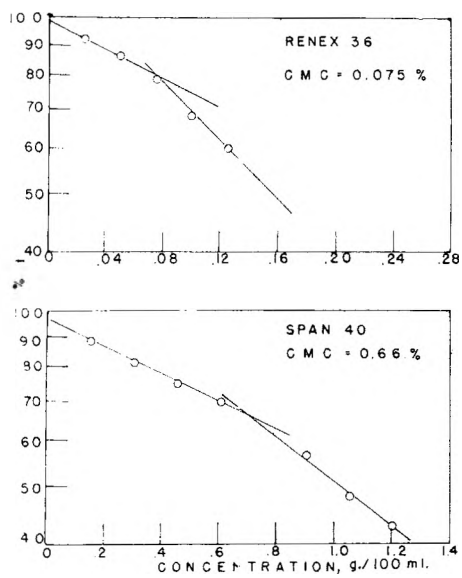


Fig. 3.—Log per cent. transmittance at 360 mμ of benzene solutions of Renex 36 with iodine and Span 40 with iodine, as a function of concentration.

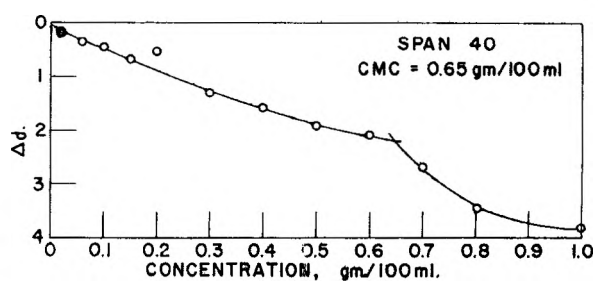


Fig. 4.—Relative differential refractive index at 25° of solutions of Span 40 in benzene as a function of concentration.

A few experiments have shown us that the method can also be used with solutions of surface-active agents in petroleum ether.

In connection with the development of the method, information about a number of pertinent points was obtained. That not already reported is mentioned below.

1. The concentration of iodine in the stock solution A was selected to be as dilute as possible, consonant with the maximum precision of measurement of the spectrophotometer. For water, the concentration used is about one-tenth of the saturated concentration; in the other solvents, much less than that. We find that higher concentrations of iodine slightly lower the CMC of the agents.

2. Solutions of iodine in water, benzene and carbon tetrachloride were all found to follow Beer's law for the variation of transmittance with concentration. According to Sidgwick[7] solutions of iodine in water do not obey Beer's law, but this was not our experience.

3. The micelle–iodine complex also behaves approximately according to Beer's law on dilution, though absolute concentrations could not be determined.

4. As the absorption maximum at 360 mμ develops with increasing concentration of micelles, the normal absorption maximum due to iodine molecules in solution shows a corresponding decline. When the absorption spectra of solutions containing different concentrations of surface-active agent, both below and above the CMC, are traced on the same record (as is done by the Spectracord), an isosbestic (or isoabsorption) point develops between the two absorption maxima. In benzene, for example, the isosbestic point occurs at a wave length of 455 mμ, between the two absorption maxima at 490 mμ and 360 mμ. The presence of this point is clear-cut proof that a simple equilibrium exists between the iodine molecules in the solution and those in the micelles, and that only one type of iodine–micelle complex is present in the solution. The simplicity of the system invites a thorough physico-chemical study, which offers promise to increase our knowledge of the association micelle.

5. Even at concentrations below the CMC, the presence of surface-active agent in solutions of iodine causes a decrease in the intensity of the light transmitted and the effect is proportional to the concentration of agent present (Fig. 2 and 3). This observation is evidence of interaction between iodine and agent of the same character as that at higher concentrations; that is, micelles are detected below the CMC. This result is predicted by mass law and has been reported previously as an experimental finding.[8]

We have discussed hitherto the use of light absorption as a method for detecting the CMC of the agent. Analytical methods are equally applicable and, though slightly more troublesome, may occasionally be preferable. The quantity of iodine solubilized as a function of the concentration of the surface-active agent has been measured by Allawala and Riegelman[1]; their results show no change of iodine solubility at agent concentrations below a critical value, thus marking a point that can be taken as the CMC. The method used was a volumetric titration of the total iodine taken into the aqueous phase after equilibration with a saturated solution of iodine in mineral oil. An experimental difficulty with this method is that the oil frequently forms a stable emulsion that prevents the separation of the phases. Equilibration of the aqueous solution with solid iodine, which can be separated by filtration, might prove preferable. An analytical method of determining the amount of iodine solubilized in non-aqueous solutions has not yet been developed.

(7) N. V. Sidgwick, "The Chemical Elements and their Compounds," Clarendon Press, Oxford, 1952, Vol. 2, p. 1145.

(8) For a discussion of this controversial point, see J. L. Moilliet and B. Collie, "Surface Activity," E. and F. N. Spon, Ltd., London, 1951, pp. 19–24.

**Acknowledgment.**—The authors gratefully acknowledge a grant-in-aid of research from the Atlas Powder Company. These students assisted with the experiments: E. F. Adams, C. E. Brukl, E. C. Chen, D. Frick, R. Stein and L. Zimkiewicz.

## DISCUSSION

F. M. FOWKES (Shell Development Company).—You have explained the very low critical concentrations for micelle formation of non-ionics by suggesting that the polar group is less hydrophilic than ionic materials. One might also note that for micelles of equal aggregation number, twice as many ionic particles are required to make up a micelle and the tendency to form micelles is proportional to the square of the concentration of ionic detergent but only the first power of the concentration of non-ionic material. If the equilibrium constant were the same for both micelles, a CMC of $10^{-2}$ mole/l. for ionic substances would correspond to $10^{-4}$ mole/l. for non-ionic.

S. Ross.—I was not aware of the point you mention and I thank you for the information.

F. M. FOWKES.—Is there any indication of the acid–base interaction of iodine with the ether groups, as has been demonstrated in the classical studies of Hildebrand and coworkers? The spectra should demonstrate easily whether iodine is solvated by hydrocarbons or by ether groups: in the former case it would be violet and in the latter case brown.

S. Ross.—We obtained measurements in compounds such as the Spans where ether groups are not present. Of course these materials are commercial mixtures and ether linkages may occur in the impurities. But we have also found the characteristic iodine-micelle color developed with relatively pure quaternary ammonium salts dissolved in benzene, where no ether groups are present; so we would be inclined to rule out the possibility of the acid–base interaction to which you refer.

W. A. ZISMAN (U. S. Naval Research Laboratory).—I would like to have you discuss the effects of dissolved salts and of temperature on the ability of iodine to serve as an indicator of micelle formation.

S. Ross.—We have rather scanty information about that. We are trying to measure the c.m.c. in the presence of salts. There is sometimes a very marked dependence on the temperature.

M. B. EPSTEIN (Colgate Palmolive Company).—Have you compared the absorption spectra obtained with aqueous solutions of iodine and polyglycols with those obtained for aqueous solutions of iodine and non-ionic surface active agents?

S. Ross.—They are similar but not identical.

# NON-IONIC SURFACE-ACTIVE COMPOUNDS. I. CRITICAL MICELLE CONCENTRATIONS OF WATER-SOLUBLE ETHER-ALCOHOLS

BY PAUL BECHER

*Chemical Research Department, Atlas Powder Co., Wilmington, Delaware*

*Received March 2, 1959*

The critical micelle concentrations in aqueous solution of commercial polyoxyethylene lauryl, stearyl, oleyl and tridecyl alcohols, as well as commercial polyoxyethylene sorbitan monolaurate have been determined by means of the iodine solubilization technique of Ross and Olivier. As found by previous workers, there is a linear dependence between the logarithm of the critical micelle concentration and the ethylene oxide content. However, it is found that (with the exception of sorbitan monolaurate) these lines vary only in slope from one alcohol to another, having a common intercept at zero ethylene oxide concentration. The sorbitan monolaurate line has a much higher intercept. The difference is ascribed to the difference in hydrophobicity of the non-ethylene oxide portion of the molecule.

The critical concentration for the formation of micelles has long been considered an index of surface activity. Although there exists, in principle, a large number of ways in which to measure this phenomenon, for all practical purposes most of the data in the literature have been obtained by at most two or three methods. Most of these are inapplicable to non-ionic compounds, either owing to the non-iongenity of the compounds themselves, or to the fact that the compounds are usually inhomogeneous chemically.

Recently, however, Ross and Olivier[1] have described an elegant method for the determination of the c.m.c.'s of non-ionic compounds which depends on the solubilization of, or complex formation with, elemental iodine. This method has been used in our laboratory for an extensive study of the critical micelle concentrations of non-ionic surface-active compounds. In the present paper, we report on our findings on ethylene oxide derivatives of some fatty alcohols.

## Experimental

**Materials.**—The non-ionics investigated were either commercially available materials or similar materials prepared under commercial conditions. The ethylene oxide mole ratios are nominal values based on the known preparative conditions. No attempt at purification was made, and the results reported correspond to the heterogeneous mixture which results on oxyethylation. For this reason, all c.m.c.'s are reported in terms of grams per deciliter. Reagent grade iodine and distilled water were used in making up solutions.

**Measurements.**—The technique used was essentially that described by Ross.[1] In some determinations, the entire spectrum of the solutions between 350 and 750 mμ was obtained by the use of a Beckman model DK-2 spectrophotometer. In other cases, measurements were made only at the wave length of the complex, using a Beckman model B spectrophotometer.

## Results

Measurements were carried out on commercial polyoxyethylene lauryl, stearyl, oleyl and tridecyl (Oxo-process) alcohols, as well as commercial polyoxyethylene sorbitan monolaurates, *i.e.*, TWEEN® 20 and its analogs.

The results are presented graphically in Fig. 1. As can be seen, these values are much lower than values reported for anionic compounds of comparable surface activity. They are generally of the order of magnitude of those reported by other authors, *i.e.*, $10^{-4}$ molar, assuming that average molecular weights calculated from composition have any real validity.

(1) S. Ross and J. Olivier, THIS JOURNAL, **63**, 1671 (1959).

As an indication of the reliability of the method, the following comparison between c.m.c.'s determined by iodine solubilization and by light-scattering for a series of lauryl alcohol derivatives may be cited. The values for the ethylene oxide ratio, the iodine-solubilization c.m.c., and the light-scattering c.m.c. are, respectively, 8, 0.0059, 0.0055; 12, 0.0065, 0.0065; 18, 0.0080, 0.0085; 23, 0.011, 0.014. The c.m.c.'s are given in units of grams per deciliter.

It will be noted that the graphical data show no points for compounds containing an ethylene oxide mole ratio greater than about 25. This is due to the fact that an appreciable deviation from the straight line occurs at higher ethylene oxide contents, the extent of the deviation being roughly proportional to the mole ratio. The deviation is presumably attributable to the high heterogeneity of such compounds.

## Discussion

In the case of ionic surface-active compounds, Klevens[2] has shown that a relation exists between the c.m.c.'s of a homologous series. This relation has the form

$$\ln c_0 = \alpha - \beta N \qquad (1)$$

where $c_0$ is the critical micelle concentration, $N$ is the number of carbon atoms in the chain, $\alpha$ is a constant for a given temperature and homologous series and $\beta$ is a constant whose approximate value is the logarithm of two.

That an analogous relation holds for non-ionic systems, where one can hold the hydrophobic portion of the molecule constant and vary the hydrophilic moiety in a systematic manner, has been shown by Hsiao, Dunning, and Lorenz[3] for the case of ethylene oxide derivatives of alkyl phenol. They found the relation

$$\ln c_0 = A + BR \qquad (2)$$

where $R$ is the ethylene oxide mole ratio (*i.e.*, the number of moles of ethylene oxide added per mole of hydrophobe), $B$ is a constant whose value depends on the electrolyte content of the solution, and is, according to the authors, independent of $A$.

That a similar relation applies for the series studied in our work is obvious from an examination of Fig. 1. However, the interesting observation which arises from the data presented therein, is the

(2) H. B. Klevens, *J. Am. Oil Chemists' Soc.*, **30**, 74 (1953).

(3) L. Hsiao, H. N. Dunning and P. B. Lorenz, THIS JOURNAL, **60**, 657 (1956).

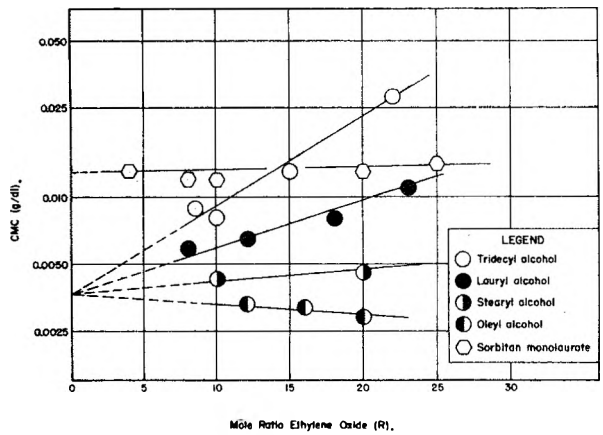


Fig. 1.—Relation between critical micelle concentrations of ether–alcohols and ethylene oxide mole ratio ($R$).

fact that the lines for the fatty alcohol derivatives apparently have a common intercept, while the intercept for the line corresponding to derivatives of sorbitan monolaurate is much higher. The equations for the lines are ($c_0$ being expressed in units of g./dl. $\times 10^4$)

Tridecyl alcohol:

$$\ln c_0 = 3.59 + 0.091R$$

Lauryl alcohol:

$$\ln c_0 = 3.72 + 0.038R$$

Stearyl alcohol:

$$\ln c_0 = 3.69 + 0.0068R$$

Oleyl alcohol:

$$\ln c_0 = 3.67 - 0.015R$$

Sorbitan monolaurate:

$$\ln c_0 = 4.87$$

The average intercept for the four fatty alcohols is $3.67 \pm 0.05$; or, putting it another way, they agree to within about 1%. This is actually better than the precision of the measurement, so the fact of a common intercept may well be accepted.

The intercept thus corresponds to a "critical micelle concentration" at zero ethylene oxide concentration of 0.0039 g./dl. It is a little difficult to ascribe a meaning to this quantity, but it is tempting to describe it as the "critical micelle concentration of a standard hydrophobic unit."

The radically different behavior of the sorbitan monolaurate derivatives is not unexpected and indeed was predicted. From one point of view, sorbitan monolaurate might be regarded as a long-chain polyhydric alcohol, and the intercept of the ln c.m.c.-$R$ line might well be expected to coincide with that of the other alcohols. However, as a result of the polyhydric character of the molecule, it possesses a fair degree of hydrophilic character, and this makes its behavior quite different from that of the ordinary alcohols. Indeed, it already has sufficiently polar properties to be surface-active, and the intercept may well correspond to a true critical micelle concentration. This fact remains to be determined.

It is interesting to note that the slope of the line is apparently a function of the chain length of the hydrophobic unit. The highly-branched tridecyl alcohol apparently has an effectively shorter chain than the lauryl alcohol, and the oleyl alcohol, with its double bond, is effectively longer than the stearyl alcohol containing an equal number of carbon atoms. Presumably ease of packing into micelles is the controlling factor here, and it appears that longer chain length is the favorable characteristic, since these corresponds to lower c.m.c.'s for a given ethylene oxide mole ratio. The high c.m.c.'s for the sorbitan monolaurate derivatives are thus probably attributable to the steric properties of the sorbitan ring.

**Acknowledgment.**—The kindness of Dr. S. Ross in describing the method of determination of critical micelle concentration prior to publication is gratefully acknowledged. Most of the measurements reported herein were carried out by Mr. M. J. Megraw and Miss Nancy K. Clifton.

## DISCUSSION

W. A. ZISMAN (U. S. Naval Research Laboratory).—What is the effect of the purity of these compounds?

P. BECHER.—The definition of purity for non-ionic surface-active agents raises a semantic problem. Obviously, they are quite heterogeneous. But they are reproducibly so. For example, if you take a given sample of, say, TWEEN 20 and examine its surface properties—surface tension lowering, c.m.c., etc., and then compare these with measurements on a second sample, one obtains the same results within quite close limits. Now if reproducibility of physical properties is a criterion of purity, I think that these may be considered pure compounds in the classical sense.

M. B. EPSTEIN (Colgate-Palmolive Company).—Would you care to comment on whether there is a relation between the points of extrapolation in Fig. 1 and the solubility of the hydrophobes?

P. BECHER.—As a matter of fact, the common intercept was somewhat surprising. What was expected, as you imply, was that the intercepts should increase with increasing solubility of the hydrophobe. Of course, this is a log plot, which would tend to obscure small differences. The very large difference for the sorbitan monolaurate shows up very well. On the other hand, we have data which show that nonylphenol and stearic acid derivatives of ethylene oxide share this common intercept.

# MECHANISM OF FORMATION AND STRUCTURE OF MICRO EMULSIONS BY ELECTRON MICROSCOPY

BY JACK H. SCHULMAN, WALTHER STOECKENIUS AND LEON M. PRINCE

*Contribution from the School of Mines, Columbia University; Department of Cytology, Rockefeller Institute for Medical Research; Emulsion Division, Reichhold Chemicals, Inc., Elizabeth, N. J.*

*Received June 8, 1959*

Optically isotropic transparent oil and water dispersions consisting of about equal volumes of the two phases from previous investigations were considered to be uniform dispersions of droplets of either water or oil in the appropriate continuous phase, whose diameters were from those somewhat greater than swollen micelles to values of approximately $^1/_{20}$ of the wave length of visible light. These systems were obtained by titrating to transparency with an amphiphile or polar hydrocarbon such as an alcohol which penetrated into the monolayer of the soap or detergent leaflet producing sufficient disorder to liquefy the interface. In the present work similar oil and water dispersions have been photographed directly in the electron microscope by staining available double bonds in the oil phase with osmium tetroxide. By this technique it has been established that such dispersions consist of uniform spherical droplets of either oil or water dispersed in the appropriate continuous phase and are, therefore, in fact, micro emulsions. It is proposed that the mechanism of formation of these micro emulsions consists of the penetration of the highly ordered soap or detergent micelles by any molecular species capable of producing sufficient disorder in, and hence liquefaction of, the bimolecular leaflets to enable the micelle to swell unlimitedly. In the presence of oil and water phases, surface tension differences across the interfacial monolayer impose the appropriate kind and degree of curvature on the dispersed droplets. A vapor condensed film is considered essential to the development of these micro emulsions. The necessary degree of disorder in the films was achieved in several ways: (a) penetration of a mixed interfacial film consisting of a complex of a soap or detergent and an amphiphile by a non-polar hydrocarbon originally derived from the oil phase. It has been demonstrated that such penetration can occur when the association between at least one member of the complex and the hydrocarbon is strong. (b) Use of large positive gegenions to make the resultant soap molecules asymmetric and thus produce disorder among the associating species in the film. (c) Penetration of a monolayer composed of asymmetric soap molecules by a molecular species derived from the oil phase which species associates with the soap monolayer but is sufficiently asymmetric therewith to produce the required disorder.

## Introduction

It had been considered by Schulman and collaborators[1,2,3,4,5] that optically isotropic, fluid, transparent oil and water dispersions consisted of uniform spherical droplets of either oil or water in the appropriate continuous phase and that the anisotropic viscoelastic birefringent systems consisted of an array of cylinders[6] under conditions where the systems were homogeneous.

The non-homogeneous systems have been studied mainly by Winsor[7] and very recently by Palit.[8] The diameters ($D$) of the droplets, where the volume of the interphase was largely calculated on the relationship $D = 6V/\text{I.A.}$ (I.A. = interfacial area, $V$ = volume of dispersed phase), are very small, of the order 100–500 Å. These could only be calculated indirectly from low angle X-ray measurements[3] giving center to center distances between droplets, from light scattering intensities at different angles[4] giving volume of the droplets, from ultracentrifuge[5] experiments giving sedimentation rates and hence again the volume of the droplets and from phase diagrams which indicated the number or ratio of the different polar molecules in the interphase, thus giving, from a knowledge of the area of the molecules, the total interfacial area.

It was considered important to establish directly the structure of these systems by a high resolution electron microscope. Recent improvements in the resolution of electron microscopes together with increased knowledge of staining techniques developed by the biologists have now made this possible, and initial electron microscope studies will be presented in this paper. These show that the droplet structures can be stained suitably to prevent them from disintegrating in the electron beam. The theory previously expressed was that soap or detergent micelles possessed an array of molecules too ordered to expand in the presence of a non-polar compound beyond certain small limits (10%), indicating that the monolayer of the bimolecular leaflet of the micelle aggregate was not truly in a liquid state and thus through surface tension differences take on a curvature. The formation of a curvature to the monolayer would permit droplets of either oil or water to form in the presence of the hydrocarbon. This previously was achieved by adding an amphiphile or polar hydrocarbon such as an alcohol which now penetrated into the monolayer of the soap or detergent leaflet producing sufficient disorder to liquify the interface, so that surface tension now could exert its influence and produce droplets of the dispersed phase, in the presence of the non-polar hydrocarbon. This dissolved between the bimolecular leaflet. These systems without the hydrocarbon form types of liquid crystals or myelenic structures.[9]

It will now be shown in this paper that the association between the molecules in the leaflet monolayer of the micelle and the molecules of the hydrocarbon in the dispersed or continuous phase is also very important for the study of the mechanism of formation of micro emulsions in general, and that certain rules can be established. This association can be controlled by changes in the

(1) T. P. Hoar and J. H. Schulman, *Nature (London)*, **152**, 102 (1943).

(2) J. H. Schulman and T. S. McRoberts, *Trans. Faraday Soc.*, **42B**, 165 (1946).

(3) J. H. Schulman and D. P. Riley, *J. Colloid Sci.*, **3**, 383 (1948).

(4) J. H. Schulman and J. A. Friend, *ibid.*, **4**, 497 (1949).

(5) J. E. Bowcott and J. H. Schulman, *Z. Elektrochem.*, **59**, Heft 4, 283 (1955).

(6) J. H. Schulman, R. Matalon and M. Cohen, *Disc. Faraday Soc.*, **11**, 117 (1951).

(7) P. A. Winsor, *Trans. Faraday Soc.*, **44**, 376 (1948); **46**, 762 (1950).

(8) S. R. Palit, V. A. Moghe and B. Biswas, *ibid.*, **55**, 463 (1959).

(9) B. J. Boffey, R. Collison and A. S. C. Lawrence, *Trans. Faraday Soc.*, **55**, 654 (1959).

detailed structure of the hydrocarbon portions of the associating molecules in the monolayer and oil phase, or by changes in the size and shape or ionization of the polar or ionic groups of the interfacial monolayer forming molecules.

## Experimental

The measurements were carried out in a manner similarly to Bowcott and Schulman,[5] where phase diagrams were composed by mixing two or three components together at a particular ratio and the whole system titrated to transparency by the addition of the final component. In previous work the soap suitably neutralized with potassium hydroxide together with the hydrocarbon such as benzene and water was titrated to transparency with a long chain hydrocarbon alcohol, and the d.c. electrical conductivity measured for phase continuity. In this work, since both water in oil and oil in water dispersions were required, the soap with alcohol and oil phase were added together and titrated to transparency with water under *p*H control. Over the high concentration range where the soap existed as an ion pair, where the ionic diffuse layer is suppressed, the system is that of water in oil dispersion and as further water is added the soap will become ionized and a high surface charge will develop and the continuous phase will invert to that of an oil in water micro emulsion.[5] For non-ionic surface active stabilizers, the solubility of the agent in either the oil or water phase controls the phase continuity[6] giving w/o or o/w, respectively. It will be shown that there is also the question of compatibility of the non-ionic agent with the chemical nature of the oil phase to be considered. Thus to emulsify a linear compound such as methyl methacrylate, a linear non-ionic agent such as a polypropylene/ethylene oxide copolymer must be used and not the single polar alkyl residue agents such as normal soaps or detergents.

**The Influences of Polar Additives on the Formation of Micro Emulsions in Relation to the Chemistry of the Oil Phase.**—In previous work[5] it has been shown that the chain length of a normal alcohol, when benzene was the oil phase and potassium oleate the micelle forming compound, was a governing factor in controlling the size of the droplets. Increasing the chain length greatly diminished the range of the phase diagram such that above decyl alcohol, no micro emulsions could be formed with this system. Only coarse emulsions could be formed of 0.5 $\mu$ diameter droplets. This occurred also with systems stabilized with cetyl alcohol or cholesterol and detergents such as the alkyl sulfates or amines when benzene was the oil phase. Now it is further known that the interfacial tension in the presence of the mixed monolayer at the interface was not greater than 0.1 dyne/cm. and thus, although the emulsions were spontaneously formed, no micro emulsions could be made. It was considered that the interfacial mixed monolayer was too highly condensed with the strong associating components and thus no great degree of curvature necessary for the very small droplets could be produced, a vapor condensed film being essential. In these considerations an important factor had been neglected, that of the association of the oil phase molecules with the components of the mixed interfacial film. Now it has been shown by Zisman[10] from measurements of the surface pressures exerted by duplex films of alkyl alcohols and hydrocarbons such as Nujol at different concentrations of the alcohols that the area per molecule of the alcohol molecule at the oil/water interface as deduced from the application of the Gibbs equation or from a two dimensional analogy of the Amagat equation of state

$$\pi(A - A_0) = xRT \quad (\pi = \text{surface pressure})$$

where a co-area $A_0$ of the molecule is determined, that the area of the alkyl alcohol is double that of the theoretical area (44–50 Å.$^2$). This indicated that the alcohol monolayer at the oil water interface was penetrated by the long chain mineral oil molecules, to form a 1:1 association; further, that surface pressures as great as 30 dynes/cm. did not force out the non-polar hydrocarbon molecule from the mixed alcohol film. On the other hand films of fatty acids at a benzene/water interface gave the correct surface area per fatty acid molecule, showing that the benzene could be ejected readily from the alkyl hydrocarbon chains in the monolayer at the benzene/water interface. It is known[11] that at the air/water interface the solvent hydrocarbon molecules used to spread monolayers can remain in the film, but can at moderate surface pressures be squeezed out and do not form stoichiometric associations even at low surface pressures.

The experiments summarized in Table I were carried out to test this idea, and show that if there is a possibility for the oil molecules to associate with the interfacial film molecules, a micro emulsion readily forms. This form of association can take place with either of the two monolayer forming components, but the micro emulsions are better if the association is with both.

Thus the system cetyl alcohol, benzene and oleate neutralized with 2-amino-2-methyl-1-propanol to *p*H 10.5 or above will give no micro emulsion, but if the oil phase is changed to a straight chain hydrocarbon varying in length from $C_7$ to $C_{18}$, micro emulsions readily form. But if the hydrocarbon chain is greater than $C_{18}$ the association with the $C_{16}$ alcohol again breaks down and no micro emulsions form, as seen with the long chain hydrocarbon paraffin waxes (see Table I).

But if now the alcohol chain is lengthened as in myricyl alcohol to $C_{32}$ or Ouricury wax and is equal to or greater than the chain length of the hydrocarbon oil, micro emulsions readily form again. In the case of the high melting waxes and alcohols, the systems solidify when cold, but the oil in water type remains transparent or with a tyndall effect although in this case the oil droplets will be solid. These latter systems were found to be very useful for the electron microscope experiments. In another example good micro emulsions could be formed when *p*-methylcyclohexanol was the alcohol, and benzene the oil phase, association taking place in this case with ring systems instead of straight hydrocarbon chains.

**Formation of the Amphiphilic Agent in Situ and Production of Lattice Disorder by Large Positive Gegenions.**—In the examples given the additive has been chosen in relation to its association with the oil molecules or with the soap or detergent molecules adsorbed at the oil/water interface. If soaps are used as the ionic agent the associated form can be used as the amphiphile additive and the system then becomes *p*H dependent. In Fig. 1 the titration curve of a standard soap such as potassium laurate, at different concentration is given with hydrochloric acid. It can be seen that there are two sharp inflections, one at *p*H 8.8 and the other at *p*H 6.8 for concentrations above the CMC. By an analysis of the acid soap at these two *p*H's, it can be shown that the composition is 1:1 and 2:1, respectively,[12] in ratio of the free fatty acid to soap molecules. The associated acid form readily dissolves in hydrocarbons leaving the soap molecules soluble in water. Thus it could be predicted that at *p*H 8.8 for soap solutions with the correct hydrocarbon (for soaps a straight chain hydrocarbon such as kerosene is essential) micro emulsions would form. This can be demonstrated in a striking manner (see Table I). The amphiphilic additive has a dual role not only of achieving association with the non-polar oil phase, but also produces disorder in the micelle lattice. This enables the micelle to swell unlimitedly in liquid form so that the interfacial tension can produce spherical droplets. In these systems, this was done by the use of large sized positive ions to produce a large polar group attached to the alkyl radical.[13] Good examples of this mechanism working are given, as with substituted amines.

Kerosene and stearic or oleic or linolenic acid + 2-amino-2-methyl-1-propanol (AMP) above *p*H 10.5 with equal quantities of oil to water gives *no* micro emulsion. On addition of boric acid to bring the *p*H to 8.7, an excellent micro emulsion is produced; 25 g. of kerosene + 10 g. of linolenic acid + 3 g. of AMP + 0.5 g. of boric acid + 25 g. of water yields a transparent water in oil dispersion. In this system at *p*H's above 10.5 a micro emulsion can be formed if an alcohol such as stearyl alcohol is added to replace the associated fatty acid, which becomes a soap molecule above *p*H 10.5 (Fig. 1).

Thus 25 g. of kerosene + 10 g. of oleyl alcohol + 8 g. of oleic acid + 2.5 g. of AMP + 25 g. of water *p*H >10.5 gives a good micro emulsion. This system can be improved if

(10) W. A. Zisman, *J. Chem. Physics*, **9**, 789 (1941).

(11) M. L. Robbins and V. K. La Mer, *J. Phys. Chem.*, **62**, 1291 (1958).

(12) F. V. Ryer, *Oil and Soap*, 23, 310 (1946).

(13) R. C. Pink, *Disc. Faraday Soc.*, **8**, 170 (1946).

TABLE I

AMP is 2-amino-2-methyl-1-propanol

| | Oil phase | Alcohols | Soap | Acid soap | *p*H | Transparent micro emulsion |
|---|---|---|---|---|---|---|
| 1 | N-$C_7$-$C_{18}$ | Cetyl, stearyl or cholesterol | AMP oleate | ..... | >10.5 | Good |
| 2 | N-$C_{10}$-$C_{12}$ kerosene | Oleyl | AMP–oleate or potassium oleate | ..... | >10.5 | None |
| 3 | N-$C_{18}$ | Cetyl or stearyl | AMP oleate | ..... | >10.5 | None |
| 4 | N-$C_{18}$-$C_{30}$ paraffin waxes | ($C_{32}$) myricyl | AMP oleate | ..... | >10 5 | Good |
| 4a | Micro-crystalline paraffin waxes $C_{18}$–$C_{30}$–$C_{80}$ | Ouricury wax | AMP oleate | ..... | >10.5 | Good |
| 5 | $C_{10}$–$C_{12}$ kerosene | ..... | ..... | AMP oleate | 8.8 | Good |
| 6 | Benzene | ..... | ..... | AMP oleate | 8.8 | None |
| 7 | Kerosene | ..... | AMP oleate | ..... | >10.5 | None |
| 8 | Benzene | ..... | AMP oleate | ..... | >10.5 | Good |
| 9 | Benzene | ..... | Ethanolamine or potassium oleate | ..... | >10.5 | None |
| 10 | Benzene | *p*-Methyl cyclohexanol | Potassium oleate | ..... | >10.5 | Good |
| 11 | Benzene | Cetyl or cholesterol | AMP oleate | ..... | >10.5 | None |

stearyl alcohol and stearic acid are used instead of the unsaturated compounds; this might be due to the solubility and stability of the amphiphile molecule in the oil phase and interfacial monolayer, respectively. None of these systems forms micro emulsions with the potassium soap unless the amphiphile molecule is strongly asymmetric with the soap molecule as in the systems previously studied, potassium oleate, *p*-methylcyclohexanol, benzene and water,[3,5] above *p*H 10.5.

An interesting case is with cholesterol, as the alcohol, no micro emulsions are formed when benzene or phenanthrene is the oil phase, and oleate is the ionic stabilizer. Micro emulsion in this case can be made if the association is made with the oleate radical in the monolayer. Thus good micro emulsions can be made if dodecane or kerosene is the oil phase and cholesterol the alcohol, the *p*H of this system should be above 10.5.

The question of disorder is important either with the nonpolar or polar portions of the associating molecules as shown in the examples given for AMP. Where disorder is required, AMP works very much better than di- or mono-ethanolamine or potassium as demonstrated. Increasing the temperature also helps this type of system as shown by Pink[13] for the monoethanolamine oleate benzene example, where heating produces the disorder. Substituting benzene for kerosene with AMP oleate again produces sufficient disorder to make good micro emulsion at *p*Hs > 10.5 (see Table I).

The fine differences in these associations or disorders are very much emphasized in Table I. It can be seen in example 5 giving a good micro emulsion, when the free fatty acid is the associating compound in the mixed acid soap interfacial monolayer. If the *p*H is increased to above 10.5 to remove the free fatty acid and oleyl alcohol is substituted no emulsion is formed (Example 2), since the polar groups of alcohol and carboxyl are not quite replaceable with one another. To achieve the fine balance of association needed, the system immediately becomes transparent on substitution of stearyl alcohol for oleyl alcohol (Example 1). It must be stressed that this example is given for kerosene as the oil phase. If this is replaced with any other oil slightly differing in constitution, the system again becomes unbalanced, as in the case (6) for benzene or case (10) for *p*-methylcyclohexanol as the associating alcohol. Continuation of the work started by Zisman on measurements of interfacial tension or spreading pressures of the different soaps or detergents in the presence of the different oils with or without the different amphiphile molecules, should put this type of investigation on a more quantitative basis.

**Phase inversion** is measured directly by the conductivity of the system (very high resistances being obtained for the oil continuous systems) or by the stability of the system to dilution with either oil or water.

In very high concentration of the soaps the system is nearly always water in oil; on dilution, for soaps below a certain value, the micro emulsion inverts and becomes charged. This necessitates an o/w emulsion.[5,14]

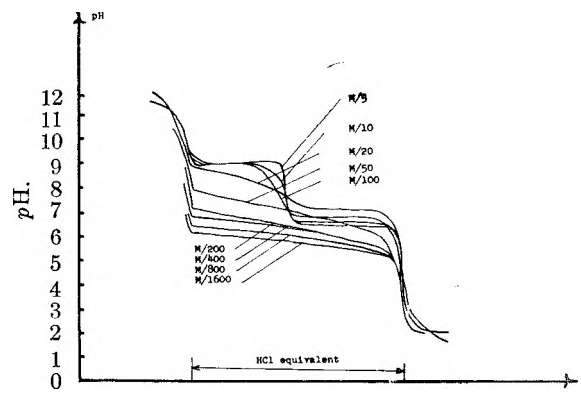


Fig. 1.—Potassium laurate titration at 25°.

During this inversion the system usually becomes strongly visco-elastic and anisotropic but again reverts back to an isotropic fluid system when in the form of an oil in water micro emulsion. The two micro emulsion forms, w/o and o/w, are isotropic and of low viscosity. Thus 20 g. of kerosene + 4 g. of oleic acid + 2 g. of AMP + less than 20 g. of water + 1.5 g. of boric acid (*p*H 8.7) gives a transparent isotropic, thin fluid, water in oil micro emulsion. On dilution to 30 g. of water the micro emulsion inverts to a transparent oil in water system, having passed through the anisotropic viscous phase. This system can be further greatly diluted with water and commences to scatter light, as the droplets are diluted.[4]

**Electron Microscope Studies of the Micro Emulsions.**—The transparent isotropic micro emulsions have been described in the first part of this paper as consisting of uniform spherical droplets of either oil or water in the appropriate continuous phase. Detailed methods of producing these systems have now been described and it should be possible to adapt the formulas to answer certain specifications.

The specifications required in order to investigate the structure of the micro emulsions by a high resolution electron microscope (Siemens EmI) is that the oil droplets in the one type of emulsion, *e.g.*, o/w must be resistant to the hot focused electron beam. In the staining of fats or proteins in biological tissue osmic tetroxide is used among other metal oxides and the tissue is bedded in a polymer such as methyl methacrylate or alkyl esters of this compound which do not change volume appreciably on polymerization. The

(14) J. H. Schulman and E. G. Cockbain, *Trans. Faraday Soc.*, 36, 661 (1940).

entire system is then microtomed to thin sections of 300–900 Å. thickness and the structure investigated direct without shadow casting.

It was considered that some of this technique might be adapted on similar lines to the study of the structure of the two classes of transparent micro emulsions. The oil in water systems could be directly stained by osmic acid if the oil phase is made reactive to this metal oxide. The water in oil systems likewise could be stained if proteins were added to the aqueous phase so that the water droplets could now be seen by the metal oxide staining adhering to the protein. In contrast to the oil in water system microtome sections would have to be made cutting through the small protein filled water droplets embedded in a standard polymer.

**Oil in Water Micro Emulsions.**—The initial reaction of osmic tetroxide with fats is primarily dependent on the availability of double bonds and only subsequently on the ionic groups such as carboxyl. The first reaction on the double bonds is extremely fast and is accelerated by the presence of a water phase and takes place in a few minutes; the second reaction on the polar group takes place in many hours or days. Most other heavy metal atoms react with the ionic polar group with the possible exception of manganese, and catalyze the oxygen uptake and bridging of the unsaturated double bonds inter-molecularly (polymerization). They also can oxidize the compounds further into breakdown products.[15] It can thus be seen that the more unsaturated the fatty acid is, together with the separation of the double bonds in the hydrocarbon chain in a non-conjugated form, the easier will the hydrocarbon chains be joined up intermolecularly in a type of osmic oxide polymer. Osmic acid interacts very poorly with oleic acid, better with linoleic and much better with linolenic. The repeat unit seen in the electron microscope pictures could be interpreted as those between the hydrocarbon portions of the molecules with osmic acid staining and between the polar groups of the fatty acid or phosphatidic molecules with other metal ions such as cobalt or barium. A combination of the electron microscope and X-ray pictures with the different metal atoms suitably placed in the polar or non-polar portion of the molecule should be a very useful device to study colloid structures, especially monolayers or systems built up from monolayer orientations, and work is now proceeding along these lines.

The simplest sources of unsaturated fatty acids are soy bean, tung oil and linseed oil glycerides. These form the basic components of alkyd resins when esterified with phthalic acid and glycerol and readily form micro emulsions with the correct stabilizers, according to the examples given in Table I. These systems take up osmic tetroxide very quickly, the oil droplets solidify in the process and can be washed or diluted and placed on a nitrocellulose film, dried and viewed in the electron microscope in the usual way.

A typical oil in water alkyd resin emulsion stabilized in this case with a mixture of linolenate and non-ionic emulsifying agents prepared with osmic acid is placed in a petri dish, inserted in a desiccator and a small vial of osmic acid powder is opened and laid on the desiccator shelf. The osmic acid vapor from the opened tube reacts in a few minutes with the emulsion system and solidifies the oil droplets. The diameter of the droplets can be assessed readily according to the previously described methods, such as $D = 6V/\text{I.A.}$, when the interfacial areas (I.A.) are taken from the area per molecule of the stabilizers as determined by Langmuir through techniques ($V$ = volume of the oil phase), and a further rough estimate also can be made from the intensity of the scattered light viewed at 90°.

The oil droplets seen in the high resolution electron microscope are completely spherical and become more uniform as the droplets are made smaller by increasing the concentration of the emulsifying agents as per the above formula. In the 1200 Å. diameter dimensions a considerable scatter is seen in the droplet diameters. In the range of 450 Å. diameter the droplets are uniform such that hexagonal packing is clearly visible on an electron microscope plate. Droplets of 250 Å. diameter can be seen clearly by the osmic acid staining technique at magnifications of 40,000 or 80,000 on the electron microscope plate. These pictures can be enlarged again by normal photographic processes.

These pictures will be published elsewhere in the appropriate journal. They were taken directly without microtoming or shadow casting. Stereo pictures could show whether this treatment causes any flattening of the oil droplets.

**Indirect Staining Methods.**—Attempts to stain oil droplets of the normal micro emulsion as shown in Table I, by addition of unsaturated hydrocarbons such as carotene to the oil phase, with osmic acid gave results in the electron microscope, which could be spurious. Strongly stained structures of uniform shape and approximately correct size were obtained. There is a possibility that these structures are osmic acid stained carotene particles uniformly dispersed by the emulsion stabilizing agents and have no relation to the size of the oil droplets of the original micro emulsion.

**Water in Oil Micro Emulsions.**—Good electron microscope pictures so far have not been obtained with these systems. Water in oil micro emulsions of osmic acid carotene stained Carnauba wax were prepared which could be microtomed. But the strains in the thin section on cutting could not be relieved in the normal way. Water in oil methyl methacrylate monomer micro emulsions were made with Pluronic F-68 and polymerized. These systems changed volume on polymerization and hardening and again proved negative in the electron microscope after microtoming. Work is now proceeding with proteins (gelatin) dissolved in the aqueous phase and the system embedded in methylmethacrylate and treated as biological tissue, the dispersed protein being made insoluble with formaldehyde.

**Acknowledgment.**—We wish to thank Dr. Henri Rosano for help on the soap titration work, Fig. 1.

(15) A. R. Gilby and A. E. Alexander, *Australian J. Chem.*, **9**, 347 (1956).

# SPREADING COEFFICIENTS AND HYDROPHILE-LIPOPHILE BALANCE OF AQUEOUS SOLUTIONS OF EMULSIFYING AGENTS

BY SYDNEY ROSS, E. S. CHEN

*Department of Chemistry, Rensselaer Polytechnic Institute, Troy, New York*

PAUL BECHER AND H. J. RANAUTO

*Atlas Powder Company, Wilmington, Del.*

*Received March 2, 1959*

It is shown that the stability of emulsions may be related to two spreading coefficients, one for water-soluble, the other for oil-soluble solutes. Since these spreading coefficients are shown to correlate with the empirical index of emulsion stability based on the hydrophile-lipophile balance (HLB) of the emulsifier, the effect of the structure of the emulsifier, the nature of the emulsion phases and the concentration of the emulsifier are explicitly considered. The spreading coefficient which is significant for the particular system relates to the spreading of the internal phase of the emulsion on the surface of a 1% solution of the emulsifying agent in the external liquid phase. Experimental data are presented indicating that for O/W emulsions instability results when the appropriate spreading coefficient is positive; optimum stability is obtained when the coefficient is barely negative, *i.e.*, *ca.* −1. For W/O emulsions, the indications are that the most negative value obtainable is the optimum one.

## Introduction

In any complete theory of emulsion stability, three factors must be explicitly introduced. These are, the structure of the emulsifier molecule, the concentration of the emulsifier used and the chemical and physical nature of the phases of the emulsion. No theory which has been developed up to now does this. The first and last of these factors have indeed been included in the somewhat empirical approach due to Griffin,[1] the so-called HLB number method. This technique has been widely used for the past decade as a guide in the formulation of emulsions, and, in spite of its pragmatic nature, represents a convenient index of emulsion stability, in the sense that an emulsion containing an emulsifier of the correct HLB for the phases involved may be expected to be intrinsically stable. Thus, even if it is possible to show that the stability of an emulsion is determined by a more fundamental property of the system, this property must correlate with HLB, and, of course, conversely. HLB numbers will be used in the subsequent discussion in this way, *i.e.*, as an index to the stability of a given emulsion system.

The present work is an attempt to demonstrate that emulsion stability, and *pari passu*, HLB number, may be correlated with a fundamental physical property of the system oil–water–emulsifier, namely, the spreading coefficient of the internal-phase liquid on the surface of a 1% solution of the emulsifying agent in the external phase. The discussion is limited mostly to oil-in-water emulsions, but sufficient data are presented to show that similar considerations apply in the case of water-in-oil systems.

**Materials and Methods.**—A series of emulsifying agents which provide a range of HLB numbers was obtained by mixing two primary agents, commercial sorbitan monooleate and polyoxyethylene sorbitan monooleate (Span[2] 80 and Tween[3] 80, respectively) in different proportions by weight. The oil phases used were: paraffinic mineral oil (Marcol GX-Esso); naphthenic mineral oil (Sun No. 91 Golden Oil); tricresyl phosphate (Celanese Cellulube 150); cottonseed oil (Wesson Oil); castor oil (Baker AA); perchloroethylene (du Pont Perclene); and xylene (Allied Chemical industrial pure grade).

The spreading coefficients were determined by the measurement of surface and interfacial tensions, using Cenco-du Nouy ring tensiometers, and applying the corrections of Zuidema and Waters.[4]

The spreading coefficients required to define the systems were calculated from the relations

$$S_1 = \gamma_{\text{soln. aq.}} - (\gamma_{\text{oil}} + \gamma_{\text{int.}})$$
$$S_2 = \gamma_{\text{soln. oil}} - (\gamma_{\text{aq.}} + \gamma_{\text{int.}})$$

where $\gamma_{\text{soln. aq.}}$ represents the surface tension of a 1% aqueous solution of the emulsifier mixture, and $\gamma_{\text{soln. oil}}$ represents the surface tension of a 1% solution of the emulsifier mixture in oil.

The measurements were made at ambient temperatures, usually about 24°. The variation of $S_1$ and $S_2$ due to a few degrees change of temperature is probably almost the same as the probable error of the calculation.

Comparative tests of emulsion stabilities at room temperature were made, using the apparatus[5] and the method[6] described by Griffin and Behrens. The emulsions were all prepared according to the formula 32% oil, 3% emulsifier, 65% water. The emulsifier was dissolved in the oil phase, and the emulsion prepared by mixing for five minutes in an Atlab shaker. Most stability observations were made after 24 hours storage at room temperature; in a few cases, shorter storage periods sufficed.

## Experimental Results

In Table I there are presented data showing the relative stabilities of a series of oil-in-water emulsions as a function of the type of emulsifier mixture used (hence of HLB), and of the spreading coefficient $S_1$ for the oil-water-emulsifier system corresponding to the given emulsion.

In Fig. 1, the same data are presented for one of the oils studied, castor oil, in a slightly different way, in order to illustrate the correlation existing between $S_1$ and HLB. Figure 2 shows the same relationship for $S_2$. The corresponding emulsion stability data for the latter curve are unavailable; however, as indicated above, a large body of earlier empirical data permits us to use the HLB as a measure of emulsion stability.

The relation between spreading coefficient and HLB shown in Figs. 1 and 2 is reproduced in its general features by all the other oils reported. The solute mixtures in the HLB range 8.6–15.0 have a linear dependence of $S_1$ with HLB; below 8.6 the

(1) W. C. Griffin, *J. Soc. Cosmetic Chem.*, **1**, 311 (1949).

(2) Registered trademark, Atlas Powder Co.

(3) Registered trademark, Atlas Powder Co.

(4) H. H. Zuidema and G. W. Waters, *Ind. Eng. Chem., Anal. Ed.*, **13**, 312 (1941).

(5) W. C. Griffin and R. W. Behrens, *Anal. Chem.*, **24**, 1076 (1952).

(6) W. C. Griffin and R. W. Behrens, *Agr. Chem.* **7**, 63 (1952).

Table I

Stability of O/W Emulsions as a Function of Spreading Coefficient, $S_1$, for Various Oil Phases[a]

| Emulsifier mixture (Tween 80/Span 80) | HLB | Paraffinic mineral oil $S_1$ | Stab. | Naphthenic mineral oil $S_1$ | Stab. | Tricresyl phosphate $S_1$ | Stab. | Cottonseed oil $S_1$ | Stab. | Castor oil $S_1$ | Stab. | Perchloroethylene $S_1$ | Stab. | Xylene $S_1$ | Stab. |
|---|---|---|---|---|---|---|---|---|---|---|---|---|---|---|---|
| 100/0 | 15.0 | 5.0 | u | 4.2 | u | 0.6 | u | 0.9 | u | 1.1 | u | 9.5 | u | 6.7 | u |
| 90/10 | 13.9 | 2.7 | u | 3.4 | u | − 1.1 | u | − 0.8 | u | − 1.4 | u | 7.6 | u | 5.0 | u |
| 80/20 | 12.9 | 2.0 | u | 1.5 | u | − 2.4 | ms | − 1.4 | u | − 3.0 | u | 6.4 | u | 2.0 | u |
| 70/30 | 11.8 | 0.0 | s | −0.7 | s | − 4.5 | u | − 3.8 | s | − 5.3 | ms | 4.4 | u | −0.3 | u |
| 60/40 | 10.7 | −0.2 | u | −1.8 | u | − 5.7 | u | − 4.9 | u | − 6.9 | ms | 2.9 | u | −1.7 | u |
| 50/50 | 9.7 | −0.9 | u | −5.2 | u | − 9.9 | u | − 9.8 | u | −10.1 | ms | −1.5 | u | −6.0 | u |
| 40/60 | 8.6 | −2.8 | u | −6.1 | u | −13.3 | u | − 8.7 | u | −11.4 | u | −2.6 | s | −5.3 | ms |
| 30/70 | 7.6 | −3.4 | u | −6.7 | u | −16.3 | u | −11.0 | u | −13.3 | u | −4.7 | si | −6.0 | si |
| 20/80 | 6.4 | −3.3 | si | −6.2 | u | −17.3 | u | − 9.5 | u | −14.7 | u | −4.8 | si | −5.9 | si |
| 10/90 | 5.4 | −3.0 | ui | −6.8 | u | −22.3 | ui | −11.4 | u | −14.7 | ui | −6.1 | u | −8.2 | si |
| 0/100 | 4.3 | −3.3 | si | −5.5 | u | −24.0 | ui | − 6.4 | u | −17.6 | ui | −6.6 | u | −3.2 | ui |

[a] s = stable emulsion; ms = most stable emulsion; u = unstable emulsion; si = stable invert emulsion; ui = unstable invert emulsion.

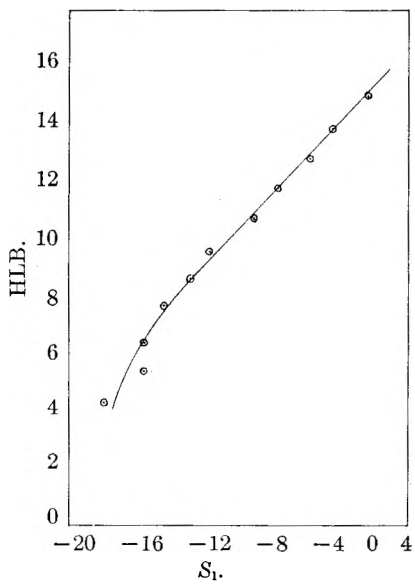


Fig. 1.—Spreading coefficients ($S_1$) of castor oil on a series of 1% aqueous solutions made with solutes of varying HLB.

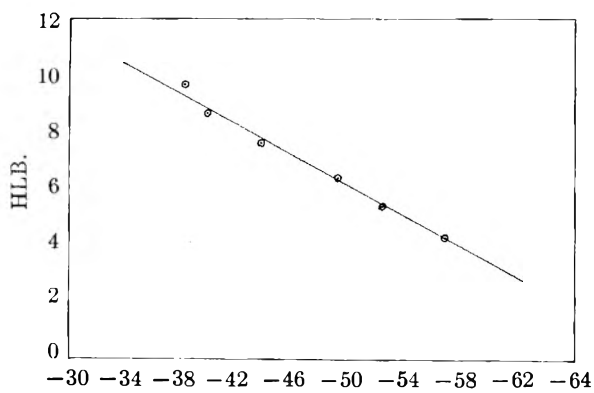


Fig. 2.—Spreading coefficients ($S_2$) of distilled water on a series of 1% solutions in castor oil of solutes of varying HLB.

solute mixture is not completely water-soluble and deviation from linearity occurs. In the HLB system of classification, the higher numbers refer to the more hydrophilic solutes. Such agents in aqueous solution do not greatly lower the surface free energy, so that oils, which *do* have low surface energies, will spread spontaneously on the aqueous subphase. This is consistent with the positive spreading coefficients shown in Fig. 1 at higher values of HLB.

The relation between the spreading coefficient $S_2$ and HLB shown in Fig. 2 is also typical of the behavior of all the oil solvents studied. A linear relation between HLB and $S_2$ holds for the solutes which can be dissolved to form 1% solutions in the oil. Here, the deviation from linearity occurs with solutes of higher HLB values, as these are progressively less soluble in oil.

## Discussion

Let us consider, for example, the fate of an oil droplet in an O/W emulsion. Imagine that this droplet rises through the emulsion (whether through creaming or as the result of random motion) until it reaches the surface. At this point one of two things will happen. In one case, the oil drop will spread on the surface and become a film of oil, losing its identity as a droplet. In the other, it will not spread and will, in due course, return to the body of the emulsion. In the first case, of course, repetition of the process leads to breaking of the emulsion. Clearly then, a negative spreading coefficient between the phases of the emulsion is necessary to ensure the stability of the emulsion.

Naively, we might suppose that stability would be ensured by a large negative spreading coefficient. However, examination of Table I shows that (within the admittedly wide limits imposed by the estimation of emulsion stability by visual observation) the most stable O/W emulsions are found when $S_1$ has a value which is only slightly negative, *i.e.*, 0 to *ca.* −5. The reason for this is not too difficult to find. Although the primitive view which correlated emulsion stability with low interfacial tension has largely been abandoned,[7] the effect of the interfacial free energy on the energetics of emulsion formation cannot wholly be disregarded. A low interfacial tension may be classed in category of what the mathematicians call a "necessary but not sufficient" condition for stability.

(7) P. Becher, "Emulsions, Theory and Practice," Reinhold Publ. Corp., New York, N. Y., 1957, p. 86.

We may therefore modify the requirement in terms of the spreading coefficient to be the *most negative spreading coefficient consistent with a low interfacial tension.*

In practice, this means, for O/W emulsions, a value which is barely negative, *i.e.*, *ca.* $-1$, as exemplified by the emulsion stability data of Table I. Although comparable stability data for W/O emulsions have not been obtained, the use of known HLB numbers as an index of emulsion stability permits the criterion here to be seen to be actually the largest negative value, a result which is consistent with the known interfacial tension data.

It should be noted that the emulsifier composition which yields the spreading coefficient of the appropriate value for stability corresponds to the HLB number which has previously been referred to as the "required HLB" for the particular oil phase under consideration.

Emulsifier concentrations of 1% have been arbitrarily used in this study. However, since the spreading coefficient varies with the concentration to some extent, it should be obvious that an undesirable value of $S_1$ may be adjusted to one corresponding to a stable emulsion by an adjustment in concentration. The effect of concentration is thus introduced in a fundamental way.

It should be noted that precisely comparable results are obtained when the HLB of the emulsifiers are varied by using different chemical types in systems containing the same oil phases.

From the practical point of view, the considerations of this paper permit us to substitute the relatively simple and precise measurement of a fundamental physical property of the system for the laborious and often imprecise determination of HLB.

## DISCUSSION

F. M. FOWKES (Shell Development Company).—Has your spreading coefficient been calculated using the surface tensions of both phases in equilibrium with the emulsifiers? Clearly this is required to fit the proposed mechanism of emulsion breaking by spreading.

P. BECHER.—No, this was not done. I agree basically with what you say; however, the question of experimental procedures arises. How would you partition the emulsifier between the phases? You could equilibrate the two phases, and then separate them and make the measurements. The resulting spreading coefficients might give us a better fit. This would be a very elegant procedure, but I don't think that it is pragmatically necessary.

F. M. FOWKES.—It would seem to me that if there were air bubbles in contact with the system during the making of the emulsion you would get spreading onto the bubbles and poor emulsion should result whenever the spreading coefficient is positive. However, if you could make the emulsion so that there was no air in contact the principle may not hold.

P. BECHER.—I think that what you are thinking about is the question of the ease of making the emulsion. Here, we are considering it after it has been made. I do think that the spreading of the two phases upon each other is a factor in the ease of emulsification, but the spreading coefficient involved there is a different one from what we have discussed in the present paper.

W. A. ZISMAN (U. S. Naval Research Laboratory).—There is plenty of evidence that emulsions are stabilized a great deal by mutual repulsion between the oil droplets, and that they break down by coalescence. However, this occurs in the bulk of the emulsion, and it does not seem possible that the mechanism you have described can make much of a contribution to the breakdown.

P. BECHER.—It is possible that there is no relation between the mechanisms. However, I must emphasize again that the view we have presented is a very much simplified one. For example, I can see—rather dimly, I must admit—that the *coalescence* of *flocculated* emulsion droplets might be controlled by the mutual spreading process.

# MONOLAYERS IN EQUILIBRIUM WITH LENSES OF OIL ON WATER. II DEPENDENCE OF EQUILIBRIUM PRESSURES ON *p*H AND ON CONCENTRATION OF SURFACTANT

By F. M. Fowkes, G. S. Ronay and M. J. Schick

*Shell Development Company, Emeryville, California*

*Received March 16, 1959*

The equilibrium spreading pressures ($\pi_w$) of oil solutions of surface-active substances on aqueous substrates can be measured easily and rapidly. These are found useful as analytical tools to determine type and concentration of surface-active substance in the oil phase. Surface active acids, bases, salts and non-ionizable substances are easily distinguished by the *p*H-dependence of $\pi_w$. The concentration dependence of $\pi_w$ can be used to determine the molecular area, and $\pi_w$ measurements of the supernatant oil can be used to measure surface areas of solids and heats of adsorption thereon.

In the preceding paper of this series[1] it was shown that the equilibrium spreading pressure $\pi_w$ of surface active substances in oil has a concentration-independent relation to $\pi_{ow}$, the equilibrium spreading pressure at the oil–water interface

$$\pi_{ow} - \pi_w = \Delta$$

These relationships apply to systems in which there is negligible depletion from the oil phase by adsorption of the surface active substance or by its solution into the aqueous substrate. The value of $\Delta$ was found to be zero for 1-*n*-octadecanol in white oil and 5.8 dynes/cm. for 1-*n*-tetradecanoic acid in the same oil on 0.01 *N* HCl at 25°. Earlier published data of Heymann and Yoffe[2] showed that for oleic acid in white oil $\Delta$ = 10.3 dynes/cm. Because $\Delta$ is independent of concentration, measurements of $\pi_w$ can be used analytically for many of the same purposes that one uses interfacial tension. Moreover, because of the greater ease and rapidity of measuring $\pi_w$, it is more useful for routine measurements.

## Experimental Details

**Methods.**—The surface film pressure of monolayers spread from lenses of oil solution on aqueous substrates was measured from the pull on a hanging vertical glass slide.[3] The glass slide was hung from one arm of a chainomatic analytical balance so that it dipped beneath the surface of water in a paraffined petri dish on the floor of the balance case. Calibration of the balance scale divisions in dynes/cm. was accomplished by adding weight to the opposite arm with the chainomatic device, with calculations based on the measured perimeter of the glass slide. Barriers of paraffined brass were used to sweep the surface clean before applying the oil solution. Usually five drops of oil solution were added and the film pressure $\pi_w$ was read every five minutes, with two more additions of two drops each within 30 minutes. Usually the pressure rose rapidly in the first three or four minutes and gradually levelled off well before 30 minutes. Petri dishes and barriers were cleaned and rewaxed prior to each measurement.

In the case of adsorption studies the supernatant liquid was separated from the adsorbent by centrifuging in a small clinical centrifuge. For studies of temperature coefficients of adsorption the centrifuge was operated in a large oven at the desired temperature.

**Materials.**—The water was twice distilled, the second time in dilute alkaline permanganate with a stream of water-pumped nitrogen to sweep out $CO_2$, and condensed in a block tin condenser. Buffered substrates of *p*H 2, 4, 6, 8, 10, 12 were prepared with HCl, sodium formate, potassium phosphate, sodium borate and sodium hydroxide. A light white oil (naphthenic), silica treated to remove oxidation products, was used as solvent for most studies, a silica-treated neutral lubricating oil in others. Silica gels or magnesia–silica gels used in adsorption studies were specially prepared in this Laboratory by L. B. Ryland. The oil-soluble amine used in adsorption studies was prepared in this Laboratory by forming the stearic amide of a dibasic amine ($NH_2CH_2$–$CHOH$–$CH_2NH_2$). Other surface active materials were obtained from usual sources, which are indicated in the text.

**Dependence of Equilibrium Pressures on *p*H.**—Values of the equilibrium pressure $\pi_w$ were determined with white oil solutions containing 0.5% by weight of (a) naphthenic acids (E. K., b.p. 160–198° (6 mm.) or (b) dodecylamine (Armour's Armeen 12D) or (c) dodecylamide (Armour's Armid 12) or a mixture of 0.5% each of both (a) and (b) on aqueous substrates buffered at *p*H 2, 4, 6, 8, 10 and 12 (Fig. 1). The shape of each curve is characteristic of the surface-active substance. The naphthenic acids and the dodecylamine are most surface-active at interfaces where dissociation of the hydrophilic group is promoted: alkaline substrates for the acids, and acidic substrates for the amine. This is interpreted to mean that the ionized molecules (soaps or salts) are much less soluble in the oil than the undissociated precursors, and back diffusion from the interface is therefore considerably reduced. On the other hand, the amide has constant $\pi_w$ values over the whole *p*H range. The mixture of surface-active acids and amines were highly surface-active over the whole *p*H range but showed maximum activity over neutral substrates.

Figure 2 shows how the *p*H-dependence of $\pi_w$ values can be used to follow interaction of surface-active substances. In this case the white oil containing 0.5% each of naphthenic acids and dodecylamine was heated at 120° for several days and the $\pi_w$–*p*H relationship was determined intermittently. The maximum characteristic of the dodecylammonium naphthenate soap is seen to disappear until a *p*H-independent relationship results. This is interpreted to mean that water was split out of the soap to give an amide.

Figure 3 shows the $\pi_w$–*p*H relationship observed with three different asphalts (diluted with oil until pourable (MC-2)) in order to illustrate how this method gives information about naturally-occurring surface active substances. Here a minimum in surface-activity is observed on neutral substrates, with greatest activity on alkaline sub-

(1) W. M. Sawyer and F. M. Fowkes, This Journal, **60**, 1235 (1956).

(2) E. Heymann and A. Yoffe, *Trans. Faraday Soc.*, **36**, 999 (1940).

(3) W. D. Harkins and T. F. Anderson, *J. Am. Chem. Soc.*, **59**, 2189 (1937).

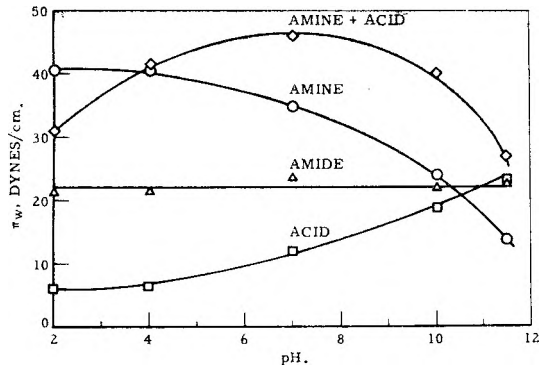


Fig. 1.—Dependence of spreading pressure of oil solutions of surface-active substances on $p$H of the substrate.

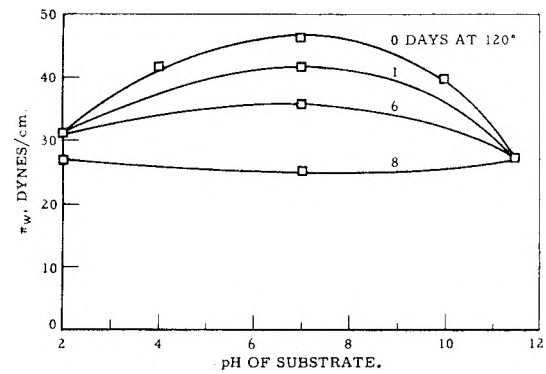


Fig. 2.—Effect of heating at 120° on $\pi_w$–$p$H relationship of white oil solution containing 0.5% of dodecylamine and of naphthenic acid.

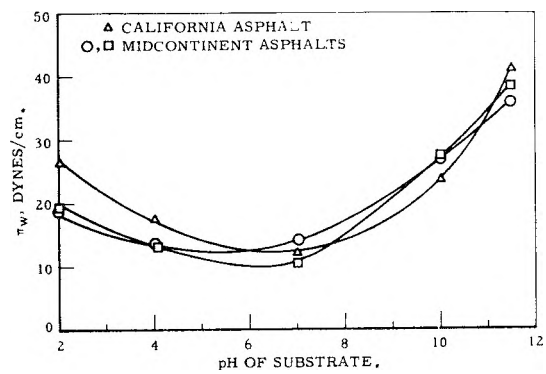


Fig. 3.—Relation of $\pi_w$ to $p$H of substrate for oil-diluted asphalts.

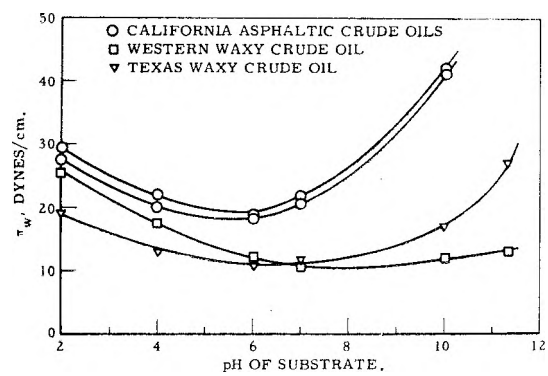


Fig. 4.—Characterization of surface-active substances in crude oils by the $\pi_w$–$p$H relation.

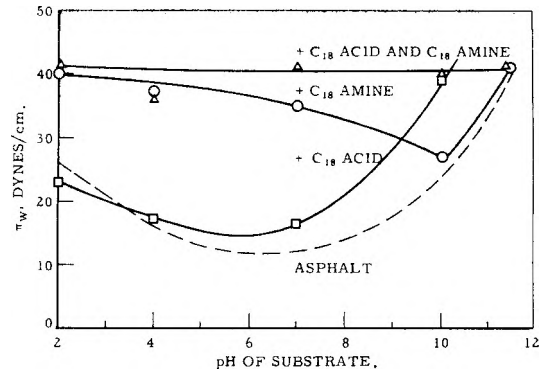


Fig. 5.—Use of $\pi_w$–$p$H relation to determine effect of additives on surface-activity of asphalts.

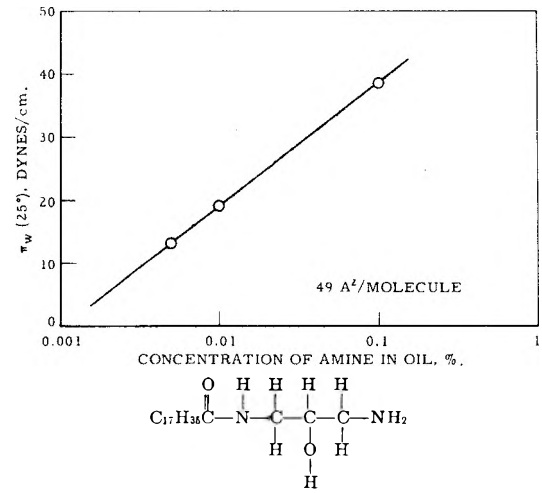


Fig. 6.—Concentration-dependence of spreading pressure $\pi_w$ of neutral oil solution of an amine.

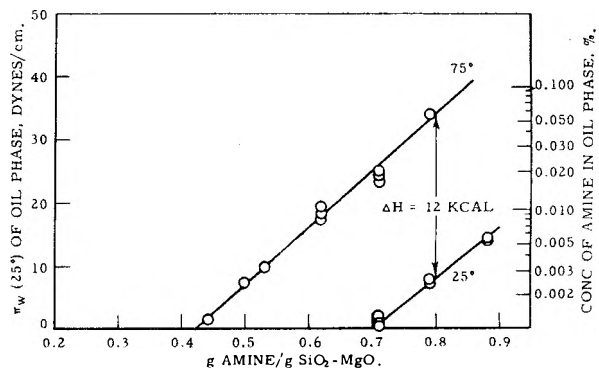


Fig. 7.—Concentration of amine in oil phase of silica-magnesia oleogel determined by $\pi_w$ measurements.

strates. It appears that asphalts contain both surface-active acids and bases, the acids being the more surface active. The minimum is quite the opposite of the maximum shown in Fig. 1 for a mixture of surface-active acids and bases. The minimum could very well result from molecules having both acidic and basic groups, such as in porphyrins or their residues.[4] These contain carboxylic groups (which over alkaline substrates give these substances the properties of surface active acids) and nitrogen-containing rings which often chelate metal ions. A ferric ion in such a ring has a

(4) H. N. Dunning, *J. Colloid Sci.*, **8**, 279 (1953).

single remaining positive charge in acidic media, but becomes a neutral hydroxide in alkaline media; it could thus act as a surface-active base.

Similar results were obtained with various crude oils (Fig. 4). Here it is seen that the $\pi_w$–$p$H relationship is characteristic of the type of crude oils; the greatest surface-activity is observed with asphaltic crudes.

The presence of added surface-active agents in oil products can sometimes be determined by the $\pi_w$–$p$H relationship. Figure 5 shows the effect of adding 1% each of oleic acid (Merck) or octadecylamine (Armour's Armeen 18), or 0.5% of both to an (oil-diluted) California asphalt. The amines raise the activity of the naturally-present bases, the acids raise the activity of the naturally-present acids, and the mixture eliminates the minimum over neutral substrates.

**Dependence of Equilibrium Pressures of Concentration.**—Figure 6 shows the dependence of $\pi_w$ on a substrate buffered at $p$H 8 of a neutral oil containing various concentrations of an oil-soluble amine derived by forming the mono-stearamide of the amine $H_2NCH_2$–$CHOH$–$CH_2NH_2$. The area per molecule can be determined from these data with the Gibbs adsorption equation[5]

$$\sigma = -kT \frac{d \ln a}{d\gamma_{ow}} = kT \frac{d \ln a}{d\pi_w}$$

if one assumes that the activity coefficient for the amine is constant in this concentration range. The results give 49 Å.$^2$ for the area per molecule of this amine.

(5) W. A. Zisman, *J. Chem. Phys.*, **9**, 789 (1941).

Measurements of $\pi_w$ are useful for determining the concentration of surface active agents. An application of this nature is illustrated in Fig. 7, showing adsorption equilibria of the above amine on a silica–magnesia gel in a neutral oil. The original aquagel had been transferred into the oil phase with a minimum of the amine used as a transfer agent and the remaining water cooked out. To several aliquots of the oleogel were added increasing increments of the amine, the aliquots equilibrated and centrifuged at a desired temperature and $\pi_w$ of the gel-free oil measured at 25° on a substrate buffered at $p$H 8. By reference to Fig. 6 the concentration of amine in equilibrium with the adsorbed monolayer can be determined. By means of the temperature coefficient of the concentration necessary in solution to give a monolayer of any desired packing, one can calculate the heat of adsorption, which in this case was 12 kcal. per mole. To determine the specific area of the gel, we must know the area per molecule in the adsorbed monolayer on the gel; Figure 7 shows this monolayer to be fairly compressible. We make the assumption that at $\pi_w = 0$ the area per molecule is 49 Å.$^2$ as was found for the oil/water monolayer under moderate to high film pressures; this value may be too small. At 49 Å.$^2$ per molecule, 0.7 g. of amine per gram of solid corresponds to 600 m.$^2$/g. for the surface area of the gel.

**Acknowledgments.**—The authors thank Miss Helen Robbins for making most of these measurements and Dr. M. W. Tamele for encouragement in these studies.

# BUBBLE STABILITY IN DIMETHYLSILICONE SOLUTIONS

BY MELVIN H. GOTTLIEB*

*The Research Laboratories, Interchemical Corporation, New York, New York*

*Received March 2, 1959*

The average lifetimes of bubbles on solutions of dimethylsilcones in benzene have been studied for four dimethylsilicone fluids of average molecular weights ranging from 162 to 30,000. The bubble lifetimes were measured from the most dilute solutions in which bubbles could be formed to concentrations greater than 10%. Surface tensions of the solutions and surface viscosity were also measured. It was found that stable bubbles were formed on solutions with less than 1% of the surface occupied by silicone molecules. There were no indications of surface viscosity at a concentration many times higher than that at which stable bubbles were formed. A loss in bubble stability was observed at high concentrations of the dimethylsilicones of molecular weights of 162 and 310. At the highest dilutions at which stable bubbles could be formed, it was necessary for the solution surface to age for a period of time before stable bubbles were obtained. This was interpreted in terms of migration of the silicone molecules to the surface.

## Introduction

The problem of the stability of foams and bubbles in organic liquids has not attracted the attention of investigators to nearly the same extent as has the corresponding problem in aqueous systems.[1] The most comprehensive work on bubbles and foams in non-aqueous systems is that of McBain.[2] Other papers on foaming in organic systems deal with empirical data regarding the foaming properties of solutions of amphipathic materials[3,4] and some data pertinent to the mechanism of bubble stability.[5,6]

This investigation was an attempt to gain an understanding of the factors involved in bubble stability in organic systems from the lifetimes of single bubbles, particular attention being paid to the concentration regions which are just sufficient for the formation of stable bubbles, in the expectation that the factors necessary for bubble stability would be accentuated under such conditions. In more concentrated solutions, a correlation between bubble stability and other measurable properties of the solution, surface tension and surface viscosity, was sought.

The systems of dimethylsilicone fluids in benzene were chosen for initial study for a variety of reasons. The effect of molecular size may be studied since the dimethylsilicone fluids are available, in pure form, over a wide range of molecular weights, ranging from what is essentially the dimer, tetramethyldisiloxane, to viscous fluids of molecular weights of the order of several hundred thousand. The silicones have low surface tensions; the relationship between bubble stability and surface tension depression should be most readily discernible in these systems. The silicones are also of intrinsic interest since in some systems they act as strong anti-foam agents while they have strong foaming properties in other systems. Benzene was chosen as a suitable solvent for the initial work because it has an intermediate surface tension, permitting an eventual comparison with solvents of both higher and lower surface tensions.

* Bell Telephone Laboratories, 463 West St., New York, N. Y.

(1) See *e.g.*, J. J. Bikerman, "Foams," Reinhold Publ. Corp., New York, N. Y., 1953.

(2) J. W. McBain, *et al.*, N.A.C.A. Wartime Report 4I05, 1943.

(3) E. J. King, THIS JOURNAL, **48**, 141 (1944).

(4) S. Ross and J. W. McBain, *Ind. Eng. Chem.*, **36**, 570 (1944).

(5) B. Y. Teitlebaum and E. E. Sidorova, *Coll. J. U.S.S.R.*, 401 (1952).

(6) J. W. Robinson and W. W. Woods, THIS JOURNAL, **52**, 763 (1948).

## Experimental

All glassware was cleaned by immersion in chromic-sulfuric acid cleaning solution, followed by rinses with tap water, distilled water and C.P. acetone. The glassware was then dried in a dust-free oven.

Bubble Lifetimes.—Bubble lifetimes were measured in an enclosed all-glass apparatus consisting of a flat bottom Pyrex dish, 15 cm. in diameter, with flanges which were ground to fit a similarly flanged cover. The dish and cover were clamped mechanically; no grease was used in any part of the apparatus. The bubbles were delivered by means of a micrometer driven syringe fitted to a 5 mm. glass tube which was drawn down at the tip to 1 mm. i.d. The bubbles were delivered about $^1/_2$ inch below the solution surface. Pressure build-up was avoided by means of a covered air outlet.

The apparatus was immersed in a constant temperature water-bath up to the flanges, about two inches above the solution surface. Erratic results were obtained when temperature gradients within the dish were sufficient to cause condensation of solvent on the walls of the dish. The temperature of the bath was 30.0 ± 0.1°.

In order to avoid spurious results due to bubbles caused by accidental contamination, two hundred ml. of pure solvent was first added to the apparatus. If no stable bubbles could be formed after the solvent had been in the apparatus for an hour, an aliquot of a stock solution was added, and the solution was thoroughly stirred. The apparatus was recleaned if stable bubbles were formed in pure solvent.

Surface Tensions.—Surface tensions of the silicone solutions were measured using both the capillary rise method and Sugden's two tube modification of the maximum bubble pressure method.[7] All measurements were done at 30.0 ± 0.1°.

The surface tensions by the capillary rise method were calculated assuming a zero contact angle between the solution and the walls of the capillary, using the expression

$$\gamma = \frac{1}{2} hdgr \qquad (1)$$

where $\gamma$ is the surface tension, $h$ the capillary rise which was measured to the nearest 0.1 mm. using a cathetometer, $g$ the acceleration due to gravity and $r$ the capillary radius. The radius of the capillary was determined from the capillary rise of pure benzene, taking the surface tension of benzene at 30° as 27.6 dynes/cm. and the density at 30° as 0.868 g./ml.[8]

The surface tensions by the maximum bubble pressure method were calculated using an alternate form of an expression given by Sugden

$$\gamma = AP + Bd \qquad (2)$$

where $A$ and $B$ are instrumental constants, $P$ is the difference in pressure needed to liberate bubbles from the small and large capillaries and $d$ the density of the solution. The constants $A$ and $B$ were determined using benzene and hexane as reference liquids, taking the surface tension of hexane at 30° as 17.4 dynes/cm. and its density as 0.652 g./ml.[8] For $P$ expressed in mm. of ethanol, the manometer fluid used, $A$ for the several capillary pairs used in this work was of the order of 0.8 and $B$ of the order of 0.2.

(7) S. Sugden, *J. Chem. Soc.*, **125**, 29 (1924).

(8) "International Critical Tables," McGraw-Hill Book Co., New York, N. Y., Vol. 3, pp. 29, Vol. 4, p. 434.

The densities of the various solutions were not measured, but were estimated from the densities of the pure components assuming a linear relation between density and volume fraction. The error resulting from this method of estimating density should not have exceeded 0.1% in any solution except possibly the 50% silicone solution, and was therefore well within the experimental accuracy desired for this work. Precision of each type of surface tension measurement was within ±0.2 dyne/cm.; accuracy on pure liquids of known surface tensions was ±0.2 dyne/cm.

**Surface Viscosity.**—Surface viscosity was measured by the oscillating disk method at 30.0°.[9] A 90 cm. length of 8 mil steel wire supported the oscillating disk. The moment of inertia of the oscillating system was 567 g. cm.²; the period was 17.3 seconds. The disk used had a radius of 2.54 cm. The measurements were made in a dish of 7.4 cm. radius, with a solution depth of 3.0 cm. Reproducibility of the instrument is such that a 10% change in the logarithmic decrement of the amplitude is significant.

Measurements were made on 1% solutions of each of the silicones over a period of at least 24 hours.

**Materials.**—C.P. grade benzene was distilled from sodium. Stable bubbles were not formed in benzene which had been treated in this way; benzene which had not been distilled from sodium gave bubble lives of the order of 5 seconds.

The silicone fluids were used as received from General Electric Corporation. Hexamethyldisiloxane (0.65 cs., mol. wt. = 162) will be referred to as the silicone dimer, decamethyltetrasiloxane (1.0 cs., mol. wt. = 310) as the silicone tetramer. The 100 cs. fluid (mol. wt. ≅ 8000)[10] is labeled SF-96 (100), the 1000 cs. fluid (mol. wt. ≅ 30,000) is labeled SF-96 (1000). The first two materials are essentially pure compounds with sharp boiling points. The higher molecular weight silicones may be expected to have the usual molecular weight distribution.

## Results

The data for bubble stability and surface tension of solutions of each silicone as a function of solution concentration are shown for the dimer and tetramer in Fig. 1A, for the 100 cs., and the 1000 cs. fluids in Fig. 1B.

**Surface Tension.**—The values for the surface tensions determined by the two methods agreed within experimental error (±0.2 dyne/cm.) for solutions of the higher molecular weight silicones and for many other solutions measured in this Laboratory. However, with solutions of the two low molecular weight silicones 1% and higher in concentration, the values by the maximum bubble pressure method were from 0.5 to 1.0 dyne/cm. lower than those from the capillary rise method. The reason for this discrepancy is not known. The qualitative conclusions to be drawn from the surface tension data are not affected. Arbitrarily, the capillary rise data were chosen for Fig. 1A.

The capillary rise was in every case independent of time from the attainment of temperature equilibrium (about ten minutes) to periods of several hours. Maximum bubble pressures were independent of rate of bubbling over a range of bubbling rates from 1 bubble every second to about 1 bubble every 30 seconds.

**Bubble Stability. A. Effect of Concentration.**—The stability of bubbles was studied as a function of solution concentration for concentrations ranging from the most dilute solutions which will give stable bubbles to solutions of concentrations of 10% and greater. No stable bubbles could be formed at concentrations less than the lowest shown.

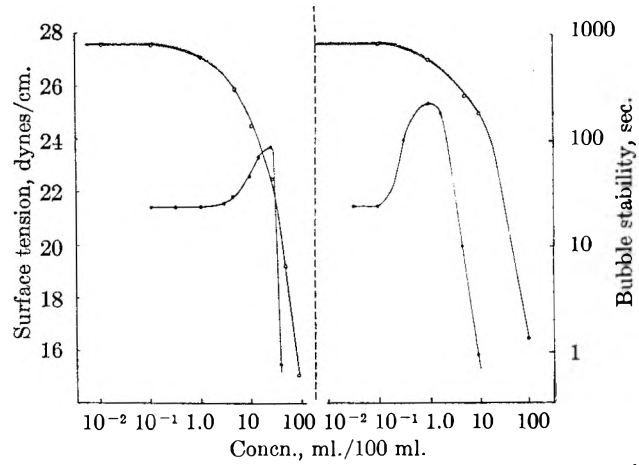


Fig. 1A.—Surface tensions (○) and mean lifetimes of bubbles (●); left for solutions of 0.65 cs. dimethylsilicone (silicone dimer); right, solutions of 1.5 cs. dimethylsilicone (silicone tetramer).

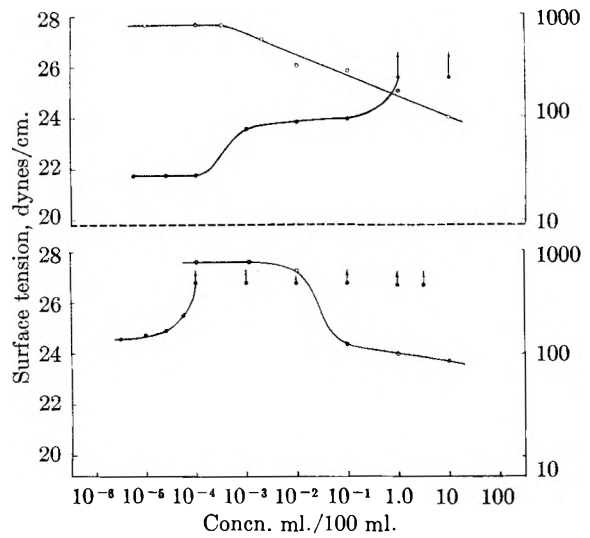


Fig. 1B.—Surface tensions and mean lifetimes of bubbles; upper for solutions of 100 cs. dimethylsilicone; lower, 1000 cs. silicones. ↑ indicates minimum value for bubble lifetime. ●

The data shown in Fig. 1 are mean lifetimes for bubbles on surfaces which are about 5 minutes old[11]; there is a small increase in bubble stability with time which does not alter the trends shown. The average deviation from the mean lifetime at each point is about ±20%.

**B. Effect of Surface Age.**—It was found that stable bubbles were not formed at fresh surfaces of the most dilute solutions in which bubbles could be formed. On standing, the probability of forming a stable bubble increased, until eventually all the bubbles which were initiated resulted in stable bubbles. The lifetimes of those bubbles which did not break immediately are, however, independent of the age of the surface. For the sake of illustration, the data for a $0.25 \times 10^{-4}$% solution of the 100 cs. fluid is presented in Table I.

(9) R. Bulas and C. A. Kumins, *J. Colloid Sci.*, **13**, 429 (1958).

(10) R. L. Merker, *J. Polymer Sci.*, **XXII**, 353 (1956).

(11) The data for the most dilute solutions studied omit the bubbles with a lifetime of zero seconds. See B, "Effect of Surface Age."

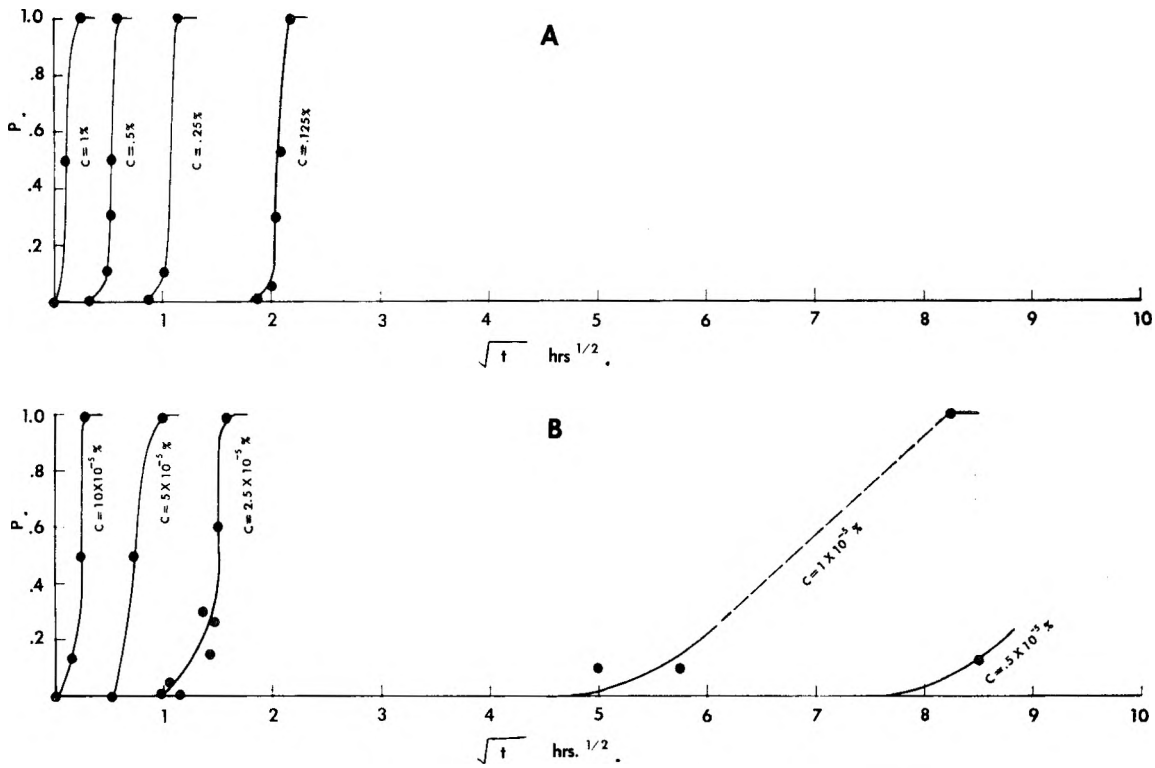


Fig. 2.—Fraction of stable bubbles formed as a function of age of surface. A, dimer; B, 100 cs. silicone.

TABLE I

EFFECT OF AGE OF SURFACE ON STABILITY OF BUBBLES
$0.25 \times 10^{-4}$ % 100 CS. SILICONE IN BENZENE
$T = 30.0°$

| Age of surface, min. | Bubble stability (sec.) | Fraction of bubbles which are stable | Mean lifetimes of stable bubbles (sec.) |
|---|---|---|---|
| 0 | 0 (10×) | 0.00 | .... |
| 30 | 0 (10×) | .00 | .... |
| 60 | 0 (10×) | .00 | .... |
| 75 | 0, 0, 0, 34, 0 (16×) | .05 | 34 |
| 85 | 0 (20×) | .00 | .... |
| 95 | 0, 0, 32, 0, 28, 0, 0, 32, 0 (4×), 27, 0 (4×), 33 | .28 | 30 ± 2 |
| 105 | 0 (3×), 34, 0 (6×), 37, 0 (3×), 30, 0 (5×) | .15 | 34 ± 2 |
| 120 | 31, 0 (5×), 33, 0, 31, 0 (3×), 35, 0 (6×), 32 | .25 | 32 ± 1 |
| 130 | 30, 39, 0, 40, 0, 40, 32, 25, 0, 38, 0, 39, 0 | .62 | 35 ± 5 |
| 150 | 42, 40, 37, 36, 24, 40 | 1.0 | 37 ± 4 |

The first column of Table I indicates the age of the surface, that is, how long the solution has remained undisturbed after a thorough stirring. The second column indicates the actual data for the lifetimes of consecutive bubbles at the various times. (0(10×) indicates that ten consecutive bubbles had lifetimes of zero seconds.) The third column is the number of bubbles with lifetimes greater than zero seconds divided by the total number of bubbles initiated at the respective time. The fourth column is the average of the lifetimes of those bubbles which did not break immediately.

If the solution is thoroughly stirred, the time course of the probability of forming stable bubbles is repeated accurately. Moderate disturbance of the solution surface, from ripples on the surface from vibrations due to the stirring motor in the thermostat bath, or from the breaking of bubbles, does not appear to affect the bubble stability properties. Stable bubbles appear at the same time regardless of the number of bubbles previously initiated or whether the stirring bath motor is on or off.

The fractions of stable bubbles, $P$, formed after various aging periods in dimer and 100 cs. silicone solutions of a range of concentrations are shown in Figs. 2A and 2B.

No stable bubbles were formed in pure benzene which had aged in the apparatus for up to 120 hours.

Analogous data were obtained with the tetramer and 1000 cs. materials. However, the data for the tetramer differed from that of the other systems in one important respect. At zero time, the bubbles had lifetimes of 1 to 3 seconds; with increased time the fraction of 1 to 3 second bubbles decreased and that of longer lived bubbles increased. There was a sharp separation in life-times between bubbles with lifetimes of 1 to 3 seconds and those with lifetimes of the order of 30 seconds, with no bubbles of intermediate lifetimes observed. Bubbles with lifetimes of 1 to 3 seconds in the solutions of the tetramer were considered to correspond to those with lifetimes of zero seconds in solutions of the other silicones.

In Fig. 3 the time necessary for the formation of stable bubbles ($P = 0.1$) is shown as a function of solution concentration for each system.

In order to determine the generality of the

previous results several experiments were performed at other temperatures and with bubbles of a smaller size. The aging phenomena were observed for a $5 \times 10^{-5}\%$ solution of the 100 cs. fluid at 20 and 40°. Qualitatively, the results were similar to those obtained at 30°: a gradual increase in the fraction of stable bubbles with increased age of the surface, with the mean lifetimes of the stable bubbles independent of the age of the surface. Similarly, measurements made on 0.1 and 1% solutions of the dimer and tetramer, reducing the bubble diameter from about 5 to 1 mm. by reducing the size of the capillary, indicated similar aging phenomena and the same nondependence of mean bubble life on solution concentration in this region. Quantitatively, a 10° increase in temperature resulted in about a 1.5-fold decrease in the aging period and about a twofold increase in mean bubble life. The reduction in bubble size resulted in a two- to threefold decrease in the aging period and a twofold decrease in mean bubble lifetime.

**Surface Viscosity.**—The damping characteristics of the surfaces of the silicone solutions were found to be identical with that exhibited by pure benzene. The surface viscosity was also measured at 25° in order to preclude the possibility that the surface viscosity might be critically dependent on temperature in the region in which bubble stability was measured. No increased surface viscosity was found at the lower temperature. The logarithmic decrement of the amplitude was found to be 0.041 ± 0.002 in all cases. This leads to a maximum value of 0.3 surface centipoises for the surface viscosity which might be present due to the silicones.[12] Cridle and Meader[13] have reported the absence of a surface viscosity of a 0.01% solution of a 350 cs. dimethylsilicone in a hydrocarbon oil.

## Discussion

The most noteworthy aspect of the data presented in Figs. 1A-1B is the formation of stable bubbles at very low concentration, indeed at concentrations from ten to a thousand times less than those at which a lowering of surface tension can be discerned by ordinary methods. The quantity of silicone which is at the surface in these solutions can be estimated in an indirect manner from the surface tension data of Fig. 1. Using the Gibbs adsorption isotherm

$$\Gamma = -\frac{1}{2.3RT}\frac{d\gamma}{d \log c} \qquad (1)$$

where $\Gamma$ is the surface excess in moles/cm.$^2$, $d\gamma/d \log c$ the slope of the surface tension log concentration plot of Fig. 1, $R$ the gas constant in ergs per mole per degree and $T$ the absolute temperature, we may calculate the surface excess for a dilute solution in which there is a measurable surface tension depression. Thus the slopes of Fig. 1A at 1% solution concentration are each about 1.6. Substitution of this quantity for $d\gamma/d \log c$ in equation 1 gives a surface excess of $2.7 \times 10^{-11}$ mole/cm.$^2$ for a 1% solution. A close-packed monolayer of molecules with a cross sectional area of 20 Å.$^2$ per molecule would correspond to a surface concentration of approximately $80 \times 10^{-11}$ mole/cm.$^2$ Even if the dimer and tetramer occupied the unreasonably high cross-sectional area of 100 Å.$^2$ per molecule, no more than 20% of the surface would be covered by these silicones in a 1% solution. It may therefore be assumed that the surface coverage is proportional to solution concentration at concentrations below 1%. Thus at the 0.1% solution of the dimer which is just sufficient for the formation of stable bubbles there are only $0.3 \times 10^{-11}$ mole /cm.$^2$ of the silicone; at the 0.03% solution of the tetramer there are only $0.1 \times 10^{-11}$ mole/cm.$^2$. Stable bubbles can then be formed when the order of magnitude of 1% of the surface is occupied by the low molecular weight silicones.

An identical calculation cannot be made for the higher molecular weight materials for several reasons. The Gibbs adsorption isotherm cannot be applied in a simple form as in equation 1 since this equation refers to two component systems; because of the wide molecular weight distribution present in polymers these solutions are multicomponent systems. Further, no estimate of the area occupied by the polymer molecules at the surface is available. Nevertheless, it is reasonable to assume that the solutions which indicate no surface tension depression do not have a complete monolayer adsorbed at the surface. As seen from Fig. 1B, stable bubbles are formed in solutions of the higher molecular weight silicones at concentrations of the order of one hundredth to one thousandth of those at which there is a measurable

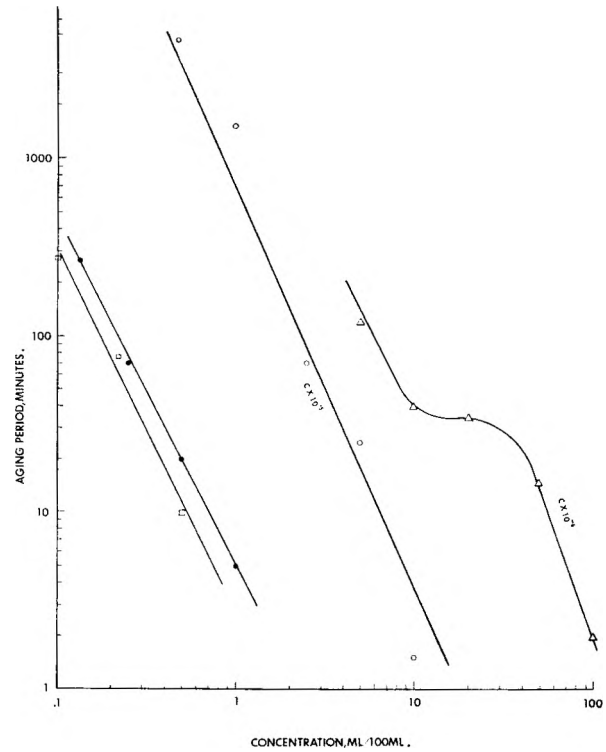


Fig. 3.—Aging period necessary before formation of stable bubbles as a function of solution concentrations: ●, dimer; □, tetramer; ○, 100 cs. fluid; △, 1000 cs. fluid.

(12) R. J. Myers and W. L. Harkins, *J. Chem. Phys.*, **5**, 601 (1937).
(13) D. W. Cridle and A. L. Meader, *J. Appl. Phys.*, **26**, 838 (1938).

surface tension lowering. If the adsorption at the surface is again assumed to be proportional to solution concentration at low surface coverage, we again reach the conclusion that stable bubbles can be formed when no more than 1% of the surface is occupied by silicone molecules.

As indicated by Fig. 1, the mean bubble lifetime is independent of solution (and hence surface) concentration at the concentration regions just sufficient for bubble stability in the silicone–benzene solutions. It thus appears that the role of the small quantities of silicone adsorbed at the surface in the very dilute solutions is to determine whether or not stable bubbles are formed, the lifetimes of the bubbles being only prolonged by larger amounts of silicone at the surface. With the exception of the 1000 cs. silicone resin, the mean bubble lifetime in the dilute solutions is about 30 seconds and the increase in mean bubble lifetime with solution concentration occurs at the concentration at which the surface tension lowering is first measurable.

Ross and Butler[14] have studied the role played by surface structure in foaming and anti-foaming action in aqueous systems. The effect on the bubble stability of the extremely small amounts of silicone which are present at the surface in the most dilute solutions is especially surprising in view of the fact that these materials were found to have no measurable effect on the surface viscosity at concentrations many times greater than those required for stable bubbles. Thus apparently the two factors usually assumed to be necessary for stable bubbles, surface structure and a significant difference in concentration between surface and bulk phases (ref. 1, p. 168) are not responsible for stability of bubbles in the dilute silicone–benzene solutions.

The sharp drop in bubble stability in concentrated solutions of the dimer and tetramer occurs in the same concentration region in which the surface tension falls most sharply with concentration. This is the concentration region in which the solution surface probably consists only of silicone molecules. Burcik[15] has observed a loss of bubble stability on aqueous sodium laurate solutions at a concentration at which the surface might be expected to be saturated with soap molecules. A decrease in the average lifetimes of bubbles under insoluble unimolecular films of ethyl palmitate and ethyl oleate on water with increase in surface coverage has been observed (ref. 1, p. 73). No work is known on bubble stability in organic solvents with adsorbed monolayers.

The induction period required for bubble formation in the dilute solutions indicates that a given quantity of silicone must migrate to the surface at these concentrations before stable bubbles can be formed.

According to the treatment of Ward and Tordai,[16] the quantity of material $M$ which has diffused to the surface after a period of time $t$ neglecting back diffusion is

$$M = 2n_0 (Dt/\pi)^{1/2} \quad (2)$$

where $n_0$ is the bulk solution concentration and $D$ the diffusion coefficient of the surface active material. If we assume that for each silicone a given quantity $M_0$ of material must diffuse to the surface before stable bubbles can be formed, the time for the formation of stable bubbles as a function of solution concentration should be given by

$$t_0 = \frac{M_0^2}{4n_0^2} \frac{\pi}{D} \quad (3)$$

Indeed, as seen in Fig. 3, a straight line, with a slope of approximately 2, was obtained when the logarithm of the time delay necessary for bubble formation in the dilute solutions was plotted as a function of the logarithm of solution concentration for the dimer, tetramer and 100 cs. silicone solutions.

However, if diffusion of surface active material to the surface is the rate-determining step in the formation of a surface on which stable bubbles can be formed, a reasonable value for the diffusion coefficient should be obtained from equation 3 and the data of Fig. 3. A simple calculation will indicate that values of $D$ obtained in this manner are unreasonably low. The surface of a 0.5% solution of the dimer must age for 10 minutes before stable bubbles can be formed. We assumed that 1% of a monolayer, *i.e.*, $10^{-11}$ mole/cm.$^2$ or $10^{-9}$ g./cm.$^2$ of silicone, has migrated to the surface in this period. Using equation 3 with $n_0 = 0.005$ g./cm.$^3$, $M_0 = 10^{-9}$ g./cm.$^2$ and $t_0 = 600$ seconds, a value of $D = 10^{-16}$ cm.$^2$/second is obtained. If it is assumed that a complete monolayer must migrate to the surface before stable bubbles can be formed, *i.e.*, $M_0 = 10^{-7}$ g./cm.$^2$, a value of $D$ of $10^{-12}$ cm.$^2$/second is obtained. Diffusion coefficients in liquids are usually of the order of $10^{-5}$ cm.$^2$/second. Thus the aging periods found are far too long for diffusion to the surface to be the rate-determining step in the formation of a surface on which stable bubbles can be formed.

It should be emphasized that equilibration times of the surfaces of dilute solutions which are too long to be accounted for by diffusion to the surface have been observed by many workers.[17] Addison,[18] for example, has observed equilibration times of the order of minutes for 0.001% solutions of decanoic acid in water. The problem of the rate of equilibration of dilute solutions of surface active materials is essentially unresolved. It is believed that the long aging periods required for the formation of stable bubbles on the dilute silicone solutions is a result of this general phenomenon and is not a peculiarity of the silicone solutions.

If, as postulated, the aging period is a result of the necessity for a sufficient quantity of solute to migrate to the surface, a decrease in aging period with increasing temperature would be anticipated. For the one solution studied over a temperature range, the $5 \times 10^{-5}$% solution of the 100 cs. fluid at 20, 30 and 40°, such a decrease was observed. Indeed a plot of the logarithm of the aging period as a function of the reciprocal of the absolute tempera-

(14) S. Ross and J. N. Butler, THIS JOURNAL, **60**, 1255 (1956).
(15) E. J. Burcik, *J. Coll. Sci.*, **5**, 421 (1950).
(16) A. Ward and L. Tordai, *J. Chem. Phys.*, **14**, 453 (1946).
(17) S. Ross, *J. Am. Chem. Soc.*, **67**, 990 (1945).
(18) C. C. Addison, *J. Chem. Soc.*, 579 (1946).

ture gave a straight line with a slope corresponding to an activation energy of 8 kcal./mole. This value is about twice that which would be expected if diffusion were the rate governing process.

**Acknowledgments.**—The author wishes to express his appreciation to Mr. R. Bulas for the surface viscosity measurements, and to Mr. H. F. Lamoreaux of the General Electric Corporation for his assistance in providing the various silicone fluids.

## DISCUSSION

W. A. ZISMAN (U. S. Naval Research Laboratory).—I can't help but think that the long diffusion periods are due to small quantities of an impurity, possibly a higher homolog, which must migrate to the surface before stable bubbles can be formed.

M. GOTTLIEB.—This is, of course, possible, but I think not likely. To obtain reasonable values for the diffusion coefficient, in the case of the dimer, for example, the concentration of the "impurity" would have to be about one ten thousandth that of the dimer (from equation 3). The "impurity" would have to have an extremely low surface tension in order to be appreciably adsorbed at the surface in the presence of this large excess of silicone. One of the reasons that these materials were chosen for this study was because it was considered unlikely that trace impurities would be more surface active than the silicones. Also, the method of preparation of the dimethyl siloxanes makes it improbable that higher homologs are formed.

J. J. BIKERMAN (Massachusetts Institute of Technology).—In interpreting the formation of stable bubbles in the very dilute solutions, did you consider that the concentration in the surface region might be appreciably greater than in the bulk because of evaporation of solvent?

M. GOTTLIEB.—The measurements were made in a closed system, so that the atmosphere was saturated with solvent. The silicone dimer has about the same vapor pressure as benzene; nevertheless, similar effects were found with the dimer as with the higher molecular weight materials. It is not believed that evaporation of solvent plays a significant role in the phenomena discussed.

# THE DESORPTION OF SODIUM DODECYL SULFATE SPREAD ON AN AQUEOUS SUBSTRATE

BY HENRI L. ROSANO AND GERHART KARG

*Contribution of Lever Bros. Co. Research Center, Edgewater, New Jersey*

*Received March 2, 1959*

Sodium dodecyl sulfate was spread on distilled water and on 5% and 20% NaCl solutions, and surface pressures were measured as functions of time. It was attempted to apply an empirical equation for rate of desorption of a soluble monolayer, extrapolating the pressure back to the time of initial spreading. This should permit calculation of the molecular weight of the detergent from the two-dimensional gas law, provided the measurements are made at sufficiently low surface concentrations. It was found that this approach is valid only when the rate of desorption is decreased by having sufficient electrolyte present in the substrate. A discussion of the mechanism of desorption of soluble monolayers is presented.

## Introduction

In 1955, it was demonstrated[1] that the surface micromanometer technique[2] could be used to determine the molecular weights of slightly-soluble substances from their film pressures. Saraga[3,4] has shown that lauric acid, which is slightly soluble in water, forms films whose surface pressure is a linear function of the square root of time shortly after spreading. It is therefore possible to obtain the surface pressure of the substance by extrapolating surface pressure *versus* square root of time to zero time. This suggested the possibility of studying spread surface films of relatively soluble substances by employing this extrapolation method.

Subsequently one of us (HLR) used this technique for measuring the molecular weight of dodecylbenzenesulfonic acid spread on water at very low pressures. The result obtained (323) was close to the expected value. In another study, this method was used for the determination of molecular weights of long-chain alcohol–ethylene oxide condensates. Our results were in good agreement with those determined by cryoscopic and infrared techniques.

The molecular weight of bovine serum albumin in water and in solutions of increasing amounts of sodium decyl-dodecyl-tetradecyl sulfates was determined. Bovine serum albumin spread on water gave stable film. However, solutions of bovine serum albumin in detergent gave surface films whose pressures diminished with the surface pressure of the film at time = 0, *i.e.*, the pressure which the film would exert if it were insoluble (no desorption). These studies will be published elsewhere.

Once the method had been proved useful, it appeared very desirable to define its limits. To what extent can we treat a soluble monolayer as an insoluble monolayer? Surface chemists classify monolayers as insoluble or soluble (adsorbed). The techniques used in studying these are different. The borderline between soluble and insoluble monolayers has not been investigated extensively. Better understanding of the similarities and distinctions between these two types of monolayers will greatly improve the utilization of our techniques. The present investigation was undertaken to determine whether sodium dodecyl sulfate could be spread at the water–air interface and studied as a surface film despite its solubility.

**Method of Calculating Initial Pressures of Soluble Films.**—Saraga[3,4] has found experimentally that for films of lauric acid at constant area there is a linear relationship between the logarithm the surface pressure and the square root of the time. Saraga developed a theory which can be summarized as follows: the desorption of the fatty acid molecules may be diffusion controlled, the diffusion

(1) H. L. Rosano, *J. Colloid Sci.*, **10**, 362 (1955).

(2) J. Guastalla, Cahiers de Physique. n°13. March 1943–1–17.

(3) L. Ter Minassian-Saraga, *Mem. Services Chimi. Etat (Paris)*, 3728 (1952). *J. chim. phys.*, **52**, 181 (1955).

(4) L. Ter Minassian-Saraga, *J. Colloid Sci.*, **11**, 398 (1956).

proceeding through a very thin layer immediately below the film. During desorption, an extremely thin layer of substrate adjacent to the film has a concentration $c$ in equilibrium with the spread film. The variation of the film area at constant pressure as a function of time was predicted and the correct value of the diffusion constant calculated. It appears, therefore, that in this case the possible potential barrier to desorption must be very low. Ward and Brooks[5] were led to an analogous conclusion when studying the transfer of fatty acids of low molecular weight across an oil–water interface.

In the case of desorption of a film at constant area, Saraga states that during a short time interval the pressure exerted by a film is a function of the density as

$$L_D p = \alpha \ln \delta + \beta$$

where $\alpha$ and $\beta$ are constants. From this she derived

$$\ln p/p_0 = -2\alpha \frac{C_\alpha(t)}{\delta(t)} \frac{\sqrt{D}}{\sqrt{\pi}} \sqrt{t}$$

where $C_\alpha$ is the concentration of a homogeneous solution in equilibrium with a film of $\delta$ surface density and $D$ is the diffusion constant. If the film loses molecules, it is only because the molecules of the liquid layer diffuse, the flux of the desorption being identical to a flux of diffusion. We have found that at pressures above 1 dyne/cm., our data fitted the equation $\log p/p_0 = K + K'\sqrt{t'}$. At pressures under 1 dyne/cm., satisfactory straight lines were obtained by plotting $p$ rather than $\ln p$ against $t_{1/2}$. Thus, it is possible to plot surface pressures as linear functions which may conveniently be extrapolated back to $t = 0$ in order to determine the initial surface pressure.

Since the plot of $\ln p$ against $t_{1/2}$ is a straight line, it is obvious that during the desorption process the ratio $C_\alpha(t)/\delta_{(t)}$ of the Saraga equation remains constant. This simply expresses the initial hypothesis that the solution below the film is in equilibrium with the film, so that $C_\alpha(t)/\delta_{(t)} = \text{const.}$

**Materials.**—The sodium dodecyl sulfate was recrystallized from alcohol. Its purity was indicated by the absence of any minimum in its surface tension curve. The water used was distilled and its purity was tested in the following way: calcined talcum powder was dusted on the water surface. The talcum particles were blown in one corner of the frame and removed two or three times with a fine glass tube connected to a vacuum line. After 4 minutes the amount of impurities was negligible as shown by close packing of the talcum particles when the surface was cleaned.

**Exploratory.**—It is possible to demonstrate the spreading of a detergent solution by dusting the surface of distilled water with talcum powder and allowing a droplet of solution to hit the surface. The powder will be observed to move away from the point of impact of the droplet. It is also possible by using a detergent solution dyed with methylene blue to show that the solution does not pass through the surface but rather that it spreads. After trying various concentrations of SDS, it was found that $M/10$ was satisfactory. This concentration was high enough to give surface pressures of up to ten dynes on distilled water without requiring use of an inordinately large amount of solution to obtain adequate surface pressure.

It was observed that different volumes of water containing the same amount of sodium dodecyl sulfate deposited on water gave fairly reproducible results for variation of surface pressure *vs.* time. It was also found that similar results were obtainable when water was replaced by 99% alcohol as solvent. The maximum volume of solution never exceeded 1 ml. and generally was less than 0.5 ml. At first glance, this result seemed puzzling because the thickness of the liquid layer varies with the volume of solution spread. But, the evaporation of water which is a continuous process, should bring all the molecules to the surface within a short period of time. The loss of water under ordinary conditions for 500 cm.$^2$ in 15 sec. will be 0.064 g., which means that 0.064 ml. of solution spread have evaporated, leaving only detergent on the surface. It is apparent that 0.25 ml. will evaporate in one minute. Hence, due to the evaporation of the water, the SDS should be on the surface within a short time.

(5) Ward and Brooks, *Trans. Faraday Soc.*, **48**, 1124 (1952).

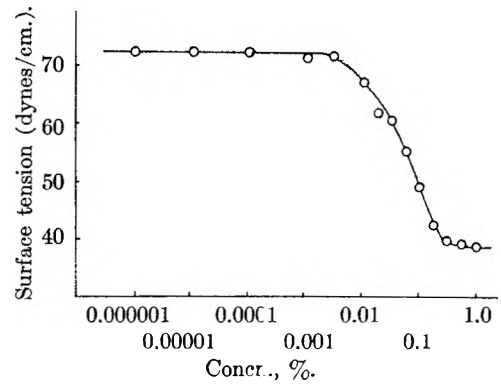


Fig. 1.—Surface tension *vs.* concentration; $t = 25°$; sodium dodecyl sulfate.

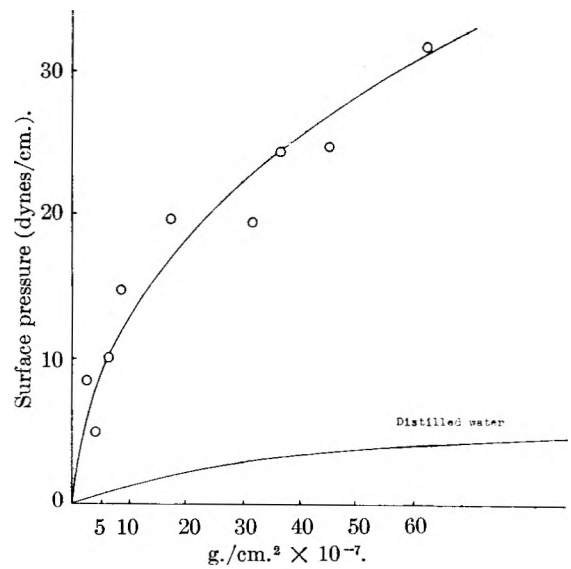


Fig. 2.—Sodium dodecyl sulfate on 5% sodium chloride.

**Determination of Force–Area Curve of Adsorbed SDS at Water Surface.**—Figure 1 shows the surface tension *vs.* concentration curve of SDS at 25°. The Wilhelmy plate method was used. Provided the adsorption process is a reversible one, which is usually the case with ordinary surface active agents, the area per solute molecule in the adsorbed film can be calculated from the Gibbs adsorption isotherm. The surface tension ($\gamma$) is plotted against the logarithm of the concentration, and then the slope d $\gamma$/d log ($C$) at any required value of the concentration is measured. The number of molecules per cm.$^2$ ($n$) is given by the expression

$$n = \frac{-1}{2.3kT}\left(\frac{\partial\gamma}{\log C}\right) = \frac{10^{16}}{3.2T} \times \text{slope}$$

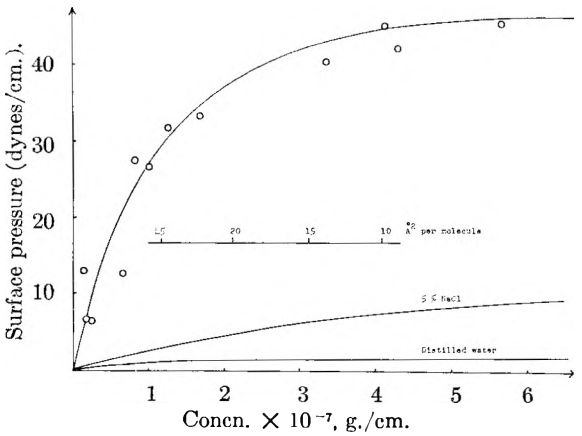


Fig. 3.—Sodium dodecyl sulfate on 20% sodium chloride.

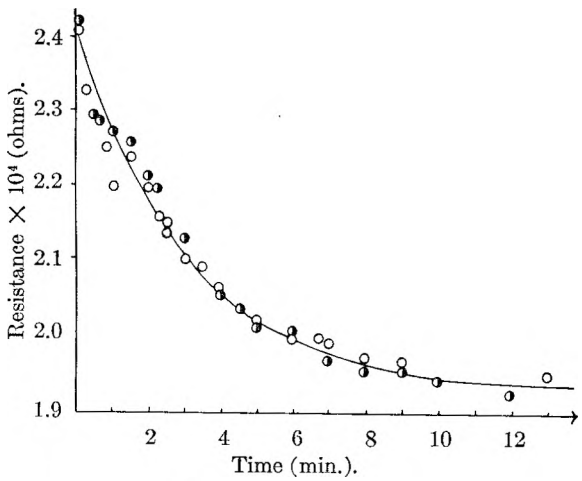


Fig. 4.—Surface concentration 1.27 × $10^{-5}$ g./cm.²; $t$ = 25°.

and at 25°, $\sigma$ = 953.6 × 1/slope (Å.²/molecule) where $\sigma$ is the surface area per adsorbed molecule. $\sigma$ was calculated by this method for several bulk concentrations and the corresponding surface pressures were calculated from the well known relationship

$$p = \gamma_0 - \gamma$$

where $\gamma_0$ is the surface tension of pure water and $\gamma$ is the surface tension of the solution. It has been claimed that one must take into account the dissociation of SDS.

**Desorption of Spread SDS at Constant Area.**—Since a spread film of SDS is soluble, its surface pressure tends to diminish with time. The experiment is performed point-by-point, *i.e.*, for each film concentration the substance is spread.

The assumption of complete dissociation led to a calculated surface isotherm with a high surface pressure portion corresponding to a molecular area of approximately 20 Å.² per molecule. Results close to this would be expected for this type of molecule. The surface pressure is plotted as a function of time, and the resulting curve is extrapolated to zero time.

The $p_0$ values (surface pressure at time = 0) thus obtained are then plotted as a function of the areas per molecule ($\sigma$) in the original spread films, and the isotherm is thus established. Saraga found good agreement between the isotherm of lauric acid determined in this manner and the isotherm determined by applying the Gibbs equation to the curve of surface tension *vs.* concentration.

The variation of surface pressure *vs.* square root of time for various surface concentrations of SDS spread on water were found to produce satisfactory straight lines. This suggests that the desorption may be diffusion controlled. But, the spread films led to a surface isotherm very different from the one calculated from the surface tension–concentration curve, giving unreasonable surface pressures as low as 1 Å.²/molecule.

The foregoing refers to the high-pressure portion of the surface isotherms which we established with the Wilhelmy-plate apparatus. We used the micromanometer (sensitivity 1/1000 dyne/cm.) in order to study very low surface pressures (in the gaseous region). It was found necessary to use $M/10{,}000$ SDS in 99% alcohol instead of water in order to obtain a satisfactory spreading at this low surface concentration. It was observed that even at low surface concentrations the SDS desorbed fairly rapidly. It was found that it was not necessary to plot log pressure *vs.* square root of time, since pressure *vs.* square root of time gave a satisfactory straight line.

The force–area isotherm was obtained from extrapolated $p$ *vs.* $t_{1/2}$ curves in the low-pressure region, where the adsorbed molecules should resemble an ideal two-dimensional gas. The theoretical surface pressures (from the ideal gas equation in two dimensions) for various molecular areas have been calculated. The results are shown in Table I. It can be seen that as the surface concentration decreases the difference between the experimental and theoretical values become smaller. Since the molecular weight is calculated from the extrapolated value of $C/p$ for zero concentration, the portion of the surface isotherm in which we are interested is that in which the experimental and the theoretical surface isotherms coincide. It is clear from the data for SDS on distilled water that the surface pressures did not extrapolate to correct values for time = 0. It would be desirable to carry these measurements to lower surface concentrations than 10,000 Å.² per molecule, but this is not feasible experimentally.

TABLE I

| Mol. area, Å.² | No. of molecules/ cm.² | Surface concn., g./cm.² | Theor. pressure $P = RT \times C/M$ (mdynes/ cm.) | Pressure extrapd. to $T$ = 0 from meas. on spread layer of SDS (mdynes/ cm.) |
|---|---|---|---|---|
| 10,000 | $1 \times 10^{12}$ | $4.75 \times 10^{-10}$ | 40.9 | .. |
| 5,000 | $2 \times 10^{12}$ | $9.5 \times 10^{-10}$ | 81.8 | 12 |
| 1,000 | $1 \times 10^{13}$ | $4.75 \times 10^{-9}$ | 409 | 24 |
| 500 | $2 \times 10^{13}$ | $9.5 \times 10^{-9}$ | 818 | 32 |
| 100 | $1 \times 10^{14}$ | $4.75 \times 10^{-8}$ | 4090 | 78 |
| 50 | $2 \times 10^{14}$ | $9.5 \times 10^{-8}$ | 8180 | 102 |

Apparently the rate of desorption is too fast even at these very low surface concentrations. In order to reduce the rate of desorption we repeated the ex-

periments spreading the SDS on 5 and 20% sodium chloride solution.

**Desorption of SDS Films on a 5% NaCl Solution.**—Sodium chloride solution was freed of surface active impurities by aerating the solution in a sintered glass funnel and removing the froth with a spatula. When the saline solution is free of surface active impurities, the froth is very unstable, breaking as soon as the filtered air flow is stopped. The purified solution then was placed in a glass trough of surface area = 244 cm.$^2$.

Various volumes of 0.2% SDS solution were spread on the surface of the 5% NaCl solution. The changes in surface tension were recorded as functions of time, using the Wilhelmy plate method. Before each spreading, fresh NaCl solution was placed in the trough and the surface was cleaned with the help of a capillary tube attached to a vacuum system, the surface being dusted with calcined talcum powder to follow the cleaning operation.

Log $p$ *vs.* $t_{1/2}$ was plotted for various surface concentrations. We extrapolated the upper portion of the curve to zero time, and from these extrapolated values we plotted the surface isotherm of SDS spread on a 5% NaCl solution (Fig. 2).

Similar measurements were made at low concentrations of SDS on purified 5% NaCl solution using the surface micromanometer. From the extrapolated values of surface pressure *vs.* $t_{1/2}$ we were able to obtain the surface isotherm (in the gaseous region) of SDS on 5% NaCl. By applying a modified van der Waals equation[1] we calculated a molecular weight (288 ± 10) very close to the expected one (288). Our conclusion is that the extrapolation is applicable to SDS in the gaseous region when the rate of desorption has been reduced by including sufficient electrolyte in the substrate. Using the same method for a 20% NaCl solution we obtained similar types of desorption curves.

Figure 3 shows the nominal surface isotherms obtained on 20 and 5% NaCl solutions and distilled water in the high-pressure region. The comparison of the three surface isotherms shows the salting-out effect of NaCl. The area per molecule is also shown on this figure. It was found that for concentrations greater than $1 \times 10^{-5}$ g./cm.$^{-2}$ a plateau is reached at a surface pressure of 45 dynes/cm.

**Explanation of the Shape of the Desorption Curves of SDS Spread on Distilled Water and on 5 and 20% NaCl Solution.**—On distilled water the curve of log $p$ *vs.* $t_{1/2}$ is a straight line for at least 7 to 8 minutes, whereas on a 5% NaCl solution there is a change in slope after approximately 4 minutes and on a 20% NaCl solution the change occurs at about 2.8 minutes. The explanation is apparent if one considers the dissociation phenomena involved. Before spreading, SDS *in* distilled water has a given degree of dissociation which is not changed appreciably when SDS molecules are spread on distilled water. On the contrary, when these SDS molecules are spread on a saline solution the degree of dissociation may become less because of the effective charge neutralization due to the presence of sodium ions. Since the surface pressure is due to the sum of the attractive and repulsive forces between the molecules in the surface, the presence of more and more neutralized (non-ionized) SDS molecules spread on a saline substrate will tend to produce a lower surface pressure than the identical surface concentration on distilled water.

**Change in Resistance of Distilled Water Covered by a Spread Film of SDS.**—In the first part of our study we followed the variation of surface pressure of sodium dodecyl sulfate monolayers as a function of time. In the second part we measured the conductivity of distilled water on which a film of detergent was spread as previously described. It was hoped that by measuring the change in conductivity, with the aid of a pre-established calibration curve, it would be possible to determine the change in concentration during the desorption process.

Two platinum electrodes 3.6 cm. in diameter were maintained at 8.7 cm. distance apart. The distance from the center of the electrodes to the water surface was 3.7 cm. The determination of the cell constant with 0.02 $M$ KCl solution gave a value of $K_{25}^{\circ} = 0.45478$. The cell was set up in a Pyrex trough which was in turn placed in an oil-bath maintained at 25°. The trough was filled with 1250 ml. of water. The free surface of the water was 226 cm.$^2$.

It was found that if a given volume of SDS solution (for example 1 ml. of $M/10$ SDS at 25°) was spread on distilled water, the curve of resistance *vs.* time was reproducible (Fig. 4). We spread different volumes of SDS solutions ($M/10$, $M/100$, $M/200$) and each time we obtained a similar type of curve. The rate of decrease of the resistance of the water changed rapidly at first, then the change became slow. We were unable to calculate any quantitative results from these experiments.

When the logarithm of the resistance of the solution was plotted against $t_{1/2}$ it was found that all the curves were similar, showing first a rapid decrease followed by a marked slowing down of the change of the resistance with time.

It is believed that the shapes of the curves can be explained as follows. First, the SDS molecules (which are spread on the surface following the capillary explosion) desorb from the surface into the water. Due to the convection currents in the bulk of the solution, a mixing effect takes place and the rate of change of the resistance of the solution slows down. The existence of these convection currents can be demonstrated by placing aluminum powder in a glass trough containing water.

## Conclusions

It is concluded that the desorption of SDS from aqueous surfaces follows the Saraga equation. At low surface pressures one can apply a simplified version of this equation, obtaining a linear plot of pressure *vs.* $t_{1/2}$. Provided sufficient electrolyte is present in the substrate, it is feasible to extrapolate the surface pressure of the SDS back to time = 0 and thus obtain the pressure exerted when all the SDS is at the surface. Surface isotherms of detergents can be established in this way. Molecular weights of detergents also can be determined.

# LIGHT SCATTERING BY SOME LAURYL SULFATE SOLUTIONS[1,2]

BY KAROL J. MYSELS AND L. H. PRINCEN

*Contribution from the Department of Chemistry of the University of Southern California, Los Angeles 7, California*

*Received October 2, 1958*

Light scattering from solutions of pure sodium dodecyl (lauryl) sulfate in water and in salt solutions and of the lithium and tetramethylammonium lauryl sulfates in water are reported. The solutions were clarified by filtration under conditions which greatly reduced hydrolysis of the ester link and contamination with lauryl alcohol. The effect of the interaction of the charged micelles with the other electrolytes present, in particular with the dimer of the lauryl sulfate ion, upon the meaning of the results is discussed, and the effect of the polydispersity of the micelles is considered. It appears likely that the weight average of the micelles is determined and that this varies from about 18,000 in water to 40,000 in 0.5 *M* salt. When lithium is substituted for sodium there is little effect on the micellar weight, while tetramethylammonium increases it appreciably.

The measurement of light scattering can be a powerful tool in the study of the size and charge of micelles of association colloids such as sodium lauryl (dodecyl) sulfate, but it is also beset with pitfalls which can lead to very substantial errors. One of us has previously reported with Phillips[3] measurements leading to a micellar weight whose accuracy was estimated at some 10%. The same system has been studied by others,[4-8] and results differing by up to a factor of two have been reported. While the present study was originally undertaken to explore other aspects of light scattering by these solutions, it discovered and overcame a number of potential sources of error in previous work. In view of the importance of absolute micellar weights in the interpretation of the nature and other properties of micelles, we are now reporting values which are believed to be much closer to reality but differ up to 25% from the previous ones. We also include measurements showing the effect of replacing the sodium ion by lithium and by tetramethylammonium ions.

## Experimental

**Apparatus.**—Our apparatus is a commercial[9] one based on the design of Brice and Halwer.[10] It has been carefully realigned and modified in a number of details: additional partitioning to reduce stray light was provided, and also an opening to permit direct observation of the solution along the 45° direction. The latter permits visual detection of dust particles which are too small to affect the measured turbidity and also examination of the homogeneity of the solution. The galvanometer was calibrated for linearity.

An important source of error was found in the insufficient monochromaticity of the original colored glass filters and an uneven absorbancy of the neutral light filters. As a result, the filter factors were non-additive and the constant *H* uncertain. Addition of interference filters (Baird Associates, Cambridge, Mass.) improved the monochromaticity to the point where only a single mercury line was visible in a pocket spectroscope, and an attenuation by a factor of at least $10^{-3}$ was measured in a recording spectrophotometer at the wave lengths of other strong lines of mercury. An additional criterion was provided by the identity of the filter factor of each neutral filter, whether it was measured alone or superimposed on the remaining filters. The combined filter factor of the latter varied from about $10^{-3}$ to $2 \times 10^{-5}$, depending on the particular combination and on the wave length.

**Standardization.**—We used as our standard a 0.25 g./ml. sucrose solution in water, for which we accepted Maron and Lou's[11] values $\tau = 3.38 \times 10^{-4}$ for $\lambda = 435$ Å. and $\tau = 1.32 \times 10^{-4}$ for $\lambda = 5461$ Å. Small deviations in concentration were corrected by using $\partial\tau/\partial C = 8.07 \times 10^{-4}$ and $3.08 \times 10^{-4}$, respectively, which are also based on their values. The solutions were clarified easily by their procedure of filtration after mixing with about 0.1 g./cc. of powdered active charcoal (Nuchar C-N). Several other procedures which were tried to avoid the use of charcoal were less successful. Bureau of Standards sample 17 and J. T. Baker C.P. sucrose gave identical results.

The concentration of the sucrose was determined on the filtered solution after the light scattering measurement because the charcoal adsorbs a significant amount of sucrose. Polarimetric determination was found sufficient after repeated checks with a refractometer showed that no hydrolysis occurs.

Our values of turbidity are therefore given by the expression

$$\tau_x = \frac{\left[\left(\frac{I_{90}}{I_0}\right)_x - \left(\frac{I_{90}}{I_0}\right)_w\right]}{\left[\left(\frac{I_{90}}{I_0}\right)_s - \left(\frac{I_{90}}{I_0}\right)_w\right]} \frac{f(n_x)}{f(n_s)} \tau_s = S\left[\left(\frac{I_{90}}{I_0}\right)_x - \left(\frac{I_{90}}{I_0}\right)_w\right] f(n)_x \quad (1)$$

where $\tau_s$ is the corrected turbidity of the sugar solution as given above. $I$ is the measured intensity on an arbitrary scale along the angle given by the subscript, $n$ is the refractive index, s refers to sucrose, w to water including any stray light, x to the solution studied, S is an apparatus constant obtained by this standardization

$$f(n) = n^2 [1.070 + 0.217 (n - 1.3340)] \quad (2)$$

Here the bracket expresses the $R_w/R_s$ refractive index correction of Brice, Halwer and Speiser[10] using the later and slightly different values given in the manufacturer's manual.[9]

This method of standardization has the following advantages. It involves the same procedure as the measurement, the turbidity of the standard is of the same order as that of the unknown; the refractive indices differ by little; the scattered light is similarly polarized; above all, the standard is universally accessible and easily reproducible. If Maron and Lou's values are revised, our results can be adjusted accordingly.

The apparatus constant S did not have a constant ratio to the constant *a* obtained by standardization with an opal glass.[10] Variations amounted to as much as 5%. Both constants as well as their ratio varied when the mercury lamp had to be replaced and also slowly during the lifetime of the lamp. This was probably due to changes in the distribution of light intensity in the mercury arc and conse-

(1) This work forms part of the doctoral dissertation of L. H. P., Utrecht, The Netherlands, 1959. Additional details may be found therein or in the 11th Technical Report ONR, project NR-051-254. It was presented in part at the 133rd National Meeting of the American Chemical Society, San Francisco, California, in April, 1958.

(2) This work was supported in part by the Office of Naval Research. Reproduction in part or in whole for the purposes of the United States Government is permitted.

(3) J. N. Phillips and K. J. Mysels, THIS JOURNAL, **59**, 325 (1955).

(4) E. Hutchinson and J. C. Melrose, *Z. physik. Chem.* (*N.F.*), **2**, 363 (1954).

(5) H. V. Tartar and A. L. M. Lelong, THIS JOURNAL, **59**, 1185 (1955); see also ref. 30.

(6) L. M. Kushner and W. D. Hubbard, *J. Colloid Sci.*, **10**, 428 (1955).

(7) W. Prins and J. J. Hermans, *Proc. Kon. Neder. Akad. Wet.* **B59**, 298 (1956).

(8) W. Prins, Thesis, Leiden, 1955.

(9) Phoenix Precision Optical Co., Philadelphia, Pa.

(10) B. A. Brice, M. Halwer and R. Speiser, *J. Opt. Soc.*, **40**, 768 (1950).

(11) S. H. Maron and S. R. L. Lou, THIS JOURNAL, **59**, 231 (1955).

TABLE I

REFRACTIVE INDEX DATA AND $H$ VALUES

| Solvent | Solute | $\lambda = 4358$ $\Delta\nu/\Delta C$ | $\lambda = 4358$ $\nu_0$[a] | $\lambda = 4358$ $H \times 10^6$ | $\lambda = 5461$ $\Delta\nu/\Delta C$ | $\lambda = 5461$ $\nu_0$[a] | $\lambda = 5461$ $H \times 10^6$ |
|---|---|---|---|---|---|---|---|
| $H_2O$ | LiLS | 0.1234 | 1.3397 | 4 161 | 0.1221 | 1.3339 | 1.638 |
| $H_2O$ | $(CH_3)_4$ NLS | .1207 | 1.3397 | 3.981 | .1193 | 1.3339 | 1.564 |
| $H_2O$ | NaLS | .1208 | 1.3397 | 3.988 | .1194 | 1.3339 | 1.567 |
| 0.03 $M$ NaCl | NaLS | .1205 | 1.3400 | 3.956 | .1192 | 1 3342 | 1 567 |
| .20 $M$ NaCl | NaLS | .1166 | 1.3418 | 3 714 | .1157 | 1.3359 | 1.479 |
| .50 $M$ NaCl | NaLS | .1097 | 1 3449 | 3.300 | .1095 | 1 3390 | 1.332 |

[a] Based on $(\Delta\nu/\Delta n)_{NaCl} = 0.01040$ and 0.01015 for blue and green light.

quently in the collimated beam. Standardization was therefore repeated after every important series of measurements.

**Preparation of Solutions.**—The solutions were clarified by filtration through ultrafine fritted Pyrex glass filters (max. pore size 0.9–1.4 $\mu$). The method previously employed of repeated filtration through a seasoned filter proved a serious source of difficulty when it was found that the fritted glass catalyzed the ester hydrolysis of the lauryl sulfate ion with formation of lauryl alcohol, especially after the glass has been treated with acid during cleaning. This was established by recovering traces of a material melting between 5 and 16° (presumably the alcohol) from an acid-washed filter through which a dilute solution of NaLS has been filtered, and also by finding a benzene-insoluble precipitate (presumably $BaSO_4$) upon addition of barium chloride to a lauryl sulfate solution filtered slowly through such a filter. While the amount of this hydrolysis is minute, it results in erratic higher turbidities of concentrated solutions and in dissymmetry and "milkiness" (when observed along the 45° direction) of solutions near or below the c.m.c.

A satisfactory procedure was the use of a filter which has not ever been exposed to acid, and which was cleaned by thorough washing with alcohol and ether and heating it overnight to 200°. This last treatment was found essential to remove traces of organic impurities. Water was then passed through the filter until completely clear. The lauryl sulfate solution was then filtered and the filter immediately rinsed with water. After some 5 or 10 portions of the solution had been filtered, the cleaning procedure was repeated. If any dissymmetry or milkiness was noted, the solution was discarded and the filter recleaned.

In order to avoid sources of dust, the filter was sealed to a bell-jar and the air entering the latter after filtration passed through a cotton-fritted glass filter. A rubber O-ring served to seal the base of the bell-jar to a glass plate and no grease was used. While dust still occasionally entered the solution during manipulation this was reduced to about once in five filtrations.

**Dissymmetry.**—The dissymmetry $(I_x - I_w)_{45}/(I_x - I_w)_{135}$ was determined for all solutions, and only those for which it did not differ significantly from unity were used. The uncertainty here stemmed mainly from the variation of straight light produced by external contamination of cell windows and amounted to no more than 0.02 for solutions of higher turbidity and 0.05 for those near the c.m.c.

**Depolarization.**—The depolarization

$$\rho^\mu = (I^v_x - I^v_{solvent})/(I^h_x - I^h_{solvent})$$

was determined for a 0.25% solution of NaLS considering water as the solvent and found to be appreciable (0.035 and 0.064 for green and blue light, respectively). This is presumably due to monomeric ions and unsolubilized impurities. A similar determination for a 0.5% solution considering the 0.25% solution as the solvent, showed no significant depolarization (0.006 and 0.000, respectively). This is the effect of micelles.

The sensitivity of the phototube varied only about 2% with the plane of polarization. In view of our method of standardization this required no correction.

**Refractive Increment.**—The refractive increment was determined using a differential refractometer similar to that of Brice and Halwer.[12] It was standardized with KCl solutions, assuming[13] $\Delta\nu_{blue} \times 10^{-3} = 0.1431C - 0.0001433C^2$ and $\Delta\nu_{gr} = \Delta\nu_{blue}/1.0350$. The results are shown in Table I. For NaLS our result agrees closely with those of Kushner and Hubbard[6] and of Tartar and Lelong.[5] Our values are based on the difference in refractive index between the solvent and a solution containing about 2% of the surfactant. The effect of the c.m.c. was corrected for by assuming a 3% change in $d\nu/dc$ at that point by analogy with the value found for sulfonates by Klevens.[14] The residual error should be quite small compared to the over-all accuracy.

**Materials.**—The NaLS used was completely independent of the samples previously studied in this Laboratory. The $n$-$C_{12}$ alcohol was a commercial sample of high purity prepared by fractional distillation and obtained from Applied Research Laboratories, State College, Pa. It was sulfonated with gaseous stabilized $SO_3$ ("Sulfan") in a stream of nitrogen, neutralized with NaOH, and repeatedly recrystallized and extracted with ether. Its conductivity was indistinguishable from that of the previously described samples[15] even in the c.m.c. region where it is most sensitive to impurities.[16] It may be noted also that the c.m.c. value found is exactly the same (0.234%) as reported by Wilson, Epstein and Ross.[17]

The lithium and tetramethylammonium salts were prepared by the method described elsewhere[18] by careful double decomposition of the corresponding halide with silver lauryl sulfate. To avoid traces of impurities which gave high turbidities at the c.m.c., the precipitation was conducted in water and the product recovered by freeze-drying (lyophilization) followed by extraction with ether to remove any remaining alcohol.

The presence of small amounts of lauryl alcohol in the compounds has little effect on the turbidity as long as it is all solubilized, *i.e.*, as long as the dissymmetry is substantially unity. Its effect is overwhelming, however, once it leaves the micelle.[1,19]

Commercial distilled water was used for preparing all solutions. After clarification by filtration, its apparent turbidity—which includes all stray light—was $4.75 \times 10^{-5}$ and $1.83 \times 10^{-5}$ cm.$^{-1}$, respectively, for $\lambda$ 4358 Å. and $\lambda$ 5461 Å. This is only about 26 and 20% over the theoretical values of $3.77 \times 10^{-5}$ and $1.53 \times 10^{-5}$ estimated on the basis of compressibility[20] and depolarization,[21] and compares with $4.84 \times 10^{-5}$ and 1.76 obtained experimentally in the determination of the turbidity of pure water by Kraut and Dandliker.[21]

**Selection of Values.**—A very large number of measurements have been discarded for definite reasons such as high dissymmetry, visible dust, or presence of impurities revealed upon further dilution to the c.m.c. A few stray values, both high and low, also have been discarded without a definite basis when they differed markedly from the bulk of the results or from the measurement at another wave length on the same solution. The retained values represent for each system at least two separate series of dilutions plus at least one check on a directly prepared more dilute solution.

## Results

The results of the turbidity measurements are plotted in Fig. 1 as $H(c - c_0)/(\tau - \tau_0)$ values. A

(12) B. A. Brice and M. Halwer, *J. Opt. Soc.*, **41**, 1033 (1951).

(13) Interpolated from Landolt-Börnstein's "Physikalisch-Chemische Tabellen," Springer, Berlin, 5th ed.

(14) H. B. Klevens, THIS JOURNAL, **52**, 130 (1948).

(15) P. Mukerjee, K. J. Mysels and C. I. Dulin, *ibid.*, **62**, 1390 (1958).

(16) P. Mukerjee and K. J. Mysels, *J. Am. Chem. Soc.*, **77**, 2937 (1955).

(17) A. Wilson, M. B. Epstein and J. Ross, *J. Colloid Sci.*, **12**, 345 (1957).

(18) P. Mukerjee and K. J. Mysels, THIS JOURNAL, **62**, 1400 (1958).

(19) L. H. Princen and K. J. Mysels, *ibid.*, **63**, 1781 (1959).

(20) C. I. Carr and B. H. Zimm, *J. Chem. Phys.*, **18**, 1616 (1950).

(21) J. Kraut and W. B. Dandliker, *ibid.*, **23**, 1544 (1955).

summary of the constants used and slopes and intercepts obtained is given in Table II. The critical micelle concentrations, c.m.c. or $c_0$, are based on conductometric data,[22,23] except in the two highest salt concentrations for which a linear extrapolation was used. For these latter solutions the use of the quite different value of Pethica[24] would not affect the results significantly because of the smallness of $c_0$.

For $\tau_0$ we used the turbidity at the c.m.c. This cannot be measured directly with the required precision in our systems because it is here that any impurity causes the greatest error. Hence $\tau_0$ was calculated by adding to the turbidity of the solvent the very small, computed turbidity of the solute, assuming that it behaves as an ideal electrolyte. This correction amounted to at most $0.135 \times 10^{-5}$ but increased nevertheless substantially the linearity of the $Hc/\tau$ plot at low concentration .

TABLE II

THE OBSERVED INTERCEPTS $A$ AND SLOPES $B$ OF THE LINES OF FIG. 1 AND THE CHARGES $p$ AND DEGREES OF ASSOCIATION $m$ CALCULATED THEREFROM ASSUMING PARTIAL DIMERIZATION

| Solute | NaCl, $M$ | C.m.c., % | $A \times 10^5$ | $B \times 10^3$ | $p$ | $m$ |
|---|---|---|---|---|---|---|
| LiLS | 0 | 0.239 | 77.3 | 37.55 | 14.2 | 63 |
| $(CH_3)_4NLS$ | 0 | .188 | 47.8 | 26.83 | 14.0 | 76 |
| NaLS | 0 | .234 | 69.5 | 20.61 | 10.4 | 62 |
| NaLS | .03 | .090 | 51.0 | 3.75 | 10.2 | 72 |
| NaLS | .20 | .026 | 36.0 | 0.75 | 15.6 | 101 |
| NaLS | .50 | .015 | 25.7 | 0.30 | 21.9 | 142 |

## Interpretation

In a two-component uncharged system the intercept of the $Hc/\tau$ line gives directly the particle weight. In our case of a charged colloidal particle in the presence of small ions—the unmicellized ions and any added salt—the situation is more complicated. It can be treated rigorously if one assumes that the small ion has a constant concentration above the c.m.c. and that the micelles have a constant *effective* charge $p$. The meaning of effectiveness in this case is that it takes care of all the nonidealities of the system. Mysels[25] and, more rigorously, Prins and Hermans[26,6] have thus treated the case of monodisperse micelles in the presence of monovalent ions.[27] We have pointed out elsewhere[28] how this can be applied and how it is changed if the small similiions are divalent. The latter point became important when detailed study of dilute solutions showed[15] that the $LS^-$ ions could only exist in equilibrium with their dimer $(LS)_2^{--}$.

Better insight into the meaning of our results required the solution of the basic equations for the remaining three component systems: micelles–monomer–dimer and micelles–dimer–salt. These were obtained following the procedure outlined previously[8] and starting from basic equations analogous to those given by Prins and Hermans.[8,26] The result gives the micellar degree of association $m$ and effective charge $p$ in terms of the experimental intercept $A$ and limiting slope $B$ of the $H(c - c_0)/(\tau - \tau_0)$ line.

For micelles in the presence of a mixture of monomer and dimer we find

$$p = \frac{\sqrt{2(n_1 + 3n_2)B} + 2(n_1 + 3n_2)BM_1E}{A - A^2M_1E} \tag{3}$$

$$m = \frac{1}{AM_1} + \frac{2E\sqrt{2(n_1 + 3n_2)B} - E^2AM_1\sqrt{2(n_1 + 3n_2)B} + 2(n + 3n_2)BE^2M_1}{A - A^2EM_1} \tag{4}$$

For micelles in the presence of dimer and salt we find

$$p = \frac{\sqrt{2(3n_2 + n_3)B} + 2(3n_2 + n_3)BM_1F}{A - A^2M_1F} \tag{5}$$

$$m = \frac{1}{AM_1} + \frac{2F\sqrt{2(3n_2 + n_3)B} - F^2AM_1\sqrt{2(3n_2 + n_3)B} + 2F^2M_1(3n_2 + n_3)B}{A - A^2M_1F} \tag{6}$$

where

$p$ = effective charge
$m$ = aggregation number
$M_1$ = molecular weight of the monomer molecule
$n_1$ = molar concn. of the monomer
$n_2$ = molar concn. of the dimer } per ml.
$n_3$ = molar concn. of the salt

$$F = \frac{4n_2 + fn_3}{6n_2 + 2n_3} \qquad E = \frac{n_1 + 4n_2}{2n_1 + 6n_2}$$

$$f = \left(\frac{\partial \nu}{\partial n_3}\right) \Big/ \left(\frac{\partial \nu}{\partial n_1}\right)_{p,T}$$

While the dimerization constant of $LS^-$ has been estimated for very dilute solutions,[15] it is not known at present how it varies with the ionic strength. We have therefore based our calculations on the assumption that it is equal to $10^2$. The results are included in Table II, while Fig. 2 shows also values obtained for no dimerization and for complete dimerization. The effect of dimerization is pro-

(22) R. J. Williams, J. N. Phillips and K. J. Mysels, *Trans. Faraday Soc.*, **51**, 728 (1955).

(23) P. Mukerjee, Dissertation, University of Southern California, 1957, and unpublished measurements of P. Kapauan.

(24) E. Matijevic and B. A. Pethica, *Trans. Faraday Soc.*, **54**, 587 (1958).

(25) K. J. Mysels, *J. Colloid Sci.*, **10**, 507 (1955), for corrections see 28.

(26) W. Prins and J. J. Hermans, *Proc. Neder. Akad. Wet.*, **B59**, 162 (1956).

(27) Prins and Hermans[8,26] prefer to introduce in addition an excluded volume correction in which the micelle is considered as a charged hard sphere whose volume includes one double layer thickness. The charge of this sphere is necessarily even smaller than $p$ (roughly by 40 to 80%) and the hard sphere does not introduce any corrections in the optical efficiency of fluctuations.[26] The degree of association is calculated as about halfway between $m$ and $m'$.

(28) L. H. Princen and K. J. Mysels, *J. Colloid Sci.*, 12, 594 (1957).

nounced in water but, as would be expected, decreases rapidly in the presence of salt.

Of the three salts studied here, the tetramethylammonium is the only one in which the oppositely charged ions form neutral ion pairs.[18] Using the ionization constant 0.080 determined conductivimetrically gives a reduction of less than 10% in the number of simple ions present at the c.m.c. If this is taken into account in the calculation, it reduces the degree of association $m$ and the charge $p$ by about 0.15, which is negligible.

## Discussion

**The Validity of the Model.**—The micellar weights given in Table II and Fig. 2 depend on three assumptions: (i) the concentration of small ions is constant above the c.m.c., (ii) the micelles are monodisperse, and (iii) the size and effective charge of the micelles is constant above the c.m.c.

(i) The effect of the change in the concentration of small ions under ideal conditions if they are monovalent has been discussed[25] and leads to a reduction by about 3% in the degree of association in water and is negligible in the presence of salt. Thus this assumption is unlikely to lead to serious error.

The linearity of the $Hc/\tau$ in water plot of Fig. 1

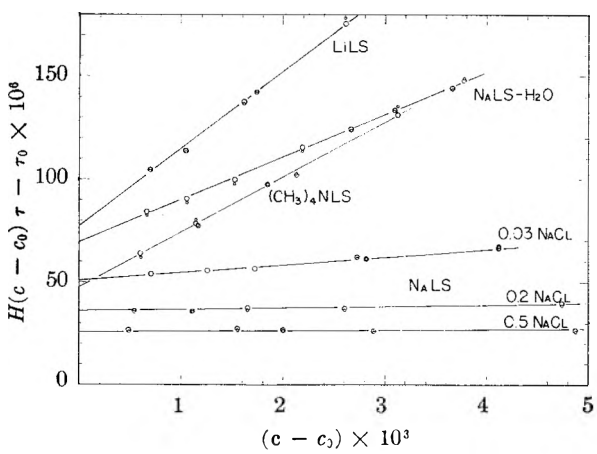


Fig. 1.—The reduced turbidity of solutions of lauryl sulfates, $H(c - c_0)/(\tau - \tau_0)$: larger circles, blue line of mercury; smaller circles, green line.

is in better agreement with a slight variation in the concentration of small ions according to the above discussion[25] than with a constant concentration. The latter should lead to a definitely noticeable curvature in the upper part of the range studied.

(ii) That the micelles cannot be monodisperse is evident from the fact that their size varies upon addition of salt. This can only be due to the gradual shifting of the relative concentration of existing species and not to the sudden complete disappearance of some and appearance of others. In other words, a small change in the composition of the intermicellar liquid should correspond to a correspondingly small change in the relative free energies of closely related micellar species and therefore to correspondingly small changes in their relative concentration ratios. The observed changes in average weight must therefore result from finite shifts in a distribution of weights. Hence a single

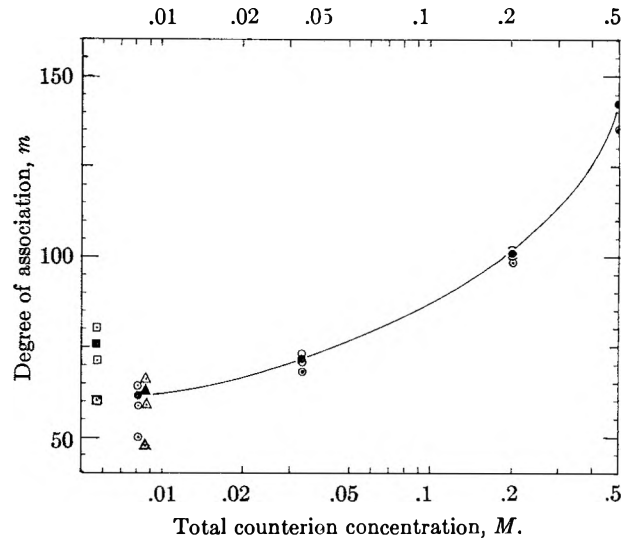


Fig. 2.—The variation of association number of lauryl sulfates with total counterion concentration at the c.m.c.: circles, Na; triangles, Li; squares, $(CH_3)_4N$ salt; filled figures; assuming partial dimerization; upper open, complete dimerization; lower open, no dimerization; central dot, uncorrected for charge effects.

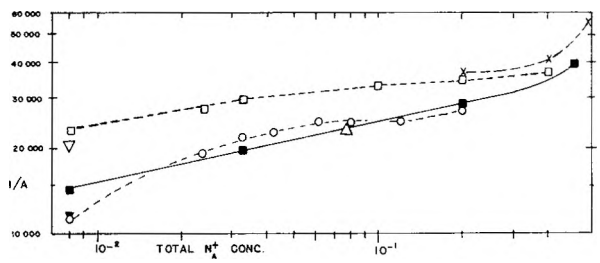


Fig. 3.—Comparison of the experimental quantity—the apparent micellar weight = the inverse of the intercept $A$—obtained by different investigators for NaLS: ■ This work; □ Phillips and Mysels; ▽ Tartar and Lelong; △ Prins and Hermans; ○ Kushner and Hubbard; X centrifugal data of Granath, ▼ Tartar.[30]

value of micellar size can represent only an average, and the weighting of this average depends on the method of investigation.

If $\beta_i$, the proportion by weight of species i to the total of large particles, is constant—the case of simple polymers—it is well known that light scattering gives a weight average for uncharged particles of the same refractive increment. For charged particles the problem is again more complicated. We have calculated the turbidity of a charged polydisperse system in the presence of monomer, again, following the same general procedure[28] and find for the average charge

$$p_{av} = \frac{\sum_1^N (2m_i - p)\beta_i}{\sum_1^N \frac{(2m_i - p_i - 1)(2m_i - p_i)}{2m_i}\beta_i} \sum_1^N \frac{2m_i - p_i - 1}{2m_i}\beta_i p_i \quad (7)$$

and for average aggregation number

$$m_{av} = \sum_1^N \beta_i \left\{ d_i m_i + \frac{2m_i - p_i - 1}{4m_i} p_i \frac{\sum_1^N \frac{(2m_i - p_i)(4m_i - p_i - 1)}{2m_i} \beta_i}{\sum_1^N \frac{(2m_i - p_i)(2m_i - p_i - 1)}{2m_i} \beta_i} \right\} \quad (8)$$

The expressions simplify greatly if the effective degree of ionization $p/m$ is the same for all species. Such an assumption should be close to reality, as the present work as well as that of others[3,7,8] shows little change in this degree of ionization upon addition of salt despite large variations in both $p$ and $m$. Under these conditions the above equations show that it is again the simple weight average that is obtained.

(iii) The nature of the solution bathing each micelle changes somewhat with total concentration, and the nature of the average micelle can be expected to change accordingly. Our interpretation is confined, however, to the extrapolated intercept and initial slope. It therefore pertains to the extrapolated micelle—the one that would exist at the c.m.c. if its properties would change smoothly from the measured range. In the present work the extrapolation is based on measurements which cover the range of about 0.04–0.6% above the c.m.c., and shows no deviations from linearity. The slope is therefore constant and the intercept readily established.

That the changes in the micelle are not very large in the region studied is made plausible by a comparison of the small ion concentration at higher concentrations of micelles and upon addition of salt. Thus in water the concentration of free $Na^+$ ions increases between the c.m.c. and the highest concentration used in the extrapolation (0.6% = $2.1 \times 10^{-2} M$) by only $2 \times 10^{-3} M$ based on $p/m = 0.15$, or at most twice as much using the true charge[29] of the micelle. This is less than one tenth or one fifth of the increase produced by the presence of $3 \times 10^{-2} M$ NaCl, and the latter produces only about a 20% change in the degree of aggregation. In the presence of salt, the change in the bathing solution becomes completely negligible.

The same argument suggests that the proportion, $\beta_i$, of micelles of a given molecular weight does not change much in this range, so that the assumption of its constancy which underlies eq. 8 and 9 may not introduce a substantial error.

Thus the micelles are not expected to change much over the range used in the extrapolation, nor would such a change affect the values obtained. The values themselves are likely to be close to the weight averages.

(29) D. Stigter and K. J. Mysels, THIS JOURNAL, **59**, 45 (1955); K. J. Mysels and C. I. Dulin, *J. Colloid Sci.*, **10**, 461 (1955).

**The Absolute Values.**—The precision of the individual measurement of turbidity is about $\pm 1.5 \times 10^6$ and corresponds to about 2% in the uncorrected molecular weight $M' = 1/A$ and to about $5 \times 10^{-5}$ in the slope $B$. In view of past experience it may be preferable not to comment about accuracy, although every effort was made to keep it of the same order.

A comparison of the above results with previously reported ones is best made in terms of the direct experimental quantity $M' = 1/A$, the inverse of the intercept of the $Hc/\tau$ line. Figure 3 shows these values. It may be seen that the discrepancy is largest in water while in the presence of higher salt concentrations the values tend to converge. On the other hand the plot of our results against the logarithm of the total counterion concentration at the c.m.c. is curved upward while previous results tended to show a downward curvature[3,6,25,30] except for some micellar weights obtained by Granath[31] by centrifugation[32] and diffusion which also indicated an upward curvature. The increase in micellar size upon addition of salt results presumably from a reduction of electric repulsions entering the balance of forces which determine micellar size as discussed for example by Overbeek and Stigter.[33] The fact that simple electrolytes affect the micellar size of all association colloidal electrolytes[3] but not of the corresponding non-ionics[34] shows clearly the importance of the electric term in the former case. A more detailed interpretation, especially any meaning of the reported curvature, does not seem feasible at present.

Because of the many improvements introduced we cannot pinpoint the reason for the difference from previous light scattering measurements in this Laboratory. It should be noted, however, that self-diffusion measurements obtained in fritted glass[35] probably are vitiated by the hydrolysis catalyzed by the glass surface as discussed above.

(30) H. V. Tartar, *J. Colloid Sc.*, **14**, 115 (1959).

(31) K. Granath, *Acta Chem. Scand.*, **7**, 297 (1953).

(32) P. F. Mijnlieff, Thesis, Utrecht, 1958, obtains from centrifugal experiments $m = 58$ for NaLS in water.

(33) J. T. G. Overbeek and D. Stigter, *Rec. trav. chim. Pays Bas*, **75**, 1263 (1956).

(34) L. M. Kushner and W. D. Hubbard, THIS JOURNAL, **58**, 1163 (1954).

(35) D. Stigter, R. J. Williams and K. J. Mysels, *ibid.*, **59**, 330 (1955).

# NUCLEAR MAGNETIC SHIELDING OF $F^{19}$ IN SOME CHLOROFLUOROCARBONS[1]

BY T. S. SMITH[2] AND E. A. SMITH

*Goodyear Atomic Corporation, Portsmouth, Ohio*

*Received December 12, 1958*

The positions of the nuclear magnetic resonance lines of the various $F^{19}$ groups in dichlorotetrafluoroethane ($CCl_2FCF_3$ and $CClF_2CClF_2$), trichlorotrifluoroethane ($CCl_2FCClF_2$), trichlorofluoromethane ($CCl_3F$), perfluorodimethylcyclohexane ($C_8F_{16}$), and trichloroheptafluorobutane ($CF_3CCl_2CClFCF_3$) have been measured with respect to the $F^{19}$ line of trifluoroethanoic acid ($CF_3COOH$). The magnetic shielding constant for the $F^{19}$ groups increases with an increase of the total electronegativity of the atoms associated with the nearest carbon atom.

## Introduction

Since Knight[3] first reported that the external conditions for nuclear magnetic resonance of a particular nucleus depended upon the chemical compound in which the nucleus resided, many investigators[4-16] have made experimental and theoretical studies of the effect.

The chemical shift is caused by a magnetic shielding of the nucleus due to the electron distribution about the nucleus of interest. Ramsey[11] has developed a formal procedure for calculating the shielding as a function of the externally applied magnetic field. It consists of two terms: (a) Lamb's[17] diamagnetic correction and (b) a paramagnetic term arising from a spherical asymmetry of the electrical potential at the nucleus due to the electrons. Unfortunately, the results of Ramsey's study can only be used to calculate the shielding for linear molecules for which spin–rotational interaction data are known.

A series of binary covalent compounds was examined by Gutowksy and Hoffman[12] in an attempt to determine the effect of the electronic structure associated with bond formation and of the electronic configuration of the other atoms in the molecule. The results of their examination showed a decrease of the nuclear magnetic shielding of the $F^{19}$ nucleus with increased electronegativity[18] of the adjacent atom. Investigations by Gutowsky and others[13] on the substituent effects in some fluorobenzene derivatives led to an apparent direct relation between the Hammett substituent constant[19] and the magnetic shielding constant for the $F^{19}$ nucleus in the number one position on the benzene ring.

Fluorine magnetic resonance shifts also have been measured in the halomethanes.[14] The relation between the shielding constant $\partial$ and the sum of the electronegativities of the atoms present exhibits a simple relation which is shown in Fig. 1. The shielding constant $\partial$ is defined as $(H_R - H_C)/H_R \times 10^6$ where $H_R$ is the externally applied magnetic field for which resonance occurs at a fixed frequency for a reference nucleus, and $H_c$ is the externally applied field for which resonance occurs at the same frequency for the nucleus of interest. This allows a direct comparison to be made of shielding effects without regard to the magnitude of the magnetic field. Shoolery[15] studied the effect of substituting various atomic groups for one of the hydrogen atoms of $C_2H_6$. He found a direct relationship between $(\partial_{CH_2} - \partial_{CH_3})$ and the electronegativity of the substituent; where $\partial_{CH_2}$ is the shielding constant for the protons in the $CH_2$-plus-substituent group and $\partial_{CH_3}$ is the shielding constant for the protons in the $CH_3$ group.

Saika and Slichter[16] simplified the procedure devised by Ramsey[11] for calculating the second-order paramagnetic term and were able to calculate the shift between $F_2$ and HF. Their calculations agree well with the experimental results.

In view of the evidence presented above, an examination was undertaken to investigate the $F^{19}$ shielding constants for some of the more complicated molecules.

## Apparatus and Materials

Measurements were made at 30 Mc. by means of a Varian Associates High Resolution Nuclear Magnetic Resonance Spectrometer. For calibration purposes side-bands[20-23] were created by subjecting the steady magnetic field to a 600 cycle sine wave modulation from a Hewlett–Packard Function generator Model 202A. The 600 cycles per second frequency was checked by means of a Hewlett–Packard Electronic timer Model 524B whose accuracy had been checked against the frequency signal from WWV radio. This permitted a frequency regulation of the side-bands accurate to five significant figures. The spectra were recorded on a Minneapolis–Honeywell Model 153 variable span, strip chart recorder running at 2.75 inches per minute.

The materials investigated include: 1. A mixture of 93% 1,2-dichloro-1,1,2,2-tetrafluoroethane ($CClF_2CClF_2$) and

(1) This work was performed under Contract AT-(33-2)-1 with the United States Atomic Energy Commission, and was presented at the Annual Meeting of the American Physical Society, New York, January 30, 1958.

(2) Department of Physics, Ohio University, Athens, Ohio.

(3) W. D. Knight, *Phys. Rev.*, **76**, 1259 (1949).

(4) H. S. Gutowsky and B. R. McGarvey, *J. Chem. Phys.*, **20**, 1472 (1952).

(5) N. Bloembergen and T. J. Rowland, *Acta Metallurgia*, **1**, 731 (1953).

(6) W. C. Dickenson, *Phys. Rev.*, **77**, 736 (1950).

(7) H. S. Gutowsky and C. J. Hoffman, *ibid.*, **80**, 110 (1950).

(8) W. G. Proctor and F. C. Yu, *ibid.*, **77**, 717 (1950).

(9) W. C. Dickenson, *ibid.*, **81**, 717 (1951).

(10) J. E. Wertz, *Chem. Revs.*, **55**, 829 (1955).

(11) N. F. Ramsey, *Phys. Rev.*, **78**, 699 (1950).

(12) H. S. Gutowsky and C. J. Hoffman, *J. Chem. Phys.*, **19**, 1259 (1951).

(13) H. S. Gutowsky, *et al.*, *J. Am. Chem. Soc.*, **74**, 4809 (1952).

(14) L. H. Meyer and H. S. Gutowsky, THIS JOURNAL, **57**, 481 (1953).

(15) J. N. Shoolery, *J. Chem. Phys.*, **21**, 1899 (1953).

(16) A. Saika and C. P. Slichter, *ibid.*, **22**, 26 (1954).

(17) W. E. Lamb, Jr., *Phys. Rev.*, **60**, 817 (1941).

(18) L. N. Ferguson, "Electron Structures of Organic Molecules," Prentice–Hall, Inc., New York, N. Y., 1952.

(19) L. P. Hammett, "Physical Organic Chemistry," McGraw–Hill Book Co., New York, N. Y., 1940

(20) C. H. Townes and F. R. Merritt, *Phys. Rev.*, **72**, 1266 (1947).

(21) R. Karplus, *ibid.*, **73**, 1027 (1948).

(22) J. H. Burgess and R. M. Brown, *Rev. Sci. Instr.*, **23**, 334 (1952).

(23) J. N. Shoolery and B. J. Alder, *J. Chem. Phys.*, **23**, 805 (1955).

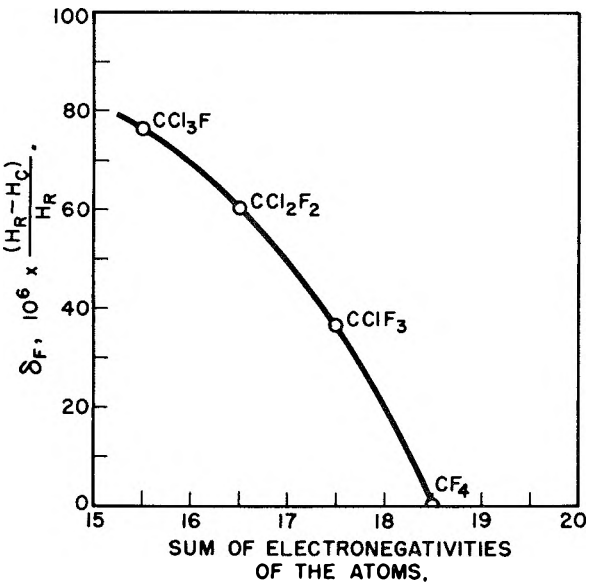


Fig. 1.—Relation of $\delta$ to total electronegativities of adjacent atoms (data from Meyer and Gutowsky[14]).

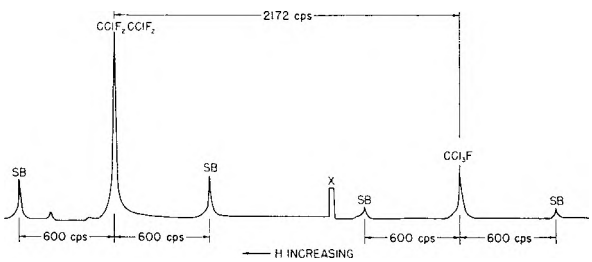


Fig. 2.—N.m.r. spectrum of $CCl_2FCF_3$, $CClF_2CClF_2$, and $CCl_3F$.

7% 1,1-dichloro-1,2,2,2-tetrafluoroethane ($CCl_2FCF_3$) (determined by infrared analysis) supplied by E. I. du Pont de Nemours and Co. under the trade name "Freon-114." In this paper the mixture is referred to as F-114. 2. A mixture of 85.5% 1,1-dichloro-1,2,2,2-tetrafluoroethane ($CCl_2FCF_3$) and 14.5% 1,2-dichloro-1,1,2,2-tetrafluoroethane ($CClF_2CClF_2$) supplied by General Chemical Company under the trade name "Genetron." The isomer concentrations were also determined by infrared analysis. 3. Trichloromonofluoromethane ($CCl_3F$) supplied by Olin Mathieson Company. Infrared analysis of this material showed 98% $CCl_3F$ and 2% $CCl_2F_2$. 4. 1,1,2-Trichloro-1,2,2-trifluoroethane ($CCl_2FCClF_2$) supplied by E. I. du Pont de Nemours and Company under the trade name "Freon-113." Mass spectroscopic analysis indicated this compound to be 99% pure. The only impurity detected was $N_2$. 5. 2,2,3-Trichloroheptafluorobutane ($CF_3CCl_2$-$CClFCF_3$) supplied by the Hooker Electrochemical Company. A mass spectroscopic analysis of this material indicated less than one per cent. $N_2$ as the only impurity. 6. Perfluorodimethylcyclohexane ($C_8F_{16}$) supplied by E. I. du Pont de Nemours and Company. This compound contained only traces of $N_2$, A and $O_2$ as indicated by mass spectroscopic analysis. 7. Trifluoroethanoic acid ($CF_3$-$COOH$) supplied by the Minnesota Mining and Manufacturing Company as chemically pure.

Each sample was prepared by condensing the material from the vapor phase into a 5 mm. o.d. Pyrex glass sample tube. The spectra were obtained while each sample was in an atmosphere of its own vapor and at room temperature.

### Procedure

All observed $F^{19}$ resonance lines were measured relative to the line of $CClF_2CClF_2$. The position of the $CClF_2CClF_2$ line was then measured relative to the line of trifluoroethanoic acid. These data were used to compare the results of this work with previous efforts in which trifluoroethanoic acid had been used as a reference.[14]

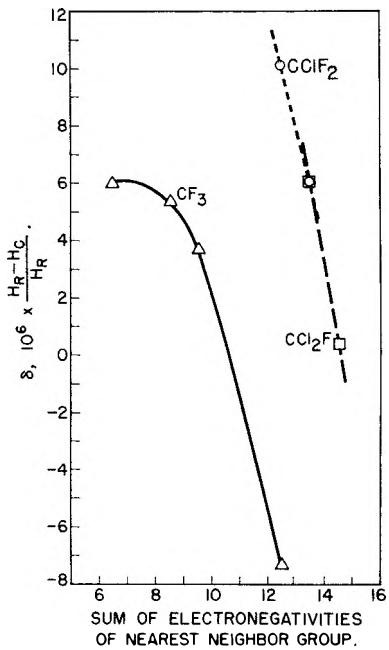


Fig. 3.—Influence of total electronegativities of neighboring groups on $\delta$ for $F^{19}$.

The general procedure in obtaining scans of the $F^{19}$ spectra was one of a continuous, slow sweep of the magnetic field while the reference sample and the test sample were alternately placed in and removed from the field. Figure 2 shows a typical spectrum thus obtained. The zero of the recorder is on the far left of the scale; therefore, the scan was obtained with the recorder paper moving from left to right. The direction of increasing field is indicated by an arrow.

Figure 2 is a scan of $CCl_3F$ and F-114. The position marked x indicates where the $CCl_3F$ sample was removed and the F-114 sample inserted in the probe as the field was being swept. The two small signals upfield from the $CClF_2CClF_2$ line are the lines of $CCl_2FCF_3$ which are present in F-114. (A series of runs on various concentrations of $CClFCF_3$ in $CClF_2CClF_2$ showed no effect on the positions of their respective lines.) The side-bands (SB) of each line are separated by 1200 cycles per second. In actual practice this distance on a tracing is about 300 mm. This measurement provided a direct calibration on every scan. No attempt was made to eliminate drift in the magnetic field during this experiment because uniform drift would not affect the results. In order to check the uniformity of drift it was necessary to measure the separations between different pairs of side-bands on a single scan such as those shown in Fig. 2. Since the distance between the side-bands around the line of $CClF_2CClF_2$ was found to be equal to the distance between the side-bands around the line of $CCl_3F$, the total magnetic field sweep rate was the same during the recording of both pairs of side-bands. Uniformity of drift was all that was necessary because of the method of calibration used. A direct measurement of the distance between lines in Fig. 2 determined their separation in cycles per second. By use of the rate of precession of $F^{19}$, 30 megacycles per second in a field of 7500 gauss or $^1/_4$ milligauss per cycle per second, the shift in cycles per second can be expressed in milligauss.

The spectra of the other compounds were obtained in the same manner as the spectrum shown in Fig. 2. In cases where the reference line fell upon, or very near, a line in the spectrum of the sample, only the side-bands of the reference line were recorded by substituting and removing the reference sample at the proper times. Thus very small field shifts could be measured. The various lines in a particular spectrum were identified easily by means of their multiplets caused by spin–spin interactions through the valence bond electron spins.[24,25] The spectrum of $C_8F_{16}$

(24) H. S. Gutowsky, D. W. McCall and C. P. Slichter, *J. Chem. Phys.*, **21**, 270(1953).

(25) J. T. Arnold, *Phys. Rev.*, **102**, 136 (1956).

TABLE I

POSITIONS OF LINES RELATIVE TO $CClF_2CClF_2$ IN CYCLES PER SECOND, POSITIONS OF LINES RELATIVE TO $CF_3COOH$ IN MILLIGAUSS, AND NUCLEAR MAGNETIC SHIELDING CONSTANTS WITH RESPECT TO $CF_3COOH$

| No. of obs. | Source of $F^{19}$ signal | $\Delta H$(c.p.s.) with respect to $CClF_2CClF_2$ | $\Delta H$(mgauss) with respect to $CF_3COOH$ | $\partial\ 10^6 \left(\frac{H_R - H_C}{H_R}\right)$ |
|---|---|---|---|---|
| 10 | $CCl_3F$ | $-2172 \pm 4$ | $-588 + 1$ | $+ 78.4$ |
| 11 | $CF_3COOH$ | $181 \pm 3$ | 0.00 | |
| 73 | $F_3C\diagdown CCl_2F$ | $400 \pm 1$ | $55 \pm 0.8$ | $- 7.33$ |
| 16 | | $171 \pm 2$ | $-2.5 \pm 0.9$ | $+ 0.33$ |
| 11 | $CClF_2—CClF_2$ | 0.0 | $-45 \pm 0.75$ | $+ 6.00$ |
| 13 | $Cl_2FC\diagdown CClF_2$ | $0 \pm 3$ | $-45 \pm 1.0$ | $+ 6.00$ |
| 13 | | $-122 \pm 2$ | $-76 \pm 0.9$ | $+ 10.1$ |
| 14 | $CF_3\diagdown CCl_2\diagdown CClF\diagdown CF_3$ | $20 \pm 2$ | $-40 \pm 0.9$ | $+ 5.33$ |
| 14 | | $1455 \pm 4$ | $318 \pm 6$ | $- 42.4$ |
| 14 | | $68 \pm 3$ | $-28 \pm 1$ | $+ 3.73$ |
| 11 | 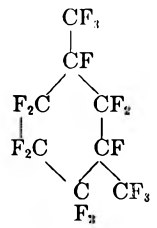 | $0.0 \pm 3$ | $-45 \pm 1.0$ | $+ 6.00$ |
| 11 | | $3472 \pm 18$ | $822 \pm 18$ | $-109.6$ |
| 11 | | $1617 \pm 8$ | $359 \pm 8$ | $- 47.9$ |

was complicated by the presence of a mixture of isomers with the meta and para components predominating,[26] but the large groups as indicated in Table I could be distinguished.

## Results

The data derived from all observations are shown in Table I. The values in the third column, shifts in field in cycles per second with respect to $CClF_2$-$CClF_2$, are expressed with 95% confidence limits.

TABLE II

NUCLEAR MAGNETIC SHIELDING CONSTANTS OF VARIOUS $F^{19}$ NUCLEI, NEAREST NEIGHBOR ATOMIC GROUP, AND TOTAL ELECTRONEGATIVITY OF NEAREST NEIGHBOR GROUP

| $10^6 \times \frac{H_R - H_C}{H_R}$ | $F^{19}$ producing signal | Neighbor group | Electronegativity of neighbor group |
|---|---|---|---|
| 10.1 | $CClF_2—$ | $CCl_2F$ | 12.5 |
| 6.00 | $CClF_2—$ | $CClF_2$ | 13.5 |
| 6.00 | $CF_3—$ | $CF—$ | 6.5 |
| 5.33 | $CF_3—$ | $CCl_2—$ | 8.5 |
| 3.73 | $CF_3—$ | $CClF—$ | 9.5 |
| $-7.33$ | $CF_3—$ | $CCl_2F$ | 12.5 |
| 6.00 | $CCl_2F—$ | $CClF_2$ | 13.5 |
| 0.33 | $CCl_2F—$ | $CF_3$ | 14.5 |

(26) C. Slesser and S. R. Schrane (editors), "Preparation, Properties and Technology of Fluorine and Organic Fluoro Compounds." McGraw-Hill Book Co., New York, N. Y., 1951, (National Nuclear Energy Series, Div. vii, Vol. I).

The large number of observations of the line from the $CF_3$ group in $CCl_2FCF_3$ were obtained because $CCl_2FCF_3$ was an impurity in the secondary standard used ($CClF_2CClF_2$) and this line appeared frequently.

Table II illustrates the effect on similar $F^{19}$ nuclei attached to one carbon by various atoms attached to a nearby carbon in the compound. An increase of $\partial$ indicates a decrease in the shielding. In every case an increase in the total electronegativity of the atoms in the neighboring group results in an increase in the shielding of the $F^{19}$ of interest as is shown in Fig. 3.

These results are the reverse of what might be expected from a study of the measurements made on binary fluorides.[13] In the case of the binary fluorides an increase in electronegativity of the atom bonded to the fluorine produced a decrease in the shielding of the fluorine nucleus. Since the shielding effect for the fluoride ion is small, a decrease in the shielding indicates an increase in the ionic character of the bond.

The shielding effect shown in Fig. 3 is consistent with the results obtained for the chlorofluoromethanes[14] (Fig. 1) and with some recent measurements made on solid $MnF_3$.[27] A covalent bond or double-bond mechanism between the fluorine and carbon atom is essential to explain the change in $\partial$. The electron removed from the fluorine is one which has its spin aligned antiparallel to the applied magnetic field.

(27) R. G. Shulman and V. Jaccarino, *Phys. Rev.*, **109**, 1084 (1958).

# INTEGRATION OF THE RATE EQUATION FOR A SECOND-ORDER REACTION IN AN ADIABATIC FLOW SYSTEM

BY ERIC BAUM

*Department of Engineering, University of California, Los Angeles, Calif.*

*Received January 19, 1959*

The rate equation for a second-order reaction in an adiabatic flow system was integrated, subject to the following conditions: 1, the ideal gas equation describes the reacting mixture; 2, the molar flow rate through the system is unchanged as the reaction proceeds; 3, heat transfer within the reacting mixture can be neglected; 4, pressure can be considered constant; 5, $C_p$ can be considered constant.

The second-order rate equation

$$-\frac{dC_a}{d\theta} = A\sqrt{T}\,e^{-\epsilon/RT}C_aC_b \qquad (1)$$

can be solved for an adiabatic flow system if the following conditions are satisfied.

1. The ideal gas equation describes the reacting mixture.
2. The molar flow rate through the system is unchanged as the reaction proceeds; that is, the number of moles of products formed is the same as the number of moles of reactants consumed.
3. Heat transfer within the reacting mixture has a negligible effect on the temperature distribution; that is, each incremental volume of reacting mixture flowing through the system can be considered to be adiabatic.
4. Pressure is essentially constant.
5. $C_p$ is essentially constant.

Equation 1 can be more conveniently handled if these substitutions are made

$$C_a = \frac{X_aP}{RT} \qquad (2)$$

$$C_b = \frac{X_bP}{RT} \qquad (3)$$

$$d\theta = \frac{P}{\omega RT}\,dV \qquad (4)$$

where

$X$ = mole fraction
$\omega$ = molar flow rate
$V$ = vol. of reactor system traversed by the reacting mixture

Equation 1 now reads

$$-\frac{dX_a}{X_a} = \frac{A\sqrt{T}\exp(-\epsilon/RT)P^2X_b}{\omega R^2T^2}\,dV \qquad (5)$$

$X_b$ can be written as

$$X_b = X_{bi} - \beta(X_{ai} - X_a) \qquad (6)$$

where the subscripts i denote the initial conditions and $\beta$ is the number of moles of b consumed by reaction with one mole of a.

$T$ can be written as

$$T = T_i + \alpha(X_{ai} - X_a) \qquad (7)$$

where

$$\alpha = \Delta H_{reaction}/C_p.$$

When equations 6 and 7 are substituted into equation 5, one obtains

$$\frac{[T_i + \alpha(X_{ai}-X_a)]^{3/2}}{[X_{bi} - \beta(X_{ai} - X_a)]X_a}\exp\{\epsilon/R[T_i + \alpha(X_{ai}-X_a)]\}\,dX_a = \frac{-AP^2}{\omega R^2}\,dV \qquad (8)$$

The factor $\sqrt{T_i + \alpha(X_{ai} - X_a)}$ can be written as

$$\sqrt{T_i + \alpha X_{ai}}\sqrt{1 - \frac{\alpha X_a}{T_i + \alpha X_{ai}}}$$

When $\alpha X_a/(T_i + \alpha X_{ai}) << 1$, the approximation

$$\sqrt{1 - \frac{\alpha X_a}{T_i + \alpha X_{ai}}} \approx 1 - \frac{\alpha X_a}{2(T_i + \alpha X_{ai})} \qquad (9)$$

is very good. Even when this approximation is not a good one, the effect on the result of this term ($\sqrt{T}$) is quite small compared to that of the exponential ($e^{-\epsilon/RT}$). Substituting equation 9 into 8

$$\frac{\left[\frac{2}{\alpha}(T_i + \alpha X_{ai}) - X_a\right][T_i + \alpha(X_{ai} - X_a)]}{[X_{bi} - \beta(X_{ai} - X_a)]X_a}\exp\{\epsilon/R[T_i + \alpha(X_{ai} - X_a)]\}\,dX_a = -\frac{2AP^2(T_i + \alpha X_{ai})^{1/2}}{\alpha\omega R^2}\,dV \qquad (10)$$

To change the integral on the left to a more familiar form, the change in variable

$$\lambda = \epsilon/R\,[T_i + \alpha(X_{ai} - X_a)] \qquad (11)$$

is made, giving

$$\frac{\left(\lambda + \frac{1}{u}\right)e^{\lambda}}{\left(\lambda - \frac{1}{u+y}\right)\left(\lambda - \frac{1}{u}\right)\lambda^2}\,d\lambda = -u(u+y)\times\frac{2AP^2\beta}{\omega R^2\alpha}\sqrt{\frac{R}{\epsilon u}}\,dV \qquad (12)$$

where

$$u = \frac{R}{\epsilon}(T_i + \alpha X_{ai}) \qquad (13)$$

$$y = \frac{R\alpha}{\epsilon\beta}(X_{bi} - \beta X_{ai}) \qquad (14)$$

When the left-hand side of equation 12 is expanded by partial fractions, it becomes

$$\left\{\frac{-(u+y)(2u+y)}{uy}\left[\frac{1}{\lambda - \frac{1}{u+y}}\right] + \frac{2u}{y}\left[\frac{1}{\lambda - \frac{1}{u}}\right] + \frac{(3u+y)}{u}\left[\frac{1}{\lambda}\right] + \frac{1}{u}\left[\frac{1}{\lambda^2}\right]\right\}e^{\lambda}\,d\lambda = \frac{-2AP^2\beta}{\omega R^2\alpha}\sqrt{\frac{R}{\epsilon u}}\,dV \qquad (15)$$

The integrals of the left-hand side of equation 15 can be recognized to be exponential integral functions, the values of which have been tabulated. The exponential integral function of $\lambda$ is written in the contracted form $E_i(\lambda)$.

Equation 15, when integrated, yields

$$\left[-u^{-1/2}\lambda^{-1}e^{\lambda} + u^{-1/2}(3u + y + 1)E_i(\lambda) + 2u^{3/2}y^{-1}\right.$$

$$\exp\left(\frac{1}{u}\right) E_i\left(\lambda - \frac{1}{u}\right) - (u+y)(2u+y)u^{-1/2}y^{-1}\exp\left(\frac{1}{u+y}\right) E_i\left(\lambda - \frac{1}{u-y}\right)\Bigg]_{\lambda_i}^{\lambda} = -\frac{2P^2A\beta}{\omega R^2\alpha}\sqrt{\frac{R}{\epsilon}}V \quad (16)$$

The parameters included in this equation are

$$P,\ \omega,\ V,\ T_i,\ X_{ai},\ X_{bi},\ X_a$$

Equation 16 can be used to determine $P$, $\omega$ or $V$ directly if all the other parameters are known. $T_i$, $X_{ai}$, $X_{bi}$ or $X_a$ can be determined by iteration.

# HYDROGEN BOND LENGTHS AND ANGLES OBSERVED IN CRYSTALS

By W. Fuller

*Medical Research Council Biophysics Research Unit, Wheatstone Laboratory, King's College, London*

*Received February 3, 1959*

Hydrogen bond lengths observed in crystals have been classified according to the chemical groups participating in the hydrogen bond. Histograms have been drawn for those types of bond for which there is sufficient data and the mean values of bond length for the various types of bond are given. Taking into consideration the accuracy of the data, the histograms are fairly sharp indicating that the length of a hydrogen bond (Y–H...Z) is largely determined by the nature of the hydrogen donor (Y–H) and acceptor (Z) groups. By contrast there appears to be little correlation between the length of a hydrogen bond and the angle at the donor atom between the hydrogen bond direction and the expected direction of the bond to the hydrogen atom. However hydrogen bonds are rarely formed if this angle is greater than 20°. If the mean values of bond length for bonds between a particular acceptor and various donors are arranged in order of increasing size, it is found that with few exceptions the resulting arrangement of donor groups is the same for all acceptors. The corresponding arrangements of various acceptor groups for each donor group are not quite so similar and suggest that the nature of the hydrogen donor may be more important than that of the acceptor in determining the hydrogen bond length.

## Introduction

Since Donohue surveyed the observed values of hydrogen bond lengths and angles[1] many new structures have been determined. In some of these it has been possible to locate the hydrogen atoms by using new techniques, *e.g.*, X-ray diffraction difference synthesis, neutron and electron diffraction. The present paper uses this new information in an attempt to narrow the limits that have been accepted for: (a) the lengths of the various types of hydrogen bond; (b) the angle at the hydrogen donor atom between the hydrogen bond direction and the expected direction of the bond between the donor atom and the hydrogen atom.

Such limits have three main applications in molecular structure studies. First, they are a useful guide when deducing which atoms have hydrogen atoms attached to them in a structure for which the coördinates of only the heavier atoms have been determined. Second, many large molecules give X-ray diffraction patterns which indicate only the more general features of the molecular structure. By assuming reasonable values for bond lengths and angles it is possible to deduce probable configurations for these molecules, *e.g.*, deoxyribose nucleic acid[2,3] and collagen.[4–6] Third, in some cases where X-ray diffraction data are not available other evidence may suggest the existence of hydrogen-bonded macromolecular complexes, *e.g.*, intermediates in the synthesis of ribonucleic acid. Possible schemes may be tested by building molecular models based on accepted values for bond lengths and angles.[7]

**Treatment of the Data.**—A preliminary survey of the data indicated that, although the range of bond length for any type of bond, *e.g.*, the N–H...O bond was similar to that given by Donohue's data, the range for each kind of N–H...O bond, *e.g.*, $NH_3^+$ to $COO^-$ or $NH_2$ to C=O was less. Therefore, hydrogen bonds have been classified according to the chemical groups participating in them (Tables I to XXI). Intramolecular bonds have been distinguished from intermolecular bonds; and bifurcated bonds (where it is suggested that one hydrogen atom takes part in two hydrogen bonds) have also been treated separately. As in Donohue's review, all the bond lengths in Tables I to XXI are believed to have limits of error of less than 0.1 Å., and those lengths indicated by * have limits of error of less than 0.05 Å. A more precise classification of the data than this was felt to be unjustified in view of the difficulty of comparing the various ways in which workers estimate the accuracy of their determinations. All bond lengths were determined by X-ray diffraction except those indicated by † and ‡ which are from neutron and electron diffraction studies, respectively.

For those types of bond which had sufficient data available histograms were drawn (Fig. 1), determinations with limits of error of less the 0.05 Å. being represented by black rectangles. The interval used in the histograms was 0.05 Å., a smaller interval would have made the histogram unduly sensitive to errors in the bond lengths. The mean values, $d$, of the bond lengths in each histogram and the standard deviation from $d$ are shown in Fig. 1. In the calculation of $d$ each determination was given equal weight.

It is generally believed that for hydrogen bond

(1) J. Donohue, This Journal, **56**, 502 (1952).

(2) F. H. C. Crick and J. D. Watson, *Proc. Roy. Soc.* (*London*), **A223**, 80 (1954).

(3) R. Langridge, W. E. Seeds, H. R. Wilson, C. W. Hooper, M. H. F. Wilkins and L. D. Hamilton, *J. Biophys. Biochem. Cytol.*, **3**, 767 (1957).

(4) G. N. Ramachandran and G. Kartha, *Nature*, **174**, 269 (1954).

(5) A. Rich and F. H. C. Crick, *ibid.*, **176**, 915 (1955).

(6) P. M. Cowan, S. McGavin and A. C. T. North, *ibid.*, **176**, 1062 (1955).

(7) G. Zubay, *ibid.*, **182**, 1290 (1958).

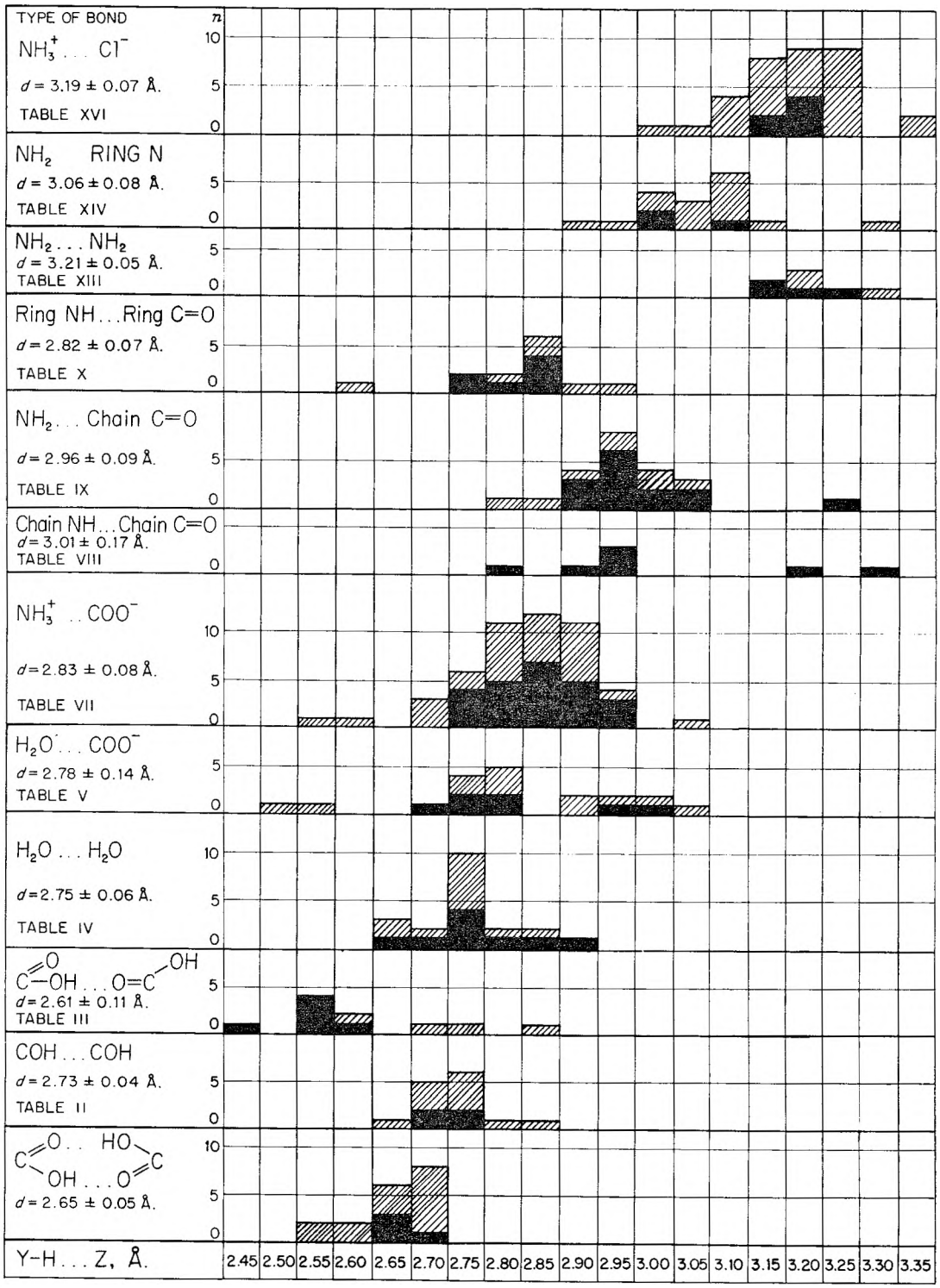


Table I

Fig. 1.—The distribution with respect to hydrogen bond length, Y–H...Z, for the more frequently occurring types of hydrogen bond. $n$ is the number of bonds in a given range of length. Bond lengths with estimated limits of error of less than 0.05 Å. in length are represented by black rectangles. The mean value of bond length in each histogram, $d$, is given with its standard deviation.

formation the angle at the hydrogen donor atom between the hydrogen bond direction and the expected direction of the bond from the donor to the hydrogen atom should be less than about 25°. The hydrogen bond direction is defined by <X–Y...Z where Y is the donor atom, Z the acceptor atom and X an atom covalently bonded to Y. If there are no atoms other than hydrogen covalently bonded to Y (as in water) it is convenient to let X denote another atom hydrogen bonded to Y. <X...Y...Z is then the angle between the two hydrogen bonds. For the three most common hydrogen donor groups, *i.e.*, $-NH_3^+$, the water oxygen and $-NH_2$ (for this group only those ex-

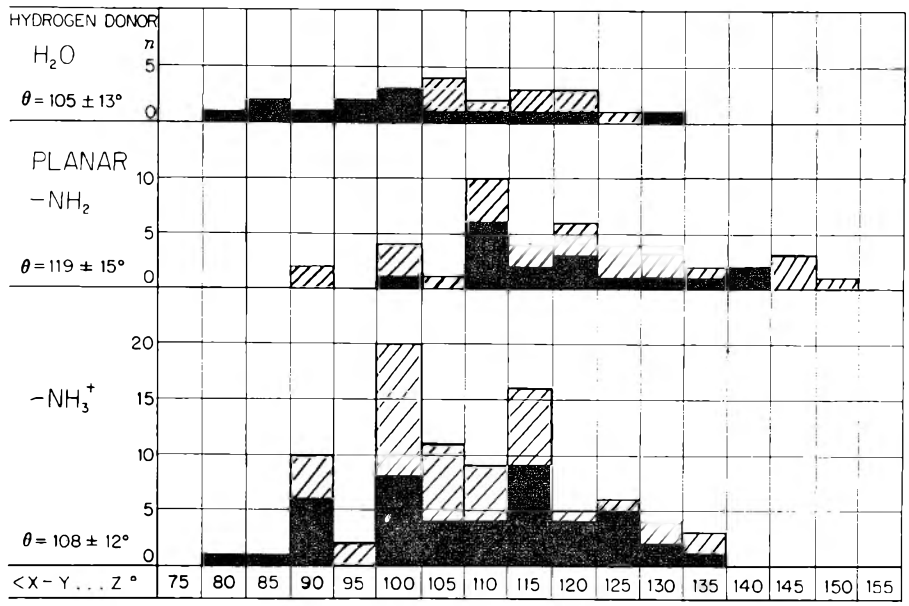


Fig. 2.—The distribution with respect to the hydrogen bond angle, <X–Y...Z (defined in the section on Treatment of Data), for three of the more common hydrogen donor groups. $n$ is the number of bonds in a given range of angle. The more accurate examples are represented by black rectangles and the mean value of bond angle in each histogram, $\theta$, is given with its standard deviation.

amples where the bonds of the nitrogen atom are expected to be coplanar are considered, *e.g.*, amides) the values of <X–Y...Z or <X...Y...Z are included in brackets after the corresponding values of Y...Z in Tables I to XIX, whenever these angles were given by the original workers. It should be noted that in general each angle for bonding at the water oxygen occurs twice in the tables, *i.e.*, once with each of the two bonds from the oxygen atom. Using these data histograms were drawn (Fig. 2). The black areas represent the more accurate determinations. The mean values, $\theta$, and standard deviations of the angles in each histogram are shown in Fig. 2. In the calculation of $\theta$ each determination was given equal weight. Two main points may be noted from these histograms: (a) the mean value, $\theta$, for each donor group is within 1° of the value it would have had if the hydrogen bonds were in the expected direction of the hydrogen atom, *i.e.*, 109, 120 and 104° for bonding at the $NH_3^+$ and $NH_2$ groups and the water oxygen, respectively, (b) the standard deviation from $\theta$ in each case is about 13°, and few values of <X–Y...Z differ by more than 20° from $\theta$.

**Comparison of Various Donor and Acceptor Groups.**–The values of $d$ for types of bond for which sufficient data exist are collected in Table XXII. The donor groups have been arranged in the table so that for a particular acceptor, *e.g.*, $COO^-$, the values of $d$ increase from left to right. From Table XXII it can be seen that with few exceptions such an arrangement of donor groups for one particular acceptor results in a similar increase in $d$ for the other acceptors. The change in $d$ in moving from one donor to the next for a particular acceptor in Table XXII is often less than the standard deviations in the values of $d$. However, since the arrangement of donor groups that places the values of $d$ for any particular acceptor group in ascending order is very similar for all nine acceptors it is felt that the arrangement of donor groups in Table XXII is significant.

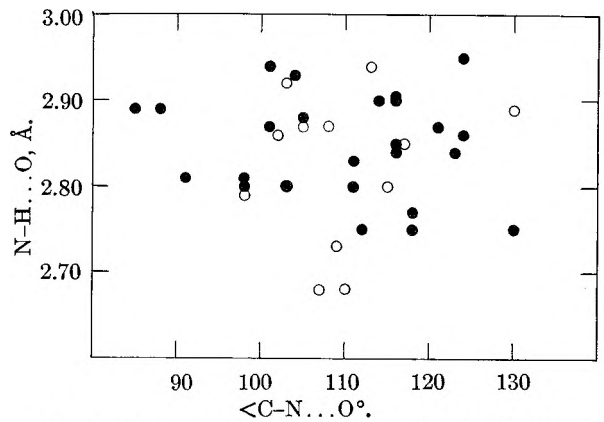


Fig. 3.—The variation of the bond length, N–H...O, with the bond angle, <C–N...O, for the hydrogen bond $NH_3^+...COO^-$. The more accurate examples are represented by filled circles.

EXPLANATORY CAPTION TO TABLES I–XXI

* indicates an estimated limit of error of 0.05Å., † a neutron diffraction and ‡ an electron diffraction determination. Titles of journals have been abbreviated as follows:

| | |
|---|---|
| *Acta Cryst.* | *A.* |
| *Current Sci.* | *C.* |
| *J. Am. Chem. Soc.* | *J.* |
| *J. Chem. Soc.* | *JC.* |
| *J. Chem. Phys.* | *JP.* |
| *Nature* | *N.* |
| *Proc. Roy. Soc.* (London) *Series A* | *P.* |
| *Structure Reports* | *S.* |
| *Travaux de l'Institut Crist.* | *T.* |
| *Z. Krist.* | *Z.* |

The values of the hydrogen bond angle X–Y...Z (defined in the section on Treatment of Data) which were used in Fig. 2 appear in parentheses against the corresponding hydrogen bond distances in Tables I–XIX.

TABLE I

O–H...O BONDS OF THE TYPE 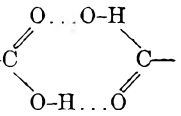

| Compound | O–H...O, Å. | Ref. |
|---|---|---|
| Adipic acid | 2.68 | *JC.*, **2**, 987 (1949) |
| *$p$-Aminosalicylic acid | 2.70 | *A.*, **7**, 808 (1954) |
| *11-Aminoundecanoic acid hydrobromide hemihydrate | 2.64 | *A.*, **8**, 833 (1955) |
| *Benzoic acid | 2.64 | *A.*, **8**, 157 (1955) |
| $p$-Chlorobenzoic acid | 2.62 | *A.*, **4**, 71 (1951) |
| Furoic acid | 2.53 | *A.*, **7**, 166 (1954) |
| $\beta$-Glutaric acid | 2.69 | *JC.*, **2**, 1001 (1949) |
| Hydrate racemic acid | 2.72 | *A.*, **4**, 131 (1951) |
| Lauric acid | 2.56 | *A.*, **4**, 324 (1951) |
| Malonic acid | 2.71 | *A.*, **10**, 125 (1957) |
| | 2.68 | |
| $\beta$-Nitropropionic acid | 2.66 | *A.*, **7**, 767 (1954) |
| Phenyl-propiolic acid | 2.60 | *A.*, **8**, 487 (1955) |
| $\alpha$-Pimelic acid | 2.68 | *A.*, **11**, 289 (1958) |
| | 2.67 | |
| *Salicylic acid | 2.63 | *A.*, **6**, 260 (1953) |
| Sebacic acid | 2.68 | *JC.*, **2**, 993 (1949) |
| $\beta$-Succinic acid | 2.64 | *JC.*, **2**, 980 (1949) |

TABLE II

O–H...O BONDS OF THE TYPE 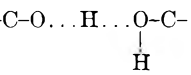

| Compound | O–H...O, Å. | Ref. |
|---|---|---|
| Dialuric acid monohydrate | 2.68 | *A.*, **9**, 501 (1956) |
| $\alpha$-Glucose | 2.78 | *A.*, **5**, 654 (1952) |
| | 2.74 | |
| | 2.70 | |
| | 2.74 | |
| Hydrate racemic acid | 2.75 | *A.*, **4**, 131 (1951) |
| | 2.83 | |
| Methanol | 2.66 | *A.*, **5**, 606 (1952) |
| †*Pentaerythritol | 2.74 | *A.*, **11**, 383 (1958) |
| | | *A.*, **11**, 389 (1958) |
| †*$\alpha$-Resorcinol | 2.69 | *P.*, **235**, 552 (1956) |
| | 2.75 | |
| $\beta$-Resorcinol | 2.70 | *P.*, **167**, 122 (1938) |
| | 2.75 | |
| *$\alpha$-Rhamnose monohydrate | 2.69 | *A.*, **10**, 227 (1957) |

TABLE III

O–H...O BONDS BETWEEN CARBOXYL GROUPS (EXCLUDING THOSE IN TABLE I)

| Compound | O–H...O, Å. | Ref. |
|---|---|---|
| *Acetic acid | 2.61 | *A.*, **11**, 484 (1958) |
| *Ammonium hydrogen D-tartrate | 2.55 | *A.*, **11**, 61 (1958) |
| *Diglycine hydrobromide | 2.46 | *Z.*, **108**, 130 (1956) |
| *Diglycine hydrochloride | 2.57 | *Z.*, **108**, 419 (1957) |
| Formic acid | 2.58 | *A.*, **6**, 127 (1953) |
| L-Glutamic acid | 2.54 | *A.*, **8**, 637 (1955) |
| *DL-Glutamic acid hydrochloride | 2.57 | *A.*, **6**, 81 (1953) |
| Maleic acid | 2.75 | *A.*, **5**, 763 (1952) |
| $\alpha$-Oxalic acid | 2.71 | *JC.*, **4**, 4854 (1952) |
| †*Potassium hydrogen bis-phenylacetate | 2.54 | *A.*, **10**, 524 (1957) |
| Tartaric acid | 2.87 | *A.*, **3**, 341 (1950) |

Similarly, the acceptor groups may be arranged in order of increasing $d$ for each donor group. Although these arrangements are not so similar to each other as those of the different donor groups the arrangement in Table XXII puts most values of $d$ for each donor group in increasing size. The variation in length of N–H...O bonds appear to be greater for a given acceptor with various donors than for a given donor with various acceptors. O–H...O bonds appear to behave similarly although values of $d$ for a number of these bonds are

TABLE IV

O–H...O BONDS BETWEEN WATER MOLECULES

| Compound | O–H...O, Å. | Ref. |
|---|---|---|
| Caffeine (structure still being refined) | 2.18 | *A.*, **11**, 453 (1958) |
| | 2.36 | |
| †*Chromium potassium alum | 2.66(102°) | *P.*, **246**, 78 (1958) |
| Colemanite | 2.73 | *A.*, **11**, 761 (1958) |
| *Creatine monohydrate | 2.87 | *A.*, **7**, 443 (1954) |
| Cupric formate tetrahydrate | 2.74 | *A.*, **7**, 482 (1954) |
| | 2.78 | |
| *N,N-Diglycyl-L-cystine dihydrate | 2.91(118°) | *A.*, **7**, 291 (1954) |
| 4,6-Dimethyl-2-hydroxypyrimidine | 2.73 | *A.*, **1**, 168 (1948) |
| *$HNO_3 3H_2O$ | 2.81(99°) | *A.*, **6**, 157 (1953) |
| ‡Ice (cubic) | 2.75 | *A.*, **10**, 710 (1957) |
| Ice (Hexagonal) | 2.76(109°) | *P.*, **125**, 670 (1929) |
| †*Ice (Heavy) | 2.75(110°) | *A.*, **10**, 70 (1957) |
| | 2.77(110°) | |
| $NaOH \cdot 4H_2O$ | 2.64 | *A.*, **10**, 37 (1957) |
| | 2.83 | |
| | 2.76 | |
| Phloroglucinol dihydrate | 2.74 | *A.*, **10**, 48 (1957) |
| *trans*-Potassium dioxalatodiaquo chromiate | 2.72 | *A.*, **4**, 35 (1951) |
| | 2.66 | |
| *Theophylline | 2.76 | *A.*, **11**, 83 (1958) |
| | 2.70 | |

TABLE V

O–H...O BONDS BETWEEN $H_2O$ AND $COO^-$

| Compound | O–H...O, Å. | Ref. |
|---|---|---|
| Chromous acetate·$2H_2O$ | 2.82 | *A.*, **6**, 501 (1953) |
| | 2.89 | |
| Copper proline dihydrate | 2.94 | *A.*, **5**, 599 (1952) |
| | 3.00 | |
| *Creatine monohydrate | 2.71 | *A.*, **7**, 443 (1954) |
| Cupric acetate·$2H_2O$ | 2.82 | *A.*, **6**, 227 (1953) |
| | 2.89 | |
| Cupric formate tetrahydrate | 2.82 | *A.*, **7**, 482 (1954) |
| Glycyl-L-alanine hydrochloride | 2.62 (105°) | *N.*, **177**, 37 (1956) |
| *Glycyl-L-tryptophan dihydrate | 2.77 (103°) | *A.*, **9**, 341 (1956) |
| | 2.78 (103°) | |
| | 2.99 (83°) | |
| *Histidine hydrochloride monohydrate | 2.76 (102°) | *A.*, **9**, 655 (1956) |
| *L-Leucyl-L-prolyl-glycine | 2.81 (82°) | *A.*, **11**, 17 (1958) |
| | 2.94 (82°) | |
| Nickel acetate·$4H_2O$ | 2.66 | *A.*, **6**, 609 (1953) |
| | 2.64 | |
| | 2.59 | |
| *trans*-Potassium dioxalatodiaquo chromiate | 2.65 | *A.*, **4**, 35 (1951) |
| | 2.75 | |
| | 3.04 | |
| Zinc acetate dihydrate | 2.49 | *A.*, **6**, 720 (1953) |
| | 2.74 | |
| Zinc salicylate dihydrate | 2.55 | *A.*, **11**, 41 (1958) |

not available. If this difference is significant it may be concluded that the nature of the donor is more important than the nature of the acceptor in determining the hydrogen bond length.

When classifying hydrogen bonds according to the chemical groups participating in them it is assumed that there is an optimum hydrogen bond distance between any two groups and that deviations from this distance are the result of a compromise between the action of the hydrogen bond force and of other forces that determine molecular configuration and packing. The histograms for the lengths of the various types of hydrogen bond (Fig. 1) will now be considered from this point of view.

**O–H...O Bonds.**—Donohue was able to make a rough classification of these bonds according to the group which contained the donor oxygen. This classification was elaborated for some types of O–H...O bonds by Ubbelohde and Gallagher.[8] For all but two of the compounds listed in Table I the only hydrogen bonds in the structure are those between the carboxyl groups. Therefore, these

(8) A. R. Ubbelohde and K. J. Gallagher, *Acta Cryst., Camb.*, **8**, 71 (1955).

TABLE VI

MISCELLANEOUS O–H...O BONDS

| Compound | Donor O in | Acceptor O in | O–H...O, Å. | Ref. |
|---|---|---|---|---|
| Glycyl-L-tyrosine hydrochloride | COOH | C–OH | 2.65 | *A.*, **6**, 531 (1953) |
| L-Tyrosine hydrobromide | COOH | C–OH | 2.50 | *C.*, **27**, 46 (1958) |
| *N-Acetylglycine | COOH | Chain C=O | 2.56 | *J.*, **72**, 2315 (1950) |
| Glutathione | COOH | Chain C=O | 2.66 | *A.*, **11**, 632 (1958) |
| Urea oxalate | COOH | Chain C=O | 2.50 | *S.*, **13**, 477 (1950) |
| *Oxalic acid dihydrate | COOH | Water | 2.49 | *A.*, **6**, 385 (1953) |
| *Ammonium hydrogen D-tartrate | C–OH | $COO^-$ | 2.74 | *A.*, **11**, 61 (1958) |
| | C–OH | $COO^-$ | 2.81 | |
| *Hydroxy-L-proline | C–OH | $COO^-$ | 2.80 | *A.*, **5**, 419 (1952) |
| *DL-Serine | C–OH | $COO^-$ | 2.67 | *A.*, **6**, 241 (1953) |
| *Threonine | C–OH | $COO^-$ | 2.66 | *J.*, **72**, 2328 (1950) |
| Tartaric acid | C–OH | COOH | 2.87 | *A.*, **3**, 341 (1950) |
| Phenoquinone | C–OH | Ring C=O | 2.64 | *A.*, **6**, 791 (1953) |
| α-Glucose | C–OH | Ring O | 2.86 | *A.*, **5**, 654 (1952) |
| α-Rhamnose monohydrate | C–OH | Ring O | 2.83 | *A.*, **10**, 227 (1957) |
| Glycyl-L-tyrosine hydrochloride | Water | C=O of COOH | 2.87 (123°) | *A.*, **6**, 531 (1953) |
| *Oxalic acid dihydrate | Water | C=O of COOH | 2.89 (84°) | *A.*, **6**, 385 (1953) |
| | Water | C=O of COOH | 2.88 (84°) | |
| Zinc salicylate dihydrate | Water | C–OH | 2.77 | *A.*, **11**, 41 (1958) |
| *N,N′-Diglycyl-L-cystine dihydrate | Water | Chain C=O | 3.13 (118°) | *A.*, **7**, 291 (1954) |
| Glycyl-L-alanine hydrochloride | Water | Chain C=O | 2.77 (105°) | *N.*, **177**, 37 (1956) |
| *Glycyl-L-tryptophan dihydrate | Water | Chain C=O | 2.74 (83°) | *A.*, **9**, 341 (1956) |
| Glycyl-L-tyrosine hydrochloride | Water | Chain C=O | 2.87 (123°) | *A.*, **6**, 531 (1953) |
| Dialuric acid monohydrate | Water | Ring C=O | 2.74 | *A.*, **9**, 501 (1956) |
| *Xanthazol·$H_2O$ | Water | Ring C=O | 2.84 (129°) | *Z.*, **106**, 339 (1955) |
| | Water | Ring C=O | 2.87 (129°) | |
| Colemanite | Water | Hydroxyl | 2.76 | *A.*, **11**, 761 (1958) |
| Zinc hydroxychloride·$H_2O$ | Water | Hydroxyl | 2.79 | *A.*, **10**, 787 (1957) |
| Callaghanite | Water | $CO_3$ | 2.52 | *A.*, **10**, 759 (1957) |
| †*Sodium sesquicarbonate | Water | $CO_3$ | 2.78 (114°) | *A.*, **9**, 82 (1956) |
| | Water | $CO_3$ | 2.76 (114°) | |
| *$HNO_3$·$3H_2O$ | Water | $NO_3$ | 2.73 (92°) | *A.*, **6**, 157 (1953) |
| | Water | $NO_3$ | 2.75 (99°) | |
| | Water | $NO_3$ | 2.79 (92°) | |
| $HNO_3$·$H_2O$ | Water | $NO_3$ | 2.61 (120°) | *A.*, **4**, 239 (1951) |
| | Water | $NO_3$ | 2.54 (120°) | |
| Sodium pyrophosphate decahydrate | Water | $PO_4$ | 2.73 | *A.*, **10**, 428 (1957) |
| | Water | $PO_4$ | 2.74 | |

TABLE VI (*Continued*)

| Compound | Donor O in | Acceptor O in | O-H...O, Å. | Ref. |
|---|---|---|---|---|
| | Water | $PO_4$ | 2.77 | |
| | Water | $PO_4$ | 2.61 | |
| | Water | $PO_4$ | 2.81 | |
| | Water | $PO_4$ | 2.84 | |
| | Water | $PO_4$ | 2.80 | |
| Cupric tetramine sulfate monohydrate | Water | $SO_4$ | 2.67(122°) | *A.*, **8**, 137 (1955) |
| †*Chromium potassium alum | Water | $SO_4$ | 2.66(102°) | *P.*, **246**, 78 (1958) |
| | Water | $SO_4$ | 2.64(94°) | |
| | Water | $SO_4$ | 2.72(94°) | |
| Zinc *p*-toluenesulfonate hexahydrate | Water | $SO_3$ | 2.78(107°) | *A.*, **10**, 191 (1957) |
| | Water | $SO_3$ | 2.79(105°) | |
| | Water | $SO_3$ | 2.77(113°) | |
| | Water | $SO_3$ | 2.82(105°) | |
| | Water | $SO_3$ | 2.81(107°) | |
| | Water | $SO_3$ | 2.73(113°) | |
| Colemanite | Hydroxyl | $Be_2O_4$ | 2.74 | *A.*, **11**, 761 (1958) |
| | Hydroxyl | $Be_3O_4$ | 2.73 | |
| *$HNO_3 \cdot 3H_2O$ | $H_3O^+$ | Water | 2.49 | *A.*, **6**, 157 (1953) |
| | $H_3O^+$ | Water | 2.57 | |
| | $H_3O^+$ | $NO_3$ | 2.62 | |
| Urea hydrogen peroxide | $H_2O_2$ | Chain C=O | 2.63 | *J.*, **63**, 1507 (1941) |
| Hydrogen peroxide | $H_2O_2$ | $H_2O_2$ | 2.78 | *A.*, **4**, 15 (1951) |
| $\beta$-$SrO_2 \cdot 2H_2O_2$ | $H_2O_2$ | $H_2O_2$ | 2.62 | *A.*, **10**, 778 (1957) |
| *Orthoboric acid | B–OH | B–OH | 2.72 | *A.*, **7**, 305 (1954) |
| $HNO_3 \cdot H_2O$ | NOH | Water | 2.68 | *A.*, **4**, 239 (1951) |
| Ammonium trinitrate | –NOH | $-NO_3$ | 2.63 | *A.*, **3**, 305 (1950) |
| Selenic acid | $H_2SeO_4$ | $H_2SeO_4$ | 2.68 | *JC.*, **2**, 968 (1951) |
| | | | 2.61 | |
| $HCrO_2$ | $HCrO_2$ | $HCrO_2$ | 2.55 | *A.*, **10**, 423 (1957) |
| †*Diaspore | | | 2.65 | *A.*, **11**, 798 (1958) |
| Potassium dihydrogen arsenate | | Acid Salt | 2.54 | *J.*, **64**, 354 (1942) |
| Potassium bicarbonate | | Acid Salt | 2.61 | *A.*, **5**, 292 (1952) |
| Sodium bicarbonate | | Acid Salt | 2.55 | *JP.*, **1**, 634 (1933) |
| †*Sodium sesquicarbonate | | Acid Salt | 2.50 | *A.*, **9**, 82 (1956) |
| †*$NH_4H_2PO_4$ | | Acid Salt | 2.48 | *A.*, **11**, 505 (1958) |
| †*$KH_2PO_4$ | | Acid Salt | 2.49 | *P.*, **220**, 397 (1953) |
| | | | | *P.*, **230**, 359 (1955) |
| *Potassium bisulfate | | Acid Salt | 2.68 | *A.*, **11**, 349 (1958) |
| | | | 2.67 | |

TABLE VII

N-H...O BONDS BETWEEN $NH_3^+$ AND $COO^-$

| Compound | N-H...O, Å. | <X-N...O° | Ref. |
|---|---|---|---|
| *DL-Alanine | 2.88 | 105 | *J.*, **72**, 949 (1950) |
| | 2.84 | 116 | |
| | 2.80 | 103 | |
| Cysteylglycine sodium iodide | 2.55 | | *A.*, **4**, 42 (1951) |
| | 3.03 | | |
| *Diglycine hydrobromide | 2.94 | 101 | *Z.*, **108**, 130 (1956) |
| | 2.90 | 116 | |
| *Diglycine hydrochloride | 2.90 | 114 | *Z.*, 108, 419 (1957) |
| | 2.93 | 102 | |
| *N,N'-Diglycyl-L-cystine dihydrate | 2.89 | 85 | *A.*, **7**, 291 (1954) |
| | 2.75 | 130 | |
| | 2.75 | 112 | |
| L-Glutamic acid | 2.86 | 102 | *A.*, **8**, 637 (1955) |
| | 2.92 | 103 | |
| | 2.94 | 113 | |
| *DL-Glutamic acid hydrochloride (carboxyl group un-ionized) | 2.89 | 88 | *A.*, **6**, 81 (1953) |
| L-Glutamine | 2.79 | 98 | *A.*, **5**, 644 (1952) |
| | 2.85 | 117 | |

| | | | |
|---|---|---|---|
| Glutathione | 2.89 | 130 | *A.*, **11**, 632 (1958) |
| | 2.68 | 107 | |
| *Glycine | 2.77 | 118 | *A.*,11, 654 (1958) |
| | 2.85 | 116 | |
| *γ-Glycine | 2.80 | 111 | *A.*, 11, 225 (1958) |
| | 2.81 | 91 | |
| | 2.95 | 124 | |
| Glycyl-L-alanine hydrochloride | 2.87 | | *N.*, **177**, 37 (1956) |
| *Glycyl-L-asparagine | 2.75 | 118 | *A.*, **7**, 225 (1954) |
| β-Glycylglycine | 2.68 | 110 | *J.*, **71**, 2618 (1949) |
| | 2.80 | 115 | |
| *Glycyl-L-tryptophan dihydrate | 2.86 | 124 | *A.*, **9**, 341 (1956) |
| Glycyl-L-tyrosine hydrochloride | 2.91 | | *A.*, **6**, 531 (1953) |
| Hexamethylenediammonium adipate | 2.75 | | *A.*, **7**, 87 (1954) |
| | 2.88 | | |
| | 2.72 | | |
| *L-Leucyl-L-prolyl-glycine | 2.84 | 123 | *A.*, **11**, 17 (1958) |
| | 2.87 | 101 | |
| | 2.83 | 111 | |
| DL-Methionine | 2.92 | | *A.*, **5**, 332 (1952) |
| | 2.59 | | |
| | 2.80 | | |
| | 2.82 | | |
| | 2.80 | | |
| | 2.78 | | |
| DL-Norleucine | 2.73 | 109 | *A.*, **6**, 399 (1953) |
| | 2.87 | 108 | |
| | 2.87 | 105 | |
| *DL-Serine | 2.87 | 121 | *A.*, **6**, 241 (1953) |
| | 2.81 | 98 | |
| *L-Threonine | 2.90 | 116 | *J.*, **72**, 2328 (1950) |
| | 2.80 | 98 | |

TABLE VIII

N-H...O BONDS BETWEEN CHAIN N-H AND CHAIN C=O

| Compound | N-H...O, Å. | Ref. |
|---|---|---|
| *Acetanilide | 2.97 | *A.*, **7**, 711 (1954) |
| *Cyclopropane carbohydrazide | 2.94 | *A.*, **11**, 413 (1958) |
| *N,N'-Diacetylhexamethylenediamine | 2.88 | *A.*, **8**, 575 (1955) |
| *N,N'-Diglycyl-L-cystine dihydrate | 3.31 | *A.*, **7**, 291 (1954) |
| *Diformylhydrazine | 2.80 | *A.*, **11**, 774 (1958) |
| *N,N'-Hexamethylenebispropionamide | 2.95 | *A.*, **10**, 528 (1957) |
| *L-Leucyl-L-prolyl-glycine | 3.19 | *A.*, **11**, 17 (1958) |

TABLE IX

N-H...O BONDS BETWEEN $-NH_2$ AND CHAIN C=O

| Compound | N-H...O, Å. | Ref. |
|---|---|---|
| Acetamide | 2.83 (127°) | *J.*, **62**, 2008 (1940) |
| | 2.89 (128°) | |
| Chloroacetamide | 3.01 | *A.*, **8**, 851 (1955) |
| | 2.82 | |
| Chloroacetamide (unstable form) | 3.05 | *A.*, **9**, 986 (1956) |
| *Cyclopropanecarbohydrazide | 3.26 | *A.*, **11**, 413 (1958) |
| *Decanamide | 2.88 | *A.*, **11**, 729 (1958) |
| | 2.90 | |
| *Formamide | 2.94 (119°) | *A.*, **7**, 559 (1954) |
| | 2.88 (109°) | |
| L-Glutamine | 2.94 (145°) | *A.*, **5**, 644 (1952) |
| *Nicotinamide | 2.99 (123°) | *A.*, **7**, 283 (1954) |
| *Oxamide | 2.95 (117°) | *A.*, **7**, 588 (1954) |
| | 2.94 (142°) | |
| *Succinamide | 2.94 (120°) | *A.*, **9**, 334 (1956) |
| | 2.94 (119°) | |
| Tetradecanamide | 2.99 | *A.*, **8**, 551 (1955) |
| | 2.93 | |
| *Urea-hydrocarbon complexes | 2.93 (136°) | *A.*, **5**, 224 (1952) |
| | 3.04 (116°) | |
| †*Urea | 2.99 (99°) | *A.*, **5**, 530 (1952) |
| | 3.04 (129°) | *A.*, **10**, 319 (1957) |

TABLE X

N-H...O BONDS BETWEEN RING NH AND RING C=O

| Compound | N-H...O, Å. | Ref. |
|---|---|---|
| Cyanuric acid | 2.83 | *J.*, **74**, 6156 (1952) |
| | 2.88 | |
| Dialuric acid monohydrate | 2.80 | *A.*, **9**, 501 (1956) |
| ‡Diketopiperazine | 2.84 | *T.*, **10**, 128 (1954) |
| Guanine hydrochloride monohydrate | 2.62 | *A.*, **4**, 92 (1951) |
| Isatin | 2.93 | *A.*, **3**, 294 (1950) |
| *Parabanic acid | 2.87 | *A.*, **8**, 129 (1955) |
| | 2.84 | |
| *α-Pyridone | 2.77 | *A.*, **6**, 591 (1953) |
| *Succinimide | 2.85 | *A.*, **9**, 405 (1956) |
| *Theophylline | 2.76 | *A.*, **11**, 83 (1958) |
| *Uracil | 2.86 | *A.*, **7**, 313 (1954) |
| | 2.81 | |
| *Xanthazol·$H_2O$ | 2.82 | *Z.*, **106**, 339 (1955) |

bonds are dominant in determining the molecular packing and as a result the histogram is sharp. A similar situation exists for the bonds between hydroxyl groups (Table II). Examples of this type of bond in which the carbon atom of the –COH group is in an unsaturated ring have $d$ equal to $2.71 \pm 0.03$ while $d$ for the remaining examples is $2.74 \pm 0.03$. Some difference would have been expected on theoretical grounds.[9] Many of the bonds between carboxyl groups listed in Table III occur in structures where the carboxyl group, and often other groups in the molecule are involved in

(9) L. Pauling, "The Nature of the Chemical Bond," 2nd Ed., Cornell University Press, Ithaca, N.Y., 1948, p. 322.

TABLE XI

MISCELLANEOUS N–H...O BONDS

| Compound | Donor N in | Acceptor O in | N–H...O, Å. | Ref. |
|---|---|---|---|---|
| Ammonium trinitrate | $NH_4^+$ | $NO_3$ | 3.01 | *A.*, **3**, 305 (1950) |
| †*Ammonium hydrogen phosphate | $NH_4^+$ | Phosphate | 2.92 | *A.*, **11**, 505 (1958) |
| Ammonium tetrametaphosphate | $NH_4^+$ | Phosphate | 2.79 | *A.*, **4**, 114 (1951) |
| | $NH_4^+$ | Phosphate | 2.79 | |
| | $NH_4^+$ | Phosphate | 3.03 | |
| | $NH_4^+$ | Phosphate | 3.03 | |
| | $NH_4^+$ | Phosphate | 2.80 | |
| | $NH_4^+$ | Phosphate | 2.85 | |
| | $NH_4^+$ | Phosphate | 2.82 | |
| | $NH_4^+$ | Phosphate | 2.82 | |
| *DL-Serine | $NH_3^+$ | C–OH | 2.79 (99°) | *A.*, **6**, 241 (1953) |
| *L-Threonine | $NH_3^+$ | C–OH | 3.10 (132°) | *J.*, **72**, 2328 (1950) |
| L-Glutamine | $NH_3^+$ | Chain C=O | 2.91 (115°) | *A.*, **5**, 644 (1952) |
| Glutathione | $NH_3^+$ | Chain C=O | 2.81 (115°) | *A.*, **11**, 632 (1958) |
| β-Glycylglycine | $NH_3^+$ | Chain C=O | 2.81 (91°) | *J.*, **71**, 2618 (1949) |
| *Glycyl-L-asparagine | $NH_3^+$ | Chain C=O | 2.86 (117°) | *A.*, **7**, 225 (1954) |
| | $NH_3^+$ | Chain C=O | 3.03 (133°) | |
| *11-Aminoundecanoic acid hydrobromide hemihydrate | $NH_3^+$ | Water | 2.92 (123°) | *A.*, **8**, 833 (1955) |
| *Glycyl-L-tryptophan dihydrate | $NH_3^+$ | Water | 2.68 (115°) | *A.*, **9**, 341 (1956) |
| | $NH_3^+$ | Water | 2.75 (114°) | |
| *Histidine hydrochloride monohydrate | $NH_3^+$ | Water | 2.82 (102°) | *A.*, **9**, 655 (1956) |
| D(−)-Isoleucine hydrobromide | $NH_3^+$ | Water | 2.82 | *A.*, **7**, 703 (1954) |
| | $NH_3^+$ | Water | 2.84 | |
| D(−)-Isoleucine hydrochloride | $NH_3^+$ | Water | 2.85 | *A.*, **7**, 703 (1954) |
| | $NH_3^+$ | Water | 2.96 | |
| Monosodium phosphoramidate | $NH_3^+$ | $PO_3^-$ | 2.84 (108°) | *A.*, **6**, 621 (1953) |
| $2NH_3 \cdot H_2O$ | $NH_3$ | Water | 3.13 | *A.*, **7**, 194 (1954) |
| | $NH_3$ | Water | 3.22 | |
| | $NH_3$ | Water | 3.22 | |
| *Hydroxy-L-proline | $NH_2^+$ | Carboxyl | 2.69 | *A.*, **5**, 419 (1952) |
| | $NH_2^+$ | Carboxyl | 3.17 | |
| *Creatine monohydrate | $NH_2$ | Carboxyl | 2.86 | *A.*, **7**, 443 (1954) |
| | $NH_2$ | Carboxyl | 2.79 | |
| | $NH_2$ | Carboxyl | 2.85 | |
| L-Glutamine | $NH_2$ | Carboxyl | 2.91 (125°) | *A.*, **5**, 644 (1952) |
| *Glycyl-L-asparagine | $NH_2$ | Carboxyl | 2.88 (109°) | *A.*, **7**, 225 (1954) |
| | $NH_2$ | Carboxyl | 2.93 (111°) | |
| 6-Amido-3-pyridazone | $NH_2$ | Ring C=O | 2.84 | *A.*, **7**, 199 (1954) |
| | $NH_2$ | Ring C=O | 2.92 | |
| Creatinine | $NH_2$ | Ring C=O | 2.85 (124°) | *A.*, **8**, 311 (1955) |
| *Creatine monohydrate | $NH_2$ | Water | 2.94 | *A.*, **7**, 443 (1954) |
| Urea·$H_2O_2$ | $NH_2$ | $H_2O_2$ | 2.94 (132°) | *J.*, **63**, 1507 (1941) |
| | $NH_2$ | $H_2O_2$ | 3.04 (112°) | |
| *Methylguanidinium nitrate | $NH_2$ | $NO_2$ | 3.00 | *A.*, **8**, 675 (1955) |
| | $NH_2$ | $NO_2$ | 2.98 | |
| | $NH_2$ | $NO_2$ | 3.06 | |
| | $NH_2$ | $NO_2$ | 3.09 | |
| Nitramide | $NH_2$ | $NO_2$ | 3.04 | *A.*, **10**, 34 (1957) |
| | $NH_2$ | $NO_2$ | 3.12 | |
| *p*-Nitroaniline | $NH_2$ | $NO_2$ | 3.03 (149°) | *A.*, 9, 960 (1956) |
| | $NH_2$ | $NO_2$ | 3.08 (119°) | |
| *Nitroguanidine | $NH_2$ | $NO_2$ | 2.97 | *A.*, 9, 573 (1956) |
| | $NH_2$ | $NO_2$ | 3.28 | |
| *Sulfamide | $NH_2$ | $SO_2$ | 3.02 (111°) | *A.*, 9, 628 (1956) |
| *N-Acetylglycine | Chain NH | Carboxyl | 3.03 | *J.*, **72**, 2315 (1950) |
| Glutathione | Chain NH | Carboxyl | 2.98 | *A.*, **11**, 632 (1958) |
| β-Glycylglycine | Chain NH | Carboxyl | 3.07 | *J.*, **71**, 2618 (1949) |
| *Glycyl-L-asparagine | Chain NH | Carboxyl | 2.88 | *A.*, **7**, 225 (1954) |
| *Glycyl-L-tryptophan dihydrate | Chain NH | Carboxyl | 2.89 | *A.*, **9**, 341 (1956) |
| *Methylguanidinium nitrate | Chain NH | $NO_2$ | 2.88 | *A.*, **8**, 675 (1955) |
| Copper proline dihydrate | Ring NH | Carboxyl | 2.86 | *A.*, **5**, 599 (1952) |
| *Histidine hydrochloride monohydrate | Ring NH | Carboxyl | 2.83 | *A.*, **9**, 655 (1956) |

| | | | | |
|---|---|---|---|---|
| | Ring NH | Carboxyl | 2.64 | |
| 6-Amido-3-pyridazone | Ring NH | Chain C=O | 2.84 | *A.*, **7**, 199 (1954) |
| *Adenine hydrochloride hemihydrate | Ring NH | Water | 2.87 | *A.*, **4**, 87 (1951) |
| *Xanthazol·$H_2O$ | Ring NH | Water | 2.74 | *Z.*, **106** 339 (1955) |

TABLE XII

MISCELLANEOUS O–H...N BONDS

| Compound | Donor O in | Acceptor N in | O–H...N, Å. | Ref. |
|---|---|---|---|---|
| 4-Isopropylidene-aminophenol | C–OH | Chain N | 2 66 | *A.*, 6, 256 (1953) |
| Ammonium oxide | Water | $NH_3$ | 2.85 (116°) | *A.*, **7**, 194 (1954) |
| | Water | $NH_3$ | 2.84 (116°) | |
| Caffeine | Water | Ring N | 2.85 | *A.*, **11**, 453 (1958) |
| *Theophylline | Water | Ring N | 2.89 | *A.*, **11**, 83 (1958) |
| ‡$K_2Cd(SCN)_4·2H_2O$ | Water | CN | 2.72 | *T.*, **10**, 79 (1954) |
| $NaCN·2H_2O$ | Water | CN | 2.81 | *A.*, **11**, 770 (1958) |
| *sym-p*-Chlorobenzaldoxime | Oxime OH | Oxime N | 2.84 | *N.*, **180**, 1410 (1957) |
| Dimethylglyoxime | Oxime OH | Oxime N | 2.83 | *A.*, **5**, 811 (1952) |
| Formamidoxime | Oxime OH | Oxime N | 3.01 | *A.*, 9, 108 (1956) |
| | Oxime OH | Oxime N | 2.81 | |

TABLE XIII

N–H...N BONDS BETWEEN $-NH_2$ AND $-NH_2$

| Compound | N–H...N, Å. | Ref. |
|---|---|---|
| *Cyclopropanecarbohydrazide | 3.16 | *A.*, **11**, 413 (1958) |
| Hexamethylenediamine | 3.21 | *A.*, **3**, 424 (1950) |
| Hydrazine | 3.19 | *A.*, **4**, 10 (1951) |
| | 3.30 | |
| *Hydrazine salt of 5-aminotetrazole | 3.14 (98°) | *A.*, **11**, 31 (1958) |
| *Methylamine | 3.18 | *A.*, 6, 770 (1953) |
| | 3.27 | |

TABLE XIV

N–H...N BONDS BETWEEN $-NH_2$ AND RING N

| Compound | N–H...N, Å. | Ref. |
|---|---|---|
| *Adenine hydrochloride hemihydrate | 2.99 | *A.*, **4**, 81 (1951) |
| 4-Amino-2,6-dichloropyrimidine | 3.09 (116°) | *A.*, 2, 46 (1949) |
| | 3.28 (107°) | |
| 4,5-Diamino-2-chloropyrimidine | 3.16 | *A.*, **9**, 586 (1956) |
| | 3.11 | |
| 5-Bromo-4,6-diaminopyrimidine | 2.96 (143°) | *A.*, **2**, 46 (1949) |
| | 3.07 (122°) | |
| Creatinine | 2.92 (117°) | *A.*, **8**, 311 (1955) |
| Guanine hydrochloride monohydrate | 3.08 | *A.*, 4, 92 (1951) |
| *Hydrazine salt of 5-aminotetrazole | 3.00 (112°) | *A.*, **11**, 31 (1958) |
| Melamine | 3.00 (136°) | *J.*, **63**, 1737 (1941) |
| | 3.02 (98°) | |
| | 3.05 (92°) | |
| | 3.10 (112°) | |
| 2-Methyl-5-aminotetrazole | 3.08 (108°) | *A.*, **9**, 874 (1956) |
| | 3.04 (108°) | |
| *Nicotinamide | 3.09 (110°) | *A.*, **7**, 283 (1954) |

other hydrogen bonds. Consequently the length of this bond may be altered from the optimum value and as a result the histogram is more diffuse. *d* for these bonds is significantly shorter than those in Table I.

The hydrogen bond length in ice (2.76 Å.) lies close to *d* for hydrogen bonds between water molecules (Table IV) and may be taken as the optimum hydrogen bond distance for this type of bond. The more accurately determined examples of the bond between a water molecule and an ionized carboxyl group (Table V) are mainly from amino acids and simple peptides. These compounds frequently crystallize in the zwitterion condition where the hydrogen bonding about the $NH_3^+$ group is dominant in determining the packing and as a result the histogram is rather broad. Of the various types of bonds collected in Table VI those from the acid salts are of interest on account of uncertainty concerning the position of the hydrogen atom. There are two possibilities: either the hydrogen atom is statistically distributed between the two oxygen atoms or it is situated symmetri-

TABLE XV

MISCELLANEOUS N–H...N BONDS

| Compound | Donor N in | Acceptor N in | N–H...N, Å. | Ref. |
|---|---|---|---|---|
| Hydrazinium chloride | $NH_3^+$ | $NH_2$ | 2.95 | *A.*, **5**, 293 (1952) |
| *Hydrazine salt of 5-aminotetrazole | $NH_3^+$ | Ring N | 2.90 (90°) | *A.*, **11**, 31 (1958) |
| | $NH_3^+$ | Ring N | 2.88 (127°) | |
| | $NH_3^+$ | Ring N | 2.90 (91°) | |
| *Azo-bis-N-chloroformamidine | $NH_2$ | Chain N | 2.96 (140°) | *A.*, **11**, 158 (1958) |
| Dicyandiamide | $NH_2$ | Chain N | 2.94 (120°) | *J.*, **62**, 1258 (1940) |
| | $NH_2$ | Chain N | 3.02 (98°) | |
| | $NH_2$ | Chain N | 3.04 (146°) | |
| | $NH_2$ | Chain N | 3.16 (91°) | |
| *Nitroguanidine | $NH_2$ | Chain N | 3.12 | *A.*, **9**, 573 (1956) |
| Isocyanic acid | Chain NH | Chain NH | 3.07 | *A.*, **8**, 646 (1955) |
| Formamidoxime | Chain NH | Oxime N | 3.12 | *A.*, **9**, 108 (1956) |
| *$S_4N_4H_4$ | Ring NH | Ring NH | 3.16 | *A.*, **11**, 497 (1958) |
| *3-Hydrazino-5-thiol-1,2,4-triazole | Ring NH | Ring N | 2.88 | *A.*, **11**, 808 (1958) |
| *Xanthazol·$H_2O$ | Ring NH | Ring N | 2.90 | *Z.*, **106**, 339 (1955) |

TABLE XVI

N-H...Cl BONDS BETWEEN $NH_3^+$ AND $Cl^-$

| Compound | N-H...Cl, Å. | <X-N...Cl° | Ref. |
|---|---|---|---|
| Cyclohexylamine hydrochloride | 3.14 | 116 | *A.*, **8**, 819 (1955) |
| | 3.20 | 102 | |
| | 3.25 | 118 | |
| Cycloserine hydrochloride | 3.14 | 91 | *A.*, **10**, 480 (1957) |
| | 3.17 | 97 | *A.*, **10**, 383 (1957) |
| | 3.25 | 98 | |
| *Diglycine hydrochloride | 3.13 | 115 | *Z.*, **108**, 419 (1957) |
| | 3.22 | 99 | |
| Geranylamine hydrochloride | 3.17 | 101 | *P.*, **183**, 388 (1945) |
| (Angles calcd. by Donohue) | 3.22 | 102 | |
| | 3.22 | 102 | |
| *DL-Glutamic acid hydrochloride | 3.18 | | *A.*, **6**, 81 (1953) |
| | 3.18 | | |
| Glycyl-L-alanine hydrochloride | 3.36 | | *N.*, **177**, 37 (1956) |
| Glycyl-L-tyrosine hydrochloride | 3.24 | | *A.*, **6**, 531 (1953) |
| | 3.24 | | |
| Hexamethylenediamine dihydrochloride (recalcd. by Donohue) | 3.15 | 104 | *A.*, **2**, 180 (1949) |
| | 3.25 | 104 | |
| | 3.25 | 98 | |
| | 3.01 | 128 | |
| | 3.07 | 115 | |
| | 3.33 | 88 | |
| *Histidine hydrochloride monohydrate | 3.17 | 92 | *A.*, **9**, 655 (1956) |
| | 3.21 | 120 | |
| Hydrazine dihydrochloride | 3.10 | 100 | *JP.*, **15**, 115 (1947) |
| Hydrazinium chloride | 3.12 | | *A.*, **5**, 293 (1952) |
| | 3.12 | | |
| D(−)-Isoleucine Hydrochloride | 3.18 | | *A.*, **7**, 703 (1954) |
| Hydroxylammonium chloride | 3.16 | 99 | *A.*, **1**, 21 (1948) |
| | 3.23 | 90 | |
| | 3.26 | 95 | |
| *m*-Tolidine dihydrochloride | 3.10 | 108 | *A.*, **3**, 81 (1950) |
| | 3.22 | 105 | |
| | 3.26 | 101 | |

TABLE XVII

MISCELLANEOUS N-H...Cl BONDS TO $Cl^-$

| Compound | Donor N in | N-H...Cl, Å. | Ref. |
|---|---|---|---|
| 1,3-Dimethyl-5-iminotetrazole hydrochloride | $NH_2^+$ | 3.21 | *A.*, **8**, 211 (1955) |
| | $NH_2^+$ | 3.17 | |
| *Adenine hydrochloride hemihydrate | $NH_2$ | 3.18 | *A.*, **4**, 81 (1951) |
| Guanine hydrochloride monohydrate | $NH_2$ | 3.38 | *A.*, **4**, 92 (1951) |
| Hydrazinium chloride | $NH_2$ | 3.26 | *A.*, **5**, 293 (1952) |
| Aminoguanidine hydrochloride | Chain NH | 3.13 | *A.*, **10**, 677 (1957) |
| Ephedrine hydrochloride | Chain NH | 3.12 | *A.*, **7**, 159 (1954) |
| Triaminoguanidinium chloride | Chain NH | 3.19 | *A.*, **10**, 681 (1957) |
| Glycyl-L-alanine hydrochloride | Chain NH | 3.23 | *N.*, **177**, 37 (1956) |
| *Adenine hydrochloride hemihydrate | Ring NH | 3.11 | *A.*, **4**, 81 (1951) |
| Guanine hydrochloride monohydrate | Ring NH | 3.20 | *A.*, **4**, 92 (1951) |

TABLE XVIII

MISCELLANEOUS O-N...Cl BONDS TO $Cl^-$

| Compound | Donor O in | O-H...Cl, Å. | Ref. |
|---|---|---|---|
| *DL-Glutamic acid hydrochloride | Carboxyl | 3.06 | *A.*, **6**, 81 (1953) |
| D(−)-Isoleucine hydrochloride | Carboxyl | 3.05 | *A.*, **7**, 703 (1954) |
| Ephedrine hydrochloride | C–OH | 3.06 | *A.*, **7**, 159 (1954) |
| Glycyl-L-tyrosine hydrochloride | C–OH | 3.04 | *A.*, **6**, 531 (1953) |
| *Adenine hydrochloride hemihydrate | Water | 3.12 | *A.*, **4**, 81 (1951) |
| Guanine hydrochloride monohydrate | Water | 3.16 | *A.*, **4**, 92 (1951) |
| *Histidine hydrochloride monohydrate | Water | 3.19 (102°) | *A.*, **9**, 655 (1956) |
| D(−)-Isoleucine hydrochloride | Water | 3.07 | *A.*, **7**, 703 (1954) |
| | Water | 3.24 | |
| Zinc hydroxychloride | Hydroxyl | 3.09 | *A.*, **10**, 787 (1957) |

TABLE XIX

MISCELLANEOUS HALOGEN HYDROGEN BONDS

| Compound | Hydrogen donor | Halogen | X-H...Y, Å | Ref. |
|---|---|---|---|---|
| Hydrazinium difluoride | $NH_3^+$ | F | 2.62 | *JP.*, 10, 309 (1942) |
| *Hydrogen fluoride | HF | F | 2.49 | *A.*, 7, 173 (1954) |
| *11-Aminoundecanoic hydrobromide hemihydrate | $NH_3^+$ | Br | 3.44 (92°) | *A.*, 8, 833 (1955) |
| | $NH_3^+$ | Br | 3.30 (104°) | |
| *Diglycine hydrobromide | $NH_3^+$ | Br | 3.37 (110°) | *Z.*, 108, 130 (1956) |
| | $NH_3^+$ | Br | 3.37 (81°) | |
| | $NH_3^+$ | Br | 3.33 (103°) | |
| D(−)-Isoleucine hydrobromide | $NH_3^+$ | Br | 3.35 | *A.*, 7, 703 (1954) |
| *Monoethylamine hydrobromide | $NH_3^+$ | Br | 3.38 | *A.*, 11, 626 (1958) |
| | $NH_3^+$ | Br | 3.37 | |
| L-Tyrosine hydrobromide | $NH_3^+$ | Br | 3.46 (101°) | *C.*, 27, 46 (1958) |
| | $NH_3^+$ | Br | 3.46 (136°) | |
| | $NH_3^+$ | Br | 3 50 (107°) | |
| D(−)-Isoleucine hydrobromide | Carboxyl | Br | 3.29 | *A.*, 7, 703 (1954) |
| L-Tyrosine hydrobromide | C-OH | Br | 3.23 | *C.*, 27, 46 (1958) |
| *11-Aminoundecanoic hydrobromide hemihydrate | Water | Br | 3.38 (93°) | *A.*, 8, 833 (1955) |
| D(−)-Isoleucine hydrobromide | Water | Br | 3.30 | *A.*, 7, 703 (1954) |
| | Water | Br | 3.35 | |
| Muscarine | C-OH | I | 3.57 | *A.*, 10, 277 (1957). |

TABLE XX

INTRAMOLECULAR HYDROGEN BONDS

| Compound | Type of Bond | X-H...X, Å. | Ref. |
|---|---|---|---|
| *p-Aminosalicylic acid | O-H...O | 2.62 | *A.*, 7, 808 (1954) |
| *Salicylic Acid | O-H...O | 2.59 | *A.*, 6, 260 (1953) |
| Zinc salicylate dihydrate | O-H...O | 2.51 | *A.*, 11, 41 (1958) |
| Maleic acid | O-H...O | 2.46 | *A.*, 5, 763 (1952) |
| *Nickel dimethylglyoxime | O-H...O | 2.44 | *A.*, 6, 487 (1953) |
| Nickel salicylaldoxime | O-H...O | 2.52 | *A.*, 9, 253 (1956) |
| *Nitroguanidine | N-H...O | 2.57 | *A.*, 9, 573 (1956) |

TABLE XXI

BONDS WHICH ARE BELIEVED TO BE BIFURCATED

| Compound | Type of bond | X-H...X, Å. | Ref. |
|---|---|---|---|
| *Nitroguanidine | $NH_2...NO_2$ | 2.57 | *A.*, 9, 573 (1956) |
| | $NH_2...NO_2$ | 3.03 | |
| *Diglycine hydrobromide | $NH_3^+...COO^-$ | 3.04 | *Z.*, 108, 130 (1956) |
| | $NH_3^+...COO^-$ | 3.10 | |
| *Diglycine hydrochloride | $NH_3^+...COO^-$ | 2.98 | *Z.*, 108, 419 (1957) |
| | $NH_3^+...COO^-$ | 3.04 | |
| *Glycine | $NH_3^+...COO^-$ | 2.95 | *A.*, 11, 654 (1958) |
| | $NH_3^+...COO^-$ | 3.07 | |

cally between them. In most of the acid salts that have been studied by neutron diffraction, the evidence indicates that the hydrogen atom is statistically distributed.

**N-H...O Bonds.**—The evidence available on bonds between the X-$NH_3^+$ and $COO^-$ groups led Donohue to suggest that the longer bonds were generally associated with the greater deviations of <X-N...O from the tetrahedral value of 109° (X is the atom to which N is covalently bond and <X-N...O is therefore the angle between the hydrogen bond and this covalent bond). Figure 3 shows that the data in Table VII do not support this conclusion. If there was a correlation between angle and length a U-shaped curve with the minimum at <X-N...O equal to 109° would be expected. A similar lack of correlation between bond angle and bond length exists for other types of hydrogen bond, *e.g.*, $NH_3^+...Cl^-$ (Table XVI).

With one exception all the examples of the bond between $NH_3^+$ and $COO^-$ are taken from structure determinations of amino acids and simple peptides. This type of bonding is particularly abundant in these compounds because they mostly crystallize in the zwitterion condition. Bonding about the $NH_3^+$ group has a dominant effect in determining the structure and as a result the histogram is narrow compared with those for some of the other hydrogen bonds in these structures, *e.g.*, $COO^-$ . . . $H_2O$. By contrast the typical polypeptide bond, N-H . . . O=C (Table VIII) is rarely formed in these structures. Of the examples in Table VIII those from N,N'-diacetylhexamethylenediamine, N,N'-hexamethylenebispropionamide and diformylhydrazine are most analogous to the hydrogen bond which is assumed to be formed in the β-configuration of polypeptides. Most of the examples of the bond between $NH_2$ and chain C=O (Table IX) are taken from structures of the amides where these two groups are often the only hydrogen bond forming groups in the molecule. It is not surprising therefore that this bond dominates the packing in these structures and a sharp histogram results. A sharp histogram also is obtained for bonds between the NH and C=O groups of heterocyclic compounds (Table X).

**O-H...N Bonds.**—As was noted by Donohue these bonds (Table XII) occur infrequently because of the preferential formation of the O-H...O bond. In a number of structures it has not been possible to decide whether the oxygen or the nitrogen donates the proton, *e.g.*, hydroxylamine.[10,11]

**N-H...N Bonds.**—It can be seen from Tables XIII, XIV, and XV that this bond is rarely formed by molecules that contain oxygen. This is because N-H . . . O bonds form preferentially. The longest N-H . . . N bonds are those between amino groups (Table XIII). They are considerably longer than the bonds between an amino group and a ring nitrogen (Table XIV) presumably because of the repulsion between hydrogen atoms in the amino groups.

(10) J. Donohue, *Acta Cryst., Camb.*, **11**, 512 (1958).
(11) B. Jerslev, *ibid.*, **11**, 511 (1958).

TABLE XXII

The Mean Value, $d$ (with Standard Deviation) of Observed Bond Length for Various Types of Hydrogen Bond. The number in parentheses is the number of determinations on which $d$ is based.

| Hydrogen acceptor | Hydrogen Donor –COOH | –COH | Water | Ring NH | $-NH_3^+$ | $-NH_2$ | Chain NH |
|---|---|---|---|---|---|---|---|
| $-COO^-$ | | 2.74 ± 0.06 (5) | 2.78 ± 0.14 (24) | 2.78 ± 0.10 (3) | 2.83 ± 0.08 (50) | 2.87 ± 0.05 (6) | 2.97 ± 0.08 (5) |
| Water | 2.49 (1) | | 2.75 ± .06 (20) | 2.81 ± .07 (2) | 2.83 ± .08 (8) | 2.94 (1) | |
| Ring C=O | | 2.64 (1) | 2.82 ± .06 (3) | 2.82 ± .07 (14) | | 2.87 ± .04 (3) | |
| –COH | 2.58 ± .08 (2) | 2.73 ± .04 (14) | 2.77 (1) | | 2.95 ± .16 (2) | | |
| Chain C=O | 2.57 ± .07 (3) | | 2.88 ± .15 (4) | 2.84 (1) | 2.89 ± .08 (5) | 2.96 ± .09 (22) | 3.01 ± .17 (7) |
| –COOH | 2.61 ± .11 (11) | 2.87 (1) | 2.88 ± .01 (3) | | | | |
| Ring N | | | 2.87 ± .02 (2) | 2.89 ± .01 (2) | 2.89 ± .01 (3) | 3.06 ± .08 (17) | |
| $Cl^-$ | 3.06 ± .01 (2) | 3.05 ± .01 (2) | 3.16 ± .06 (5) | 3.16 ± .05 (2) | 3.19 ± .07 (34) | 3.27 ± .08 (3) | 3.17 ± .04 (4) |
| $Br^-$ | 3.29 (1) | 3.23 (1) | 3.34 ± .03 (3) | | 3.39 ± .06 (11) | | |

**Halogen Hydrogen Bonds.**—The majority of N–H . . . Cl bonds are of the form $NH_3^+ \ldots Cl^-$ (Table XVI) and are usually found when compounds containing an amino group have formed a salt with hydrogen chloride. This type of bond is dominant in determining the packing in these structures and as a result the histogram is well defined. Other hydrogen bonds involving halogens are collected in Tables XVII, XVIII and XIX.

**Bifurcated Bonds.**—Bonds of this type (Table XXI) are often postulated when the number of intermolecular close approaches exceeds the number of hydrogen atoms available for hydrogen bonding. That this is not always the best interpretation has been shown by Donohue for a number of structures, *e.g.*, cycloserine hydrochloride.[12] In the structure of maleic acid (Table III) a bifurcated bond was originally suggested by the author but in view of the length of the longer of the two "bonds" and the angles involved, it is more reasonable to believe that there exists a normal hydrogen bond (2.75 Å.) and a normal van der Waals contact (J. Donohue, private communication). However, in the recently refined structure of glycine the coördinates of the hydrogen atoms were determined and show that one hydrogen atom of the $NH_3^+$ group is less than the normal van der Waals distance from two oxygen atoms. Therefore it is reasonable to suppose that a bifurcated bond exists in this structure. In X-ray structure determinations where the data are insufficient to enable the hydrogen atoms to be located, stereochemical arguments may be sufficient to suggest the existence of a bifurcated bond, *e.g.*, diglycine hydrochloride.

## Conclusions

(1) The recent structure determinations described in this paper are consistent with Donohue's observation that only in very exceptional cases does a hydrogen atom bonded to nitrogen or oxygen occupy a position such that hydrogen bonding is impossible. The fact that, almost without exception, molecules in a crystal arrange themselves so that the maximum number of hydrogen bonds is formed, indicates the important role that hydrogen bonding plays in crystal structure.

(2) Table XXII and the histograms in Fig. 1 indicate that the length of a hydrogen bond is largely determined by the chemical groups participating in it.

(3) The histograms in Fig. 2 indicate that for the three most important hydrogen donor groups, the angle at the donor atom, between the hydrogen bond direction and the expected direction of the bond from the donor to the hydrogen atom, can be as large as 20°. Few examples have been observed where this angle is greater than 20°.

(4) Figure 3 indicates that for bonding about the $NH_3^+$ group there is little correlation between the distortions in length and direction for a particular hydrogen bond. A similar lack of correlation has been observed for other types of hydrogen bond and it therefore appears likely that the angle and length of a hydrogen bond can vary almost independently.

(12) J. Donohue, *ibid.*, **10**, 383 (1957).

(5) The spread in the histograms has been interpreted as being due to two effects: (a) errors in the hydrogen bond length determinations; (b) the effect on the packing of intermolecular forces other than those due to the particular hydrogen bond in question. Therefore it might be expected that the spread would be greater for larger than for smaller molecules. Tables I–XXI support this view. Most "unexpected" lengths have been observed in the structures of amino acids, di- and tripeptides, probably because the structures of other types of molecule of comparable size have seldom been determined accurately.

(6) Examples have been given indicating that bifurcated bonds can exist though infrequently.

The need for more data with a limit of error in the hydrogen bond length of less than 0.05 Å. is apparent from Table XXII and Fig. 1. Such data will help to separate the spread in the histograms due to errors in the structure determinations from that due to variations in length of a particular type of hydrogen bond in different structures. It will then be possible to give more reliable values of $d$ (see diagram 1 for definition) and its standard deviation and to draw more detailed conclusions than those given.

I would like to thank Dr. M. H. F. Wilkins, Mr. G. R. Wilkinson and Dr. M. Spencer for much helpful discussion and suggestions during this work. Also, I am very grateful to Professor J. Donohue who read the manuscript and made a number of valuable criticisms. During the period of this work I have been the holder of a Medical Research Council Scholarship.

---

# COLLECTOR-DEPRESSANT EQUILIBRIA IN FLOTATION

By K. L. Sutherland

*Division of Physical Chemistry, Commonwealth Scientific and Industrial Research Organization, Box 4331, G.P.O., Melbourne*

*Received February 7, 1959*

It is shown that the competition in flotation between collector ions and depressant for a mineral surface can be expressed in the same form as an expression developed for collector–depressant competition in the neutral molecule theory. Accurate measurements over a wide $p$H range are made using a stable sulfur-containing collector (mercaptobenzthiazole) for pyrite. Both theories fail to describe the relation between the $p$H value and the amount of collector required to cause flotation, but accurately describe the relation between $p$H value and cyanide addition at constant collector addition.

In the flotation process minerals are differentially floated by using depressants to prevent the adsorption of a collector on certain minerals. This collector, a polar–non-polar substance, is adsorbed on the wanted mineral making its surface hydrophobic. The collectors usually contain an ionic group such as $C_{15}H_{31}COO^-$, $C_2H_5O{\cdot}CS{\cdot}S^-$, $C_{12}H_{25}SO_4^-$, $C_{16}H_{33}(CH_3)_3N^+$ or $C_{12}H_{25}NH_3^+$ and depressants usually contain inorganic ions such as $OH^-$, $CN^-$, $SH^-$, $H^+$ or $Ca^{++}$. Depressants have the same ionic sign as the collector and compete with it for the mineral surface. Wark and Cox[1] and others have considered the competition between collector ion, $X^-$, and depressant ion, $D^-$, such that

$$\frac{[X^-]}{[D^-]} = \text{constant}$$

This relation appears to hold approximately for a number of simple systems, *e.g.*, Sutherland and Wark.[2]

Last and Cook[3] have proposed an alternative mechanism in which it is postulated that the active collector is not the ion but the free acid or free base, *e.g.*, $C_{15}H_{31}COOH$, $C_2H_5OCSSH$, $C_{12}H_{25}SO_4H$, $C_{16}H_{33}(CH_3)_3NOH$ or $C_{12}H_{25}NH_2$; and that the active depressant is HCN, $H_2S$ or presumably, $Ca(OH)_2$. They also show that, for many collectors related to the xanthates or dithiophosphates, account should be taken of the extent of ionization of these collectors—a factor neglected by Wark and Cox who mostly considered solutions where such a correction is unnecessary.

In examining the mechanism of ion competition, Last and Cook suggest that the equilibria involved are

$$S'' + X^- \rightleftarrows S''X^- \quad (1)$$
$$S'' + OH^- \rightleftarrows S''OH^- \quad (2)$$
$$S'' + D^- \rightleftarrows S''D^- \quad (3)$$
$$S' + H^+ \rightleftarrows S'H^+ \quad (4)$$

where S″ is an electropositive site on the mineral and S′ an electronegative site, the surface remaining electrically neutral after adsorption. These four relations have only three unknowns, since the concentration of $H^+$ determines that of the $OH^-$. They then go on to show that the equations are mathematically inconsistent in this form, but this does not constitute proof of their assertion that the experimental facts are incompatible with an ionic mechanism.

The hypothesis of neutral molecule adsorption is examined by Last and Cook who find the relation arising from the equilibria

$$S + HX \rightleftarrows SHX \quad (5)$$
$$S + HD \rightleftarrows SHD \quad (6)$$

as

$$[HX] - [HX]_0 = \frac{K''K_2}{K_1}[HD] \quad (7)$$

where [HX] is the concentration of collector acid required to induce contact (flotation) at the concentration [HD] of depressant. $[HX]_0$ is the concentration required in the absence of HD and $K_1$

(1) I. W. Wark and A. B. Cox, *Trans. Am. Inst. Mining Met. Engrs.*, **112**, 267 (1934); **134**, 7 (1939).

(2) K. L. Sutherland and I. W. Wark, "Principles of Flotation," Australasian Inst. Mining Met., 1955, Chapter IX.

(3) A. W. Last and M. A. Cook, This Journal, **56**, 637 (1952).

and $K_2$ are equilibrium constants for equations 5 an 6. The constant $K''$ depends on the amount collector adsorbed and may be directly related to the contact angle (Wadsworth, Conrady and Cook[4]). The agreement of the experimental data to the *form* of the relation 7 is excellent although it is necessary to adjust the dissociation constants of some collectors by factors of up to twenty-five.[5]

**The Ionic Mechanism.**—Mineral for flotation is ground *under water* and then collector or depressant is added. The following simultaneous ionic equilibria will be established

$$S''_{aq} + S'_{aq} + OH^- + H^+ \rightleftharpoons S''OH^- + S'H^+ \quad (8)$$

$$S''_{aq} + S'_{aq} + D^- + H^+ + Na^+ \rightleftharpoons S''D^- + S'H^+ + Na^+ \quad (9)$$

$$S''_{aq} + S'_{aq} + X^- + H^+ + Na^+ \rightleftharpoons S''X^- + S'H^+ + Na^+ \quad (10)$$

That is, there are three simultaneous competitions for the S″ sites and the equations automatically satisfy the condition that whenever an ion of one sign is taken up electroneutrality is ensured. By subtraction of each equation from another the re-

$$\left.\begin{aligned} S''D^- + OH^- &\rightleftharpoons S''OH^- + D^- \\ S''X^- + OH^- &\rightleftharpoons S''OH^- + X^- \\ S''D^- + X^- &\rightleftharpoons S''X^- + D^- \end{aligned}\right\} \quad (11)$$

lations are obtained which give the exchange between added ion and occupied sites.

The equilibrium constants for equations 8, 9 and 10 are given by equations 12, 13 and 14 assuming the activity coefficients in solution are unity and that the activity of the solid surface is given by the mole fraction ($\theta$) of occupied sites, all sites having equal (but not necessarily unit) activity coefficients.

$$K_{H,OH} = \frac{\theta_H\theta_{OH}}{(1-\theta_H)(1-\theta_{OH}-\theta_X-\theta_D)[OH^-][H^+]} \quad (12)$$

$$K_{H,D} = \frac{\theta_H\theta_D}{(1-\theta_H)(1-\theta_X-\theta_D-\theta_{OH})[D^-][H^+]} \quad (13)$$

$$K_{H,X} = \frac{\theta_H\theta_X}{(1-\theta_H)(1-\theta_X-\theta_D-\theta_{OH})[X^-][H^+]} \quad (14)$$

In a solution free from $D^-$ define a concentration $[HX]_0$ or $[X^-]_0$ at which flotation is just possible. Introducing this and rearranging the equations the following relation is obtained

$$[HX] - [HX]_0 = \frac{K_D}{K_X}\frac{K_{H,D}}{K_{H,X}}\frac{1}{\phi}[HD] \pm \{[1 + 4\phi(1+\phi)[K_{H,D}K_D[HD] + K_{H,OH}K_W]]^{1/2} - [1 + 4\phi(1+\phi)K_{H,OH}K_W]^{1/2}\} \quad (15)$$

where $\phi = 1/\theta_X - 1$ and $[HX]_0$ is the concentration of collector required to give a collector cover of $\theta_X$ in the absence of $D^-$ and $K_D$ and $K_X$ are the equilibrium ionization constants of HD and HX, respectively.

It is now required to find the condition in which relation 15 describes data which Last and Cook find to be "reasonably" fitted by equation 7. This requires that the last term in equation 15 shall be negligible or that all the terms reduce to the form of equation 7. Equation 15 is not tractable to simplification but from equations 12 and 14

$$\frac{K_{H,OH}}{K_{H,X}} = \frac{\theta_{OH}}{\theta_X}\frac{[X^-]}{[OH^-]} \quad (16)$$

$$\frac{K_{H,D}}{K_{H,X}} = \frac{\theta_D}{\theta_X}\frac{[X^-]}{[D^-]} \quad (17)$$

and 13 and 14 form (16) and (17) and *now assume that nearly all positive sites are occupied by anions.* The condition for flotation is that

$$\frac{\theta_X}{\theta_D + \theta_{OH}} = \frac{1}{\lambda} \quad (18)$$

shall exceed a critical constant ratio.[10] From (16), (17) and (18)

$$\lambda = \frac{K_{H,D}[D^-]}{K_{H,X}[X^-]} + \frac{K_{H,OH}[OH^-]}{K_{H,X}[X^-]} \quad (19)$$

For $[D^-] = 0$ then

$$\lambda = \frac{K_{H,OH}}{K_{H,X}}\frac{[OH^-]_0}{[X^-]_0} \quad (20)$$

and by substituting for $\lambda$ in (19)

$$[HX] = [HX]_0 + \frac{K_{H,D}K_D[HX]_0}{K_{H,OH}K_W}[HD] \quad (21)$$

which is precisely the form of relation given in equation 7. *The single assumption of nearly all sites being occupied is sufficient to enable one to describe the data.* It would appear therefore that a crucial test between the two theories would be to examine a system where much less than all sites were occupied and in which the total number varied with the composition of the solution.

Wadsworth, Conrady and Cook[4] have also examined the free energy of adsorption. Considering only the equilibria given in equations 1 and 2, they find the energies of adsorption of xanthate and hydroxyl on galena to be improbable. However the method of separating the thermodynamic quantities is quite arbitrary. From their equation 33 and figure 4 the adsorption potential for the reaction (22) is $-RT$ ln 2.67. They now determine

$$SX^- + OH^- \rightleftharpoons SOH^- + X^- \quad (22)$$

the adsorption potential for an experiment conducted by Taggart and Hassialis[11] in which a clean, polished specimen of galena is immersed in $5 \times 10^{-9}$ $M$ solution of potassium ethyl xanthate. The solution is about 90% depleted and the surface coverage is about 16%. Since the solution would have a

(4) M. E. Wadsworth, R. G. Conrady and M. A. Cook, THIS JOURNAL, **55**, 1219 (1951).

(5)

| Acid | Dissociation constants: Dissociation constant for best fit to flotation data | Dissociation constant by measurement |
|---|---|---|
| Ethylxanthic | $3 \times 10^{-3}$ (18°) | $5 \times 10^{14}$ (3°)[6] |
| *n*-Amylxanthic | $1 \times 10^{-6}$ (18°) | $2.5 \times 10^{-5}$ (3°)[6] |
| Diethylphosphoric | $2.3 \times 10^{-5}$ | No measurements |
| Diethylcarbamic | $1.6 \times 10^{-7}$ | No measurements |
| $H_2S$ | $5.7 \times 10^{-8}$[7] | $9.1 \times 10^{-8}$ (18°)[8] |
| HCN | $7.2 \times 10^{-10}$ | $4.79 \times 10^{-10}$ (18°)[9] |

(6) M. A. Cook and J. C. Nixon, *ibid.*, **54**, 455 (1950).

(7) N. A. Lange, "Handbook of Chemistry," 6th Edition, Handbook Publishers, Inc., Sandusky, Ohio, 1946.

(8) I. M. Kolthoff, THIS JOURNAL, **35**, 2715 (1931).

(9) H. T. S. Britton and R. A. Robinson, *Trans. Faraday Soc.*, **28**, 536 (1932).

(10) In particular if $\theta_X + \theta_D + \theta_{OH} = 1$ then $1/\lambda = \theta_X/(1-\theta_X)$ and $\theta_X = 1/(1+\lambda)$.

(11) A. F. Taggart and M. D. Hassialis, *Trans. Am. Inst. Mining Met. Engrs.*, **169**, 259 (1946).

$p$H value of about 6, then the adsorption potential for equation 22 is given by

$$-RT \ln \frac{0.16 \times 10^{-8}}{0.84 \times 5 \times 10^{-10}} = -RT \ln 4$$

which is in good agreement with the preceding calculation and not, as they state, in contradiction.

The free energies of exchange between adsorbed depressants and collectors are from about one to several kilocalories per mole. These seem entirely reasonable as judged, for example, from free energies of exchange on clays. Thus, Merriam and Thomas,[12] who studied the exchange of $Li^+$, $Na^+$, $K^+$, $Cs^+$ on attapulgite, find values ranging from 0.2 to 2 kcal. per mole.

**Mercaptobenzthiazole as Collector.**—One of the difficulties presented by the data of Wark and Cox lies in the instability of the free acids produced from their collectors at low $p$H values. Sutherland and Wark[13] have shown that galena, pyrite, chalcopyrite and copper-activated sphalerite respond to mercaptobenzthiazole in the same way as the other thio-collectors such as the xanthates which are unstable. The dissociation constant of mercaptobenzthiazole was found to be $3.2 \times 10^{-7}$ at 35° and the response of pyrite over a wide $p$H range is shown in Fig. 1. The broken curves are lines of constant free acid concentration or of constant ratio of collector ion to hydroxyl ion based on ionization of the SH group alone. Clearly neither the theory of constant free acid nor the ionic theory, when subjected to the restriction of nearly all sites occupied, is able to describe the results. Nor is it possible to obtain agreement between theory and experiment by "adjusting" the dissociation constant of the collector acid.

The increased solubility (see Experimental section) of mercaptobenzthiazole in acid solution indicated that an amine ion (IV) is also formed

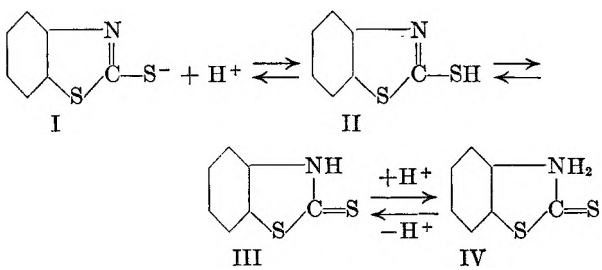


Assuming no salt effect and that the solubility (170 mg./l.) of the free acid II is the same as for the tautomer III, the acid dissociation constant for the amine is calculated as $5 \pm 3 \times 10^{-3}$ but is probably lower than this. If the free acid was the collector, then at a $p$H value of 2 a large increase in added amount of collector would be required: this is not found. However even if the only data considered are in the $p$H range 6 to 9, where the influence of amine ion must be vanishingly small, the quantity $[X^-]/(OH^-)$ or [HX] decreases rapidly as shown in Table I. Neither theory is satisfactory.

(12) C. N. Merriam and H. C. Thomas, *J. Chem. Phys.*, **24**, 99 (1956).

(13) K. L. Sutherland and I. W. Wark, *Trans. Am. Inst. Mining Met. Engrs.*, **134**, 53 (1939).

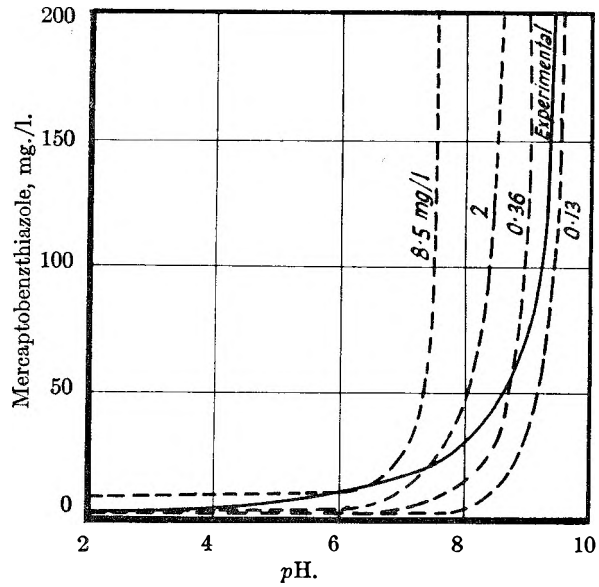


Fig. 1.—Flotation of pyrite at 35° by mercaptobenzthiazole. The full curve is a line of 30% flotation. The broken curves are for constant free acid. Concentration (in mg./l.) for lines of constant ratio of collector ion to hydroxyl ion.

TABLE I

RELATION BETWEEN $p$H VALUE AND ADDITION OF MERCAPTOBENZTHIAZOLE [X] TO CAUSE 30% FLOTATION OF PYRITE AT 35° ($pK_w$ = 13.6, $pK_a$ = 6.5)

| $p$H | $[X] \times 10^5$, mole/l. | $\frac{[X^-]}{[OH^-]} \times 10^2$ | $[HX] \times 10^5$, mole/l. |
|---|---|---|---|
| 6.0 | 6.0 | 5.7 | 4.6 |
| 6.5 | 7.8 | 4.9 | 3.9 |
| 7.0 | 10.2 | 3.1 | 2.5 |
| 7.5 | 12 | 1.37 | 1.1 |
| 8.0 | 18 | 0.69 | 0.55 |
| 8.5 | 30 | .37 | .30 |
| 9.0 | 45 | .18 | .14 |
| 9.5 | 132 | .17 | .13 |

It can be readily shown from equations 12 and 14 that, when the adsorption sites are not entirely covered by one of the species $OH^-$ or $X^-$ that

$$\frac{[X^-]}{[OH^-]} = \frac{1 + \phi K_W K_{H,OH} \pm (1 + 2\phi K_W K_{H,OH} - 4\phi^2 K_W K_{H,OH})^{1/2}}{2\phi^2 K_{H,X} K_W} \quad (23)$$

where $\phi = 1/\theta_X - 1$. The term on the right-hand side is constant so that partial *constant* occupation of sites provides no explanation of the inconstancy of the ratio.

In this and other systems, *e.g.*, dodecylamine as collector, it appears that both forms of the collector—ion and free acid or free base—may act as collectors. It is entirely logical to suppose that at the $p$H value concerned it is the predominant species which is the collector. This behavior is apparent for dodecylamine or octylamine adsorbed on platinum where a constant contact angle, presumably due to the amine ion, arises in solutions more acid than a $p$H value of 8 and then increases considerably in the neighborhood of the $pK_a$ (= 10.4) of the amine (see Zisman and Shafrin[14]: presumably due now to adsorption of free base.

Sutherland and Wark[13] studied the depressant action of cyanide on pyrite with mercaptobenzthiazole as collector. Table II shows the data (columns 1 and 2) determined from Fig. 2 in their paper.

TABLE II

MERCAPTOBENZTHIAZOLE (20 MG./L.) AS A COLLECTOR FOR PYRITE

Temp. 35°; cyanide as depressant; [HX] = free acid

| pH | NaCN, mole/l. × $10^5$ | [HCN], mole/l. × $10^5$ | [HX], mole/l. × $10^5$ | [HX] − $[HX]_0$ | (HX] − [HX]$_0$/ [HCN] × $10^2$ |
|---|---|---|---|---|---|
| 9.3 | 0 | 0 | 0.019 | 0 | .. |
| 9.0 | 1 | 0.25 | .038 | 0.019 | 7.6 |
| 8.5 | 3 | 2.8 | .121 | .102 | 3.6 |
| 8.0 | 8 | 7.8 | .37 | .35 | 4.5 |
| 7.5 | 20 | 20 | 1.11 | 1.09 | 5.4 |
| 7.0 | 47 | 47 | 2.9 | 2.9 | 6.2 |
| 6.5 | 102 | 102 | 6.1 | 6.1 | 6.0 |
| 6.0 | 184 | 184 | 9.2 | 9.2 | 5.0 |
| | | | | Mean | 5.5 |

The ratio $[OH^-]_0/[X^-]_0 - [OH^-]/[X^-] \times [D^-]/[X^-]$ is constant as required by the ionic theory: this ratio is more succinctly written as in the last column of Table II. Thus we have the apparent contradiction that, in terms of the model, competition between $OH^-$ and mercaptobenzthiazole ions is quite inadequately described but that the competition between $OH^-$ and $CN^-$ ions with this collector can be accurately described! This feature is common to many flotation systems including a wide range of types of collectors and depressants. It suggests either that the adsorption of collector ions (or molecules) is quite different from that of the competing depressant ions, *e.g.*, the activity coefficient of the surface species varying greatly with the extent of occupation of the surface or that $OH^-$ and $CN^-$, say, can compete simply with one another and provided the sum of these is large enough, flotation is inhibited.

(14) W. A. Zisman and E. G. Shafrin, *J. Colloid Sci.*, **4**, 571 (1949).

## Experimental

The mercaptobenzthiazole was purified by partial precipitation from a solution of the sodium salt by addition of acid followed by two crystallizations from hot alcohol. The melting point was 177°.

The dissociation constant of the mercaptobenzthiazole was determined from the e.m.f. of a hydrogen–calomel cell and solutions of the free acid and sodium salt of the thiazole. The solutions were prepared from conductivity water free from carbon dioxide. The method was checked by determining the $pK_a$ of pure benzoic acid at 25° which gave 4.3 ± 0.1. The $pK_a$ of mercaptobenzthiazole was found to be 7.0 at 25° and 6.5 at 35° both ± 0.2 unit.

The solubility of the mercaptobenzthiazole was determined by shaking with water or $10^{-3}$ *N* HCl solutions for periods up to a month. The total solubility in water was 180 ± 5 mg. per liter and the final *p*H value of the solution was 5.45. The calculated solubility of the free acid is 170 ± 5 mg. per liter at 35°. In solutions containing $10^{-3}$ *N* HCl the total solubility was 200 ± 10 mg. per liter.

The flotation tests were performed by shaking mineral with solution in a closed cylinder (Edwards and Ewers[15]). The pyrite was ground and elutriated to give a sized fraction between 100 and 200 mesh. The solution was adjusted to the *p*H value required using either NaOH, $K_2CO_3$ or HCl. Terpineol (40 mg. per liter) was used as frother: it produced no flotation without addition of mercaptobenzthiazole. The curve recorded in Fig. 1 was the result of 114 tests and is the line representing 30% flotation. The *p*H value of the solution was measured with a glass electrode.

**Acknowledgments.**—I wish to thank Mr. L. F. Evans and Mr. F. Meadows for the experimental determinations of flotation, dissociation constant and solubility.

(15) G. R. Edwards and W. E. Ewers, *Australian J. Sci. Research*, **A4**, 637 (1951).

# CONFIGURATIONAL TRANSITIONS IN GELATINS IN NON-AQUEOUS SOLUTIONS

BY ARTHUR VEIS AND JOAN ANESEY

*Central Research Laboratories, Armour and Company, Chicago, Illinois*

*Received February 28, 1959*

In aqueous solutions, disordered gelatin molecules cannot be returned to the ordered helical structure of native collagen. However, since synthetic polypeptides and some proteins can be made to go through the helix–coil transformation reversibly by the appropriate choice of solvent systems, a similar attempt has been made with gelatins. The behavior of gelatin in formic acid (FA)–dimethylformamide (DMF) and in ethylene dichloride–dichloroacetic acid has been examined. The studies cover (1) an analysis of the optical rotatory power and rotatory dispersion as a function of solvent composition; (2) the configurational changes as described by viscosity measurements; and (3) the roles of aggregation and degradation as determined by light scattering. $[\alpha]^{25.5}D$ is −116° for gelatin in FA and becomes more positive as the DMF content is increased, reaching a value of −58° at 5% FA in DMF. There is a discontinuity in a plot of $[\alpha]D$ *vs.* FA concentration at the molar mixing ratio FA/DMF = 1. Similarly, there is a discontinuity in a plot of $[\eta]$ *vs.* FA concentration at FA/DMF = 1, with a sharp rise in $[\eta]$ when FA/DMF <1. The light-scattering data indicate that no aggregates are formed in the FA–DMF mixtures. These data are consistent with the assumption that a hydrogen-bonded helical structure is formed when FA/DMF <1 but this helix is not the same as that of native collagen. The implications of these data are discussed.

Synthetic polypeptides and some proteins have been shown to undergo marked changes in chain conformation in solution as the solvent properties and temperature are varied.[1,2] In most instances these changes have been ascribed to the existence of internally hydrogen-bond-stabilized α-helixes

(1) J. T. Yang and P. Doty, *J. Am. Chem. Soc.*, **79**, 761 (1957).
(2) W. Kauzmann, *Ann. Rev. Phys. Chem.*, **8**, 413 (1957).

in poor solvents in contrast to more or less random structures in good solvents. In model polypeptide systems such configurational changes have been found to coincide with characteristic variations in the optical rotatory power and in the rotatory dispersion. The rotatory power changes from negative values in the random form to more positive values in the ordered $\alpha$-helical form while the dispersion constant becomes larger as more order is attained. In general, most proteins exhibit these same related changes in conformation and optical rotation, though the extent of the variations is usually less.

Notably, however, the soluble collagens, which do not exist in the form of $\alpha$-helixes, do not follow this typical course. In the native state acid-extract collagens have $[\alpha]_D$ $-350°$, which sharply falls to $\sim$ $-110°$ when the collagen is disordered in aqueous solutions by increase of the temperature above 30° or by addition of reagents such as urea or KCNS.[3] When the temperature of a solution of disordered gelatin is lowered, then $[\alpha]_D$ rises to $-290°$ or so.[3] This transition is reversible but the original change from $-350$ to $-110°$ is not reversible. These differences from the behavior of the globular proteins have been ascribed to: (1) the peculiar three-chain, coiled-coil structure of native collagen; (2) the high content of hydroxyproline and proline in collagen; and (3) *cis–trans* isomerization about the frequent pro-hypro bonds.

Because of the central role of proline residues in collagen it is of interest to consider the behavior of synthetic polyprolines. Poly-L-proline exists in two forms.[4] Polyproline I is insoluble in water but soluble in glacial acetic acid with $[\alpha]_{5460}$ $+40°$. With time, I mutarotates to form II, with $[\alpha]_{5460}$ varying from $-510$ to $-860°$. Polyproline II is water soluble. Harrington and Sela[5] have proposed that polyproline I is in a right-handed helix with the peptide bonds all in the *cis* configuration while polyproline II is in a left-handed coil with the imide linkage in the *trans* configuration. Since polyproline cannot be internally hydrogen-bonded all the configurational changes appear to be related to these *cis–trans* isomerizations.[5]

There have been several indications, particularly from optical rotation and polarized infrared anisotropy studies on gelatin films, that a polypeptide chain "fold" similar to the native structure could be induced in gelatins in aqueous solutions.[6] We set out to see whether we could take a randomized gelatin and induce it to take up a more native, ordered configuration by the use of non-aqueous solvent systems, the more native form presumably being characterized by a highly negative optical rotation. In a preliminary investigation of a commercial alkali-precursor gelatin we found that, contrary to expectations, $[\alpha]_D$ varied from $-115°$ in formic acid to substantially more *positive* rather than more negative values as non-solvent dimethylformamide was added.[7] In view of these interesting data we undertook a more complete investigation of the system. The studies reported here cover three areas: (1) an analysis of the optical rotatory properties of the gelatin as a function of solvent composition; (2) the configurational changes as described by viscosity measurements; and (3) the roles of aggregation and degradation as determined by light-scattering measurements.

(3) C. Cohen, *J. Biophys. Biochem. Cytology*, **1**, 203 (1955).

(4) E. R. Blout and G. D. Fasman, "Recent Advances in Gelatine and Glue Research," Pergamon Press, London, 1958, pp. 122–130.

(5) W. F. Harrington and M. Sela, *Biochim. Biophys. Acta*, **27**, 24 (1958).

(6) C. Robinson, "Nature and Structure of Collagen," Academic Press, Inc., New York, N. Y., 1953, pp. 96–105.

## Experiments and Results

**A. Materials and Methods. 1. Materials.**—An acid-precursor pig-skin gelatin (Grayslake Gelatin Company), A, was used. After the first few experiments pointed out the pronounced influence of even trace amounts of salts, the subsequent work was carried out using A deionized by the technique of Janus, Kenchington and Ward.[8] The deionized preparation, denoted as A-D, was ash free and had a nitrogen content of 18.20%.

Merck's reagent grade formic acid, 89.9%, and Eastman Kodak's N,N-dimethylformamide were used without further purification. For a few experiments, reagent grade dichloroacetic acid and ethylene dichloride were also used. The dichloroacetic acid was dried over anhydrous sodium sulfate before use.

**2. Refractive Index.**—Refractive index measurements were employed as a rapid and convenient method for the determination of protein concentration. The refractive indexes, $n^{25.5}D$, of the mixtures of formic acid (FA) and dimethylformamide (DMF) were measured in an Abbé refractometer and found to vary linearly from $n^{25.5}D_{100\%\ FA}$ 1.3692 to $n^{25.5}D_{5\%\ FA\ in\ DMF}$ 1.4253. The refractive index increments, $dn/dc$, required for the concentration determinations and light-scattering computations were determined in a Hilger Rayleigh interferometer at $\lambda$-436 m$\mu$ and 25.5°. For the determinations, portions of dried A-D were weighed into 5-ml. volumetric flasks and about 4 ml. of the appropriate, previously prepared FA–DMF mixture was added to each. The gelatin dissolved at 40° in about 1.5 hours, but each mixture was kept at that temperature for 2 hours. The flasks were then cooled at 25.5° and diluted to volume. The final solutions were read in the interferometer against the solvent mixture used for the dilution. Plots of the interferometer dial reading differences *vs.* the A-D concentration were linear. The refractive index increments calculated from the slopes of these lines were 0.1765, 0.1515, 0.1423, 0.1267 and 0.1223, respectively, when the FA contents were 100, 80, 60, 40, 10 and 5%. The concentrations are expressed as grams protein/cc. of solution.

It is worth pointing out that the order of preparation of the gelatin solutions affected the $\Delta n$ values. When the gelatin was dissolved in 100% FA (solution complete in less than 5 minutes) and then diluted with the proper amount of DMF, the results at 60, 40 and 10% FA were not reproducible and did not agree with those obtained by the solution process outlined above. The $\Delta n$ values were always greater than those calculated for the corresponding cases when the solutions were made up directly, the greatest discrepancies appearing at 40% FA. At first it was thought that these results could be explained on the basis of a strong binding of FA by the protein and a slow attainment of equilibrium on the addition of DMF, but this did not prove to be the case. Any changes which did occur as the solutions aged served to increase rather than decrease $\Delta n$. Other alternatives are discussed later. In view of these results, most solutions used in subsequent experiments were made up in the appropriate solvent mixture directly.

**3. Specific Rotation and Rotatory Dispersion.**—A Schmidt–Haensch Polarimeter and a jacketed, thermostated, 2-decimeter cell were used for all measurements. The various wave lengths required for the rotatory dispersion measurements were obtained by the use of the following lamp and filter combinations: $\lambda_{4360}$, Hg vapor lamp, Corning Filters No. 5113, 3389; $\lambda_{5460}$, Hg vapor lamp, Corning Filters No. 5120, 4303; $\lambda_{5893}$, Na lamp, Schmidt–Haensch

(7) A. Veis and J. Anesey, "Recent Advances in Gelatine and Glue Research," Pergamon Press, London, 1958, p. 269.

(8) J. W. Janus, A. W. Kenchington and A. G. Ward, *Research*, **4**, 247 (1951).

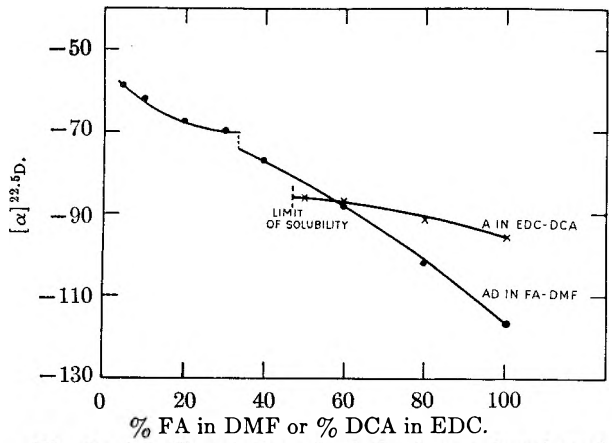


Fig. 1.—Specific rotation of gelatin A as a function of solvent composition: ●, A-D in FA–DMF mixture; X, A in EDC–DCA mixtures.

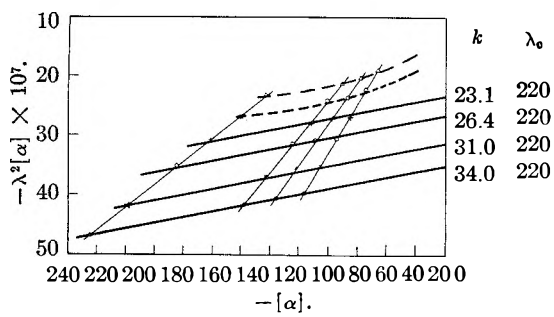


Fig. 2.—Optical rotatory dispersion plot for A-D in FA–DMF mixtures: ●, 100% FA; X, 80% FA; O, 60% FA; ✚, 40% FA; ◑, 20% FA; △, 5% FA. $k$ = rotation constant, $\lambda_c$ = dispersion constant in m$\mu$.

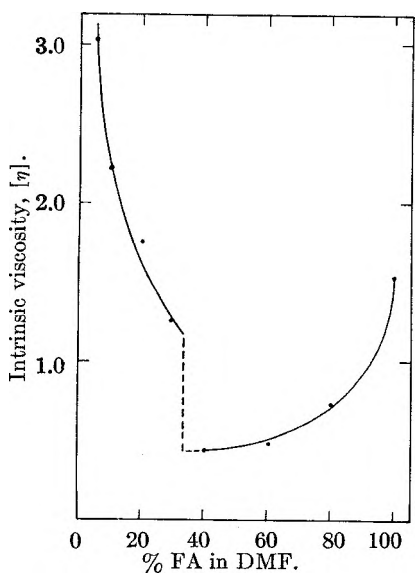


Fig. 3.—Intrinsic viscosity of A-D as a function of solvent composition in FA–DMF mixtures.

"D" filter; $\lambda_{6400}$, Zr lamp, Corning Filters No. 2408, 4784. Each specific rotation reported is the average of 10 readings taken approaching the null point from each side.

$[\alpha]^{25.5}D$ is plotted in Fig. 1 as a function of solvent composition for A-D in FA–DMF and DCA–EDC mixtures. Because of dissolution difficulties the DCA–EDC solutions had to be prepared by dissolving the gelatin in the DCA first.

The rotatory-dispersion data are shown in Fig. 2. With most proteins the dispersion can be represented by a one-term Drude equation 1

$$[\alpha] = \frac{k}{\lambda^2 - \lambda_c^2} \quad (1)$$

where $\lambda_c$ is the dispersion constant and $k$ is the rotation constant. Accordingly, as Yang and Doty point out,[1] a plot of $[\alpha]\lambda^2$ *vs.* $[\alpha]$ should give a straight line from which $\lambda_c$ and $k$ may be evaluated, as indicated in Fig. 2. In spite of the limited range of wave lengths available without the use of a photoelectric polarimeter, it is clear that the dispersion remains simple in solvent mixtures containing 40% or more FA and the dispersion constant does not vary with solvent composition. On the other hand in mixtures containing <40% FA the dispersion becomes complex.

4. **Viscosity.**—All viscosity measurements were made with Cannon–Fenske viscometers with flow times from 200 to 300 seconds for each of the solvent systems. The temperature was controlled at 25.50 ± 0.05°. After each solution was prepared and allowed to stand at 40° for two hours, it was filtered without suction through a dry, coarse, sintered-glass filter. The filtrate was transferred to the viscometer and equilibrated at the measurement temperature for at least one-half hour. In order to standardize each preparation, the flow times were recorded at 3- and 4-hour intervals from the time of initial introduction of solvent to the gelatin. The viscosity proved to be a function of time, always decreasing. Therefore, all calculations were made with the earliest possible data—those taken after 3 hours. The intrinsic viscosities so obtained, $[\eta]^{25.5}$, are plotted as a function of solvent composition in Fig. 3.

The dramatic variations in intrinsic viscosity with solvent composition are related directly to the competition between FA–DMF and FA–protein interactions. The nature of the FA–DMF interaction is described in Fig. 4a, which shows the viscosities of FA–DMF mixtures relative to that of the 5% FA–DMF solution. There is no significant volume change on mixing but the process is highly exothermic. Figure 4b, a plot of specific conductance *vs.* solution composition, shows another aspect of the solvent properties. Between 30 and 40% FA there is a sharp increase in conductivity and then only a gradual increase as the FA content is further raised. From 40 to 100% FA the conductivity is in the range of that of aqueous 0.01 $M$ KCl solutions.

5. **Light Scattering.**—The molecular weight of A-D was determined by light-scattering measurements in FA–DMF mixtures containing 5 and 40% FA, in 100% FA, all at 25.5°, and in 0.1 $M$ aqueous KCl or KCNS solution at 40°. The scattering photometer was constructed in this Laboratory but was patterned after the basic design of Aughey and Baum.[9] A principal feature of this instrument is that the photomultiplier tube is turned in synchronization with a recorder chart so that the angular scattering envelope may be traced directly and examined as the run proceeds. This is especially advantageous when working with solutions which are difficult to clean and handle, as in the present case.

After the solutions were prepared at 40°, as before, they were spun for 1.5 hours at 40,000 × $G$ in a Spinco preparative ultracentrifuge. A portion of each supernate was withdrawn from the upper third of the centrifuge tube and transferred directly to the light-scattering cell. After the scattering envelope had been recorded, the contents of the cell were analyzed interferometrically and the concentration determined. Each measurement was, therefore, an independent experiment. Zimm plots were constructed from data taken at several gelatin concentrations in each solvent. The appropriate extrapolated parameters are recorded in Table I.

Since our difficulties with the refractive index measurements had indicated that some permanent—or at least partly irreversible changes—might occur in FA–DMF mixtures, we also examined the light-scattering behavior of the A-D recovered by dialysis from 5% FA–DMF mixtures and from 100% FA solutions. The aqueous solutions were lyophilized and the recovered A-D then dissolved in 0.1 $M$ aqueous KCNS and the scattering measured at 40°. These results are also recorded in Table I. The increase in $M_w$ upon recovery of A-D from 5% FA is only a partial indication of the extent of aggregation. Large plugs, comprising about one-third of the protein, were obtained on centrifugation. This was the only case in which any significant insoluble material was found.

The Zimm plots and scattering envelopes were normal in each case except 5 and 40% FA in DMF. In these latter

(9) W. H. Aughey and F. J. Baum, *J. Opt. Soc. Am.*, **44**, 833 (1954).

TABLE I

LIGHT-SCATTERING PARAMETERS

| Gelatin | System | $M_w \times 10^{-5}$ | Interaction coefficient, $B$ | $Z$-av. radius of gyration, A. | $[\eta]$ |
|---|---|---|---|---|---|
| A-D, original | 0.1 $M$ KCNS, aq., 40° | 1.60 ± 0.05 | $6.2 \times 10^{-4}$ | 250 | 0.445 |
| A-D, recovered from 100% FA | 0.1 $M$ KCNS, aq., 40° | 1.20 – 1.35 | ..... | 230 | 0.377 |
| A-D, recovered from 5% FA in DMF mixture | 0.1 $M$ KCNS, aq., 40° | 2.5 – 3.0 | $2.2 \times 10^{-3}$ | 180 | 0.470 |
| A-D, original | 100% FA, 25.5° | 1.6 ± 0.4 | $8.8 \times 10^{-2}$ | 1000 | 1.55 |
| A-D, original | 40% FA in DMF, 25.5° | 1.6 ± 0.2 | $4.6 \times 10^{-2}$ | .. | 0.45 |
| A-D, original | 5% FA in DMF, 25.5° | 1.6 ± 0.2 | $3.6 \times 10^{-2}$ | .. | 3.20 |

situations repulsive solute–solute interactions led to external interference. (This behavior is illustrated in Fig. 5.) Consequently, $R(\theta)$ was less at low than at high angles and resulted in a negative slope for the extrapolated $[R(\theta)]_{c=0}$ *vs.* $\sin^2(\theta/2)$ line. A characteristic molecular dimension could not, therefore, be determined. However, the excluded volume can be related to the interaction coefficients and these do give some indication of molecular dimension even though complicated by charge and shape effects.

## Discussion

In the systems under discussion three factors in addition to thermal effects are operating to regulate the equilibrium configuration of the dissolved gelatin molecules. These are (1) the net electrical charge density per molecule and the dielectric constant of the medium, (2) the *cis–trans* isomerization equilibrium at each pro-hypro peptide linkage, and (3) the direct competition between protein–solvent hydrogen bonds and internal protein–protein hydrogen bonds.

Before assessing the relative effects of these factors, however, we must consider the nature of the solvent mixtures themselves. DMF has a dielectric constant of 26.6[10] and in the general sense is considered to be a weakly basic solvent. FA and DMF interact strongly with a negative heat of mixing. Two possibilities for this interaction are the formation of hydrogen bonded FA–DMF aggregates or the formation of ion pairs in stoichiometric amounts[11]

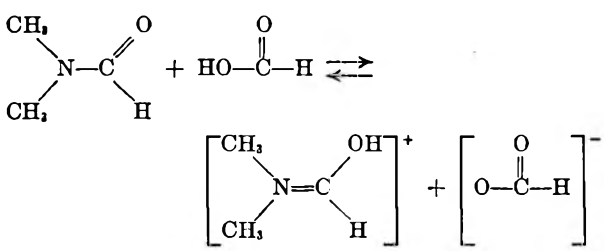

It is difficult to distinguish between these possibilities from our data. As shown in Fig. 4a the viscosity increases over that of DMF as the concentration of FA is raised until one has about 40% FA in the mixture. When FA <40%, as seen in Fig. 4b, the conductivity of FA–DMF mixture is very low. On a molar basis the ratio FA/DMF = 1 in a mixture containing 33.5% FA. Thus, the sharp rise in conductivity coincides with the presence of excess FA. The dielectric constant of FA is 57. If ion pairs were formed the dissociation of the salt would be negligible because of the low dielectric constant when DMF is in excess. The logarithm of the dissociation constant of an electrolyte decreases linearly with the reciprocal of the dielectric constant. Accordingly, when the dielectric constant is halved, the dissociation constant is decreased by a factor of 100.

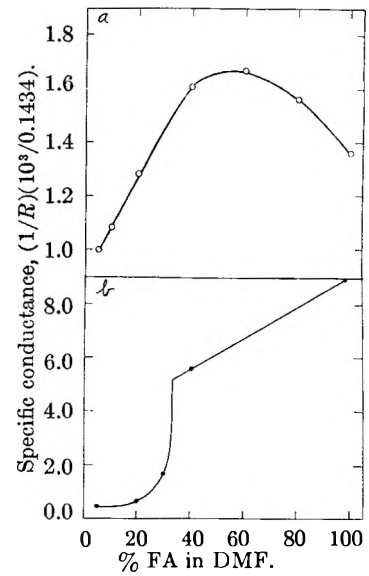


Fig. 4.—(a) Viscosity of FA–DMF mixtures relative to the viscosity of 5% FA in DMF as a function of mixture composition. (b).—Specific conductance of FA–DMF mixtures at 25.5° as a function of mixture composition.

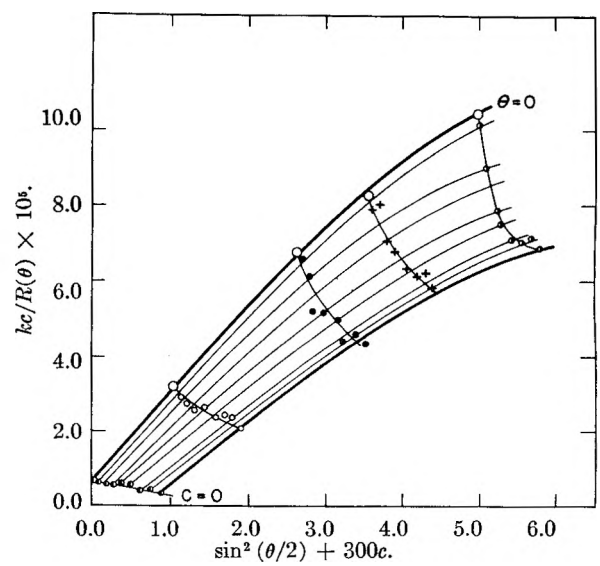


Fig. 5.—Zimm plot of light-scattering data for A-D in 5% FA in DMF.

(10) E. D. Rees and S. J. Singer, *Nature*, **176**, 1072 (1955).

(11) A. Berger, A. Loewenstein and S. Meiboom, *J. Am. Chem. Soc.*, **81**, 62 (1959).

The FA–DMF mixtures are sufficiently acid at every mixing ratio used here to suppress the ionization of the gelatin carboxyl groups. At the same time each basic group on the protein, being more basic than DMF, is in the cation form as the formate salt. Because of the low dielectric constant when DMF is in excess, this salt must be essentially undissociated. Consequently, electrostatic effects are relatively unimportant in this range. When FA/DMF >1, dissociation of the protein salt can occur and the electrostatic repulsion between the positively charged groups of the gelatin side chains lead to chain expansion. It is possible that in this range the amide linkages themselves are also in the ionic form similar to that indicated above for the DMF. The high value of $[\eta]$ and the very large value of the interaction coefficient $B$ in 100% FA are measures of these two effects and show that they predominate in very concentrated FA mixtures. As the FA content is decreased, the protein effective charge also decreases and consequently, thermal bombardment of the gelatin by the solvent molecules leads to chain contraction, ultimately to that state corresponding to what might be the equilibrium extension of an uncharged (actually charge-shielded) gelatin molecule in a nearly random coil form.

This behavior apparently explains the course of the $[\eta]$–solvent composition plot of Fig. 3 from 100% FA down to the minimum at ~40% FA. There is a gratifying agreement between $[\eta]_{40\%\ \mathrm{FA}}$ and $[\eta]_{0.1\ M\ \mathrm{KCNS},\ \mathrm{aq.},\ 40°}$, though the large value of $B$ in 40% FA and the negative slopes of the $KC/R(\theta)$ *vs.* $\sin^2(\theta/2)$ plots indicate that the intermolecular electrostatic repulsions are still considerable.

The intrachain electrostatic repulsions lead to a breakdown of what small amount of configurational chain regularity the gelatin molecules might still retain. This can be seen in the following way. The specific rotation of the polypeptide chain is a composite of the intrinsic residue rotations of each of the component amino acids, $[\alpha]_i$, and an additive configurational term $[\alpha]_{\mathrm{config}}$. From the amino-acid composition of typical gelatins, Harrington[12] has estimated $[\alpha]_i$ −92°. In aqueous 0.1 *M* KCNS at 40° $[\alpha]_{D,\mathrm{obsd}}$ −136° for A-D, or, in other words, there is a "native collagen fold"[7] or "order" persisting that contributes $[\alpha]_{D,\ \mathrm{config}}$ −44° to the observed rotation. This configurational term is further reduced in 100% FA since $[\alpha]^{25.5}_{D,\ \mathrm{obsn}}$ is only −116° in that solvent.

As the gelatin is dissolved in mixtures containing progressively more DMF (but still with FA >40%), the viscosity data show that each molecule becomes relatively more compact. Since this does not allow for the formation of asymmetric and space-filling helical structures, one would guess that $[\alpha]_{D,\ \mathrm{obsd}}$ would remain constant at about −100° over this entire DMF concentration range. In actual fact, as we have described in Fig. 1, $[\alpha]_{D,\ \mathrm{obsd}}$ steadily assumes more positive values. The most likely explanation of this behavior appears to be that the pro-hypro peptide linkages are assuming the *cis* configuration, since such linkages tend to fold the peptide chain back upon itself whereas *trans* linkages are extended in the chain direction. The *cis* form imparts a right-handed sense to the peptide chain and leads to positive values of $[\alpha]_D$. The *cis* form of poly-L-proline, polyproline I has $[\alpha]_D$ +45°. In 100% FA the *trans* imide form is more stable. Kurtz, Berger and Katchalski[13] have shown that in FA poly-proline I rapidly mutarotates to polyproline II, but that I is the more stable form in basic solvents such as pyridine.

Internal protein H-bonds cannot play any important role in the solvent mixtures containing more than 40% FA, both because of the above-mentioned electrostatic factors and because there is an excess of free FA to compete for H-bonds.

However, just as electrostatic interactions control the spatial distribution of the gelatin peptide chains when FA/DMF >1, hydrogen bonds control the ordering of these chains when FA/DMF <1, and helical chain segments are built. The abrupt increase of intrinsic viscosity at FA/DMF ≤1 indicates the formation of asymmetric structures, aggregation being ruled out by the light-scattering data. Similarly, the interaction constants, and hence the excluded volumes, remain large though the charge effect is reduced, the specific rotation becomes more positive showing an increased contribution from $[\alpha]_{D\ \mathrm{config}}$, and the dispersion plots become complex.

The most important question to pose at this point is that of the nature of the asymmetric units. Since the imino nitrogen of both proline and hydroxyproline cannot participate in intrachain hydrogen bonds, the helical segments can contain these amino acids only at their ends. Further, at least four, and probably six, amino-acid residues in sequence are required to form a stable helix segment. This is quite in agreement with amino-acid sequence studies[14,15] that show the common occurrence of the tripeptide gly-pro-hypro. From the over-all amino-acid analysis, then, the gelatin chains must contain many non-imino-acid segments with at least four amino acids between pro-hypro groupings (*e.g.*, -gly-pro-hypro-X-Y-Z-gly-pro-hypro-). As a corollary to this argument, in order to get a configurational contribution to $[\alpha]_D$ from the *cis* or *trans* imide structures, there must be several such imide linkages in close sequential proximity. Since, as mentioned earlier, the *cis* pro-hypro configuration appears to be favored in the solutions containing more DMF, the asymmetric hydrogen-bonded structures do not take up the same orientation as they do in cooled gelatin in aqueous solution. The new structure is apparently quite stable and not very water soluble. When an attempt was made to displace the FA–DMF with $H_2O$, and then with 0.1 *M* KCNS, about one-third of the gelatin was no longer soluble at 40° and what did remain in solution were aggregates of nearly double the molecular weight of the initial A-D. Thus, the configuration

(12) W. F. Harrington, *Nature*, **181**, 997 (1958).

(13) J. Kurtz, A. Berger and E. Katchalsky, "Recent Advances in Gelatine and Glue Research," Pergamon Press, London, 1958, pp. 131–135.

(14) T. D. Kroner, W. Tabroff and J. J. McGarr, *J. Am. Chem. Soc.*, **77**, 3356 (1955).

(15) W. A. Schroeder, L. M. Kay, J. LeGette, L. Honnen and F. C. Green, *ibid.*, **76**, 3556 (1954).

about the pro-hypro peptide linkage sets the hydrogen-bonded configuration which the remainder of the chain may assume. The so-called "collagen fold" is thus directly related to the *trans* pro-hypro form.

The data presented here cannot answer another important question—whether the proline and hydroxyproline are concentrated in only one of the three collagen peptide chains, as has been suggested in connection with X-ray diffraction data.[16] However, this seems to be unlikely in view of the viscosity data in the 40–100% FA range. On the basis of our data it does appear that there is a decided possibility that long segments of each of the polypeptide chains are essentially free of proline and hydroxyproline. Grassman has found large peptide fragments in gelatin that do not have a full complement of hydroxyproline. This means that other parts of the chain must have more than their average share.[17]

(16) P. M. Cowan, S. McGavin and A. C. J. North, *Nature*, **176**, 1062 (1955).

(17) W. Grassman, K. Hannig, H. Endres and A. Riedel, *Z. physiol. Chem.*, **306**, 123 (1956).

# SONIC DEGRADATION OF HIGH POLYMERS IN SOLUTION

By J. R. Thomas

*California Research Corporation, Richmond, California*

*Received February 10, 1959*

The rates of sonic degradation of polymethyl methacrylate, polyisobutene, polylauryl methacrylate and polystyrene are determined by use of 2,2-diphenyl-1-picryl hydrazyl to measure free radical fragments. Using fractionated samples it is found (1) that the rate of degradation per polymer backbone bond, under constant conditions of cavitation, is directly proportional to the degree of polymerization; (2) that large side chains accelerate the rate of degradation; and (3) that a 10–20% change in the carbon–carbon bond dissociation energy of the polymer chain has little effect upon the rate. A simple model is proposed whereby the rupturing stress arises from the radial velocity gradient surrounding a collapsing cavity. The model yields a kinetic expression in agreement with the experimental results.

It has been shown that the degradation of high polymers in solution by sonic or ultrasonic radiation is primarily due to hydrodynamic forces arising from cavitation of the fluid.[1]

Henglein[2] has reported the use of 2,2-diphenyl-1-picryl hydrazyl (DPPH) to detect free radical fragment products from the degradation of polymethyl methacrylate in solution by ultrasonics. We have confirmed his observation and have used this technique to study the degradation of polymethyl methacrylate, polystyrene, polyisobutene and polylauryl methacrylate. This paper describes the results of this study and presents a simple model to account for the observed rates of degradation.

## Experimental

Degradation of the polymer solutions was carried out in a Raytheon DF 101 sonic oscillator operating at 10 kc. The machine was equipped with Teflon gaskets to avoid reaction of DPPH with the rubber commonly used. Standard runs were included in each series of experiments so that daily variations in the power output of the oscillator could be corrected for. Samples were degassed and run under dry nitrogen since oxygen is known to interfere with the quantitative use of DPPH as a radical trap. Small aliquots were withdrawn as a function of time and analyzed for DPPH by optical density measurements at 5250 Å.

Polystyrene, polymethyl methacrylate and polylauryl methacrylate were prepared by bulk polymerization with dibenzoyl peroxide. The polybutene was a commercial polymer (Paratone N). The polymers were fractionated in the usual fashion with appropriate non-solvents. The fractionations were conducted in dilute solution (0.5% or less). Initial precipitates were redissolved by warming the solutions, and the fractions taken were reprecipitated by cooling the solution to its original temperature. The fractions taken were all less than 10% of the total material initially present. The molecular weights of the polystyrene, polymethyl methacrylate and polyisobutene were determined from intrinsic viscosity measurements. The molecular weights of the polylauryl methacrylate fractions were determined from ultracentrifuge sedimentation rates. Sedimentation data on the polybutene polymers gave molecular weights in agreement with those determined by viscosity measurements.

DPPH was prepared by the method of Lyons and Watson[3] and was purified by recrystallization from hexane. Optical density measurements were made with either a Cary Model 14 or Beckman DU spectrophotometer. C.P. benzene, dried with calcium hydride, was used as solvent in all cases.

## Results

Typical results are shown in Fig. 1 where the DPPH consumption is plotted against time of sonic irradiation. In the absence of polymer, the DPPH consumption was essentially zero during the time of these experiments. While the DPPH-radical adduct has a much lower extinction coefficient than the DPPH, its extinction coefficient is not zero. The small correction necessary for this was made by determining the extinction coefficient of the adduct in a sample of DPPH and polymer irradiated to the point that no further change in optical density took place.

**Effect of DPPH Concentration.**—The rate of DPPH consumption was found to be independent of DPPH concentration over the range 5 to 80 mg./100 cc. In all experiments reported here the DPPH concentration was 20 mg./100 cc.

**Effect of Polymer Concentration.**—The effect of polymer concentration is shown in Fig. 2 where the initial rate of DPPH consumption (determined as described below) is plotted *versus* weight concentration of polyisobutene. The failure of the rate to be strictly first order in polymer concentration probably results from the influence of viscosity upon the cavitation process. In very viscous solutions, cavitation cannot be induced at all,[1] and polymer degradation ceases. In the following experi-

(1) H. H. G. Jellinek, "Degradation of Vinyl Polymers," Chapter 4, Academic Press, Inc., New York, N. Y., 1955, p. 231.

(2) Von Arnim Henglein, *Makromol. Chem.*, **15**, 188 (1955).

(3) J. A. Lyons and W. F. Watson, *J. Polymer Sci.*, **18**, 141 (1955).

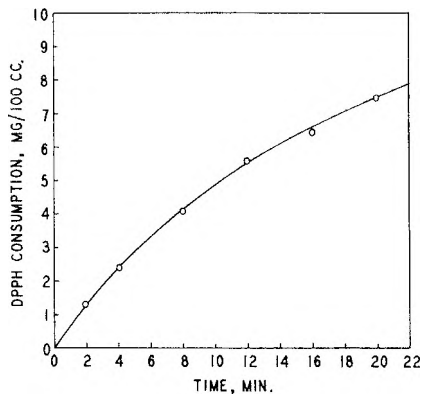


Fig. 1.—DPPH consumption *versus* time of sonic irradiation —2% polyisobutene (mol. wt. = $1.3 \times 10^6$).

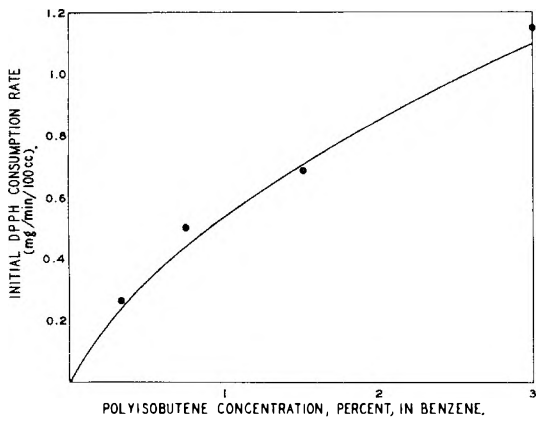


Fig. 2.—Effect of polymer concentration (polyisobutene) upon rate of DPPH consumption.

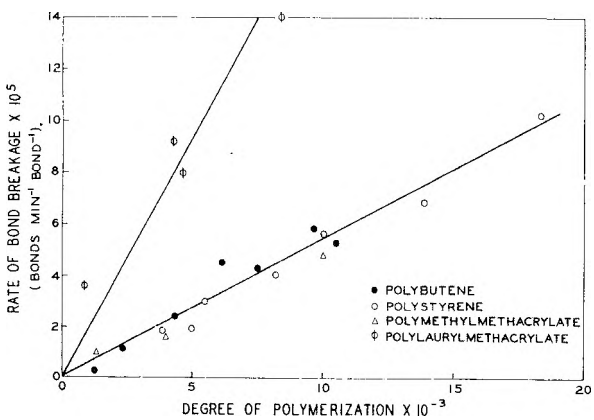


Fig. 3.—Rate of bond breakage *versus* degree of polymerization.

ments, all solutions were prepared to have the same initial viscosity so that the cavitational intensity would be constant. The polymer concentrations ranged from about 3% by weight for the lowest degree of polymerization samples to 0.2% by weight for the highest degree of polymerization samples.

**Treatment of Data.**—The decrease in rate of DPPH consumption as a function of time noted in Fig. 1 is primarily due to the decrease in average degree of polymerization of the polymer, as will be discussed later. In order to obtain rates under conditions where the degree of polymerization is known, the initial slopes were taken from data such as those given in Fig. 1. With low molecular weight fractions, where the rate of degradation is low and the rate of change of the degree of polymerization is small, the initial slopes could be extracted quite accurately. With the high molecular weight samples, the initial slope is good to about $\pm 10\%$. In all cases rate data refer to initial rates.

The initial rates of carbon–carbon bond breakage in the various polymer fractions are plotted in Fig. 3 *versus* the degree of polymerization of the polymer. The rates are given in terms of bonds broken per minute per polymer backbone bond available, assuming the destruction of two DPPH molecules per broken bond. As discussed above, it is expected that the rate of bond rupture would be first order with respect to polymer concentration at constant solution viscosity. Each point represents the average of at least two independent determinations. In the interpretation of the data, it is assumed that the counting efficiency of DPPH is the same for all polymer radicals studied.

## Discussion

Three points of interest are disclosed by the data given in Fig. 3. First, for all four polymers the rate of degradation per polymer backbone bond is directly proportional to the degree of polymerization. Second, the rate of degradation of polylauryl methacrylate is 3.5 times as fast as that of polymethyl methacrylate of similar degree of polymerization showing an influence of side chain length. Third, the rates of degradation of polymethyl methacrylate, polyisobutene and polystyrene are the same within experimental error, indicating at most a small effect of the dissociation energy of the backbone bonds upon the rate.

While there has been considerable discussion of possible mechanisms of polymer degradation in a cavitating fluid,[1] no specific detailed mechanism has been proposed. Most of the published data which might be used to determine the mechanism of degradation are based upon viscosity change as a result of degradation. The complicated dependence of viscosity upon molecular weight distribution makes it very difficult to interpret the results from such studies. The experiments reported here give a direct measure of the important quantity, namely, the rate of carbon–carbon bond breakage. Henglein's results, also obtained by use of DPPH, are difficult to interpret because his measurements were made after considerable degradation had occurred, during which time in many cases the average degree of polymerization changed manyfold, and because the measurements were not made at constant solution viscosity. Recently, Ovenall, Allen, *et al.*[4,5] reported a study of polymer degradation using DPPH. They arrive at the conclusion, based upon their own data and their interpretation of Henglein's data that the fundamental rate equation for polymer degradation is

$$\frac{dB_i}{dt} = k(P_i - P_e)n_i \qquad (1)$$

(4) D. W. Ovenall, G. W. Hastings and P. E. M. Allen, *J. Polymer Sci.*, **33**, 207 (1958).

(5) P. E. M. Allen, G. M. Burnett, G. W. Hastings, H. W. Melville and D. W. Ovenall, *ibid.*, **33**, 213 (1958).

where $dB_i/dt$ is the rate of breakage of molecules of degree of polymerization $P_i$, $n_i$ is the number of such molecules and $P_e$ is a degree of polymerization below which molecules no longer degrade. The assumptions made in use of equation 1 are that only $P_i$-$P_e$ units are capable of degradation and that all bonds within this degradable section are equally likely to break.

Our data, plotted in Fig. 3, are not consistent with this rate expression but fit instead the expression

$$\frac{dB_i}{dt} = kP_i^2 n_i = k'P_i n_b \qquad (2)$$

where $n_b$ is the number of polymer bonds. For this discussion, the existence of a degree of polymerization $P_e$ below which degradation does not take place is unimportant and $P_e$ has been assumed small with respect to $P_i$. Equation 2 is of the form originally proposed by Schmid.[6]

It is difficult to reconcile the discrepancy between the results of Ovenall, Allen, *et al.*, and those of the present study. For the reasons stated above, the use of Henglein's data to determine the functional dependence of the rate of degradation upon the degree of polymerization appears hazardous. The interpretation of the results of the present study with regard to the functional dependence of rate upon the degree of polymerization appears to be more straightforward and more free of *ad hoc* assumptions than that which Ovenall, Allen, *et al.*, were forced to use.

Having obtained experimental data which appear to show correctly the effects upon the rate of bond rupture of the degree of polymerization, the length of the side chains, and change in the carbon–carbon bond dissociation energy of the polymer backbone bonds due to changes in chemical composition, it is reasonable to consider the mechansm of degradation in some detail. The principal point of interest concerns the manner by which the stresses arising in a cavitating fluid are able to rupture the chemical bonds in a macromolecule. We propose the following mechanism which accounts reasonbly well for the experimental observations.

The collapse of a cavity, or a void, in a liquid is a process wherein very high velocities of collapse can be obtained resulting in large hydrodynamic pressures and velocity gradients in the surrounding fluid.[7,8] Since a polymer molecule in solution occupies a relatively large volume (a region of diameter several hundred to several thousand Angstroms), it is apparent that, with sufficiently large velocity gradients, the side of the polymer coil near a collapsing cavity will move at a higher velocity than the side away from the collapsing cavity. Assuming that the relaxation time of the polymer segments is short, the velocity gradient existing over the volume of the polymer will distort it from its initial spherical shape along a radius of the collapsing cavity. The unfolding of the polymer coil will continue until a geometry is reached which is incapable of further relaxation At this time, a tensive force operates on the polymer chain due to the relative

(6) G. Schmid, *Z. physik. Chem.*, **A186**, 113 (1939).

(7) Lord Rayleigh, *Phil. Mag.*, **34**, 94 (1917).

(8) B. E. Noltingk and E. A. Neppiras, *Proc. Roy. Soc.* (*London*), **B63** 674 (1950); **B64**, 1032 (1951).

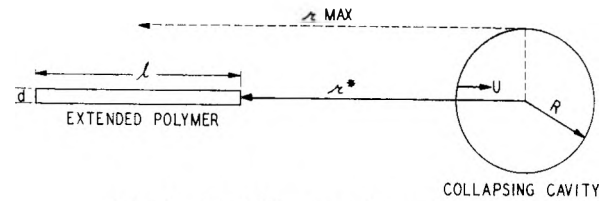


Fig. 4.—Model for degrading polymer.

motion of polymer segments and solvent. For simplicity, we assume that this critical geometry can be approximated by the linearly extended polymers presented in Fig. 4.

The extended polymer will flow through the solution at a velocity intermediate between the solvent velocities at the two ends. At the point of maximum tension, designated as $r_{max}$ in Fig. 4, the polymer velocity and solvent velocity will be equal. Making the usual assumptions that the hydrodynamic behavior of the polymer resembles that of a string of spherical beads,[9] the frictional force $dF$ on a polymer segment of length $ds$ is

$$dF = 3\pi d\eta V_{rel} \frac{ds}{a} \qquad (3)$$

where $\eta$ is the viscosity, $V_{rel}$ is the relative velocity of solvent with respect to polymer, $d$ is the diameter of the polymer, and $a$ is the length of a monomer unit in the polymer chain. This treatment assumes that each monomer unit has the frictional behavior of an independent macroscopic sphere of diameter $d$.

At any point, $r$ distant from the center of the cavity, the solvent velocity is

$$v = UR^2/r^2 \qquad (4)$$

where $U$ is the velocity of the collapse of the cavity and $R$ is the cavity radius. Integrating (3) from $r^*$ (defined in Fig. 4) to $r_{max}$, the total force on this part of the polymer is seen to be

$$F = \frac{3\pi\eta dUR^2}{a}\left[\frac{(r_{max} - r^*)^2}{r^2_{max}r^*}\right] \qquad (5)$$

Integrating the force on the other part of the molecule from $r_{max}$ to $r^* + l$ and equating the two forces, one obtains, where $l$ is extended polymer length

$$r^2_{max} = r^*(r^* + l) \qquad (6)$$

For $r^* > l$ it is readily seen that the position of $r_{max}$ is near the center of the molecule and that the tensive force is

$$F_T = \frac{3\pi\eta dUR^2}{a}\left[\frac{l^2}{4r^{*3}}\right] \qquad (7)$$

The rate of polymer degradation will be determined by the product of: (a) the volume of solution surrounding the cavity where $F_T > F^*$ (the yield strength of the polymer), (b) the number concentration of the polymer molecules, and (c) a quantity defining the rate and intensity of cavitation. That is

$$\frac{dB}{dt} = n_i V_{F_T > F^*} K \qquad (8)$$

where $dB/dt$ is the rate of bond rupture, $n_i$ is the number concentration of polymer, $V_{F_T>F^*}$ is the solution volume where the tensive force is greater

(9) P. J. Flory, "Principles of Polymer Chemistry," Cornell University Press, Ithaca, N. Y., 1953, p. 602.

than the yield strength and $K$ is a constant defining the cavitation. From equation 7

$$V_{F_T>F^*} \propto \frac{dl^2}{F^*} \tag{9}$$

For the degrees of polymerization under consideration $n_b$, the number of concentration of polymer bonds, is

$$n_b \propto n_i l \tag{10}$$

and the rate of bond rupture per polymer bond is from (8)

$$\frac{1}{n_b}\frac{dB}{dt} \propto \frac{dl}{F^*} \tag{11}$$

This expression gives the linear dependence of rate upon degree of polymerization which is found experimentally as shown in Fig. 3. Further it correctly predicts the influence of increasing the side chain length in changing from methyl methacrylate to lauryl methacrylate. Assuming that the side chains are fully extended, the diameter of the lauryl methacrylate should be about 4.7 times that of the methyl methacrylate. This agrees well with the experimentally observed variation in degradation rate of 3.5.

With regard to the influence of the C–C bond dissociation energy upon the rate, equation 11 predicts an inverse relationship. Using dissociation energies from simple molecules having somewhat similar structures, it is reasonable to expect the D(C–C) for polyisobutene to be about 70–75 kcal./mole; whereas that of polystyrene would be expected to be about 60 kcal./mole.[10] With similar diameters one would only expect a 10–20% difference in rate. While the data shown in Fig. 3 are not precise enough to show this difference, it is clear that a difference in D(C–C) the order of 10–15 kcal./mole causes very little effect upon the rate. This is confirming evidence that polymer degradation is not a thermally activated reaction. The influence of side chain length further substantiates this conclusion.

With the assumption $r^* > l$, which appears reasonable for a majority of the degradation events, equation 6 predicts that the molecule will break very near the center. On this assumption the change in reduced specific viscosity, $\eta_{sp}/C$, as a function of degradation can be calculated from the number of bonds broken as determined by DPPH consumption. Calculated values of $(\eta_{sp}/C)/(\eta_{sp}/C)_0$ at 1% are compared in Table I with observed values for a polylauryl methacrylate and a polymethyl methacrylate fraction.

TABLE I

CALCULATED AND OBSERVED CHANGES IN $(\eta_{sp}/C)/(\eta_{sp}/C)_0$ WITH DEGRADATION

| Polymer | Time, min. | $(\eta_{sp}/C)/(\eta_{sp}/C)_0$ Obsd. | Calcd. |
|---|---|---|---|
| PLMA | 1 | 0.981 | 0.984 |
| | 3 | .884 | .926 |
| | 6 | .752 | .860 |
| PMM | 1 | 0.959 | 0.964 |
| | 3 | .844 | .927 |
| | 6 | .719 | .871 |

(10) J. S. Roberts and H. A. Skinner, *Trans. Faraday Soc.*, **45**, 339 (1949).

The calculated values, assuming the consumption of two DPPH's per broken bond, are only in fair agreement with the observed values with the observed loss being twice that of the calculated loss. Hammond, *et al.*,[11] and Bevington[12] have shown that DPPH is only about 65% effective in trapping the radicals produced by decomposition of azo-bis-isobutyronitrile. Using this lower trapping efficiency the calculated viscosity loss is only about 30% higher than that observed. If the bond cleavage is random, the loss in viscosity caused by a given number of breaks will be only about 60% that observed for cleavage restricted to the center of the polymer chain. Uncertainty in the trapping efficiency and lack of knowledge about the polydispersity of the fractionated samples precludes a choice between random and center of the chain cleavage. However, the data are consistent with the idea of largely center cleavage and are good enough to exclude a mechanism whereby the cleavage takes place selectively near the ends of the polymer chain.

While the proposed model gives kinetic behavior consistent with experiment, it is difficult to say with certainty that the shear gradient over the region occupied by a polymer molecule is large enough to rupture a C–C bond. Using de Boer's[13] value of the force necessary to rupture a C–C bond, *i.e.*, $6 \times 10^{-4}$ dynes, it can be seen from (7) that sufficient force is available for a polymer of degree of polymerization of 2000 at about $10^6$ Å. from the cavity if the collapsing cavities can achieve near sonic velocities at radii the order of $10^6$ Å. The calculations of Noltingk and Neppiras[8] indicate that these values may be realized.

The notion that a random coil polymer is considerably distorted at the time of its rupture receives qualitative support from the observation that a polylauryl methacrylate fraction and a polyisobutene fraction suffered the same relative loss in $(\eta_{sp}/C)/(\eta_{sp}/C)_0$ in a solvent where their intrinsic viscosities differed by 50% as they did in a solvent where their intrinsic viscosities were identical.

The pearl necklace hydrodynamic model used here is highly idealized and cannot be rigorous. In addition to the simplifying assumptions normally introduced in its application to polymer solutions, we have explicitly assumed that each monomer unit behaves as a sphere, with macroscopic fractional coefficient, of radius equal to the side chain length. A better representation might be thought to be the identification of a "bead" as a polymer segment of length equal to the side chain length. This, however, leads to the implausible result that the frictional force is independent of the polymer diameter. Treatment of the polymer chain as a string of connected non-interacting cylinders leads to essentially the same results as found above except that the polymer diameter appears in a log function. Treatment of the polymer chain as a single macroscopic cylinder in a velocity gradient appears to involve formidable mathematical problems. The kinetic treatment used here is also highly idealized since it

(11) G. S. Hammond, J. N. Sen and G. E. Boozer, *J. Am. Chem. Soc.*, **77**, 3244 (1955).

(12) J. C. Bevington, *Nature*, 478 (1955).

(13) J. H. de Boer, *Trans. Faraday Soc.*, **32**, 10 (1936).

correlates observed rate data with a model based upon monodisperse cavities of uniform size; whereas, actually, a distribution of initial cavity sizes probably exists. Throughout, we have ignored molecular entanglements between polymer molecules which have been considered important by various investigators. Our justification is that the polymer concentrations are moderately low and that the proposed mechanism gives satisfying results without considering this additional complication.

Allen, Burnett, *et al.*,[5] discuss at some length the limiting degree of polymerization below which a polymer will not degrade in a cavitating fluid and the discrepancies in the determination of this quantity by various investigators. Since this discrepancy involves a range in the limiting degree of polymerization of 200–2000, it is obvious from the scatter in Fig. 3 that our data will not aid in answering this question. It seems worthwhile to point out, however, that the mechanism we propose would predict a strong dependency of this limiting value upon the intensity and characteristics of the cavitational process. It is not surprising, on this basis, that the different experimental conditions of the various investigators lead to different values of the limiting degree of polymerization.

# A RADIOACTIVE TRACER STUDY OF THE ADSORPTION OF FLUORINATED COMPOUNDS ON SOLID PLANAR SURFACES. I. PERFLUOROÖCTANOIC ACID[1]

BY J. W SHEPARD AND JOHN P. RYAN

*Contribution No. 146 from Central Research Department, Minnesota Mining and Manufacturing Company, St. Paul, Minnesota*

*Received March 10, 1959*

A method for measuring areas of flat surfaces involving solution adsorption techniques is described and its limitations discussed. A carbon-14 labeled fluorochemical acid ($C_7F_{15}C^*OOH$) was used. Isotherms for the adsorption of the acid onto plane surfaces of glass, quartz, aluminum and platinum have been determined. The adsorption is not reversible. Desorption studies showed that the rate and extent of desorption was a function of the polarity of the desorbing solvent. Contact angles using hexadecane were found to be a poor measure of the extent of surface coverage by the adsorbate. Surfaces of platinum and quartz were unreactive and surface area measurements corresponded closely to the geometric area. Soft glass and aluminum showed signs of chemical reaction with the perfluoro acid. An exchange phenomenon was observed between the adsorbed acid molecules and those in solution. The rate and extent of exchange for the surfaces studied increased in the order: glass, aluminum, platinum.

## Introduction

The use of radioactive tracer techniques in studying surface phenomena has expanded considerably in recent years.[2] One technique which has considerable merit since it lends a quantitative aspect to the usual measurements of surface properties is the adsorption of long chain polar organic compounds labled with C-14 or H-3 onto solid surfaces. These "oleophobic" films, when properly prepared, have the interesting property of not being wetted by the solution or the pure solvent.[3] When the film-covered surfaces are withdrawn from the solution, the liquid recedes, leaving a dry surface made up, in most cases, of a closely packed monolayer of the organic compound oriented with the polar group on the surface of the solid and the hydrocarbon chain perpendicular to the substrate.

Preliminary work in our laboratory with a benzene solution of C-14 labeled stearic acid indicated that this adsorbed acid imparted only a low degree of "oleophobic" character to the surface and the samples emerged from the adsorption cell wet with solution. Other workers have also noted this behavior.[4] In view of this difficulty, a system was chosen which would eliminate this "carry-out" problem. A surface composed of closely packed, oriented $-CF_3$ groups has extreme oleophobic character[5] and fluorocarbons as a class have the lowest free surface energy of any known compounds.[6] A solution of C-14 labled perfluoroöctanoic acid ($C_7F_{15}C^*OOH$) in *n*-decane[7] was chosen as the adsorption system.

The initial objective of this research was to develop a simple method for measuring the specific surface area of plane solid surfaces. The importance of the actual surface area when studying adhesion, catalysis, lubrication, etc., is well known.

Techniques for measuring specific surface areas of flat surfaces have found limited application. Gas adsorption techniques have been explored[8,9] but the method is primarily limited by low sensitivity.

(1) Presented at the Symposium on "Surface Chemical Properties of Fluorochemicals," 134th Meeting of the American Chemical Society, Division of Colloid Chemistry, Chicago, September, 1958.

(2) F. P. Bowden and A. C. Moore, *Trans. Faraday Soc.*, **47**, 900 (1951); J. E. Willard, THIS JOURNAL, **57**, 129 (1953); D. E. Beischer, *ibid.*, **57**, 134 (1953); E. Rideal and J. Tadayon, *Proc. Roy. Soc. (London)*, **225A**, 346 (1954); J. E. Young, *Astr. J. Chem.*, **8**, 173 (1955); H. A. Smith and T. Fort, Jr., THIS JOURNAL, **62**, 519 (1958); H. D. Cook and H. E. Ries, Jr., Miami ACS Meeting, April, 1957.

(3) W. C. Bigelow, D. L. Pickett and W. A. Zisman, *J. Colloid Sci.*, **1**, 513 (1946).

(4) W. C. Bigelow and L. O. Brockway, *ibid.*, **11**, 60 (1956); H. A. Smith and K. A. Allen, THIS JOURNAL, **58**, 449 (1954).

(5) F. Schulman and W. A. Zisman, *J. Colloid Sci.*, **7**, 465 (1952); E. F. Hare, E. G. Shafrin and W. A. Zisman, THIS JOURNAL, **58**, 236 (1954).

(6) H. M. Scholberg, R. A. Guenthner and R. I. Coon, *ibid.*, **57**, 923 (1953).

(7) J. W. Shepard and John P. Ryan, *ibid.*, **60**, 127 (1956).

(8) P. H. Emmett, "Pittsburgh Conference on Surface Reactions," Corrosion Publishing Co., Pittsburgh 12, Pa., 1948, p. 82.

(9) C. Brown and H. H. Uhlig, *J. Am. Chem. Soc.*, **69**, 462 (1947); R. L. Burwell, P. A. Smudski and T. P. May, *J. Am. Chem. Soc.*, **69**, 1925 (1947); T. Rhodin, *ibid.*, **72**, 4343 (1950); W. Rausch, *Z. physik. Chem.*, **201**, 32 (1952).

O'Connor and Uhlig, however, did obtained reasonable values on stainless steel sheet and abraded iron foil.[10] Solution adsorption has long been used to determine the specific surface area of powders.[11-18] At maximum adsorption two general assumptions are made: (1) the surface is occupied by a close-packed unimolecular film, and (2) the area occupied by each molecule is the same as on an aqueous substrate. The results obtained have shown good agreement with values obtained by independent methods such as the photomicrographic and the BET.

## Experimental

**Materials. A. Labeled Acid.**—The labeled perfluorooctanoic acid[19] was prepared by electrofluorination of octanoic-1-$C^{14}$ acid. The latter was synthesized from $BaC^{14}O_3$ (Oak Ridge National Laboratory) and $C_7H_{15}MgBr$. The acid was purified by fractional distillation and the fraction boiling in the range 187–192° was used in this study. The melting point was 38–43°. The neutralization equivalent was 414 (theo. 414) and the amount of free fluoride was found by analysis to be 0.003%. The tagged acid contained approximately 25% $C_8$-acid isomers.

The specific activity of the acid (0.12 millicuries/g.) was determined by gas counting the $CO_2$ obtained by combusting the acid. This value was checked by measurements of known samples in a Liquid Scintillation Counter.

A saturated "stock" solution of the perfluoro acid in *n*-decane was prepared by dissolving excess acid in 50 cc. of the solvent. The solutions used in this study were prepared by appropriate dilution of this "stock" solution.

**B. Solvents.**—Polar impurities were removed from all non-polar solvents by passing the liquid through a column of activated alumina–silica gel. The solvents were checked for absence of polar impurities by placing a drop on neutral, acidic and basic substrate.

**C. Surfaces.**—The surfaces used in this study were: 1. Glass—ordinary microscope slides cut to fit our Q-gas sample counting holders. Edges were polished on a lapping machine. 2. Quartz—$^1/_{16}$″ ground and polished quartz plates. 3. Aluminum—40 mil Alcoa flat sheet—2S, 4. Platinum—20 mil rolled.

**Procedure.**—The steps in the adsorption of tagged acid on a surface and the subsequent measurements were as follows.

1. The samples were pretreated before immersion in the active solution by heat treating at 450° in a pure $N_2$ atmosphere. When it was necessary to use the same samples for repeat runs, the adsorbed active acid was removed from the sample by rinsing in acetone or water before the heat treatment. This technique was not designed to give a perfectly "clean" surface, but a reproducible one. It also was suitable for a wide variety of surfaces.

2. The active solutions of perfluoroöctanoic acid, which were prepared by dilution to 100 ml. of an aliquot from the "stock" solution, were placed in a 200-cc. test-tube (adsorption cell) immersed in a constant temperature bath (28.5°). The adsorption cell was covered with a standard tapered cap containing an outlet and inlet tube so that a dry $N_2$ atmosphere could be maintained over the solution at all times. The concentrations of the adsorption solutions were determined by removing aliquots with a micropipet, evaporating to dryness on stainless steel planchets and measuring the activity. To eliminate the error caused by absorption of tagged acid on the walls of the pipet, the pipet was rinsed three times with acetone and this solution added to the original aliquot. Triplicate samples from each cell were prepared.

3. After pretreatment, the samples were placed in a special holder and lowered into the adsorption cell. After the desired immersion time, the holder was slowly withdrawn from the solution at a rate of about one millimeter per second by means of a small motor. In most cases the solution did not wet the surface and the meniscus rolled back uniformly leaving no droplets behind. In the few cases where minute drops of "carry-out" solution were observed, they were removed by touching a corner of tissue paper to the drops.

4. **Radioactive Measurement.**—The amount of acid adsorbed on a surface was ascertained by measuring the radioactivity in a Q-gas flow counter connected to a conventional scaler. To eliminate any "edge effect" and to obtain an accurate knowledge of the exact area being counted, the samples were placed in a masked holder (counting area 2.45 cm.$^2$) before introduction into the counter. Contamination of the counter by the "tagged" acid was never observed.

Samples were usually counted for a time period long enough to give a 9/10's statistical error of less than 5%.

The distribution of tagged acid on a surface was determined by the autoradiographic technique using Eastman No-Screen X-ray plates (1″ × 3″).

5. **Contact Angle Measurement.**—Contact angle measurements were determined by the sessile drop or drop on plate method using hexadecane. The drops were formed on the samples with a hypodermic syringe which was operated through micrometer screw controls. To ensure measurement of advancing angles, the syringe tip was withdrawn slowly from the drops while the liquid was being ejected and the drops were growing in size. Contact angles were calculated from drop height values ($h$) and widths ($w$) using the formula: $\tan \theta/2 = 2h/w$. Mack[20] has shown the validity of this equation for drops which are less than 0.5 mm. in diameter and for contact angles less than 90°. All values reported are the average of three measurements.

## Experimental Results

**A. Rate of Adsorption.**—The rate of adsorption of perfluoroöctanoic acid was studied as a function of adsorbate concentration and the solid surface upon which the acid was being adsorbed. For unreactive solids such as quartz and platinum, 90% of the adsorption took place in less than one hour except for the most dilute solution (Fig. 1). For glass and aluminum, however, a plateau was not reached until several hours of immersion time had elapsed—except for the more concentrated solution where the curves continued to rise with increasing dip time (Fig. 2). The significance of this will be discussed later.

**B. Isotherms. Glass.**—Isotherms at 28.5° for glass samples were obtained for various dip times in the active cells (Fig. 3). The concentrations are plotted as a ratio of the actual cell concentration ($C$) to the concentration of a saturated solution ($C_0 = 8.1 \times 10^{-4}\ M$). At dip times of six hours or less, the amount of acid adsorbed became independent of adsorbate concentration over a range from 0.3 to 0.5 $C/C_0$. At higher adsorbate concentrations and longer dip times, the activity of the samples increased rapidly. It should be pointed out that for a unimolecular film on a perfectly smooth glass surface (roughness factor of 1.0) the curves should have leveled off at an activity reading of 93 counts/minute.

Autoradiographs of samples immersed in an 0.5 saturated solution for various dip times showed a gradual build-up of localized layers of activity over

(10) T. L. O'Connor and H. H. Uhlig, THIS JOURNAL, **61**, 402 (1957).

(11) W. D. Harkins and D. M. Gans, *J. Am. Chem. Soc.*, **53**, 2804 (1931).

(12) W. E. Ewing, *ibid.*, **61**, 1317 (1939).

(13) H. A. Smith and J. F. Fuzek, *ibid.*, **68**, 229 (1946).

(14) E. B. Greenhill, *Trans. Faraday Soc.*, **45**, 625 (1949).

(15) W. Hurst and J. K. Lancaster, *Research*, **3**, 336 (1950).

(16) S. H. Maron, *J. Colloid Sci.*, **11**, 21 (1956).

(17) C. Orr, Jr., and P. T. Bankston, *J. Am. Ceram. Soc.*, **35**, 58 (1952).

(18) C. Orr, Jr., and H. G. Blocker, *J. Metals*, **4**, Trans. 657 (1952).

(19) We are indebted to R. R. Burford of the Fluorochemical Division of our Company for the labeled acid used in this study.

(20) G. L. Mack, THIS JOURNAL, **40**, 159, 169 (1936).

a fairly uniform background level (Fig. 4). The uniform background level would represent about three monolayers of the acid if the glass were assumed to be perfectly smooth. Autoradiographs of samples immersed in solutions within the adsorbate concentration range from 0.3 to 0.7 $C/C_0$ were similar in appearance to the ones shown in Fig. 4.

These data suggest either a chemisorption process in which the perfluoro acid and constituents in the glass react to produce an insoluble product or the glass surface is not as smooth as one expects.

**Aluminum.**—Isotherms (28.5°) obtained for various dip times using aluminum samples (Fig. 5) are similar in general appearance to those obtained for the glass samples except the "apparent" reaction is not as noticeable between the 5 minute and the 24 hour dips (Fig. 3). For short dip times, the amount adsorbed became independent of adsorbate concentration over the concentration range 0.3 to 0.5 of a saturated solution. At longer dip times and higher adsorbate concentrations, sample activity increased continuously. Autoradiographs of some typical aluminum samples after immersion in a 0.5 $C/C_0$ solution of $C_7F_{15}C^*OOH$ are shown in Fig. 6.

The distribution of the acid on the aluminum surfaces is much more uniform than on glass. The striations in the rolled aluminum are plainly visible and it is quite possible that a true monolayer has been adsorbed for the short dip times. It is likely that a chemisorption process is responsible for the monolayer formation, but that longer dip times and higher concentrations allow penetration of this protective monolayer and further adsorption.

**Platinum and Quartz Samples.**—Platinum and quartz isotherms (28.5°) for various dip times were different in general characteristics from those for the other two surfaces studied (Figs. 7 and 8). Even for long dip times, adsorption became independent of concentration for all concentrations greater than 0.5 $C/C_0$. Autoradiographs showed uniform activity distribution over the sample surface for both short and long dip time samples.

These data suggest that monolayer formation takes place by the expected mechanism of physical adsorption.

**C. Measurement of Surface Area.**—The initial objective of this study was to develop a simple technique for measuring the surface area of plane surfaces. The acid used in this study appears useful only for non-reactive surfaces or for surfaces where the reaction product formed between the surface and the acid prevents further adsorption. The usual manner of expressing surface areas of plane surfaces is in terms of a "roughness factor"—ratio of the true surface area to the geometrical area. To convert a radioactive count to roughness factor requires a knowledge of: (1) the area occupied by the adsorbed molecule, (2) the specific activity of the radioactive acid, (3) the counting efficiency of the counter, and (4) the area of the sample counted. The figure used for the molecular area[21] of

(21) The actual average area of our perfluoro acid was undoubtedly somewhat larger than the value given due to the presence of branched isomers. Construction of molecular models showed that the presence of a branched methyl group would increase the area only a few Å.² units.

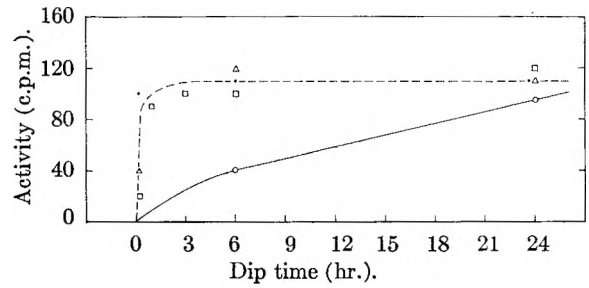


Fig. 1.—Rate of adsorption of $C_7F_{15}C^*OOH$ on platinum (temp. 28.5°). Solution concentrations: – – –, 0.03, 0.13, 0.5 $C/C_0$; ———, 0.0035 $C/C_0$; $C_0 = 8.1 \times 10^{-4}$ $M$.

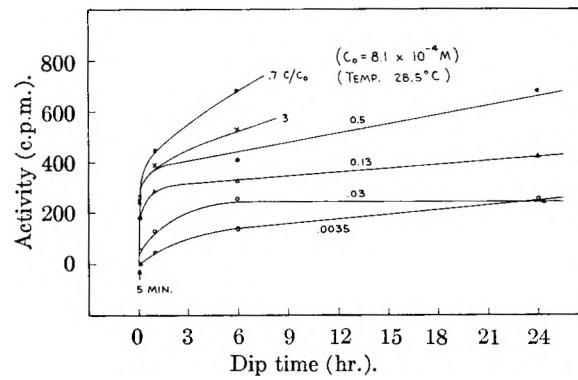


Fig. 2.—Rate of adsorption of $C_7F_{15}C^*OOH$ on glass.

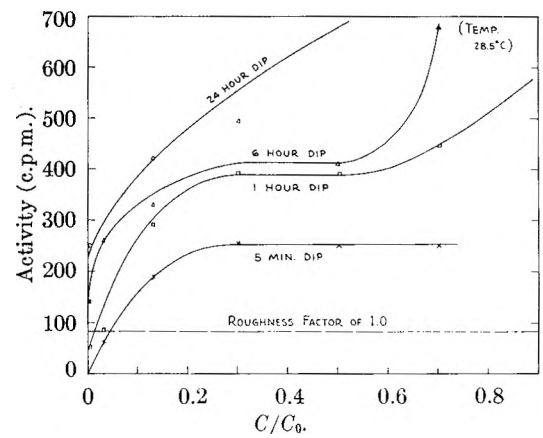


Fig. 3.—Isotherm for adsorption of $C_7F_{15}C^*OOH$ on glass.

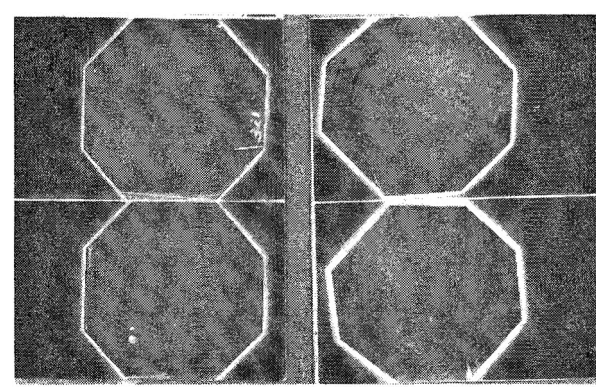

Dip time, 5 min. Activity, 243 c.p.m. 245 c.p.m.

Dip time, 1 hr. Activity, 403 c.p.m. 352 c.p.m.

Fig. 4.—Autoradiographs of $C_7F_{15}C^*OOH$ on glass (solution concentration, 0.5 $C/C_0$).

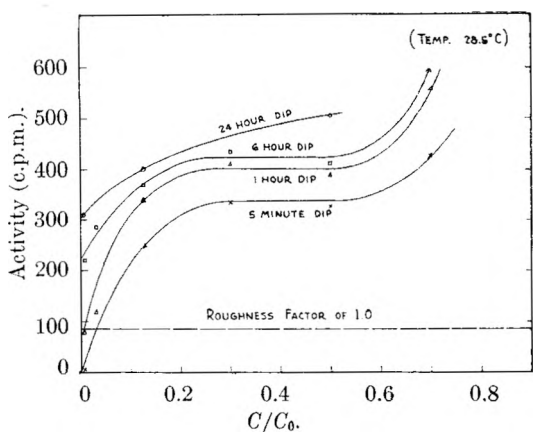


Fig. 5.—Isotherm for adsorption of $C_7F_{15}C^*OOH$ on aluminum.

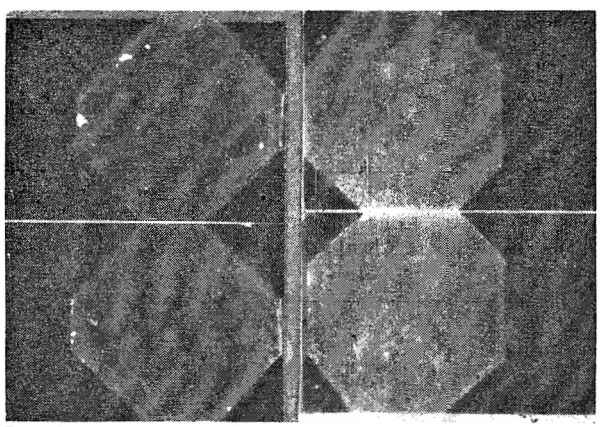

Dip time, 5 min. Activity, 274 c.p.m. 247 c.p.m.

Dip time, 1 hr. Activity, 508 c.p.m. 456 c.p.m.

Fig. 6.—Autoradiographs of $C_7F_{15}C^*OOH$ on aluminum (solution concentration, 0.5 $C/C_0$).

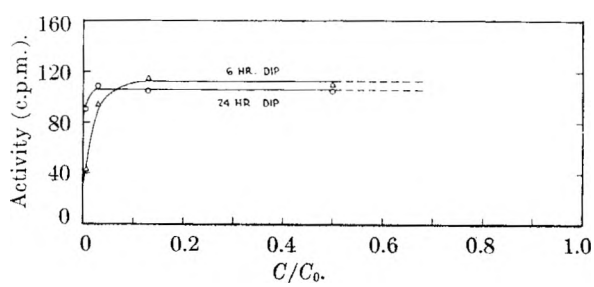


Fig. 7.—Isotherm for adsorption of $C_7F_{15}C^*OOH$ on platinum (temp. 28.5°).

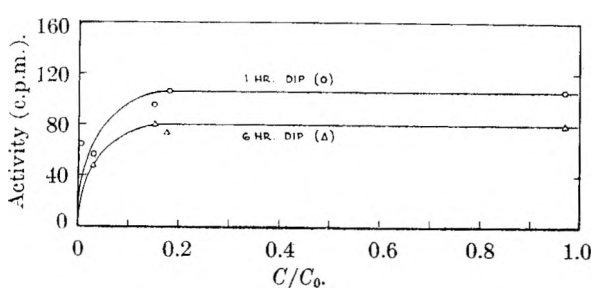


Fig. 8.—Isotherm for adsorption of $C_7F_{15}C^*OOH$ on quartz (temp. 28.5)°.

perfluorooctanoic acid was 29 Å.[2,22] The specific activity of the acid was 0.12 millicurie per gram or 264 dis./min./microgram. The counting efficiency of the Q-gas flow counter was calculated using a 50% geometry correction and backscattering factors[23] of 23% for aluminum, glass and quartz, and 52% for platinum. The unmasked area of the samples was 2.45 cm.$^2$. Using these data, one arrives at a figure of 93 counts/minute/monolayer for aluminum, glass and quartz; and 115 c.p.m./monolayer for platinum.

Roughness factors for glass, quartz, aluminum and platinum are given in Table I. Only the data for quartz and platinum can be considered to actually represent the "true" surface area.[24] Glass certainly appears to react continuously with the acid, and aluminum shows a tendency in that direction also. It is possible that the 5 minute dip for an aluminum sample gives a true measure of the surface area. A roughness factor of 3.3 for "rolled" aluminum seems reasonable.

TABLE I

ROUGHNESS FACTOES

| Surface | Soln. concn. $C/C_0$ | Dip time | Amount acid adsorbed (c.p.m.) | "Apparent" roughness factor |
|---|---|---|---|---|
| Glass | 0.5 | 5 min. | 250 | 2.7 |
| | | 1 hr. | 390 | 4.2 |
| | | 6 hr. | 410 | 4.5 |
| | | 24 hr. | 680 | 7.3 |
| Platinum | 0.5 | 6 hr. | 120 | 1.04 |
| | | 24 hr. | 110 | 0.96 |
| Aluminum | 0.5 | 5 min. | 310 | 3.3 |
| | | 1 hr. | 380 | 4.1 |
| | | 6 hr. | 390 | 4.2 |
| | | 24 hr. | 410 | 4.4 |
| Quartz | 0.2 | 5 min. | 80 | 0.86 |
| | | 1 hr. | 106 | 1.10 |
| | | 6 hr. | 74 | 0.80 |
| | | 24 hr. | 76 | 0.81 |

**D. Desorption by Solvents.**—Data on desorption as a function of dip time in a number of solvents were obtained. A typical set of curves for films on glass is shown in Fig. 9. Polar solvents were found to be extremely efficient "desorbers." An aromatic hydrocarbon (benzene) was considerably less effective, and an aliphatic hydrocarbon (decane) desorbed only a negligible amount of the adsorbed film. The adherence of the perfluoro acid film to the substrate increased in the order: platinum, aluminum, glass. The greater adherence to glass than aluminum was somewhat surprising, but furnishes further evidence for reaction between the perfluoro acid and the glass surface.

The surface distribution of an adsorbed film on glass after a prolonged rinse in benzene showed a peculiar behavior. A clean glass sample was

(22) Value reported in literature for $H(CF_2)_{10}CH_2OH$ is 29 Å.[2] C. H. Arrington, Jr., and G. D. Patterson, THIS JOURNAL, **57**, 247 (1953).

(23) H. Sobotka, "Monomolecular Layers," Am. Assn. Adv. Sci., 113 (1954). The backscattering correction is necessary when counting monomolecular layers because some of the $\beta$-particles emitted in a downward direction are deflected back into the counting zone.

(24) Quartz values tend to fall below 1.0 which might be due to using a low value for the molecular area of our acid.

dipped in a $C_7F_{15}COOH$/*n*-decane solution for five minutes and then immersed in benzene for eighteen days. The activity over the area counted actually increased from an average of 230 c.p.m. for the two sides to 353 c.p.m. after the benzene treatment. This is undoubtedly due to migration of the acid from the rough cut edges of the sample to the center. It should be noted (Fig. 9) that a one day rinse in benzene removed approximately 10% of the acid from the counting area.

On the other hand, no such behavior was noted when *n*-decane was the rinse solvent. Glass samples were dipped in a $C_7F_{15}COOH$/*n*-decane solution for 24 hours and then immersed in pure *n*-decane for 72 hours. There was no change in activity and the autoradiographs were quite similar to those taken on adsorbed films only. Apparently the adsorbed film can undergo surface migration in the presence of benzene but remains stationary in the presence of *n*-decane.

The failure of adsorbed films of perfluoroöctanoic acid to desorb in pure *n*-decane solvent suggests that the adsorption is not a reversible process. In the case of glass and aluminum, where a chemisorption process is likely, this might be due to the insolubility of the salt formed. But with quartz and platinum, the adsorption process itself is apparently not reversible.

Cook and Hackerman[25] observed an irreversible isotherm for the adsorption of fatty acids in benzene solution onto steel powder. The normal reversible isotherm increased with increasing concentration and exceeded the calculated amount necessary for a close packed monolayer by 20–70%. Calculated surface coverage for the irreversible adsorption was only 10–50%. This behavior differs considerably from perfluoroöctanoic acid isotherms which show only the irreversible behavior and do so for both reactive and non-reactive surfaces.

**E. Exchange.**—This phenomenon was first observed while investigating "carry-out" of solution from the adsorption cell when the samples were withdrawn. It seemed pertinent to establish that none of the solution was carried out with the samples even though the film appeared to be perfectly dry. A monolayer of non-radioactive perfluoroöctanoic acid was adsorbed on platinum and the samples dipped into a solution of the radioactive acid for one minute and withdrawn. If carry-out were occurring, some activity should be found on the samples. Surprisingly, a great deal of activity was found on the samples. The experiment was repeated and the results verified, but the amount of activity present appeared too large to be accounted for by mere carry-out. One alternate explanation was that the adsorbed molecules on the surface of the platinum were exchanging with the radioactive molecules in the solution. To check this, platinum samples containing an adsorbed film of radioactive acid were dipped for one minute into a solution of non-radioactive acid and slowly withdrawn. Activity measurements revealed that a majority of the adsorbed molecules had been removed but contact angle measurements gave no indication of a depleted monolayer. Thus exchange was established.

(25) E. L. Cook and N. Hackerman, THIS JOURNAL, **55**, 549 (1951).

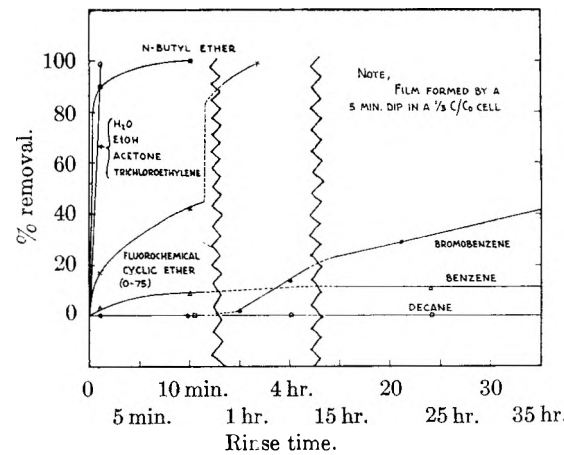


Fig. 9.—Desorption of $C_7F_{15}C^*OOH$ films from glass.

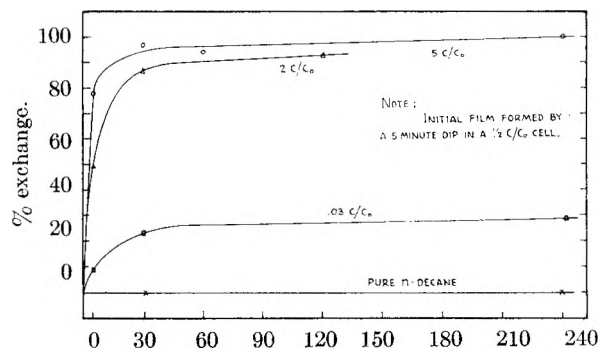


Fig. 10.—Exchange: $C_7H_{15}C^*OOH$ on glass.

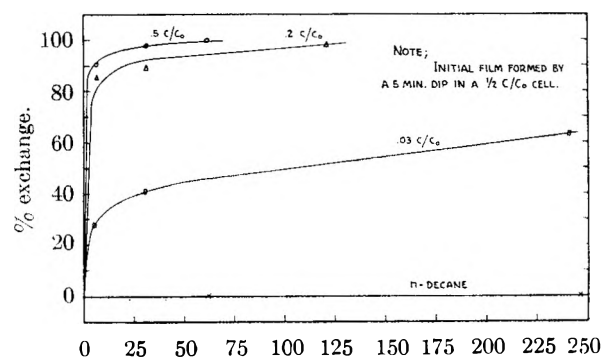


Fig. 11.—Exchange: $C_7F_{15}C^*OOH$ on aluminum.

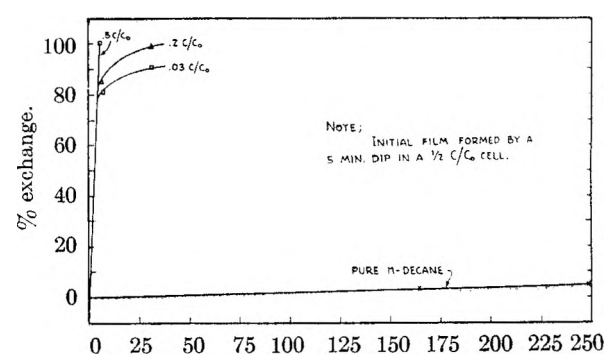


Fig. 12.—Exchange: $C_7F_{15}C^*OOH$ on platinum.

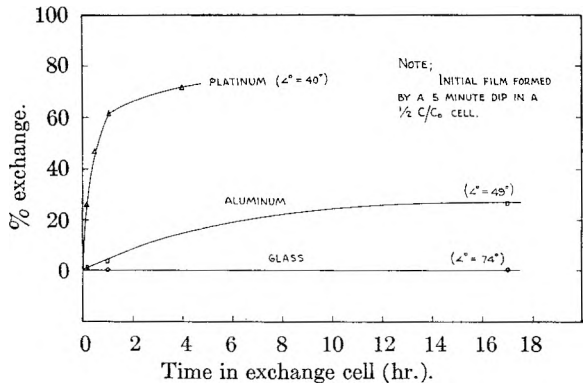


Fig. 13.—Exchange of adsorbed films of $C_7F_{15}C^*OOH$ with non-tagged stearic acid.

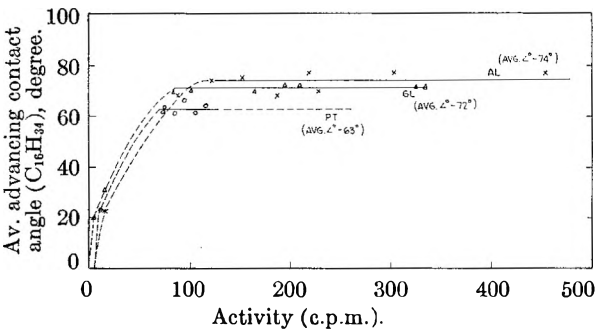


Fig. 14.—Contact angle *vs.* surface coverage.

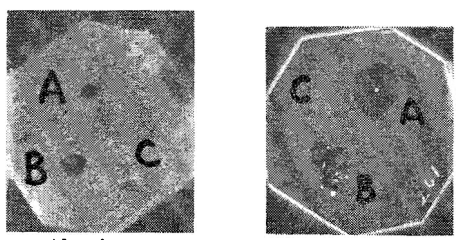


Aluminum Glass

Fig. 15.—Autoradiographs of adsorbed films of $C_7F_{15}C^*OOH$ after contact angle measurements: A, spot left by water contact angle drop; B, spot left by glycerol contact angle drop; C, no removal by hexadecane contact angle drop.

The extent of the exchange process was investigated as a function of solution concentration, time and nature of the surface. Data for platinum, glass and aluminum are plotted in Fig. 10, 11 and 12. The samples were dipped in an 0.5 $C/C_0$ active cell for 5 minutes before the exchange experiments. It is important to note that even after 40 hours in pure solvent (*n*-decane) there is no loss of the adsorbed film from glass and aluminum and only a 5% loss from platinum. The effect of solution concentration on the rate and extent of exchange is especially noteworthy. The rate and extent of exchange for the surfaces studied increase in the following order: glass, aluminum and platinum.

It is obvious that the presence of the perfluoro acid in solution has a pronounced effect on the exchange process. The question arose as to whether or not a weaker acid, such as stearic, would have the same effect. When a glass sample with an adsorbed layer of tagged perfluoroöctanoic acid was immersed in an *n*-decane solution of non-radioactive stearic acid, no exchange took place. With aluminum a slow exchange occurred, while with platinum the rate of exchange was very much faster (Fig. 13). The rates are much slower, however, than those with untagged perfluoroöctanoic acid in solution. It should be noted how the contact angle values reflect the replacement of the perfluoro acid by the less oleophobic stearic acid.

Smith and Fort[26] observed a type of exchange with a hydrocarbon acid that differs in many respects from the type we are reporting. They reported that an adsorbed film of C-14 tagged *n*-nonadecanoic acid on mechanically activated metal surfaces was undergoing continuous renewal by the acid in solution. Analysis showed that the adsorbed acid was coming off as the metal salt. The rate-determining step in the exchange is apparently the desorption process which is certainly not the case in the exchange involving a perfluoro acid. Further, the rate of exchange with an adsorbed hydrocarbon acid was greatest for the active metals, which is just the reverse of our observations.

**F. Contact Angle *versus* Surface Coverage.**—Contact angles using hexadecane were measured on most of the adsorbed films. The contact angles of water and glycerol were measured on some of the perfluoro acid films also.

The comparison of hexadecane contact angles *versus* amount adsorbed on glass, aluminum and platinum is shown in Fig. 14. These values are for pure hexadecane. The difference in contact angle for the various substrates should be noted. The values for hexadecane saturated with perfluoroöctanoic acid are approximately 8° higher. Hexadecane contact angle values are not sensitive to changes in surface concentration once a certain threshold is reached. Optical examination of the aluminum samples used in this study indicates that the roughness factor is probably more than 2.0. Thus, a monolayer of adsorbed perfluoro acid would give a count of about 200 c.p.m. A glance at Fig. 14 shows that with about 50% of complete coverage the contact angle has reached its maximum value. These results agree qualitatively with those reported by Bartell and Ruch[27] who used the optical method of Drude to determine surface concentration of octadecylamine. Smith and McGill[28] noted on magnesium, lead and silver that the surface became oleophobic after 55 to 60% of a monolayer of *n*-nonadecanoic acid has been adsorbed.

The contact angles of both the pure and the saturated hexadecane on perfluoro acid films on quartz were the same —70°.

The contact angles obtained with water and glycerol were very erratic—even on films adsorbed on platinum. The range of values obtained are shown in Table II.

TABLE II

| Substrate | $H_2O$ | Glycerol |
|---|---|---|
| Platinum | 46–85° | 46–81° |
| Glass | Spread | Spread |
| Aluminum | 61–77° | 58–90° |

The drops of liquid used in measuring the contact angles were removed by carefully touching a corner

(26) H. A. Smith and T. Fort, Jr., *ibid.*, **62**, 519 (1958).
(27) L. S. Bartell and R. J. Ruch, *ibid.*, **60**, 1231 (1956).
(28) H. A. Smith and R. M. McGill, *ibid.*, **61**, 1025 (1957).

of tissue paper to them. Autoradiographs were then prepared and the results (Fig. 15) show that the adsorbed film is not measurably disturbed by hexadecane but is completely desorbed by the polar liquids, water and glycerol.

Zisman and Levine[29] used methylene iodide as a measure of surface coverage and found it to be more sensitive to the orientation and packing of molecules in the adsorbed layer than the hexadecane which they had used in previous studies. The methylene iodide was chosen because of its large molecular diameter, high boiling point (180°) and low viscosity at ordinary temperature. It is conceivable that methylene iodide contact angle values would correlate better with our surface coverage data than the hexadecane values.

## Discussion

**A. Surface Area Measurements.**—There are a number of pertinent factors which must be considered when using solution adsorption to study surface phenomena. True surface area in terms of atomic dimensions is rather an indeterminate quantity. The areas measured by solution adsorption techniques are always relative and the values obtained are dependent on the physical and chemical properties of the adsorbate molecule.

**Molecular Configuration and Size.**—Surface area calculations, using solution adsorption data, are based on the assumption that the adsorbed molecule assumes the same configuration as at the liquid–air interface. The data in the literature indicate that this assumption is valid for long chain acids adsorbed on polar substrates.[11-18] Electron diffraction studies have shown that in oleophobic films of long chain acids, the molecules appear to be adsorbed in clusters.[30] The average tilt of the axes of the polar molecules from the normal to the substrate was related to the lengths of the molecules and varied from 2° for behenic acid to 8° for myristic acid. The average tilt angle also varies with the roughness of the substrate surface. It must be remembered that the tilt is measured relative to the average surface, and the tilt at the actual point of attachment may be much less. For cerotic acid films on rough rolled platinum, the observed maximum tilt was 30°, while for metallographically polished platinum the tilt angle decreased to nearly 0°. Specific area values for Raney nickel powders did not depend on the chain length of the fatty acid ($C_7$ to $C_{22}$) used.[13] The assumption that the orientation is similar to that on a water substrate is a good approximation and apparently the film follows the contours of the solid surface.

The relative size of a molecule can influence the surface area value also. Ewing[12] found twice as many methyl stearate molecules were adsorbed on a given zinc oxide powder when compared to the number of glycol dipalmitate molecules adsorbed. This agrees with the ratio of their surface areas as measured on an aqueous substrate. On rough or porous surfaces this relationship would not be found if the larger molecules failed to enter pores or fissures on the surface.

**Chemical Reactions within the System.**—The surface used in the adsorption and the chemistry involved must be considered in interpreting results. Bowden and Moore[31] and Daniel[31] showed that fatty acids react continuously with Zn, Cu and Cd surfaces with dissolution of reaction products into the surrounding liquid, but found no evidence of a similar action on Au or Pt.

Dobry and Mahncke[32] studied the adsorption of stearic acid on copper foil with and without an oxide surface. They also found evidence of a reaction with this oxide surface, but none with pure copper. Tabor points out that the latter observation may be due to absence of water rather than a non-oxide surface.

As a result of surface studies on various metals, using hydrocarbon carboxylic acids, Tingle[33] has divided metals into three categories on the basis of reactivity: I. Metals which form thick permeable oxide layers capable of reacting with fatty acids to form soaps; *i.e.*, cadmium, copper and zinc. II. Metals whose oxides, although capable of reaction with fatty acids, are formed on the surface as tough, compact films; *i.e.*, aluminum, chromium and nickel. III. Metals which form no oxide film, or only a very thin film; *i.e.*, platinum, gold and silver. Since the oxide films formed by Group II metals are tough and impermeable, hydrocarbon carboxylic acids are considered to form only a monolayer on these surfaces. Reliable surface area values for Groups II and III metals can be obtained from adsorption using these acids. Because of the permeability of the oxide layer and subsequent reaction, considerable caution is necessary in using adsorption data for Group I metals.

The results for perfluoroöctanoic acid give evidence of a considerable build-up of adsorbed material on glass and some build-up of adsorbed material on aluminum surfaces. The autoradiographic data supports this. It would appear that the oxide film on both glass and aluminum falls into class I for perfluoro acids. It has been suggested[34] that glass normally has a surface layer, possibly of silicic acid, which is different chemically from the bulk of the glass and protects the latter from contact with the solution. The reaction between the perfluoro acid and glass resulting in built-up layers of adsorbed material was certainly not expected. Perfluoroöctanoic acid is a strong acid (the dissociation constants of the fluorocarboxylic acids are all of the order of $2.5 \times 10^{-3}$) and it is possible that even with only minute amounts of water present on the surface of glass, a reaction takes place between the acid and the reactive surface layer. The results indicate that considerable care must be exercised in interpreting adsorption data obtained with perfluoro acids on both powdered and plain surfaces of reactive materials.

(29) O. Levine and W. A. Zisman, *ibid.*, **61**, 1068 (1957).

(30) W. C. Bigelow and L. O. Brockway, *J. Colloid Sci.*, **11**, 60 (1956); L. O. Brockway and J. Karle, *ibid.*, **2**, 277 (1947); J. Karle, *J. Chem. Phys.*, **17**, 500 (1949).

(31) F. P. Bowden and A. C. Moore, *Trans. Faraday Soc.*, **47**, 900 (1951); S. G. Daniel, *ibid.*, **47**, 1345 (1951).

(32) A. Dobry and H. E. Mahncke, *Nature*, **174**, 507 (1954); D. Tabor, *ibid.*, **174**, 507 (1954).

(33) E. D. Tingle, *Trans. Faraday Soc.*, **46**, 93 (1950).

(34) J. E. Willard, THIS JOURNAL, **57**, 129 (1953); P. F. Holt and D. T. King, *J. Chem. Soc.*, 773 (1955).

The results on platinum and quartz indicate that a monolayer is formed and that there is no reaction between the surface and the adsorbate. Reliable surface area data can thus be obtained from adsorption measurements on such surfaces.

**B. Exchange.**—Any explanation of the exchange process must account for the following observations: 1. essentially no desorption of adsorbed molecules by pure solvent (*i.e.*, irreversible adsorption); 2. rapid exchange of adsorbed molecules on all substrate studied with molecules in solution—both the free acid and salts of the acid undergo exchange; 3. extent and rate of exchange increases with increasing solution concentration; 4. extent of exchange does not approach 100% for all surfaces; 5. Slower exchange for adsorbed perfluoro acid with stearic acid than with perfluoro acid; 6. polar solvents (water, alcohol) desorb film rapidly while nonpolar solvents (decane, benzene), either do not desorb the film or desorb it very slowly.

Since this is an exchange process, the adsorbed untagged acid molecules, as well as the adsorbed tagged molecules, are exchanging with molecules in the solution. The radiochemical technique is limited to the detection of the decrease in the number of adsorbed tagged molecules. The data obtained could be explained by a process in which the activation energy for exchange is the same for all molecules on the surface. As the concentration of adsorbed tagged acid decreases, the probability of an exchange between a non-tagged solution molecule and an adsorbed tagged molecule decreases. It is assumed that once desorbed, the probability of readsorption of a tagged molecule is very small since the ratio of adsorbed molecules to molecules in even the most dilute solution used (0.03 $C/C_0$ )was approximately 1:500. Another alternative would be to assume the existence of differences in chemical structure between the rapidly removed fraction and the less rapidly removed molecules; *i.e.*, free acid *versus* aluminum salt.

A mechanistic explanation of the exchange process might be that the presence of the polar perfluoro acid molecules in the solution provide the driving force necessary for the adsorbed molecules to invert and leave the surface. Thus, the greater the concentration of acid molecules in the solution, the faster the rate of exchange. The fact that no exchange takes place between stearic acid in solution and perfluoro acid adsorbed on glass, and very slow exchange with adsorbed films on aluminum, while a measurable exchange is found with platinum, might be explained by both a difference in the chemical species of the adsorbed acid on these surfaces and the lower degree of polarity of stearic acid. Platinum undoubtedly contains adsorbed free acid but it is very likely that both glass and aluminum contain salts of the acid. The isotherm data give additional evidence of the reactive nature of the glass surface. It is likely that stearic acid is not polar enough to "induce" the acid salts to leave the surface. Other evidence for this explanation lies in the fact that the contact angle of hexadecane on an adsorbed film has no effect on the film. Autoradiographs show that the adsorbed layer is not disturbed. However, when polar molecules such as water and glycerol are used to measure contact angles, the adsorbed monolayer turns over and the film is disturbed. Further evidence for this polar effect on molecules is provided by the data of Rideal and Tadayon.[35] They measured the contact angle of water on a paraffin–stearic acid mixture and found that the contact angle decreased with time and also with increasing concentration of stearic acid. They stated that the randomly oriented stearic acid molecules in the paraffin were reoriented with their carboxyl groups in the water phase—thus causing a decrease in contact angle.

Additional experimental studies with other types of labeled polar organic molecules are planned.

(35) E. Rideal and J. Tadayon, *Proc. Roy. Soc.* (*London*), **225A**, 346 (1954).

---

# SHOCK TUBE STUDIES ON THE PYROLYSIS AND OXIDATION OF METHANE

BY GORDON B. SKINNER AND ROBERT A. RUEHRWEIN

*Monsanto Chemical Company, Research and Engineering Division, Dayton 7, Ohio*

*Received March 11, 1959*

A shock tube has been used to study the pyrolysis and oxidation of methane in the range 1200–1800°K. under homogeneous reaction conditions. The experimental activation energy in pyrolysis is 101,000 cal., which suggests that the initiating reaction is $CH_4 \rightarrow CH_3 + H$, and that the chain length in reaction is only 2. With addition of oxygen, the activation energy decreases, suggesting that the initiating reaction is $CH_4 + O_2 \rightarrow CH_3 + HO_2$. Quantitative product yields of $C_2H_6$, $C_2H_4$, $C_2H_2$ and $H_2$ are recorded for pyrolysis experiments, and these plus CO for oxidation experiments. Induction times were measured for several $CH_4$–$O_2$ mixtures of 40% or less $O_2$ content, in the range of 1 to 10 milliseconds.

## Introduction

The shock tube has recently become a popular tool for the study of high temperature gas reactions,[1-3] largely because it is one of the few techniques which can yield entirely homogeneous reaction data. We have built a shock tube similar to that of Glick, Squire and Hertzberg[2] and used it to study the high temperature reactions of methane and methane–oxygen mixtures by the reflected shock wave technique.

(1) E. F. Greene, R. L. Taylor and W. L. Patterson, Jr., THIS JOURNAL, **62**, 238 (1958).

(2) H. S. Glick, W. Squire and A. Hertzberg, 5th Symposium on Combustion, Pittsburgh, 1954, p. 393.

(3) H. S. Glick, J. J. Klein and W. Squire, *J. Chem. Phys.*, **27**, 850 (1957).

Experiments on the pyrolysis of methane have been done mostly with tubular flow reactors, where wall effects could be important. The earlier work has been summarized by Storch,[4] while more recent studies have been made by Gordon[5] and Germain and Vaniscotte.[6] There still seems to be doubt as to the mechanism of methane pyrolysis.[7]

Numerous studies of the methane–oxygen reaction have been made below 600°, but the only data at temperatures and compositions comparable to ours are those of Sachsse,[8] who measured induction times of 62:38 mole ratio methane–oxygen mixtures up to 920°. Our studies of the methane–oxygen reaction were of two kinds. We measured induction times by heating samples until a rapid reaction set in, and we quenched samples which had been heated for less than the induction time, to analyze for reaction products.

## Experimental

The shock tube was made from 7.6-cm. stainless steel pipe, generally resembling that of Glick, Squire and Hertzberg. The reaction section was 3.66 m. long, while the driver section could be adjusted in length between 1.83 and 8.53 m., so dwell times up to 15 milliseconds could be obtained with helium driver gas. The expansion tank had a volume of about 1.4 m.[3]

For measuring the incident shock speed, SLM pressure transducers spaced 1.22 m. apart near the downstream end of the reaction section were used. Two identical trigger circuits amplified the transducer signals, while thyratron elements with manual reset assured that only one signal was emitted from each amplifier in an experiment. The amplified signals were used to start and stop a timer accurate to one microsecond (Hewlett–Packard type 523-B) and also to start two oscilloscopes. One of these measured the pressure, by means of a third SLM gauge mounted on top of the shock tube, 7.6 cm. from the downstream end, while the other measured the output from a photocell mounted outside a window in the side of the shock tube, also 7.6 cm. from the end. Directly opposite the photocell window was a small tube leading to a quick-opening valve, from which samples of gas could be drawn for analysis.

Gas mixtures to be studied were made up beforehand by pressure, and the concentration of each gas was known within 1 to 2% of its value. Argon, oxygen and helium from the Air Reduction Co., and 99% methane from the Matheson Co., were used without further purification. Gas samples were analyzed before and after reaction by a vapor chromatograph designed in these laboratories, which had a limit of detection of about 30 p.p.m. for most of the gases analyzed. In spite of the fact that the driver gas was in direct contact with the sample during the experiments, no more than 5% driver gas was found in the reactant gas after the runs, and in most cases the amount was less than 1%. As would be expected, the longer time runs showed the greatest contamination.

In a typical run, all sections of the shock tube were first evacuated, and then the sample and driver gases were added. Since the "tailored interface" technique[2] was used to give a pulse of uniform temperature, small amounts of nitrogen were usually added to the helium driver gas, to match it with the sample and pressure ratio. The two diaphragms were then ruptured at the proper times, by the plungers operated by the auxiliary shock tube, and a sample of gas taken for analysis a few seconds later. The oscilloscope traces were recorded with Polaroid cameras.

Strehlow and Cohen[9] have recently published a discussion of the reflected shock wave technique. They found that the most nearly ideal conditions for kinetic studies occurred when the sample gas was nearly all monatomic, while diatomic gases could be studied with some accuracy if measurements were taken near the end wall of the shock tube. With polyatomic gases, perturbations in the reflected shock wave due to boundary layer interactions were so great that temperatures could not be calculated with any accuracy. Since our polyatomic gas samples were diluted with argon, the average properties of the gas mixtures used in the shock tube were about the same as those of diatomic gases, and our method of sampling gave a sample for analysis which had been fairly near the end plate during the high temperature pulse.

Strehlow and Cohen also point out that since measured reflected shock speeds in argon are about 4% less than theoretical, the actual temperatures behind the reflected shock will be lower than the calculated values. However, their estimate of 300–500° for the temperature error seems to be about ten times too high. Moreover, the observed weaker reflected shock should cause a lower reflected pressure as well as a lower temperature, and our method of correcting for pressure variations would take care of over half the temperature error. Therefore the possibility of error in temperature due to the weaker reflected shock will be in the neighborhood of 10–20°, rather than 300–500°.

The over-all uncertainty in the absolute temperature of the experiments may be as large as 20–30°, largely because of the type of perturbations which Strehlow and Cohen have pointed out. Since the instrumental errors in measuring the shock speeds and pressures introduce only a few degrees uncertainty in temperature, the precision within a group of experiments will be 5–10°. The uncertainty in the residence time at high temperature was in the range of 10–20%. For pyrolysis and oxidation experiments, there is uncertainty because all parts of the gas were not heated for exactly the same time, and it was not known exactly from which part of the gas the analytical sample came. For induction times, the uncertainty came in defining the end of the induction period, which is signalled by a rapid rise in the rate of reaction (and light emission), rather than by a sudden explosion.

## Calculation of Results

For each experiment the incident shock speed, the pressure record and the photocell record were obtained. For induction time experiments, the end of the induction time was signalled by a rapid rise in photocell output, corresponding to a flash of light.

From the shock speed, the temperature ($T_3$) and pressure ($P_3$) behind the reflected shock wave were calculated, using the known thermal functions of the $CH_4$, $O_2$ and argon in the gas mixtures, assuming the gases behaved ideally and that no chemical reaction occurred ahead of the reflected shock wave.

It was also assumed that full rotational and vibrational relaxation of the $CH_4$ and $O_2$ were achieved in calculating $T_3$. Strehlow and Cohen, among others, have shown that the vibrational relaxation time of $O_2$ at one atmosphere is about 10 microseconds at 1500°K., which is typical of our experiments, while Chesick and Kistiakowsky[10] have shown that the relaxation time for $CH_4$ is less than 1 microsecond at 2500° K., so it can hardly be more than 10 microseconds at 1500°K. Since our reaction times were several milliseconds, it seems clear that vibrational equilibration was complete before much else happened.

The pressure record showed that the pressure during a run varied somewhat and was generally in the neighborhood (±10–20%) of $P_3$. It was assumed that $T_3$ and $P_3$ were actually realized just behind the reflected shock wave, and that subsequent pressure changes caused changes in temperature given by the isentropic equation

(4) H. H. Storch, *Ind. Eng. Chem.*, **26**, 56 (1934).
(5) A. S. Gordon, *J. Am. Chem. Soc.*, **70**, 395 (1948).
(6) J. E. Germain and C. Vaniscotte, *Bull. soc. chim. France*, 692 (1957); 319 (1958).
(7) F. W. Cagle, Jr., *J. Chem. Phys.*, **25**, 1300 (1956).
(8) H. Sachsse, *Z. physik. Chem.*, **B33**, 229 (1936).
(9) R. A. Strehlow and A. Cohen, *J. Chem. Phys.*, **30**, 257 (1959).
(10) J. P. Chesick and G. B. Kistiakowsky, *J. Chem. Phys.*, **28**, 956 (1958).

$$\frac{T}{T_3} = \left(\frac{P}{P_3}\right)^{(\gamma-1)/\gamma}$$

This is reasonable since small shock changes of 10 or 20% in pressure have negligible entropy changes. A graph of $T$ *versus* time was plotted for each run, and the arithmetic average temperature taken as the temperature of the run. Usually this average temperature was within 30° of $T_3$.

Vapor chromatographic analyses were made for $CH_4$, $H_2$, $C_2H_6$, $C_2H_4$ and $C_2H_2$ in pyrolysis experiments, and for CO and $CO_2$ as well in oxidation experiments. We were unsuccessful in making accurate determinations of water vapor, partly because the gas samples picked up traces of water vapor in handling. Also, since only a few per cent. of the methane and oxygen reacted, it was not possible to get accurate analyses of the amounts of these used up. Therefore the amounts of $CH_4$ and $O_2$ used up, and of $H_2O$ produced, were calculated from the other analytical data, assuming that no other substances were involved.

In some pyrolysis experiments the amount of $H_2$ found was greater than that calculated from the observed $C_2H_6$, $C_2H_4$ and $C_2H_2$. This was probably due to the formation of higher hydrocarbons or carbon (although no carbon was actually observed), and for purposes of calculation these were assumed to have the formula $(CH_{1.5})_n$ and to have zero heat of formation. In a few others of these runs, the hydrogen found was less than the calculated amount, probably because of experimental error. Here the average of the observed and calculated amounts was taken as the true value, and only the $C_2$ hydrocarbons were assumed to be formed, in the ratio in which they were found experimentally.

**Calculations for Methane Pyrolysis.**—The experiments of Kassel[11] and others suggest that the pyrolysis of methane is a first-order reaction, so that

$$\frac{d(CH_4)}{dt} = -k(CH_4)$$

where $(CH_4)$ is the partial pressure of methane, $t$ the time and $k$ the rate constant. The rate constant $k$ is given by an equation of the type

$$\log k = A + B/T$$

where $A$ and $B$ are constants. We used equations of this type in our calculations. The procedure was to assume "reasonable" values for $A$ and $B$, calculate the conversion of methane to be expected in each run, and compare the observed and calculated yields. The calculations took into account the actual time–temperature history of the run obtained from the pressure record and corrected for the heat absorbed by the pyrolysis reaction. Successive approximations to $A$ and $B$ were made until the average of the observed/calculated ratios was unity and independent of temperature.

**Calculations for Methane Oxidation.**—This method of calculation resembled that for methane pyrolysis, with a few variations. If the per cent. of methane converted in an experiment was $\alpha$, then an equation of the type

$$\log \alpha = A + B/T$$

was assumed. For a first approximation, $A$ and $B$ were determined from a plot of log $\alpha$ *versus* $1/T$, the temperature being the average temperature of the run ($T_{av}$), and all the runs being for about the same time at high temperature. A first approximation to the rate constants (in % of methane converted per millisecond, for example) was given by dividing the experimental conversion by the run time. These rate constants were used to calculate the methane conversion to be expected from the individual runs, allowance now made for temperature variations due to pressure and to heat of reaction, and for the decrease in concentration of reactants, assuming the rate to be proportional to the product of the $CH_4$ and $O_2$ concentrations. Another calculation was made for each point, assuming a constant temperature $T_{av}$, a constant hold time which was the average time for the group of experiments, and no reduction in reactant concentrations. The experimental $CH_4$ conversions were multiplied by the ratio of the above calculated values, to give a second approximation which more nearly approached what one would expect from an isothermal experiment of very low conversion. A third approximation was made in the same way, by which time each experimental conversion was corrected to the value for an isothermal experiment of fixed time, corrected for decrease in reactant concentration. Actually the concentration effect was rather small, since the largest conversion of methane was less than 10%.

**Calculations for Induction Times.**—Here calculations were simpler since no attempt was made to correct for the decrease in reactant concentrations or the heat evolved by the reaction. A plot of log $\tau$ (where $\tau$ is the induction time) *versus* $1/T_{av}$ gave a straight line, and this graph was used as a first approximation. For a second approximation, the arithmetic average temperature $T_{av}$ was retained, and the correction for temperature variations during the run applied by calculating an "effective time" which allowed for the logarithmic dependence of induction time on $1/T$. A further correction was made to account for pressure variations during the runs. It was found for mixtures of 60–40 methane–oxygen ratio that the induction time was inversely proportional to the pressure. Therefore corrections were made to the induction times by multiplying the observed times by $p'/p$, where $p'$ is the observed average pressure for a run, and $p$ is a standard pressure for a group of runs. These pressure corrections were as high as 20%.

Once these corrections were made, a least-squares curve was calculated for log $\tau$ *versus* $10^4/T$.

## Results

**Pyrolysis of Methane.**—Most of the pyrolysis experiments were carried out with a mixture of 12% methane and 88% argon, with a total pressure of 5 atmospheres. Three runs were made with a 1% methane mixture at the same total pressure. The experimental data are summarized in Table I. The first-order rate constant is given by the equation

$$\log k = 14.71 - \frac{22{,}070}{T}$$

(11) L. S. Kassel, *J. Am. Chem. Soc.*, **54**, 3949 (1932).

which corresponds to an activation energy of 101,000 cal. A graph of $k$ *versus* $10^4/T$ is shown in Fig. 1. The temperatures of the experimental points are those at which an isothermal experiment would give the calculated conversion in the experimental time, while the "experimental" $k$'s show the variations from the average curve required to give the observed methane decompositions. This method of plotting was needed since the temperature varied during the experimental runs, and no unequivocal "experimental temperature" can be assigned to a run.

**Methane Oxidation.**—Measurements were made with $CH_4$–$O_2$–Ar mole ratios of 12–8–80 and 12–2–86, at dwell times of 1.5 and 9.7 milliseconds. The product yields are listed in Table II, in terms of moles of product per 100 moles of methane originally present. Table II also includes the calculated values for water produced, and methane and oxygen used up. All these values are corrected, as described above, to isothermal conditions at the indicated temperatures. The constants $A$ and $B$ of the corrected empirical equations for the conversion of methane are given in Table III, along with the derived $\Delta H$ values.

TABLE I

PRODUCT DISTRIBUTION IN METHANE PYROLYSIS

| Temp., °K. | Moles of product / 100 mole methane originally present: $C_2H_6$ | $C_2H_4$ | $C_2H_2$ | $H_2$ |
|---|---|---|---|---|
| Group 1. $CH_4$:Ar = 12:88, av. dwell time 1.5 msec. | | | | |
| 1593 | 0.26 | 0.26 | 0 | 0.62 |
| 1602 | .26 | .27 | 0 | 0.99 |
| 1635 | .33 | .63 | 0.19 | 2.87 |
| 1673 | .33 | .99 | .33 | 4.80 |
| 1676 | .37 | 1.38 | .90 | 3.92 |
| 1678 | .33 | 1.17 | .81 | 7.5 |
| 1715 | .29 | 1.95 | 2.33 | 14.8 |
| 1733 | .20 | 1.94 | 4.04 | 12.8 |
| 1739 | .29 | 1.93 | 3.31 | 16.2 |
| Group 2. $CH_4$:Ar = 12:88, av. dwell time 10 msec. | | | | |
| 1430 | 0.07 | 0.02 | 0 | 0.12 |
| 1442 | .10 | 0 | 0 | 0.12 |
| 1468 | .16 | 0.10 | 0 | 0.32 |
| 1518 | .24 | 0.32 | 0 | 1.29 |
| 1561 | .32 | 0.50 | 0.20 | 2.34 |
| 1618 | .32 | 1.19 | 1.08 | 9.33 |
| Group 3. $CH_4$:Ar = 1:99, av. dwell time 10 msec. | | | | |
| 1630 | 0.8 | 1.8 | 1.9 | 14.7 |
| 1705 | 1.5 | 1.5 | 13.1 | 63.5 |
| 1785 | 0 | 0.9 | 22.0 | 87.5 |

**Induction Times.**—Induction times were measured for several $CH_4$–$O_2$–Ar mixtures. The corrected experimental points are shown in Table IV, where the methane–oxygen–argon mole ratio is shown as the "composition." Table V lists the empirical constants $A$ and $B$ of the equation

$$\log t = A + B/T$$

where $t$ is the induction time in milliseconds.

## Discussion

**Pyrolysis of Methane.**—The temperature dependence of the pyrolysis rate constant strongly

$$CH_4 \longrightarrow CH_3 + H \qquad (1)$$

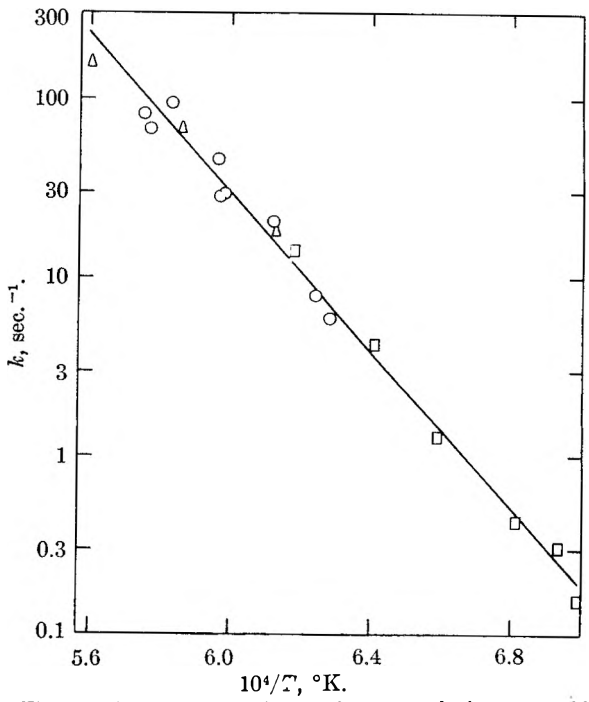


Fig. 1.—Rate constant for methane pyrolysis: △, 1–99 $CH_4$–Ar mole ratio, 10 msec. dwell time; ○, 12–88 $CH_4$–Ar mole ratio, 1.5 msec. dwell time; □, 12–99 $CH_4$–Ar mole ratio, 10 msec. dwell time.

TABLE II

PRODUCT DISTRIBUTION IN METHANE OXIDATION

| $10^4/T$, °K. | Moles of product/100 moles methane originally present: $C_2H_6$ | $C_2H_4$ | $C_2H_2$ | $H_2$ | CO | $H_2O$ | $CH_4$ used up | $O_2$ used up |
|---|---|---|---|---|---|---|---|---|
| Group 1. $CH_4$:$O_2$:Ar = 12:8:80, dwell time 1.5 msec. | | | | | | | | |
| 7.46 | 0.19 | 0 | 0 | 0.07 | 0.05 | 0.22 | 0.43 | 0.14 |
| 7.12 | .35 | .07 | 0 | 0.18 | 0.13 | 0.59 | 0.98 | 0.36 |
| 6.97 | .95 | .55 | 0.08 | 1.92 | 1.43 | 3.23 | 4.59 | 2.33 |
| 6.82 | .65 | .36 | 0 | 1.52 | 1.14 | 2.14 | 3.17 | 1.64 |
| Group 2. $CH_4$:$O_2$:Ar = 12:8:80, dwell time 9.7 msec. | | | | | | | | |
| 8.08 | 0.26 | 0.02 | 0 | 0.10 | 0.07 | 0.34 | 0.63 | 0.21 |
| 7.72 | .52 | .15 | 0 | 0.55 | 0.43 | 1.13 | 1.77 | 0.78 |
| 7.56 | .77 | .48 | 0 | 1.58 | 1.27 | 2.70 | 3.78 | 1.99 |
| Group 3. $CH_4$:$O_2$:Ar = 12:2:86, dwell time 1.5 msec. | | | | | | | | |
| 6.94 | 0.24 | 0 | 0 | 0.12 | 0.04 | 0.21 | 0.53 | 0.13 |
| 6.70 | .34 | 0.13 | 0 | 0.35 | .12 | .51 | 1.07 | 0.32 |
| 6.67 | .38 | .10 | 0 | 0.43 | .15 | .44 | 1.10 | 0.29 |
| 6.51 | .67 | .27 | 0 | 1.10 | .38 | .76 | 2.25 | 0.57 |
| 6.33 | .75 | .94 | 0 | 4.05 | 1.26 | 1.12 | 4.58 | 1.15 |
| Group 4. $CH_4$:$O_2$:Ar = 12:2:86, dwell time 9.7 msec. | | | | | | | | |
| 7.45 | 0.14 | 0.04 | 0 | 0.08 | 0.04 | 0.21 | 0.39 | 0.12 |
| 7.26 | .29 | .09 | 0 | 0.45 | .15 | 0.32 | 0.91 | .30 |
| 7.12 | .34 | .12 | 0 | 0.55 | .24 | 0.47 | 1.16 | .35 |
| 6.90 | .64 | .49 | 0 | 1.74 | .68 | 1.25 | 2.94 | .97 |
| 6.62 | .80 | 1.36 | 0.38 | 6.8 | 2.3 | 2.5 | 8.8 | 2.4 |

TABLE III

CONSTANTS IN THE EMPIRICAL RATE EQUATION FOR METHANE OXIDATION

| Composition $CH_4$:$O_2$:Ar | Time, msec. | $A$ | $-B$ | $\Delta H$(cal./mole) |
|---|---|---|---|---|
| 12-8-80 | 1.5 | 11 425 | 15,804 | 72,300 |
| | 9.7 | 11 479 | 14,474 | 66,200 |
| 12-2-86 | 1.5 | 10 444 | 15,518 | 71,000 |
| | 9.7 | 11.539 | 16,031 | 73,400 |

suggests that the rate-determining step is the decomposition of methane which is known to have a dissociation energy of about 101,000 cal.[12] The reaction could then proceed by the simple steps

$$H + CH_4 \longrightarrow CH_3 + H_2 \qquad (2)$$

and

$$2CH_3 \longrightarrow C_2H_6 \qquad (3)$$

Our experiments support this view in various ways. First, the same first-order rate constants applied for 12–88 and 1–99 mixtures at the same total pressure, so the first-order mechanism seems correct. Second, changing the dwell time from 1.5 to 10 milliseconds at a constant temperature changed the product distribution, but not the rate of decomposition of methane. This infers that methane decomposition is not much affected by the presence of the decomposition products. Third, ethane is found to be the first pyrolysis product, followed by ethylene and acetylene. A comparison of the data in Table I for short and long dwell times certainly suggests that the unsaturated hydrocarbons come from the ethane, and not directly from the methane. Finally, there is the agreement of the experimental and theoretical $\Delta H$ values.

This suggested mechanism can be checked semi-quantitatively by the absolute reaction rate theory. The rate of activation of methane molecules will be given by the equation[13]

$$k_a = \frac{kT}{h} e^{\Delta S/R} e^{-\Delta H/RT}$$

If we consider the activated complex to be a methane molecule with 101,000 cal. of energy in one of the vibrational modes (frequency between 1300 and 3000 cm.$^{-1}$) then the excess entropy at 1600°K. would be between 6.4 and 7.1 e.u. If we take an average of 6.7 e.u., then at 1600°K., $k_a = 15$ sec.$^{-1}$. From Fig. 1 we find $k$ for the disappearance of methane to be 8.2 sec.$^{-1}$ at 1600°K., but since the chain length is two the rate of methane dissociation would be 4.1 sec.$^{-1}$. It seems reasonable that the rate of activation should be a few times greater than the rate of reaction.

Several recent papers have given rate constant values for reactions 2 and 3. For (2), Pritchard, Pyke and Trotman-Dickenson[14] gave the activation energy as 9,000 cal., and calculated a frequency factor of $10^{13.3}$ at 140°, compared to a measured value of $10^{12.5}$ at the same temperature. Since the frequency factor is proportional to the absolute temperature, we may write the measured value as

$$k_2 = 10^{9.9} Te^{-9,000/RT} \text{ mole}^{-1} \text{ cc. sec.}^{-1}$$

For reaction 3 Moseley and Robb[15] give $k_3 = 3.8 \times 10^{13}$ at room temperature; Shepp[16] found $k_3 = 2.2 \times 10^{13}$ at 150°, while Ingold and Lossing[17] found that $k_3$ decreased from $1.36 \times 10^{13}$ to $0.48 \times 10^{13}$ as the temperature was increased from 434° to 1087°K. The value of $k_3$ is about $10^{12.9}$ at 1600°K.

At 1600°K. and one atmosphere methane pressure, the concentration of methane, $(CH_4)$, is $10^{-5.1}$ mole cc.$^{-1}$ and the experimental $k_1$ is 4.1 sec.$^{-1}$. The rates of reactions 1, 2 and 3 are all $10^{-4.5}$ mole cc.$^{-1}$ sec.$^{-1}$, so the steady-state concentration of H atoms is $10^{-11.3}$ mole cc.$^{-1}$, while that of $CH_3$ radicals is $10^{-8.7}$ mole cc.$^{-1}$. This is in agreement with results of Rice and Dooley,[18] who found $CH_3$ radicals but not H atoms in mirror removal experiments.

We should now consider reaction (4) which has

$$CH_3 + CH_4 \longrightarrow C_2H_6 + H \qquad (4)$$

been suggested by Rice as a reaction which could lead to longer reaction chains for methane decomposition. Steacie[12] states that the activation energy is 40–50 kcal., but the frequency factor has not been estimated. Pritchard gives the factor for reaction (5) as $10^{11.5}$ at room temperature. The

$$CH_3 + CH_4 \longrightarrow CH_4 + CH_3 \qquad (5)$$

factor for reaction 4 will probably be less than this since a closer approach of the reactants is required. If we take his value as a first approximation, then

$$k_4 = 10^{9.0} Te^{-45,000/RT}$$

and for the value of $(CH_3)$ obtained above for 1600° K., the rate of reaction 4 will be $10^{-8.4}$ mole cc. sec.$^{-1}$, which is much less than the rate of reactions 1, 2, and 3. Therefore we conclude that reaction 4 can be neglected.

It is hard to compare our results with other experimental work, since the other studies employed quartz or porcelain reactors, lower temperatures and longer dwell times. On the whole, reaction rates obtained at the lower temperatures were higher than those obtained by extrapolating our curve, while the activation energy found at low temperatures was lower. This suggests that the low temperature results may have been affected by catalysis at the walls. Gordon[5] and Germain and Vaniscotte[6] reported some effects of surface on the reaction rates. Kassel[11] reported no surface effects, but on the other hand he found that even at low methane conversions all the decomposed methane went to carbon, which could itself have acted as a heterogeneous catalyst, while in our work almost all of the decomposed methane remained as $C_2$ hydrocarbons.

**Methane Oxidation.**—Since the $\Delta H$ of the overall oxidation reaction is near 70 kcal. (Table III), it seems unlikely that reaction 1 is the chief initiating step. A likely candidate is

$$CH_4 + O_2 \longrightarrow CH_3 + HO_2 \qquad (6)$$

which has been suggested by Semenov[19] and others, with a $\Delta H$ of about 54,000 cal. The further steps in the reaction remain open to speculation, and we are not now in a position to assign reaction rates for them. However, a few general comments will be made.

(12) E. W. R. Steacie, "Atomic and Free Radical Reactions," 2nd ed., Reinhold Publ. Corp., New York, N. Y., 1956.

(13) S. Glasstone, "Textbook of Physical Chemistry," D. Van Nostrand Co., New York, N. Y., 1946.

(14) H. O. Pritchard, J. B. Pyke and A. F. Trotman-Dickenson, *J. Am. Chem. Soc.*, **77**, 2629 (1955).

(15) F. Moseley and J. C. Robb, *Proc. Roy. Soc.* (*London*), **A243**, 130 (1957).

(16) A. Shepp, *J. Chem. Phys.*, **24**, 939 (1956).

(17) K. U. Ingold and F. P. Lossing, *ibid.*, **21**, 368 (1953).

(18) F. O. Rice and M. D. Dooley, *J. Am. Chem. Soc.*, **56**, 2747 (1934).

(19) N. N. Semenov, *Chim. & ind.* (*Paris*), **79**, 3 (1958).

TABLE IV

INDUCTION TIMES FOR METHANE–OXYGEN–ARGON MIXTURES

| Composition $CH_4:O_2:Ar$ | Pressure, atm. | $10^4/T$, °K. | Time, msec. |
|---|---|---|---|
| $CH_4:O_2:Ar$ | | | |
| 6-4-90 | 5 | 6.30 | 0.8 |
| | | 6.34 | 0.8 |
| | | 6.44 | 1.2 |
| | | 6.56 | 2.3 |
| | | 6.86 | 6.9 |
| | | 6.92 | 6.2 |
| | | 6.99 | 6.6 |
| | | 7.05 | 8.0 |
| | | 7.06 | 8.8 |
| | | 7.08 | 10.6 |
| | | 7.12 | 11.1 |
| | | 7.21 | 13.1 |
| | | 7.21 | 16.1 |
| 6-4-90 | 10 | 6.48 | 0.8 |
| | | 6.52 | 0.7 |
| | | 6.61 | 1.4 |
| | | 6.75 | 2.6 |
| | | 6.94 | 4.9 |
| | | 7.11 | 5.6 |
| | | 7.23 | 7.1 |
| | | 7.32 | 8.0 |
| 12-8-80 | 5 | 6.37 | 0.4 |
| | | 6.73 | 1.4 |
| | | 6.97 | 2.6 |
| | | 7.17 | 3.4 |
| | | 7.41 | 6.5 |
| | | 7.45 | 9.7 |
| | | 7.50 | 8.3 |
| | | 7.67 | 12.8 |
| | | 7.70 | 18.6 |
| $20\text{-}13^1/_3\text{-}66^2/_3$ | 3 | 6.54 | 0.6 |
| | | 6.59 | 0.6 |
| | | 6.96 | 1.6 |
| | | 7.06 | 2.6 |
| | | 7.21 | 2.8 |
| | | 7.21 | 4.1 |
| | | 7.25 | 7.4 |
| | | 7.33 | 5.1 |
| | | 7.37 | 3.8 |
| | | 7.40 | 6.3 |
| 60-40-0 | 6 | 7.53 | 0.4 |
| | | 7.69 | 0.8 |
| | | 7.85 | 1.3 |
| | | 7.99 | 2.1 |
| | | 8.30 | 3.1 |
| | | 8.33 | 4.1 |
| | | 8.56 | 5.5 |
| | | 8.57 | 3.4 |
| | | 8.57 | 5.0 |
| | | 8.57 | 8.4 |
| | | 8.64 | 4.5 |
| | | 8.64 | 5.5 |
| | | 8.68 | 6.4 |
| 7-3-90 | 10 | 5.86 | 0.7 |
| | | 5.89 | 0.7 |
| | | 5.96 | 0.6 |
| | | 6.18 | 2.3 |
| | | 6.38 | 2.2 |
| | | 6.41 | 3.1 |
| | | 6.41 | 3.1 |
| | | 6.52 | 3.2 |
| | | 6.54 | 3.0 |
| | | 6.55 | 3.0 |
| | | 6.60 | 3.6 |
| | | 6.60 | 3.9 |
| | | 6.62 | 3.7 |
| | | 6.68 | 4.0 |
| | | 6.69 | 5.2 |
| | | 6.71 | 5.6 |
| | | 6.75 | 4.3 |
| | | 6.76 | 6.0 |
| | | 6.98 | 8.2 |
| 14-6-80 | 5 | 6.26 | 0.8 |
| | | 6.31 | 0.8 |
| | | 6.41 | 1.5 |
| | | 6.44 | 1.0 |
| | | 6.53 | 2.1 |
| | | 6.65 | 2.3 |
| | | 6.92 | 4.8 |
| | | 7.02 | 4.9 |
| | | 7.11 | 5.9 |
| | | 7.11 | 7.0 |
| | | 7.12 | 7.7 |
| | | 7.19 | 8.0 |
| | | 7.22 | 10.2 |
| $23^1/_3\text{-}10\text{-}66^2/_3$ | 3 | 6.38 | 0.7 |
| | | 6.50 | 1.4 |
| | | 6.52 | 1.6 |
| | | 6.64 | 2.0 |
| | | 6.81 | 2.9 |
| | | 6.84 | 3.4 |
| 16-4-80 | 5 | 5.76 | 0.8 |
| | | 5.78 | 0.9 |
| | | 6.23 | 2.0 |
| | | 6.28 | 2.0 |
| | | 6.52 | 4.1 |
| | | 6.66 | 4.3 |
| | | 6.71 | 5.1 |
| | | 6.74 | 5.4 |

First, the rate of disappearance of methane for the 12–2–86 mixture at 1600°K. is 37 sec.$^{-1}$, while the rate of reaction 1 is 4.1 sec.$^{-1}$. Thus the maximum chain length is about 10; and if any chain initiation occurs by reaction 6, it will be correspondingly shorter. From the intermediate value of the experimental $\Delta H$, we might guess that the rates of (1) and (6) are roughly comparable in this temperature range. For the 12–8–80 runs, which were studied at lower temperatures, the rate of (6) will be substantially higher than that of (1), particularly since the rate of (6) should be proportional to the oxygen concentration.

Second, the lowest temperature experiment in each series gave almost equal amounts of water and ethane as the chief products. This means that the initial stage of the oxidation is

$$4CH_4 + O_2 \longrightarrow 2C_2H_6 + 2H_2O \qquad (7)$$

A simple sequence of reactions will give these products, starting with reaction 6, but it is necessary to assume that $CH_3$ reacts only slowly with $O_2$ to form formaldehyde, since this reaction will lead to CO and $H_2$

$$CH_3 + O_2 \longrightarrow HCHO + OH \qquad (8)$$
$$HCHO \longrightarrow H_2 + CO \qquad (9)$$

Reaction 8 is favorable energetically, but it may be slow because it involves a rather complicated rearrangement of atoms, which would require the $CH_3$ and $O_2$ to stay together as an active complex for a long time.

Third, it is likely that the average chain length (defined as the ratio of the rate of disappearance of methane to the sum of the rates of reactions 1 and 6) increases as the reaction proceeds. This is shown experimentally, for example, by noting that at $10^4/T = 7.60$, 0.26% of the methane in a 12–8–80 mixture is converted in 1.5 milliseconds, 3% in 9.7 milliseconds, while the induction time is only 12 milliseconds. The induction time is not strictly comparable, since it was not measured isothermally; but a calculation which assumes that the rate of reaction increases only because of heat evolution fails to correlate the experiments. The increase in chain length probably involves the oxidation of the intermediate products (ethane, ethylene and acetylene), the radicals involved in these reactions reacting with methane molecules. We plan to study the oxidation and pyrolysis of the $C_2$ hydrocarbons, with the hope of formulating the over-all mechanism leading to induction.

**Induction Times.**—The precise meaning of the induction times will remain unknown until more complete kinetic data on the chain branching reactions are available, so only a few comments will be made here.

From the results of Table IV it is seen that the induction times increased only slightly when argon was added to a given $CH_4$–$O_2$ mixture, the observed increase being due largely to the increased heat capacity of the mixture, which kept the temperature from rising as rapidly as it would without dilution. We could not heat undiluted mixtures hot enough at one atmosphere to measure induction times, but values for one atmosphere were calculated by a short extrapolation of the data with argon dilution, using the average slope of the diluted mixtures. There is a quite noticeable pressure effect on the induction time. Comparison of the 12–8–80 and 6–4–90 mixtures at 5 and 10 atmospheres suggests that the time is inversely proportional to the pressure, while comparison of 60–40 mixtures at 1 and 6 atmospheres suggests a somewhat higher power of pressure dependence.

TABLE V

CONSTANTS IN THE EMPIRICAL INDUCTION TIME EQUATIONS

| Composition $CH_4$:$O_2$:Ar | Pressure, atm. | $-A$ | $B$ | $\Delta H$ (cal./mole) |
|---|---|---|---|---|
| 6-4-90 | 5 | 8.810 | 13,852 | 63,400 |
| 6-4-90 | 10 | 8.203 | 12,578 | 57,600 |
| 12-8-80 | 5 | 7.731 | 11,601 | 53,100 |
| 20-13$^1/_3$-66$^2/_3$ | 3 | 8.123 | 12,045 | 55,100 |
| 60-40 (extrap.) | 1 | 8.236 | 12,080 | 55,300 |
| 60-40 | 6 | 6.785 | 8,720 | 39,900 |
| 7-3-90 | 10 | 5.957 | 9,905 | 45,300 |
| 14-6-80 | 5 | 6.911 | 10,906 | 49,900 |
| 70-30 (extrap.) | 1 | 6.750 | 10,400 | 47,600 |
| 16-4-80 | 5 | 4.833 | 8,329 | 38,100 |
| 80-20 (extrap.) | 1 | 5.050 | 8,330 | 38,100 |

The activation energy of induction is fairly close to 56,000 cal. for the 60–40 type mixtures, but decreases when the oxygen content is reduced. This is so far unexplained, since one would expect the activation energy to increase as the reaction changed from oxidation to pyrolysis.

**Acknowledgment.**—The authors wish to thank Mr. Carl Gerdes, who designed and built the electronic trigger circuit, and Mr. Edward Sokoloski, who assisted in the experiments and calculations.

# ULTRACENTRIFUGAL MOLECULAR WEIGHT AVERAGES DURING THE APPROACH TO EQUILIBRIUM[1,2]

BY DAVID A. YPHANTIS

*Biological and Medical Research Division, Argonne National Laboratory, Lemont, Illinois, and The Rockefeller Institute, New York, New York*

*Received March 16, 1959*

Concentrations at the meniscus $r_1$ of the ultracentrifuge cell may be approximated by $-\ln c/c(0) = a\sqrt{t} + bt$, where $a = 1.1284\ \omega^2 s r_1/\sqrt{D}$ and $b = 0.1366\ \omega^4 s^2 r_1^2/D$. This relation has been verified experimentally using ribonuclease A purified by countercurrent distribution. The concentrations at the base of the cell $r_2$ may be approximated by $\ln c/c(0) = a'\sqrt{t} - bt$, where $a' = 1.1284\omega^2 s r_2/\sqrt{D}$ and $b' = 0.1336\ \omega^4 s^2 r_2^2/D$. These approximations lead to expressions for the average molecular weights given by the Archibald and Trautman approach to equilibrium methods. The molecular weight averages are functions of both molecular weights and sedimentation coefficients. It is recommended that the Archibald molecular weights be extrapolated to zero time as a function of the square root of the time to obtain the weight average molecular weight. The difficulties in obtaining the molecular weight of a lighter component in the presence of heavier components are illustrated.

It is of considerable importance to know the type of molecular weight average given by a method of determining molecular weight. The techniques of determining molecular weight during the approach to equilibrium ultracentrifugation[3–6] are being used widely. However, little is known of the types

(1) Presented at the 135th American Chemical Society national meeting, Boston, Massachusetts, April 1959.

(2) Work performed under the auspices of the U. S. Atomic Energy Commission and supported, in part, by a grant, #A-2493, from the U. S. Public Health Service.

(3) W. J. Archibald, THIS JOURNAL, **51**, 1204 (1947).

(4) S. M. Klainer and G. Kegeles, *ibid.*, **59**, 952 (1955).

(5) A. Ginsburg, P. Appel and H. K. Schachman, *Arch. Biochem. Biophys.*, **65**, 545 (1956).

(6) R. Trautman, THIS JOURNAL, **60**, 1211 (1956).

of averages given by these techniques, except that the initial value given by the Archibald technique is the refractive weight average molecular weight. Some consideration has been given to the problem, but only on the experimental level.[5,7] If one had analytical expressions or approximations for the behavior of the concentration at the meniscus and base of the ultracentrifuge cells, one should then be able to specify the types of averages.

In calculating transient distributions in the ultracentrifuge, one usually assumes that the kinetic behavior of the solutes can be described by constant sedimentation and diffusion coefficients. This is assumed here also. Since molecular weights are only infrequently calculated for the base of the cell, the meniscus will be the primary consideration here.

**Concentrations at the Meniscus: Theoretical.**— The computation of exact solute distributions in the sector cell with a radially increasing field is difficult. If one assumes the cell to be rectangular and in a uniform field, one can use modifications of the solution, obtained by Mason and Weaver,[8] for the settling of spherical particles under gravity in a finite, bounded cell. This approximation has been shown applicable to approach to equilibrium runs where no distinct boundary is formed.[9] The solution of Mason and Weaver[8] for the sedimentation in a semi-infinite rectangular cell, bounded at the meniscus and in a uniform field should also be a good approximation to the behavior in the ultracentrifuge, provided the plateau region still exists. After introducing the sedimentation and diffusion coefficient $s$ and $D$, their solution for this case gives the concentration $c$ at any time $t$ as

$$\frac{c(x,t)}{c(0)} = -\frac{\omega^2 s r_1 \sqrt{t}}{\sqrt{\pi D}} \exp[-(\omega^2 s r_1 t - x)^2/4Dt] + \frac{1}{2}\left[1 - \Phi\left(\frac{\omega^2 s r_1 t - x}{\sqrt{4Dt}}\right) + \frac{1}{2}\exp(\omega^2 s r_1 x/D)[1 + \frac{\omega^2 s r_1}{D}(\omega^2 s r_1 t + x)]\left[1 - \Phi\left(\frac{\omega^2 s r_1 t + x}{\sqrt{4Dt}}\right)\right]\right] \quad (1)$$

Here $c(0)$ is the original concentration, $\omega$ is the angular velocity, $r_1$ is the meniscus radius, $x = r - r_1$ is the distance from the meniscus and $\Phi(z)$ is the probability integral. In obtaining eq. 1 the centrifugal field has taken as that at the meniscus, $\omega^2 r_1$. Setting $\lambda = {}^1/_2\omega^2 s r_1 \sqrt{t/D}$, then for $x = 0$, *i.e.*, at the meniscus, the concentration is given by

$$c/c(0) = [1 + 2\lambda^2][1 - \Phi(\lambda)] + \frac{1}{2}\Phi''(\lambda) \quad (2)$$

where $\Phi''(\lambda) = \partial^2\Phi(\lambda)/\partial\lambda^2$ is the second derivative of the probability integral.

An IBM 650 computer [10] was used to obtain values of $c/c$ (0) for various $\omega^2 s/D$ and $\tau = 2\omega^2 s t$ and for various positions in the cell from the rectangular approximation for the complete cell.[9,11] Comparison of the values found for the meniscus for this bounded cell case with eq. 2 for the semi-infinite cell, showed them to be identical for considerable periods of time even after the plateau was lost. Since loss of the plateau showed only a rather delayed effect on meniscus concentrations, it is valid to compare the available exact solutions of the Lamm equation for the ultracentrifuge,[12] in which the plateau is at most only indicated, with the values given by eq. 2. Figure 1 shows concentrations at the meniscus as a function of $\lambda$. The curve is from eq. 2 and the points are the differential analyzer values. It can be seen that the maximum difference is about 0.02 in $c/c(0)$.

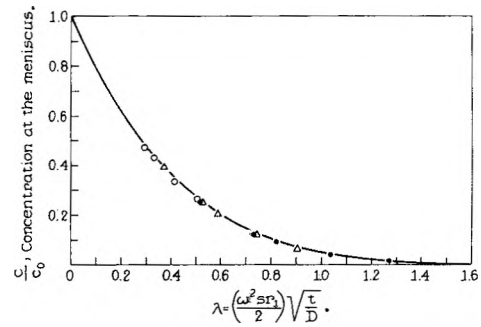


Fig. 1.—Meniscus concentration as a function of $\lambda$. The curve is that given by eq. 2 for a semi-infinite rectangular cell in a uniform field and the points are differential analyzer solutions of the Lamm equation for $\omega^2 s/D = 0.467$ (○), $\omega^2 s/D = 0.933$ (△), and $\omega^2 s/D = 1.399$ (●).

Fujita and MacCosham[13] have recently developed an approximation for the initial stage of ultracentrifugation that is similar to eq. 1. The concentration at the meniscus given by their approximation is

$$c/c(0) = e^{-\tau}\left\{[1 + 2\lambda^2][1 - \Phi(\lambda)] + \frac{1}{2}\Phi''(\lambda)\right\} \quad (3)$$

This differs from eq. 2 only by a factor $e^{-\tau}$. Values of $\omega^2 s/D$ and $\lambda$ determine values of $\tau$; thus eq. 2 and 3 may be compared for different $\omega^2 s/D$. In Table I columns 1, 2, 3 and 4 present values of the meniscus concentration for $\omega^2 s/D = 0.1$, 0.5, 1.5 and 5.0 calculated from eq. 3 for various values of $\lambda$. Column 5 gives the values calculated from eq. 2. It can be seen that eq. 2 and 3 are in agreement except under conditions where, in practical cases, almost complete equilibrium would be approached. Thus, eq. 2 is a reasonable approximation for the meniscus concentration.

More tractable forms of eq. 2 can be obtained. The expansion of ln $c/c$ (0) yields, neglecting terms in $\lambda^3$ and higher powers

$$-\ln c/c(0) = 4\lambda/\pi^{1/2} + (8/\tau - 2)\lambda^2 = 2.2568\lambda + 0.5465\lambda^2 \quad (4)$$

If only the first term of eq. 4 is retained, the concentration at the meniscus is approximated by

$$c/c(0) = \exp(-4\lambda/\pi^{1/2}) = \exp(-2.2568\lambda) \quad (5)$$

Colum 6 of Table I gives the values calculated from this single term approximation and column 7, the values from eq. 4, the two term approximation. It can be seen that the single term approximation is valid for the initial stages of centrifugation,

(7) S. Erlander and J. F. Foster, Abstracts 133rd Meeting Am. Chem. Soc., San Francisco, 46C (1958). Also *J. Polymer Sci.*, **37**, 103 (1959).

(8) M. Mason and W. Weaver, *Phys. Rev.*, **23**, 412 (1924).

(9) D. A. Yphantis and D. F. Waugh, THIS JOURNAL, **60**, 623 (1956).

(10) The author would like to express his appreciation to Miss Joan Gurian for the programming and carrying out of these computations.

(11) Equation 8a of reference 9 contains a misprint: the term $e^{1/2\alpha}$ should be $e^{-1/2\alpha}$.

(12) D. F. Waugh and D. A. Yphantis, THIS JOURNAL, **57**, 312 (1953).

(13) H. Fujita and V. J. MacCosham, *J. Chem. Phys.*, **30**, 291 (1959).

TABLE I

COMPARISON OF MENISCUS CONCENTRATIONS, $c/c(0)$ GIVEN BY THE VARIOUS APPROXIMATIONS

| | Sectoral cell, varying field. Eq. 3 with $r_1$ = 6.067 cm. and with | | | | Rectangular cell, uniform field | | |
|---|---|---|---|---|---|---|---|
| $\lambda$ | $\frac{\omega^2 s}{D} = 0.1$ | $\frac{\omega^2 s}{D} = 0.5$ | $\frac{\omega^2 s}{D} = 1.5$ | $\frac{\omega^2 s}{D} = 5.0$ | Complete approx. eq. 2 | Single term approx. eq. 5 | Two term approx. eq. 4 |
| 0.05 | 0.888 | 0.891 | 0.892 | 0.892 | 0.892 | 0.893 | 0.892 |
| .1 | 0.777[a] | .790 | .792 | .794 | .794 | .798 | .794 |
| .2 | 0.670 | .612 | .619 | .622 | .623 | .637 | .623 |
| .3 | | .465 | .477 | .481 | .483 | .508 | .484 |
| .4 | | .345 | .361 | .367 | .370 | .406 | .372 |
| .6 | | .179[b] | .198 | .206 | .209 | .258 | .212 |
| .8 | | 0.085 | .102 | .109 | .112 | .164 | .116 |
| 1.0 | | | .049 | .054 | .057 | .104 | .061 |
| 1.4 | | | .009 | .011 | .012 | .042 | .015 |

[a] Equilibrium concentration at meniscus for $r_2 - r_1 = 1$ cm. is $c/c(0) = 0.707$. [b] Equilibrium concentration at meniscus for $r_2 - r_1 = 1$ cm. is $c/c(0) = 0.128$.

$c/c\ (0) > 0.5$–$0.6$, while the two term approximation differs at most by only 0.004 in $c/c(0)$ from eq. 2 and is a simple approximation to the ultracentrifuge behavior, provided one is not too close to equilibrium.

**Concentrations at the Meniscus: Experimental.**—Equation 4 has been verified experimentally, using bovine ribonuclease A isolated by countercurrent distribution[14] from Armour crystalline ribonuclease, lot No. 381-059, and generously supplied by Dr. T. P. King. This ribonuclease A was over 99% pure, as determined by column chromatography, countercurrent distribution, amino acid composition and nitrogen content. The meniscus experiments were performed with an 0.5% solution, exhaustively dialyzed against a $p$H 7.7[5] buffer containing 0.1 $M$ NaCl, 0.035 $M$ $K_2HPO_4$ and 0.004 $M$ $KH_2PO_4$. The Spinco model E ultracentrifuge used was equipped with an automatic temperature control and with Rayleigh interference optics for simplicity in determining meniscus concentrations. Care was taken so that the light source was on axis and in the focal plane of the collimating lens. The contrast mask was centered so that there was only a single meniscus image. One could then measure the Rayleigh fringes to within 0.15 mm. of the center of the meniscus image on the plates. Spectroscopic plates with emulsion type II-G were used for increased sensitivity over the usual metallographic plates with very little loss of resolving power. "Fluorochemical FC-43"[15] was used as a base fluid. It has the advantage of being volatile as well as dense and inert.

The sedimentation coefficient of ribonuclease A was measured in a standard synthetic boundary cell at 59,780 r.p.m. using the schlieren optics. One run was made on the same solution used in the meniscus experiments and another on an undialyzed solution of same concentration in the same buffer; the values found were $1.775 \pm 0.015 \times 10^{-13}$ sec. and $1.785 \pm 0.015 \times 10^{-13}$ sec., respectively. Several synthetic boundary runs on Armour ribonuclease, lot No. 381-059, under similar conditions gave values of $1.83 \pm 0.02 \times 10^{-13}$ sec. The difference is possibly due to aggregated material in the commercial sample.

(14) T. P. King and L. C. Craig, *J. Am. Chem. Soc.*, **80**, 3366 (1958).

(15) Perfluorotributylamine supplied through the courtesy of Minnesota Mining and Manufacturing Co., Saint Paul 6, Minnesota.

Initial concentration was determined, in terms of Rayleigh fringes, using a double sector Kegeles type[16] synthetic boundary cell at low speed. The decrease with time in the number of these fringes at 12,590 r.p.m. agreed very closely with that predicted from the sedimentation coefficient, showing the absence of aggregated material in the preparation. With Armour ribonuclease, lot No. 381-059, that had not been purified by countercurrent distribution, the number of fringes decreased much more rapidly than predicted from the sedimentation coefficient, showing the presence of what is presumed to be aggregated material.

Two meniscus concentration runs were performed, one at 23,150 r.p.m. and one at 12,590 r.p.m. with the menisci in the solution and solvent sectors accurately aligned. Concentration differences, in terms of Rayleigh fringes, were measured between the plateau region and the center of the meniscus images. Plateau concentrations were obtained from

$$c_{\text{plateau}} = c(0) \exp(-2\omega^2 s t) \qquad (6)$$

using the initial concentration and the sedimentation coefficients for the experimental conditions. The lowest plateau concentration was calculated to be 2.5% less than the original concentration. Concentrations at the menisci were taken as the plateau concentrations less the meniscus-plateau differences. A zero time correction for the sedimentation occurring during acceleration was estimated as

$$\Delta t = \int_{\omega=0}^{\omega=\omega_0} (\omega/\omega_0)^4 \, dt \qquad (7)$$

where $\omega_0$ is the angular velocity at operating speed. This correction amounted to 45 sec. in the run at 23,150 r.p.m. and to 23 sec. in the run at 12,590 r.p.m.

In order to consolidate the experimental results, the Svedberg relation was introduced into eq. 4 along with a normalizing factor to give

$$-\ln c/c(0) = 2.2568[s_{20,w} M(1 - \bar{V}\rho_{20,w})]^{1/2}\gamma t^{1/2} + 0.5465[s_{20,w} M(1 - \bar{V}\rho_{20,w})]\gamma^2 t \qquad (8)$$

Variations of angular velocity, meniscus radius, temperature and solvent properties were taken into account by the normalizing factor

(16) G. Kegeles, *J. Am. Chem. Soc.*, **74**, 5532 (1952).

$$\gamma = \frac{\omega^2 r_1}{2(RT)^{1/2}} \frac{(1 - \bar{V}\rho)}{(1 - \bar{V}\rho_{20,w})} \left(\frac{\eta_{20,w}}{\eta}\right)^{1/2} \quad (9)$$

The density and viscosity of the solvent at the temperatures of the experiments are $\rho$ and $\eta$, the corresponding quantities for water at 20° are $\rho_{20,w}$ and $\eta_{20,w}$, $S_{20,w}$ is the sedimentation coefficient reduced to water at 20°, $\bar{V}$ is the partial specific volume (assumed constant), $R$ is the gas constant and $T$ is the absolute temperature.

Equation 8 suggests that a plot of $-\ln c/c(0)/\gamma t^{1/2}$ *versus* $\gamma t^{1/2}$ should be linear and that the slope and intercept should give the molecular weight. A least squares treatment of the data, weighing each point inversely to its estimated error, and covering the ranges $1 \geq c/c(0) \geq 0.81$ at 12,590 r.p.m. and $1 \geq c/c(0) \geq 0.47$ at 23,150 r.p.m. gave values for the intercept and slope. These were then combined with values of 0.695 cm.$^3$ g.$^{-1}$ for $\bar{V}$[17,18] and $1.78 \times 10^{-13}$ sec. for $S_{20,w}$ to calculate molecular weights of 12,800 ± 500 from the intercept and 15,100 ± 1,500 from the slope of the least squares line. These values are to be compared with the molecular weights of 13,683 from the amino acid composition[19] and 13,500–13,800 found by equilibrium ultracentrifugation in ultrashort columns[20] for the same sample of ribonuclease and in the same buffer.

**Molecular Weight Averages Given by the Archibald Method.**—In the Archibald techique[3-5] the molecular weight is determined from the relation

$$M^* = \beta \frac{\partial c}{\partial r}/rc \quad (10)$$

where $\beta = RT/\omega^2$, and $M^*$ is the reduced molecular weight $M(1 - \bar{V}\rho)$, and where $\partial c/\partial r$, $r$ and $c$ are evaluated at the meniscus. The average reduced molecular weight $\bar{M}^*$ is given by

$$\bar{M}^* = \beta \frac{\overline{\partial c}}{\partial r}/\bar{c} \quad (11)$$

where

$$\bar{c} = \sum_i c_i(t) \quad (11a)$$

and

$$\frac{\overline{\partial c}}{\partial r} = \sum_i \frac{\partial c_i(t)}{\partial r} \quad (11b)$$

From eq. 4 and the Svedberg relation, it is seen that

$$c_i(t) = c_i(0) \exp\left[-k_1(M_i^* s_i t)^{1/2} - k_2(M_i^* s_i t)\right] \quad (12)$$

where $k_1 = 2.2568\ \omega^2 r_1/(4RT)^{1/2}$, $k_2 = 0.5465\ \omega^4 r^2/4RT$, and where the $c_i(0)$ are the initial concentrations of the various components. Substituting eq. 11a, 11b and 12 in eq. 11 we have

$$\bar{M}^* = \frac{\sum_i M_i^* c_i(0) \exp\left[-k_1(M_i^* s_i t)^{1/2} - k_2(M_i^* s_i t)\right]}{\sum_i c_i(0) \exp\left[-k_1(M_i^* s_i t)^{1/2} - k_2(M_i^* s_i t)\right]} \quad (13)$$

as the molecular weight average given by the Archibald method. Substitution of the simpler eq. 5, valid for $c/c(0) > \sim 0.5$, gives

$$\bar{M}^* = \frac{\sum_i M_i^* c_i(0) \exp\left[-k_1(M_i^* s_i t)^{1/2}\right]}{\sum_i c_i(0) \exp\left[-k_1(M_i^* s_i t)^{1/2}\right]} \quad (13a)$$

Equations 13 show that the Archibald molecular weight average involves the sedimentation coefficients, except at $t = 0$ when it reduces to the weight average molecular weight.

**Molecular Weight Averages Given by the Trautman Method.**—In the Trautman method[6] the molecular weight is given by

$$M^* = \frac{\beta}{r} \left\{ \frac{\frac{\partial c}{\partial r}(t_2) - \frac{\partial c}{\partial r}(t_1)}{c(t_2) - c(t_1)} \right\} \quad (14)$$

where the terms involving $c$, $r$ and $\partial c/\partial r$ are again evaluated at the meniscus. The average reduced molecular weight at any time $t$ is

$$\bar{M}^* = \frac{\beta}{r} \frac{\sum_i \frac{\partial^2 c_i(t)}{\partial r \partial t}}{\sum_i \frac{\partial c_i(t)}{\partial t}} = \frac{\sum_i M_i^* \frac{\partial c_i(t)}{\partial t}}{\sum_i \frac{\partial c_i(t)}{\partial t}} \quad (15)$$

Differentiating eq. 12 with respect to $t$ and substituting the result in eq. 15, it is seen that

$$\bar{M}^* = \frac{\sum_i M_i^{*3/2} s_i^{1/2} c_i(0) \exp\left[-k_1(M_i^* s_i t)^{1/2} - k_2(M_i^* s_i t)\right] \left[1 + \frac{2k_2}{k_1}(M_i^* s_i t)^{1/2}\right]}{\sum_i M_i^{*1/2} s_i^{1/2} c_i(0) \exp\left[-k_1(M_i^* s_i t)^{1/2} - k_2(M_i^* s_i t)\right] \left[1 + \frac{2k_2}{k_1}(M_i^* s_i t)^{1/2}\right]} \quad (16)$$

Using the simpler eq. 5, the Trautman average molecular weight is approximated by

$$\bar{M}^* = \frac{\sum_i M_i^{*3/2} s_i^{1/2} c_i(0) \exp\left[-k_1(M_i^* s_i t)^{1/2}\right]}{\sum_i M_i^{*1/2} s_i^{1/2} c_i(0) \exp\left[-k_1(M_i^* s_i t)^{1/2}\right]} \quad (16a)$$

The initial Trautman average molecular weight at $t = 0$ is

$$\bar{M}^* = \frac{\sum_i c_i(0)\ M_i^{*3/2} s_i^{1/2}}{\sum_i c_i(0)\ M_i^{*1/2} s_i^{1/2}} \quad (17)$$

If now $s_i$ is assumed proportional to $M_i^{*2/3}$, as would be the case for solutes having the same frictional ratio, $f/f_0$, then eq. 17 becomes

$$\bar{M}^* = \frac{\sum_i c_i(0)\ M_i^{*11/6}}{\sum_i c_i(0)\ M_i^{*5/6}} \quad (18)$$

which is practically the $Z$ average

$$\bar{M}_z = \frac{\sum_i c_i M_i^2}{\sum c_i M_i} \quad (19)$$

(17) W. F. Harrington and J. A. Schellman, *Compt. rend. trav. Lab. Carlsberg, Ser. Chim.*, **30**, 21 (1956).

(18) K. E. Van Holde and R. L. Baldwin, THIS JOURNAL, **62**, 734 (1958).

(19) C. H. W. Hirs, W. H. Stein and S. Moore, *J. Biol. Chem.*, **221**, 151 (1956).

(20) By a technique similar to method III of Van Holde and Baldwin.[18]

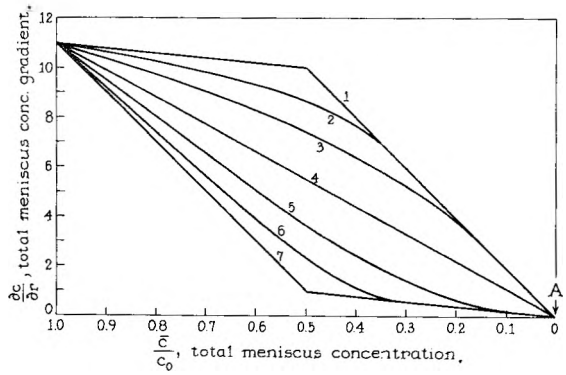


Fig. 2.—Trautman plots for $M_2^* = 10M_1^*$: curve 1, $s_1 \rangle\rangle\rangle s_2$; curve 2, $s_1 = 10^3 s_2$; curve 3, $s_1 = 10^2 s_2$; curve 4, $s_1 = 10 s_2$; curve 5, $s_1 = s_2$; curve 6, $s_1 = s_2/10$; and curve 7, $s_1 \langle\langle\langle s_2$.

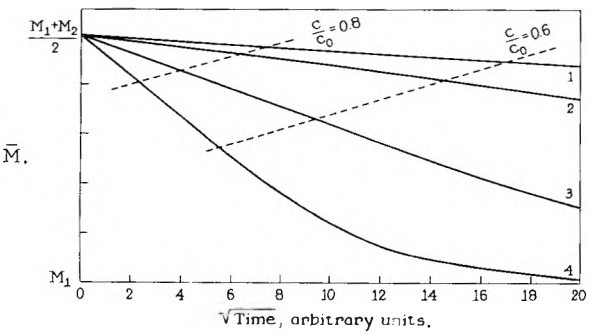


Fig. 3.—Archibald average molecular weight as a function of the square root of time: curve 1, $M_2^* s_2 = 2.25 M_1^* s_1$; curve 2, $M_2^* s_2 = 4M_1^* s_1$; curve 3, $M_2^* s_2 = 16M_1^* s_1$; curve 4, $M_2^* s_2 = 64M_1^* s_1$.

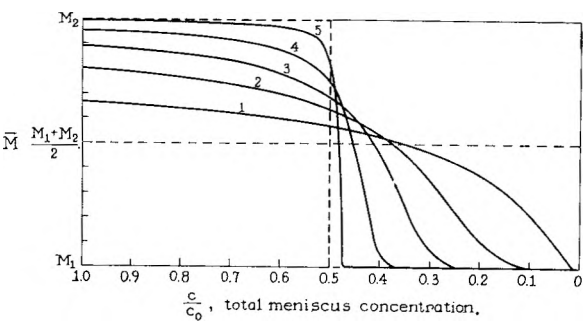


Fig. 4.—Trautman average molecular weight as a function of the total meniscus concentration: curve 1, $M_2^* s_2 = 4M_1^* s_1$; curve 2, $M_2^* s_2 = 16M_1^* s_1$; curve 3, $M_2^* s_2 = 64 M_1^* s_1$; curve 4, $M_2^* s_2 = 400M_1^* s_1$; curve 5, $M_2^* s_2 = 10^4 M_1^* s_1$.

The $Z$ average would be obtained exactly if $s$ were proportional to $M^*$. Equations 16 show that the average molecular weight from the Trautman method is more strongly dependent on the sedimentation coefficient than is the average molecular weight from the Archibald method.

**Molecular Weight Averages at the Base of the Cell.**—A slight modification of Mason and Weaver's derivation yields a solution corresponding to eq. 1 for a semi-infinite rectangular cell bounded at the base and in a uniform field. The concentration at the base of the cell, at $r_2$, is then given by

$$[c/c(0)]_{\text{base}} = [1 + 2(\lambda')^2][1 + \Phi(\lambda')] - \frac{1}{2}\Phi''(\lambda') \quad (20)$$

where

$$\lambda' = \frac{1}{2}\omega^2 s r_2 \sqrt{t/D}$$

The values given by eq. 20 are identical with the IBM computation for the base of a finite, bounded rectangular cell for considerable times after loss of the plateau. The expansion of $\ln c/c(0)$ for the base yields

$$\ln[c/c(0)]_{\text{base}} = 4\lambda'/\pi^{1/2} - (8/\pi - 2)\lambda'^2 = 2.2568\lambda' - 0.5465\lambda'^2 \quad (21)$$

This approximation is valid to 0.05 in $c/c(0)$ for $\lambda' = 0.6$, ($c/c(0) = 3.23$), and is better for lower values of $\lambda'$; thus it encompasses almost every practical case. Using eq. 21 it can be shown that the Archibald and Trautman average molecular weights at the base of the cell are given by eq. 13 and 16 with $r_2$ replacing $r_1$ and with the sign of the coefficient $k_1$ altered wherever $k_1$ appears.

## Discussion

The dependence of the various molecular weight averages on the sedimentation coefficients of the components is illustrated in Fig. 2 where the total concentration gradient at the meniscus is plotted against the total concentration. This is the plot suggested by Trautman.[6] The Archibald method gives a molecular weight proportional to the slope of a straight line from point A (on Fig. 2) where the total concentration is zero to some point on the curves, while the Trautman method gives an average proportional to the tangent to the curves at any point. The curves presented were calculated through eq. 2; they are for a series of theoretical two component systems in which the molecular weight of component (2) is ten times that of component (1). Weight concentrations of the two components were taken as initially equal. The different curves were obtained for different ratios of sedimentation coefficients.

Curve 1 is given when the sedimentation coefficient of the smaller molecular weight solute, $s_1$, is infinitely larger than $s_2$, the sedimentation coefficient of the larger molecular weight solute; this would correspond to all of the smaller components sedimenting completely before any sedimentation of the larger component (1), a rather fictitious case. For curve 7, on the other hand, $s_2$ is infinitely larger than $s_1$ and all of the heavier component has sedimented away from the meniscus before any sedimentation of the smaller component (2). For curve 2, $s_1 = 10^3 s_2$; curve 3, $s_1 = 10 s_2^2$; curve 4, $s_1 = 10 s_2$; curve 5, $s_1 = s_2$; and curve 6, $s_1 = s_2/10$. Most cases encountered in practice for this system would lie between curves 5 and 6. It can be seen that the result of both the Archibald and Trautman methods depend on the sedimentation coefficients. The Trautman plot does not give an absolute indication of dispersity. For example, a system in which all the ($M_i s_i$) are equal will give a straight line for this plot over the complete range, a behavior corresponding to a single component. If the sedimentation coefficients are sufficiently different one can, of course, observe the dispersity of this system at other points in the cell than the meniscus and base. Conversely, a curved Trautman plot would be given by a non-ideal single component system in which $s/D$, the apparent reduced

molecular weight, was a function of concentration or time.

It is instructive to examine the time dependence of the molecular weight averages. Archibald average molecular weights were calculated for two component systems with initially equal weight concentrations and for different ratios of $(M_1s_1):(M_2s_2)$. Values for the initial period are presented in Fig. 3 as a function of the square root of the time. The dashed lines indicate the times at which the total meniscus concentrations are $0.8c(0)$ and $0.6c(0)$. It can be seen that the extrapolation to zero time is almost linear over a considerable range. On the other hand, if the Archibald average molecular weights are plotted as a function of time, there is considerable curvature at low times and extrapolation to the true zero time average may be difficult. The graph of the Archibald average molecular weight as a function of the total meniscus concentration, gives a reliable extrapolation to zero time, although it is not as linear as that of Fig. 3. It is recommended that extrapolation to zero time to obtain the weight average molecular weight be made as a function of the square root of the time.

Similar calculations have been made for the Trautman average molecular weight of the same set of systems. Figure 4 shows these averages as a function of the total meniscus concentrations for various ratios of $(M_1s_1):(M_2s_2)$. The dashed curves indicate the two extremes of equal values of $Ms$, and of $M_2s_2$ infinitely greater than $M_1s_1$. This figure illustrates the difficulty in obtaining the molecular weight of the slow component. If $M_2s_2 = 4M_1s_1$ there is only a rather limited range, $0.015 \geq c/c(0) > 0$, where the smaller component is free of the larger component at the meniscus. If $M_2s_2 = 16M_1s_1$ this range is $0.11 \geq c/c(0) > 0$. These ranges are not influenced by angular velocity, nor by any other factor that does not change the ratio of $M_2s_2$ to $M_1s_1$.

A number of "short-cuts" in the calculation of approach to equilibrium runs are evident from the functional dependence of the meniscus concentration on the square root of the time. For example, in the determination of the Archibald molecular weight of a monodisperse system, the meniscus or base concentrations need not be calculated; one can simply extrapolate the logarithm of the concentration gradient at the meniscus or base of the cell as a function of the square root of the time to zero time where the initial concentration can be used directly in the Archibald equation. In multicomponent systems, where the total initial meniscus and base concentrations and gradients are linear functions of the square root of the time, one can extrapolate the total concentration gradients themselves to zero time; in this case, however, the linear range is limited.

Observations of approach to equilibrium systems are usually performed with the schlieren and occasionally with the interference optics, both of which depend on the refractive index increments of the solutes. The concentrations to be used in evaluating molecular weight averages should therefore be in terms of refractive index, rather than in weight units. In almost every practical case, however, the refractive index increments of the various components are essentially identical and this distinction may then be neglected.

# THE VARIATION OF LATTICE PARAMETER WITH CARBON CONTENT OF NIOBIUM CARBIDE[1]

BY E. K. STORMS AND N. H. KRIKORIAN

*Contribution from the University of California, Los Alamos Scientific Laboratory, Los Alamos, New Mexico*

*Received March 21, 1959*

A lattice constant of $a_0 = 4.4702 \pm 0.0001$ Å. has been determined for $NbC_{0.994 \pm 0.002}$ at 25°. The equation $a_0 = 4.4704 - 0.0239\,(1 - C/Nb) - 0.3586\,(1 - C/Nb)^2$ has been calculated relating composition to lattice parameter of NbC. Solution of this equation for $NbC_{1.000}$ gives a lattice-parameter of $4.4704 \pm 0.0005$ Å.

## Introduction

NbC forms a face centered cubic crystal lattice for which the lattice constant, $a_0$ decreases as the crystal becomes deficient in carbon. An exact knowledge of the relationship between $a_0$ and the NbC composition provides not only an analytical tool but, by extrapolation, gives an $a_0$ value for the tenuous composition $NbC_{1.000}$. Brauer, Renner and Wernet[2], and Umansky[3] have measured values for the lattice constants while studying phase changes in the system Nb–C. However, there is a lack of agreement between them. Lattice parameters for NbC have also been reported by Becker and Ebert[4]; Kovalskii and Umansky[5]; Norton and Mowry,[6] and Duwez and Odell.[7] The lack of complete analytical data on the material measured leaves most of the reported values in question.

## Experimental

Fansteel high-purity niobium powder and AUC graphite powder, outgassed at 2000°, were used as starting materials. After a thorough mixing, the materials were cold pressed without binder at 100,000 to 200,000 p.s.i. into a plug $^3/_8$" in diameter and $^3/_4$" long. A 0.040 by 0.4 inch hole was

(1) This work done under the auspices of the Atomic Energy Commission.

(2) G. Brauer, H. Renner and J. Wernet, *Z. anorg. allgem. Chem.*, **277**, 249 (1954).

(3) Ya. S. Umansky, *J. Phys. Chem. USSR*, **14**, 332 (1940).

(4) K. Becker and F. Ebert, *Z. Physik*, **31**, 268 (1925).

(5) A. E. Kovalskii and Ya. S. Umansky, *J. Phys. Chem. USSR*, **20**, 769 (1946).

(6) J. T. Norton and A. L. Mowry, *Trans. Am. Inst. Mining Met. Eng'rs.*, **185**, 133 (1949).

(7) P. Duwez and F. Odell, *J. Electrochem. Soc.*, **97**, 299 (1950).

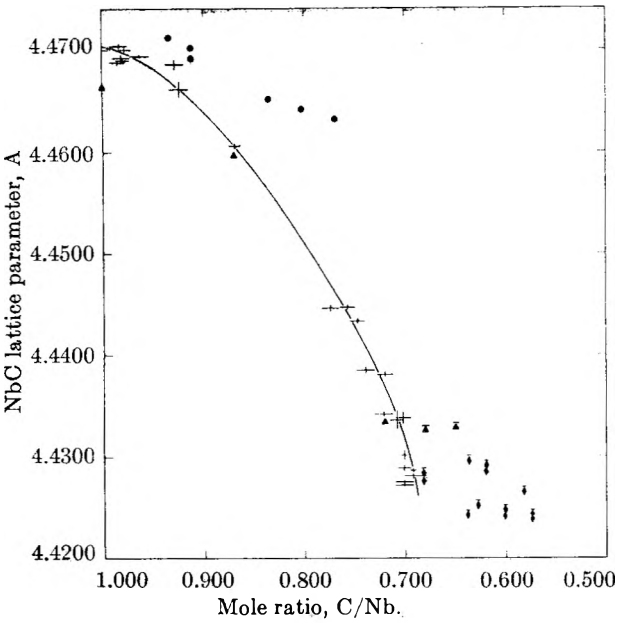


Fig. 1.—Variation of NbC lattice parameter with composition: + (one phase) and ◆ (two phase), this work; ▲ (one phase) and ▲ (two phase), Brauer; ●, Umansky.

drilled in the top to provide for blackbody temperature measurement. During induction heating a small tantalum rod was used to support the sample within an eddy current concentrator. In this way, contact with foreign materials was kept to a minimum. The heatings were started after the system had been evacuated to approximately $10^{-3}$ mm. and continued at a pressure of about $10^{-5}$ mm. during the bulk of the heating. Heatings were made for sufficient time to ensure complete reaction. For example, at 3000° only one-half hour was needed, but at 1800° the temperature had to be maintained for at least 38 hours. After heating the sample was pulverized. An X-ray powder pattern was taken and the remainder was analyzed separately for niobium (by ignition to $Nb_2O_5$), total carbon (by weighing the $CO_2$ evolved during ignition) and free carbon (by dissolution of the NbC in acid).

The stock niobium powder was analyzed both chemically and spectroscopically. Chemical analysis showed the powder to be 99.24% niobium. The spectroscopic data of the niobium is listed in Table I, along with the spectroscopic data for $NbC_{0.994}$. The graphite was analyzed and found to be 99.4% carbon.

Two of the niobium carbide samples were analyzed for nitrogen and gave values of 205 and 240 p.p.m. The absence of major impurities and the fact that in all cases the sums of the analyses of niobium and total carbon were within 0.2% of 100% and many times within 0.05% gives assurance as to the high purity of the resulting NbC.

The error in the analytical values was estimated to be less than 1%. Repeated analysis allowed a statistical error to be assigned to the composition value of the following samples: $NbC_{0.994\pm0.002}$; $NbC_{0.977\pm0.003}$; and $NbC_{0.983\pm0.003}$.

The X-ray patterns were made in a 114.6 mm. Debye–Scherrer camera using copper radiation with a nickel filter. The $a_0$ values were obtained from the back-reflection lines by applying the least-squares extrapolation of Cohen[8] as modified by Hess[9] using an IBM 704. A standard deviation was calculated from each film. In addition, the complete procedure, from mounting the sample to reading the film, was repeated on the same material six times. Deviation from the mean of these values gave another measure of the random error. From these two methods an average standard deviation of ±0.0003 Å. was estimated for samples above composition $NbC_{0.90}$. Samples of lower carbon content produced sufficiently diffused X-ray patterns in the back-reflection region that the uncertainty was increased to an average value of ±0.001 Å. The standard deviation in the individual points are noted in Fig. 1.

(8) M. U. Cohen, *Rev. Sci. Instr.*, **6**, 68 (1935); **7**, 1955 (1950); *Z. Krystallogr.*, **94A**, 288 (1936); **94A**, 306 (1936).

(9) J. B. Hess, *Acta Cryst.*, **4**, 209 (1951).

## Results

The experimental data are summarized in Fig. 1 as a plot of lattice parameter, $a_0$ at 25 ± 2° *vs.* the mole ratio, C/Nb, of combined carbon in the total sample. The data are also listed in Table II. The following equation was computed by an IBM 704 to be a least-square fit to the single phase points. The curve in Fig. 1 is based on the equation

$$a_0 = 4.4704 - 0.0239(1 - X) - 0.3586(1 - X)^2$$

A solution of this equation for the $a_0$ value of composition $NbC_{1.000}$ gives 4.4704 ± 0.0005 Å. It should be emphasized that confidence in this value is limited mainly by the uncertainty in the analyses.

TABLE I

SPECTROSCOPIC DATA

Spectroscopic analysis of niobium metal and $NbC_{0.994}$. Values are based on sample after conversion to $Nb_2O_5$ and reported in parts per million.

| Element | Nb | NbC | Element | Nb | NbC |
|---|---|---|---|---|---|
| Li | <3 | <3 | Co | <10 | <10 |
| Be | <1 | 1 | Ni | 10 | <10 |
| B | <1 | 1 | Cu | 10 | 10 |
| Na | <3 | <3 | Zn | <300 | <300 |
| Mg | 1 | 1 | Sr | <30 | <30 |
| Al | <10 | 10 | Zr | <300 | <300 |
| Si | <10 | 20 | Mo | <100 | <100 |
| K | <30 | <30 | Ag | <1 | <1 |
| Ca | 10 | 5 | Sn | <50 | <50 |
| Ti | <50 | 10 | Ba | <10 | 10 |
| V | <50 | 50 | Ta | <500 | 500 |
| Cr | <10 | 10 | W | <1000 | <1000 |
| Mn | 3 | 3 | Pb | <30 | |
| Fe | 100 | 10 | Bi | <50 | |

TABLE II

SUMMARY OF THE DATA

| One phase points | | | Two phase points | | |
|---|---|---|---|---|---|
| Composition | Error | $a_0$ | Error | Composition | $a_0$ |
| 0.692 | 0.010 | 4.4281 | 0.0001 | 0.574 | 4.4244 |
| .692 | .005 | 4.4287 | .0020 | .574 | 4.4238 |
| .701 | .010 | 4.4272 | .0001 | .582 | 4.4265 |
| .701 | .010 | 4.4275 | .0004 | .601 | 4.4241 |
| .701 | .005 | 4.4289 | .0003 | .601 | 4.4247 |
| .701 | .005 | 4.4301 | .0005 | .619 | 4.4292 |
| .702 | .010 | 4.4338 | .0005 | .620 | 4.4285 |
| .708 | .005 | 4.4336 | .0009 | .628 | 4.4252 |
| .720 | .008 | 4.4381 | .0003 | .638 | 4.4242 |
| .721 | .010 | 4.4342 | .0003 | .637 | 4.4295 |
| .739 | .010 | 4.4385 | .0003 | .682 | 4.4284 |
| .747 | .010 | 4.4433 | .0002 | .682 | 4.4276 |
| .757 | .010 | 4.4447 | .0002 | | |
| .774 | .010 | 4.4446 | .0004 | | |
| .869 | .005 | 4.4605 | .0003 | | |
| .924 | .010 | 4.4661 | .0004 | | |
| .929 | .010 | 4.4686 | .0004 | | |
| .963 | .010 | 4.4694 | .0001 | | |
| .977 | .003 | 4.4700 | .0002 | | |
| .980 | .010 | 4.4690 | .0002 | | |
| .981 | .010 | 4.4692 | .0003 | | |
| .983 | .003 | 4.4704 | .0003 | | |
| .985 | .010 | 4.4688 | .0003 | | |
| .992 | .010 | 4.4702 | .0002 | | |
| .994 | .002 | 4.4702 | .0001 | | |

This value gives an X-ray density of 7.80 g./cm.$^3$. The closest experimental approach to this composition was $NbC_{0.994 \pm 0.002}$ with $a_0 = 4.4702 \pm 0.0001$ Å.

## Discussion

The values reported by Umansky (closed circles), and the values of Brauer, *et al.* (triangles), are shown in Fig. 1 for comparison. It is interesting to observe that the values of Brauer agree with the present work except for his composition $NbC_{1.00}$. This composition is no doubt in error because of Brauer's failure to analyze for free carbon. In the present work, all compositions above $NbC_{0.93}$ contained free carbon. Umansky's values, when converted to Angstrom from kX units, show very little agreement. This discrepancy can be improved somewhat if corrections are applied for the reported presence of ~2% oxygen, 0.25% Ti and 0.5% Ta in the niobium metal. Furthermore, since the samples were heated at 1200–1500° for a maximum of 4 hours, it is doubtful that the reaction had been completed.

The curve drawn in Fig. 1 relates the composition of the NbC lattice to the lattice parameter. When the sample contains two phases, indicated by a line drawn over the points, the composition of the NbC phase is not identical with the overall composition. The presence of some $Nb_2C$ makes the total composition richer in Nb than the NbC phase. However, a horizontal projection from the two-phase points to the curve enables one to determine the composition of the NbC phase.

In the single phase region the decrease in lattice constant with decreasing carbon content is independent of the temperature at which the sample was heated. However, when the experimental conditions fall within the two phase region, the composition of the NbC phase will follow, under equilibrium conditions, the phase boundary as the heating temperature is changed. This will cause the measured lattice constant to be sensitive to the heating temperature. Reference to Fig. 2, which shows a portion of the NbC–$Nb_2C$ phase diagram, will make this clearer.[10]

Experimentally, below approximately 2500°, equilibrium between phases is established so slowly compared to the cooling time, that the composition of the phases at the heating temperature is the same as that measured at 25°. But above 2700° equilibrium is rapid even when compared to a 600°/second cooling rate. As a result, samples experiencing conditions which lie within the area ABC (Fig. 2) will contain, upon cooling, a NbC phase of a composition between $NbC_{0.67}$ and $NbC_{0.69}$. The exact value will depend on the cooling rate and the particular heating temperature. This behavior makes the location of the phase boundary in this region uncertain.

(10) Unpublished work by the authors.

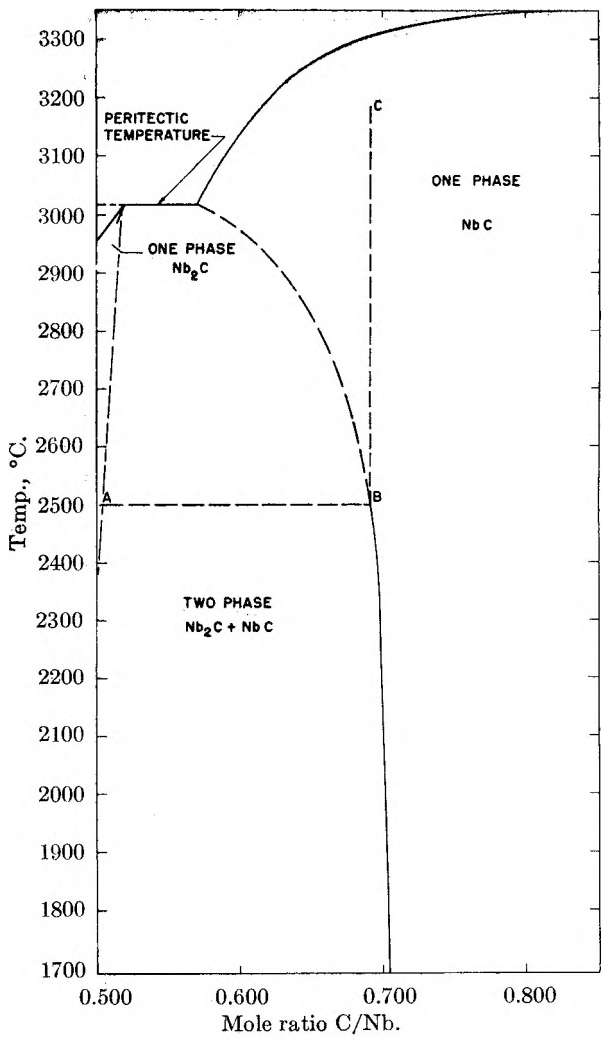


Fig. 2.—Portion of NbC–$Nb_2C$ phase diagram.

**Acknowledgment.**—We gratefully acknowledge the advice and support of Dr. Melvin G. Bowman during the course of this work. Acknowledgment is also due Dr. Don T. Cromer for programming crystallographic data, and Dr. R. K. Zeigler for programming the least-squares fit of the derived curve for the IBM 704 computer. Thanks are due Dr. E. Van Kooten for the analyses and Mrs. Mary Jane Jorgensen for reading the many X-ray diffraction patterns.

# PREPARATION AND DIELECTRIC PROPERTIES OF SYNTHETIC BORACITE-LIKE COMPOUNDS

BY F. JONA

*Westinghouse Research Laboratories, Pittsburgh, Pennsylvania*

*Received March 28, 1959*

The dielectric properties of boracite ($Mg_3B_7O_{13}Cl$) and some isomorphous compounds were investigated. The preparation of synthetic magnesium, nickel, zinc and cadmium boracite is described, the pseudo-cubic lattice constants of these compounds being 12.10, 12.08, 12.08 and 12.49 Å., respectively, and the transition from the (room temperature) orthorhombic to the cubic phase occurring at 265, 340, 450 and 525°, respectively. The dielectric constant of every compound exhibits a small anomaly at the corresponding transition temperature.

## Introduction

Boracite, a magnesium chloroborate, $Mg_3B_7O_{12}Cl$, is one of the most investigated minerals, as it presents interesting aspects both from the crystallographic and mineralogic point of view as well as from that of solid state physics. The crystal habit of the natural crystals is cubic, dodecahedral or pseudo-octahedral. Above 265°, the symmetry is isometric hextetrahedral ($4\bar{3}m$). Below this temperature, the paramorphic isometric crystals have orthorhombic pyramidal symmetry (mm2) with $a:b:c = 1:1:0.7072$.[1]

Very extensive investigations of the chemical, crystallographic, optical and twinning characteristics of boracite are reported by Mehmel,[2,3] according to whom the pseudo-cubic lattice constant of natural crystals (often containing Fe in partial substitution for Mg) varies between 12.05 and 12.18 Å. A small discontinuity in the value of the lattice constant of about 0.25% is found at the transition temperature of 265°, corresponding to a volume increase for increasing temperature. A weak piezoelectric effect is found in the high-temperature phase and a strong pyroelectric effect in the low-temperature phase. The relation between the lattices of the high and low-temperature phases of boracite is depicted schematically in Fig. 1.

The crystal structure of boracite was recently determined by Ito, *et al.*,[4] by means of X-ray powder diffraction data at 300°, for the high temperature phase, and Weissenberg–Buerger photographs at room temperature for the low temperature phase. The former phase, cubic, belongs to space group $T_d^5 - F\bar{4}3c$, with $a = 12.1$ Å. and $Z = 8$, the latter phase, orthorhombic, to space group $C_{2v}^5 - Pca$ with $a = b = 8.54$ Å., $c = 12.07$ Å. and $Z = 4$. The high and low temperature structures are essentially the same, both containing the same boron-oxygen network and differing only in the position of magnesium and chlorine atoms. In contrast to Mehmel,[3] Ito, *et al.*, report little or no change of lattice dimensions, in that powder photographs of the high and low temperature phases are practically identical. Owing to this fact, the latter authors suggest that the phase change occurring at 265° could be adequately explained by the freezing-in of the chlorine atoms, which are in thermal agitation above the transition temperature.

The characteristics of this transition are very highly suggestive of ferroelectric properties of boracite in the low temperature phase. This possibility was first recognized by Cady and Jaffe,[5] who, however, failed to detect any dielectric anomaly at the transition temperature and were only able to investigate qualitatively the piezoelectric response of small crystals, concluding that boracite has an elastic stiffness even greater than that of quartz. A recent optical and dielectric study of boracite by Le Corre[6] reveals a few interesting points, *viz.*: (a) in the immediate vicinity of the transition temperature, a small motion of the twin boundaries can be induced by an electric field of 2 kv./cm.; (b) a small anomaly of the dielectric constant along cubic [110] is observed at the transition temperature; (c) a very small remanent polarization $P_r = 0.002$ microcoulomb/cm.$^2$ is measured immediately below the transition temperature. On the basis of these observations, Le Corre claims that boracite is ferroelectric below 265°. Obviously, the experimental data do not completely justify such a statement, but the author suggests that the ferroelectric activity may be hindered or hidden by the presence of impurities in the natural crystals (mainly $Fe^{2+}$).

Accordingly, the present investigation is concerned with the preparation of synthetic boracite and its dielectric behavior. The investigation is extended to the preparation and the properties of compounds isomorphous to boracite, where Mg is substituted by other divalent metals.

## Preparation of Materials

**Previous Syntheses of Boracite.**—A summary of the numerous attempts to synthesize boracite is found in Mellor's Treatise.[7] One of the most successful methods is that developed by Heintz and Richter,[8] who melted a mixture of 55 g. of $MgCl_2$, 145 g. of NaCl, 5 g. of basic magnesium borate and 10 g. of anhydrous boric acid in a platinum crucible and obtained a mixture of microscopic crystals of complex magnesium borates and boracite, from which the latter could be separated by treatment with cold hydrochloric acid, which does not attack boracite. de Gramont[9] obtained boracite crystals by heating a mixture of one part $Na_2B_4O_7$ with two parts $MgCl_2$ with a little water for 2 or 3 days in a tube at 275–280°. A very detailed investigation of this preparative problem was done by Rousseau and

(1) C. Palache, H. Berman and C. Frondel, "Dana's System of Mineralogy," Vol. II, John Wiley and Sons, Inc., New York, N. Y., 1957, p. 378.

(2) M. Mehmel, *Z. Krist.*, **87**, 239 (1934).

(3) M. Mehmel, *ibid.*, **88**, 1 (1934).

(4) T. Ito, N. Morimoto and R. Sadanaga, *Acta Cryst.*, **4**, 310 (1951).

(5) W. G. Cady, "Piezoelectricity," McGraw-Hill Book Co., New York, N. Y., 1946, p. 230.

(6) Y. Le Corre, *J. phys. radium*, **18**, 629 (1957).

(7) J. W. Mellor, "A Comprehensive Treatise on Inorganic and Theoretical Chemistry," Vol. V, Longmans, Green and Co., New York, N. Y., 1924, p. 137.

(8) W. Heintz, *Pogg. Ann. Phys.*, **110**, 613 (1860).

(9) A. de Gramont, *Bull. soc. min.*, **13**, 245 (1890).

Allaire,[10] who prepared a series of chloroborates isomorphous with boracite by the action of the vapors of metallic chlorides on native calcium borate or boronatrocalcite (also called ulexite, $NaCaB_5O_9 \cdot 8H_2O$). Heintz and Richter's method for boracite gave negative results except in the case of zinc chloroborate. Rousseau and Allaire also report the preparation of bromoborates (brom.ted boracite) of iron and zinc by the action of bromine vapors on a mixture of the corresponding metal and boronatrocalcite. The corresponding iodoborates are reportedly also possible.[1]

**Magnesium Boracite.**—Attempts to synthesize magnesium boraeite by firing a stoichiometric mixture of MgO, $B_2O_3$ and $MgCl_2$ were unsuccessful. Even traces of water lead to the production of oxychlorides and the eventual loss of chlorine by vaporization. In this case, the yield was generally a mixture of magnesium oxide and complex magnesium borates in various ratios.[11] Good yields were obtained by the following procedure: 13 g. of $B_2O_3$ + 73 g. of $MgCl_2$ + 190 g. of NaCl were ground and thoroughly mixed in dry atmosphere. The mixture was introduced in a magnesia crucible, heated to 900°, soaked for 1 hour and cooled at the rate of 20°/hour. Under these conditions, a good portion of NaCl evaporated; the resulting mass was washed in boiling water and dried. Impurities like magnesium oxide and magnesium borates remaining in the end product could be eliminated by washing for a few hours in cold hydrochloric acid.

**Zinc Boracite.**—This preparation was complicated by the low boiling point of zinc chloride (732°). A successful run involved firing a mixture of 25 g. of $B_2O_3$ and 50 g. of $ZnCl_2$ in a covered alumina crucible to 700° and cooling rapidly. The end product was washed in boiling water and dried.

**Nickel Boracite and Cadmium Boracite.**—These compounds were prepared from stoichiometric mixtures of the appropriate oxides and chlorides with boric oxide by heating them to 900° in a covered alumina crucible and cooling at the rate of 100°/hr.

**Lead Boracite and Barium Boracite.**—Mixtures of 5PbO (or 5BaO) + $7B_2O_3$ + $1PbCl_2$ (or $BaCl_2$) fired at 900° in covered alumina crucibles exhibit an X-ray powder diffraction pattern which is very similar to that of magnesium boracite. In both cases, cubic indexing of high-angle lines is possible, leading to values of $a$ = 11.37 Å. for the Pb compound and $a$ = 11.55 Å. for the Ba compound. These values, however, are doubtful, owing to the presence of a low-angle extra line which could either indicate the presence of unknown impurities or a doubling of the above lattice constants.

## Experimental Methods

Identification of all the compounds prepared was done by comparison of X-ray powder diffraction photographs, taken with Cu K$\alpha$ radiation at room temperature, with the corresponding pattern of natural (magnesium) boracite crystals. The lattice constant of each compound was measured from high-angle lines (cubic $h^2 + k^2 + l^2$ = 228 to 253) of the powder patterns and averaged.

Samples for the dielectric measurements were obtained by compressing the fine crystalline powder of each compound, prepared as described above, in the form of disks of about 13 mm. diameter and 0.5 mm. thickness. The disks were sintered in an electric furnace at 750° in air, then coated on both sides out to the edge with conductive silver paint. In each case, the density of the samples was measured and compared with the theoretical value computed from the X-ray data in order to determine the porosity. The latter quantity was found to vary between 25% for the magnesium and zinc boracite samples to 32% for the samples of nickel and cadmium boracite.

The dielectric study of natural boracite was carried out on four crystals from Germany (source: Ward's Natural Science Establishment, Inc., Rochester, New York). They were rhombic dodecahedra about 3.5 mm. in the largest dimensions, colorless to light green, free from visible faults. Thin plates were cut and ground parallel to the pseudo-cubic (110) face.

(10) G. Rousseau and H. Allaire, *Compt. rend.*, **116**, 1195 (1893); **116**, 1445 (1893).

(11) The obtainable magnesium borates are found in the phase diagram of magnesium oxide and boric oxide investigated by Davis and Knight.[12]

(12) H. M. Davis and M. A. Knight, *J. Am. Ceram. Soc.*, **28**, 97 (1945).

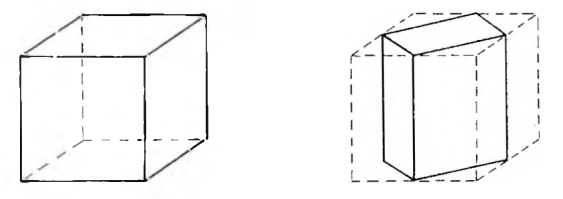


Fig. 1.—Relation between the lattices of the two phases of boracite.

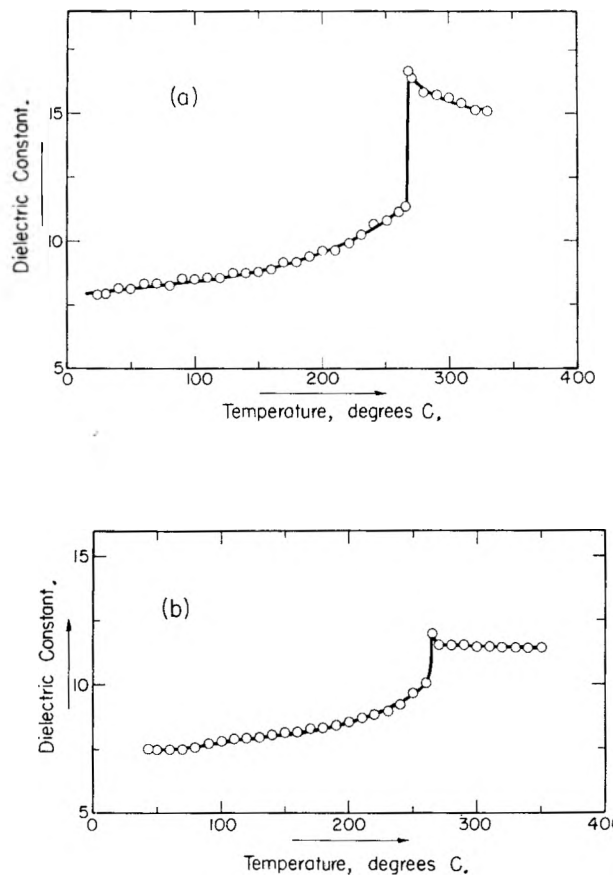


Fig. 2.—Temperature dependence of dielectric constant of: (a) single crystal of natural magnesium boracite along cubic [110]; (b) polycrystalline sample of synthetic magnesium boracite.

The dielectric constant of each specimen was measured as a function of temperature with a frequency of 100 Kc. and a field of approximately 15 v./cm. The data of the sintered samples were corrected for porosity by the method discussed by Rushman and Strivens.[13]

Tests for non-linearity and dielectric hysteresis were done with a modified Sawyer and Tower circuit as described by Diamant, *et al.*,[14] with a frequency of 60 c.p.s. and fields varying between 2 and 8 kv./cm.

## Results

The temperature dependence of the dielectric constant of natural and synthetic magnesium boracite is depicted in Fig. 2a, b, that of synthetic nickel,

(13) D. F. Rushman and M. A. Strivens, *Proc. Phys. Soc.* (*London*), **59**, 1011 (1947).

(14) H. Diamant, K. Drenck and R. Pepinsky, *Rev. Sci. Instr.*, **28**, 30 (1957).

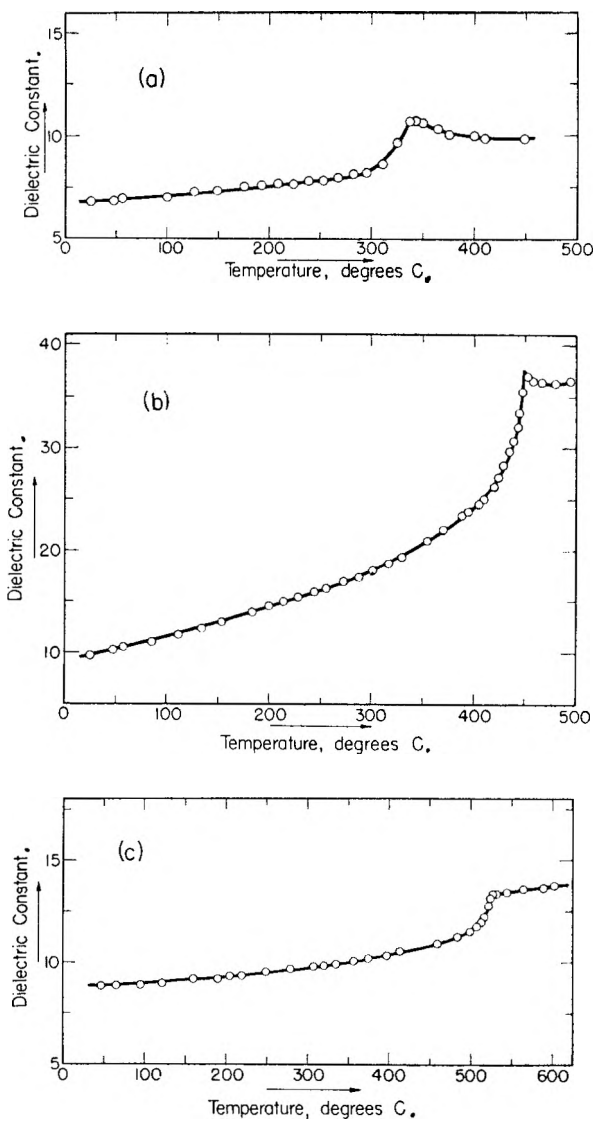


Fig. 3.—Temperature dependence of dielectric constant of polycrystalline samples of: (a) synthetic nickel boracite; (b) synthetic zinc boracite; (c) synthetic cadmium boracite.

zinc and cadmium boracite in Fig. 3a, b, c. In all cases, a distinct anomaly of the dielectric constant is found at higher temperatures, which is indicative of the orthorhombic–cubic transition already known in natural magnesium boracite crystals.

The transition temperature and the pseudo-cubic lattice constant of each compound are listed in Table I.

TABLE I

| Compound | Pseudo-cubic lattice constant (Å.) | Transition temp. (°C.) |
|---|---|---|
| Natural Mg boracite | 12.10 | 268[a] |
| Synthetic Mg boracite | 12.10 | 265 |
| Synthetic Ni boracite | 12.08 | 340 |
| Synthetic Zn boracite | 12.08 | 450 |
| Synthetic Cd boracite | 12.49 | 525 |

[a] The transition temperature of natural crystals was found to vary between 268 and 275° in different specimens. This variation is due to varying impurity content of different crystals.

No dielectric anomaly was found in the samples of lead and barium chloroborates, prepared as described above, up to 600°.

All samples were subjected to hysteresis tests in the temperature interval investigated. Especially at higher temperatures, the 60 c.p.s. losses were very substantial; after compensation, however, no evidence for ferroelectricity was found in any of the samples investigated.

It is possible that the synthetic materials contained small amounts of impurities, such as unreacted metal oxides and/or metal borates in concentrations not detectable by X-ray methods. However, the maximum amounts which could be present would not be expected to mask the ferroelectric activity of the specimens.

## Discussion

It is interesting to confirm that the crystal lattice of (magnesium) boracite allows the substitution of Mg with a variety of divalent metals. In addition to the isomorphous compounds investigated here, boracite-like crystals can reportedly be synthesized with Co, Mn of Fe instead of Mg, and with Br or I instead of Cl.[7] According to the structure of magnesium boracite reported by Ito, *et al.*,[4] the Mg–O distances are equal to 2.04 Å., which is between the sum of the ionic radii (1.99 Å.) and that of the covalent radii (2.15 Å.); and the Mg–Cl distances, 3.02 A., are remarkably larger than both the sum of ionic (2.48 Å.) and covalent radii (2.50 Å.), implying that the lattice should allow the replacement of Mg with larger atoms, like Cd and probably even Pb and Ba.

The difference between the structures of the high and low temperature phases of magnesium boracite is indicative of small relative shifts of the magnesium and chlorine atoms. Above 265°, the magnesium atoms are fairly symmetrically surrounded by two chlorine and four oxygen atoms in octahedral arrangement, while, at room temperature, the magnesium atom is found closer to one chlorine atom than to the other. Reversal of these relative displacements by means of an externally applied electric field is not confirmed by the present experiments on polycrystalline specimens.

The piezoelectric effect of the high temperature phase of boracite is characterized by the non-zero piezomoduli $d_{14} = d_{25} = d_{36}$. If a polarization is created along, say, the cubic [001] axis, a shear deformation $x_y$ would result. Since the pyroelectric polarization of the low-temperature phase lies along the twofold screw axis, the expected symmetry of the lower phase would be monoclinic. Actually, this symmetry is orthorhombic, and the fact that $a = b$ indicates that the spontaneous shear is vanishingly small. The latter is similar to the situation in the room temperature phase of $PbZrO_3$.[15] As in that case, it is possible that the energy barrier opposed to the reversibility of the polarity requires the application of electric fields higher than the breakdown, a question which could only be answered by experiments on large (synthetic) single crystals.

**Acknowledgments.**—The author wishes to thank Drs. G. Shirane, W. J. Takei and E. C. Subbarao for their helpful discussions.

(15) F. Jona, G. Shirane, F. Mazzi and R. Pepinsky, *Phys. Rev.*, **105**, 849 (1957).

# THE KINETICS OF OXIDATION OF HBr[1]

BY WILLIS A. ROSSER, JR., AND HENRY WISE

*Stanford Research Institute, Menlo Park, California*

*Received March 28, 1959*

The oxidation of gaseous HBr has been studied in the temperature range 700 to 800°K. When the concentration of HBr is much greater than that of $O_2$, the over-all reaction stoichiometry is $4HBr + O_2 = 2H_2O + 2Br_2$, and the reaction is a homogeneous, gas-phase reaction. The rate of reaction varies with the concentration of each reactant as shown by the equation $d(Br_2)/dt = 2k(HBr)(O_2)$. The temperature variation of the specific reaction rate $k$ may be summarized as $k = 10^{12.6} e^{-37,700/RT}$ cc./mole sec. A reaction mechanism is proposed.

## I. Introduction

In a study of the effect of bromine compounds on the oxidation of hydrocarbons and on hydrocarbon combustion, it was found that $O_2$ and HBr react at moderate temperatures. By virtue of this reaction, a small percentage of HBr in a mixture of $CH_4$ and $O_2$ eliminates the induction period which normally precedes the onset of observable reaction. Illustrative pressure–time curves are shown in Fig. 1. The oxidations of hydrocarbons other than $CH_4$ have also been catalyzed by HBr.[2] Consequently, a knowledge of the oxidation of HBr is required to interpret observations made on systems containing both $O_2$ and either HBr or substances from which HBr can be derived.

## II. Experimental

The various experiments were carried out using the apparatus schematically shown in Fig. 2. The essential elements of the system are: (a) a reaction vessel housed in a cylindrical resistance furnace, (b) a tungsten lamp, (c) a Beckman DU monochromator to select light of the desired wave length which then is detected by a photomultiplier tube, (d) a silicone–oil manometer for measuring low pressures, and (e) a Bourdon gauge for measuring higher pressures. The Bourdon gauge consisted of a Vycor spiral to which was attached a small mirror. Movement of the mirror was detected by means of a reflected light beam. The course of the reaction was followed by photometric measurement of the concentration of $Br_2$ at a wave length of 4200 Å.

Two cylindrical reaction vessels of a comparable size were used, one of quartz and the other of Pyrex. The dimensions of the quartz vessel (diameter $\approx$ 4 cm., length $\approx$ 60 cm.) correspond to a surface to volume ratio of 1 cm.$^{-1}$. The Pyrex vessel, of similar dimensions, was partially filled with borosilicate–glass beads to give an over-all surface to volume ratio of about 5 cm.$^{-1}$. The monitoring light beam passed 1 to 2 mm. above the bed of beads which occupied the lower third of the reaction vessel.

In order to obtain temperature uniformity within the reaction vessel, the furnace was heated by four resistance windings, each independently regulated by hand adjustment of a variable voltage supply; and the reaction vessel was housed within a heavy-walled aluminum liner. The temperature of the reaction vessel was measured by six eternal chromel–alumel thermocouples distributed uniformly along the length of the reaction vessel. By adjusting the voltage applied to each of the four heater windings, one could easily limit the temperature range indicated by these six thermocouples to less than two degrees. The temperature within the reaction vessel was considered to be the average of the temperatures indicated by the external thermocouples.

The rate of reaction was measured by observing the rate of production of $Br_2$ as a function of time, of reactant concentrations and of temperature. The pressure change associated with the reaction was also observed; the total pressure change is quite small (1 to 2 mm.) and is not suitable for quantitative measurement of the reaction rate. The reaction was studied at temperatures from 700 to 800°K. and for reactant concentrations in the range $10^{-7}$ to $10^{-5}$ mole/cc. Extra dry $O_2$ (> 99.6%) was used as supplied by the Matheson Co., Inc. Anhydrous HBr (> 99.8%), from the same source was used after impurities non-condensable at the temperature of liquid nitrogen had been removed by vacuum distillation.

The reactants were introduced separately into the reaction vessel from a small manifold attached to the gas storage vessels. (The concentration of one component, either $O_2$ or HBr, was always much greater than that of the other.) The minor component was introduced first and its initial pressure measured with the oil manometer attached to the apparatus. The oil manometer connection was then closed and the major component added. The total pressure and the pressure change were measured by means of the Bourdon gauge.

## III. Experimental Results

**A. Reaction in a Quartz Vessel.**—When the concentration of HBr is much greater than that of $O_2$, the experimental results are uncomplicated. For extensive reaction the pressure change is one-half the pressure of $Br_2$ produced by the reaction, *i.e.*, $-\delta p = (1/2)(p_{Br_2})$. The pressure measurements are only semi-quantitative since the precision of measurement (0.2 mm.) is an appreciable part of the total pressure change (1 to 2 mm.). The ratio, $Br_2$ produced/$O_2$ initially present, is precisely 2 ($\pm 2\%$) for complete reaction. These facts indicate that the over-all stoichiometry is given by

$$4HBr + O_2 = 2H_2O + 2Br_2 \qquad (1)$$

The rate of production of $Br_2$ was found to be proportional to the product of the concentrations of HBr and $O_2$. For presentation of the data, however, it is convenient to convert the differential rate expression

$$\frac{d(Br_2)}{dt} = 2k(HBr)(O_2) \qquad (2)$$

to an integral form. The integral expression corresponding to eq. 1 and 2 has the form

$$-\log [1 - (Br_2)/2(O_2)_i] = (\log e)2k(HBr)_i t \qquad (3)$$

where the subscript "i" refers to initial concentrations. As shown in Fig. 3, as well as by eq. 3, the left-hand side of eq. 3 is proportional to time. The rate constant $k$, derived by means of eq. 3 from the slope of curves like that in Fig. 3, varies with temperature but not with the initial concentrations of the reactants, as long as these concentrations satisfy the condition $(HBr) >> (O_2)$.

When the initial concentrations of the reactants satisfy the condition $(O_2) >> (HBr)$, the experimental results involve features that differ from those associated with the inverse condition

(1) This research was supported by the Engineer Research and Development Laboratories, U. S. Army, Corps of Engineers, under contract DA-44-009-ENG-2863; and by the Division of Physical Sciences, Stanford Research Institute, Menlo Park, California.

(2) F. F. Rust and W. E. Vaughan, *Ind. Eng. Chem.*, **41**, 2595 (1949).

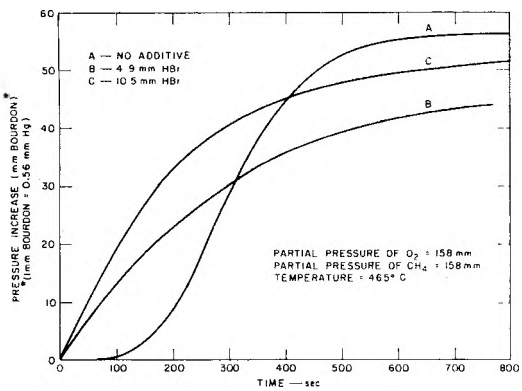


Fig. 1.—The effect of HBr on the oxidation of $CH_4$.

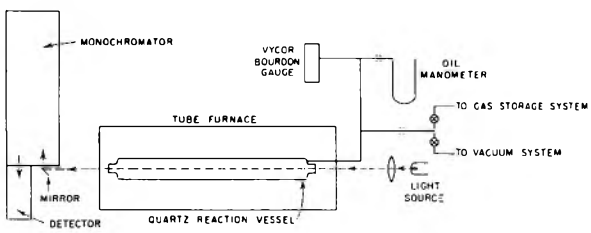


Fig. 2.—Schematic diagram of apparatus.

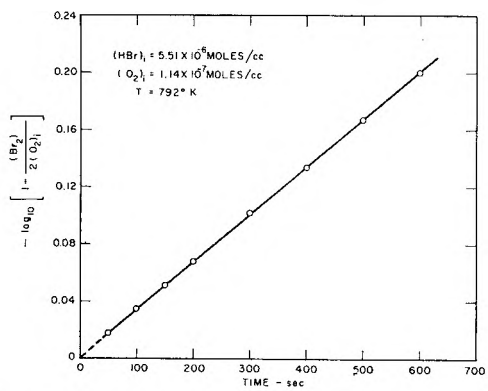


Fig. 3.—The rate of production of bromine when (HBr) >> ($O_2$).

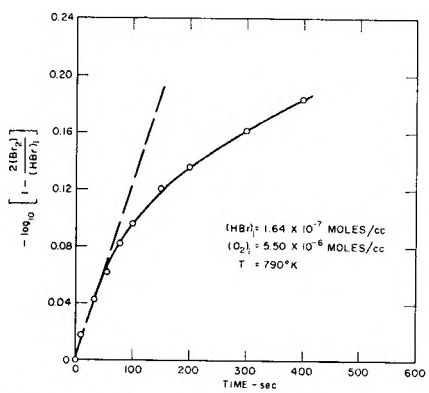


Fig. 4.—The rate of production of bromine when (HBr) << ($O_2$).

(HBr)>>($O_2$). In particular, the observed pressure drop for extensive reaction is considerably less than $^1/_2$ the pressure of $Br_2$ produced. The results of several determinations may be summarized by $-\delta p = (0.2 \text{ to } 0.3)p_{Br_2}$. These observations indicate that a portion of the observed $Br_2$ has been produced by reactions which lead to the stoichiometry of eq. 4

$$2HBr = H_2 + Br_2 \qquad (4)$$

Because eq. 4 proceeds without pressure change, the observed pressure drop will be less than $^1/_2$ $p_{Br_2}$, the value when the reactions lead exclusively to the stoichiometry of eq. 1. Other possible stoichiometries not involving $H_2$ as a product but rather such unstable intermediates as $H_2O_2$, BrO, etc., all lead to the relation $-\delta p > {}^1/_2\ p_{Br_2}$. Accordingly it may be concluded that some $H_2$ is produced by the reaction between $O_2$ and HBr when the concentrations of the reactants satisfy the condition ($O_2$)>>(HBr).

Even for the condition ($O_2$)>>(HBr), eq. 2 describes the initial rate of production of $Br_2$ although not the rate of production of $Br_2$ for extensive reaction. To illustrate this behavior, the rate expression is converted to the integral form

$$-\log [1 - 2(Br_2)/(HBr)_i] = (4 \log e)k(O_2)_i t \qquad (5)$$

As shown in Fig. 4, the left hand-side of eq. 5 does not increase linearly with time for extensive reaction. The initial slope of the curve shown in Fig. 4 may still be used to derive a value for the specific reaction rate $k$

$$k = \lim_{t \to 0} \frac{d}{dt}\left[\frac{-\log \{1 - 2(Br_2)/(HBr)_i\}}{4 \log e\,(O_2)_i}\right] \qquad (6)$$

Values of $k$ derived in this manner agree with the values derived from eq. 3 (see Table I for comparison). The failure of eq. 2 and 5 to describe the experimental results for prolonged reaction is attributed to the presence of $H_2$ in the system. A reaction between $H_2$ and $Br_2$, known to occur at these temperatures, will consume the product $Br_2$ and regenerate the reactant HBr. Consequently, the net rate of disappearance of $Br_2$ will be less than it would be if $H_2$ were not present.

The temperature variation of $k$ is presented in Fig. 5. The line shown is intended to fit the data for the condition (HBr)>>($O_2$) because these data were determined with greater precision than those for the opposite condition, (HBr)<<($O_2$). The Arrhenius expression for $k$ is given in eq. 7

$$k = 10^{12.6}\, e^{-37{,}700/RT} \text{ cc./mole sec.} \qquad (7)$$

**B. Reaction in a Packed Pyrex Vessel.**—When (HBr)>>($O_2$) the observed pressure change during reaction in a packed reaction vessel is larger than can be accounted for by eq. 1. It was found that a reaction between HBr and the glass surfaces within the vessel results in a small pressure decrease. Since HBr is the major component of the mixture, a slight reaction, while it does not significantly affect the concentration of HBr, is sufficient to prevent a determination of the pressure change resulting from the oxidation of HBr.

The time variation of the concentration of $Br_2$ followed eq. 3 and the values of the specific reaction rate derived from eq. 3 agree with those found for reaction in the quartz vessel (see Fig. 5). It was therefore concluded that the oxidation of HBr for the cited experimental conditions is a homogeneous reaction.

The packed bessel was not used in experiments

TABLE I

THE OXIDATION OF HBr
$T$=762° K. (Quartz Reaction Vessel)

| $(O_2)$, mole/cc. | $(HBr)_i$, mole/cc. | Specific reaction rate $k$, cc./mole sec. |
|---|---|---|
| $5.12 \times 10^{-6}$ | $5.09 \times 10^{-7}$ | 47 |
| $5.20 \times 10^{-6}$ | $2.65 \times 10^{-7}$ | 49 |
| $5.26 \times 10^{-6}$ | $3.56 \times 10^{-7}$ | 53 |
| $2.68 \times 10^{-6}$ | $3.45 \times 10^{-7}$ | 49 |
| $7.28 \times 10^{-6}$ | $3.47 \times 10^{-7}$ | 44 |
| | Av. = | 48.4 ± 2.9[a] |
| $3.46 \times 10^{-7}$ | $5.43 \times 10^{-6}$ | 50.8 |
| $1.99 \times 10^{-7}$ | $5.45 \times 10^{-6}$ | 51.3 |
| | Av. = | 51.1 |

[a] Standard deviation.

for which $(HBr) << (O_2)$ because the HBr–glass reaction would make them difficult to interpret.

## IV. Discussion

The various experimental observations may be interpreted in terms of the following reaction mechanism. When $(HBr) >> (O_2)$

$$HBr + O_2 \longrightarrow HO_2 + Br \quad (8)$$
$$HO_2 + HBr \longrightarrow H_2O_2 + Br \quad (9)$$
$$Br + Br \longrightarrow Br_2 \quad (10)$$
$$H_2O_2 \longrightarrow 2OH \quad (11)$$
$$OH + HBr \longrightarrow H_2O + Br \quad (12)$$

When $(O_2) >> (HBr)$, it is necessary to include reactions 13 and 14 both of which compete with

$$HO_2 \longrightarrow H + O_2 \quad (13)$$
$$HO_2 \longrightarrow \text{destruction at walls} \quad (14)$$

reaction 9. The hydrogen resulting from reaction 13 or possibly from reaction 14 will react with $Br_2$ to give the features associated with the condition $(O_2) >> (HBr)$.

The decomposition of $H_2O_2$ has been recently studied[3,4] and it is known that above 700°K. the decomposition is primarily homogeneous and begins as written in eq. 11.

(3) P. A. Giguere and I. D. Lin, *Can. J. Chem.*, **35**, 283 (1957).
(4) C. N. Satterfield and T. W. Stein, THIS JOURNAL, **61**, 537 (1957).

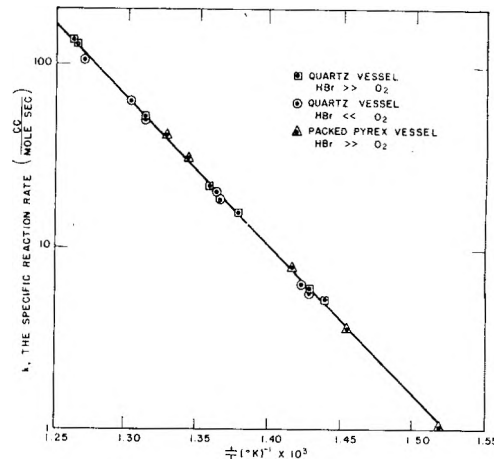


Fig. 5.—The specific reaction rate as a function of temperature.

According to the mechanism outlined above, the specific reaction rate $k$ refers to the initiation reaction, eq. 8. The Arrhenius expression for $k$ (eq. 7) then implies a steric factor of about $10^{-2}$ and an activation energy of 38 kcal. for reaction 8. This activation energy requires that the heat of formation of the $HO_2$ radical be no greater than about 2.5 kcal. This maximum value, $\Delta H_f$ = 2.5 kcal., compares reasonably well with the energy of dissociation $D(H–O_2)$ = 47 ± 2 kcal.[5] or $\Delta H_f$ = 4.5 ± 2 kcal.

The reaction between $O_2$ and HBr is undoubtedly responsible for the absence of an observable induction period during the sensitized reaction between $CH_4$ and $O_2$ (see Fig. 1). The reaction pair

$$HBr + O_2 \longrightarrow HO_2 + Br \quad (8)$$
$$Br + CH_4 \longrightarrow CH_3 + HBr \quad (15)$$

is formally equivalent to the reaction

$$CH_4 + O_2 \longrightarrow CH_3 + HO_2 \quad (16)$$

and apparently provides radicals at a rate much greater than does the initiation reaction associated with the unsensitized reaction.

(5) S. N. Foner and R. L. Hudson, *J. Chem. Phys.*, **23**, 1364 (1955).

# RADIATION CHEMISTRY OF POLYVINYL CHLORIDE

BY A. A. MILLER

*Research Laboratory, General Electric Company, Schenectady, New York*

*Received March 28, 1959*

The irradiation, with high-energy electrons, of the polyvinyl chloride structure, $-CH_2CH(Cl)-$ was studied. Radiation yields for HCl were determined as a function of temperature. Post-irradiation changes *in vacuo* and in air, were measured by electron paramagnetic resonance and by visual observation of color. It is concluded that the major primary chemical processes are the formation of $-CH_2\dot{C}H-$ + Cl· and $-CH{=}CH-$ + HCl. A free-radical chain dehydrochlorination, involving the unstable $-\dot{C}HCH(Cl)-$ radical, appears to explain the development of conjugated unsaturation. The radiation yield for HCl increases with temperature from a minimum value of $G$ = 5.6 at −90° and below, to $G$ = 23 at 70°.

## Introduction

This paper discusses some aspects of the radiation chemistry and related free-radical chemistry of polyvinyl chloride (PVC), $-CH_2CH(Cl)-$. A study of the chemical effects of $\gamma$-radiation in this polymer has already been reported by Chapiro[1] and, although similar over-all results were observed in the present work, the interpretation is somewhat different. Much more research has been done on the

(1) A. Chapiro, *J. Chim. phys.*, **53**, 895 (1956).

thermal degradation and stabilization of polyvinyl chloride,[2,3] but the mechanisms still are not completely defined. (These two papers list extensive references.) In particular, there is some question regarding the manner in which successive units of HCl are expelled along the polymer chain to produce conjugated unsaturation and the accompanying discoloration. Generally, an allyl-activated, and presumably molecular, elimination of HCl has been accepted as the most probable mechanism.[4] However, in a review of the degradation and stabilization of PVC, Winkler has suggested a free-radical chain reaction in which the propagation is sustained by the unstable –CHCH-(Cl)– radical.[2]

In conjunction with previous results on this system, the post-irradiation effects described here appear to support a free-radical dehydrochlorination mechanism of the type proposed by Winkler. In addition, this paper discusses primary radiation chemical processes and subsequent free-radical reactions in PVC, particularly as related to grafting and crosslinking and to the use of PVC as a radiation dosimeter.

## Experimental

The polyvinyl chloride used in this work was Geon 101 powder (B. F. Goodrich Company) with an average particle size of about 75 $\mu$. The limiting equivalent viscosity, measured in cyclohexanone at 25°, was $\lambda_0 = 7.2$ l./mole of $-CH_2CH(Cl)-$ and on the basis of the relation derived by Mead and Fuoss,[5] $\lambda_0 = 7 \times 10^{-5} M$, a weight average molecular weight of 103,000 was derived for this polymer. Unoriented polyvinyl chloride is largely amorphous with a glass transition temperature of about 75°.[6]

Irradiations were done with 800 Kv. (peak) electrons from a G. E. resonant transformer unit. For such radiation, the depth of uniform ionization is about 0.1 g. cm.$^{-2}$ and sample thicknesses were always well below this value. Dosimetry was based on the calibration of the beam current by measurements with a special air-ionization chamber. The irradiation doses are expressed as megaroentgens (1 Mr. = $10^6$ r.) and radiation yields ($G$ values) are based on the conversion factor: 1 r. = 84 ergs g.$^{-1}$ = $5.2 \times 10^{13}$ e.v. g.$^{-1}$.

**Radiation Yield of HCl.**—A stainless-steel irradiation cell, attached to a mercury manometer and equipped with a thin (1 mil) steel removable window, was used to measure the HCl evolved under irradiation. A 1-gram sample of the PVC powder was sealed into the cell and outgassed by vacuum-pumping at 1 $\mu$ pressure for several hours while the temperature was raised to 70°, just below the glass point. The sample was irradiated at a dose rate of 14 Mr./minute to doses of 5 to 20 Mr., in increments of 5 Mr. to avoid a temperature rise. Following irradiation, the cell was allowed to stand for one hour at room temperature allowing diffusion of the HCl out of the PVC particles to a constant pressure reading. The irradiated sample was not heated because of post-irradiation effects to be described later. Cooling of the evolved gas into a liquid nitrogen trap showed that at least 95% was condensable and that little or no hydrogen (non-condensable) was formed. The amount of HCl was calculated from the pressure and the previously calibrated volume of the irradiation cell. HCl yields were determined on separate 1-gram samples over a temperature range of −145 to 70°. In the irradiation at 70°, a 5 Mr. dose was given in 21.7 sec. and the irradiation cell was immediately quenched in liquid nitrogen to cool the sample to room temperature in less than five minutes.

**Electron Paramagnetic Resonance (e.p.r.) Measurements.**—A sample of PVC powder was outgassed, as described earlier, and irradiated at −190° (liquid nitrogen temperature) at a dose of 10 Mr. The sample was transferred to a culture-tube which was then tightly sealed and stored in liquid nitrogen. All transfer operations, before and after irradiation, were done under anaerobic conditions in a "dry box" filled with pure nitrogen. For the e.p.r. measurements, irradiated samples, which had been stored in liquid nitrogen, were transferred to standard 3 mm. Pyrex tubes, evacuated and sealed-off. This transfer required about 10 minutes, during which time the samples were at room temperature but never exposed to air. The sealed e.p.r. sample tubes were again stored in liquid nitrogen prior to measurement. The e.p.r. measurements were made at room temperature on a Varian Spectrometer, Model V-4500. For the semi-quantitative results described here, gross changes in e.p.r. intensity could be estimated from the peak-to-peak heights of the differential curves rather than by measurement of areas under the integrated absorption curves. Concurrently with the e.p.r. measurements, visual observations of color changes in the PVC samples were made.

**Crosslinking Measurements.**—Estimates of the radiation-induced crosslinking in the PVC were made on 5-mil films of the polymer, cast from a 10% solution in tetrahydrofuran. The films were thoroughly dried and outgassed at 1 $\mu$ pressure and 70° and stored in a pure nitrogen atmosphere. For one experiment, a 5-mil film of PVC containing 10% by weight of a non-volatile, tetrafunctional monomer, polyethylene glycol dimethacrylate (Monomer MG-1, Union Carbide Chemicals Co.) was prepared from solution. Following irradiation under a nitrogen atmosphere, gel yields were measured by extraction of the PVC films in a large excess of dimethylformamide solvent at 90° for 4 hours. The extracted gels were then swollen in fresh solvent at room temperature and the swollen length and width dimensions were measured. The relative swelling is reported as an *area* swelling ratio.

## Results

The yields of HCl as a function of irradiation temperature are shown in Fig. 1. At 30°, $G$(HCl) = 13 and this increases to a value of $G = 23$ at 70°, just below the glass point. Below room temperature, the yield decreases to a minimum of $G = 5.6$.

The post-irradiation changes in e.p.r. intensity and visible color are summarized in Fig. 2 for samples irradiated at 10 Mr. and −190°. Under these conditions, irradiation produced a strong e.p.r. signal but with no visible discoloration of the PVC. Furthermore, such samples could be stored in liquid nitrogen for many days with no change in e.p.r. activity or color. However, when the sample was warmed to room temperature in the absence of oxygen, shielded or unshielded from ordinary light, color slowly developed to a brown in a period of about 24 hours while the e.p.r. intensity remained relatively constant (Fig. 2, vacuum). If the sample was restored to room temperature while exposed to air, only a slight discoloration to a gray developed and the e.p.r. signal rapidly decayed (Fig. 2, air). A sample which was stored for 24 hours *in vacuo* at room temperature, to allow the development of the brown color, and then exposed to air showed a rapid bleaching to an olive-gray color and a simultaneous decrease in e.p.r. intensity. These changes were observable within a few minutes after exposure of the sample to air.

PVC powder irradiated at room temperature, rather than at −190°, showed post-irradiation effects similar to those just described, except that for the same 10 Mr. dose, the initial e.p.r. intensity was higher and a slight initial discoloration (tan color) was produced. Following irradiation, this color

(2) D. E. Winkler, *J. Polymer Sci.*, **35**, 3 (1959).

(3) C. F. Bersch, M. R. Harvey and B. G. Achhammer, *J. Research Natl. Bur. Standards*, **60**, 481 (1958).

(4) B. Baum and L. H. Wartman, *J. Polymer Sci.*, **28**, 537 (1958).

(5) D. J. Mead and R. M. Fuoss, *J. Am. Chem. Soc.*, **64**, 277 (1942).

(6) P. J. Flory, "Principles of Polymer Chemistry," Cornell University Press, Ithaca, N. Y., 1953, p. 52.

slowly intensified to a brown *in vacuo* or was quickly bleached to an olive-gray in air.

Volumetric oxygen-absorption measurements indicated that the rate and amount of oxygen absorption were significantly greater for an irradiated PVC sample in which the brown color had been allowed to develop than in one which was exposed to the oxygen immediately after warming to room temperature and before development of color. For a sample irradiated at 10 Mr. and −190° and stored *in vacuo* at room temperature for 24 hours to allow the development of the brown color, about $2 \times 10^{-5}$ moles of oxygen per gram of PVC was absorbed within 20 minutes. This corresponds to $-G'(O_2) \simeq 2$ for the post-irradiation consumption of oxygen by PVC.

The effect of temperature on the rate of e.p.r. decay was examined briefly. PVC samples, irradiated at 10 Mr. and −190° and sealed under vacuum in e.p.r. tubes, were annealed by immersion in a heated oil-bath. At an annealing temperature of 90°, about 15° above the glass point, the e.p.r. signal decrease to 25% of its initial value in 3 minutes while the color changed from white to violet. At 150°, the e.p.r. intensity decreased to about 5% in 30 seconds with the development of an intense purple color. Subsequent exposure of these annealed, and more highly colored, samples to air did not result in the rapid bleaching which was characteristic of the unannealed samples described earlier. In fact, no bleaching occurred in the annealed samples even after several months exposure to air at room temperature.

In view of the entrapment of radicals demonstrated by the e.p.r. observations for samples irradiated in the glass state below 75°, radiation-crosslinking was measured only at elevated temperatures, on outgassed films in nitrogen and at a dose rate of 14 Mr./minute. At 90°, incipient gelation was observed at a dose of 12 Mr. At 20 Mr. a gel yield of 44% was obtained, with an area swelling ratio of 9.3. Irradiations at 150° gave incipient gelation between 2 and 5 Mr. and at 10 Mr. the gel yield was 80%, with an area swelling ratio of 5.3. These results show that the crosslinking, as measured by gel yields and swelling, increases with temperature. However, in all cases the crosslinked PVC was severely discolored and this discoloration increased with dose and/or irradiation temperature.

The addition of 10% dimethacrylate monomer caused a pronounced enhancement of the radiation-crosslinking. At 90°, incipient gel was observed at a dose of only 0.5 Mr. and at 1 Mr. a 44% gel yield, with an area swelling ratio of only 4.3, was obtained. Also, this degree of crosslinking at 1 Mr. was achieved with little or no discoloration of the PVC.

## Discussion

The radiation and post-irradiation effects observed for PVC can be explained on the basis of a free-radical, chain dehydrochlorination reaction which is initiated by the radiation. The several phases of this mechanism will be discussed in sequence.

**Initiation and Primary Chemical Processes.**—

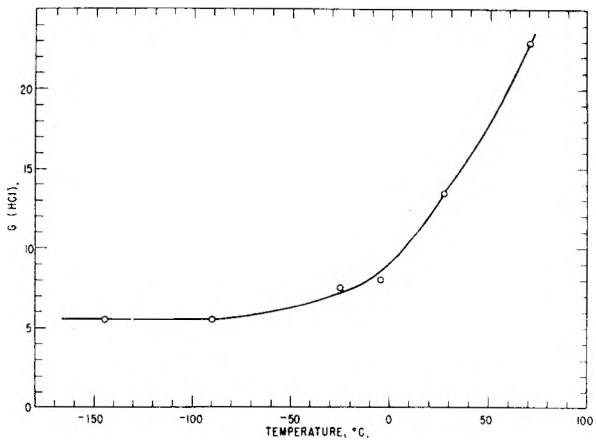


Fig. 1.—Effect of irradiation temperature on yield of HCl.

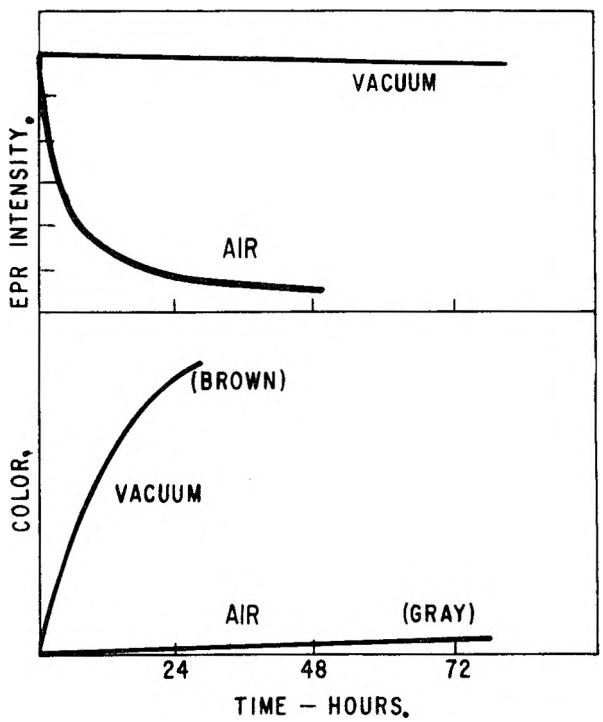


Fig. 2.—Post-irradiation changes in e.p.r. intensity and color in polyvinyl chloride powder. Irradiations at −190° and 10 Mr.; observations at room temperature.

In the radiolysis of the polyvinyl chloride structure, $-CH_2CH(Cl)-$, cleavage of an H or Cl substituent from the main chain could lead to three possible types of polymer radicals: (A) $-CH_2\dot{C}(Cl)-$; (B) $-\dot{C}HCH(Cl)-$; and (C) $-CH_2\dot{C}H-$. Since the C–Cl bond dissociation energy is about 20 kcal./mole less than that of either of the C–H bonds,[7] preferred scission of this bond to produce polymer radical (C) may be expected. More direct evidence for preferred scission of the C–Cl bond in this type of structure may be derived from results on the $\gamma$-irradiation of solid ethyl chloride, $C_2H_5Cl$, at liquid nitrogen temperature. From an e.p.r. analysis of the frozen product, Smaller and Matheson[8] concluded that the ethyl radical, $C_2H_5\cdot$, is produced.

(7) T. L. Cottrell, "The Strengths of Chemical Bonds," Butterworths, London, 1954, p. 277.

(8) B. Smaller and M. S. Matheson, *J. Chem. Phys.*, **28**, 1169 (1958).

It is proposed that the major primary free-radical process in the radiolysis of PVC is

$$-CH_2CH(Cl)- \longrightarrow -CH_2\dot{C}H- + Cl\cdot \quad (1)$$

This process may occur even at $-190°$ but at this low temperature the resulting polymer radical may remain trapped without reaction. When the sample is warmed up to room temperature after irradiation, or irradiated at room temperature, free-radical reactions of the type suggested by Winkler[2] may ensue

$$Cl\cdot + -CH_2CH(Cl)- \begin{cases} \longrightarrow HCl + -CH_2\dot{C}(Cl)- \quad (2a) \\ \qquad\qquad (A) \\ \longrightarrow HCl + -\dot{C}HCH(Cl)- \quad (2b) \\ \qquad\qquad (B) \end{cases}$$

Of the two processes shown above, evidence from the chlorination of aliphatic chlorides[9] suggests that attack on the methylene group (*i.e.*, process 2b) is preferred. Also, as Winkler points out, in the free-radical chlorination of PVC itself, methylene groups disappear.[10] Reaction 2b produces polymer radical (B), which, in contrast to radicals (A) or (C), is quite unstable and can undergo a spontaneous dissociation. The chlorine atom then attacks the activated adjacent methylene group to regenerate the unstable radical (B). Thus, a chain reaction leading to the formation of HCl and *conjugated* unsaturation is propagated

$$-\dot{C}HCH(Cl)- \longrightarrow -CH{=}CH- + Cl\cdot$$

$$Cl\cdot + -CH{=}CHCH_2CH(Cl)- \longrightarrow HCl + -CH{=}CH\dot{C}HCH(Cl)-, \text{ etc.}$$

(B)

It is also possible that this propagation may not involve a "free" Cl atom but rather a simultaneous dissociation and abstraction

$$-\dot{C}HCH(Cl)CH_2CH(Cl)- \longrightarrow HCl + -CH{=}CH\dot{C}HCH(Cl)-, \text{ etc.}$$

It is apparent that, according to these mechanisms, the evolution of HCl and the concurrent development of conjugated unsaturation can proceed without the loss of radicals and this is consistent with the observations summarized in Fig. 2 (vacuum). Also, this chain reaction can propagate only along a regular $-CH_2CH(Cl)-$ sequence. If this sequence is interrupted by imperfections, such as branches or double bonds, the dehydrochlorination chain will be terminated by the formation of a more stable, trapped polymer radical. Should the Cl· atom abstract a *tertiary* hydrogen from an adjacent polymer molecule, the reaction chain would again be terminated as a stable radical (A). If, on the other hand, the propagating Cl atom should abstract a *methylene* hydrogen from an adjacent polymer molecule, a new conjugated sequence would be initiated. This process is analogous to chain-transfer in ordinary free-radical chain reactions.

Oxygen can suppress the chain dehydrochlorination by reacting with the propagating radicals, Cl or polymer radical (B). This explains the post-irradiation effect of oxygen in preventing the development of color while causing a rapid decay in e.p.r. intensity (Fig. 2, air). The slight discoloration to a gray in the presence of oxygen may be attributed to an autoxidation of the polymer radicals. The oxygen-bleaching of the color previously developed in irradiated PVC by vacuum storage must be due to reaction of the conjugated double bonds with $O_2$, peroxy radicals or peroxides. A rapid bleaching reaction directly between molecular $O_2$ and the conjugated unsaturation seems least likely since vacuum-annealed, intensely colored samples, no longer containing trapped radicals, are not noticeably bleached even after several months exposure to air.

The low radiation yield for crosslinking of PVC at room temperature has been noted by Chapiro.[1] In the present work, at 90°, gelation was first observed at a dose of about 12 Mr. Based on the criterion that one crosslink is required for two initial "weight-average" molecules to produce incipient gelation,[11] the present polymer ($\bar{M}_w$ = 103,000) should require about $3 \times 10^{18}$ crosslinks per gram. Thus, at 90° the crosslinking yield is only $G = 0.5$ compared to $G = 3$ for polyethylene.[12] At 150°, the crosslinking yield is increased several-fold. It should be emphasized, however, that under these high temperature conditions, a considerable amount of conjugated unsaturation, as evidenced by severe discoloration, was also formed and this could contribute to crosslinking by reactions of the type indicated by previous workers.[2,13] Therefore, the estimated crosslinking yields are not true radiation yields but also include secondary (*i.e.*, thermal) crosslinking processes.

An added vinyl monomer, such as the dimethacrylate employed here, can suppress the chain dehydrochlorination by reacting with the propagating radicals. In this case, the polymer radical initiates a graft-polymerization of the added monomer to produce graft-crosslinks between PVC molecules. At an irradiation temperature of 90°, the over-all effect of the added monomer is to increase the crosslinking yield by at least 10-fold while preventing the discoloration of the PVC.

**Mass Spectral Data.**—In relation to the radiolysis of polyvinyl chloride, it is of interest to compare the mass spectral pattern of a structurally similar model compound, ethyl chloride. It is not intended here to use mass spectra, obtained for very dilute gaseous systems, to substantiate radiolysis mechanisms in the condensed state but rather as preliminary evidence regarding the primary processes.[14]

For ionizing and accelerating voltages of 70 and 3000 volts, respectively, the following principal ions and their relative intensities were observed for $C_2H_5Cl$[15]: $C_2H_5Cl^+ = 97$; $C_2H_5^+ = 61$; $C_2H_4^+ = 100$; $C_2H_3^+ = 56$; $C_2H_2^+ = 22$; and $C_2H_4Cl^+ = 6$. The $C_2H_5^+$ ion, corresponding to C–Cl scission, is about 10 times as abundant as

(9) C. Walling, "Free Radicals in Solution," John Wiley and Sons, Inc., New York, N. Y., 1957, p. 362.

(10) V. W. Fuchs and D. Louis, *Makromol. Chem.*, **22**, 1 (1957).

(11) See ref. 6, p. 359.

(12) E. J. Lawton, J. S. Balwit and R. S. Powell, *J. Polymer Sci.*, **32**, 257 (1958).

(13) D. Druesedow and C. F. Gibbs, "Polymer Degradation Mechanisms," Nat. Bur. Standards, 1953, p. 69.

(14) See, for example, J. G. Burr, THIS JOURNAL, **61**, 1483 (1957).

(15) F. J. Norton, private communication.

the $C_2H_4Cl^+$ ion which is formed by C–H scission. The parent ion, $C_2H_5Cl^+$, is also present at a high relative intensity. In radiolysis, such an ion might produce further scission of the weaker C–Cl bond by direct decomposition: $C_2H_5Cl^+ \rightarrow C_2H_5^+ + Cl\cdot$, or following neutralization: $C_2H_5Cl^+ + e \rightarrow (C_2H_5Cl)^* \rightarrow C_2H_5\cdot + Cl\cdot$.

The predominant ion in the mass spectrum of ethyl chloride is $C_2H_4^+$ and this must arise from the loss of H + Cl (or HCl) in a single interaction with an ionizing electron. Accordingly, it is suggested that, concurrently with C–Cl scission, a non-radical, "molecular" expulsion of HCl may occur in the radiolysis of these aliphatic structures to produce unsaturation: $-CH_2CH(Cl)-\sim\rightarrow -CH{=}CH- + HCl$. Based on similar mass spectrometric evidence, *i.e.*, the predominance of $C_2H_4^+$ in the mass spectrum of *ethane*, an analogous molecular expulsion of $H_2$ from the polyethylene structure to produce vinylene unsaturation: $-CH_2CH_2-\sim\rightarrow -CH{=}CH- + H_2$, was proposed some time ago.[16] More recent results on the effects of temperature[12] and additives[17] in the irradiation of polyethylene appear to support this idea. In other hydrocarbon systems definite evidence that a significant fraction of the $H_2$ is formed by molecular elimination is provided by the work of Dorfman with $C_2H_6$–$C_2D_6$ mixtures in the gas phase[18], paraffin-deuterated paraffin mixtures in the condensed phase[19] and by Dewhurst for solid and liquid *n*-hexane.[20]

In polyvinyl chloride, infrared absorption analysis at 10.35 $\mu$ for vinylene unsaturation is complicated by an existing band in the 10.3–10.4 $\mu$ region for the unirradiated polymer.[21] At present, therefore, there is no direct measurement of possible vinylene formation by a molecular expulsion of HCl.

The $C_2H_3^+$ and $C_2H_2^+$ ions, which result from the loss of three and four atoms from the parent molecules, are present in appreciable quantities in the mass spectra of both ethane and ethyl chloride. At the present time, it is not known whether the analogous processes are important in the radiolysis of polyethylene and polyvinyl chloride.

## Conclusion

It is concluded that in the radiolysis of polyvinyl chloride, the predominant primary free-radical process is C–Cl scission to produce the stable $-CH_2\dot{C}H-$ (C) polymer radical. On the other hand, evidence from liquid phase free-radical studies indicates that attack by alkyl radicals (from peroxides, for example) on this type of structure results in a preferential abstraction of a tertiary hydrogen atom[22,23] to produce the $-CH_2-\dot{C}(Cl)-$ (A) type radical. It is not unlikely that as the reaction temperatures are increased, the hydrogen abstraction would become less specific and increasing attack on the methylene hydrogens would occur, producing the unstable $-\dot{C}HCH(Cl)-$ (B) polymer radical as well. This suggests that for free radical processes in PVC, such as cross-linking and graft-copolymerization, initiation by radiation at ordinary temperatures is fundamentally different and may be more effective than initiation by chemical agents (*i.e.*, peroxides) at elevated temperatures. It is clear that in this regard, PVC differs from the polyethylene structure, where the same polymer radical, $-CH_2\dot{C}H-$, is presumably formed by either method (radiation or peroxide) of initiation.

Apart from its radiation chemical aspects, this work also suggests that ionizing radiation may be used as a tool for studying the decomposition mechanisms, under controlled conditions, in PVC and related polymers, such as polyvinylidene chloride. Of particular significance is the ease with which the chain dehydrochlorination occurs even at room temperature, once the reaction is initiated and provided that no free-radical scavengers are present.

Finally, some conclusions regarding the use of PVC as a radiation dosimeter[24,25] may be made. The present results, as well as previous work,[1] show that the radiation-induced discoloration and HCl formation are quite sensitive to temperature, oxygen and other free-radical inhibitors, and to post-irradiation storage conditions. For reproducible dosimetry, it would appear, therefore, that the following factors are critical and should be specified: grade of PVC (purity, and possible copolymer content), temperature and atmosphere during exposure. In an air atmosphere, where diffusion of oxygen into the PVC film can become important, even the film thickness and radiation intensity may influence the changes produced in the PVC film dosimeter.

**Acknowledgment.**—The author is indebted to R. S. Powell for the e.p.r. measurements, J. S. Balwit for the irradiations, and to Dr. F. J. Norton for the determination of the ethyl chloride mass spectrum.

(16) A. A. Miller, E. J. Lawton, J. S. Balwit, THIS JOURNAL, **60**, 599 (1956).

(17) M. Prober, Abstracts ACS Meeting, Chicago (1958), Paper No. 94, Div. of Polymer Chem.

(18) L. M. Dorfman, THIS JOURNAL, **60**, 826 (1956); **62**, 29 (1958).

(19) L. M. Dorfman, private communication.

(20) H. A. Dewhurst, THIS JOURNAL, **62**, 15 (1958).

(21) R. R. Stromberg, S. Straus and B. G. Achhammer, *J. Research Natl. Bur. Standards*, **60**, 147 (1958).

(22) M. S. Kharasch and G. Buchi, *J. Am. Chem. Soc.*, **73**, 632 (1951).

(23) A. S. Kenyon, "Polymer Degradation Mechanisms," Natl. Bur. Standards, 1953, p. 81.

(24) E. J. Henley and A. Miller, *Nucleonics*, **9** [6], 62 (1951).

(25) C. Artandi and A. A. Stonehill, *ibid.*, **16** [5], 118 (1958).

# THE EFFECT OF MONOCARBOXYLIC ACIDS AND THEIR DERIVATIVES ON THE TRICHLOROACETATE ION

BY LOUIS WATTS CLARK

*Contribution from the Department of Chemistry, Saint Bonaventure University, Saint Bonaventure, N. Y.*

*Received April 2, 1959*

Kinetic data are reported on the decomposition of potassium trichloroacetate in acetic acid, propionic acid, butyric acid and monochloroacetic acid. The constants of the Eyring equation are evaluated. The data support the hypothesis previously enunciated that a transition complex is formed, prior to cleavage, involving coördination between the electrophilic carbonyl carbon atom of the trichloroacetate ion and the unshared pair of electrons on the nucleophilic atom of the solvent molecule.

Kinetic studies by Verhoek and others[1] on the decomposition of trichloroacetic acid and its salts in various solvents revealed that the reaction velocity is dependent upon the concentration of the trichloroacetate ion and is first order in the presence of an excess of solvent. Verhoek found that the salts of trichloroacetic acid decompose in isoamyl alcohol, ethyl alcohol, ethyl acetate, acetic acid and acetone, but that trichloroacetic acid itself does not decompose in boiling acetic acid.[1a]

Kinetic studies on the decomposition of trichloroacetic acid in aromatic amines[2] indicated that a transition complex is probably formed, prior to cleavage, involving coördination of the electrophilic carbonyl carbon atom of the trichloroacetate ion and the unshared pair of electrons on the nucleophilic nitrogen atom of the amine.

The fact that the salts of trichloroacetic acid undergo decarboxylation in acetic acid appeared to offer a means of further testing the transition complex theory of the decomposition of the ion. The oxygen atom in the hydroxyl group of acetic acid and its homologs would be expected to possess the characteristics of a Lewis base, offering opportunity for attack by a strongly electrophilic agent. Inductive and steric effects could be tested by introducing suitable substituents into the acetic acid molecule. With this in view kinetic studies were carried out in this Laboratory on the decomposition of potassium trichloroacetate in acetic acid, propionic acid, butyric acid and chloroacetic acid. The results of these experiments, which are recorded herein, afford additional evidence in support of the transition complex theory and likewise reveal some interesting properties of the reagents used in the investigation.

## Experimental

**Reagents.**—(1) Potassium trichloroacetate, reagent grade, 1000.0% assay, was used in this investigation. (2) The solvents, acetic acid, propionic acid, butyric acid and monochloroacetic acid, were reagent grade chemicals which were freshly distilled, at atmospheric pressure, directly into the reaction flask, immediately before the beginning of each decarboxylation experiment.

**Apparatus and Technique.**—The apparatus and technique used in this investigation, involving measuring the volume of $CO_2$ evolved with time at constant pressure, were the same as those used in studying the decarboxylation of trichloroacetic acid in glycerol.[3-4] Temperatures were determined by means of a thermometer calibrated by the U. S. Bureau of Standards. In each experiment a 330-mg. sample of potassium trichloroacetate (the amount required to produce 40 ml. of $CO_2$ at STP on complete reaction) was introduced in the usual manner into the reaction flask containing approximately 50 ml. of solvent saturated with dry $CO_2$ gas.

## Results

When the corrected volumes of $CO_2$ were plotted against time and graphs made of the log $(a - x)$ *vs.* $t$ (where $a$ is the maximum theoretical yield of $CO_2$ and $x$ is the volume evolved at time $t$) from representative points on the smoothed experimental plots, straight lines resulted for the first 75% or so of the reaction. The value of the specific reaction velocity constant appeared to decrease somewhat during the latter part of the reaction, due, perhaps, to a partial transformation of the trichloroacetate ion into the stable trichloroacetic acid molecule by the taking up of a proton from the medium. No appreciable difference in the specific reaction velocity constant for the reaction at a given temperature could be observed when the quantity of solvent used was varied from 45 to 65 ml. (see ref. 2). Generally two experiments were carried out at each temperature. The average rate constants calculated in the usual manner from the slopes of the experimental logarithmic plots are brought together in Table I. The parameters of the Eyring equation, based upon the data in Table I, are shown in Table II. Data for the decomposition of the trichloroacetate ion in water, and of trichloroacetic acid in aniline, previously reported, are included in the table for purposes of comparison.

TABLE I

APPARENT FIRST-ORDER RATE CONSTANTS FOR THE DECARBOXYLATION OF POTASSIUM TRICHLOROACETATE IN VARIOUS LIQUIDS

| Solvent | Temp. (°C. cor.) | $k \times 10^4$ (sec.$^{-1}$) |
|---|---|---|
| Acetic acid | 100.89 | 0.396 |
| | 106.70 | 0.835 |
| | 115.20 | 2.380 |
| Propionic acid | 117.96 | 1.470 |
| | 126.44 | 4.080 |
| | 135.81 | 9.660 |
| Butyric acid | 109.80 | 0.440 |
| | 123.16 | 2.170 |
| | 138.04 | 11.200 |
| Monochloroacetic acid | 156.96 | 1.560 |
| | 163.27 | 3.570 |
| | 168.10 | 6.720 |

## Discussion of Results

As seen in Table II, lines 1, 2 and 3, the enthalpy of activation for the decomposition of the trichloroacetate ion changes only slightly on going from acetic acid to propionic acid, and from propionic acid to butyric acid. This is to be expected in view of the fact that all the fatty acids except formic acid are known to have very nearly the same ionization constants, hence all have about the

(1) (a) F. H. Verhoek, *J. Am. Chem. Soc.*, **56**, 571 (1934); (b) **67**, 1062 (1945); (c) G. A. Hall, Jr., and F. H. Verhoek, *ibid.*, **69**, 613 (1947); (d) C. N. Cochran and F. H. Verhoek, *ibid.*, **69**, 2987 (1947).

(2) L. W. Clark, THIS JOURNAL, **63**, 99 (1959).

(3) L. W. Clark, *J. Am. Chem. Soc.*, **77**, 3130 (1955).

(4) L. W. Clark, THIS JOURNAL, **60**, 1150 (1956).

TABLE II

KINETIC DATA FOR THE DECARBOXYLATION OF THE TRICHLOROACETATE ION IN VARIOUS LIQUIDS

| Solvent | $\Delta H^{\ddagger}$ (cal.) | $\Delta S^{\ddagger}$ (e.u.) | $\Delta F_{90^\circ}^{\ddagger}$ (cal.) | $k_{90^\circ} \times 10^4$ (sec.$^{-1}$) |
|---|---|---|---|---|
| Acetic acid | 35,500 | +15.6 | 29,800 | 8.5 |
| Propionic acid | 35,300 | +13.8 | 30,300 | 4.8 |
| Butyric acid | 35,100 | +12.7 | 30,500 | 2.9 |
| Monochloroacetic acid | 48,900 | +36.9 | 35,500 | 0.004 |
| Water[1a] | 34,800 | +20.9 | 27,200 | 30.0 |
| Aniline[2] | 24,500 | − 2.57 | 25,400 | 33.0 |

same acid strength, which is equivalent to saying that they all are about equally basic in the Lewis sense. In propionic acid we have a methyl group added to acetic acid, which would be expected to exert a small positive inductive effect, increasing the effective negative charge on the hydroxyl oxygen atom. Since an increase in the attraction between two reagents lowers the enthalpy of activation,[5] the fact that $\Delta H^{\ddagger}$ is lower for the decomposition of the trichloroacetate ion in propionic acid than for the reaction in acetic acid suggests that a transition complex is formed between the unshared pair of electrons on the oxygen atom of the hydroxyl group and the electrophilic carbonyl carbon atom of the trichloroacetate ion. In butyric acid we have an ethyl group added to acetic acid. Since the +I effect of the ethyl group is larger than that of the methyl group we would expect the effective negative charge on the oxygen of the hydroxyl group of butyric acid to be slightly greater than that in the case of propionic acid—this would manifest itself by a slight decrease in $\Delta H^{\ddagger}$, which is actually observed.

For the decomposition of the trichloroacetate ion in acetic acid $\Delta S^{\ddagger}$ has a rather large positive value (line 1, Table II). This may be interpreted as representing a rather high probability of formation of the activated state and is related to the complexity of the molecule. In the case of acetic acid we are dealing with a relatively small molecule and the observed value of $\Delta S^{\ddagger}$ is correspondingly large. In the case of aniline, a relatively more complex molecule than acetic acid, the value of $\Delta S^{\ddagger}$ is seen to be much lower (line 6, Table II). The addition of a methyl group to acetic acid to form propionic acid increases the complexity of the molecule. This would be expected to act to sterically hinder the approach of the electrophilic agent and hence lower the probability of formation of the activated state, resulting in a decrease in $\Delta S^{\ddagger}$. The experimental results are observed to be in accordance with this prediction (line 2 of Table II). The addition of an ethyl group to the acetic acid to form butyric acid would be expected to increase the steric effect still more, resulting in a further decrease in $\Delta S^{\ddagger}$ which is actually observed (line 3, Table II).

Alkyl groups exert a +I effect. It was thought of interest to investigate the effect on the reaction of a substituent which can exert a −I effect. The compound selected for this study was monochloroacetic acid. A chlorine atom introduced into the methyl group of acetic acid would be expected to exert a very strong −I effect. This would greatly decrease the effective negative charge on the oxygen atom of the hydroxyl group, thereby greatly increasing the acid strength and correspondingly lowering the basicity. It would be expected, therefore, that $\Delta H^{\ddagger}$ for the reaction in monochloroacetic acid should be considerably greater than in acetic acid. Such indeed is seen to be the case, as $\Delta H^{\ddagger}$ increases from 35,480 cal. in acetic acid to 48,860 cal. in monochloroacetic acid (lines 1 and 4, Table II).

In monochloroacetic acid it is observed that $\Delta S^{\ddagger}$ has a much larger positive value than in acetic acid, despite the fact that the halogen substituted acid is a more complex molecule than acetic acid itself. One would expect that the attacking agent would encounter more steric hindrance in approaching the nucleophilic center of the monochloroacetic acid than in the case of acetic acid, giving rise to a decrease in $\Delta S^{\ddagger}$ instead of the large increase which is actually observed. The explanation of this apparent anomaly is probably connected with the fact that the weaker acids such as acetic acid, propionic acid, etc., exist largely in dimer form in the pure liquid state, where also extensive coassociation obtains, whereas a stronger acid such as monochloroacetic acid cannot dimerize and coassociation is probably negligible in the liquid state. Actually, therefore, monochloroacetic acid represents a simpler molecular species than acetic acid in spite of the symbolism conveyed by the structural formulas.

Comparing the results of the present investigation with data calculated on the basis of information reported by Verhoek for the decomposition of the trichloroacetate ion in water, it is seen that $\Delta H^{\ddagger}$ for the reaction in water is only very slightly less than that for acetic acid or its homologs (line 5, Table II). This would appear to indicate that the acyl group exerts a rather small −I effect with respect to hydrogen and shows that the effective negative charge on the oxygen atom of the water molecule is only slightly greater than that in the case of the hydroxyl group of acetic acid.

Comparing the $\Delta S^{\ddagger}$ values for the reaction in monochloroacetic acid and in water it is seen that, although water is a smaller and much simpler molecule than the monochloroacetic acid the $\Delta S^{\ddagger}$ for the reaction in water is much smaller than in the case of the chloroacetic acid. Again this apparent anomaly is probably tied up with the coassociation of water molecules and the absence of coassociation in molten monochloroacetic acid.

It is interesting to note that the trichloroacetic acid ion decomposes in water at about the same rate as in aniline at 90° (lines 5,6, Table II). Aniline is a much stronger base than water as revealed by the very large lowering of $\Delta H^{\ddagger}$ on going from water to aniline. However, aniline is a more complex molecule than water as shown by the low negative value of $\Delta S^{\ddagger}$ in the amine. Despite the weakly basic character of the water substance as compared with aniline, the smaller size of the water molecule, by enhancing the probability of the formation of the activated state, acts to overcome the disadvantage occasioned by the higher heat of activation,

(5) K. J. Laidler, "Chemical Kinetics," McGraw-Hill Book Co., Inc., New York, N. Y., 1950, p. 138.

so that $\Delta F^{\ddagger}$ in the two liquids is roughly comparable and the reaction is able to proceed at nearly the same rate in these two diverse liquids.

The data in Table II appear, therefore, to substantiate fully the transition complex theory of the mechanism of the decomposition of the trichloroacetate ion. Further studies of this interesting reaction are contemplated.

**Acknowledgments.**—(1) The potassium trichloroacetate used in this research was kindly supplied by Dr. James D. Solomon, St. Elizabeth's Hospital, Washington, D. C. (2) Assistance in running some of the kinetics experiments was rendered by Edward Luke and Richard A. Ymilik. (3) This research was supported in part by the National Science Foundation, Washington, D. C.

# ATOMS AND FREE RADICALS BY $\gamma$-IRRADIATION AT 4.2°K.[1]

BY LEO A. WALL, DANIEL W. BROWN AND ROLAND E. FLORIN

*National Bureau of Standards, Washington 25, D. C.*

*Received April 10, 1959*

In nitrogen, hydrogen and deuterium at 4.2°K. radiolysis produces atoms which are immobilized. They were identified by electron spin resonance (e.s.r.). In irradiated methane both hydrogen atoms and methyl radicals were found in approximately equal amounts. Repeated irradiation of the same samples in all cases led to more efficient production of active species. Added oxygen (0.07%) reduced the nitrogen atom yield of the initial run. Yields were studied as a function of irradiation dose. The maximum nitrogen atom concentration attained in solid nitrogen was 0.06%, while in irradiated methane 0.15% of hydrogen atoms and 0.14% of methyl radicals were attained. Because of saturation of the e.s.r. spectra, the results with hydrogen and deuterium are low. High-energy radiation at low temperatures in general appears to be a useful and promising method for the production of stabilized free radicals or atoms.

## Introduction

For the elucidation of the mechanism of the processes induced by high-energy radiation, information about the identity and kinetic properties of the short-lived intermediates is essential. Quite a number of investigators[2-4] have shown that radicals are produced in various irradiated substances. At 300°K. radicals in irradiated polymers have in many cases exhibited extremely long lifetimes.[5-7] It was anticipated that at liquid helium temperatures very small and active radicals or atoms would be immobilized or stabilized, although the efficiency for their production might decrease with temperature. In the present investigation the main objective was to identify species produced by irradiation and to measure the efficiency of production and the concentrations attained.

The materials studied were nitrogen, methane, hydrogen and deuterium. Mixtures of rare gases containing nitrogen were also investigated. At the beginning of this work considerable evidence[8-10] was available for the presence of atoms in the condensation products from electrical discharges in various gases. Accurate estimates of concentrations in such systems, however, are rarely, if ever, available. Electron spin resonance (e.s.r.) spectroscopy, which has been used to indicate atoms and radicals in various solids,[9,10] was used in this work to detect the radical species. In the major portion of the work both the $\gamma$-irradiation and the e.s.r. measurement were carried out at 4.2°K. The samples were also in general maintained at 4.2°K. between the time of their irradiation and e.s.r. study.

## Experimental

Irradiation Source.—The irradiations to be described were performed with a 2000-curie cobalt-60 source shielded by water. The dose rate was determined with a ferrous sulfate dosimeter; a $G$-value of 15.5 was used. On January 31, 1957, the rate of energy deposition in water was $0.41 \times 10^{20}$ e.v./g. hr. and was corrected to current dates in accordance with the known decay rate of the cobalt. It was assumed that the rate of energy deposition varied as the electron density (e.v./g.) of the irradiated material.

Dewar System.—The irradiation vessel is sketched to scale in its position in the source in Fig. 1. The dewars are separate glass vessels whose capacities are such that 5.5 l. of liquid helium is surrounded by 6 l. of liquid nitrogen. More liquid nitrogen capacity would have been desirable since the level of nitrogen dropped faster than that of the helium.

The outer polyethylene hose and inner Tygon hose carry the evolved gases up through the surrounding water. The use of two hoses as shown and two gas meters permits measurement of the individual amounts of helium and nitrogen evolved. From these measurements one knows at all times how much of each coolant is left in the dewars. Rubber tubing fails very quickly in these applications because the liquid nitrogen contains enough oxygen to form ozone. Some of this ozone is evolved with the nitrogen and severely atacks the rubber tubing.

The evaporation rate of the helium in liters of liquid/hour was about 0.090 in the source and 0.030 out of it. The difference results largely from energy absorbed from the radiation by the dewar walls. Experiments with a 1.5-liter cryostat that did not incorporate the lead shielding gave a value about twice as high. After about 4 months intermittent use the rate in the source had increased by 30% while the value out of the source was unchanged. Apparently diffusion of helium occurs into the vacuum space. The unchanged rate out of the source would follow if the diffused helium were slowly adsorbed on the wall at low temperatures but desorbed by radiation.

By filling the nitrogen jacket every 12 hours, runs could be extended to more than 48 hours with one filling of liquid helium. Even then, more liquid helium could be added without warming up the samples if the helium transfer siphon

(1) This research project under the Free Radical Research Program has been supported by the Department of the Army.

(2) R. Livingston, H. Zelde and E. H. Taylor, *Disc. Faraday Soc.*, **19**, 166 (1955).

(3) E. E. Schneider, *ibid.*, **19**, 158 (1955).

(4) M. S. Matheson and B. Smaller, *J. Chem. Phys.*, **23**, 521 (1955).

(5) W. B. Ard, H. Shields and W. Gordy, *ibid.*, **23**, 1727 (1955).

(6) R. J. Abraham and D. H. Whiffen, *Trans. Faraday Soc.*, **54**, 1291 (1958).

(7) L. A. Wall and D. W. Brown, *J. Research Natl. Bur. Standards*, **57**, 131 (1956).

(8) H. P. Broida, *Endeavour*, **17**, 68 (1958).

(9) C. K. Jen, S. N. Foner, E. L. Cochran and W. A. Bowers, *Phys. Rev.*, **104**, 846 (1956).

(10) S. N. Foner, C. K. Jen, E. L. Cochran and W. A. Bowers, *J. Chem. Phys.*, **28**, 351 (1958).

were precooled and not allowed to dip below the helium level in the radiation dewar.

The samples were prepared on a high-vacuum line, and the quantities were calculated from the perfect gas laws. According to manufacturers' data the purities were: nitrogen, 99.996%; methane, 99.83%; argon 99.9%; xenon, 99.92%; hydrogen, 99.9%; and deuterium, 99.5%. The sample tubes were made of quartz; that part which fitted into the e.s.r. cavity was the high purity type, which develops little signal when irradiated. About $3 \times 10^{-3}$ mole of sample were used. About seven samples were irradiated simultaneously.

A glass liquid helium dewar, shown in Fig. 2, was used for the e.s.r. determinations. Its capacity of about 1 liter of liquid helium permitted e.s.r. measurements to be continued for about 2 hours. All e.s.r. spectra reported here have been determined in liquid helium.

Samples were transferred from the radiation dewar to the resonance dewar by removing the transfer dewar with samples and placing it in the resonance dewar after the latter had been partially filled with helium. The height of helium in the resonance dewar was such that the samples could be lifted over the edge of the transfer dewar and placed as shown without removing the lower 10–15 cm. portion of the sample tubes from liquid helium. The transfer dewar was removed and the polyethylene bag put in place.

The chief difficulty was that small particles of air condensed in the resonance dewar during the transfer operation. The packing, inverted funnel and cap prevented the air from collecting in the tip. On occasion this air prevented helium from circulating around the sample tube in the tip and such samples warmed up. Once the polyethylene bag was in place, air no longer condensed. The cap was removed and the samples inserted in the tip as desired with the bag in place. This dewar could also be refilled without warming up the samples if the precautions previously mentioned were followed.

**Electron Spin Resonance.**—The e.s.r. machine was a standard Varian-4500, which plots the derivative of the absorption curve if small modulating amplitudes are used. The tip of the resonance dewar fitted into a rectangular cavity with an enlarged hole. The cavity was kept at room temperature, which permitted easy adjustment of the iris and eliminated seals in the wave guide. The frequency was about 9086 megacycles with the dewar shown. Line spacings, widths and positions were estimated from manufacturers' data and standard resonances such as the hydrogen doublet and diphenyl-picrylhydrazyl (DPPH). The resonances were obtained at the lowest power convenient, around 1 milliwatt, to minimize saturation effects. Several spectra were obtained at different powers in order to estimate the effect of saturation.

Quantitative estimates were made by integrating the recorder plots to obtain the absorption curve, correcting them for saturation where data had been taken with different powers, and then integrating the absorption curves. The resulting area is related to that obtained at the same machine conditions from a calibrating material such as DPPH at room temperature by the expression[11]

$$N_s = \frac{T_s A_s (S_0)(S_0 + 1) N_0}{T_0 A_0 (S_s)(S_s + 1)}$$

$S$ = total spin quantum number
$A$ = area under the absorption curve
$T$ = absolute temperature
$N$ = number of atoms or radicals

The subscripts s and o refer to sample and calibrating material, respectively. The total spin was 3/2 for nitrogen atoms and 1/2 for all the other species considered here.

When the absorption curve was calculated by integrating the recorder plots from the outside to the center of the resonance, it was usually found that areas under the two halves of the absorption curve differed by 10–20%. This implies that the composite area is probably inaccurate by about this percentage. The resonance from the quartz does not contribute appreciably to the calculated areas except with the weakest resonances.

The magnitude of $N_0$ appreciably affects the result since it was observed that the sensitivity, measured in area under the absorption curve per spin, decreases by 50% as $N_0$ is initially increased and then becomes independent of $N_0$. There is a reversible change in the crystal leakage current between non-resonant and resonant conditions which parallels the change in $N_0$, and the decrease in sensitivity occurs between maximum leakage current changes of 5 and 30 μ amp. The region of constant sensitivity extends up to a leakage current change during resonance of 200 μamp. Since most of the sample resonances changed the leakage current by 30 to 280 μamp. the $N_0$ used in the calculations was of such size that it brought about a leakage current change in this range.

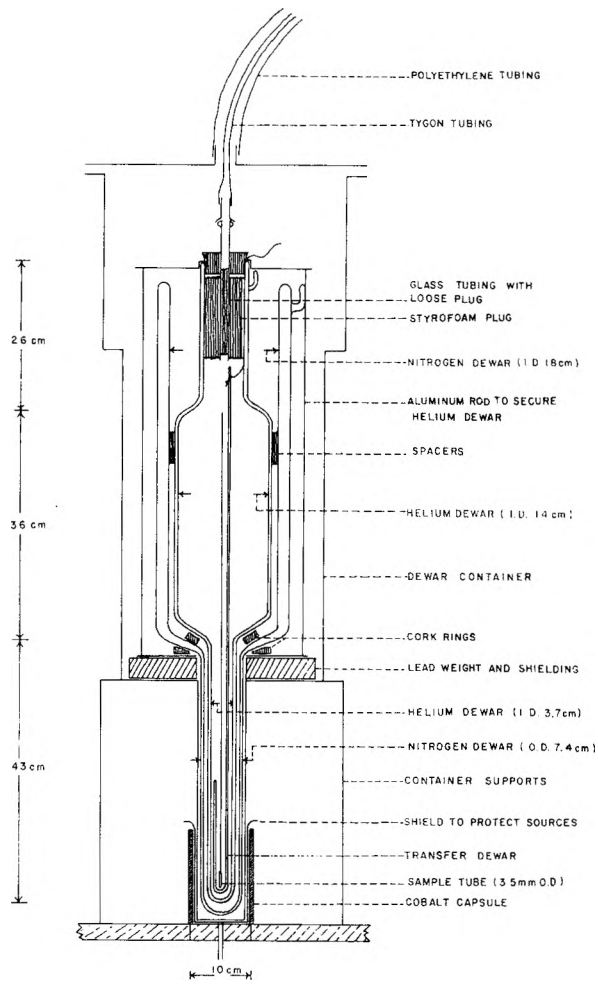


Fig. 1.—Dewar system for γ-irradiation at 4.2°K.

In the calculations $T$s and $T_0$ were taken to be 4.2 and 298°K., respectively. Attempts were made to determine the actual temperature in the tip by measuring the voltage from a thermocouple in a typical sample tube placed in the tip and also by comparing the areas under the absorption curves of a sample of DPPH in liquid helium and at room temperature. The former method indicated only that the temperature was less than 6°K. while the latter method indicated it was 4.6° K. if the effect of the increased leakage current change during the low temperature run was included in the calculation. The difference between 4.2 and 4.6° K. is less than the uncertainty in the double integrations so 4.2°K. was used as the sample temperature. The calculated concentration is directly proportional to the temperature assumed. Substitution of $CuSO_4 \cdot 5H_2O$ as a calibrating material changes the results of the calculations by about 10%. From the above observations it is concluded that the real concentrations should be within 40% of the calculated values when the extent of saturation is known.

By applying voltage to a widely spaced nichrome coil wound on the tip of the resonance dewar, samples could be heated up even though surrounded by liquid helium. The irradiated nitrogen samples emitted light when so treated.

(11) D. J. E. Ingram, "Free Radicals," Academic Press, Inc., New York, N. Y., 1958.

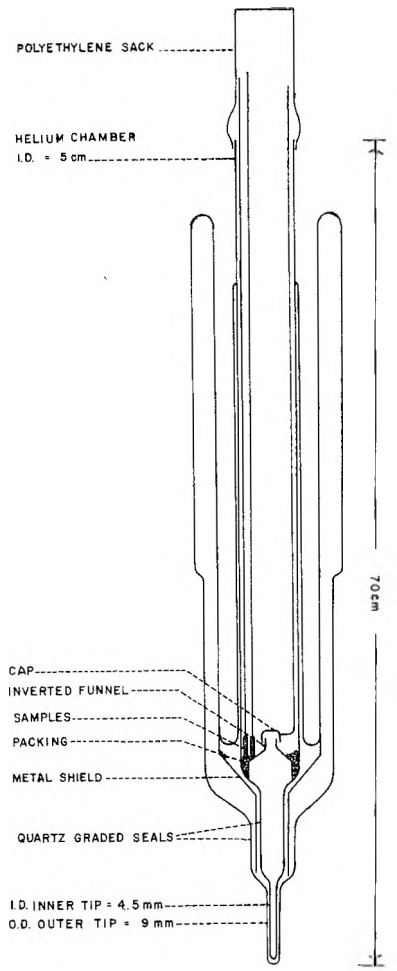


Fig. 2.—Dewar system for e.s.r. measurements at 4.2°K.

The spectrum was substantially the same as that emitted by condensed discharged $N_2$.[8] Similarly an irradiated mixture of nitrogen and argon was found to emit blue light as do discharged nitrogen and argon.

## Results

**Irradiation of Nitrogen.**—The e.s.r. spectra (see Fig. 3) observed for $\gamma$-irradiated nitrogen showed more than the three expected hyperfine lines,[10] centered around g of about 2, due to the introduction of the $N^{14}$ nuclear spin. An additional four small satellites were seen.[12] These have also been recently observed in the condensed discharge products of nitrogen,[13] and an interpretation was advanced[14] based on a zero field splitting due to crystal field effects. Also shown in Fig. 3 are the spectra for $\gamma$-irradiated $N^{15}_2$ and $N_2$ in xenon and in argon. Nitrogen-15 gives six lines. The small line in the center is very likely due to the $N^{14}$ impurity, which was 8.2 atom %. In xenon at low doses and also in neon and hydrogen, which are not shown, $N^{14}$ atoms give resonances like spectrum D, Fig. 3. These are identical with that for irradiated nitrogen, except for intensity. Between 3.7 and 13.4 $\times$ $10^{20}$ e.v./g. the N-atom resonance in the xenon mixture changes to forms in which broadening causes the larger satellites to appear as shoulders on the major peaks. Spectrum C is the most extreme version of this type obtained so far. None of the other atom spectra, either of N atom-containing samples or of irradiated $H_2$, $D_2$ or $CH_4$, had lines whose width was dose-dependent over the ranges studied. The intensities, of course, increased markedly with dose.

In the argon mixture irradiated at 4.2°K. only three broad lines are seen. The sample irradiated at 20°K., which gave a considerably less intense spectrum, shows definitely 9 lines with less splitting of the weak lines, suggesting a different crystal field effect.

In Fig. 4 the concentrations of atomic nitrogen in irradiated bulk nitrogen are plotted as a function of dose. For nitrogen, a $M_R$. is equivalent to 0.54 $\times$ $10^{20}$ e.v. absorbed/g. Spectra at two different powers were obtained at both 33.6 and 6.4 $\times 10^{20}$ e.v./g. The saturation correction, which is included in Fig. 4, amounted to 10 and 25% of the plotted values at 33.6 and 6.4 $\times$ $10^{20}$ e.v./g., respectively. A linearly interpolated saturation correction was applied to intermediate points. Increased spin–spin interaction should decrease saturation effects at higher atom concentrations.

One of the first general observations made was that samples used a second or third time produced stronger e.s.r. signals. For all runs on the upper line the nitrogen sample had been irradiated previously. Fresh samples, which had no prior dose of irradiation, produced the lower line in Fig. 4. Although usually the points at high doses had more preirradiation than those at low doses, the two points at about 19 $\times$ $10^{20}$ e.v./g. were obtained before and after the large 33.6 $\times$ $10^{20}$ e.v./g. dose.

Between irradiations the sealed sample tubes were stored at room temperature, where their contents were in the gaseous state. Hence, it is safe to assume that no atoms or radicals could survive under these conditions.

However, preirradiation causes what appears to be a removal or a consumption of impurities that have an initial inhibiting effect on the production of atom or radical species. This phenomenon was found with all the materials studied. Since traces of oxygen were suspected, a definite amount, 0.07%, of $O_2$ was added to one sample of $N_2$ and a very low yield of N atoms was found (see closed triangle point in Fig. 4). Storage at 4.2°K. produced no observable decay in N-atom concentration. The highest point in Fig. 4 was obtained 19 hr. after its companion point just below it. During this period the sample was stored in the absence of $\gamma$-radiation at 4.2°K. The apparent increase is very suggestive and invites numerous speculations. However, until further work is carried out it is assumed that the e.s.r. technique is subject to this degree of fluctuation. The average $G$ for the 33.6 $\times$ $10^{20}$ e.v./g. points is about 0.4 N atoms/100 e.v.

Table I shows the effect of added materials on the yield of N-atoms in mixtures of $N_2$ and other materials. From left to right the table headings give the concentration of $N_2$ in mole and electron fraction, the other component, the dose, the over-all

(12) L. A. Wall, D. W. Brown and R. E. Florin, *J. Chem. Phys.*, **30**, 602 (1959).

(13) C. K. Jen and S. N. Foner, private communication.

(14) T. Cole and H. M. McConnell, *J. Chem. Phys.*, **29**, 451 (1958).

mole % of N-atoms, the over-all $G$, and a relative efficiency factor $\phi$, which is the fraction of $N_2$ converted to atoms in the mixture divided by the fraction of $N_2$ converted to atoms in bulk nitrogen at the same dose and temperature. These figures in Table I are not corrected for saturation except where indicated, and so the factor $\phi$ as calculated may be in error to a certain extent. The measurements with bulk nitrogen indicated the denominator of $\phi$ would be increased by less than 25% because of saturation. Hence $\phi$ would be decreased by less than this percentage. The saturation correction increased the concentration obtained in the argon and $N_2$ mixture by 50% and so is more important than with bulk $N_2$. Saturation was not measured with the other mixtures. Where $\phi$ is more than 1, the fraction of available nitrogen converted to N atoms has been increased relative to the same fraction from bulk nitrogen.

TABLE I

NITROGEN ATOMS FORMED BY γ-RADIATION OF MIXTURES AT 4.2°K.

| System mf$N_2$ | ef$N_2$ | Other component | Dose,[a] e.v./g. × $10^{-20}$ | Concn. of N % of total molecules | $G$, N/100 e.v. over-all | $\phi$[b] |
|---|---|---|---|---|---|---|
| 0.2 | 0.062 | Xe | 15.8[c] | 0.013 | 0.049 | 2.8 |
| .2 | .062 | Xe | 11.1 | .0096 | .051 | 3.5 |
| .2 | .062 | Xe | 16.6 | .018 | .064 | 3.8 |
| .2 | .062 | Xe | 28.9 | .022 | .045 | 1.8 |
| .01 | .008 | Ar | 16.5[c] | .00054[d] | .0049 | 2.5 |
| .01 | .008 | Ar | 30.3 | .00069[d] | .0034 | 1.1 |
| .05 | .039 | Ar | 18.2[c,e] | .00017 | .0014 | 100 |
| .05 | .068 | Ne | 18.3[c] | .0024 | .038 | 2.2 |
| .05 | .068 | Ne | 4.0 | .00051 | .031 | 3.3 |
| .14 | .53 | $H_2$ | 23.5[c] | .00017 | .00077 | 0.058 |

[a] Dose rate 0.57 Mr./hr. = 0.33 × $10^{20}$ e.v./g. hr. [b] $\phi$ = fraction of $N_2$ decomposed in mixture/fraction of $N_2$ decomposed in pure $N_2$ at the same dose and temperature. [c] First irradiation. [d] Saturation correction included. [e] Irradiated at 20°K.

**Irradiation of Methane.**—The e.s.r. spectrum of irradiated methane consisted of a quartet, centered about $g = 2.0$ and a pair of lines, obviously the hydrogen doublet with a separation near 500 gauss (see top spectrum in Fig. 5). When this methane sample was accidentally warmed slightly during a helium refill and then observed again at 4.2°K., the hydrogen lines had disappeared. The quartet (see second spectrum, Fig. 5) was somewhat diminished and considerably sharpened. The fully shaped lines in these spectra suggest less power saturation than in the hydrogen experiments. A somewhat puzzling aspect is that while the line widths in irradiated methane spectra did not change between 1.5 and 24.6 × $10^{20}$ e.v./g. the line width of the methyl radical decreased during warm up. The line shapes suggest overlapping spectra and possibly hyperfine dipolar broadening.

Although considerably more elusive, signals were observed for hydrogen and deuterium atoms in hydrogen and deuterium irradiated at 4.2°K. However, the lines did not have the correct derivative form[15] and were fairly weak (see lower two spectra, Fig. 5). The center line in these two spectra has the general characteristics of the quartz resonance. It probably obscures the center line of the D-atom spectra since the other hyperfine components are weak. We have observed that lines having a rough derivative appearance are obtained if large modulating amplitudes are used. The appearance of the hydrogen lines in the deuterium run suggests some energy transfer leading to preferential dissociation of the weaker H–H or H–D bonds rather than the D–D bonds, since these lines, though small, are relatively greater than would be expected on the basis of the concentration of hydrogen impurity in the deuterium.

In Table II the results on 4.2°K. irradiated methane, hydrogen and deuterium are listed. The $G$-values in the case of H atoms in irradiated $H_2$ and

(15) C. K. Jen, S. N. Foner, E. L. Cochran and V. A. Bowers, *Phys. Rev.*, **112**, 1169 (1958).

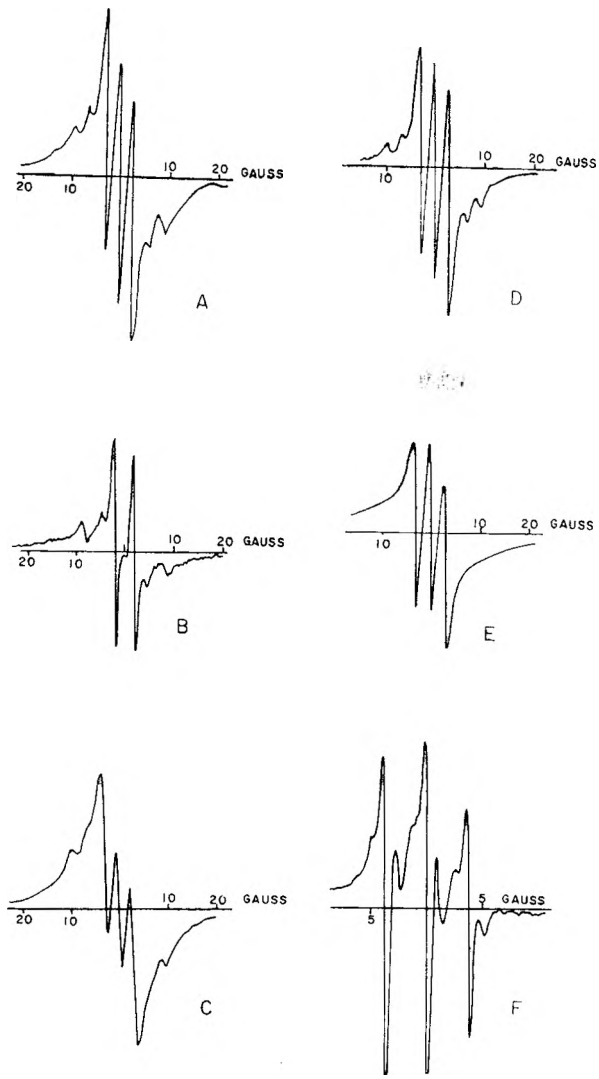


Fig. 3.—E.s.r. spectra found with nitrogen-containing specimens.

| | Sample | Irradiation temp., °K. | (Signal/noise)$_{max}$ | Modulating field amplitude, gauss |
|---|---|---|---|---|
| A | $N_2$ | 4.2 | >100 | 0.22 |
| B | $N_2^{15}$ | 4.2 | 20 | .035 |
| C | $N_2$/Xe-1/5 | 4.2 | >100 | .22 |
| D | $N_2$/Xe-1/5 | 4.2 | 25 | .22 |
| E | $N_2$/Ar-1/99 | 4.2 | 20 | .9 |
| F | $N_2$/Ar-1/19 | 20 | 20 | .9 |

TABLE II

RADICALS FORMED BY γ-RADIATION AT 4.2°K.

| System | Pretreatment | Dose, (e.v./g.) × $10^{-20}$ | Radical, % H | Radical, % $CH_3$ | Radicals/100 e.v. |
|---|---|---|---|---|---|
| $CH_4$ | Melted after 52 × $10^{20}$ e.v./g. | 1.5 | 0.0027 | 0.0029 | 1.4 |
| | Melted after 44 × $10^{20}$ e.v./g. | 7.7 | .026 | .015 | 2.0 |
| | Partial warm-up | | .000 | .007 | |
| | Melted after 61 × $10^{20}$ e.v./g. | 24.6 | .11 | .14 | 3.8 |
| | | | H | | |
| $H_2$ | None | 13.2 | (0.0001)[a] | | (0.02)[a] |
| | Melted after 39.4 × $10^{20}$ e.v./g. | 37.2 | ( .0006) | | ( .05) |
| | Melted after 87 × $10^{20}$ e.v./g. | 68 | ( .0003) | | ( .01) |
| | Stored 19 hr. at 4.2°K. | 0 | ( .00015) | | |
| | | | H + D | | |
| $D_2$ | None | 6.7 | (0.0001) | | (0.02) |
| | Melted after 6.6 × $10^{20}$ e.v./g. | 7.4 | ( .0003) | | ( .07) |
| | Melted after 14 × $10^{20}$ e.v./g. | 18.3 | ( .0007) | | ( .06) |

[a] Values in parentheses are minimum estimates.

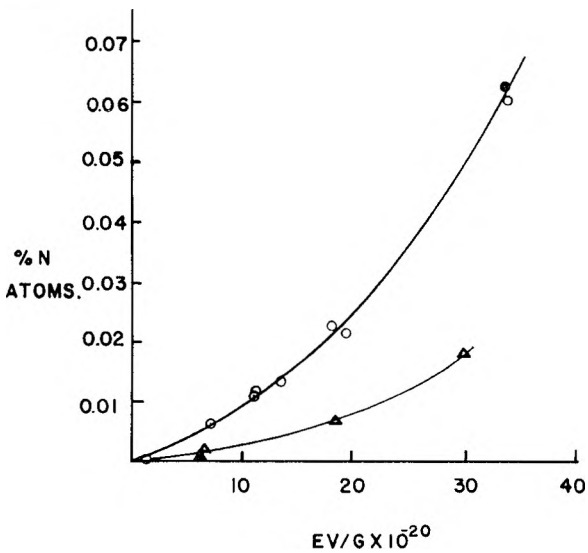


Fig. 4.—Yield of nitrogen atoms with γ-ray dose: ○, sample preirradiated; ●, after 19 hr. storage at 4.2°K.; △, freshly prepared samples; ▲, fresh sample + 0.07% added oxygen.

$D_2$ were calculated by assuming the observed spectrum is half the derivative and calculating by integration in the usual manner. This should give values which are low because of the high degree of power saturation of the spectra, and hence they are listed in parentheses.

Power saturation data were taken with only one sample here — on an H line in the methane sample given the largest dose. The H-atom concentration corrected for saturation would be 0.15% instead of the tabulated 0.11%. Under the second methane entry there is shown the amount of methyl radical remaining after an accidental partial warm up. This result graphically points up the difference in the mobility of the hydrogen atom and methyl radical and implies rapid recombination of H atoms, some recombination of H atoms and methyl radicals and little or no recombination of methyls. Another observation is that at 7.7 × $10^{20}$ e.v./g. there are decidedly more H-atoms than methyl radicals. It is difficult to accept this latter result as meaning that hydrogen atoms are produced or stabilized better than methyl radicals, particularly in view of the reverse observation in the partial warm up. It is more reasonable to suspect saturation effects in the e.s.r. measurements result in relatively less signal from the methyl radical than from the H-atom at the atom concentration achieved at 7.7 × $10^{20}$ e.v./g. The saturation effects became less important at higher concentrations, and a more reasonable ratio of methyl radical to H atom concentrations was observed at 24.6 × $10^{20}$ e.v./g.

The H-atom concentration in irradiated hydrogen was observed to have decayed after storage for 19 hr. at 4.2°K. The sample was handled side by side in the same operation with the sample containing N-atoms, which increased slightly during storage. It is certain no accidental warm up occurred. Considering the system, this was actually slower decay than might have been expected and points to a fairly long lifetime for H-atoms at this temperature. Quite long lifetimes for H atoms in other matrices would then appear to be possible.

## Discussion

**Irradiation of Nitrogen.**—The various e.s.r. spectra give considerable evidence about the nature of the environment of the atoms. For irradiated nitrogen the spectrum is consistently as shown in the top spectrum of Fig. 3. In deposition experiments from electrical discharges the satellite lines were not at first seen[10,16] and do not consistently show up.[13] This suggests that the appearance of satellites reflects the nature of the matrix. In the deposition work the nitrogen lattice is unlikely to be as dense and uniform as in the γ-ray work where the solid nitrogen is formed by freezing the liquid phase.

The irradiated nitrogen spectrum is substantially the same as that published very recently by Cole and McConnell.[14] It is centered about $g = 2.0$ with peak separations of 4.1 ± 0.2 gauss and a total spread of 53 gauss. They advanced the reasonable interpretation that the satellites arise as a result of a zero field splitting due to the crystal field. From this treatment there should be a total of 9 lines, two hidden by the two outer intense lines. The zero field splitting parameter

(16) T. Cole, J. T. Harding, J. R. Pellam and D. M. Yost, *J. Chem. Phys.*, **27**, 593 (1957).

$D$, used in this treatment, is equal to the separation of the first satellite and the first intense line, and correspondingly to other pairs of lines. Its value in our work for $N^{14}$ was 9 ± 1 gauss which corresponds to their 11 ± 2 gauss. Any possibility of species other than nitrogen atoms being present is rather conclusively ruled out by our spectrum (see second spectrum, Fig. 3) produced by irradiated $N_2^{15}$. This material contained 8.2 atom % of $N^{14}$. The prominent central lines are now 2 in number instead of 3, and 2 pairs of satellites are still present on either side of the two intense lines. The central small line is probably from the $N^{14}$ present. A $N_3$ species of 3 equivalent nitrogen atoms should yield a 4-line spectrum with nitrogen-15.

A 6-line spectrum composed of 3 pairs of lines would be obtained, however, by the zero-field splitting treatment, if the parameter $D$ were greater than the line separations. The observed value for $D$, *i.e.*, the separation of the first weak and first intense line, is 9 ± 1 gauss as in our $N^{14}$. The line separations are 5.7 ± 1 gauss. The line separation value is in good agreement with the value 5.8 ± 0.2 gauss obtained from the product of the $N^{14}$ line separation and the ratio of the quotients of the magnetic moment and nuclear spin for $N^{15}$ and $N^{14}$.

Additional spectra obtained for $N^{14}$ from irradiated mixtures with xenon and argon are shown in Fig. 3. As explained above, the spectra of N atoms in irradiated mixtures of nitrogen with neon or hydrogen are the same, except for intensity, as in the mixture with xenon at low dose or in bulk nitrogen over the entire experimental dose range. Presumably this implies that these mixtures exist largely as crystals of $N_2$ mixed with crystals of the other component. The broadening observed in the xenon–$N_2$ mixture indicates that the concentration of N-atoms in the nitrogen crystallites is higher than any obtained in bulk $N_2$. This is borne out by the data on this mixture in Table I. The percentage of nitrogen decomposed to atoms is almost twice as high as the highest obtained with bulk nitrogen.

With argon the mixing is very likely on a molecular scale, and here the spectrum is quite different. With irradiation at 4.2°K. a fair concentration of $N^{14}$ atoms was attained in argon (Table I). The spectrum (Fig. 3) showed only 3, though broad, lines which suggests something different in the way of crystal field interactions. On irradiating at 20°K. and measuring spectra at 4.2°K. a lower concentration of N atoms occurred, and with sharper lines it was possible to resolve and obtain the spectrum shown at the bottom of Fig. 3. Here the 9 lines anticipated by the zero-field treatment are observed. However, the effect of the crystal field is weaker, and parameter $D$ has the low value of 1.2 ± 0.5 gauss.

Bulk nitrogen and nitrogen mixed with xenon and neon were irradiated at 20°K. with the above-mentioned argon mixture. The concentrations obtained were less than $^1/_{1000}$ of those obtained by irradiation of these mixtures at 4.2°K. but could not be calculated unambiguously because of the quartz resonance. This supports the idea that these mixtures have little solid solution character since one would expect different stabilizing effects if the N atoms were in different matrices. In argon, where the spectra imply a different environment for the trapped atoms, the concentration was measurable and found to be much greater than for bulk $N_2$ irradiated at the same temperature (see value of $\phi$, Table I, for this mixture).

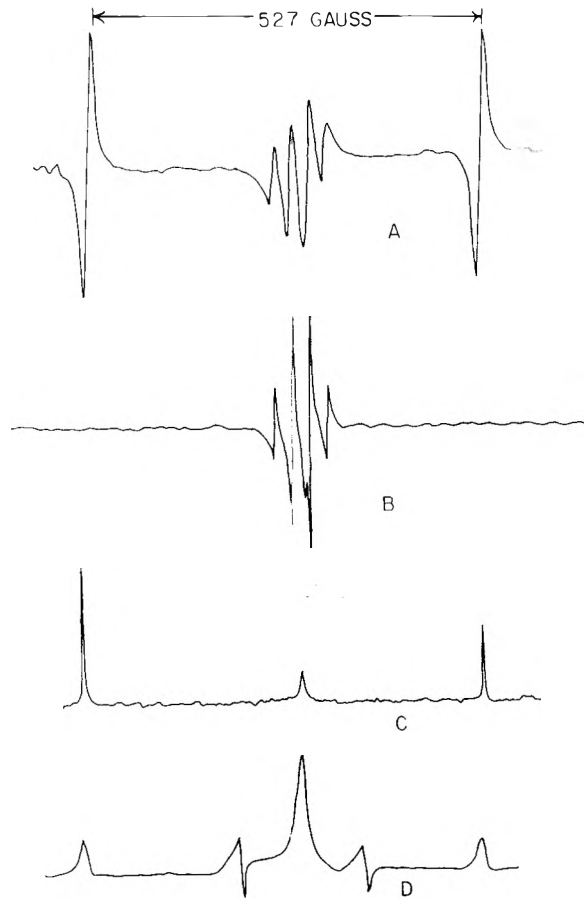


Fig. 5.—E.s.r. spectra of irradiated (4.2°K.) methane, hydrogen and deuterium.

| Sample | (Signal/Noise)$_{max}$ | Modulating amplitude (gauss) |
|---|---|---|
| A methane | 8:1 | 0.22 |
| B methane (after partial warm up) | 8:1 | 0.22 |
| C hydrogen | 25 | 1.8 |
| D deuterium | 4 | 1.8 |

The yield of nitrogen atoms with increasing amounts of γ-radiation (Fig. 4) behaves in an entirely unexpected manner. Although no back reaction is observed on storage at 4.2°K., in the presence of radiation it may be occurring. In a simple system such as this, one would expect a mechanism comprised of a dissociation of nitrogen molecules proportional to the intensity of the radiation competing with the recombination of N-atoms. Thus one would expect a curve rising to a limiting value. Its curvature would be the reverse of that found, and until the N-atom concentration reached a third of its limiting value it would be essentially linear. Initially it was thought that the preirradiation effect and greater power saturation at the low

concentration values were responsible for the increasing rate of atom production. However, corrections based on the saturation measurements available failed to eliminate the curvature. The preirradiation effect also is not responsible since one point at about $19 \times 10^{20}$ e.v./g. (Fig. 4) was obtained before and one after the $33.6 \times 10^{20}$ e.v./g. The slight increase on storage is consistent with the upward curvature. Together these observations suggest a mechanism involving a precursor for the N-atoms. The highest point corresponds to an average of 0.4 atom produced per 100 e.v. absorbed energy. The maximum slope corresponds to a value of about 0.8.

The data in Fig. 4 suggest that the ultimate achievable concentrations of N-atoms are considerably higher than those found. Several theoretical papers have been published suggesting that concentrations as high as 10% are possible.[17,18] A more recent treatment[19] assumes an autocatalytic mechanism in which, at a certain critical concentration, the recombination of 2 atoms leads to a self-propagating chain reaction for the consumption of N-atoms. For N-atoms in $N_2$ this concentration is estimated to be of the order of 0.3%. With this mechanism limiting values in curves such as shown in Fig. 4 may be reached with little warning.[19] Thus we can only say that the maximum concentration achievable is higher than that observed.

The concentration-dose studies on the mixtures are less complete, but the values in Table I indicate that both the preirradiation effect and the subsequent efficiency increase are less than with bulk nitrogen. The xenon–$N_2$ and argon–$N_2$ mixtures appear to be leveling off at the highest doses listed. In the case of the xenon mixture where one can regard the nitrogen content as being in a separate crystalline phase, this may imply that the N-atom concentration in bulk nitrogen would level off at about 0.11%. The observed leveling off in the argon mixture is not believed to be the result of mere depletion of nitrogen molecules by conversion to atoms. Neon was not given as large a dose, and a limiting concentration does not seem to be approached. The values of $\phi$ when neon, argon and xenon are additives are all greater than 1. No correlations seem possible on the basis of simple charge transfer processes. The ionization potentials of the rare gases are 21.6, 15.8 and 12.1 e.v., respectively, while that of $N_2$ is 15.6 e.v. It is thought the high value of $\phi$ found in the xenon–$N_2$ mixture occurs because the density is about 3 times that of bulk nitrogen. For a given exposure the mixture therefore absorbs more energy than does bulk nitrogen. If electronic equilibrium is not established between the crystalline phases of different densities, the energy absorbed by the nitrogen would be greater than in the same amount of bulk nitrogen. The value of $\phi$ is therefore higher but the over-all $G$-value is low because most of the energy dissipated in the xenon does not produce N-atoms. The $G$-values for N atoms from $N_2$ based on energy absorbed by the nitrogen can be estimated from the electron fraction of nitrogen. For the xenon–nitrogen mixture these $G$-values are about 16 times the over-all $G$-values and are higher than corresponding values for bulk nitrogen. This supports the proposition that the energy absorbed by the nitrogen is greater than that calculated from its electron fraction. The ratios of such $G$-values to the corresponding values for bulk nitrogen are less than $\phi$ because the $G$-values are averages whereas the $\phi$'s come from individual points.

The high value of $\phi$ in the neon mixture is compatible with charge transfer, provided most of the molecules of $N_2$ are isolated in the neon matrix.

With the $H_2$–$N_2$ mixture the matrix can yield H atoms. These are thought to be mobile at 4.2°K. and hence could scavenge N atoms and account for their low yield.

**Irradiation of Methane.**—The hydrogen lines in $\gamma$-irradiated methane (see Fig. 5) were quite broad with Lorentz half widths of about 19 gauss. Concentrations estimated from this broadness[15] were higher than those obtained with DPPH.

However, the broadening did not change in our experiments with a variation in H atom concentration of about 50. Since there is ample evidence of some saturation, it is probable that saturation broadening is also occurring and renders such estimates extremely unreliable here. The quartet of lines due to the methyl radical contained components of Lorentz half width roughly 11 gauss and separations of 23 gauss. The derivative peaks had the intensity relationship 1–2.4–2.8–1.1. In all respects their appearance matches Smaller and Matheson's irradiated methane[20] and Gordy's irradiated zinc dimethyl.[21] The theoretical distribution of intensities is 1–3–3–1. This spectrum was observed at 4.2°K. although Smaller and Matheson[20] mention that they found nothing until warming to 20°K. because of power saturation.

The changes in the methyl quartet during accidental warm up call for further comment. During this warm up the hydrogen doublet disappeared totally and the methyl quartet was reduced in intensity and sharpened. At first sight the sharpening seems a natural consequence of the lowered concentration and lessened spin–spin interaction. However, equally low concentrations of methyl, produced in the course of simple irradiation at 4.2°K. uncomplicated by warmup, display much greater line widths—the line width being apparently independent of dose. The observed great line width before warmup is not therefore a simple concentration effect due to spin–spin interaction. Several possible explanations can be put forward.

(1) Radicals are formed in closely-associated pairs or clusters, in which high local concentrations and consequent spin–spin interactions prevail from the start, with little increase at higher doses. The observed broadening is due to the spin–spin interaction only, at high and relatively constant local concentrations. After warmup, only the most isolated radicals remain, with much lower spin–

(17) S. Golden, *J. Chem. Phys.*, **29**, 61 (1958).
(18) J. L. Jackson and E. W. Montroll, *ibid.*, **28**, 1101 (1958).
(19) J. L. Jackson, private communication.
(20) B. Smaller and M. S. Matheson, *J. Chem. Phys.*, **28**, 1169 (1958).
(21) W. Gordy and C. G. McCormick, *J. Am. Chem. Soc.*, **78**, 3243 (1956).

spin interactions. This account is somewhat unrealistic for $\gamma$-irradiation, although it might apply to some extent in the case of radicals produced by radiation with more densely ionizing particles.

(2) Saturation broadening and spin–spin broadening compensate as dose is increased. This, of course, explains the constancy of line width, but not the narrowing after the warm-up.

(3) The sample before warm-up contains an assortment of lattice sites with associated spread in $g$-values and hyperfine coupling parameters. Warm-up produces a more regular crystal lattice with uniform sites.

(4) In the sample before warm-up, the radical is not free to rotate, and broadening is due to the combination of randomly oriented hyperfine dipolar interactions plus the Fermi contact interaction of the electron with the 3 methyl protons. After annealing, the hole occupied by the methyl radical is enlarged and the radical is free to rotate.

(5) At least one quantum of rotational angular momentum is acquired by nearly every methyl radical during warm-up, and is retained upon recooling for a period long enough to make the resonance measurement. Long storage before measurement would presumably regenerate the original broad lines.

(6) Other species superimposed broaden the original spectrum. Warm-up destroys these more labile radicals.

Deuterium and hydrogen spectra similar to those in Fig. 5 have been reported in discharge deposition work.[15] The incomplete shape of the lines is believed to be a fast passage phenomenon resulting from a long spin-lattice relaxation time for the sample and a relatively high modulation frequency.[15] The deuterium lines should be equal in intensity, but the center one has a contribution from the quartz. The central line in the hydrogen spectra is also from the irradiated quartz of the sample tube.

The most efficient atom and radical production, as well as the highest concentration, was found in the methane experiments. From the best data and the appropriate dissociation energies one calculates that 10% of the absorbed $\gamma$-ray energy was stored in irradiated methane while 4% was stored in the nitrogen. The results in general show that high-energy radiation is promising as a means of producing atoms and radicals and suggests that these species are important and plentiful intermediates in chemical transformations induced by radiation.

# THE OXIDATION OF IODIDE IONS IN AQUEOUS SOLUTION BY ATOMIC HYDROGEN

BY GIDEON CZAPSKI, JOSHUA JORTNER AND GABRIEL STEIN

*Department of Physical Chemistry, Hebrew University, Jerusalem, Israel*

*Received April 15, 1959*

Iodide ions in aqueous solution are oxidized by atomic hydrogen produced in an electrodeless high frequency discharge and introduced into the solution. The influence of hydrogen ion and iodide ion concentration on the reaction was investigated in the $p$H range of 0.4–7.0. Various possible mechanisms are discussed and it is shown that of these only the mechanism involving the $H^+_{2aq}$ ion as the actual oxidizing species agrees with all the results. Some rate constants are estimated.

Investigations of the radiation chemistry of $Fe^{2+}$ ions in acid solution led to the conclusion that hydrogen atoms oxidize ferrous to ferric ions,[1-3] probably through the intermediate formation of $H^+_{2\ aq}$ ions. The results obtained in the radiation chemistry of acid iodide solutions[4] and the $p$H dependence of the quantum yield in the photochemistry of the iodide ion[5] may also be interpreted best by assuming oxidation of iodide ions by H atoms in acid solution.

The oxidation of ferrous ions in acid solution by H atoms, which were produced as such in the gaseous phase and then introduced into the solution, was recently demonstrated.[6-8] Although the oxidative properties of H atoms in acid solution are now well established, the actual mechanism of the reaction is still a matter of controversy.[3,6-12] We have now investigated the oxidation of iodide ions by H atoms. Here the practicable $p$H region is wider than in the case of ferrous ion solutions and complications arising from a $p$H dependent back-reaction—as is the case with the ferrous–ferric system—are absent.

## Experimental

**Generation of Atomic Hydrogen.**—A high frequency electrodeless discharge was used, operated at 27–30 Mc., at 2200 v. and 0.42 a., as described previously.[6,8] The hydrogen pressure used was 27 ± 1 mm. and the pumping velocity was 50 liters per minute.

**Experimental Procedure.**—The discharge tube was cleaned with $CrO_3$–$H_2SO_4$, followed by $HNO_3$, then 10% HF and rinsed finally several times with triply distilled water. To avoid photochemical oxidation of iodide by the ultraviolet light emitted by the discharge, there was a 90° bend in the vacuum line between the quartz discharge tube and the

(1) J. Weiss, *Nature*, **165**, 728 (1950).
(2) T. Rigg, G. Stein and J. Weiss, *Proc. Roy. Soc. (London)*, **A211**, 375 (1952).
(3) W. G. Rothschild and A. O. Allen, *Rad. Research*, **8**, 101 (1958).
(4) H. A. Schwartz, J. P. Losee and A. O. Allen, *J. Am. Chem. Soc.*, **76**, 4693 (1954).
(5) T. Rigg and J. Weiss, *J. Chem. Soc.*, 4198 (1952).
(6) G. Czapski and G. Stein, *Nature*, **182**, 598 (1958).
(7) T. W. Davis, S. Gordon and E. J. Hart, *J. Am. Chem. Soc.*, **80**, 4487 (1958).
(8) G. Czapski and G. Stein, THIS JOURNAL, **63**, 850 (1959).
(9) J. H. Baxendale and G. Hughes, *Z. physik. Chem. N.F.*, **14**, 323 (1958).
(10) H. L. Friedman and A. H. Zeltman, *J. Chem. Phys.*, **28**, 878 (1958).
(11) M. Lefort, *Ann. Rev. Phys. Chem.*, **9**, 123 (1958).
(12) C. A. Coulson, *J. Chem. Soc.*, 778 (1956).

TABLE I

OXIDATION OF IODIDE ION BY ATOMIC HYDROGEN

| KI, $M$ | $H_2SO_4$, $N \rightarrow 0.64$ | 0.4 | 0.2 | 0.13 | 0.056 | 0.032 |
|---|---|---|---|---|---|---|
| 0.6 | 1.75 ± 0.13 | 1.4 ± 0.09 | 0.71 ± 0.12 | 0.48 ± 0.07 | 0.21 ± 0.05 | 0.13 ± 0.04 |
| .3 | 1.6 ± .14 | 1.28 ± .11 | 0.68 ± .14 | .44 ± .05 | .22 ± .04 | .13 ± .04 |
| .15 | 1.2 ± .05 | 0.98 ± .10 | .52 ± .08 | .38 ± .05 | .18 ± .03 | .10 ± .02 |
| .06 | 0.78 ± .12 | .61 ± .08 | .41 ± .11 | .29 ± .04 | .12 ± .02 | .06 ± .01 |
| .03 | .48 ± .09 | .45 ± .08 | .24 ± .04 | .19 + .02 | .048 ± .015 | .032 ± .01 |
| .012 | .32 ± .05 | .31 ± .04 | .12 ± .03 | .05 ± .01 | .033 ± .013 | .025 ± .002 |
| .006 | .09 ± .03 | .09 ± .02 | ——— | .025 ± .006 | ——— | ——— |

reaction vessel, which was made of Pyrex glass, and light shields were placed between the two vessels. The outer face of the reaction vessel was blackened. The inner bubbler tube itself was made of glass opaque to light below 3000 Å. and there were bends of 90° along the bubbler tube to prevent reflected ultraviolet light from the discharge reaching the solution. Blank experiments were carried out with solutions of 0.6 $M$ KI in 0.64 $N$ $H_2SO_4$, with the discharge in operation but without the $H_2$ being pumped along. No oxidation could be detected. When the discharge was operated and the $H_2$ was pumped so that instead of passing through the solution it was passed over its surface only, the oxidation rate obtained was 1% of that obtained under full operating conditions. Thus we conclude that the oxidation observed in our normal experimental conditions is not caused by light. No oxidation was observed when $H_2$ was bubbled through the solution without the discharge being operated. For our regular experiments, with the solution in the reaction vessel, the system was evacuated and without discharge $H_2$ passed through the solution for 10 minutes. Traces of $I_2$ formed by thermal oxidation were thus carried off. Only then was the discharge switched on and the trap beyond the reaction vessel immersed in liquid air, to retain the $I_2$ formed in the reaction vessel. Control experiments using $I_2$–KI solution, containing up to $10^{-3}$ mole/l. $I_2$ in the reaction vessel showed, that sweeping in this manner, not less than 90% of the $I_2$ was retained in $T_2$. The concentration of $I_2$ remaining in the reaction vessel in our experiments did not exceed $5 \times 10^{-7}$ mole/l. For each experiment 25 ml. of solution was used. The reaction vessel was always maintained at 5 ± 3°. The discharge was operated for 5 minutes. After this the iodine in the trap was dissolved in 25 ml. of 0.06 $M$ KI, and appropriately diluted for analysis with KI solution.

**Analysis.**—Iodine was determined at 3500 Å. using 1 cm. cells in a Beckman Model B spectrophotometer. We found the absorption coefficient of $I_2$ in 0.06 $M$ KI at 20°, $\epsilon$ 25000 l. mole$^{-1}$ cm.$^{-1}$.

**Materials.**—The KI used was C.P. The $H_2SO_4$ was B. D.H. Reagent Grade. The water used was triply distilled, ordinary distilled water being redistilled from alkaline permanganate and phosphoric acid in an all-glass still. The $H_2$ was Matheson's Electrolytic. It was further purified by passage over palladized asbestos at 400°.

**Reproducibility of Results.**—Every experimental value represents the average of 4–10 separate runs. Values are given with the appropriate standard deviations. The reproducibility is comparable with that obtained by Littman, *et al.*[13] and is now somewhat better than that obtained by Davis, *et al.*,[7] or by ourselves previously.[8]

## Experimental Results and Their Evaluation

Using constant pressure, discharge and flow conditions and thus a constant dose of H atoms, the concentration of iodide ions and hydrogen ions in the solution was varied. The experimental results are summarized in Table I.

The quantity of H atoms reaching the solution is low enough ($\sim 2 \times 10^{-6}$ mole l.$^{-1}$ sec.$^{-1}$) to assume that practically all H atoms reaching the solution will react within it, and that there will be in this respect no solubility limitation which may be $p$H dependent. We tested for and could not detect any H atoms in the gas leaving the solution. We do not assume equilibrium with the gas phase, regarding H atoms.

Irrespective of its actual mechanism, the formation of $I_2$ may be represented by assuming I atom formation

$$I^- + H + H^+ \longrightarrow I + H_2$$

The I atoms yield $I_2$ and $I_3^-$ by [14]

$$I + I^- \rightleftharpoons I_2^-$$
$$2I \longrightarrow I_2$$
$$I + I_2^- \longrightarrow I_3^-$$
$$2I_2^- \longrightarrow I_3^- + I^-$$

Under our experimental conditions the concentration of $I^-$ is much greater than of I, $I_2^-$, $I_3^-$ or of $I_2$, which is constantly swept out by the gas stream. We neglect any competitive back reactions and assume that every I atom formed yields finally $^1/_2I_2$. We shall assume that we may treat our system on the basis of homogeneous kinetics and shall apply the steady-state assumption for transient species occurring in the system.

Our results show that H atoms oxidize iodide ions, the yield depending on $[H^+]$ and $[I^-]$. The quantitative dependence on these factors enables us to differentiate amongst several possible mechanisms.

Let us denote by $A$ moles l.$^{-1}$sec.$^{-1}$ the rate of introduction of H atoms into the solution, and by $k_1$ the rate constant of the recombination process

$$2H \xrightarrow{k_1} H_2 \qquad (1)$$

Uri[15] considered the possibility of the oxidation of inorganic ions in aqueous solution by H atoms through H atom transfer from the hydration layer of the ion. This mechanism was applied by Lefort and Douzou[16] to interpret the photochemistry of ferrous ions. In this case the oxidation will proceed by what we denote as mechanism I.

$$I^- \cdot H_2O + H \xrightarrow{k_2} I + OH^- + H_2 \qquad (2)$$

Steady-state treatment for H atoms gives

$$d[H]/dt = A - k_1[H]^2 - k_2[H][I^-] = 0$$

and $Y$ — the yield of iodine is

$$Y = d\left[\frac{1}{2} I_2\right]/dt = k_2[H][I^-] =$$
$$\{(k_2[I^-])^2/2k_1\}\left\{\left(1 + \frac{4k_1A}{(k_2[I^-])^2}\right)^{1/2} - 1\right\} \qquad (a)$$

According to this mechanism the yield is independent of $p$H and should increase with increasing

(13) F. E. Littman, E. M. Carr and A. P. Brady, *Rad. Research*, **7**, 107 (1957).

(14) L. I. Grossweiner and M. S. Matheson, THIS JOURNAL, **61**, 1080 (1957).

(15) N. Uri, *Chem. Revs.*, **50**, 376 (1952).

(16) M. Lefort and P. Douzou, *J. chim. phys.*, **53**, 536 (1956).

$[I^-]$ to the same limiting value, which equals $A$, at all $p$H values. Neither of these conditions is fulfilled experimentally and so mechanism I is excluded.

The second mechanism proposed[17,7] postulates oxidation through a triple collision between H, $H^+$ and $I^-$

$$I^- + H + H^+ \xrightarrow{k_3} I + H_2 \qquad (3)$$

so that

$$d[H]/dt = A - k_1[H]^2 - k_3[H][H^+][I^-] = 0$$

and

$$Y = \{(k_3[H^+][I^-])^2/2k_1\}\left\{\left(1 + \frac{4k_1A}{(k_3[H^+][I^-])^2}\right)^{1/2} - 1\right\} \qquad (b)$$

In this case the yield does depend on both $[H^+]$ and $[I^-]$, being a function of the product $[H^+][I^-]$. However, it should be constant for a constant value of the product, and should tend to the asymptotic value of $A$ whether the value of the product is increased by increasing $[H^+]$ or $[I^-]$.

We have also considered the possibility of oxidation through the interaction of an H atom with some complex formed between $I^-$ and $H^+$.[15] The investigation of the absorption spectra of $I^-$ in acid solution[18] did not yield any evidence for the existence of such a species. The kinetic scheme would in this case be

$$H^+ + I^- \underset{k_4'}{\overset{k_4}{\rightleftharpoons}} H^+ \ldots I^- \qquad (4)$$

$$H^+ \ldots I^+ + H \xrightarrow{k_5} H_2 + I \qquad (5)$$

When $k_4[H^+][I^-] >> k_5[H^+ \ldots I^-][H]$ the concentration of the complex will be determined by equilibrium 4, and the yield will be a function of the product $[H^+][I^-]$ once again. When the concentration of the complex is low

$$d[H]/dt = A - k_1[H]^2 - k_5[H][H^+ \ldots I^-] = 0$$

$$d[H^+..I^-]/dt = k_4[H^+][I^-] - (k_4' + k_5[H])[H^+..I^-] = 0$$

and this third mechanism leads to the same asymptotic trend as the second one, depending on the product $[H^+][I^-]$ alone.

The plot of our experimental results according to this test is presented in Fig. 1. A unified curve is not obtained except at the lowest $I^-$ and $H^+$ concentrations. At higher concentrations a large divergence is observed. Thus mechanism II and III are inadequate for the interpretation of the experimental results.

We shall show however that the results are consistent with mechanism IV, involving the intermediate formation of the $H_2^+{}_{aq}$ ion. This mechanism, proposed by Weiss[1] and applied in detail previously,[2] is based on a charge transfer reaction between $I^-$ and $H_2^+$.

$$H + H^+ \underset{k_6'}{\overset{k_6}{\rightleftharpoons}} H_2^+ \qquad (6)$$

$$H_2^+ + I^- \xrightarrow{k_7} H_2 + I \qquad (7)$$

(17) J. P. Ethier and F. Haber, *Naturwiss.*, **18**, 266 (1930).
(18) G. Stein and A. Treinin, to be published.

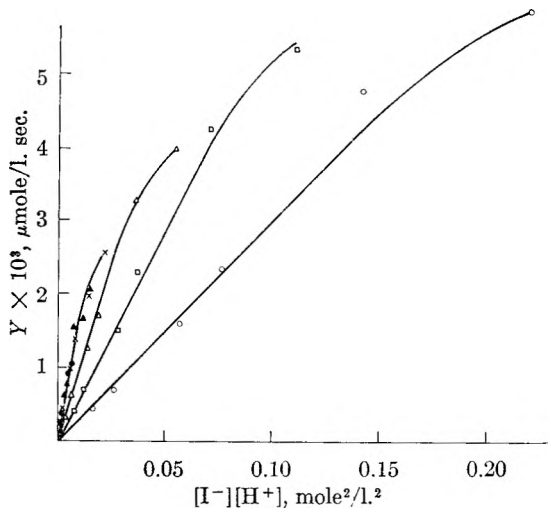


Fig. 1.—Dependence of the yield on the concentration product $[I^-][H^+]$. Experimental points: ○, 0.6; □, 0.3; △, 0.15; ×, 0.06; ▲, 0.03; ●, 0.012; ■, 0.006 $M$ $[I^-]$.

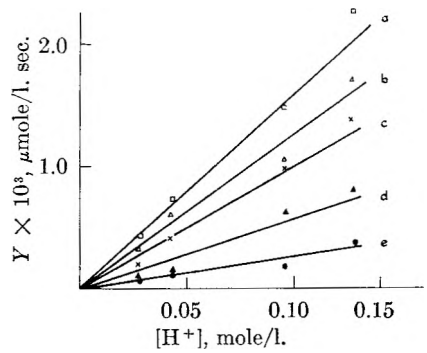


Fig. 2.—Dependence of the yield on $[H^+]$ at low and intermediate $[I^-]$ and $[H^+]$. Notation as in Fig. 1. (a) 0.3; (b) 0.15; (c) 0.06; (d) 0.03; (e) 0.012 $M$ $[I^-]$.

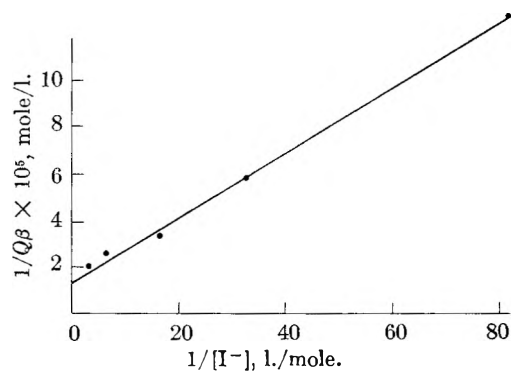


Fig. 3.—Graphical determination of $\beta$.

Steady-state treatment for H and $H_2^+$ leads to

$$d[H_2^+]/dt = k_6[H][H^+] - (k_6' + k_7[I^-])[H_2^+] = 0$$

$$d[H]/dt = A - k_1[H]^2 - k_6[H][H^+] + k_6'[H_2^+] = 0$$

thus

$$Y = \alpha\beta^2[H^+]^2\left\{\left(1 + \frac{2A}{\alpha\beta^2[H^+]^2}\right)^{1/2} - 1\right\} \qquad (c)$$

where $\alpha = k_6^2/2k_1$ and $\beta = [I^-]/((k_6/k_7) + [I^-])$. This mechanism thus also predicts the dependence of the yield on both $[H^+]$ and $[I^-]$ but in a manner different to mechanisms II and III. Namely at constant $[H^+]$ the yield increases with increasing $[I^-]$ to the limiting value of

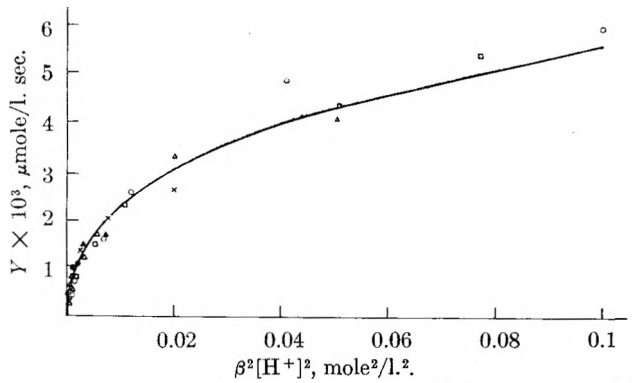


Fig. 4.—Dependence of the yield on $(\beta[H^+])^2$. Notation as in Fig. 1. Curve, calculated.

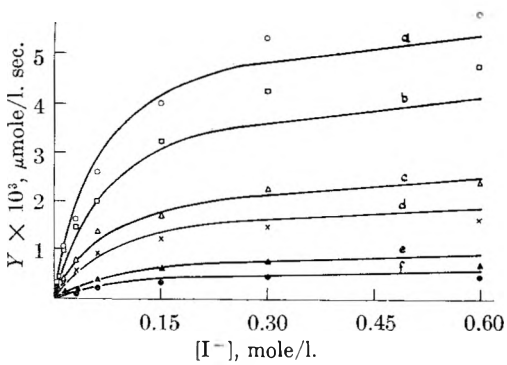


Fig. 5.—Dependence of the yield on $[I^-]$ at different $[H^+]$: (a) ○, 0.64; (b) □, 0.4; (c) △, 0.2; (d) ×, 0.13; (e) ▲, 0.056; (f) ●, 0.032 $N$ $H_2SO_4$. Curves, calculated.

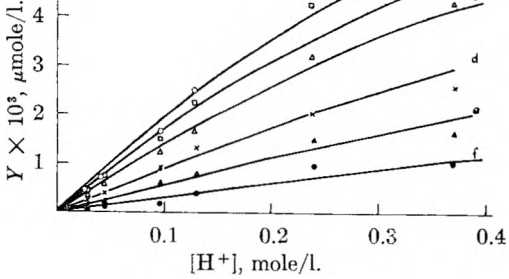


Fig. 6.—Dependence of the yield on $[H^+]$ at different $[I^-]$. Notation as in Fig. 1. Curves, calculated. (a) 0.6; (b) 0.3; (c) 0.5; (d) 0.06; (e) 0.03; (f) 0.012 $M$ $[I^-]$.

$$Y = \alpha[H^+]^2 \left\{ \left(1 + \frac{2A}{\alpha[H^+]^2}\right)^{1/2} - 1 \right\}$$

when $\beta \rightarrow 1$. Only at high $[H^+]$, where $2A/\alpha[H^+]^2 << 1$, does the limiting yield tend to the value of $A$. Thus in this case an asymptotic value of the yield achieved at constant $[H^+]$ by increasing $[I^-]$, does not necessarily mean the complete utilization for oxidation of all H atoms entering the solution. At low $[H^+]$ the limiting yield at high $[I^-]$ is determined by the rate of formation of $H_2^+$, while at low $[I^-]$ the rate-determining step is the oxidation by $H_2^+$.

In mechanism IV the yield depends on the product $([H^+]\beta)$ only. When both $[I^-]$ and $[H^+]$ are low, the yield approaches $Y = (k_7/k'_6)(2\alpha A)^{1/2}[H^+][I^-]$, in agreement with the results of Fig. 1.

We can now estimate the value of $(k'_6/k_7)$. At relatively low $[H^+]$, $Y = Q\beta[H^+]$, where $Q = (2\alpha A)^{1/2}$. Plotting $Y$ *versus* $[H^+]$ at constant $[I^-]$, at low $[H^+]$ we can obtain (Fig. 2) the value of $Q\beta$. Then plotting $1/Q\beta$ *versus* $1/[I^-]$ (Fig. 3) we obtain from the ratio of slope to intercept, $(k'_6/k_7) = 0.1 \pm 0.02$ mole $l.^{-1}$ and from the intercept $\alpha A = 3.1 \pm 0.3 \times 10^{-11}$ sec.$^{-2}$. Hence $\beta = [I^-]/(0.1 + [I^-])$.

To test the correctness of mechanism IV in Fig. 4 the yield is plotted as a function of the product $(\beta[H^+])^2$. It will be seen that within the entire experimental region a good fit with a single curve is obtained, and no dependence on $[H^+]$ or $[I^-]$ alone is observed. The best agreement with the experimental results was obtained by setting $\alpha = 1.2 \times 10^{-5}$ l. mole$^{-1}$ sec.$^{-1}$ and $A = 2.6 \times 10^{-6}$ mole $l.^{-1}$ sec.$^{-1}$.

Using these values, we could now calculate theoretical curves to represent the dependence of the yield on $[H^+]$ and on $[I^-]$. In Fig. 5 and Fig. 6 our experimental results are plotted and the calculated theoretical curves drawn. Good agreement (within about 10% difference at most) is obtained.

From the value of $\alpha$ obtained from Fig. 4 the rate constant of the formation of $H_2^+$, $k_6$, can be calculated. $k_1$, the rate constant of the H atom recombination, is[10] of the order of $10^{10}$ l. mole$^{-1}$-sec.$^{-1}$. In aqueous solution at $p$H 2 Friedman and Zeltman found a value of only $10^8$ liter mole$^{-1}$-sec.$^{-1}$ for "$k_1$". We proposed[8] an explanation for this, according to which "$k_1$" of Friedman and Zeltman is a composite constant. Taking this uncertainty into account $k_6$ has a value of 50–500 l. mole$^{-1}$sec.$^{-1}$. This value is in agreement with the value of about 200 l. mole$^{-1}$ sec.$^{-1}$ which can be derived from the work of Friedman and Zeltman,[10] as will be discussed later.

## Discussion

Our experimental results are thus consistent only with the mechanism of oxidation involving the intermediate formation of $H_{2aq}^+$, which is the actual oxidizing species. It remains to be seen whether other experimental results in systems where reactions of H atoms in solution are postulated, support or contradict this conclusion.

**(a) *p*H Dependence of the Oxidation by H Atoms.**—It was shown[8] that the oxidation of $Fe^{2+}$ by H atoms proceeds by a $p$H dependent mechanism. The yield was nearly constant in the $p$H region of 0.4–1.3, whilst above $p$H 1.7 a sharp drop in yield occurred. The careful reinvestigation of the radiation induced oxidation in air-free ferrous sulfate solutions in which $H_2^+$ was assumed as an intermediate, indicates[3] that up to $p$H 2.1 the $p$H dependence of the yield can be adequately explained by assuming that it is due to the $p$H dependence of the primary yield of H atoms. Rigg and Weiss[19] found the photochemical oxidation of ferrous sulfate in air-free solution to be $p$H dependent, and assumed a mechanism involving $H_2^+$. Photochemical experiments carried out in our laboratories[20] confirm these results, rather than

(19) T. Rigg and J. Weiss, *J. Chem. Phys.*, **20**, 1194 (1952).
(20) J. Jortner and G. Stein, to be published.

those of Lefort and Douzou.[16] However, we found that the *p*H dependence of the quantum yield is largely due to the effect of *p*H on the primary formation of H atoms.

Similarly, the photochemical oxidation of $I^-$ was found by Rigg and Weiss[5] to be *p*H dependent in the absence of $O_2$. They attributed this *p*H dependence to be due to $H_2^+$, formed in competition with the efficient back reaction between H and I. The primary photochemical formation of H they considered to be *p*H independent, according to the Franck–Haber mechanism. However, Farkas and Farkas[21] and Platzman and Franck[22] indicated that the primary photochemical formation of H may also be *p*H dependent.

If so, the different region of *p*H dependence due to $H_2^+$ observed by us in our work using H atoms externally generated and by, *e.g.*, Allen and Rothschild, who also assume $H_2^+$ as the active intermediate is determined by the steady-state concentration of the H atoms. The higher this concentration, the lower the *p*H at which pronounced competition between oxidation and recombination will be observed. In the experiments with radiation chemistry[3] the rate of formation of H atoms is $\sim 3 \times 10^{-8}$ mole $l.^{-1}sec.^{-1}$; in our experiments it is about 100-fold higher. In our work on the oxidation of $Fe^{2+}$ *p*H dependence is observed some one *p*H unit lower than in the radiation chemistry. Thus experiments performed under different conditions are self-consistent in this respect.

(b) **Competitive Reactions.**—Evidence derived from the investigation of competition between $Fe^{2+}$ and scavengers such as $O_2$ methanol for H atoms[3,9] showed that the ratio of the rate constants is not *p*H dependent. These results can be explained by assuming that $H_2^+$ ions react with these scavengers.

(c) **Investigations Using Isotope Exchange.**—The evidence obtained from work on the radiation induced hydrogen–deuterium exchange in aqueous solution[10,23] indicated the absence of chain propagated exchange reactions in acid solution. This was held to exclude the possibility of $H_2^+$ being present in significant concentrations,[7] Friedman and Zeltman[10] came to the conclusion that this absence of fast exchange could be explained on the basis of an acid prompted reaction only if the rate of formation of $H_2^+$ is as slow as about 200 $l.\ mole^{-1}sec.^{-1}$. We have shown that this value is in agreement with the rate constant obtained by us by a completely different method. Thus the existence of $H_2^+$ does not necessarily contradict the results of the isotopic exchange reactions. The slowness of its formation prevents it being a path for a fast and efficient isotopic exchange.

Thus the experimental results of this paper show that oxidation by H atoms in acid solution may proceed by a mechanism involving $H_2^+$; this is consistent with the available experimental evidence from other fields.

One of our conclusions is that $H_2^+{}_{aq}$ is not in rapid equilibrium with H and $H^+{}_{aq}$; $k_6$ is relatively slow. No reliable estimation of $k'_6$ or of the *p*K of $H_2^+$ is possible at present.

The proof of the role of $H_2^+{}_{aq}$ as the actual oxidizing species in acid solutions where H atoms occur would account for a number of phenomena, which are difficult to explain otherwise. Thus Ives[24] very recently summarized the evidence to show that a number of reactions where H atoms are formed at an electrode receive their best explanation by assuming that in this case too it is the $H_2^+{}_{aq}$ ion as such that is the actual reactive species formed from H atoms.

**Acknowledgment.**—This work was partly supported by grant from the Israel Atomic Energy Commission.

## Appendix

**The Application of the Steady-state Treatment to a Kinetic System where an Active Reactant is Generated at a Constant Rate.**—The adequacy of the application of the steady-state approximation to our system where hydrogen atoms are formed at a constant rate and homogeneously distributed in the solution is shown. In the absence of a scavenger for the hydrogen atoms the kinetic equation will be presented by

$$\frac{d[H]}{dt} = A - k_1[H]^2 \qquad (A1)$$

The exact solution of this equation is

$$[H] = \left(\frac{A}{k_1}\right)^{1/2} \frac{\exp\{2(k_1A)^{1/2}t\} - 1}{\exp\{2(k_1A)^{1/2}t\} + 1} \qquad (A2)$$

Hence the concentration of the hydrogen atoms will tend to a stationary value

$$[H]_s = (Ak_1^{-1})^{1/2} \qquad (A3)$$

Under our experimental conditions $A \sim 2 \times 10^{-6}$ mole $l.^{-1}sec.^{-1}$, $k_1 = 10^{10}$ $mole^{-1}\ l.^{-1}\ sec.^{-1}$ and thus $[H]_s \sim 10^{-8}$ mole $l.^{-1}$. This steady state concentration will be reached after a time given by the condition

$$t_c >> (4k_1A)^{-1/2}\ 10^{-2}\ \text{sec.} \qquad (A4)$$

which is much smaller than the duration of our experiments ($\sim$10 min.).

In the presence of a scavenger S for hydrogen both the steady-state concentration and $t_c$ are lower than in the former case. The kinetic equation is

$$\frac{d[H]}{dt} = A - k_1[H]^2 - k_s[S][H] \qquad (A5)$$

This differential equation can be integrated leading to the final result

$$[H] = \frac{(4Ak_1 + k_s^2[S]^{1/2}[F + 1) - k_s[S](F - 1)}{2k_1(F - 1)} \qquad (A6)$$

where

$$F = \frac{k_s[S] + (4Ak_1 + k_s^2[S^2)^{1/2}}{k_s[S] - (4Ak_1 + k_s^2[S^2)^{1/2}} \exp(4Ak_1 + k_s^2[S]^2)^{1/2}t$$

The stationary concentration is

$$[H]_s = \left(\frac{A}{k_1} + \frac{k_s^2[S]^2}{4k_1^2}\right)^{1/2} - \frac{k_s[S]}{2K_1} \qquad (A7)$$

and will be obtained after a period when

(21) A. Farkas and L. Farkas, *Trans. Faraday Soc.*, **34**, 1113 (1938).

(22) R. Platzman and J. Franck, "Farkas Memorial Volume," Jerusalem, 1952, p. 21.

(23) S. Gordon and E. J. Hart, *J. Am. Chem. Soc.*, **77**, 3981 (1955).

(24) D. J. G. Ives, *Can. J. Chem.*, **37**, 213 (1959).

$$F >> 1 \quad \text{(A8)}$$

which is equivalent to

$$l_c >> (4Ak_1 + k_3^2[S]^2)^{-1/2} \quad \text{(A8')}$$

Hence the steady-state treatment to this system appears to be justified since the time taken here to reach it is even shorter than before.

# PHASE EQUILIBRIA IN THE BINARY SYSTEMS $PuCl_3$–NaCl AND $PuCl_3$–LiCl[1,2]

BY C. W. BJORKLUND, J. G. REAVIS, J. A. LEARY AND K. A. WALSH

*Contribution from the University of California, Los Alamos Scientific Laboratory, Los Alamos, New Mexico*

*Received April 18, 1959*

Equilibrium diagrams for the binary systems $PuCl_3$–LiCl and $PuCl_3$–NaCl were studied over the temperature range 100–825° by thermal and differential thermal analysis techniques. A single eutectic was observed in each system with no evidence of solid solution or compound formation. The eutectic occurred at 461° and 28 mole % $PuCl_3$ in the $PuCl_3$–LiCl system and at 453° and 36 mole % $PuCl_3$ in the $PuCl_3$–NaCl system. The melting points of LiCl, NaCl and $PuCl_3$ in equilibrium with an atmosphere of anhydrous HCl were 607 ± 2°, 802 ± 2° and 767 ± 2°, respectively. Within experimental error, the same values were obtained for the melting points of these salts under vacuum.

## Introduction

Information concerning the equilibrium diagrams for the binary systems $PuCl_3$–LiCl and $PuCl_3$–NaCl was required for a proposed study of fused salt methods for processing irradiated plutonium–alloy fuels. Since only the melting points of the three compounds have been reported, it was necessary to investigate the entire composition range in both systems. The techniques of thermal and differential thermal analysis were adopted for this work.

Although the terms melting point and freezing point are used synonymously in this paper, all data are based solely on freezing points obtained from cooling curves.

## Experimental

**Materials.**—LiCl was purified in the quartz apparatus shown in Fig. 1. The evacuation–hydrochlorination technique developed by Laitinen, Ferguson and Osteryoung[3] for the preparation of LiCl–KCl eutectic mixtures was adapted for this purpose. The purified salt was then cast in the form of rods 4–14 mm. in diameter and was stored in an atmosphere of dry argon. Since molten commercial LiCl invariably was discolored by a suspension of black particles,[4] it was necessary to filter the salt between the hydrochlorination and casting steps. The equipment was designed so that the entire purification procedure could be carried out without exposure of the LiCl to atmospheric moisture. In a typical procedure, LiCl (Mallinckrodt, analytical reagent grade) was dried by evacuation (0.05–0.1 mm.) at room temperature for a period of 48–72 hr. Evacuation was continued for a 12 hr. period during which the temperature was increased to 400° at 0.5°/min. Anhydrous HCl was then admitted at a flow rate of 3 l./hr. through the filter tube embedded in the powder as shown in Fig. 1, and the temperature was raised to 650° at 1°/min. The salt melted at ~607°. The flow of HCl was continued for 30 min., after which argon was bubbled through the melt for 5 min., and the system was evacuated. Argon pressure was then used to force part of the molten salt successively into the filter tube and into the casting tube. The filled casting tube was raised to the cooler upper region of the filter tube to permit the LiCl to solidify completely. Additional castings were made by exchanging casting tubes. To prevent the entry of air during this exchange, a positive pressure of argon was maintained in the filter tube. The system was then evacuated, and the procedure was repeated. After their removal, the filled casting tubes were sealed with a torch and were stored in an atmosphere of dry argon.

Two modifications of the LiCl purification procedure were also tested. In one modification, LiCl prepared by the procedure described above was distilled under vacuum at 750°; in the other, commercial analytical reagent grade LiCl was recrystallized from aqueous solution prior to the evacuation–hydrochlorination–filtration procedure. Qualitative spectrographic analyses were obtained for samples of each product. The results are given in Table I.

TABLE I

QUALITATIVE SPECTROGRAPHIC ANALYSES OF PURIFIED LiCl SAMPLES

| Element | Filtered LiCl, % | Filtered and distilled LiCl, % | Recrystallized and filtered LiCl, % |
|---|---|---|---|
| Na | ~0.1 | ~0.1 | 0.01–0.1 |
| Mg | ~ .01 | < .001 | ND[a] |
| Ca | ~ .01 | < .001 | .001– .01 |
| Si | < .001 | < .001 | < .001 |
| Fe | 0.001–0.01 | 0.001–0.01 | .001– .01 |
| K | ND | 0.001–0.01 | ND |

[a] ND = not detected. Other elements not detected: Ag, Al, B, Ba, Be, Bi, Cd, Co, Cu, Cr, In, Mn, Mo, Ni, P, Pb, Sb, Sn, Sr, Ti, V, Zn, Zr.

A significant result of the purification procedure, in addition to the removal of carbonaceous material, was the elimination of constituents which promoted etching of the quartz containers. Purified LiCl could be held in quartz vessels under dry HCl or argon for several days at 650° with no appreciable effect on the vessels. Molten LiCl which had been dried at room temperature but which had not been treated with HCl etched the quartz vessels severely within a few hours. Corrosion was most pronounced on surfaces immediately above the melt.

$PuCl_3$ was prepared from plutonium hydride by reaction with anhydrous HCl at 450°. The hydride was obtained by reacting pure plutonium metal with hydrogen at about 200°. Since $PuCl_3$ prepared in this manner may still contain small amounts of oxide, hydride or unreacted metal, the $PuCl_3$ used in these experiments was subjected to further treatment. Anhydrous HCl was passed through the $PuCl_3$ powder in the quartz apparatus shown in Fig. 1 as the temperature was increased to 800° at 2–4°/min. The stream of HCl was bubbled through the molten salt at 800° for 45 min., after which the $PuCl_3$ was filtered and cast by the same procedure used in the LiCl preparation. Analytical data for

(1) Presented at the 135th meeting of the American Chemical Society in Boston, April, 1959.

(2) This work was done under the auspices of the Atomic Energy Commission.

(3) H. A. Laitinen, W. S. Ferguson and R. A. Osteryoung, *J. Electrochem. Soc.*, **104**, 516 (1957).

(4) Some tiny black specks could also be observed in unopened bottles of analytical reagent grade LiCl. Suspensions of black particles observed in molten LiCl-KCl mixtures by C. T. Brown, H. J. Gardner, C. Solomons and G. J. Janz (NP-6483, Oct., 1957) were attributed to organic impurities which they suggested might decompose with heat in the same manner as sugar to give carbon and water.

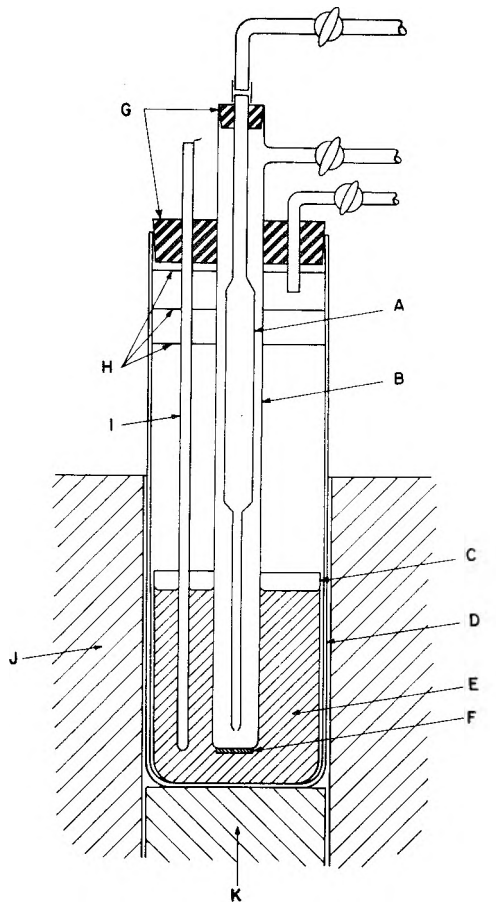


Fig. 1.—Purification apparatus: (A) casting tube, 60 × (0.4 to 1.4 cm.) i.d.; (B) filtration tube, 56 × 2 cm. i.d.; (C) melt container, 12 × 4.5 cm. i.d.; (D) furnace tube, 50 × 5 cm. i.d.; (E) fused salt; (F) quartz filter 15–40 $\mu$ porosity; (G) neoprene stoppers; (H) nickel radiation shields; (I) thermocouple well; (J) Hevi-Duty type M2012 tube furnace; (K) fire brick support.

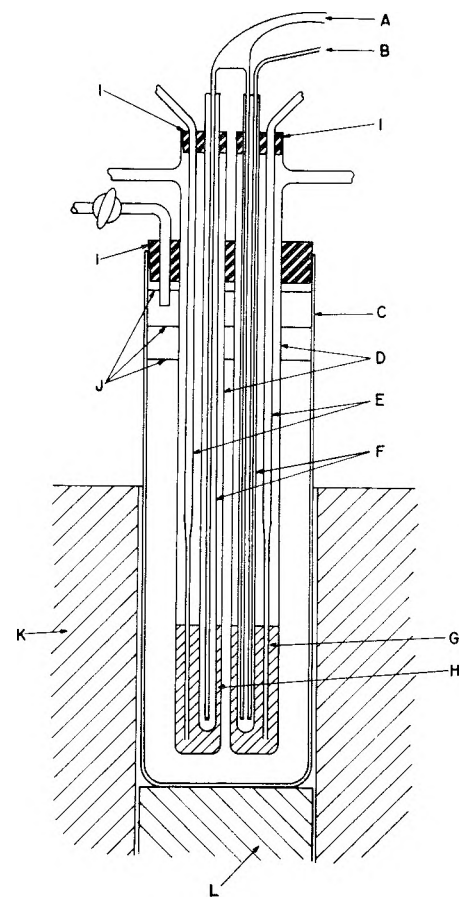


Fig. 2.—Freezing point apparatus: (A) differential Cr–Al thermocouple leads; (B) Cr–Al thermocouple leads; (C) furnace tube, 38 × 5.0 cm. i.d.; (D) freezing point tubes, 45 × 1.6 cm. i.d.; (E) gas inlet tubes, upper end 3 mm. i.d., lower end 2 mm. i.d.; (F) thermocouple wells, 4 mm. i.d.; (G) fused salt; (H) LiCl–KCl eutectic; (I) neoprene stoppers; (J) nickel radiation shields; (K) Hevi-Duty type M2012 tube furnace; (L) fire brick support.

a typical sample of the filtered $PuCl_3$ are given in Table II. The stoichiometry of the filtered salt was the same, within experimental error, as that of $PuCl_3$ purified by vacuum distillation at 900°.

TABLE II

TYPICAL ANALYSIS OF FILTERED $PuCl_3$

| Element | Wt., % | Element | Wt., % |
|---|---|---|---|
| Pu[a] | 69.2 (±0.1) | Mg | 0.004 |
| Cl[a] | 30.8 (±0.1) | Fe | .003 |
| Si | 0.07 | Cr | .001 |
| Ni | 0.005 | Al | < .001 |

[a] Calcd. for $PuCl_3$: Pu, 69.20; Cl, 30.80.

NaCl (J. T. Baker, analytical reagent grade) was heated in a quartz tube to 825° at 1°/min. in a stream of dry HCl. The HCl was bubbled through the molten salt at 825° for 30 min., after which the salt was cooled and stored in a desiccator over anhydrous $Mg(ClO_4)_2$.

Argon (Linde Air Products) was passed over hot copper turnings to remove traces of $O_2$. Both the argon and HCl (Matheson Co., 99.0% min.) were passed through anhydrous $Mg(ClO_4)_2$ to remove any moisture that might have been present.

**Freezing Point Apparatus.**—Cooling curves were obtained by a combination of thermal and differential thermal analysis techniques using the quartz apparatus shown in Fig. 2. The furnace tube was supported on a cylinder of fire-brick located approximately 9 in. below the top of the furnace so as to center the melt in the hottest zone. The furnace temperature was regulated by a Brown Type 153 Elektronic Proportioning Controller. The detecting unit was a chromel–alumel thermocouple located between the furnace winding and the quartz furnace tube with the thermocouple bead at approximately the same level as the fused salt. A Brown Elektr-O-Line Relay with automatic reset operated from the controller to vary the position of a Beck No. 2521 proportioning motor which, in turn, drove the 7.5 k.v.a. Powerstat transformer which furnished power to the furnace. Linear heating and cooling rates from 0.4 to 8.3°/min. were obtained by adjusting percentage timers in the circuits of the two motors which drove the set point index of the controller.

Temperatures were measured with chromel–alumel thermocouples and were recorded by either Brown or Leeds and Northrup 0 to 1000° strip chart recording potentiometers. The thermocouples were calibrated by comparison with a standard Pt *vs.* Pt–Rh thermocouple. The recorders were calibrated by frequent comparison with a Leeds and Northrup Type 8662 portable potentiometer which, in turn, had been calibrated against a Rubicon potentiometer standardized by the National Bureau of Standards.

The chromel–alumel differential thermocouple shown in Fig. 2 provided a means for detecting liquidus temperatures with greater accuracy than was possible by the use of cooling curves alone. The temperature difference between the two junctions was recorded by either Brown or Leeds and Northrup strip chart recording potentiometers with a full-scale range of 4 mv. Since the chart speeds of these potentiometers were identical with those of the 0–1000° recording potentiometers, the differential temperature record could be superimposed on the cooling curve record for easy comparison.

In a typical run, an accurately weighed charge of 15–20 g.

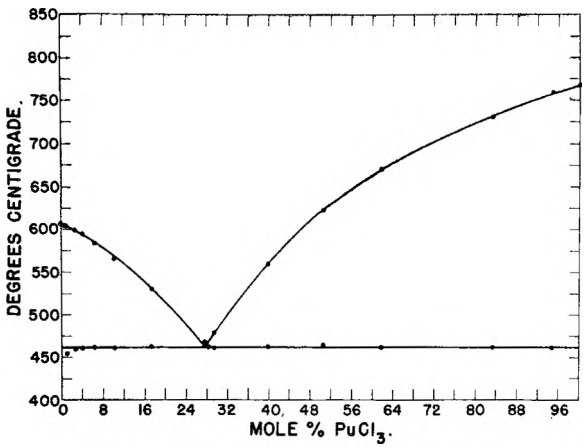


Fig. 3.—$PuCl_3$–LiCl equilibrium diagram.

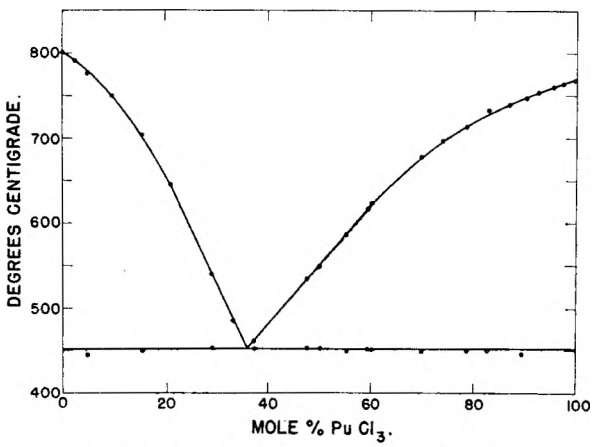


Fig. 4.—$PuCl_3$–NaCl equilibrium diagram.

of the fused salt or salts to be studied was added to one of the freezing point tubes shown in Fig. 2. An equivalent amount of LiCl–KCl eutectic mixture was added to the second tube, or, as was frequently the case, the second tube was replaced by a ceramic crucible which surrounded the lower end of the second thermocouple well. Each tube was evacuated to remove any moisture which might have entered during the loading operation. HCl was then passed through the tube at a rate of 40–60 ml./min. as the furnace temperature was raised through the heating cycle. The gas inlet tube and the thermocouple well were pushed into the salt as soon as it had melted. During each cooling cycle the HCl flow was continued in order to provide the stirring required to ensure a uniform temperature throughout the melt. The gas was preheated sufficiently in the upper part of the inlet tube at the flow rate used so that no deleterious cooling effects were encountered. After the desired number of cooling curves had been recorded for a given salt mixture, the composition could be changed by the addition of an accurately weighed pellet of one of the components through a second side-arm (not shown in Fig. 2) at the upper end of the freezing point tube.

## Results

Equilibrium diagrams for the $PuCl_3$–LiCl and $PuCl_3$–NaCl systems are plotted in Figs. 3 and 4 from the data in Tables III and IV. The melting points of LiCl, NaCl and $PuCl_3$ are 607, 802 and 767°, respectively. The estimated maximum error in each case is ±2°. A eutectic point occurs at 461° and 28 mole % $PuCl_3$ in the $PuCl_3$–LiCl system and at 453° and 36 mole % $PuCl_3$ in the $PuCl_3$–NaCl system. All data were based on results obtained from cooling curves.

TABLE III

$PuCl_3$–LiCl SYSTEM

| Mole % $PuCl_3$ | Liquidus, degree | Eutectic, degree | Mole % $PuCl_3$ | Liquidus, degree | Eutectic, degree |
|---|---|---|---|---|---|
| 100.0 | 767 | .. | 17.4 | 530 | 462 |
| 94.8 | 759 | 461 | 10.3 | 565 | 461 |
| 83.3 | 731 | 462 | 6.5 | 583 | 461 |
| 61.9 | 670 | 462 | 4.1 | 595 | 460 |
| 50.6 | 622 | 464 | 2.7 | 598 | 459 |
| 39.6 | 564 | 463 | 1.1 | 603 | 454 |
| 29.5 | 479 | 461 | 1.0 | 604 | 460 |
| 28.0 | 469 | 464 | 0.0 | 607 | .. |

TABLE IV

$PuCl_3$–NaCl SYSTEM

| Mole % $PuCl_3$ | Liquidus, degree | Eutectic, degree | Mole % $PuCl_3$ | Liquidus, degree | Eutectic, degree |
|---|---|---|---|---|---|
| 100.0 | 767 | .. | 51.0 | 556 | [a] |
| 97.6 | 765 | [a] | 50.2 | 549 | 452 |
| 95.7 | 761 | [b] | 49.9 | 550 | [a] |
| 92.7 | 755 | [a] | 48.4 | 541 | [a] |
| 89.6 | 746 | 446 | 47.7 | 534 | 453 |
| 87.2 | 741 | [a] | 43.9 | 511 | 454 |
| 82.8 | 734 | 450 | 37.4 | 466 | 453 |
| 78.7 | 715 | 450 | 33.2 | 485 | [a] |
| 70.1 | 676 | 447 | 29.2 | 541 | 453 |
| 64.4 | 648 | 451 | 21.0 | 646 | 451 |
| 60.3 | 624 | 451 | 15.6 | 704 | 450 |
| 59.4 | 617 | 452 | 9.8 | 751 | [a] |
| 55.3 | 587 | 449 | 5.1 | 777 | 445 |
| 54.1 | 579 | 448 | 2.5 | 792 | [a] |
| 51.8 | 562 | [a] | 0.0 | 802 | .. |

[a] Salt was not cooled through eutectic region. [b] No thermal arrest appeared below the liquidus.

## Discussion

The binary systems $PuCl_3$–LiCl and $PuCl_3$–NaCl are characterized by simple equilibrium diagrams in the temperature range 100–825° with a single eutectic in each system and no evidence of solid solutions. Compound formation was not observed in either system. (Indications of an irregularity in the $PuCl_3$-rich region of the $PuCl_3$–NaCl diagram were observed, but the evidence was too indefinite for interpretation and was not included in the diagram.) A comparison was made of the melting points of pure LiCl, NaCl and $PuCl_3$ after prolonged evacuation at 0.1 mm. with the melting points of the same compounds in equilibrium with an atmosphere of anhydrous HCl. The results in each case were found to be the same within experimental error.

The value 767 ± 2° for the melting point of $PuCl_3$ was obtained independently by two of the authors using different equipment and separate batches of $PuCl_3$ purified by the hydrochlorination–filtration technique. The results agreed within one degree. Phipps, Sears, Seifert and Simpson[5] have reported 760 ± 5° as the melting point based on the unpublished work of H. P. Robinson. Their $PuCl_3$ was purified by a vacuum sublimation of relatively impure $PuCl_3$ prepared by treating dried plutonium hydroxide with $CCl_4$ at 750–800°. The data in Table II indicate that the filtered $PuCl_3$ used in the present work contained less than

(5) T. E. Phipps, G. W. Sears, R. L. Seifert and O. C. Simpson, *J. Chem. Phys.*, **18**, 713 (1950).

0.1% total impurities. Moreover, the Pu:Cl ratio of the filtered $PuCl_3$ was in excellent agreement with the theoretical value.

The melting point of NaCl agreed, within experimental error, with the values 800.4, 801 and 804° reported in several recent references.[6-9]

A considerable amount of time was devoted to the determination of the melting point of LiCl because of the wide variation in the values reported in the literature. The melting points most commonly quoted, 613°[7,9] and 614°,[6,8,10] apparently are based on some of the work published between 1910 and 1925.[11] Numerous other values ranging from 600–609° were also reported[11,12] during this same period. More recent measurements[13-17] range from 603–610°. The value consistently obtained for all samples of LiCl prepared in the present work was 607°. It was not affected by changing the rate of stirring, the rate of cooling over the range 0.4–3°/min., or by changing the container from quartz to Pyrex or platinum. The melting point of LiCl under vacuum was the same as that of LiCl in equilibrium with an atmosphere of either dry argon or HCl. It is estimated that a freezing point depression of 6° (from 613 to 607°) would require at least 2 wt. % of an impurity such as NaCl. In view of the analytical data in Table I, it is highly unlikely that such a concentration of impurities could have been present in the LiCl used in this work.

**Acknowledgments.**—The authors are indebted to W. J. Maraman of this Laboratory for many productive discussions and to the members of the analytical group under the direction of C. F. Metz for the analytical data.

(6) N. A. Lange, "Handbook of Chemistry," 9th ed., Handbook Publishers, Inc., Sandusky, Ohio, 1956.

(7) "Handbook of Chemistry and Physics," 40th ed., Chemical Rubber Publishing Co., Cleveland, Ohio, 1958.

(8) O. Kubaschewski and E. L. Evans, "Metallurgical Thermochemistry," John Wiley and Sons, Inc., New York, N. Y., 1956.

(9) G. W. C. Kaye and T. H. Laby, "Tables of Physical and Chemical Constants," 11th ed., Longmans, Green and Co., New York, N. Y., 1956.

(10) K. K. Kelley, Bull. U. S. Bur. Mines, No. 393, 1936.

(11) R. J. Meyer, "Gmelins Handbuch der Anorganischen Chemie," 8th ed., Vol. 20, Verlag Chemie, Berlin, Germany, 1927.

(12) E. M. Levin, H.F. McMurdie and F. P. Hall, "Phase Diagrams for Ceramists," The American Ceramic Society, Columbus, Ohio, 1956.

(13) E. Elchardus and P. Laffitte, *Bull. soc. chim.*, **51**, 1572 (1932).

(14) A. S. Botschwar, *Z. anorg. allgem. Chem.*, **210**, 163 (1933).

(15) Metalloy Corp. Minneapolis, Minn., 1944; *cf.* 12, p. 242.

(16) G. A. Bukhalova and A. G. Bergman, *Doklady Akad. Nauk, S.S.S.R.*, **66**, 69 (1949).

(17) G. Munzhakov, *Doklady Akad. Nauk*, **87**, 791 (1952).

# VISCOSITY OF AQUEOUS SODIUM FLUORIDE AND SODIUM PERIODATE SOLUTIONS. IONIC ENERGIES AND ENTROPIES OF ACTIVATION FOR VISCOUS FLOW

BY E. R. NIGHTINGALE, JR., AND R. F. BENCK

*Department of Chemistry, University of Nebraska, Lincoln 8, Nebraska*

*Received April 22, 1959*

The viscosities of aqueous sodium fluoride and sodium periodate solutions have been measured in the concentration range 0.0005 to 1 molar. The viscosity data have been interpreted in terms of the Jones–Dole equation for strong electrolytes. Using this relation, the viscosity *B*-coefficients for the fluoride and periodate ions at 25° are calculated to be +0.0965 and −0.0647, respectively. The energies and entropies of activation for viscous flow at 25° have been calculated for a number of ionic species. Large ions such as $Ba^{+2}$, $IO_3^-$ and $SO_4^{-2}$, which exhibit a minimal hydration for their respective charge types, are observed to decrease the activation energy for viscous flow in the solution from that for the pure solvent even though the ion itself increases the bulk viscosity of the solution. The influence of such ions upon the water structure is discussed. Experimental evidence for the hydration of the $IO_3^-$ ion is cited.

Accurate viscosity data for aqueous sodium fluoride solutions and sodium periodate solutions are not available in the literature. The viscosity *B*-coefficients from the Jones–Dole equation for the viscosity of strong electrolytes have not been reported for any of the fluoride or periodate salts. In conjunction with recent studies in these laboratories concerning the nature and relative sizes of hydrated ions,[1] the viscosities of sodium fluoride and sodium periodate solutions have been measured at 25° in the concentration range 0.0005 to 1 *M*. These data are interpreted in terms of the Jones–Dole equation, and the viscosity *B*-coefficients have been determined for the fluoride and periodate ions. The influence of strong electrolytes upon the viscosity of the solvent is interpreted as a rate process, and the energies and entropies of activation for viscous flow have been calculated for a number of salts. From these data the influence of the individual ions upon the energy and entropy of activation for viscous flow has been estimated. The nature of the ion–solvent interaction is considered, and it is demonstrated that for a given charge type, those ions which exhibit a minimal hydration at 25° may decrease the activation energy for viscous flow in the solution even though the ion itself is sufficiently large to increase the viscosity of the solution over that of the pure solvent.

(1) E. R. Nightingale, Jr., THIS JOURNAL, **63**, 1381 (1959).

## Experimental

Reagent grade sodium fluoride and sodium metaperiodate were each purified by twice recrystalling the salts from conductivity water. After recrystallization, the salts were dried at 110° for four hours. The salt solutions were prepared on the molal basis by dissolving weighed quantities of salt into weighed volumes of conductivity water. The densities of the solutions were measured at 25.00 ± 0.05° using

25-ml. specific gravity bottles, and the densities are precise to 0.0001 g./ml.

The viscosities of the solutions were measured at 25.00 ± 0.02° using an Ostwald viscometer with a flow time of 170 seconds for water. Flow times were measured to 0.01 sec. with a calibrated stopwatch. The average deviation for six to ten measurements of a single sample of a solution did not exceed ± 0.03 sec. The average flow times for replicate samples of a single solution agreed within ± 0.04 sec. The viscometer was calibrated with water at 20, 25 and 30°, and at 25° with 20 and 30% sucrose solutions by means of equation 1

$$\eta/\rho = Kt - L/t \qquad (1)$$

where $\eta$ is the absolute viscosity, $\rho$ is the density, and $t$ is the flow time of the calibrating solution. The characteristic viscometer constants $K$ and $L$ were 0.00005251 and 0.00011, respectively. The absolute viscosities of water at 20, 25 and 30°, and of the 20 and 30% sucrose solutions were taken as 0.01002, 0.008903, 0.007976[2] and 0.01701 and 0.02741[3] poise, respectively. The densities of the solutions were taken as 0.99823, 0.99707, 0.99568[4] and 1.07940 and 1.12517[3] g./ml., respectively.

## Results

The viscosities of the salt solutions were computed by means of equation 1. The relative and absolute viscosities at 25° for eight sodium periodate solutions in the concentration range 0.0005 to 0.1 $M$ are presented in Table I. The data have been analyzed using the Jones–Dole equation[5]

$$\eta/\eta_0 = 1 + A\sqrt{C} + BC \qquad (2)$$

where $\eta/\eta_0$ is the viscosity of the salt solution relative to that of the solvent, water, $C$ is the molar concentration, and $A$ and $B$ are constants characteristic of the electrolyte. The $A$-coefficient represents the contribution from interionic electrostatic forces.[6] The $B$-coefficient measures the order or disorder introduced by the ions into the solvent structure; this constant is a specific and approximately additive property of the ions of a strong electrolyte at a given temperature,[7] although no satisfactory theoretical treatment has yet been given.

TABLE I

RELATIVE AND ABSOLUTE VISCOSITIES OF AQUEOUS SODIUM PERIODATE SOLUTIONS AT 25°

| $C$, moles/l. | $\eta/\eta_0$ | $\eta$, poise |
|---|---|---|
| 0.000506 | 1.00017 | 0.0089045 |
| .000997 | 1.0002 | .008905 |
| .003906 | 1.0004 | .008907 |
| .01007 | 1.0010 | .008912 |
| .01712 | 1.0013 | .008915 |
| .03527 | 1.0021 | .008922 |
| .06184 | 1.0031 | .008931 |
| .09680 | 1.0044 | .008942 |

Plotting $(\eta/\eta_0 - 1)/\sqrt{C}$ *vs.* $\sqrt{C}$, the $A$-coefficient is the ordinate intercept, and the $B$-coefficient given by the slope of the resulting straight line. The experimental value for the $A$-coefficient for sodium periodate of 0.0072 compares well with the theoretical value of 0.00718 calculated according to the theory of Falkenhagen and Vernon.[6] The $B$-coefficient is observed to be 0.0216. Taking the value for the $B$-coefficient for the sodium ion to be +0.0863,[8] we calculate −0.0647 as the magnitude of the $B$-coefficient for the periodate ion at 25°. The periodate ion is similar in size to the perchlorate ion, and its behavior in disrupting the local structure of water in the cosphere about the ion and increasing the fluidity of the solution is identical with that of the perchlorate ion.[9]

The absolute viscosities for ten sodium fluoride solutions in the concentration range 0.0005 to 1 $M$ are given in Table II. The fluoride ion is the conjugate base of a moderately weak acid, and the $p$H of these solutions increases with concentration. The effect of hydrolysis upon the viscosity of the solution is negligibly small, however, and $(\eta/\eta_0 - 1)/\sqrt{C}$ is linear in $\sqrt{C}$ in the concentration range zero to 0.1 $M$. The experimental value for the $A$-coefficient for this salt is 0.0073 at 25° as compared with the theoretical value of 0.0071. At 20 and 30°, the experimental values do not differ significantly from the calculated ones, 0.0078 and 0.0070, respectively. The $B$-coefficients at 20, 25 and 30° are +0.224, 0.1828 and 0.141, respectively. Assuming that the $B$-coefficient for the sodium ion is +0.0863 and independent of temperature in this range,[8] we calculate +0.138. 0.0965 and 0.055 as the magnitude of the $B$-coefficient for the fluoride ion at 20, 25 and 30°, respectively. The fluoride ion strongly orders the solvent in the cosphere about the ion. With increasing temperature, the solvent ordering is perturbed by the increase in the thermal energy, and the B-coefficient for the fluoride ion decreases in proportion to the increase in the entropy of hydration.[1]

TABLE II

ABSOLUTE VISCOSITIES OF AQUEOUS SODIUM FLUORIDE SOLUTIONS AT 20, 25 AND 30°

| $m$, moles/1000 g. | Absolute viscosity, poise 20° | 25° | 30° |
|---|---|---|---|
| 0.000568 | | 0.008906 | |
| .001030 | 1.0020 | .008907 | 0.007992 |
| .003686 | | .008913 | |
| .01022 | 1.0060 | .008926 | .008037 |
| .01696 | | .008939 | |
| .03436 | 1.0113 | .008971 | .008069 |
| .06228 | | .009020 | |
| .1014 | 1.025 | .009086 | .008153 |
| .4103 | | .009701 | |
| .9622 | | .010776 | |

## Discussion

The interpretation of viscous flow according to the theory of absolute reaction rates has been presented by Eyring and co-workers.[10] The energy of activation for viscous flow $\Delta E^*$ is given by

$$\Delta E^* = R\,\frac{\mathrm{d}\ln\eta}{\mathrm{d}(1/T)} \qquad (3)$$

(2) J. R. Coe and T. B. Godfrey, *J. Applied Phys.*, **15**, 625 (1944).

(3) E. C. Bingham and R. F. Jackson, *Bull. U. S. Bur. Standards*, **14**, 59 (1918).

(4) L. W. Tilton and J. K. Taylor, *J. Research Natl. Bur. Standards*, **18**, 205 (1937).

(5) G. Jones and M. Dole, *J. Am. Chem. Soc.*, **51**, 2950 (1929).

(6) H. Falkenhagen and E. L. Vernon, *Physik. Z.*, **33**, 140 (1932).

(7) W. M. Cox and J. H. Wolfenden, *Proc. Roy. Soc. (London)*, **A145**, 475 (1934).

(8) M. Kaminsky, *Disc. Faraday Soc.*, **24**, 171 (1957).

(9) E. R. Nightingale, Jr., THIS JOURNAL, **63**, 742 (1959).

(10) S. Glasstone, K. J. Laidler and H. Eyring, "The Theory of Rate Processes," McGraw-Hill Book Co., New York, N. Y., 1941.

For associated liquids, the plot of $\ln \eta$ *vs* $1/T$ is not linear, and the energy of activation varies with temperature. The influence of a strong electrolyte upon the viscosity of a solvent may likewise be interpreted as a rate process. Substituting equation 2 into 3

$$\Delta E^* = R \frac{\mathrm{d} \ln [\eta_0(1 + A\sqrt{C} + BC)]}{\mathrm{d}(1/T)} \quad (4)$$

For solutions that are not too dilute (*ca.* 1 *M*), the contribution of the interionic electrostatic forces to the viscosity of the solution is negligibly small (except for the fortuitous case where $B$ is identically equal to zero), and equation 4 may be rewritten as

$$\Delta E^* = R \frac{\mathrm{d} \ln \eta_0}{\mathrm{d}(1/T)} + \frac{R}{1 + BC} \times \frac{\mathrm{d}(1 + BC)}{\mathrm{d}(1/T)} \quad (5)$$

This expression is equivalent to adopting the Bingham relation[11] for moderately concentrated solutions in place of the Jones–Dole equation. In a similar manner, the free energy of activation for viscous flow is given by[10]

$$\Delta F^* = RT \ln \frac{\eta V}{hN} \quad (6)$$

where $h$ is the Planck constant and $N$ is the Avogadro number. $V$ may be regarded as the volume of one mole of solution particles and is given by

$$V = \frac{1000}{n_1 + \nu n_2} \text{ cm.}^3 \quad (7)$$

where $\nu$ is the number of species into which a solute molecule dissociates and $n_2$ is the number of moles of solute per liter of solution. The number of moles of solvent, $n_1$, per liter of solution is given by

$$n_1 = \frac{1000\rho - n_2 M_2}{M_1} \quad (8)$$

where $M_1$ and $M_2$ are the molecular weights of the solvent and solute, respectively. Assuming that the activation enthalpy does not differ appreciably from the activation energy, the entropy of activation $\Delta S^*$ may also be calculated as

$$\Delta S^* = (\Delta E^* - \Delta F^*)/T \quad (9)$$

Table III evaluates the free energy, energy and entropy of actviation for viscous flow at 25° for one molar solutions of a number of salts whose $B$-coefficients are available in the literature.[8,12] The activation free energy for these solutions is essentially constant and exhibits only a slight increase for solutions of multivalent ions over that of the pure solvent. The abnormally large energies and entropies of activation are characteristic of associated liquids and are attributed to the excess energy necessary to break the hydrogen bonds in the solutions.[10]

It is observed that the energy and entropy of activation for viscous flow are, with two exceptions, decreased as compared with the respective values for water. This usually is considered to be the general behavior for dilute aqueous salt solutions and interpreted energetically as evidence for a decrease in the hydrogen bonding in the solution. However, this behavior is directly a consequence of

(11) E. C. Bingham, THIS JOURNAL, **45**, 885 (1941).

(12) R. W. Gurney, "Ionic Processes in Solution," McGraw–Hill Book Co., New York, N. Y., 1953.

TABLE III

FREE ENERGY, ENERGY AND ENTROPY OF ACTIVATION FOR VISCOUS FLOW AT 25° ($C$ = 1 MOLE/L.)

| Salt | $\Delta F^*$, kcal. | $\Delta E^*$, kcal. | $\Delta S^\ddagger$, e.u. |
|---|---|---|---|
| Water | 2.19 | 4.01 | 6.1 |
| LiCl | 2.26 | 4.00 | 5.8 |
| NaCl | 2.20 | 3.81 | 5.4 |
| $NH_4Cl$ | 2.19 | 3.69 | 5.0 |
| KCl | 2.18 | 3.56 | 4.6 |
| RbCl | 2.17 | 3.30 | 3.8 |
| CsCl | 2.17 | 3.36 | 4.0 |
| $BeCl_2$ | 2.40[a] | 4.27 | 6.3 |
| $MgCl_2$ | 2.36 | 3.99 | 5.5 |
| $FeCl_2$ | 2.35[a] | 3.96 | 5.4 |
| $BaCl_2$ | 2.30 | 3.10 | 2.7 |
| $CeCl_3$ | 2.45 | 3.74 | 4.3 |
| NaF | 2.28 | 5.27 | 10.0 |
| NaCl | 2.20 | 3.81 | 5.4 |
| NaI | 2.20 | 3.67 | 4.9 |
| $NaNO_3$ | 2.21 | 3.79 | 5.3 |
| $NaIO_3$ | 2.22 | 3.75 | 5.2 |
| $NaClO_3$ | 2.23 | 3.70 | 4.9 |
| NaOH | 2.29 | 3.79 | 5.0 |
| $Na_2SO_4$ | 2.37 | 3.77 | 4.7 |

[a] Estimated.

the salts considered, primarily the alkali halides and should not be generalized. For this reason, it is of interest to consider the role of the individual ions rather than of the salt itself in influencing the viscosity of the solvent. For this purpose, we assume that the difference between the activation energy of the solution and the solvent is equal to the sum of the activation energies for the ionic components, and we write

$$\Delta E^* - \Delta E_0^\ddagger = \nu_+ \Delta E_+^* + \nu_- \Delta E_-^* \quad (10)$$

where $\Delta E_+^*$ and $\Delta E_-^*$ are the cation and anion activation energies, $\nu_+$ and $\nu_-$ are the number of cations and anions, respectively, per molecule of salt, and $\Delta E_0^*$, the activation energy for pure water, is identified as $R$ d ln $\eta_0/\mathrm{d}(1/T)$ in equation 5. We further assume, in a manner similar to that for the evaluation of the ionic $B$-coefficients,[8] that the influence of the potassium ion upon the activation energy for viscous flow in the solution is approximately equal to that for the chloride ion. A previous discussion[1] has demonstrated that this is a satisfactory but not necessarily rigorous approximation. Using equation 10 and a similar expression for the ionic entropy of activation, Table IV presents the energies and entropies of activation calculated for a number of ions. These data indicate that the $Li^+$, $Na^+$, $Be^{+2}$, $Mg^{+2}$, $Fe^{+2}$, $Ce^{+3}$ and $F^-$ ions increase the activation energy, while the remaining ions decrease the activation energy. These results may be correlated qualitatively with the order-producing properties of the ions at 25°: order producing ions with positive $B$-coefficients have positive activation energies, while order destroying ions with negative $B$-coefficients have negative activation energies. For ions of small size and/or large charge, the surface charge density is sufficiently large to orient the water molecules immediately adjacent to the ion more firmly than in the bulk solvent and increase the activation energy for viscous flow. Large ions

with weak electric fields collapse the normal water structure about the ion and increase the fluidity of the solvent molecules over that in bulk water.

TABLE IV

IONIC ENERGY AND ENTROPY OF ACTIVATION FOR VISCOUS FLOW AT 25° ($C$ = 1 MOLE/L.)

| Ion | $\Delta E^*$, cal. | $\Delta S^*$, e.u. |
|---|---|---|
| $Li^+$ | +210 | +0.45 |
| $Na^+$ | + 20 | +0.05 |
| $NH_4^+$ | −100 | −0.4 |
| $K^+$ | −220 | −0.75 |
| $Rb^+$ | −490 | −1.55 |
| $Cs^+$ | −430 | −1.35 |
| $Be^{+2}$ | +700 | +1.7 |
| $Mg^{+2}$ | +420 | +0.9 |
| $Fe^{+2}$ | +390 | +0.8 |
| $Ba^{+2}$ | −470 | −1.9 |
| $Ce^{+3}$ | +390 | +0.45 |
| $F^-$ | +1240 | +3.85 |
| $Cl^-$ | −220 | −0.75 |
| $NO_3^-$ | −240 | −0.85 |
| $IO_3^-$ | −290 | −0.95 |
| $ClO_3^-$ | −340 | −1.25 |
| $I^-$ | −370 | −1.25 |
| $OH^-$ | −240 | −1.15 |
| $SO_4^{-2}$ | −280 | −1.5 |

However, four ions in Table IV, $Ba^{+2}$, $IO_3^-$, $SO_4^{-2}$ and $OH^-$, exhibit the apparently anomalous relation of positive $B$-coefficients and negative activation energies. From equation 5, it is seen that the sign of $\Delta E^*$ is opposite to that for $dB/dT$. Hence the relation of the $Ba^{+2}$, $IO_3^-$ and $SO_4^{-2}$ ions may be explained by determining the conditions under which the positive $B$-coefficients may be accompanied by positive values for $dB/dT$.

The extent of hydration of an ion[13] is a function of the ionic charge, size and structure, and comparisons between ions are valid only for a given classification of charge and structure. A previous discussion has presented a set of effective hydrated radii for solvated ions in water.[1] Referring to Table I in that discussion, it may be noted that the $Ba^{+2}$, $IO_3^-$ and $SO_4^{-2}$ ions are those species, which in their respective classes, have the larger crystal radius and smaller difference between the effective hydrated radius and the crystal radius, and which therefore are minimally hydrated at 25°. As the temperature is increased, the normal ordering of the water structure is destroyed, and the water molecules are more susceptible to orientation in the relatively weak electric field about, for example, the barium ion. It should be noted that this behavior is not directly comparable with that proposed by Kaminsky[8] to explain the positive $dB/dT$ values accompanying negative $B$-coefficients. Kaminsky's explanation for positive $dB/dT$ values is that due to Cox and Wolfenden[14]: since the fluidity of the solvent immediately surrounding order destroying ions is greater than that of the bulk solvent, the decrease in the solution viscosity with increasing temperature must be less than that of the pure solvent, and the relative viscosity and hence the $B$-coefficient, increases with temperature. The recent discussion of negative hydration by Samoilov[15] suggests, however, that this explanation is inadequate and that the ion–solvent interactions must also be considered for ions with negative $B$-coefficients.

The behavior of the sulfate ion is similar to that of the barium ion except that, by virtue of its larger crystal radius and smaller surface charge density, the extent of its hydration at 25° is considerably less than for the barium ion. Nevertheless, the sulfate ion orders the solvent about the ion and evidences a positive viscosity increment.

The behavior of the iodate ion is more complex. Traditionally the iodate ion has been considered to be unhydrated, and in comparison with the chlorate and bromate ions, the positive $B$-coefficient of the iodate ion appears to result solely from the increased size of the ion. However, since the positive values of $dB/dT$ for ions with positive $B$-coefficients are interpreted to indicate an increase in ion–solvent interaction, some degree of hydration must therefore be recognized at 25°. Further evidence for this hydration is obtained by comparing the limiting equivalent conductances and the viscosity $B$-coefficients for the iodate and periodate ions. At 25°, $\lambda_0$ = 41.5 and 54.5, and $B$ = +0.140 and −0.065 for the iodate and periodate ions, respectively. Both the conductance and viscosity parameters indicate the presence of some interaction between the iodate ion and water which is present to a much lesser degree, or not at all, with the periodate ion. This effect cannot be explained solely on the basis of ion size, for the crystal radius of the iodate ion is larger than that for the periodate ion. It appears that the lack of appreciable interaction between the periodate and water stems from the double bond character present in the periodates. Both the meta- and paraperiodate ions possess an appreciable amount of double bond character in the I–O bonds[16,17] which can prevent delocalization of the charge on the iodine atom and lessen to a considerable extent the amount of bonding that otherwise might be expected between the oxygen atoms and water. In this respect, the periodate ion compares not unfavorably with the tetramethylammonium ion in which the charge is localized on the nitrogen atom. The $B$-coefficients for these latter two ions are not comparable, however, because of the difference in their crystal radii. In the iodate ion, on the other hand, the double bond character is much less pronounced (*ca.* 20%) than that in the periodate ion, and the charge is more effectively delocalized by the oxygen atoms permitting more extensive interaction with the solvent. In addition, the unshared electron pair on the iodine atom may it-

(13) Hydration is used in this sense to denote ion–solvent interactions which restrict the translational motion of water molecules in the vicinity of the ion as compared with those in the bulk solvent. A specific microscopic model is not implied.

(14) W. M. Cox and J. H. Wolfenden, *Proc. Roy. Soc.* (*London*), **A145**, 486 (1934).

(15) O. Ya. Samoilov, *Disc. Faraday Soc.*, **24**, 141 (1957).

(16) L. Pauling, "The Nature of the Chemical Bond," Cornell University Press, Ithaca, N. Y., 2nd Ed., 1948, pp. 175, 247.

(17) In neutral solution at 25°, the metaperiodate ($IO_4^-$) is the predominant species. See C. E. Crouthamel, A. M. Hayes and D. S. Martin, *J. Am. Chem. Soc.*, **73**, 82 (1951). Using the relations of Pauling, the double bond character in the metaperiodate is calculated as approximately 90%.

self promote interaction with the water molecules. Similar but less significant comparisons may be expected between the $ClO_3^-$ and $ClO_4^-$, and $SO_3^{-2}$ and $SO_4^{-2}$ ions. The predominant dioxanation reported recently by Grunwald[18] for the tetraphenylphosphonium ion in dioxane–water mixtures may be further evidence of charge localization preventing extensive hydration, although the role of the coordinating phenyl groups in dispersing the charge of the central atom is not yet satisfactorily understood.

It should be emphasized that the extent to which the water molecules are ordered about an ion with given charge and structure is a function of the temperature and hence the disorder present in the bulk solvent. If one considers the effect of ions upon water at 40° instead of 25°, the potassium, ammonium, chloride and bromate ions will also exhibit positive $B$-coefficients along with positive values for $dB/dT$. The behavior of the $Ba^{+2}$, $IO_3^-$ and $SO_4^{-2}$ ions is therefore not anomalous but may indeed be predicted if one considers that these ions are minimally hydrated at 25° and allows for the change in the water structure with temperature. A similar behavior may be expected for the $Pb^{+2}$, $SeO_4^{-2}$, $CrO_4^{-2}$, $MoO_4^{-2}$, $WO_4^{-2}$ and perhaps the $Co(NH_3)_6^{+3}$ and $Fe(CN)_6^{-4}$ ions. While the appropriate data are not available for aqueous salt solutions near the boiling point, it appears as if the effect of strong electrolytes upon the viscosity of solutions at elevated temperatures is to exhibit a common positive viscosity increment which is dependent only upon the charge of the ion and not appreciably influenced by ionic size or structure.

(18) E. Grunwald, 135th National Meeting, American Chemical Society, Boston, 1959, Abstracts p. 30R.

**Acknowledgment.**—The assistance of the Research Corporation in support of these studies is gratefully acknowledged.

# NOTES

## SOME EFFECTS OF LAURYL ALCOHOL ON LIGHT SCATTERING BY SODIUM LAURYL SULFATE[1]

By L. H. Princen and Karol J. Mysels

*University of Southern California, Los Angeles 7, California*

*Received October 2, 1958*

The turbidity of solutions of association colloids such as sodium lauryl (dodecyl) sulfate (NaLS) is known to increase sometimes suddenly upon dilution in the vicinity of the critical micelle concentration (c.m.c.). This already has been interpreted in terms of precipitation of previously solubilized and water-insoluble impurities, particularly lauryl alcohol (LOH), as the micelles disintegrate.[2,3] The purpose of the present note is to expand this interpretation and point out some complications involved.

Phillips and Mysels[2] have suggested that the precipitate may be not the alcohol itself but the alcoholate (adduct) LOH·2NaLS described by Epstein and coworkers.[4] Strong support for this is given by the fact that the precipitate is formed by anisometric particles, as evidenced by very pronounced streamers when the solution is even mildly disturbed. Lauryl alcohol alone is a liquid at 25° and cannot have such an effect.

The system is greatly complicated by its reluctance to reach equilibrium in the dilute micellar region (0.19–0.5%). It is easy to prepare two solutions of the same composition (*e.g.*, 0.36% NaLS, $1.2 \times 10^{-4}$% LOH) both giving values of scattered light which are stable for hours but differ by a large factor (5 in the above example). One solution can be prepared by simple dilution and filtering; the other by further dilution (without filtering) to about 0.2–0.19% and addition of the proper amount of a more concentrated filtered solution. None of the precipitate seems to dissolve during this last step. Conversely, seeding seems to have little effect in facilitating precipitation. Thus it is not possible at present to determine the composition of the equilibrium system in this region.

The scattered light is completely depolarized for most of these systems, and the dissymmetries are of the order of 6. The variation in the intensity of light scattered at 90° is shown in Fig. 1 as a function of concentration $c$ of NaLS and of the percentage $\alpha$ of alcohol in the sample. The concentrations are for the total system without correction for the amounts precipitated. The Rayleigh ratios for the green and blue lines of mercury (5461 and 4358 Å.) follow closely the relation

$$R_g \times 10^7 = (R_b \times 10^7)^{0.941}$$

The materials and apparatus have been described elsewhere.[5] The solutions were obtained by solubilizing the alcohol in a 12% solution of pure NaLS, diluting carefully to 0.6% and filtering into the cell. Concentration then was changed by adding filtered water but the solution itself was not filtered again.

(1) This work forms part of the doctoral dissertation of L. H. P., Utrecht, The Netherlands, 1959. It was supported in part by the Office of Naval Research. Reproduction in part or in whole for purposes of the United States Government is permitted.

(2) J. N. Phillips and K. J. Mysels, This Journal, **59**, 325 (1955).

(3) W. Prins and J. J. Hermans, *Proc. Kon. Neder. Akad. Wett.*, **B59**, 298 (1956).

(4) M. B. Epstein, A. Wilson, C. W. Jacob, L. E. Conroy and J. Ross, This Journal, **58**, 860(1954); A. Wilson, *J. Soc. Cosmetic Chem.*, **6**, 392 (1955).

(5) K. J. Mysels and L. H. Princen, This Journal, **63**, 1696 (1959).

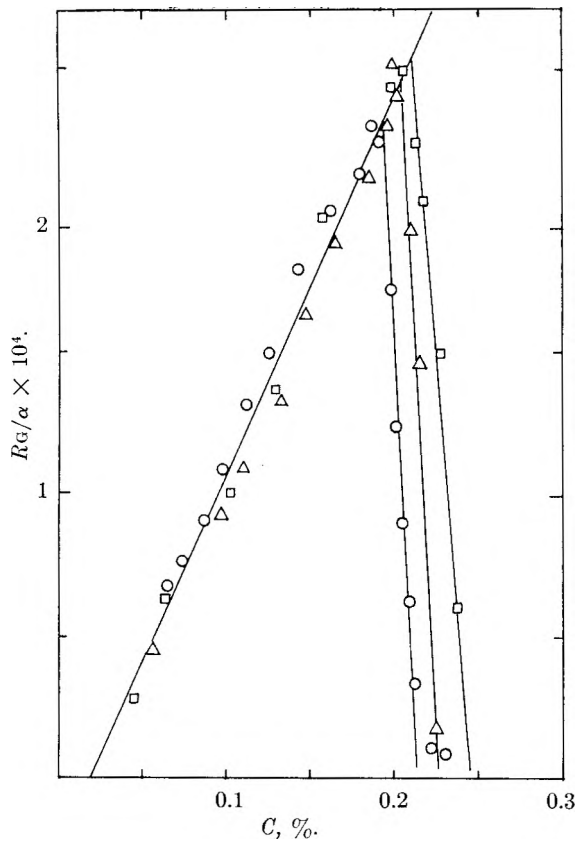


Fig. 1.—The reduced Rayleigh ratio in green light for solutions having a concentration $c$% of sodium laurylsulfate containing $\alpha$% of lauryl alcohol: ○, $\alpha$ = 0.2%; △, $\alpha$ = 1%; □, $\alpha$ = 2%.

Within experimental scatter the points fall on a single line at low concentrations, so that the scattered light is directly proportional to the alcohol content of the sample. This shows again that none of the alcohol is removed by filtration at the higher concentration and also that the method can be used for quantitative determination of alcohol under proper conditions.

At low concentrations the turbidity vanishes as the precipitate dissolves completely at a point substantially independent of the proportion of alcohol in the mixture. If the precipitate were the alcohol itself, one would expect a ten-fold change in this concentration. This seems to be beyond experimental error. On the other hand if it is the alcoholate, the solubility product, $[LOH][Na^+]^2[LS^-]^2$, is much more sensitive to the concentration of NaLS than to that of LOH and only a two-fold change in the concentration at which turbidity vanishes would be expected. This is probably within the experimental error. The solubility thus determined is appreciably lower than found previously and corresponds to a solubility product of the order of $10^{-18}$.

The peaks of the curves must correspond closely to the point where induced micelles[6] saturated with LOH begin to form—or, more precisely, where they have disintegrated completely. If correction is made for the NaLS precipitated along with the LOH as the alcoholate, the three peaks all occur at 0.197 ± 0.002%. This can be considered as the c.m.c. of the mixed system and is some 15% lower than the corresponding value for pure NaLS.

The foot of the steep branch of the graph gives the lowest concentration at which all the alcohol remained unprecipitated, presumably in a supersaturated state. If one assumes that all the $LS^-$ added between the peak and this point is micellized and that all the LOH is solubilized, one can estimate the number of $LS^-$ per LOH molecule in the supersaturated micelle. This gives about 2.5 $LS^-$/LOH for the two alcohol-richer systems, and three times more in the one which contained only 0.2% LOH. This interpretation is very uncertain, however, since these systems are very far from equilibrium. In particular, some of the alcohol may be in supersaturated molecular solution or in supersaturated association with individual $LS^-$ ions or with their dimers.[7]

(6) P. Mukerjee and K. J. Mysels, *J. Am. Chem. Soc.*, **77**, 2937 (1955).

(7) P. Mukerjee, K. J. Mysels and C. I. Dulin, THIS JOURNAL, **62**, 1390 (1958).

## THE CONVERSION OF NITROGEN DIOXIDE TO NITRIC OXIDE

BY JAMES D. RAY[1]

*Contribution from the Department of Chemistry, Stanford University, California*

*Received February 10, 1959*

In relation to the nuclear magnetic resonance program of this Laboratory involving compounds of the isotopes of nitrogen, it became desirable to convert efficiently nitrogen dioxide to nitric oxide.

Thermochemical considerations indicated that many metal oxides were capable of quantitatively reducing nitrogen dioxide to nitric oxide. However, of more importance, owing to the metastable character of the desired nitric oxide product, it was necessary to find a material that would not catalytically cause the formation of any nitrogen or nitrous oxide by product. Such reactions of many of the lower oxides of the transition metals have been summarized by Mellor.[2] It was necessary to find an oxide that would not form a mixture of nitrate and nitrite rather than just the higher oxide of the metal. It was also desirable that the higher oxide of the metal be capable of decomposition to the lower oxide at as low a temperature as possible, since it was desired to use the material in conversion of $NO^{18}_2$ to $NO^{18}$ with recovery of the oxygen isotope Cobaltous oxide was experimentally found to meet these requirements. In support of this finding, it was previously shown by Ogg and Ray[3] that alkali and alkaline earth compounds of cobalt oxides absorb nitric oxide from dilute air mixtures to form quantitatively alkali or alkaline earth nitrates.

### Experimental

Cobaltous oxide was prepared by calcining precipitated cobaltous hydroxide, with a final heating under vacuum at

(1) Department of Chemistry, University of Minnesota, Minneapolis 14, Minn.

(2) J. W. Mellor, "A Comprehensive Treatise on Inorganic and Theoretical Chemistry," Longmans, Green and Co., New York, N. Y., 1947, pp. 437–438.

(3) R. A. Ogg, Jr., and J. D. Ray, U. S. Patent 2,684,283 (July 20, 1954).

950° to evolve all oxygen in excess of the stoichiometric formula CoO. A 15-g. sample of cobaltous oxide was placed in a porcelain boat in a 30 mm. "Pyrex" tube. An electric furnace was used to heat the length of the tube containing the cobaltous oxide. The "Pyrex" tube was part of a vacuum system which had a glass helix Bourdon gage.

A nitrogen dioxide–oxygen mixture prepared by calcining 2 g. of moisture-free lead nitrate was evolved into the system with the furnace at room temperature. No absorption by the cobaltous oxide was observed to take place at room temperature over a period of 24 hours under these anhydrous conditions. The furnace temperature was raised to 450° and held there for 12 hours. During this time the brown $NO_2$ color of the gas phase slowly diminished to colorless (the rate no doubt being controlled largely by diffusion from the ends of the tube to the sample boat). The furnace was then cooled to room temperature for a final pressure observation. The pressure change corresponded to that expected for the reaction

$$2NO_2(\text{partly as } N_2O_4) + {}^1/_2O_2 + 9CoO = 2NO + 3Co_3O_4$$

An approximately fourfold excess of cobaltous oxide was found desirable for rapid reaction.

The purity of the nitric oxide product was confirmed by its vapor pressure and its subsequent quantitative conversion to sodium nitrite by the method described by Ray and Ogg.[4]

This research was supported in part by the National Science Foundation and was supported in part by the National Heart Institute. This research was supported in part by a grant from the Petroleum Research Fund administered by the American Chemical Society.

(4) J. D. Ray and R. A. Ogg, Jr., *J. Am. Chem. Soc.*, **79**, 265 (1957).

## THE VISCOSITY OF DIETHYLAMINE–WATER MIXTURES

By R. N. Barfield*

*Pure Chemistry Division, National Research Council, Ottawa, Canada*

*Received February 24, 1959*

Viscosity measurements of diethylamine–water solutions were undertaken as part of a study of the origin of the large "excess" sound absorption observed in these solutions.[1] The measurements were made with a capillary viscometer, which was modified in a novel way so as to eliminate hydrostatic "head" corrections. The viscometer consisted of two similar shallow glass bulbs of about 30-cc. volume fixed to the ends of a 0.5 mm. capillary U-tube 80 cm. long. One of the bulbs was open to the atmosphere and the other could be connected to a vacuum line or to a source of constant pressure. The latter was obtained by compressing air into a 55-gallon steel drum to about 20–60 cm. of Hg above atmospheric pressure. The pressure of the drum, $p$, as well as the atmospheric pressure, $p_0$, were accurately measured (±0.05 cm.) by means of mercury columns and a cathetometer.

In use the viscometer was thermostated to ±0.05°. The left-hand bulb was filled with liquid. The constant pressure $p$ then was applied and the time $t$ for the liquid to flow between two fiduciary marks at the top and bottom of the bulb was measured. Since the pressure difference acting on the liquid is $\Delta p = p - p_0$, the viscosity $\eta$ is given by the simple relation

$$\eta = Kt\Delta p$$

where $K$ is an apparatus constant which was determined at each temperature by calibration with distilled water.[2] Change in the applied pressure during a run was negligible, and because of the design of the viscometer the correction for the hydrostatic pressure of the liquid also was negligible. Calculations of Reynolds number showed the flow in the capillary under the conditions of the experiment to be non-turbulent.

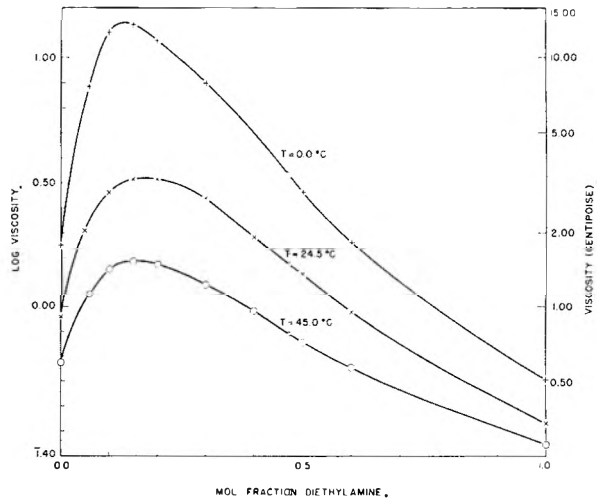


Fig. 1.

Table I

Shear Viscosity of Diethylamine–Water Solutions

| Mole % amine | Viscosity (centipoise) 0.0° | 24.5° | 45.0° |
|---|---|---|---|
| 0.0 | | 0.904 | 0.599 |
| 5.0 | 7.772 | 2.033 | 1.123 |
| 10.0 | 12.865 | 2.828 | 1.425 |
| 15.0 | 13.554 | 3.273 | 1.520 |
| 20.0 | 11.547 | 3.256 | 1.483 |
| 30.0 | 7.727 | 2.734 | 1.230 |
| 40.0 | .... | 1.905 | 1.034 |
| 50.0 | 2.893 | 1.353 | 0.714 |
| 60.0 | 1.811 | 0.943 | 0.568 |
| 100.0 | 0.505 | 0.341 | 0.280 |

Table II

Comparison of Viscosity Values of Diethylamine at 25°

| Author | Viscosity (centipoise) |
|---|---|
| Kurnakov and Zemcuzny[3] | 0.346 |
| Mussell, Thole and Dunstan[4] | .367 |
| Friend and Hargreaves[5] | .317 |
| Present work | .338 |

The solutions were made up by weighing, using distilled water and diethylamine (Eastman) purified by drying with KOH and double distilling.

* Deceased. The major part of the work reported here was completed during Dr. Barfield's tenure of a National Research Council Post-doctorate fellowship, 1954–1956.

(1) R. N. Barfield and W. G. Schneider, *J. Chem. Phys.*, in press (1959).

(2) Values of the viscosity of pure water were taken from J. F. Swindells, J. R. Coe and T. B. Godfrey, *J. Research Natl. Bur. Standards*, **48**, 1 (1952); E. C. Bingham and R. F. Jackson, *Bull. Bur. Stand.*, **14**, 59 (1918).

(3) N. Kurnakov and S. Zemcuzny, *Z. physik. Chem.*, **83**, 481 (1913).

(4) A. G. Mussell, F. B. Thole and A. E. Dunstan, *J. Chem. Soc.*, **101**, 1008 (1912).

(5) J. N. Friend and W. D. Hargreaves, *Phil. Mag.*, **35**, 619 (1944).

To obtain reproducible results, it was found necessary to de-aerate the solutions by vacuum pumping before filling the viscometer.

The results of the measurements are summarized in Table I and Fig. 1. The estimated error in the viscosity is about 0.1%. For comparison the present measurement of pure diethylamine at 25° is shown in Table II together with several literature values.

The viscosity of diethylamine–water mixtures reaches a maximum value at a composition of 13–17 mole % diethylamine. This maximum sharpens and shifts to smaller concentrations of amine as the temperature is lowered. Other hydrogen-bonded binary systems, as for example water–alcohol systems, show a similar behavior.

## CHEMICAL EFFECTS OF (n,γ) ACTIVATION OF BROMINE IN THE ALKYL BROMIDES: A NEW METHOD FOR DETERMINATION OF ORGANIC RETENTION[1]

BY W. E. HARRIS,[2] W. H. MCFADDEN AND R. G. MCINTOSH

*Chemistry and Metallurgy Division, Atomic Energy of Canada, Chalk River, Ontario*

*Received March 5, 1959*

In the study of the chemical effects of nuclear transformations in alkyl bromides it is desirable to obtain the yield of radiobromine existing in an inorganic form and the yield existing in an organic form (organic retention). These are conventionally obtained by extraction of the irradiated sample with sodium sulfite–potassium bromide solutions.[3,4] This paper reports that these analyses can be obtained with less operator effort by a gaseous absorption technique involving potassium ferrocyanide and charcoal as absorbents for the bromine–hydrogen bromide fraction and the organic fraction, respectively. The results agree well with those obtained by the extraction method and the analysis can be performed with liquids of very high vapor pressure as well as with the ordinary liquids. Samples of only 0.01 ml. are sufficient for most determinations.

In carrying out a determination of organic retention a few milligrams of alkyl bromide are sealed into a small ampoule and irradiated.[5] After irradiation, the ampoule is cooled with liquid air, opened and placed in a 50 ml. per min. air stream which carries the sample vapors through the absorption tube. This tube is made from 8 mm. glass tubing with a 2 cm. long section packed with 40 to 60 mesh potassium ferrocyanide, and a 2 cm. long section packed with about 100 mesh active charcoal. The two packings are separated and held in place with plugs of degreased glass wool. Inorganic bromine in the form of hydrogen bromide or elemental bromine reacts completely with potassium ferrocyanide at room temperature while the organic bromides pass through this section and are absorbed on the charcoal. Cooling of the charcoal section with Dry Ice is desirable to quantitatively retain methyl bromide while gas is passing through the tube. Since the radiochemical amounts of inorganic bromine produced by the "hot-atom" reaction are strongly absorbed by the glass of the radiation ampoule it is necessary to rinse the ampoule two or three times with a few microliters of ethyl bromide containing 5% bromine. The wash portions are added to the irradiation ampoule and allowed to evaporate into the air stream in the same manner as the original sample. The absorption tube is then cut into two parts and the organic yield is determined by direct counting of the activity on each absorbent with a well-type scintillation crystal and conventional counting equipment. The counting rate observed for the inorganic fraction was increased by 3% to allow for the higher γ-ray stopping power of potassium ferrocyanide relative to that of charcoal.

Table I presents the results obtained upon the irradiation of a variety of alkyl bromides or mixtures of alkyl bromides and bromine and compares these with results obtained by extraction. The organic yield data reported by Milman and Shaw[6]

TABLE I

ORGANIC RETENTION OF VARIOUS ALKYL BROMIDES MEASURED BY TWO METHODS

| Material irradiated | % organic retention: Absorption method | % organic retention: Extraction method |
|---|---|---|
| Bromoethane + 0.0 $Br_2$[a] | 44 | 35–39[6] |
| + 0.011 $Br_2$ | 23 | 26[6] |
| + 0.045 $Br_2$ | 18 | 21[6] |
| + 0.122 $Br_2$ | 16 | 16[6] |
| + 0.202 $Br_2$ | 12 | 13[6] |
| + 0.385 $Br_2$ | 9.4 | 9[6] |
| 1-Bromopropane + 0.0 $Br_2$ | 30 | 32[8,9] |
| Bromoform + 0.0 $Br_2$ | 65 | 66[8] |
| 1-Bromopropane + 0.0 $Br_2$ (not purified) | 44 | 40 |
| + trace $Br_2$ | 28 | 27 |
| + much $Br_2$ | 4.4 | 4.7 |

[a] Mole fraction of elemental bromine present in the irradiated material.

for ethyl bromide have generally been satisfactorily reproduced. The value of 44% for the irradiation of ethyl bromide without bromine is somewhat higher than the expected extraction value.[3,6] This point was not investigated further and in the absence of parallel extraction results from this Laboratory it is suggested that impurities in the bromoethane probably were responsible for this high yield. The organic yield of 30% obtained for a purified sample[7] of 1-bromopropane is in good agreement with the 32% reported by Chien and Willard[8,9] and the value obtained for bromoform also agrees with the results of these authors. The organic yields determined for three samples

(1) Issued as A.E.C.L. No. 854.

(2) Department of Chemistry, University of Alberta, Edmonton, Alberta.

(3) S. Goldhaber and J. E. Willard, *J. Am. Chem. Soc.*, **74**, 318 (1952).

(4) J. C. W. Chien and J. E. Willard, *ibid.*, **77**, 3441 (1955).

(5) The irradiation facility used in this work was the γ-ray angular correlation apparatus of the Chalk River NRX Reactor which gave a neutron flux of about $10^8$ neutrons per cm.$^2$ per sec. and a γ-ray flux of about 11 r./hr. The irradiation time varied from about 3 to 50 hours. It has been shown[4] that the threshold for measurable general radiolytic breakdown of organic bromides does not occur until the γ-ray flux is several orders of magnitude higher than in these irradiations. The authors gratefully acknowledge the cooperation of Dr. G. A. Bartholemew and Dr. G. Manning in making the irradiation facility available.

(6) M. Milman and P. F. D. Shaw, *J. Chem. Soc.*, 1303 (1957).

(7) Because only small quantities of material are necessary for this technique, purification of samples was effected with a 2.5 meter, 25 mm. i.d. gas chromatographic column packed with silicone stopcock grease on firebrick.

(8) J. C. W. Chien and J. E. Willard, *J. Am. Chem. Soc.*, **76**, 4735 (1954).

(9) J. C. W. Chien and J. E. Willard, *ibid.*, **79**, 4872 (1957).

of unpurified 1-bromopropane with different amounts of bromine indicate the agreement between the results obtained by the absorption and extraction techniques in this Laboratory.

## THE MOLECULAR WEIGHT OF SODIUM AND POTASSIUM CHLORIDE VAPORS

By J. L. Barton and H. Bloom

*Department of Chemistry, The University of Auckland, Auckland, New Zealand*

*Received April 21, 1959*

Early investigations of vapor pressure by various methods,[1] molecular weight,[2] dipole moment,[3] etc., have been interpreted to show that alkali halide vapors are monomeric. However, Ochs, Cote and Kusch,[4] from molecular beam resonance measurements, concluded that sodium halide vapors are considerably associated to the dimeric forms. Friedman[5] studied the vapor of LiI by mass spectrometry and detected ionized fragments which were consistent with the presence of $(LiI)_2$ and $(LiI)_3$. More recently Miller and Kusch[6] have made accurate determinations of the velocity distribution in molecular beams of ten alkali halide vapors. By comparing these with the theoretical distributions, they deduced the proportions of the various molecular species present. These were found to be, for NaCl and KCl, the dimeric forms, *e.g.*, in potassium chloride vapor at $10^{-2}$ mm. pressure the molar ratio of dimer to monomer was 0.087 at 897°K., while in sodium chloride vapor at 920°K. the molar ratio of dimer to monomer was 0.253. The heats of dissociation of the dimeric species were calculated from the variation of equilibrium constant of dissociation with temperature.

In this Laboratory, the absolute vapor pressures of NaCl and KCl have been measured by a boiling point method.[7] We also report now the results of transpiration experiments on these salts. These experiments yield, in combination with the vapor pressure results, the apparent molecular weight of the vapors. For NaCl vapor at pressures between 11.5 and 49.6 mm. and temperatures between 1290 and 1416°K. molecular weights between 86.9 and 83.8 are obtained (NaCl = 58.5) while for KCl vapor between 1250°K. (11.6 mm. pressure) and 1473°K. (138.0 mm. pressure) the molecular weight is between 93.9 and 98.7 (KCl = 74.55). Assuming that in these vapors association takes place to give the dimeric form in equilibrium with the monomeric form, the degree of dissociation of the dimeric form of each chloride can be calculated. Our results are shown in Tables I and II.

(1) V. Deitz, *J. Chem. Phys.*, **4**, 575 (1936); H. Hintz and K. Jellinek, *Z. Elektrochem.*, **42**, 187 (1936); B. Greiner and K. Jellinek, *Z. physik. Chem.*, **A165**, 97 (1933); B. H. Zimm and J. E. Mayer, *J. Chem. Phys.*, **12**, 362 (1944).

(2) W. Nernst, *Z. Elektrochem.*, **9**, 622 (1903).

(3) W. H. Rodebush, L. A. Murray and M. E. Bixler, *J. Chem. Phys.*, **4**, 372 (1936); L. R. Maxwell, S. B. Hendricks and V. M. Mosely, *Phys. Rev.*, **52**, 968 (1937).

(4) S. A. Ochs, R. E. Cote and P. Kusch, *J. Chem. Phys.*, **21**, 459 (1953); P. Kusch, *ibid.*, **21**, 1424 (1953).

(5) L. Friedman, *ibid.*, **23**, 477 (1955).

(6) R. C. Miller and P. Kusch, *ibid.*, **25**, 860 (1956).

(7) J. L. Barton and H. Bloom, This Journal, **60**, 1413 (1956).

Table I

Dissociation Constants of the Dimeric Forms of Sodium and Potassium Chloride Vapors

| $T$, °K. | Pressure, mm. | Apparent mol. wt. | $K_p$, atm. |
|---|---|---|---|
| | $(NaCl)_2 = 2NaCl$ | | |
| 1290 | 11.5 | 86.9 | 0.008254 |
| 1362 | 27.2 | 85.3 | .02294 |
| 1416 | 49.6 | 83.8 | .04862 |
| | $(KCl)_2 = 2\ KCl$ | | |
| 1250 | 11.6 | 97.1 | 0.02455 |
| 1333 | 32.1 | 96.1 | .07386 |
| 1416 | 78.9 | 93.9 | .2193 |
| 1416 | 78.9 | 96.8 | .1707 |
| 1416 | 78.9 | 95.5 | .1755 |
| 1416 | 78.9 | 94.7 | .2044 |
| 1473 | 138.0 | 98.7 | .2561 |

From the variation of log $K_p$ against $1/T$, the heats of dissociation of the dimeric species per mole are calculated by the method of least squares giving for $(NaCl)_2 = 2NaCl$, $\Delta H = 51.0 \pm 0.8$ kcal. and for $(KCl)_2 = 2KCl$, $\Delta H = 40.8 \pm 0.6$ kcal. The corresponding results by Miller and Kusch[6] are 46.6 ± 0.9 kcal. and 47.6 ± 0.7 kcal., respectively. The agreement between the two sets of results is satisfactory in view of the fact that the temperatures of measurement by Miller and Kusch were on the average about 400° lower than in the present work and the approximation that $\Delta H$ is independent of temperature is implicit in both cases.

We wish to acknowledge the assistance of the University of New Zealand Research Fund in the purchase of apparatus. J. L. B. was the recipient of a University of New Zealand Research Fund Fellowship.

## PURIFICATION OF LITHIUM IODIDE BY ZONE MELTING[1]

By F. Pizzarello

*Armour Research Foundation of Illinois Institute of Technology, Chicago 16, Illinois*

*Received April 2, 1959*

Since its invention, zone melting has been applied mainly to the purification of semiconductors and metals. Very pure germanium and silicon have been obtained by this method.

Pauly and Sue[2] demonstrated the general applicability of zone melting by eliminating impurities such as $Na^+$, $SO_4^=$, $Sr^{+++}$ and $PO_4^{\equiv}$ from the ionic solid, potassium nitrate. After 10 zone passes, these workers measured a $10^3$ decrease in the original concentration of $Na^+$ at the front end of an ingot.

Since zone melting is generally applicable to solids, it is possible that it may prove useful in the field of scintillator technology. To obtain information of this application, the purification of the scintillator material lithium iodide was undertaken.

The container used for the zone-melting process was a Vycor tube 11 in. long and 17 mm. o.d. It was filled in a dry box with enough chemically pure, dehydrated lithium

(1) This work was supported by the Aeronautical Research Laboratory, Wright Air Development Center.

(2) J. Pauly and P. Sue, *Compt. rend.*, **245**, 1505 (1957).

TABLE I

CONCENTRATIONS AND DISTRIBUTION COEFFICIENTS OF VARIOUS IMPURITIES IN A ZONE-MELTED LITHIUM IODIDE INGOT

| Impurity | Concentration,[a] p.p.m. 0 to 1 in. Position | 1 to 2 in. Position | 2 to 3 in. Position | 3 to 4 in. Position | 4 to 5.5 in. Position | Distribution coefficient[b] |
|---|---|---|---|---|---|---|
| Boron | 2-20 | 5-50 | 10-100 | 25-250 | 100-1000 | 0.63 |
| Calcium | 75-750 | 100-1000 | 200-2000 | 200-2000 | 100-1000 | .78 |
| Copper | 5-50 | 7-70 | 15-150 | 25-250 | 50-500 | .77 |
| Iron | 2-20 | 5-50 | 25-500 | 50-500 | 10-100 | .56 |
| Magnesium | 2-20 | 50-500 | 250-2500 | 250-2500 | 100-1000 | .23 |
| Silicon | 10-100 | 15-150 | 150-1500 | 100-1000 | 75-750 | .48 |
| Sodium | 500-5000 | 500-5000 | 500-5000 | 1000-10,000 | 2000-20,000 | [c] |

[a] Concentration measured within the limits of the indicated position. [b] $k = C_s/C_e$, where $C_s$ is the concentration of impurity in the solid phase and $C_e$ the concentration in the liquid phase. [c] Distribution coefficient not calculated

iodide to form a 7-in. ingot with a thickness less than the radius of the tube to prevent excessive radial stresses on the walls of the tube and to allow its easy removal after zone melting. About 60 g. of dehydrated lithium iodide was needed to form an ingot of the proper dimensions.

The filled tube was attached to a vacuum system, evacuated to $10^{-4}$ mm. and heated at 200° for 24 hr. Upon completion of the heat treatment, pure, dry nitrogen was introduced into the tube until a pressure of 66 cm. was reached. The tube then was sealed.

The sealed Vycor tube containing lithium iodide was clamped in a horizontal position in the zone melter. A 1-in. long molten zone was established and moved through the entire length of the ingot at a rate of 6 in./hr.

Early in the course of experimentation, it was found that the Vycor tube broke when the lithium iodide was zone melted in it. This was caused by a stress resulting when the solid lithium iodide which had adhered to the tube wall contracted on cooling. This breakage was remedied by covering the inner wall of the tube with a thin, adherent coat of carbon.

The carbon coating process was as follows. 1. The inner walls of the tube were sand-blasted with a dental sand blaster (S. S. White industrial abrasive unit, model O). Norton Abrasive Company 500 Alundum was used as the abrasive. 2. The tube ends with the desired shape were then fabricated. 3. The tube was positioned in a furnace and heated to 850°. Then a mixture of acetone vapor and nitrogen was passed through the hot tube until a dense layer of carbon was deposited on the walls.

To permit observations during the zone-melting process, a window was prepared in the following manner: a narrow longitudinal section of the inner wall of the Vycor tube was masked with tape. The unmasked portion of the wall was sandblasted and then the tape was removed. When the tube was made into the desired design, it was carbonized as described. Then, while oxygen was being passed through the tube, the section originally masked with tape was heated with an oxygen-natural gas torch to burn off the carbon.

A lithium iodide ingot in the modified tube was given 45 passes in the zone melter. Samples were taken at five positions on the length of the ingot. These samples were analyzed spectroscopically for impurities. The concentrations of the naturally occurring impurities are listed in Table I.

## Discussion

The assumption was made that 45 passes given the lithium iodide ingot yields for each species a distribution of impurities approximating an ultimate distribution. Using the relation for ultimate distribution derived by Pfann,[3] the distribution coefficients of the impurities present were calculated. The ultimate distribution is defined as

$$C_u = Ae^{Bx}$$

where $A$ and $B$ are parameters and $x$ is the distance along the ingot. The slope of each impurity curve is its $B$ value. This value was used to calculate the distribution coefficient $k$ for each impurity from the expression

$$k = \frac{Bd}{e^{Bd} - 1}$$

where $d$ is the length of the zone.

The distribution coefficients were calculated from the data given in Table I. In the calculation of the distribution coefficients the lower limit of the impurity concentration was used. Table I lists the distribution coefficients of the impurities. The coefficients calculated are more properly called effective distribution coefficients, since no attempt was made to control diffusion in the solid phase nor was there any attempt to eliminate any concentration gradient by mixing in the liquid zone. The fact that all these values are less than unity, indicates that these impurities lower the freezing point of pure lithium iodide. Thus, the impurities concentrate in the molten zone and are carried to the end of the ingot.

It is shown in Table I that the concentration of sodium is constant for approximately the beginning half of the ingot. In the remaining half of the ingot the sodium concentration increases. This concentration gradient noted at the end of the ingot is due to an actual segregation of sodium to the end of the ingot. The invariant concentration region at the beginning of the ingot can be explained by postulating a strong dependence of the distribution coefficient on concentration. Thus at low sodium concentration the distribution coefficient approaches unity.

## Conclusions

The data presented clearly show that lithium iodide can be purified effectively by zone melting. However, the purity obtained in these experiments is not the ultimate obtainable by this method. If longer ingots and shorter zone lengths are used, or if pure ends of zone-melted ingots are refined further, an even higher level of purity can be achieved.

**Acknowledgments.**—The author wishes to express his thanks to Mr. Edwin Tompkins and Major W. Downs for their many useful comments and profitable discussions. This program was sponsored by Wright Air Development Center under Contract No. AF 33(616)-3748.

(3) W. G. Pfann, *Trans. Am. Inst. Mining Met. Engrs.*, **194**, 747 (1952).

# THE HEAT OF CHLORINATION OF DIBORON TETRACHLORIDE[1]

By S. R. Gunn, L. G. Green and A. I. Von Egidy

*Lawrence Radiation Laboratory, University of California, Livermore, California*

*Received February 26, 1959*

The heat of formation of diboron tetrachloride is of interest particularly for the estimation of the thermochemical bond energy of the boron-to-boron single bond. Apple and Wartik found that at $-45°$ $B_2Cl_4$ and excess chlorine reacted rapidly to form boron trichloride in approximately 98% of the theoretical yield.[2] Since the heat of formation of $BCl_3$ is known, it seemed possible that this reaction might be performed calorimetrically to permit derivation of the heat of formation of $B_2Cl_4$.

The principal difficulty experienced in the investigation was due to the low stability of $B_2Cl_4$. With all experimental arrangements tested from 5 to 45°, small amounts of solid products were formed, presumably due to local heating produced by the reaction. Performance of the measurements at lower temperatures did not seem feasible. The system finally developed involved passing chlorine slowly into an all-glass reaction vessel containing liquid or gaseous $B_2Cl_4$.

**Materials.**—$B_2Cl_4$ was prepared by passing $BCl_3$ through a glow discharge between mercury electrodes, using a procedure similar to that of Wartik, Moore and Schlesinger.[3] It was purified by fractional condensation.

All samples used in this work were approximately 1.4 mmoles. The vapor pressure at 0° of each sample was measured individually; all were found to be in the range 44.0 ± 1.0 mm., in reasonable agreement with previously reported values. Measurements of the volume, pressure and temperature of the gaseous samples combined with subsequent weighing indicated a molecular weight equal, within experimental accuracy (about 1%), to the calculated value. The samples were condensed, sealed in glass ampoules and stored in liquid nitrogen until used.

The chlorine was purified by fractional bulb-to-bulb distillation.

**The Reaction Vessel.**—The reaction vessel (Fig. 1) consisted of a Pyrex bulb A 2.8 cm. o.d. and 21 cm. long having a re-entrant 5 mm. tube B extending to within 2 mm. of the bottom. The re-entrant tube passed through the top of the bulb to a break-seal C. Above this seal extended a 6 mm. tube D 30 cm. long, through which a close-fitting glass rod E, attached at the top with a length of rubber tube F, extended down to the break-seal. A stopcock was attached to the side of the upper tube near its top. Another tube G attached to the top of the bulb communicated to a sidearm H.

**The Calorimeter.**—The calorimeter, laboratory designation Calorimeter XV,[4] is of the twin-resistance-bridge steady-state type, designed primarily for measurement of the power of radioactive materials. The heat-distribution error, defined as the maximum spread in the values of the apparent power of a small radioactive source placed at various points throughout the 21 cm. length of the central chamber, is 0.1%. This characteristic, together with the general heat flow integrating nature of the instrument, permits use of glass reaction vessels with no difficulty due to the poor thermal conductivity of the material. The bridge output is proportional to power or heat flow; for measuring reaction heats, the power *vs.* time integral is approximated by summation at short-time intervals. About one hour was required to complete the reaction and dissipate all heat in these experiments. The precision and accuracy for the amounts of heat (about 100 cal.) liberated in these runs is 1% or somewhat better.

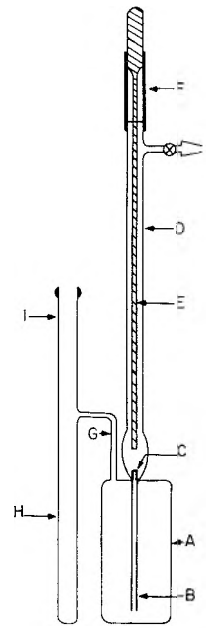


Fig. 1.—The reaction vessel (not to scale).

**Experimental Procedure.**—A new reaction vessel was required for each run. It was first evacuated and flamed and then filled with dried helium. A weighed ampoule of $B_2Cl_4$ and a glass-enveloped magnet were inserted quickly in the sidearm and the vessel was re-evacuated and sealed off at I (Fig. 1). The ampoule was then broken, the $B_2Cl_4$ condensed in bulb A with liquid nitrogen, and the sidearm sealed off at G. The fragments of the ampoule were later recovered and weighed.

The reaction vessel was placed immediately in the calorimeter and allowed to equilibrate thermally for about 45 minutes. A bulb containing chlorine at 1.5 atmospheres pressure was connected to the reaction vessel through a glass heat exchanger, immersed in the same thermostat with the calorimeter, and a fine glass capillary which served to reduce the rate of reaction. The temperature of the chlorine bulb was reduced to the point where its vapor pressure was only slightly greater than that of the $B_2Cl_4$ in the reaction vessel. The reaction was initiated by breaking the breakseal on the reaction vessel and the temperature of the chlorine bulb was then gradually raised. The time taken to admit the stoichiometric quantity of chlorine varied from about 5 to 20 minutes in various runs. After completion of the reaction and pressure equilibration, the vessel contained $BCl_3$ and $Cl_2$ in a mole ratio of approximately two to one, at a total pressure of 1.15 atmospheres.

Following the run the calorimeter was calibrated electrically. The gases then were transferred from the reaction vessel to a flask by condensation with liquid nitrogen and were subsequently hydrolyzed with water. Boric acid in the solution was determined by titration with sodium hydroxide, using mannitol and a *p*H meter.

**Results.**—Results of the measurements are given in Table I. The reaction temperature was varied in an effort to find conditions reducing the amount of side reaction as evidenced by solid residues remaining in the reaction vessel. At 10° approximately 27% of the $B_2Cl_4$ was in the gas phase; at 25°, 52%; and at 45°, 100%. All of the $BCl_3$ produced was gaseous in all runs. The observed heats are corrected for the heat effect associated with admission of the chlorine to the vessel, for the conversion from constant volume to constant pressure, and for the heat of vaporization of the gaseous portion of the $B_2Cl_4$, using a heat of va-

(1) This work was performed under the auspices of the U.S. Atomic Energy Commission.

(2) E. F. Apple and T. Wartik, *J. Am. Chem. Soc.*, **80**, 6153 (1958).

(3) T. Wartik, R. E. Moore and H. I. Schlesinger, *ibid.*, **71**, 3265 (1949).

(4) S. R. Gunn, University of California Radiation Laboratory, UCRL-5375, November, 1958.

porization[5] of 8.0 kcal. mole$^{-1}$ to give $\Delta H°$ for the reaction

$$B_2Cl_4(l) + Cl_2(g) \longrightarrow 2BCl_3(g) \quad (1)$$

TABLE I

HEAT OF REACTION OF $B_2Cl_4$ WITH $Cl_2$

| Run | Temp., °C. | $-\Delta H$, kcal. mole$^{-1}$ |
|---|---|---|
| 1 | 25 | 68.1 |
| 2 | 25 | 67.3 |
| 3 | 45 | 67.2 |
| 4 | 45 | 67.3 |
| 5 | 10 | 68.0 |
| 6 | 10 | 65.9 |

No $\Delta C_p$ correction was applied to the 10 and 45° runs. The amount of reaction is referred to the weight of the sample. The defined thermochemical calorie, 4.1840 absolute joules, is used.

In all runs a small amount of brown solid was formed in the reaction vessel. Part of this distilled very slowly into the hydrolysis flask along with the gaseous products, the remainder being lighter in color. The nature of these materials is not known. If they contain boron, it is unlikely that the part of them transferred to the hydrolysis flask would be hydrolyzed to boric acid under the mild conditions employed; hence the boric acid titration is felt to be a reasonably accurate indication of the amount of $BCl_3$ formed. The boric acid found was about 97% of the theoretical for all runs except number 6, in which it was 94%; this run also gave the lowest heat value.

In view of the side reactions occurring and the probability that their molar heat is less than that of reaction 1, it is believed that a value of $-68 \pm 2$ kcal. mole$^{-1}$ should be assigned to $\Delta H°$ for reaction 1. Using $-97.1$ for $\Delta H_f°$ $(BCl_3,g)$,[6] the standard heat of formation of $B_2Cl_4(l)$ is $-126.2$ and of $B_2Cl_4(g)$, $-118.2$.

The thermochemical-bond energy of the boron–boron single bond may be calculated if one assumes the B–Cl bond to be the same as in $BCl_3$. This assumption is supported by the observed near equality of the B–Cl distance in the two compounds.[7-9] Using $135.2 \pm 4$ for $\Delta H_f°$ (B, g),[7] and 29.012 for $\Delta H_F°$ (Cl, g),[10] $E$(B–Cl) is 106.4 and $E$(B–B) is 79.0. This value may be compared with the dissociation energy of the $B_2$ molecule; Gaydon[11] gives for this a value of 69 and Chupka[12] gives $65 \pm 7$.

**Acknowledgment.**—We wish to express our appreciation to Professor Thomas Wartik of the Pennsylvania State University for suggestion of the investigation and for provision of $B_2Cl_4$ samples used in exploratory measurements.

(5) G. Urry, T. Wartik, R. E. Moore and H. I. Schlesinger, *J. Am. Chem. Soc.*, **76**, 5293 (1954).

(6) W. H. Johnson, R. G. Miller and E. J. Prosen, *J. Research NBS*, **62**, 213 (1959).

(7) D. E. Mann and L. Fano, *J. Chem. Phys.*, **26**, 1665 (1957).

(8) M. Atoii, P. J. Wheatley and W. N. Lipscomb, *ibid.*, **27**, 196 (1957).

(9) C. Spencer and W. N. Lipscomb, *ibid.*, **28**, 355 (1958).

(10) F. D. Rossini, *et al.*, Circular of the National Bureau of Standards 500, (1952).

(11) A. G. Gaydon, "Dissociation Energies and Spectra of Diatomic Molecules," 2nd ed., Chapman and Hall, Ltd., London, 1953.

(12) W. A. Chupka, Argonne National Laboratory, private communication.

# DETERMINATION OF ASSOCIATION EQUILIBRIA BY THE METHOD OF CONTINUOUS VARIATIONS

BY T. W. GILBERT, JR.

*Chemistry Department, The Pennsylvania State University, University Park, Pa.*

*Received May 6, 1959*

The method of continuous variations, originated by Job,[1] and recently critically reviewed by Woldbye,[2] is widely used for the determination of the ratio in which two chemical species react to form a single product. Most commonly, the product is a soluble complex, the concentration of which can be determined by spectrophotometry. If the ratio of the reactants is continuously varied in a series of solutions such that the sum of the reactant concentrations is constant, then the observation of the ratio at which the maximum amount of product is obtained allows the combining ratio of the reactants to be calculated.

A common misconception about this method is that the "extended tangents" or "limiting slopes" of the experimental curve should intersect at the same ratio of reactants as the location of the maximum of the curve. Indeed, many authors have used these tangents to locate the position of the maximum in the belief that a more precise estimation could be obtained in this manner than from the maximum of a broad and often irregular experimental curve.

That such a practice has no theoretical justification and can lead to erroneous conclusions, is easily demonstrated. Consider the hypothetical case of a metal atom M reacting with a ligand A to form a complex according to the equation

$$M + 3A \rightleftharpoons MA_3 \quad (1)$$

It is assumed that no other complexes of M and A are formed to any significant extent. A value for the formation constant is assumed to be

$$K = \frac{[MA_3]}{[M][A]^3} = 10^{14} \quad (2)$$

If a continuous variations experiment is carried out to establish the formula of the complex by mixing $x$ volumes of a $10^{-4}$ $M$ solution of M with $(1 - x)$ volumes of a $10^{-4}$ $M$ solution of A, these equations, together with equation 2, describe the system.

$$10^{-4}x = [M] + [MA_3] \quad (3)$$

$$10^{-4}(1 - x) = [A] + 3[MA_3] \quad (4)$$

From (3) and (4)

$$10^{-4} = [M] + [A] + 4[MA_3] \quad (5)$$

A theoretical continuous variations curve can now be calculated. Let the quantity $R$ be defined as

$$R = [MA_3]/[M] \quad (6)$$

Equations 2 and 5 then become

$$\log R - 3 \log [A] = 14 \quad (7)$$

$$[MA_3] = R(10^{-4} - [A])/(1 + 4R) \quad (8)$$

If values of $R$ are now assumed, values of [A] can

(1) P. Job, *Ann. chim.*, [10] **9**, 113 (1928).

(2) F. Woldbye, *Acta Chem. Scand.*, **9**, 299 (1955).

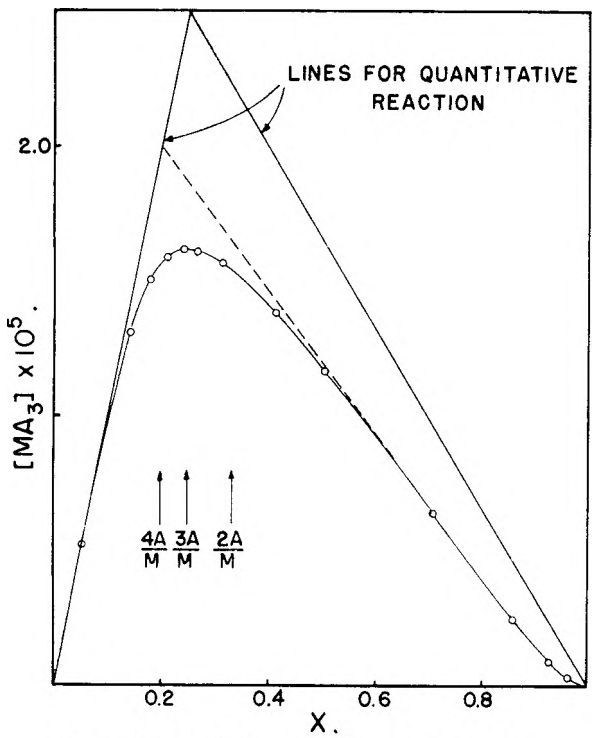


Fig. 1.—Theoretical continuous variations curve.

be found from equation 7. Substitution of these in equation 8 yields values of $[MA_3]$. The corresponding values of $x$ are found from equation 3

$$x = 10^4([M] + [MA_3]) = 10^4(R + 1)[MA_3]/R$$

A plot of $[MA_3]$ *vs.* $x$ then gives the characteristic continuous variations curve. Calculated values of $[MA_3]$ and $x$ are shown in Table I and are plotted in Fig. 1. For comparison, the lines obtained assuming that reaction 1 is quantitative are also shown (*i.e.*, the dissociation of $MA_3$ is negligible).

TABLE I

CALCULATED VALUES FOR CONTINUOUS VARIATIONS CURVE

| $R$ | $[MA_3] \times 10^5$ | $x$ |
|---|---|---|
| 50 | 0.5132 | 0.0523 |
| 10 | 1.307 | .1444 |
| 5 | 1.504 | .1805 |
| 3 | 1.591 | .2121 |
| 2 | 1.619 | .2428 |
| 1.5 | 1.615 | .2691 |
| 1.0 | 1.569 | .3138 |
| 0.5 | 1.382 | .4145 |
| .3 | 1.167 | .5057 |
| .1 | 0.6429 | .7071 |
| .03 | .2499 | .8581 |
| .01 | .09169 | .9261 |
| .003 | .02872 | .9603 |
| .001 | .00975 | .9755 |
| .0001 | .00099 | .9897 |

The position of the maximum in a continuous variations experiment in which the complex formed is $M_aA_b$ is given by $x = a/(a + b)$.[2] For the complex in this example, $MA_3$, the maximum would therefore be expected at $x = 0.25$. The curve in Fig. 1 shows that this is the case, but if the "limiting slopes" are drawn as one might do assuming that Fig. 1 represents a set of experimental data, it is seen that the lines do not intersect at $x = 0.25$ but at a value very close to $x = 0.20$. Accordingly, if this point of intersection is taken to represent the composition of the complex, the erroneous conclusion is reached that the complex formed is $MA_4$ rather than $MA_3$.

It is clear, therefore, that the practice of using "extended tangents" or "limiting slopes" has no foundation in theory, and can in fact lead to wrong conclusions even in the simple case of the formation of a single complex from two reactants. Their use in a system involving the formation of a 1:1 complex is, of course, justifiable since the curve obtained is symmetrical. However, the errors resulting when they are applied to other systems increase greatly as the ligand number of the complex increases and the curves become more and more unsymmetrical.

## THERMAL AGING OF SILICA GELS

BY A. C. MAKRIDES

*Union Carbide Metals Company, Niagara Falls, N. Y.*

*Received May 13, 1959*

There have been relatively few careful studies of thermal aging of silica gels.[1-4] In cases of dry heating it is found that although the pore volume diminishes on aging, the Kelvin radius remains essentially unaltered.[5] However, results on the relation between pore volume and surface area are contradictory. Milligan and Rachford[1] and Shapiro and Kolthoff[2] found the pore volume to decrease only slightly up to about 700° while the surface area, as calculated by them, decreased appreciably. This "anomalous" relation between porosity and surface area was attributed[2] to a decrease of surface roughness of primary particles of the gel, unaccompanied by changes in the average distance between them. According to Van Nordstrand, Kreger and Ries,[3] however, the pore volume decreases linearly with the surface area, with the possible exception of a silica aerogel for which insufficient data were reported.

Previous surface areas were obtained from BET plots of water isotherms.[1,2] It has since become apparent that reversible adsorption of water vapor on silica gel is a sensitive function of the number of tightly bound surface hydroxyl groups.[6-9]

(1) W. O. Milligan and H. H. Rachford, Jr., THIS JOURNAL, **51**, 333 (1947).

(2) I. Shapiro and I. M. Kolthoff, *J. Am. Chem. Soc.*, **72**, 776 (1950).

(3) R. A. Van Nordstrand, W. E. Kreger and H. E. Ries, Jr., THIS JOURNAL, **55**, 621 (1951).

(4) J. H. deBoer and J. M. Vleeskens, *Koninkl. Ned. Akad. Wetenschap., Proc.*, **B60**, 234 (1957).

(5) "Radius" implies pores of circular cross section. The pore structure is probably of much greater complexity. However, the geometry assumed is convenient for calculations and is used generally in the literature.

(6) V. A. Dzis'ko, A. A. Vishnevskaya and V. S. Chesalova, *Zhur. Fiz. Khim.*, **24**, 1416 (1950).

(7) (a) A. V. Kiselev, K. G. Krasil'nikov and L. N. Soboleva, *Doklady Akad. Nauk SSSR*, **94**, 85 (1954); (b) L. D. Belyakova, O. M. Dzhigit and A. V. Kiselev, *Zhur. Fiz. Khim.*, **31**, 1577 (1957); (c) S. P. Zhdanov and A. V. Kiselev, *ibid.*, **31**, 2213 (1957).

(8) (a) S. P. Zhdanov, *Doklady Akad. Nauk SSSR*, **68**, 99 (1949); (b) **100**, 1115 (1955); (c) **115**, 938 (1957).

(9) M. M. Egorov, K. G. Krasil'nikov and E. A. Syosev, *ibid.*, **108**, 103 (1956).

Above 200° –OH groups are desorbed (as $H_2O$) and subsequent reversible adsorption of $H_2O$ decreases. The decrease is approximately equal to the loss of hydroxyl groups, suggesting a one to one correspondence between adsorbed $H_2O$ molecules and surface –OH groups.[6] Surface areas obtained from $H_2O$ or other polar adsorbates are not reliable since the number of adsorption sites, and hence the apparent cross sectional area of adsorbed molecules, is strongly dependent on thermal or other pretreatment of the gel. Surface areas determined from the BET theory using nitrogen as the adsorbate are reproducible, however, and reliable results are obtained both with untreated and thermally aged gels.[10]

In view of the above, the results of Milligan and Rachford[1] were re-examined using Fu and Bartell's method for obtaining surface areas.[11] This method involves the determination of spreading pressure $\phi$ as a function of relative pressure. The calculation assigns the properties of bulk liquid to the adsorbate beyond the onset of hysteresis. For a porous adsorbent, the free energy change for adsorption beyond this point is equal to the free energy loss for destruction of $A$ cm.$^2$ of liquid–vapor interface, $\gamma A = \phi(p^0) - \phi(p')$, with $\gamma$ the surface tension of (bulk) water.

The spreading pressure–relative pressure curve consists of two sections, each obeying an equation of the form $\phi = \alpha p^\beta$. $\phi(p')$ is given by their intersection. Alternatively, $\phi(p')$ may be obtained from a log-log plot of $\phi$ *vs.* $(P/P_0)$. A more extensive discussion of the method is given in ref. 11.[12]

Results are given in Table I. The calculated decrease of surface area with aging is in general agreement with ref. 3 and 4. Van Nordstrand, Kreger and Ries[3] found with a Davisson gel a 10% reduction in area after 12 hours at 600°. The area decreased rapidly at higher temperatures (20% at 700°, 50% at 900°). deBoer and Vleeskens[4] reported that dry heating below 650° caused an initial fast (< 6 hours) decrease of about 5 to 10% followed by a slow change which was negligible in 40 days at 450° and was only 10% in 30 days at 650°. The present data also show a relatively small (10%) reduction in area below 650°, with a more rapid decrease at higher temperatures (45% at 790°). It may be concluded that aging at temperatures below 650° reduces the area by only 10 to 15% with a more rapid change occurring at higher temperatures.

The Kelvin radius is 28 ± 0.5 Å. and is independent of aging.[1] This value does not include the thickness of a layer about two molecules thick adsorbed below 0.5 relative pressure. The corrected Kelvin radius is about 34 Å. (see ref. 3). The average radius, given by $2Vs/A$, where $A$ is the area calculated here, is 36 Å. and increases slightly (to 39 Å.) on aging. In contrast, average radii calculated from BET areas are appreciably larger and increase significantly (from 47 to 72 Å.) on aging. The pore volume is approximately a linear function of $A$. Pore volume–surface area curves obtained from BET and from methyl red adsorption[2] cannot be interpreted in any simple manner.[2]

These observations suggest that areas calculated here correspond closely to the actual area of the gel. Apparent cross sectional areas which must be assigned to the $H_2O$ molecule to allow coincidence of BET areas with the present calculation are given in Table I. Values reported by others range from 11.7 to 24.6 Å.[2,9,13–15]

Heating in air above 400°, followed by rehydration, does not restore the surface to its original condition. The apparent cross sectional area of the water molecule increases by about 50%. It may be concluded that the density of adsorption sites diminishes with aging. If it is assumed that these sites are surface –OH groups, this result is in agreement with the work of Zhdanov[8a] who observed a permanent decrease in the number of –OH groups/cm.$^2$ for thermally-aged silica gels.

TABLE I[a]

| Aging temp., °C. | BET area[b] (m.$^2$/g.) | Fu and Bartell (m.$^2$/g.) | $\omega_{H_2O}$ (Å.$^2$) | $\phi = \gamma_{SO} - \gamma_{SL}$[c] (ergs/cm.$^2$) |
|---|---|---|---|---|
| 30 | 385 | 485 | 13.0 | 190 |
| 200 | 375 | 510 | 13.4 | 200 |
| 300 | 360 | 495 | 13.5 | 200 |
| 400 | 340 | 460 | 13.7 | 200 |
| 450 | 315 | 470 | 14.9 | 190 |
| 500 | 311 | 465 | 15.1 | 185 |
| 600 | 285 | 425 | 15.5 | 195 |
| 650 | 260 | 430 | 15.8 | 175 |
| 725 | 200 | 380 | 18.1 | 170 |
| 790 | 145 | 280 | 18.7 | 175 |
| 880 | (65) | (90) | .. | (238) |

[a] Results from ref. 1. Samples evacuated to $5 \times 10^{-6}$ to $1 \times 10^{-5}$ mm. and isotherms with water vapor obtained at 12 ± 0.001°. [b] BET areas calculated here differ by less than 5% from values given in ref. 1. Since interpolation at small X is relatively less precise than at higher adsorption values used in the calculation, it is estimated that interpolation errors do not exceed 3%. [c] Free energy changes for wetting $\phi$ calculated from Gibb's equation (see ref. 13).

**Temperature Dependence.**—Shapiro and Kolthoff[2] found that a plot of the logarithm of relative density against the reciprocal of aging temperature exhibited two characteristic slopes, the transition occurring at about 700°. This suggested a change in aging mechanism from surface diffusion to bulk diffusion.[2] It was also concluded, from the "anomalous" relation between porosity and surface area, that the primary particles have a very irregular surface contour which is smoothed out on heating below 700°.[2]

A plot of relative area, using values determined here, against the reciprocal of aging temperature follows closely the relative density plot.[2] Our analysis confirms, therefore, the suggestion that a

(10) K. G. Krasil'nikov, V. F. Kiselev, N. V. Kapitonova and E. A. Syosev, *Zhur. Fiz. Khim.*, **31**, 1448 (1957).

(11) Y. Fu and F. E. Bartell, THIS JOURNAL, **55**, 662 (1951).

(12) In general, areas derived by this method are in excellent agreement with BET areas. Fu and Bartell's method gives correct results even in cases where the BET calculation is not reliable because of uncertainty in the cross sectional area of the adsorbate (see, for example, butane on silica gel in ref. 11).

(13) J. J. VanVoorhis, R. G. Craig and F. E. Bartell, *ibid.*, **61**, 1513 (1957); **61**, 1520 (1957).

(14) A. V. Kiselev, N. N. Mikos, M. A. Romanchuk and K. D. Shcherbakova, *Zhur. Fiz. Khim.*, **21**, 1223 (1947).

(15) N. Hackerman and A. C. Hall, THIS JOURNAL, **62**, 1212 (1958).

change in aging mechanism occurs at about 700°. However, the area decrease at $T < 700°$ is considerably less than suggested in ref. 2. If it is attributed entirely to surface smoothing, the roughness factor of the primary particles of this gel is only 1.18.

**Free Energy Change for Wetting.**—Table I gives free energy changes for adsorption from $p = 0$ to $P/P_0 = 1$. Since the area of the liquid–vapor interface at $P/P_0 = 1$ is negligible, these are also free energy changes for wetting the gel with water, $\phi = \gamma_{SO} - \gamma_{SL}$, where $\gamma_{SO}$ and $\gamma_{SL}$ are solid–vacuum and solid–liquid interfacial energies.

The uncertainty in absolute $\phi$-values is probably about 10%. The major source of error is extrapolation to $P/P_0 = 0$. Reported free energy changes for wetting silica gels and powders with water range from 140 to 320 ergs/cm.$^2$.[2,13-16]

Below 650° $\phi(P_0)$ averages 195 ergs/cm.$^2$ and appears to be independent of aging temperature. A small decrease ($\sim$10%) is observed after aging at higher temperatures. The relatively minor dependence of $\phi$ on the temperature of heat treatment implies that changes in surface composition brought about by aging alter $\gamma_{SO}$ and $\gamma_{SL}$ to about the same extent.

(16) G. E. Boyd and H. K. Livingston, *J. Am. Chem. Soc.*, **64**, 2383 (1942).

## THE REACTION BETWEEN TITANIUM TETRACHLORIDE AND ALUMINUM TRIETHYL

BY ELMER J. BADIN

*Contribution from Central Research Laboratories, Celanese Corporation of America, Summit, New Jersey*

*Received March 16, 1959*

Previous investigations have shown that organometallic compounds are capable of reacting with halides of transition elements and that such reactions lead to reduction in the valence state of the transition element. For example, Levy[1] stated that titanium tetrachloride is reduced to titanium trichloride by heating at 100° with mercury diethyl. Challenger, Pritchard and Jinks[2] showed that titanium tetrachloride reacted with and was reduced by bismuth triphenyl or by phenylmagnesium bromide. Gilman, Jones and Woods[3] demonstrated the reaction between titanium tetrachloride and lithium methyl or ethylmagnesium bromide. The reduction of titanium tetrachloride or chromyl chloride by triethylgermanium hydride was shown by Anderson.[4] An investigation of the kinetics of the reduction of titanium tetrachloride with aluminum triisobutyl gave results[5] interpreted as a second-order reaction with an activation energy of 20 kcal. per mole. The reduction of halides such as vanadium tetrachloride or vanadium oxytrichloride, has been investigated rather thoroughly.[6,7] Each of the above reactions may be considered as an oxidation–reduction reaction. Each may be explained by postulating formation of an organo-transition element compound which on decomposition leads to a lower valent halide of the transition element.

In this paper, results of a brief investigation of the reaction between titanium tetrachloride and aluminum triethyl are reported. The research was carried out with the objective of elucidating the structure of the reaction complex formed during the reaction.

### Experimental

Experiments were carried out in a 1 liter reaction flask, equipped with a stainless steel stirrer blade revolving at high speed. The total volume of the reactants and the solvent cyclohexane was 400 ml. The reaction mixture was kept at all times under a nitrogen atmosphere. The aluminum triethyl, (1.87 *M* solution in cyclohexane), obtained from U. S. Industrial Chemicals Company, was added to the proper volume of solvent maintained at the reaction temperature (± 0.5°). The titanium tetrachloride (1.82 *M* solution in cyclohexane), obtained from Matheson Coleman and Bell, The Matheson Company, was then pipetted into the aluminum triethyl–solvent mixture. A certain error was introduced in this manner of addition since the rate of reaction depended on the ratio of titanium tetrachloride to aluminum triethyl. This ratio, of course, changed continuously during the period, about 100 seconds, of addition of the second reagent. Timing of the reaction was started at the moment of the addition of the last of the titanium tetrachloride.

Ten-ml. samples of the reaction mixture were withdrawn periodically and added to 10 ml. of 6 *N* hydrochloric acid in 20 ml. of water. The mixture then was titrated directly for Ti(III) with ferric ammonium sulfate, using KSCN as indicator.

Gas analyses (gas phase chromatography) of the gas evolved during the reaction (molar ratio of $TiCl_4$ to $Al(C_2H_5)_3$ of 2:1) showed the presence of ethane. Ethylene, if formed, was presumed to have polymerized; a further investigation of this would be of value.

### Results

The primary step in the reduction may be taken as

$$TiCl_4 + AlR_3 \longrightarrow RTiCl_3 + AlR_2Cl$$
$$\downarrow\uparrow$$
$$R + TiCl_3 \qquad (1)$$

It is to be noted that reduction of titanium does not occur until $RTiCl_3$ dissociates. Initial experiments demonstrated that, with excess of aluminum triethyl, reduction proceeded very quickly and reached a constant value. In addition, with excess of aluminum triethyl, reduction proceeded beyond the Ti(III) stage, Ti(II) being formed, an observation verified by others.[7,8] Continued reduction may be represented by equation 2 in addition to certain others that might be postulated.

$$RTiCl_3 + AlR_3 \longrightarrow R_2TiCl_2 + AlR_2Cl$$
$$\downarrow\uparrow$$
$$2R + TiCl_2 \qquad (2)$$

The existence of relatively stable compounds

(1) L. Levy, *Ann. chim. phys.*, **25**, 477 (1892).

(2) F. Challenger, F. Pritchard and J. R. A. Jinks, *J. Chem. Soc.*, **125**, 864 (1924).

(3) H. Gilman, R. G. Jones and L. A. Woods, *J. Am. Chem. Soc.*, **76**, 3615 (1954).

(4) H. H. Anderson, *ibid.*, **79**, 326 (1957).

(5) C. Feldman, L. C. Arnold and D. W. McDonald, paper presented at 131st Am. Chem. Soc. Meeting, Miami, Florida, April 1957.

(6) W. L. Carrick, W. T. Reichle, R. W. Kluiber, E. F. Bonner and J. J. Smith, paper presented at 133rd Am. Chem. Soc. Meeting, San Francisco, California, April, 1958.

(7) W. L. Carrick, A. G. Chasar and J. J. Smith, paper presented at 134th Am. Chem. Soc. Meeting, Chicago, Illinois, September, 1958.

(8) D. B. Ludlum, A. W. Anderson and C. E. Ashby, *J. Am. Chem. Soc.*, **80**, 1380 (1958).

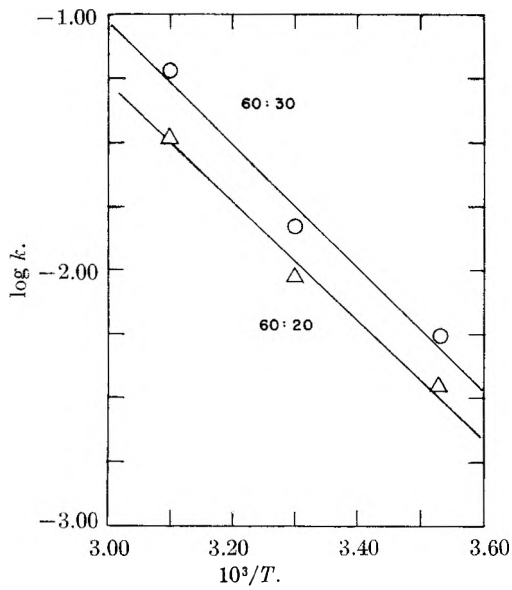


Fig. 1.—Arrhenius plot for reaction between titanium tetrachloride and aluminum triethyl. Ratios of initial concentrations, $TiCl_4$: $Al(C_2H_5)_3$, in millimoles per liter are indicated.

such as $RTiCl_2$ and $R_2TiCl_2$ has been demonstrated.[9] In view of the speed of the reaction when excess of aluminum triethyl was present, the investigation was confined to reaction mixtures containing excess of titanium tetrachloride. Ratios of titanium tetrachloride to aluminum triethyl of 2:1 and 3:1 were chosen.

In a given set of experimental data, the amount of reduction, after an initially fast rise, leveled off after about 30 minutes. The data were treated as a second-order process. A tabulation of the rate constants obtained here is shown in Table I.

TABLE I

REACTION BETWEEN TITANIUM TETRACHLORIDE AND ALUMINUM TRIETHYL

| Reactants, mmole | | | $k$ specific | | |
|---|---|---|---|---|---|
| $TiCl_4$ | Al-$(C_2H_5)_3$ | Temp., °C. | × $10^2$, l./mole/sec. | $E_a$, kcal./mole | $\Delta S^*$, e.u. |
| 60 | 20 | 10 | 0.35 | 10.5 | −35 |
| 60 | 20 | 30 | 0.94 | 10.5 | −35 |
| 60 | 20 | 50 | 3.33 | 10.5 | −35 |
| 60 | 30 | 10 | 0.55 | 11.1 | −32 |
| 60 | 30 | 30 | 1.47 | 11.1 | −32 |
| 60 | 30 | 50 | 6.03 | 11.1 | −32 |

The energy of activation was calculated from an Arrhenius plot as shown in Fig. 1, and found to be 10.5 or 11.1 kcal. per mole. The entropy of activation was determined using the absolute reaction rate equation. Data showing the rate constants, the energy of activation (10.5 or 11.1 kcal. per mole) and the entropy of activation (−32 or −35 e.u.) are shown in Table I.

## Discussion

Although it is well known that too much significance is not to be attached to entropy of activation values, some conclusions may be drawn from the relatively large negative entropy of activation, $\Delta S^*$, obtained. This figure is a measure of the association or "freezing" occurring in an activated complex. It should represent the sum of the molar entropies of fusion of the molecules in the complex. The molar entropy of fusion of titanium tetrachloride calculates to be 9.2 e.u. (cal. per mole °/K.) If the molar entropy of fusion of aluminum triethyl is estimated (heat of fusion data have not been published, but an estimate may be made on the basis of the known heat of fusion of indium trimethyl) at 10–12 e.u., the value obtained would account for an activated complex containing one molecule of titanium tetrachloride and two molecules of aluminum trialkyl. Accordingly, the primary step of the reaction is best represented as

$$TiCl_4 + Al_2R_6 \longrightarrow RTiCl_3 + AlR_2Cl + AlR_3 \quad (3)$$

The activated complex involving a negative entropy change of 32 to 35 e.u. is then postulated as structure 4

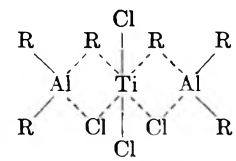


(4)

A six-membered ring coördinate structure, previously proposed as an intermediate,[10] is considered as less favorable than (4), which shows titanium with a coördination number of six and aluminum with a coördination number of four.

The dotted line bonding involving "half-bonds," "one-electron bonds" or "electron deficient bonds" is well known in the case of organometallic compounds. Thus, lithium alkyls are known to associate to hexamers,[11] beryllium alkyls form long polymer chains of associated molecules[12] and aluminum alkyls dimerize.[13] An R (alkyl) group attached to a metal by what amounts to a one-electron bond may be considered as a quasi-stabilized radical.

It is quite possible that the reaction mixture of titanium tetrachloride and aluminum trialkyl contains extended structures such as in (4). Further coördination at the ends of this compound might occur to increase the length of such chains. If some $TiCl_3$ were present, it is possible that an extended or polymeric structure, similar to (4) and with a repeating unit as in (5), would be formed. Such a speculative structure, with coordination numbers of six for titanium and four for aluminum, is very likely. It may be noted that the one odd valence electron (indicated by a dot in (5)) might influence the nature of the bonding shown. It is, of course, understood that in the stable compounds some dipoles, $Ti^{\delta+}$—$R^{\delta-}$ and $Al^{\delta+}$—$R^{\delta-}$, would exist; these might disap-

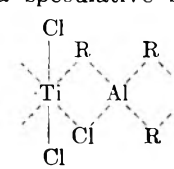


(5)

(9) Belgian Patent 553,477, Preparation of Organo-halo-titanium Compounds, December, 1956.

(10) E. J. Badin, *J. Am. Chem. Soc.*, **80**, 6545 (1958).

(11) G. Wittig, F. J. Meyer and G. Lange, *Ann.*, **571**, 167 (1951).

(12) A. I. Snow and R. E. Rundle, *Acta Cryst.*, **4**, 348 (1951).

(13) K. S. Pitzer and H. S. Gutowsky, *J. Am. Chem. Soc.*, **68**, 2204 (1946).

pear on dissociation or decomposition. The solid material formed in this reaction appeared to be somewhat gelatinous and did not exhibit a crystalline X-ray pattern, although pure reduced titanium halides did. This supplies inferential evidence regarding a polymeric structure containing "electron deficient" bonds as in (5) for the nature of the reaction mixture.

## KINETICS OF THERMAL ISOMERIZATION OF *p*-TOLYL ISOCYANIDE[1]

BY GUNDOLF KOHLMAIER[2] AND B. S. RABINOVITCH

*Contribution from the Department of Chemistry, University of Washington, Seattle*

*Received May 11, 1959*

As an exploratory study, an examination of the thermal isomerization of *p*-tolyl isocyanide has been made. The only quantitative information in the literature on isomerization of isocyanides is a mention by Ogg[3] of incomplete work on methyl and ethyl isocyanide wherein activation energies of some 40 kcal. and frequency factors $>10^{13}$ sec.$^{-1}$ are quoted.

### Experimental

**Materials.**—*p*-Tolyl isocyanide was prepared by the method of Klages and Monkemeyer.[4] Purification by recrystallization from 70% aqueous methanol gave good results. The isocyanide, white crystals with a green cast, had m.p. 20–21°. It was stored at Dry Ice temperature.

Solvent for solution studies was Nujol. It was free of water and contained no unsaturates.

**Experimental Procedure. Solution Studies.**—A Nujol solution of *p*-tolyl isocyanide was degassed by freeze–pump–melt cycles and was poured under vacuum into borosilicate tubes, 3 mm. i.d., holding 0.4 ml. of solution. The tubes were sealed leaving space for expansion. Dead space at reaction temperature was ~0.03 ml. The samples were transferred to a liquid thermostat for reaction times of 3 to 60 minutes. The temperature was controlled to better than 0.05°. A correction for the time required to heat the samples was applied.

Reacted samples were quenched in cold water and the solution was transferred with a hypodermic syringe into the liquid cell of a Beckman IR-2 spectrometer. Reaction percentage varied between 10–55%.

**Gas Phase Studies.**—With a calibrated micropipette, 0.1 mmole of isocyanide was inserted into a 1 ml. finger on each of several 100 ml. nitrogen filled bulbs and was immediately frozen. The sample was subjected to the freeze–pump–melt procedure, the bulb was sealed and was immersed in the thermostat. Reaction pressure was ~30 mm. After reaction, the finger was dipped into liquid nitrogen and all isocyanide condensed. The vessel was opened, 0.5 ml. of Nujol was injected to yield a 0.2 *M* solution of isocyanide–nitrile, comparable to the liquid-phase studies. Reaction percentage varied between 16–67%.

**Analysis.**—The C≡N stretching frequencies at 4.48 $\mu$ for *p*-tolunitrile and at 4.72 $\mu$ for *p*-tolyl isocyanide were chosen for the purpose of analysis. A calibration curve was constructed from binary isocyanide–nitrile mixtures. The sum of nitrile and isocyanide during a run always totalled 100%, within at most 5%.

### Results

Good first-order rate constants were obtained at different percentages reaction during a run; the average deviation in a run was ~4%. Decrease of concentration in solution and gas phase by a factor roughly two caused no variation in calculated rate constants. The data are summarized in Table I.

No change in the rate was observed for isomerization of non-deaerated solution.

The only product found was *p*-tolunitrile. No *meta* isomer was detected. For reaction times longer than 20 minutes the color of the solution increased from a slight yellow to a light brown. However, no new bands were identified in the infrared spectrum and the analysis was unaffected. The side product was very small since nitrile and isocyanide still added to 100%, and systematic variation of rate constant with time during a run was not observed.

Plots of log $k$ *vs.* $T^{-1}$ were made; the lines had no evident curvature and were fitted by least squares. For Nujol solution $E$ = 36.8 kcal./mole, $A_s = 10^{13.7}$ sec.$^{-1}$; for the gas phase, $E$ = 33.8 kcal./mole, $A_g = 10^{12.5}$ sec.$^{-1}$.

### Discussion

Assuming that the present reaction is unimolecular, the liquid phase studies, and possibly the gas phase work,[5] correspond to the high pressure limit. The frequency factors, $A_s = 10^{13.7}$ sec.$^{-1}$ and $A_g = 10^{12.5}$ sec.$^{-1}$, are characteristic of unimolecular processes.

The heat of isomerization of methyl isocyanide is −15 kcal./mole[6] and this serves to represent the order of magnitude of the heat of isomerization for the present reaction. The fairly large activation energy (35 kcal.) for this exothermic process indicates appreciable bond reorganization in the formation of the activated complex.

TABLE I

RATE CONSTANTS FOR ISOMERIZATION OF *p*-TOLYLISOCYANIDE

| Concentration, Molar | Concentration, Mm. Hg | Temp., °C. | $10^4k$,[a] sec.$^{-1}$ |
|---|---|---|---|
| 0.2 | | 220.0 | 21.9 |
| | | 210.0 | 10.3 |
| | | 200.0 | 4.5 |
| | | 190.0 | 1.92 |
| 0.1 | | 210.0 | 10.0 |
| | 30.0 | 210.0 | 15.6 |
| | | 200.0 | 7.5 |
| | | 190.0 | 3.6 |
| | | 180.0 | 1.65 |
| | 17.0 | 190.0 | 3.7 |

[a] Average of at least three values.

**Mechanism.**—A variety of evidence from different sources[7] indicates that the C—N≡C: configuration is linear, and bond distances[7a] indicate that the principal contribution to the structure is the linear sp-hybridized configuration. The

(1) This work was supported by the National Science Foundation. Abstracted from the M.S. thesis of G. Kohlmaier, University of Washington, 1959.

(2) Fulbright Exchange Fellow, Germany.

(3) R. A. Ogg, Jr., *J. Chem. Phys.*, **7**, 753 (1939).

(4) F. Klages and K. Monkemeyer, *Ber.*, **83**, 501 (1950).

(5) B. S. Rabinovitch and K.-W. Michel, THIS JOURNAL, **63**, in press (1959), give general discussion of unimolecular reactions.

(6) F. D. Rossini, "Selected Values of Chemical Thermodynamic Properties," Natl. Bur. Standards Circular No. 500, 1952.

(7) (a) M. Kessler, H. Ring, R. Trambarulo and W. Gordy, *Phys. Revs.*, **79**, 54 (1950); C. C. Costain, *J. Chem. Phys.*, **29**, 872 (1958). (b) G. Herzberg, "Infrared and Raman Spectra of Polyatomic Molecules," D. Van Nostrand Co., Inc., New York, N. Y., 1947, pp. 293, 332, 352.

C—N≡C: bending vibrational modes enhance the importance of the C—N⁻=C: contribution. The mechanism of isomerization may be seen as a type of "saturated" Wolff rearrangement.[8]

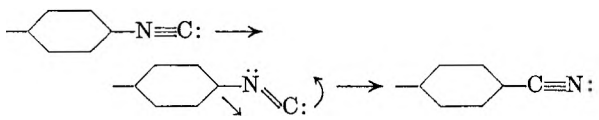

One may in a formal way invoke an intermediate ring structure such as

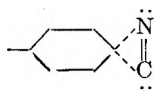

(being cognisant of the valence bond structural ellipsis implied by this single representation) to designate as activated complex. Since the C≡N group after isomerization is in *para* position to the methyl group, only the ring carbon joined to the N≡C group is assumed to take direct part in the reaction. This seems all the more evident since in the isomerization of methyl isocyanide there is no other carbon atom to take part.

**Entropy of Activation.**—Only the stretching frequencies of *p*-tolyl isocyanide have been measured in the infrared spectrum. An approximate vibrational assignment was made for it and for two types of activated complexes: an intermediate ring and a bent structure with free internal rotation. Frequencies were transferred from the analogous compounds methyl isocyanide,[7b] acetonitrile,[7b] cyanogen,[7b] cyclopropene[9] and spiropentane.[10] An internal rotation partition function was evaluated by assuming free rotation of the carbon around the molecule axis. The angle of carbon to nitrogen was taken as 120° and N=C bond length as 1.26 Å.

The entropies calculated are $\Delta S^* = -1.1$ e.u. for the ring complex, and +2.2 e.u. for the internal rotation complex. These numbers are to be construed as qualitative order of magnitude. The observed frequency factor corresponds to −4.8 e.u. for the gas phase results. A negative entropy is characteristic of tightened structure in the activated complex.[11]

The observed entropy and energy of activation are somewhat higher for the solution than for the gas phase reaction. It may be that this difference is an artifact and simply arises from undiagnosed experimental complications. If, however, it is regarded optimistically as a real effect then, using equations due to Kirkwood,[11] it may be at least partially accounted for as due to differential polarization of the solvent by the initial and activated state. A dipole moment decrease from 4.0 to 2.5 *D* results (dielectric constant 1.8 for Nujol) in a calculated entropy of activation increase of 1.0 e.u., and an increased energy of 1.2 kcal. Assumption of a smaller dipole moment in the complex produces a larger effect. But even this rationalization is complicated by the theoretical restrictions involved,[12] as well as the findings by Martin[13] of the inadequacy of the equation for benzonitrile in benzene.

It is intended to extend this work to gas phase studies of unimolecular isomerization of aliphatic isocyanides.

We thank Dr. H. J. Dauben, Jr., for an interesting discussion and Dr. W. M. Schubert for advice on purification of the isocyanide.

(8) C. K. Ingold, "Structure and Mechanism in Organic Chemistry," Cornell University Press, Ithaca, N. Y., 1953, Ch. 9.

(9) D. F. Eggers, private communication.

(10) Scott, Finke, Hubbard, McCullough, Gross, Williamson, Waddington and Huffman, THIS JOURNAL, **72**, 4664 (1950).

(11) S. Glasstone, K. Laidler and H. Eyring, "The Theory of Rate Processes," McGraw-Hill Book Co., New York, N. Y., 1941, pp. 295, 419.

(12) R. P. Bell, *Trans. Faraday Soc.*, **33**, 496 (1937).

(13) A. R. Martin, *ibid.*, **33**, 191 (1937).